TECHNISCHE UNIVERSITÄT WIEN
Vienna University of Technology

Dissertation

SYNTHESIS AND EVALUATION OF PHOTOSWITCHABLE MONOAMINE TRANSPORTER INHIBITORS

ausgeführt zum Zwecke der Erlangung des akademischen Grades eines Doktors der technischen Wissenschaften unter der Leitung von

Prof. Dr. Marko D. Mihovilovic

Institute of Applied Synthetic Chemistry, TU Wien

und unter Mitbetreuung im Rahmen des MolTag-Doktoratskollegs durch

Prof. Dr. Harald H. Sitte

Institute of Pharmacology, Medical University of Vienna

eingereicht an der Technischen Universität Wien

Fakultät für Technische Chemie

von

Dipl.-Ing. Dominik Dreier

Mondscheingasse 6/7-8, 1070 Wien

Vienna, July 22, 2018

Declaration

Hubert Kalaus contributed to the synthetic work in chapter **C I.1.1** and the data collection and interpretation in chapter **C I.1.2**. Details can be found in his bachelor thesis.

Clemens Cziegler and Philipp Miksovsky contributed to the synthetic work in chapter **C I.1.3** and the data collection and interpretation in chapter **C I.1.4**. Details can be found in their bachelor theses.

Charlie Lim contributed to the synthetic work in chapter **C II.1.2**. Details can be found in his bachelor thesis.

Konstantin Raabe contributed to the synthetic work in chapter **C II.2.2**. Details can be found in his bachelor thesis.

Danijela Kojic contributed to the synthetic work in chapter **C II.3.3**. Details can be found in her bachelor thesis.

Pontus Russegger contributed to the synthetic work in chapter **C II.4.2**. Details can be found in his bachelor thesis.

The experimental work in **C II.1.4** and **C II.3.5** was conducted by Marion Holy and Kathrin Jäntsch from the Medical University of Vienna. The experiments were supervised by Prof. Harald Sitte. The electrophysiology experiments were carried out by PhD Walter Sandtner from the Medical University of Vienna.

The computational experiments in **C II.3.6** and **C II.4.5** were carried out by Yuntao Hu (University of Vienna). Details can be found in his master thesis. The work was supervised by Stefanie Kickinger, Eva Hellsberg and Prof. Gerhard Ecker.

The UV-LED well plates (chapter **C III**) were designed and constructed by Wolfgang Tomischko (TU Wien, Institute of Chemical Technologies and Analytics) after an idea of the author (inspired by a presentation of Prof. Dirk Trauner on the work published in *Cell (Cambridge, MA, U.S.)* **2015**, *162*, 403-411.[1]

Computational studies on escitalopram based HTI analogs and subsequent synthesis of some novel derivatives were not covered in this thesis but can be found in Sophia Schnabl's master thesis and Christoph Hillisch's bachelor thesis.

Front Matter

Table of Contents

Acknowledgements

The past four years which I have spent working on this thesis and related projects have been both, challenging and rewarding beyond initial expectations. I was lucky to spend these decisive years in an environment that allowed me to develop professionally and personally in a way I am very satisfied with. I cherish the people I have met, the relationships I have built and the help and inspiration I have received.

Dear Marko. I am cordially grateful for the support and mentorship you have provided. I value the freedom you gave me to explore the world of science and the supply of opportunities and challenges alike. You not only always treated me with respect but were also a friend to me when we “enjoyed” Ouzo in Athens or dancing lessons in Sitges.

Prof. Harald Sitte served as my co-supervisor and close collaborator on the present project. I am very grateful for the joint effort in this challenging research. The pharmacological contributions of his lab boosted the prospects of this work enormously. I am very thankful for the hard work conducted by Marion Holy and Kathrin Jäntsch.

Prof. Gerhard Ecker and his team contributed significantly to this thesis on computational aspects. I am very thankful to Stefanie Kickinger, Eva Hellsberg, Yuntao Hu and Sophia Schnabl for their efforts.

Dr. Walter Sandtner carried out the electrophysiological experiments which I am very grateful for.

Flo, Michi and Christian, your numerous suggestions and inputs in various seminars have helped a lot improving my work and are very much appreciated. Flo, I admire your dedication for appealing presentations which has also motivated me to continuously work on mine. Christian, I very much enjoyed our non-scientific conversations, particularly in the past year. Keep up the good work!

I am very grateful to Wolfgang Tomischko who invested a lot of effort in the construction of the LED well plates which became quite a turning point in my PhD studies.

There have been numerous ups and downs over the years. Along the line enthusiasm and desperation were constant companions. However, one thing never changed. I always loved to come to the lab in the morning. You all created a workplace that I valued and appreciated. Most importantly – my home of the past four years – the geopolitical lab G20 was a great and enjoyable place to work in. Among other fun things, the music-genre themed weekdays (e.g. Austropop Friday) are one hallmark of the lab's unique spirit. I am grateful to all current and former G20, FGMDM, FGPG and FGHF lab members for the wonderful time. Drasi, Resi, David and Daniela, I had the most amazing time with you guys; at sailing trips, skiing trips, Oktoberfest, Prague, Dubrovnik and Pavia; to name just a few special occasions.

As a member of the doctoral program MolTag I was able to get to know many talented and smart colleagues from various disciplines. I am very thankful for the additional value the program created for its members and the opportunities that came with it. Most importantly, my stay at Columbia University was enabled by MolTag which was an incredible experience. Prof. Sames was a fantastic host and made me enjoy my time in New York.

One thing I particularly enjoyed was the supervision of young and enthusiastic students. I was lucky to spend my time in the lab regularly with committed bachelor students who contributed much of their time to this thesis. In chronological order I am very thankful to Hubert Kalaus, Clemens Cziegler, Philipp Miksovsky, Charlie Lim, Konstantin Raabe, Danijela Kojic, Pontus Russegger and Christoph Hillisch who I could convince to rather explore some mad chemistry than to enjoy their summer breaks.

Many friends have accompanied me over the years – Daniel, Drasi, Emanuel, Elias, Ferdi, Georg, Hofi, Koarl, Martin L., Martin P., Michi, Peter and Valentin – the unforgettable times spent with you balance me – thank you for being there! It has been a hell of a ride.

If lab work got too frustrating, I could always count on the members of the LaufTrUppe – Flo, Christian and Drasi – to take my mind off work by some "refreshing" interval training. Thanks for the challenge!

Last but not least, I want to express my deepest gratitude to my family who has been the most reliable support system one could ask for. My dear parents, thank you so much for your unconditional support and love. My dear sister, I know that I can be a difficult brother but you have always been there for me. Meine lieben Großeltern, ich bin euch von tiefstem Herzen dankbar, für alles was ihr für mich und die ganze Familie getan habt und noch immer Unvorstellbares vollbringt. Ihr habt mir durch eure Erziehung wichtige Werte vermittelt und eure bodenständige und aufrichtige Art beeindruckt und prägt mich. Danke für alles!

Abstract

The monoamine transporters SERT (serotonin transporter), DAT (dopamine transporter) and NET (norepinephrine transporter) are essential regulatory features in neurotransmission. These transmembrane proteins are responsible for the reuptake of released neurotransmitters (serotonin, dopamine and norepinephrine) from the synaptic cleft and thereby terminate synaptic signaling. In consequence, transporters influence important neurological processes like mood, sleep, aggression behavior and hunger. A malfunction is linked to many serious diseases like depression, anxiety, ADHD and Parkinson's disease. Over the last decades a rich collection of pharmacologically active compounds was developed to inhibit reuptake. Many reuptake inhibitors are in clinical use best known as antidepressants. Severe side effects remain a great challenge and further insights into the functionality of transporter proteins would have tremendous implications for drug discovery and a deeper understanding of brain related processes.

The precise and reversible mode of action of photoswitchable bioactives poses a great opportunity for novel tool compounds. The research field of photopharmacology has attracted enormous interest and tremendous progress was made in the past years. In this work we sought to develop photoswitchable SERT inhibitors as novel photoswitchable tool compounds to study this important transporter with light as an accurate inhibitory stimulus.

Based on well-studied SERT inhibitors escitalopram and paroxetine we rationally designed and synthesized azobenzene and hemithioindigo analogs. The compound's photophysical parameters were thoroughly investigated. For the light-dependent biological evaluation, we developed (UV) LED well plates which allowed robust and reliable photocontrolled measurements in in-vitro assays.

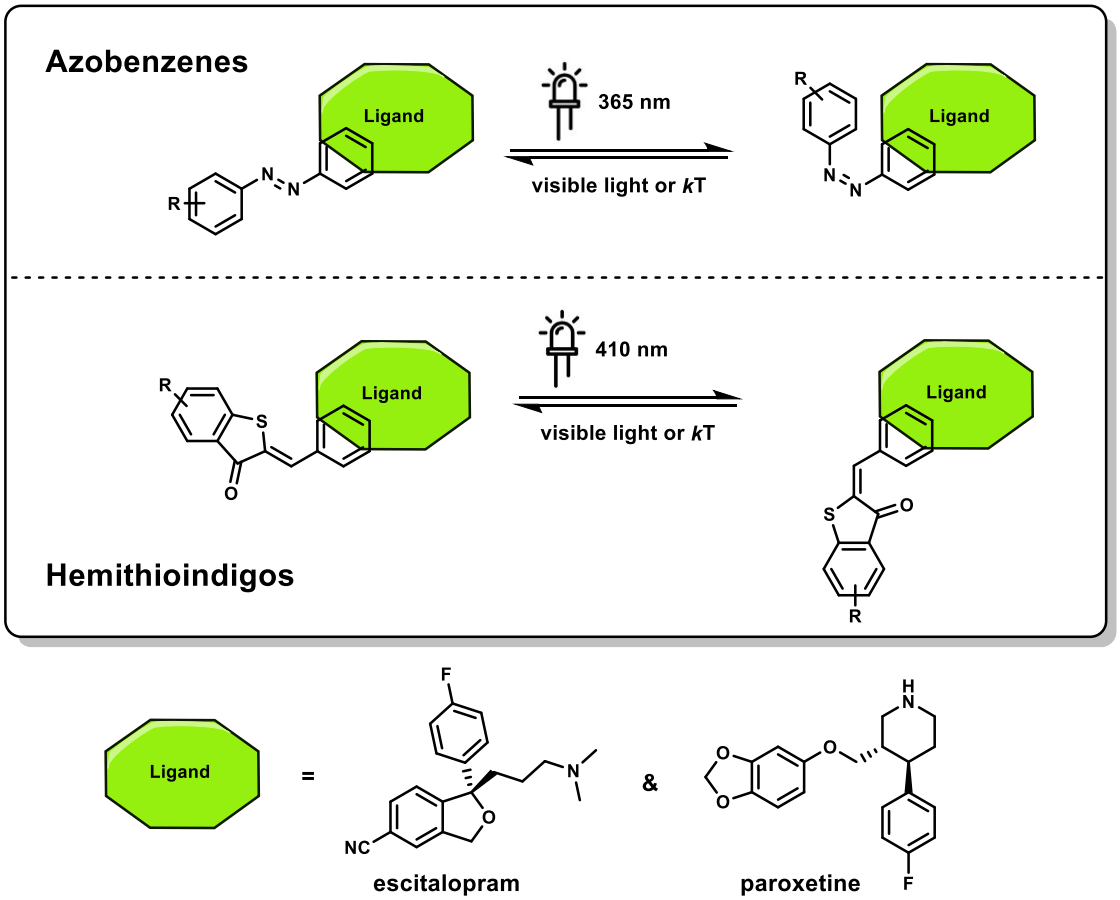

From all the assessed derivatives paroxetine based azobenzene analog **DD-482** emerged as a promising lead compound. In a cell-based uptake inhibition assay the photoswitched inhibitor displayed an 11-fold higher activity compared to its thermodynamically stable configuration when 365 nm light was used for irradiation. In electrophysiological experiments, the photo-activated form was able to block the serotonin-induced current while the natural form remained ineffective. We were able to rationalize the activity difference of the two photo-isomers by computational studies on the hSERT crystal structure. When the azobenzene moiety is isomerized with UV light, the sterical bulk in an important area of the compound decreases which otherwise hinders binding and the (*Z*)-isomer can bind to the transporter in a similar fashion as the parent compound paroxetine.

Kurzfassung

Die Monoamintransporter SERT (Serotonintransporter), DAT (Dopamintransporter) und NET (Norepinephrintransporter) sind essentielle regulatorische Elemente der Signalübertragung in Synapsen. Diese Transmembranproteine nehmen ausgeschüttete Neurotransmitter (Serotonin, Dopamin und Norepinephrin) aus dem synaptischen Spalt wieder auf und beenden dadurch die Signalübertragung. Dadurch haben Monoamintransporter großen Einfluss auf neuronale Zustände wie Stimmung, Schlaf, Aggressionsverhalten und Hunger. Eine Fehlfunktion kann zu schwerwiegenden Krankheiten wie Depression, Angststörungen, ADHS und Parkinson führen. Über die letzten Jahrzehnte wurden zahlreiche pharmakologisch aktive Substanzen entwickelt, die die Wiederaufnahme von Neurotransmitter durch Monoamintransporter inhibieren. Viele Wiederaufnahmehemmer sind vor allem als Antidepressiva klinisch im Einsatz. Schwerwiegende Nebenwirkungen stellen jedoch eine große Herausforderung dar und ein tieferes Verständnis über die Funktionsweise von Monoamintransportern hätte weitreichende Folgen für die Entwicklung von neuen Medikament aber auch für die Weiterentwicklung des Wissens über die Funktionsweise unseres Nervensystems.

Die präzise und reversible Wirkungsweise von Licht-schaltbaren biologisch aktiven Verbindungen stellt enorme Möglichkeiten für deren Entwicklung und Einsatz in Forschungsfragen dar. Das Forschungsfeld der Photopharmakologie hat in den letzten Jahren großes Interesse geweckt und riesige Fortschritte erzielt. In dieser Arbeit haben wir es uns zum Ziel gesetzt, Licht-schaltbare Inhibitoren für den Serotonintransporter zu entwickeln um Untersuchungen dieses wichtigen Proteins unter Verwendung von Licht als vielseitig kontrollierbarer Stimulus zu ermöglichen.

Basierend auf den viel-untersuchten SERT Inhibitoren Escitalopram und Paroxetin haben wir Azobenzol und Hemithioindigo Derivate konzipiert und synthetisiert. Die photophysikalischen Parameter dieser Verbindungen wurden genau untersucht. Für die lichtabhängigen Messungen der bioaktiven Verbindungen haben wir (UV) LED well plates konstruiert um robuste und verlässliche Messungen unter Lichteinfluss zu gewährleisten.

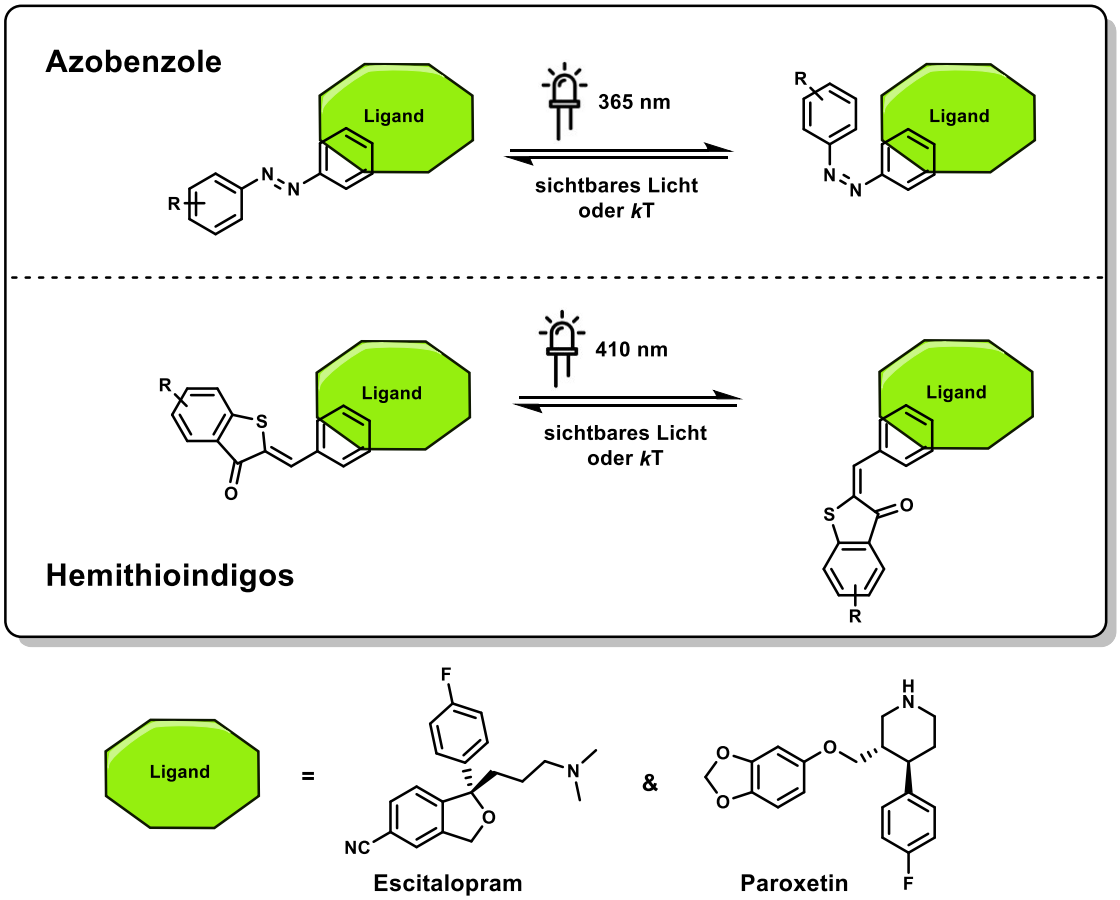

Aus allen untersuchten Verbindungen ging das Paroxetin basierte Azobenzol Derivat **DD-482** als vielversprechende Verbindung hervor. In Zell-basierten Untersuchungen zeigte der Licht-geschaltene Inhibitor eine 11-fach höhere inhibitorische Aktivität als die thermodynamisch stabile Ausgangsverbindung wenn mit 365 nm Licht bestrahlt wurde. In elektrophysiologischen Untersuchungen war die Licht-geschaltene Verbindung in der Lage, den durch Serotonin ausgelösten Strom zu hemmen während das andere Photo-Isomer inaktiv blieb. Wir konnten den Aktivitätsunterschied der beiden Isomere mit Hilfe von computergestützten Untersuchungen an der hSERT Kristallstruktur erklären. Wenn das Azobenzol Fragment mit UV Licht isomerisiert wird, so führt das zu einer Verringerung der Sterik in einem Bereich des Moleküls, der andernfalls die Bindungen an den Transporter erschwert. Dadurch kann die Licht-geschaltene Verbindung ähnlich der Basis-Verbindung Paroxetin binden.

A Synthetic schemes

All compounds prepared or used as starting materials in this thesis are numbered in bold Arabic numerals. Compounds unknown to the literature are additionally underlined. Compounds referred to the literature or presented in a hypothetical way are numbered in bold Roman numerals. Where practical, the lab-journal number based name of the compound was used additionally.

A I Arylazopyrazoles A

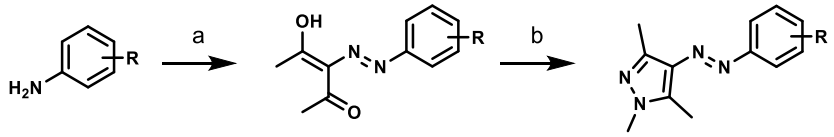

[1] R = H
[4] R = *p*-NO_2
[8] R = *p*-OH
[12] R = *p*-COOH
[19] R = *p*-CN
[23] R = *p*-NEt_2
[26] R = *p*-F
[29] R = *p*-I
[32] R = *p*-CCH

[37] R = *p*-Me
[40] R = *p*-Cl
[43] R = *p*-Br
[46] R = *p*-CF_3
[49] R = *p*-Ph
[52] R = *m*-NO_2
[55] R = *o*-NO_2

[2] R = H
[5] R = *p*-NO_2
[9] R = *p*-OH
[13] R = *p*-COOH
[20] R = *p*-CN
[24] R = *p*-NEt_2
[27] R = *p*-F
[30] R = *p*-I
[33] R = *p*-CCH
[35] R = *p*-Acetyl
[38] R = *p*-Me
[41] R = *p*-Cl
[44] R = *p*-Br
[47] R = *p*-CF_3
[50] R = *p*-Ph
[53] R = *m*-NO_2
[56] R = *o*-NO_2

[3] R = H
[6] R = *p*-NO_2
[10] R = *p*-OH
[14] R = *p*-COOH
[21] R = *p*-CN
[25] R = *p*-NEt_2
[28] R = *p*-F
[31] R = *p*-I
[34] R = *p*-CCH
[36] R = *p*-Acetyl
[39] R = *p*-Me
[42] R = *p*-Cl
[45] R = *p*-Br
[48] R = *p*-CF_3
[51] R = *p*-Ph
[54] R = *m*-NO_2
[57] R = *o*-NO_2

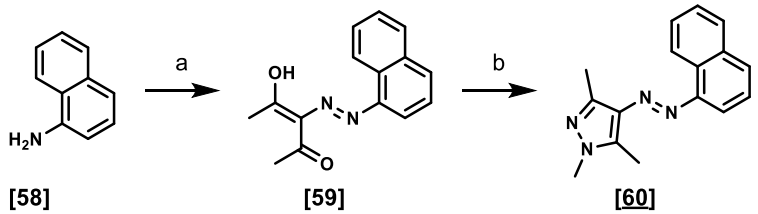

[58] **[59]** **[60]**

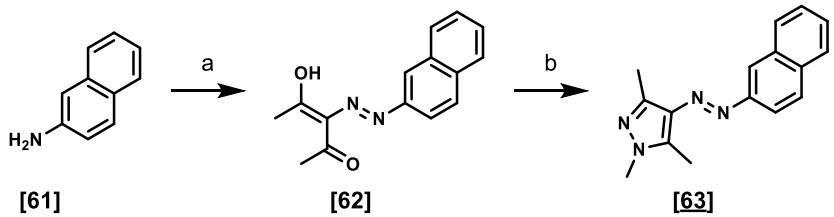

[61] **[62]** **[63]**

Scheme A I Reagents and conditions: a) 1.) $NaNO_2$, AcOH, conc. HCl, 0 °C, 1 h; 2.) acetylacetone, NaOAc, EtOH/H_2O, rt, 1 h, 73% for **[2]**, 91% for **[5]**, 66% for **[9]**, 87% for **[13]**, 91% for **[20]**, 75% for **[24]**, 87% for **[27]**, 92% for **[30]**, 34% for **[33]** & 18% for **[35]**, 95% for **[38]**, 95% for **[41]**, 94% for **[44]**, quant. for **[47]**, 44% for **[50]**, 93% for **[53]**, 92% for **[56]**, 86% for **[59]**, 90% for **[62]** b) methylhydrazine, EtOH, reflux, 3 h, quant. for **[3]**, 99% for **[6]** quant. for **[10]**, quant for **[14]**, quant. for **[21]**, 86% for **[25]**, 99% for **[28]**, 99% for **[31]**, 71% for **[34]**, 77% for **[36]**, quant. for **[39]**, quant. for **[42]**, quant. for **[45]**, 90% for **[48]**, 97% for **[51]**, 97% for **[54]**, quant. for **[57]**, quant. for **[60]**, quant. for **[63]**

A II Arylazopyrazoles B

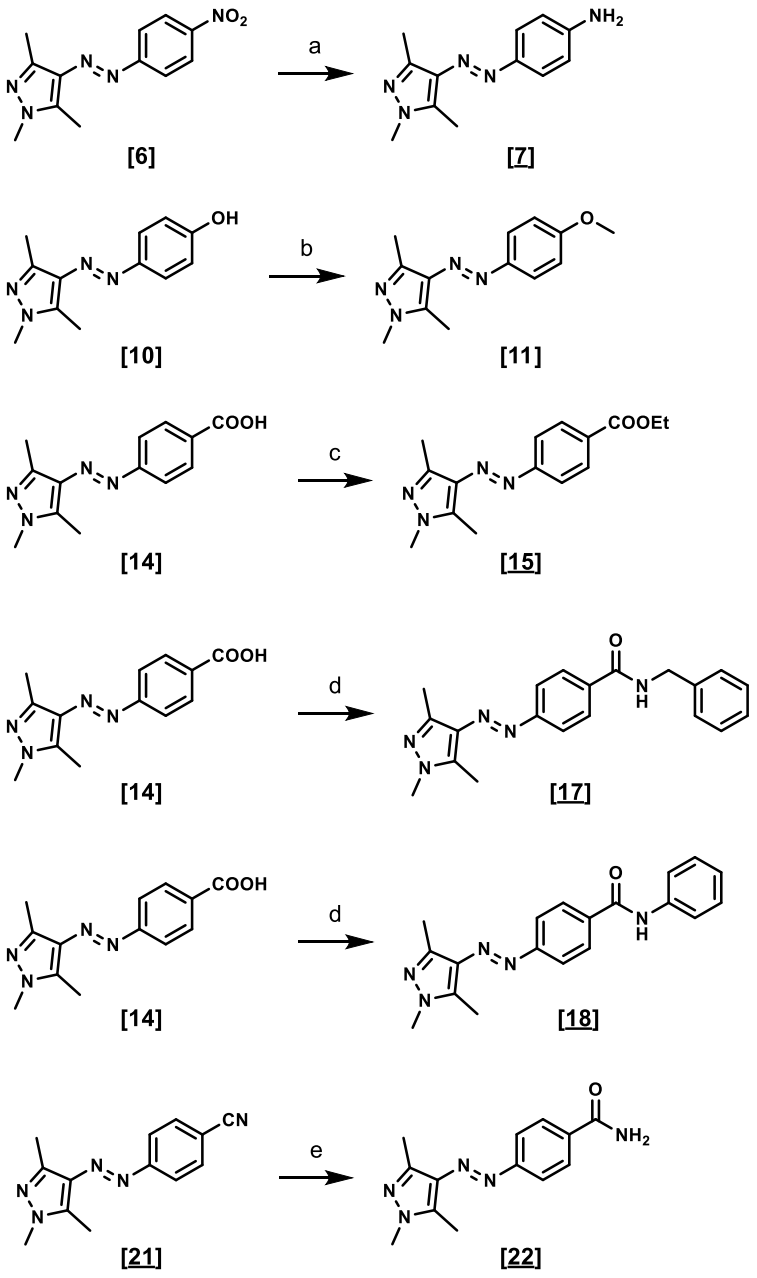

Scheme A II Reagents and conditions: a) Na_2S, THF/H_2O (3/1), reflux, 3 h, 87%,b) MeI, K_2CO_3, Cs_2CO_3, DMF, rt, 16 h, 78% c) EtOH, conc. H_2SO_4, 60 °C, 16 h, 92% d) 1.) acid, EDCI•HCl, HOBt, DIPEA, DMF, rt, 30 min; 2.) amine, rt, 16 h, 79% for **[17]**, 87% for **[18]** e) conc. H_2SO_4, 50 °C, 4 h, 68%

A III Arylazo-2-thiophenes

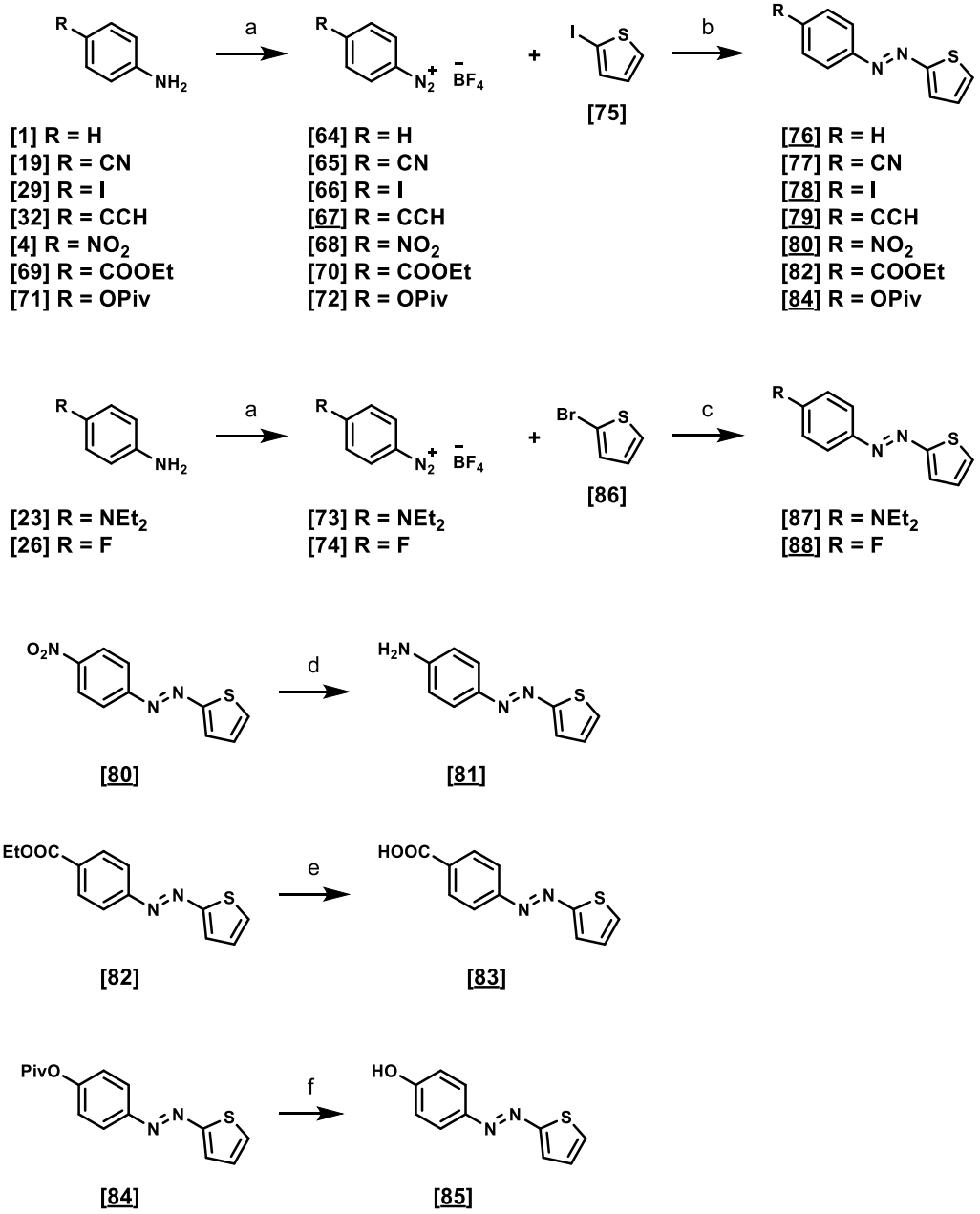

Scheme A III Reagents and conditions: a) HBF_4, $NaNO_2$, -5 °C to rt, 1.5 h, 84% for **[64]**, 77% for **[65]**, 62% for **[66]**, 85% for **[67]**, 72% for **[68]**, 99% for **[70]**, 72% for **[72]**, 99% for **[73]**, 77% for **[74]** b) 1.) 2-iodothiophene, *i*-PrMgCl•LiCl, THF, -20 °C, 30 min; 2.) $ZnBr_2$, THF, -20 °C to rt, 20 min; 3.) aryldiazonium tetrafluoroborate, THF, -78 °C to -20 °C, 1 h, 52% for **[76]**, 40% for **[77]**, 33% for **[78]**, 25% for **[79]**, 66% for **[80]**, 40% for **[82]**, 44% for **[84]** c) 2-bromothiophene, Mg, THF, 55 °C, 1 h; 2.) aryldiazonium tetrafluoroborate, THF, -78 °C to rt, 16 h, 63% for **[87]**, 47% for **[88]** d) Na_2S, THF/H_2O (3/1), reflux, 5 h, 20% e) KOH, MeOH/H_2O (2/1), 60 °C, 16 h, 93% f) LiOH, THF/H_2O (2/1), rt, 12 h, 53%

A IV Arylazo-3-thiophenes

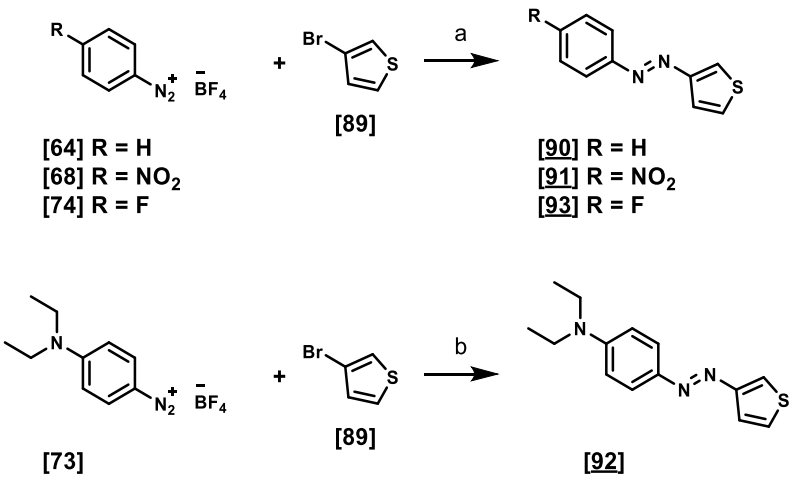

Scheme A IV Reagents and conditions: a) 1.) 3-bromothiophene, *t*-BuLi, hexane/Et_2O, -78 °C, 15 min; 2.) $ZnBr_2$, THF, -78 °C to rt, 20 min; 3.) aryldiazonium tetrafluoroborate, THF, -40 °C to rt, 16 h, 24% for **[90]**, 36% for **[91]**, 9% for **[93]** b) 1.) 3-bromothiophene, *t*-BuLi, hexane/Et_2O, -78 °C, 15 min; 2.) aryldiazonium tetrafluoroborate, THF, -40 °C to rt, 16 h, 8%

A V Escitalopram building blocks

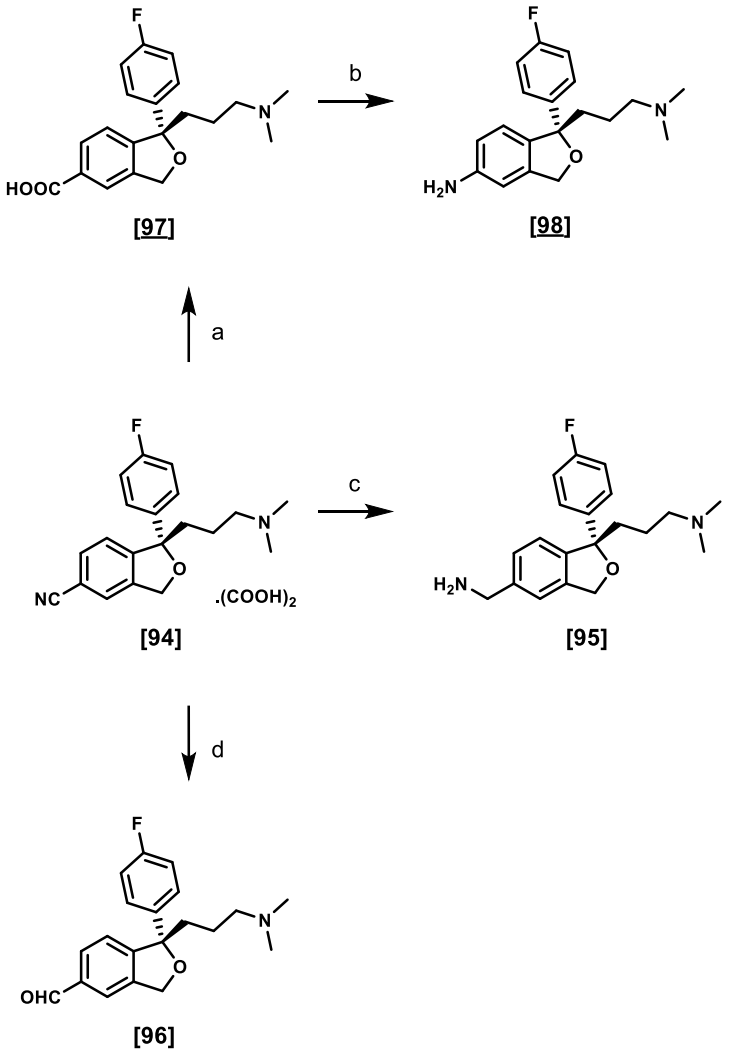

Scheme A V Reagents and conditions: a) NaOH, EtOH/H_2O (1/1), reflux, 2 d, quant. b) 1.) $(COCl)_2$, DMF (cat.), DCM, rt, 2 h; 2.) NaN_3, dioxane, rt, 1 h; 3.) DMF/H_2O (2/1), reflux, 16 h, 87% c) 1.) dil. aqu. NH_4OH; 2.) $LiAlH_4$, THF, reflux, 2 h, 94% d) 1.) dil. aqu. NH_4OH; 2.) Ni-Al alloy, HCOOH, 80 °C, 2 d, 90%

A VI Nitroso compounds

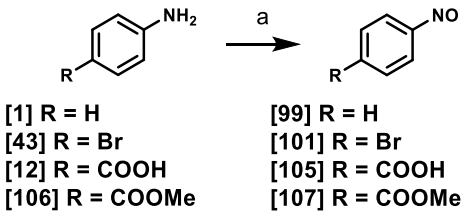

[1] R = H
[43] R = Br
[12] R = COOH
[106] R = COOMe

[99] R = H
[101] R = Br
[105] R = COOH
[107] R = COOMe

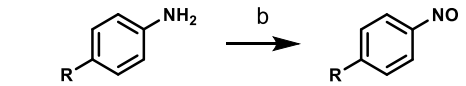

[40] R = Cl
[37] R = Me
[103] R = OMe

[100] R = Cl
[102] R = Me
[104] R = OMe

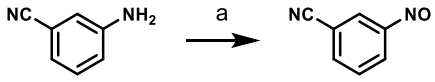

[108] **[109]**

Scheme A VI Reagents and conditions: a) Oxone®, DCM/H_2O, rt, 1 – 16 h, 50% for **[99]**, 72% for **[101]**, 92% for **[105]**, 73% for **[107]**, 80% for **[109]** b) H_2O_2, MoO_3, KOH, MeOH/H_2O, rt, 20 – 22 h, 59% for **[100]**, 81% for **[102]**, 79% for **[104]**

A VII Azo-Escitalopram derivatives A

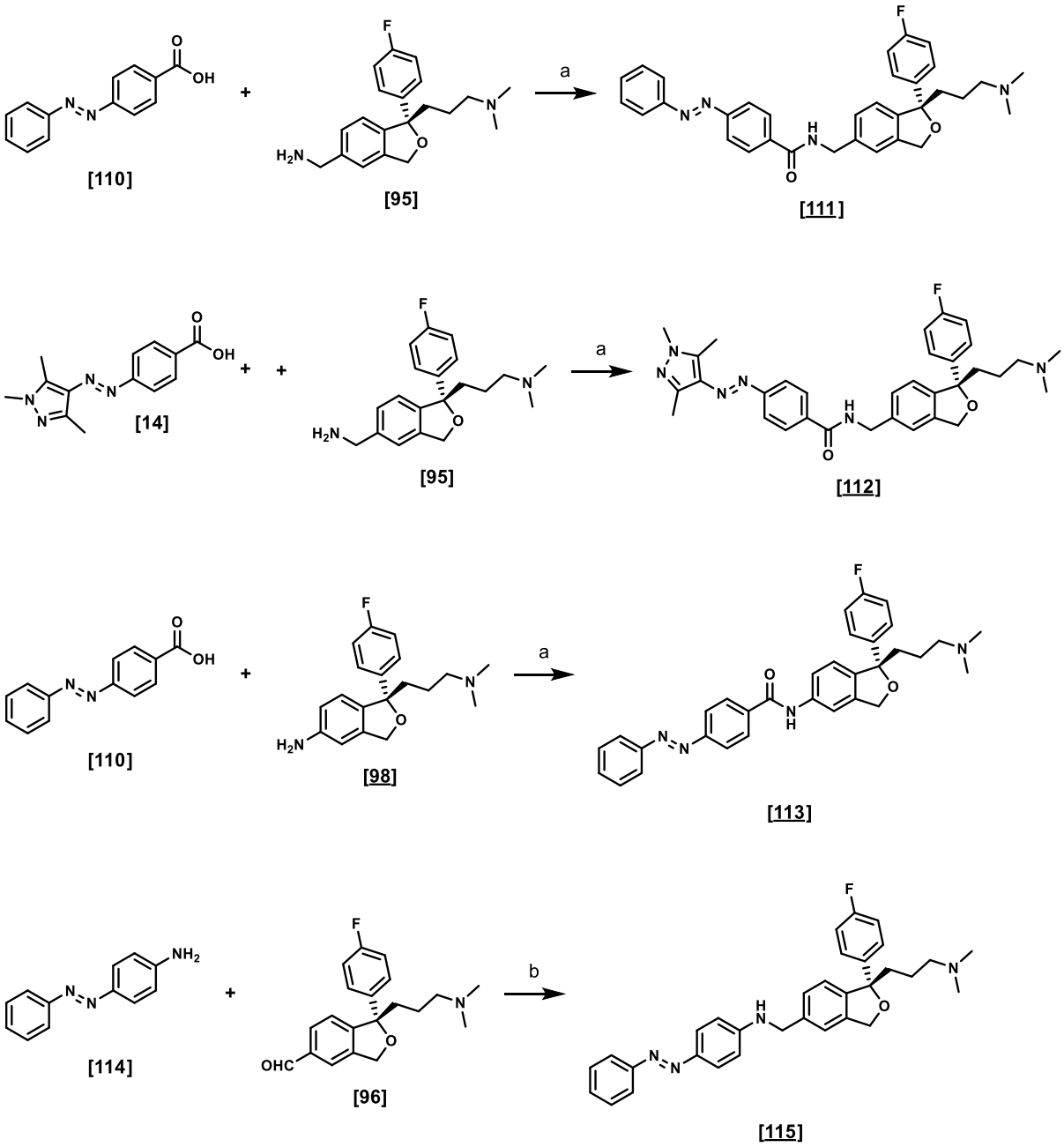

Scheme A VII Reagents and conditions: a) 1.) acid, EDCI•HCl, HOBt, DIPEA, DMF, rt, 30 min; 2.) amine, rt, 16 h, 88% for **[111]**, 66% for **[112]**, 62% for **[113]** b) $NaBH(OAc)_3$, AcOH, DCE, rt, 2 d, 54%

A VIII Azo-Escitalopram derivatives B

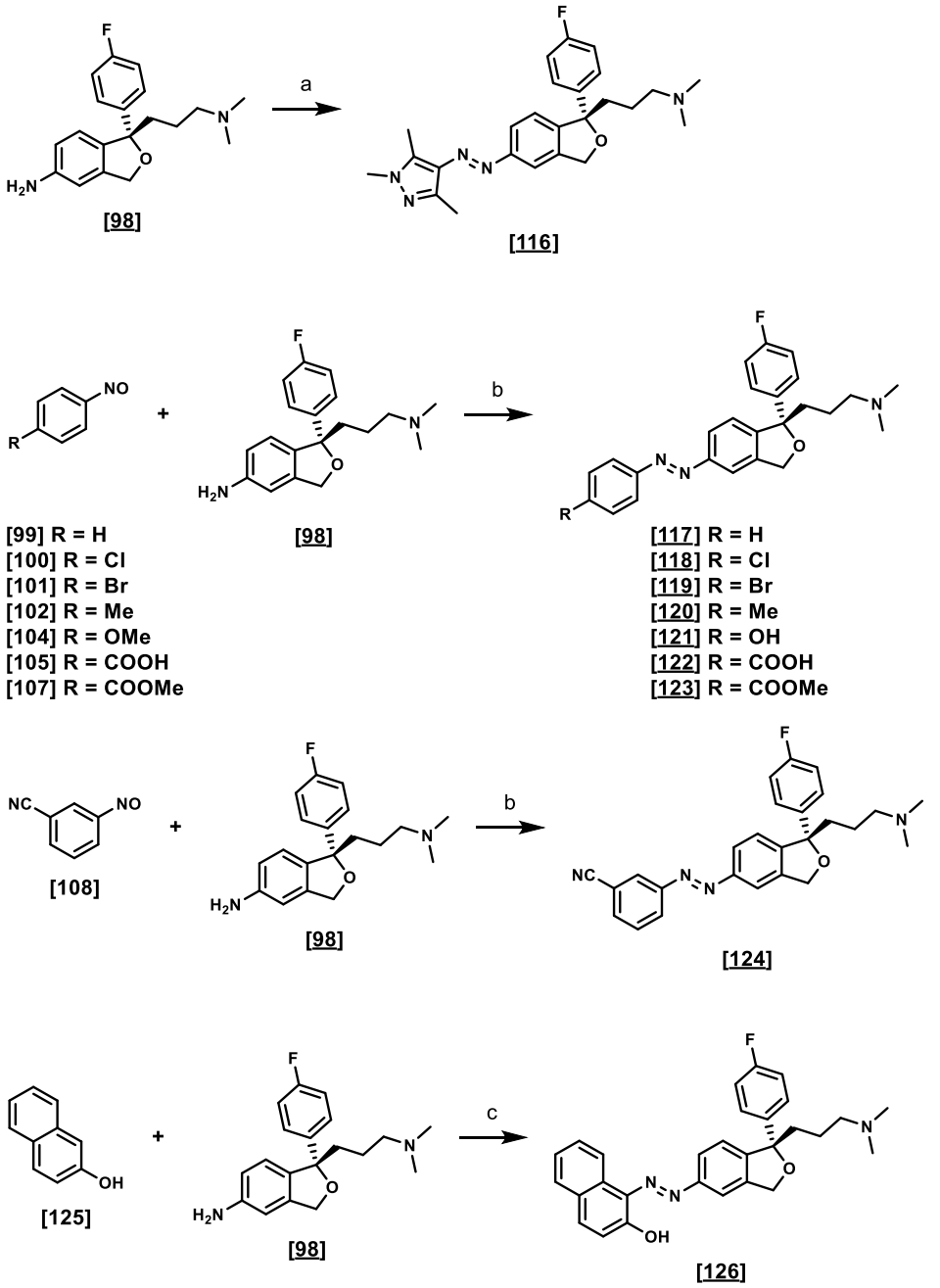

Scheme A VIII Reagents and conditions: a) 1.) $NaNO_2$, AcOH, conc. HCl, 0 °C, 1 h; 2.) acetylacetone, NaOAc, EtOH/H_2O, rt, 1 h; 3.) methylhydrazine, EtOH, reflux, 3 h, 50% b) AcOH/DMSO, rt, 1 h -48 h, 58% for **[117]**, 91% for **[118]**, 61% for **[119]**, 81% for **[120]**, 95% for **[121]**, 69% for **[122]**, 79% for **[123]**, 92% for **[124]** c) 1.) $NaNO_2$, HCl, 0 °C, 10 min; 2.) 2-naphthol, NaOH, 0 °C, 2 h, 85%

A IX HTI building blocks

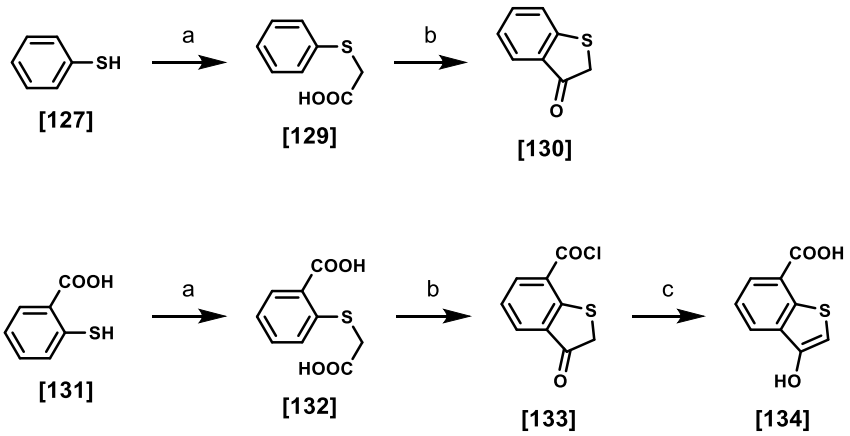

Scheme A IX Reagents and conditions: a) 1.) bromoacetic acid, NaOH, H_2O, rt, 8 h; 2.) HCl, 98% for **[129]**, 94% for **[132]** b) 1.) $SOCl_2$, DMF (cat.), reflux, 1 - 6 h; 2.) $AlCl_3$, DCE, 0 °C to rt, 1 h, 60% for **[130]**, 82% for **[133]** c) acetone/H_2O (9/1), rt, 16 h, quant.

A X HTI-Escitalopram derivatives

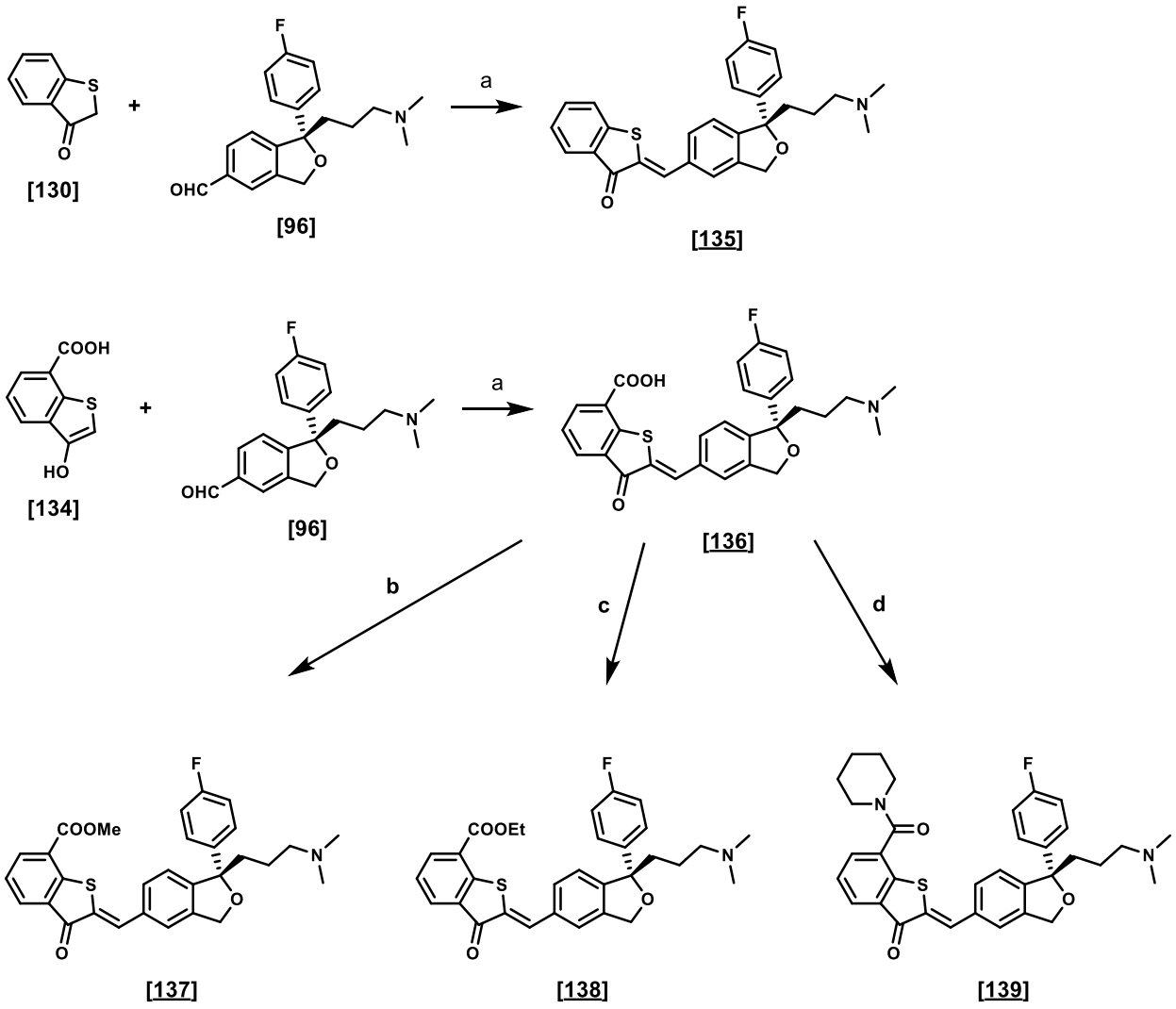

Scheme A X Reagents and conditions: a) *p*-TSA, benzene/*t*-BuOH (5/1), reflux, 6 h – 20 h, 82% for **[135]**, 78% for **[136]** b) MeOH, DMAP, EDCI•HCl, DIPEA, DCM, rt, 24 h, 78% c) EtOH, DMAP, EDCI•HCl, DIPEA, DCM, rt, 24 h, 75% d) piperidine, EDCI•HCl, HOBt, DIPEA, DMF, rt, 16 h, 81%

A XI Azo-Paroxetine

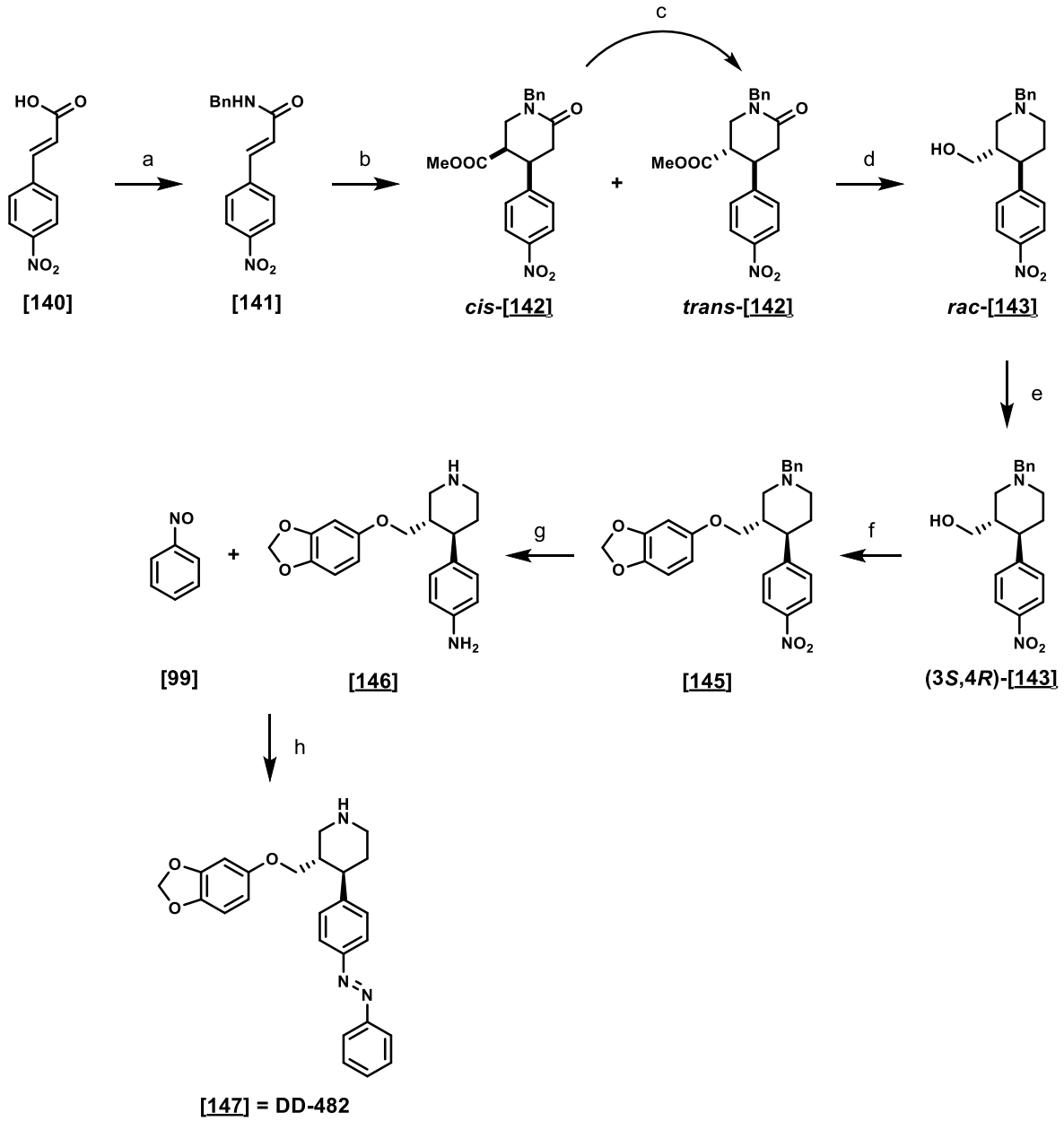

Scheme A XI Reagents and conditions: a) 1.) $(COCl)_2$, DMF (cat.), DCM, rt, 1 h; 2.) benzylamine, NEt_3, DCM, rt, 16 h, 93% b) methyl acrylate, TBSTOf, NEt_3, *t*-BuOH, DCE, rt, 16 h, 46% ***cis*-[142]**, 32% ***trans*-[142]** c) NaOMe, MeOH, 55 °C, 1 h, 62% d) 1.) $NaBH_4$, BF_3•OEt_2, THF, 0 °C to reflux, 16 h; 2.) MeOH, reflux, 1 h, 83% e) vinyl acetate, Amano Lipase, DIPE, rt, 42 h, 18%, 94% ee f) 1.) MsCl, NEt_3, DCM, 0 °C to rt, 1 h; 2.) sesamol, NaH, DMF, 90 °C, 16 h, 65% g) H_2, Pd/C, MeOH/EtOAc (4/1), 60 °C, 16 h, 84% h) AcOH, rt, 16 h, 60%

A XII HTI-Paroxetine

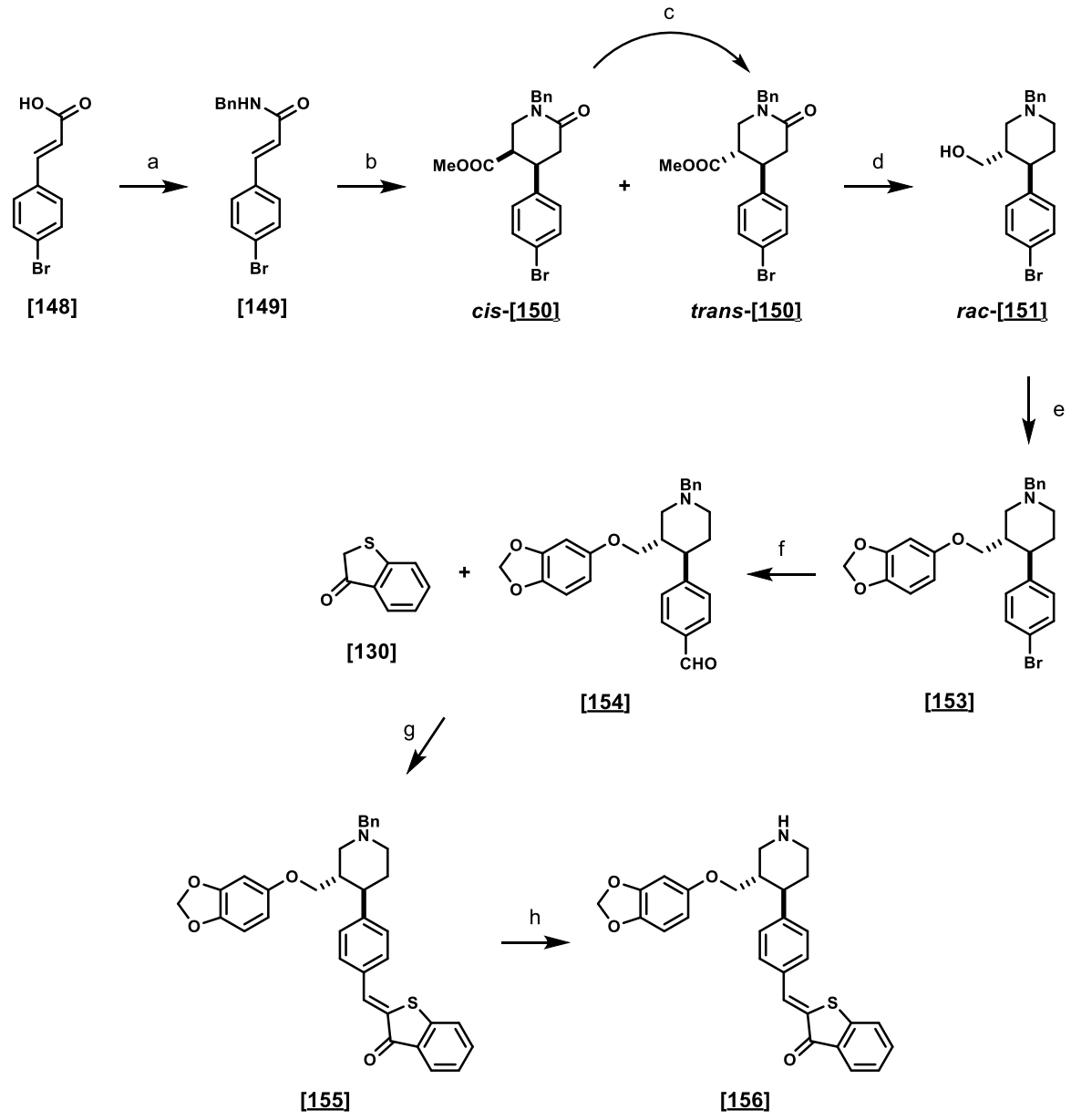

Scheme A XII Reagents and conditions: a) 1.) $(COCl)_2$, DMF (cat.), DCM, rt, 1 h; 2.) benzylamine, NEt_3, DCM, rt, 16 h, 91% b) methyl acrylate, TBSTOf, NEt_3, *t*-BuOH, DCE, rt, 16 h, 37% ***cis*-[150]**, 34% ***trans*-[150]** c) NaOMe, MeOH, 55 °C, 1 h, 71% d) 1.) $NaBH_4$, $BF_3 \bullet OEt_2$, THF, 0 °C to reflux, 16 h; 2.) MeOH, reflux, 5 h, 84% e) 1.) MsCl, NEt_3, DCM, 0 °C to rt, 1 h; 2.) sesamol, NaH, DMF, 90 °C, 16 h, 86% f) 1.) *n*-BuLi, THF, -70 °C, 1 h; 2.) DMF, -70 °C, 1 h, 55% g) *p*-TSA monohydrate, benzene/*t*-BuOH (5/1), reflux, 16 h, 71% h) 1.) 1-chloroethyl chloroformate, DCE, 90 °C, 3 h; 2.) MeOH, reflux, 1 h, 56%

B Introduction

"Understanding how the brain works is arguably one of the greatest scientific challenges of our time." – Alivisatos et al. in *Neuron*, **2012**, *74*, 970 - 974[2]

In 2013 the Obama administration announced the BRAIN initiative (brain research through advancing innovative neurotechnology), a $6 billion fund to enhance our knowledge of the brain in action, in order to better understand how we think, learn and remember.

Among the vast quantity of bio-molecules involved in brain activities, monoamine transporters (MATs) influence important neurological processes like mood, aggression behavior and hunger and their malfunction is linked to many serious diseases.[3] Eventually, this could help patients suffering from mental or neurological diseases.

B I Monoamine transporters

Membrane transporter proteins - also called solute carriers (SLCs) - transport solutes such as ions, amino acids, nutrients and signaling molecules across cellular membranes and are thus essential for life. The SLC6 family[3, 4] is a group of highly similar transporters that transport amino acids and amino acid derivatives into cells using co-transport (symport) of extracellular Na^+ as a driving force. The symport of Na^+ led to the SLC6 family being referred to as neurotransmitter sodium symporters (NSSs). Based on sequence similarity and substrate specificity, the SLC6 family is divided into four subclasses: monoamine, GABA (γ-aminobutyric acid), amino acid and amino acid/orphan (see **Figure 1**).

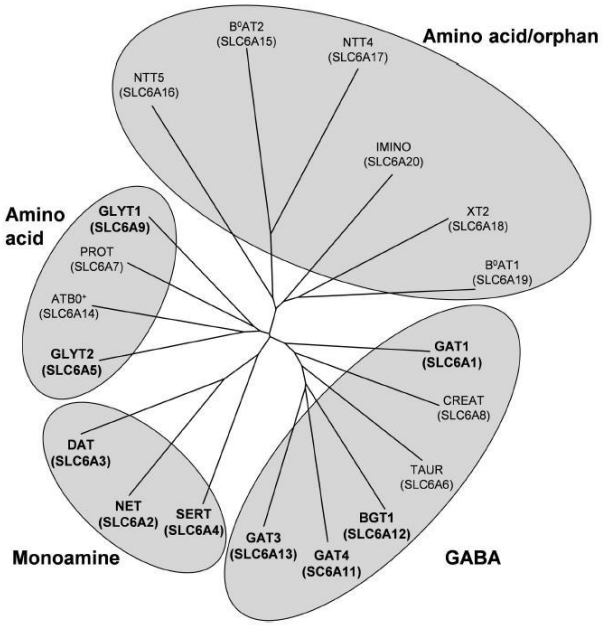

Figure 1: The SLC6 family consists of four subclasses. Picture taken from reference[3].

As neurotransmitters play essential roles in various brain functions, they pose a distinctive substrate class and their associated transporters within the SLC6 family make up the subset of SLC6 neurotransmitter transporters (NTTs, highlighted in bold in **Figure 1**). They share an average amino acid sequence identity of 40% which suggests a similar general structure. Based on their chemical structures, the corresponding neurotransmitters can be further classified into monoamine neurotransmitters (serotonin, dopamine and norepinephrine) and amino acid neurotransmitters (GABA and glycine). The cognate transporters of serotonin (serotonin transporter: SERT), dopamine (dopamine transporter: DAT) and norepinephrine (norepinephrine transporter: NET) are referred to as monoamine transporters (MATs). MATs are expressed in the central nervous system (CNS) while SERT and NET are located in other tissues, as well (see **Table 1**). They seem to be exclusively expressed in monoaminergic neurons (see **Figure 2**) and are located both in dendrites and axons, outside of synapses. Their function is to reuptake released neurotransmitters which makes them crucial to synaptic signaling.

Synaptic signaling, also called neurotransmission, is crucial for the communication between neurons. The process is initiated by the Ca^{2+} induced release of neurotransmitters into the synaptic cleft.[5] The released neurotransmitters activate associated G protein-coupled receptors and ion channels at the postsynaptic neuron which subsequently generates postsynaptic signals. MATs regulate the concentration of monoamine neurotransmitters in the synaptic cleft by reuptake. Transported neurotransmitters are partly accumulated in vesicles where they are transported into by vesicular monoamine transporters (VMATs), and partly metabolized by monoamine oxidases. In consequence, control of transport activity influences neuronal activity. Malfunctions are therefore connected to disorders like depression, attention deficit hyperactivity disorder (ADHD), Parkinson's disease and epilepsy.[6] Hence, compounds addressing MATs are of outstanding importance to study neurotransmission and furthermore, to target SERT, DAT and NET in a variety of related brain diseases as the large number of clinically applied drugs show. Additionally, MATs are also the target of many prominent illicit drugs such as cocaine, ecstasy and (meth)amphetamine.

Table 1: Members of the SLC6 neurotransmitter transporters. Modified from reference[3].

Transporter	Substrate	Tissue distribution	Link to diseases
SERT	serotonin	brain, peripheral nervous system, placenta, epithelium, platelets	anxiety, depression, autism, gastrointestinal disorders, premature ejaculation, obesity
DAT	dopamine	brain	Parkinson's disease, Tourette syndrome, ADHD, addiction
NET	norepinephrine	brain, peripheral nervous system, adrenal gland, placenta	depression, orthostatic intolerance, anorexia nervosa, cardiovascular diseases

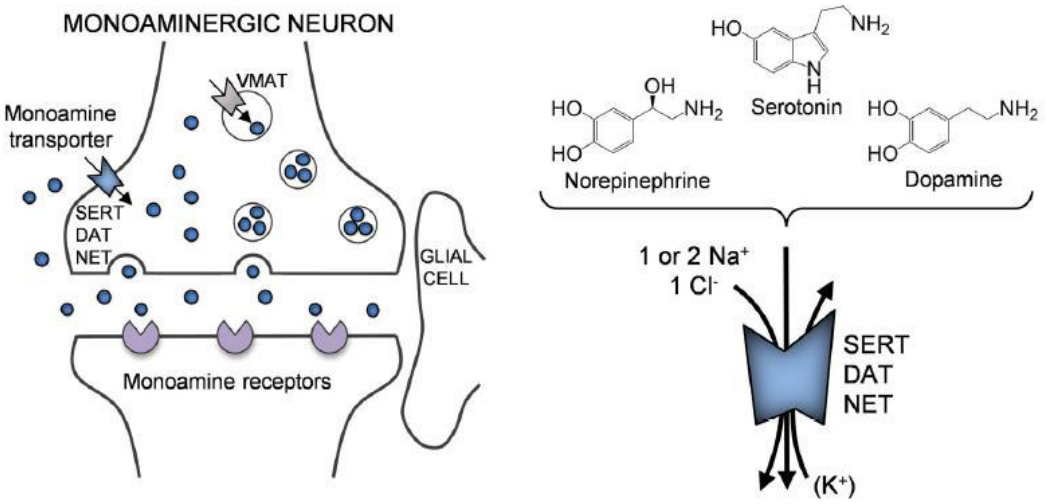

Figure 2: MATs are located in their respective monoaminergic neurons outside the synapse where they reuptake monoamine neurotransmitters into the neuron. Picture modified from reference[3].

Until very recently, the structural beliefs were based on homology to a related transporter. In 2005 Gouaux and co-workers disclosed a high-resolution (1.65 Å) X-ray crystal structure of a bacterial leucine transporter (LeuT), complexed with its substrate leucine.[7] The overall sequence identity to NTTs is only 20 – 25%, but nevertheless, the LeuT structure proved to be a valuable template for SLC6 NTTs in order to provide insight on how the transporters accommodate substrates and ions and bind inhibitors. From there on, LeuT became a very popular model protein for computational studies.

LeuT features 12 transmembrane domains (TM), almost exclusively α-helical, connected by short loops which bundle into a cylindrical shape (see **Figure 3**). The inner ring (blue helices) is formed by TMs 1, 3, 6 and 8. In the core of the inner ring a central binding site (S1) is located where the substrate leucine and two Na^+ ions are bound.

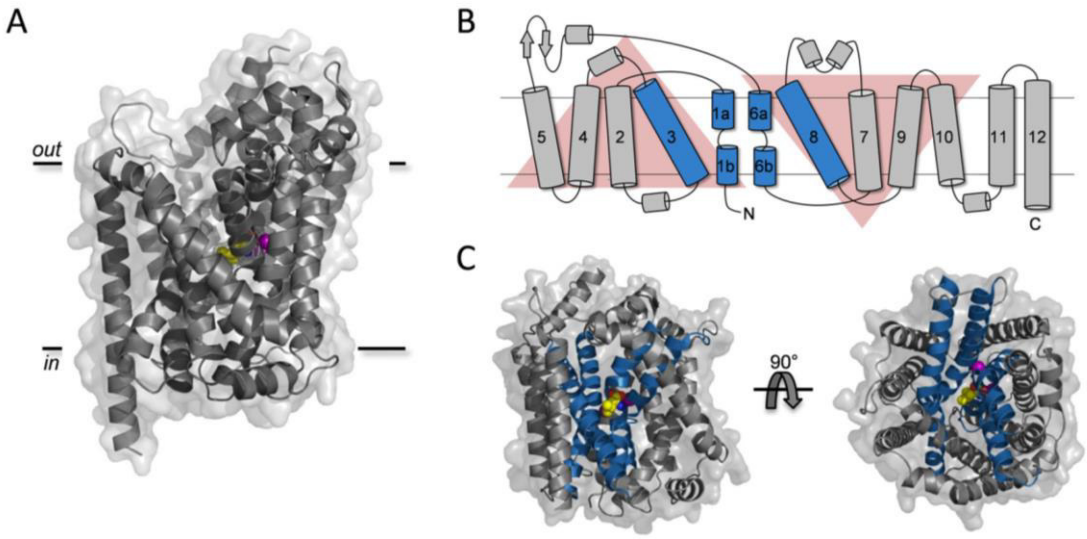

Figure 3: Crystal structure of LeuT. B: Topology with the inner ring shown in blue. C: View from the side and from the top. Picture taken from reference[3].

The amino acids Tyr108 and Phe253 form a hydrophobic lid on top of S1. Above this lid a H_2O-mediated salt bridge between the guanidium group of Arg30 and the carboxylate group of Asp404 is observed. Together they act as the external gate. The exit from S1 towards the intracellular area is blocked by a ≈20 Å layer of tightly packed TM structures forming the intracellular gating region (see **Figure 4**). These two gates undergo structural rearrangements when the protein is transporting substrates by a number of conformational changes. Noteworthy, the involved amino acids are strictly conserved across the SLC6 NTTs (except Asp404 is substituted by a glutamate in SERT). The LeuT structure depicts the transporter in an “outward-facing occluded” conformation, an early stage in the transport process. Binding of leucine and ions leads to a closure of the central binding site. While substrates were crystallized in the S1 binding site, crystal structures of inhibitors bound to LeuT have suggested that there is a second binding site at the bottom of the extracellular gating region termed S2. Binding of inhibitors in S1 and S2, respectively suggests that the required conformational change to undergo transport is blocked. This finding could be of significance for MAT inhibitors.

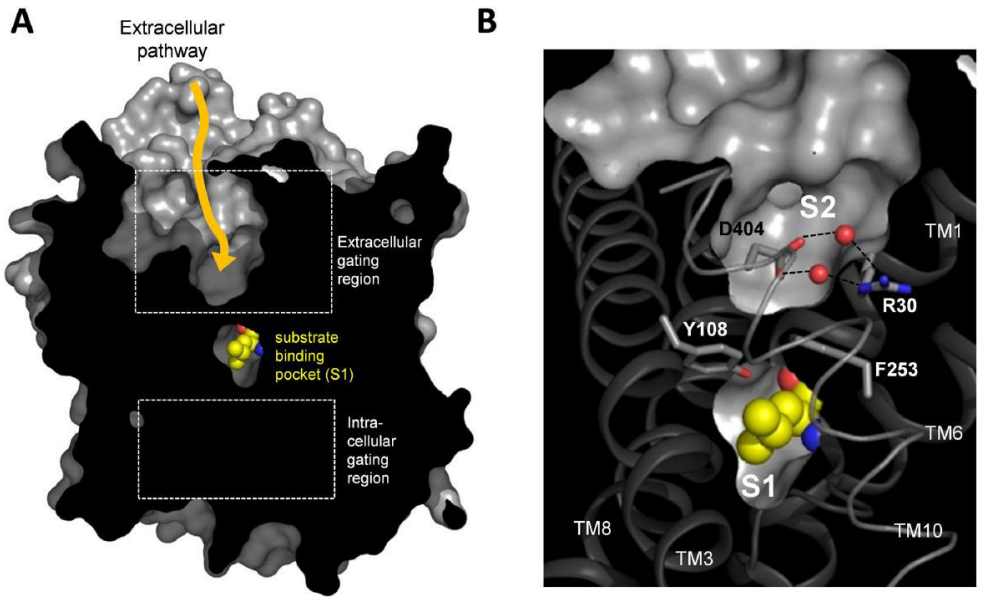

Figure 4: A: Location of bound leucine and the two gates. B: The H_2O-mediated saltbridge between Asp404 and Arg30 and the lid (Tyr108 and Phe253) form the extracellular gate. Picture taken from reference[3].

An increasing number of structures of prokaryotic transporters related to LeuT shine light on a putative transport mechanism. As various structures provide snapshots of different stages of the transport cycle, an alternating access mechanism (see **Figure 5**) is assumed. The transport cycle is believed to consist at least of three states that have been observed in a number of structures.

1) In the first state, the outward-open conformation leaves S1 accessible from the outside. The substrate and ions bind to their respective binding site which causes a conformational change.
2) In the second state, the transporter is in an outward-occluded state where S1 is blocked from both sides. Further transition leads to the third state.
3) In an inward-open conformation the substrate and ions can diffuse into the cell.

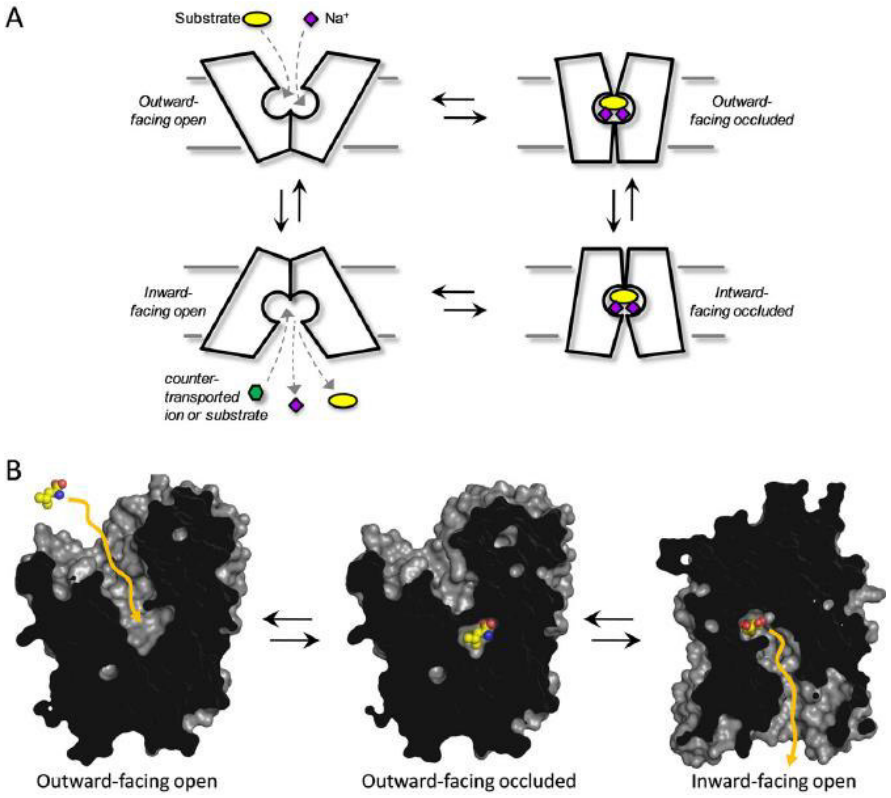

Figure 5: The transport mechanism is assumed to include alternating access to the out- and inside. Picture taken from reference[3].

LeuT and the SLC6 NTTs share a high sequence similarity (55 – 67%) in the regions that are believed to be responsible for the transport function which makes LeuT a very good template and hence, LeuT based homology models have emerged as valuable tools in absence of direct structural information. Modeling of DAT and SERT has received the most attention due to their role as outstanding drug targets.

In the important binding region, SERT, DAT and NET feature an aspartate residue (Asp98 in SERT) where all other NTTs contain a glycine. It has been shown that the acid in this position is strictly required for the correct functionality of the protein. A likely explanation is an interaction of the acid with the amino group of the monoamine substrate.

In 2013, the X-ray crystal structure of the *Drosophila melanogaster* DAT was published with a resolution of 3.0 Å, co-crystallized with the inhibitory drug nortriptyline (see **Figure 6**).[8] The dDAT structure features an overall LeuT-like structure with 12 transmembrane helices. The core of dDAT closely resembles that of LeuT while the peripheries are different. The drug-binding site is composed of TM1, TM3, TM6 and TM8 equivalent to the substrate-binding site in LeuT. Binding of the inhibitor sterically prevents the closure of the extracellular gate above the drug-binding site and thereby locking the transporter in an outward-open state. The resolution of the inhibitor binding to the central binding site (S1) served as the first structural proof that antidepressants inhibit reuptake by preventing substrate binding and stabilizing the outward-open state of the protein.

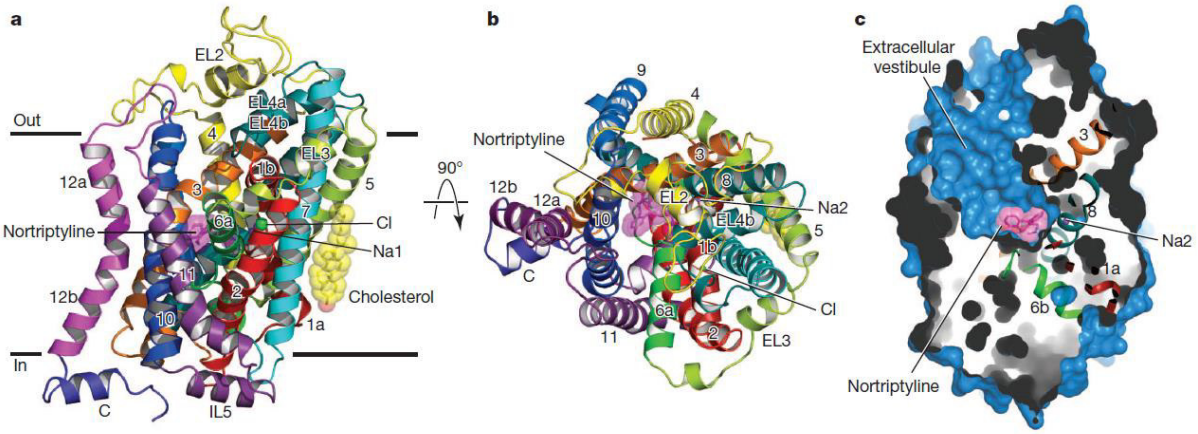

Figure 6: Crystal structure of nortriptyline bound dDAT in an outward-open state. Picture taken from reference[8].

In 2016, the first human SERT structures were reported (see **Figure 7**).[9, 10] The transporter protein was co-crystallized with two of the most widely prescribed antidepressants: escitalopram (3.24 Å resolution) and paroxetine (3.14 Å resolution). Like LeuT and dDAt, the hSERT consists of 12 transmembrane helices. The structures show the transporter in an outward-open state with the inhibitors bound to the central binding site S1 made up by residues of TM1, TM3, TM6, TM8 and TM10. In the case of escitalopram, a second molecule is observed in the allosteric binding site S2 while the allosteric maltose molecule in the paroxetine bound structure is probably an artefact of the crystallization process. In the central binding site, the amine groups of the inhibitors interact with the carboxylate group of Asp98 which was already shown to be crucial for substrate binding as well.

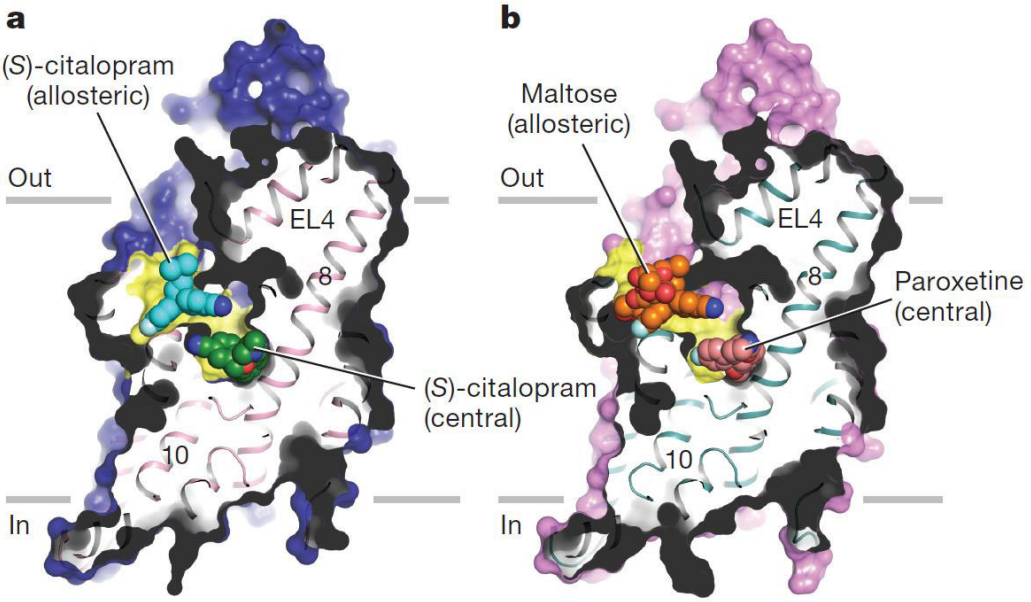

Figure 7: Crystal structure of escitalopram bound (left) and paroxetine bound (right) hSERT. Picture taken from reference[8].

As it has already been mentioned, MATs are targets of remarkable therapeutic value as they can be addressed to fight a number of serious CNS diseases (see **Table 1**). A wide range

of developed compounds are able to inhibit the reuptake. Moreover, MATs are the prime targets for naturally occurring psychostimulants like cocaine.[3] A tremendous effort by academia and the pharmaceutical industry has resulted in the development of a broad range of compounds with different affinities and selectivity profiles. Historically, tricyclic antidepressants (TCAs) like imipramine and clomipramine were the first representatives to target MATs in the 1950s but they interact with several off-targets[11] as well and, hence, cause diverse side effects. Administering selective inhibitors with diminished off-target activity led to significantly improved side effect profiles. Selective serotonin reuptake inhibitors (SSRIs) include escitalopram, fluoxetine and paroxetine. Reboxetine and atomoxetine are examples of selective norepinephrine reuptake inhibitors (NRIs). A combined selective inhibitory activity is regarded beneficial for certain diseases[12] and hence, dual inhibitors were developed as well. Dual SERT/NET reuptake inhibitors (SNRIs) include duloxetine and desvenlafaxine while nomifensine is dual NET/DAT reuptake inhibitor (NDRI). Tesofensine is a inhibiting all MATs (see **Figure 8**).

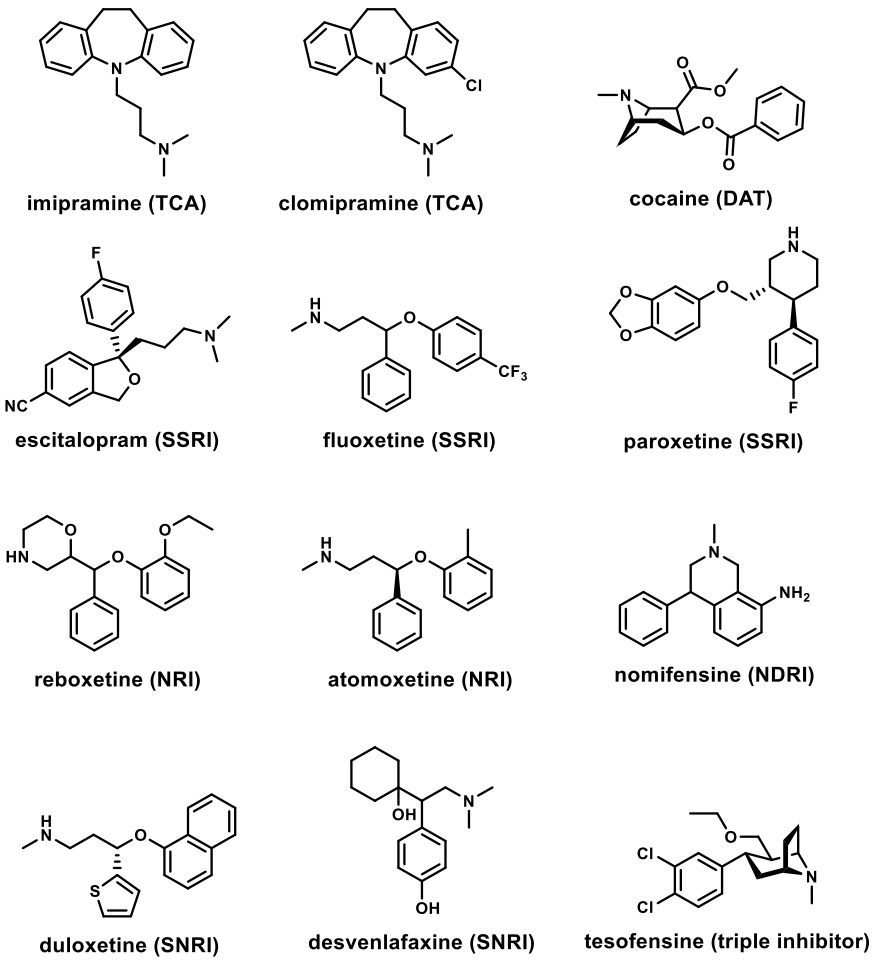

Figure 8: A wide range of MAT inhibitors is available with a wide range of affinities and selectivities.

Experimentally validated models[13] and most recently the hSERT structures suggest that the inhibitor binding site overlaps with the S1 substrate binding site. Through competitive

inhibition, the inhibitor binds to the S1 site and thereby locks the protein in an outward-facing open or occluded state. All potent inhibitors feature a structural amine that coordinates with the before mentioned aspartate residue. While the S1 site is a high-affinity binding site for this mode of action, several studies have observed a low-affinity allosteric binding site which increased the off-rate for inhibitors bound to S1. The S2 site is regularly suspected to be the putative location of binding.

Clinically, depression and anxiety can be treated with SSRIs and SNRIs. SERT and NET inhibition leads to increased levels of serotonin and norepinephrine and over a period of days to symptom relief. SNRIs have been suggested to display improved antidepressant effects while having a faster onset. ADHD can be treated by inhibiting DAT or inducing release of neurotransmitters (e.g. amphetamines). Cocaine, (meth)amphetamines[14], MDMA (3,4-methylenedioxymethamphetamine) and cathinones are nonselective MAT inhibitors and/or lead to release of neurotransmitters and are popularly used as recreational drugs. Furthermore, MAT inhibitors can be used to treat nicotine addiction and obesity. Common side effects include weight gain, sexual dysfunction and sleep disturbances.

B II Photopharmacology - concept

The phenomenon of visual perception appears truly natural to us in our daily lives. The underlying biological mechanism however, is genuinely fascinating and has inspired scientists to transfer nature's principle of photoreceptors to a broader range of applications. The resulting concepts have paved the way to unparalleled opportunities in a large array of research fields. By evolutionary means, a small number of natural chromophores like retinal, flavins and tetrapyrrols were developed. These chemical moieties are able to absorb light over a wide range of the solar spectrum and, consequently, lead to light induced processes. While being usually covalently bound to a protein, some chromophores are capable of directly activating the associated bio-molecule. For example, the light induced isomerization of 11-*cis*-retinal to all-*trans* retinal (see **Figure 9**) leads to an activation of rhodopsin which ultimately generates the neuronal response to light.[15, 16] Light of a specific wavelength is absorbed by the chromophore and, thereby, switches the molecule from its naturally more stable configuration into a less stable state of different geometry.

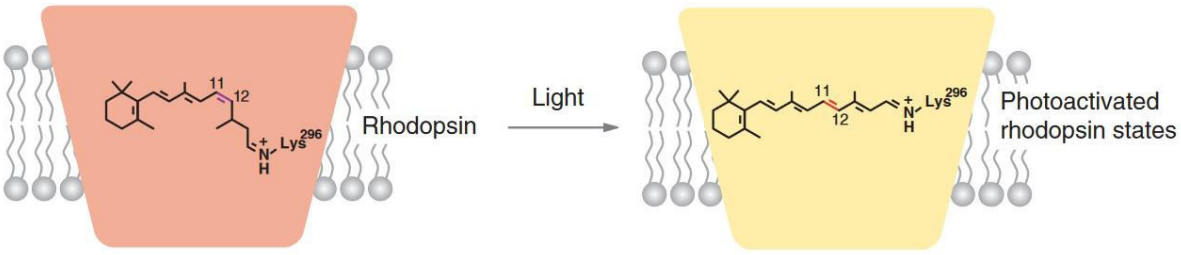

Figure 9: A Schiff base of 11-*cis*-retinal is isomerized to all-*trans*-retinal by absorbance of light. Picture modified from reference[16].

Natural and engineered systems taking advantage of these chromophores are widely applied in the field of optogenetics[17, 18] as control tools in neuroscience. In addition to their natural relatives, artificial photoswitches offer a complementary approach. This emerging field termed photopharmacology seeks to optically control biological function by the use of synthetic photoswitches and has shown great achievements in recent years.[19-24]

Light as a stimulus has unmatched potential. The light's wavelength and intensity can be broadly adjusted. The temporal and spatial precision is unsurpassed and most light exhibits no or only minor toxicity. The application of light can be realized non-invasively and in combination with other biochemical inputs; the light signal is orthogonal.[20] In this context three different principles are generally considered to introduce artificial photo dependence into biological systems.

Photolabile protecting groups in caged ligands: One related strategy that does not exploit the photon induced isomerization of a photoswitch but nevertheless, uses light to unleash a compound's potential, is the application of caged ligands.[19, 22] The usage of

photolabile protecting groups inactivates the molecular features responsible for the desired pharmacological profile. The formerly inert molecule is uncaged with light and, thereby, is transformed into its active form. For example, Zemelman et. al. demonstrated the feasibility of caged ligands to optically activate the capsaicin receptor TRPV1, a ligand-gated ion channel (see **Figure 10**).[25]

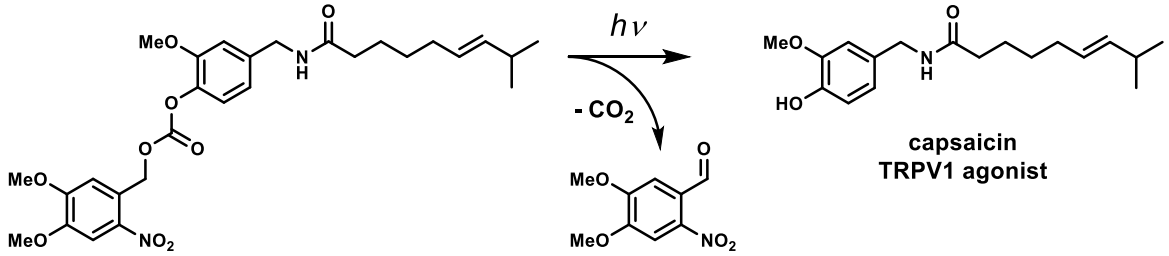

Figure 10: Irradiation of caged capsaicin led to the release of the active TRPV1 agonist.

Two-photon uncaging[26] allows the light triggered event to be caused by lasers of much higher wavelengths, as two photons combined account for the required energy transfer. Hence, long wavelength light up to infrared can be used to increase tissue penetration in adequate systems and reduce harm. Moreover, the quadratic dependence of the excitation probability versus the electric field of the exciting light allows precise spatiotemporal localization at the focal point of the laser which enhances the resolution. Two-photon uncaging of glutamate as a messenger facilitated stimulation of single synapses in vivo in mice brains.[27] The obvious drawbacks of caged ligands are their inherent irreversibility and the formation of by-products that might be toxic or lead to undesired effects.

Photochromic ligands: In contrast, the isomerization of photoswitches is a reversible process and does not generate any by-products. The application of photochromic ligands is therefore an attractive method to photodependently address ligand-protein interactions. In this case, a biologically active compound carries a photoswitchable moiety. The two photo-isomers have different properties (e.g. geometry, dipole moment, …) and hence, potentially exhibit different activities. By that, the overall protein (de)activation can be controlled by light (schematically displayed in **Figure 11**).

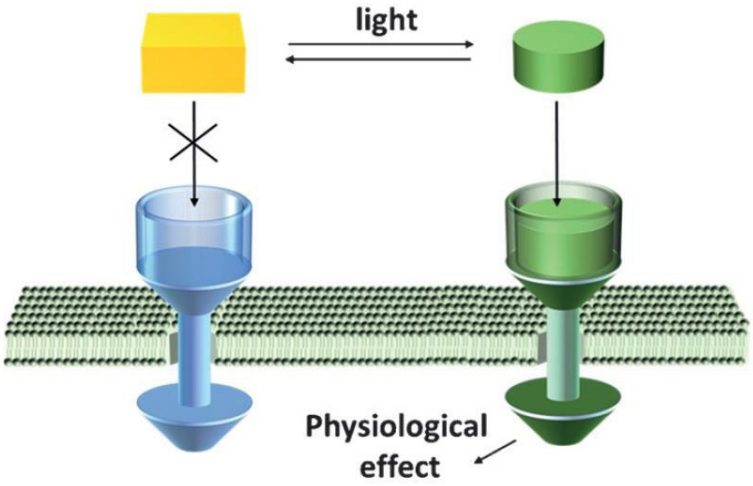

Figure 11: The two photoisomers of a photochromic ligand feature different activity. Picture taken from reference[24].

Photoswitchable tethered ligands: While photochromic ligands come with all the advantages of small molecules, they also feature the same disadvantages. Off-target activity can make this approach unfeasible and in situations where sub-type selectivity is a major concern, a related, more elaborate approach might be more attractive. Photoswitchable tethered ligands are bioactive compounds that can be covalently attached to a protein. The photoswitch is incorporated in the tether and makes the binding of the ligand dependent on the isomeric state.[28] For the covalent linkage, a variety of methods has emerged. That includes addition of native or engineered cysteine residues with maleimides, click-reactions with unnatural amino acids and a number of substitution reactions.

B III Molecular photoswitches

Besides photopharmacology, photoswitches have shown great potential in other fields like data storage[29], materials[30, 31], energy storage[32] and photoswitchable gating of chemical reactions[33]. Photoswitches are commonly categorized by their absorbance maxima of the two distinctive photo-isomers which in consequence determines the wavelength that is effectively causing the structural change. The collection of photoswitchable compound classes include azobenzenes[34-37], stilbenes[38], hemithioindigos[39, 40] and related hemiindigos[40, 41] that undergo *E*/*Z* isomerism, while spiropyranes[42], diarylethenes[43], thiophenefulgides[44] and very recently discovered stenhouse photoswitches[45, 46] interconvert between open and closed forms (see **Figure 12**). The geometrical differences can be rather large as it is the case for azobenzenes. In addition, the photoisomers' polarity can vary tremendously (e.g. spiropyrans).

Among these classes of photoswitches, azobenzenes are undoubtedly the most frequently applied ones.[34-37] The UV-Vis spectrum of the naturally more stable unsubstituted (*E*)-azobenzene features a prominent absorbance band around 320 nm resulting from the π-π^* transition and a weak signal around 430 nm caused by the symmetry forbidden n-π^*

transition. Absorbance in the region of the π-π* transition enables rotation of the N-N bond and leads to the formation of the less stable (*Z*)-isomer.[47] Irradiation with visible light (>450 nm) leads to the back isomerization which in addition takes place thermally. This thermal relaxation process follows first order kinetics and thus, a thermal half life time $\tau_{1/2}$ can be assigned which corresponds to the stability of the excited state. For unmodified azobenzene, thermal relaxation happens on the time scale of days.[48, 49] The (*Z*)-isomer has a stronger n-π* absorbance at the same location as the (*E*)-isomer and additional shorter wavelength bands (see **Figure 13**). The (*E*)-configuration is planar and has a dipole moment close to zero while the (*Z*)-isomer is bent which results in a dipole moment of 3 Debye. The end-to-end distance of the two isomers varies by 3.5 Å which is one of the compound's most important features.[50] Azobenzenes are popularly used due to their convincing set of desired properties. The photo-isomerization process takes place on a picosecond time scale. Azobenzenes have high extinction coefficients and hence, absorb light very effectively. Their photostability makes them highly fatigue resistant. Moreover, synthetic access to azobenzenes is very versatile and many methods are available. [51, 52]

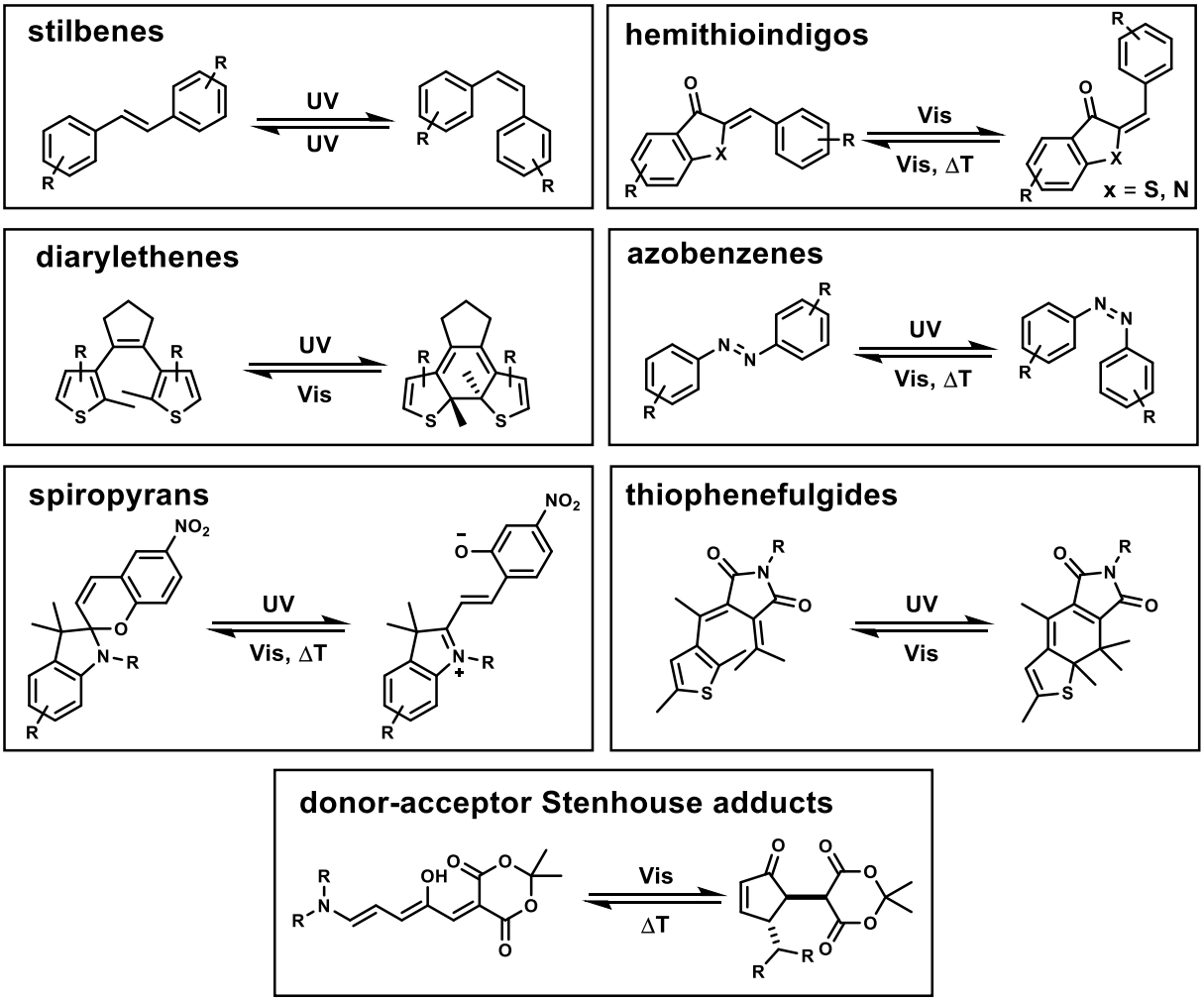

Figure 12: A number of compound classes are capable of photoinduced isomerization.

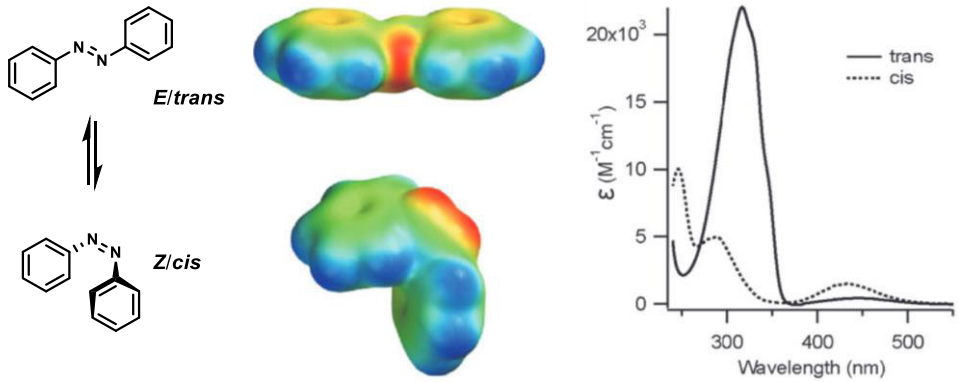

Figure 13: (*E*)-azobenzene (= *trans*-isomer) can be isomerized into (*Z*)-azobenzene (= *cis*-isomer) with UV light. The spacefilling models are colored by electrostatic potential and demonstrate the change in geometry and dipole moment. The absorbance spectra for the two isomers are very distinct. Picture modified from reference[35].

For the synthesis of symmetrical azobenzene derivatives, a reductive dimerization of aromatic nitro compounds is feasible. A wide range of reducing agents have been reported (for a comprehensive overview see review[51]). For example, nitro starting material **[I]** was treated with Zn/NaOH to afford azobenzene **[II]** by Hecht and co-workers.[53]

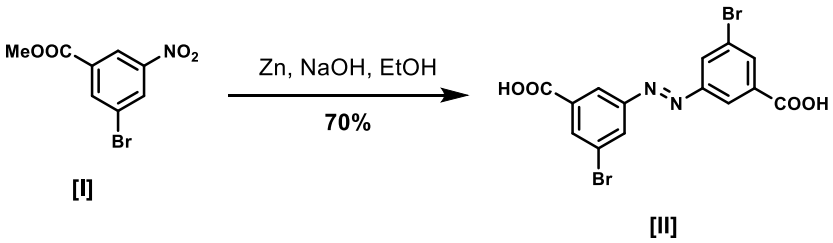

In an oxidative approach, aniline derivatives can be coupled to the corresponding symmetrical azobenzenes. MnO_2, $KMnO_4$, H_3BO_3 and Hg/I_2 are frequently applied as oxidants. Wooley and co-workers prepared azobenzene **[IV]** from aniline **[III]** to crosslink peptides.[54]

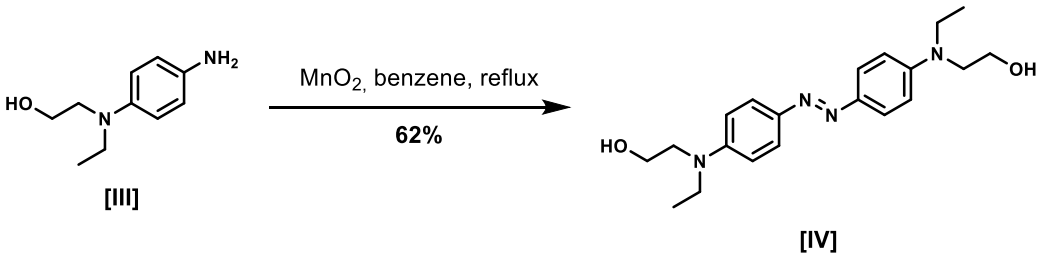

To overcome the limitations of a dimerization approach, classic azo coupling reactions can be used to obtain unsymmetric azobenzenes. In the first step a primary aniline is transformed into a diazonium salt via diazotization. Typically, HNO_2 is liberated from $NaNO_2$ under strongly acidic conditions which subsequently gives a nitrosonium cation that gets attacked by the aniline lone pair forming the diazonium species. Diazonium salts readily eliminate gaseous nitrogen. Therefore, the reaction temperature is typically kept at low temperature and the diazonium salt is subjected to the coupling step immediately after the

diazotization. Reaction with electron rich aryls yields the azobenzene in an electrophilic aromatic substitution reaction and, hence, the scope of the azo coupling reaction is subject to the limitations of electrophilic aromatic substitution chemistry (see **Figure 14**).

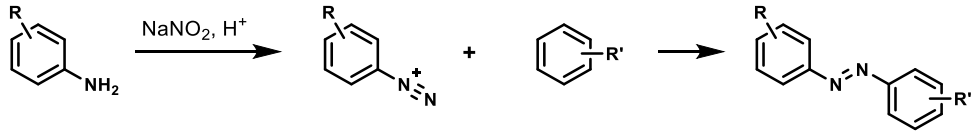

Figure 14: Azo coupling of an in situ prepared diazonium salt with an electron rich aryl gives azobenzenes.

The counter ion has a decisive influence on the stability of the diazonium salt. While chlorides have to be handled in cold solutions, non-coordinating anions like tetrafluoroborate render the diazonium salt considerably stable. They can be isolated and used in a separate reaction step. This makes them applicable in water-free environments and reaction with metal aryls readily gives the azo product. In contrast to classic azo coupling, the electrophilic center is determined by the location of the metal and, hence, regio-control gives access to a broader range of products. Very recently, this strategy was applied by Feringa and co-workers in the preparation of challenging tetra-*ortho*-substituted products which are not accessible by classic azo coupling (see **Figure 15**).[55]

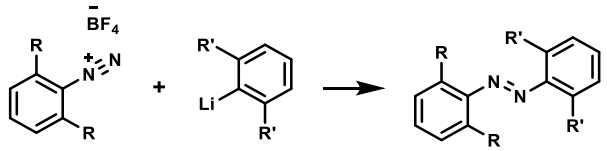

Figure 15: Diazonium tetrafluoroborates can be reacted with metal aryls to form azobenzenes.

A powerful method to synthesize unsymmetric azobenzenes with versatile functional group decoration is the condensation of an aniline with a nitroso compound known as the Mills reaction (see **Figure 16**).[56, 57] The aniline nucleophile attacks the nitroso compound and elimination of H_2O gives access to azobenzene analogs. The Mills condensation has been regularly used in the preparation of photochromic ligands.[58, 59]

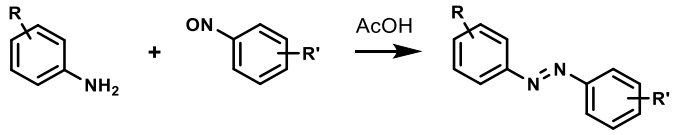

Figure 16: Aromatic nitroso compounds react with anilines to yield azobenzenes (Mills reaction).

In *N*,*N*'-diarylhydrazines the required scaffold to form azobenzenes is already in place. Dehydrogenation with various stoichiometric oxidants (for a comprehensive overview see review[51]) leads to the formation of the corresponding photoswitches. A small number of catalytic oxidations has been reported as well. The hydrazine precursor can be accessed by metal catalyzed coupling chemistry. Cho and co-workers published a coupling protocol with Pd and a subsequent oxidation with NBS/pyridine[60] or CuI[61] (see **Figure 17**).

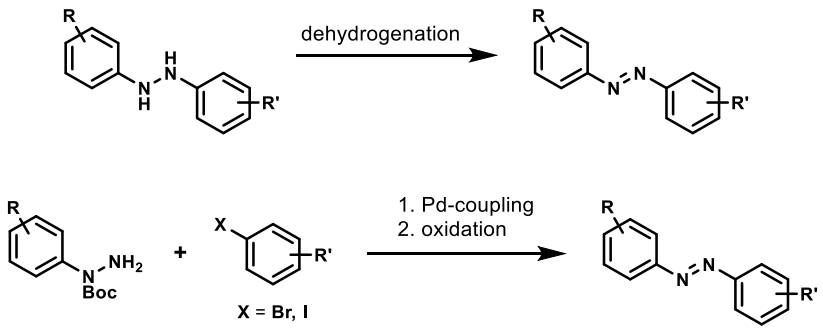

Figure 17: Metal catalyzed coupling of arylhydrazines with aryl halides gives access to diarylhydrazines which can be oxidized to azobenzenes.

Due to the corresponding absorbance band (see **Figure 13**), unmodified azobenzene can be effectively switched with UV light. This is less of a problem for in vitro studies, were short wavelength light is tolerated. As photopharmacology's ambitions seek to control biological processes in more complex environments, the required UV light poses a crucial limitation as it is absorbed and scattered by tissue and causes cell damage.[62, 63] The logic solution to this problem is the utilization of long wavelength light (red light, near-infrared) which penetrates tissue better by magnitudes.[64, 117, 118]

One strategy to redshift the absorbance is to create so called push-pull systems, where the azobenzene is substituted with an electron withdrawing group on the one phenyl ring and an electron donating group on the other one. The resulting polarized structure necessarily leads to ultra-fast relaxation which has been extensively studied.[65, 66] In general, redshifting the absorbance usually leads to a shorter half life time.[66]

Azoheteroarenes represent an underexplored area. For example, arylazoimidazoles[67] were accessed by a coupling protocol similar to **Figure 15** and displayed very effective (*E*) to (*Z*) switching with long half life times and, recently, arylazopyrazoles were reported to have well separated absorbance bands which allow high isomerization yields in both directions while exhibiting very long half life times of multiple days and a moderate redshift at the same time.[68] In a follow-up study, the authors reported on several related heterocyclic designs featuring half life times ranging from seconds to months.[69] Heterocyclic systems can therefore act as an additional handle to tailor photophysical properties in the future.

Substitution with amines in *para* and/or *ortho* position redshifts the absorbance enormously,[70] but decreases the half life time in H_2O of the switched state down to seconds. Double *ortho* substitution with amines has proven to achieve both, a strong redshift while still exhibiting moderate half life times in H_2O (see **Figure 18**).[71]

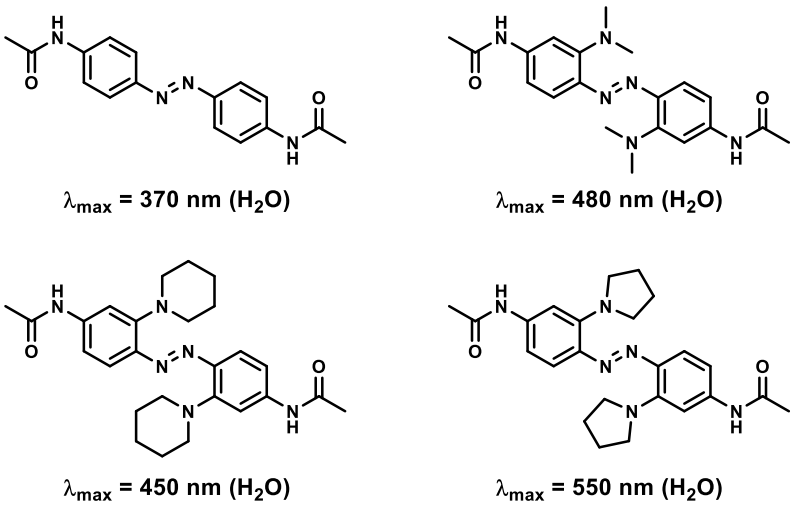

Figure 18: *Ortho*-substitution with amine leads to a strong redshift.[71]

When Wooley's lab prepared a compound carrying four methoxy substituents (compound **[V]**) in *ortho* positions following the same rationale, the π-π* transition surprisingly blueshifted while the n-π* transition was redshifted for the (*E*)-isomer but not for the excited (*Z*)-isomer.[72] Hence, the separation of the n-π* bands allowed the (*E*) to (*Z*) isomerization addressing the n-π* transition with green light (530 nm) and the backswitch with blue light (460 nm, see **Figure 19**). In addition, the molecule featured a half life time of approximately two days in H_2O. Unfortunately, the compound was reduced in 10 mM glutathione and therefore, can hardly be used in more complex biological systems. Tetra-*ortho*-chloro[73] and tetra-*ortho*–thioether[74] analogs circumvented this problem. Related tetra-*ortho*-fluoro azobenzenes were also successfully switched with green light and featured remarkably long half life times of about 700 days in DMSO.[75]

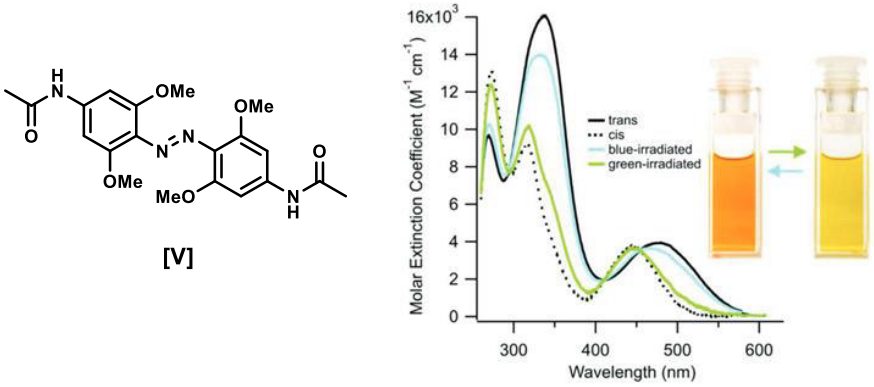

Figure 19: The tetra-*ortho*-methoxy substituted azobenzene was effectively switches with green light. Picture taken from reference.[72]

Interestingly, tetra-*ortho*-methoxy azobenzenes with additional amino substituents in *para* position[76] enabled the protonation of the azo bridge to form azonium ions at pH 7 due to a beneficial pK_a. Usually, photoswitched azonium ions relax ultra-fast[77] but the methoxy substituent seemingly led to a stabilization of the protonated state by their hydrogen bond

acceptor ability in the (*E*)-form but not in the (*Z*)-form which leads to a non-protonated excited state with a reasonable half life time. Azonium ions exhibit a significant redshift and very recently, compound **[VI]** was reported to switch with light of 720 nm (see **Figure 20**).[78]

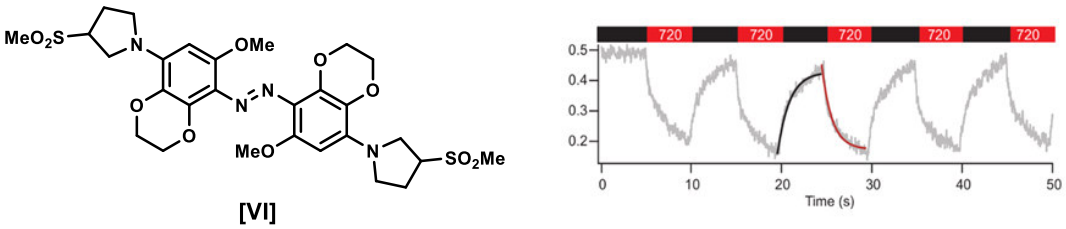

Figure 20: Compound **[VI]** could be switched with near-IR light. Picture taken from reference[78].

Apparently, *ortho*-functionalization has emerged as a promising possibility to modify azobenzene photoswitches. These representative examples are usually symmetric molecules and the implications for photopharmacological compounds are rather modest. Feringa's lab used the previously introduced method to couple an aryl lithium species with a diazonium tetrafluoroborate (see **Figure 15**) to synthesize tetra-*ortho*-fluoro and tetra-*ortho*-chloro analogs of an azobenzene based antibacterial. The switching light increased from UV light for the initial azobenzene to green light for the fluoro analog to red light for the chloro analog (see **Figure 21**).[79]

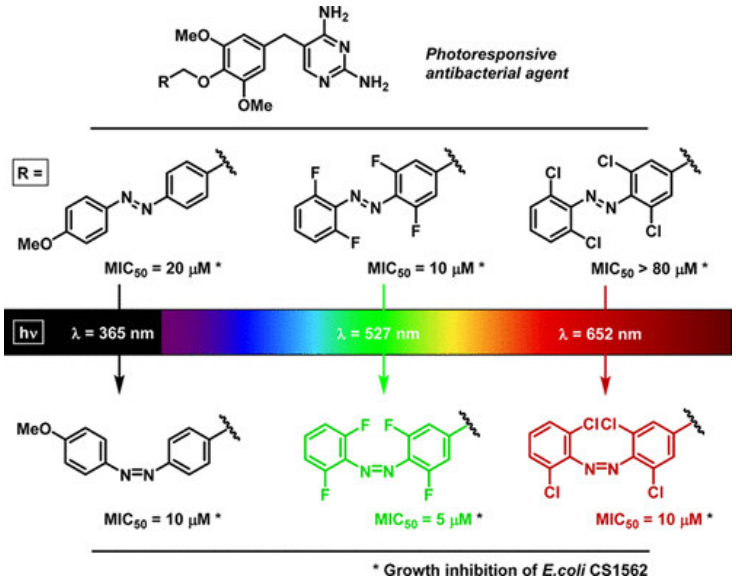

Figure 21: *Ortho*-fluoro and *ortho*-chloro versions were accessed by a modified azo coupling reaction and led to enormous redshifts in absorbance. Picture taken from reference[79].

In a complementary attempt to apply the strategy of *ortho*-functionalization to useful bioactives, Trauner and co-workers recently published a synthetic method to modify existing azobenzenes at a late stage by C-H chlorination and thereby, combining the benefits of redshifted azobenzenes with photopharamcology's ligand design principles (see **Figure 22**).[80] The group prepared the redshifted analog **[VII]** of an older photoswitchable TRPV1 agonist, and by that shifting the activation wavelength by 200 nm into the visible region. Just a while

ago, methods to directly functionalize azobenzenes by the means of metal-catalysis have been comprehensively reviewed.[81]

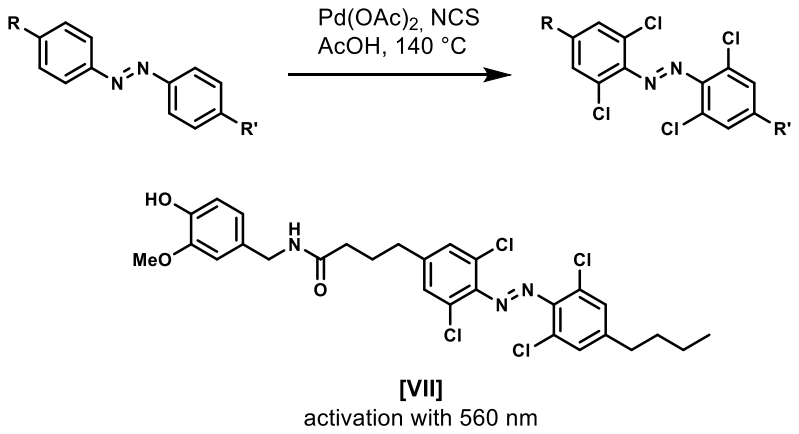

Figure 22: A C-H chlorination protocol by Trauner's lab gives access to redshifted derivatives at a late synthetic stage.

The interest in hemithioindigos (HTIs) has grown rapidly over the last years.[39, 40] While HTIs share the advantages of azobenzenes (pronounced geometrical change upon switching, high thermal stability of the excited isomer, good quantum yields and high photostabilities) they offer one additional appealing feature. In contrast to azobenzene, the unsubstituted parent HTI compound can be switched with blue light and avoids the use of biologically harmful UV light in any case.[82]

HTIs can be synthesized via an acid or base catalyzed Aldol condensation of an aldehyde and the corresponding cyclic ketone (see **Figure 23**) which is accessible in various ways (e.g. Friedel-Crafts acylation). Alternatively, an iodine mediated reaction can be used. Recently, methods have been developed for sterically demanding substrates[83] and double-bond substituted HTIs[84].

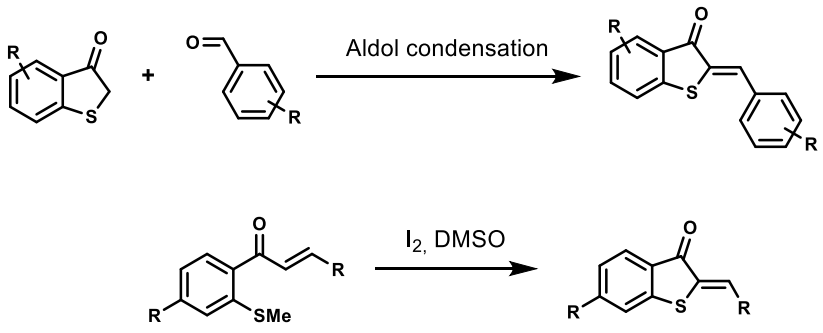

Figure 23: HTIs are readily synthesized by an Aldol condensation.

Strong donor groups in *para* position of the stilbene fragment are able to cause a profound redshift of the absorbance by promoting the donor-acceptor character of the double bond (compound **[IX]**) which in consequence leads to shorter half life times of the metastable (*Z*)-isomer.[82, 85] On the other hand, introduction of an electron donating substituent *para* to

the sulfur group (compound **[X]**) leads to a substantial redshift while a half life time of 30 days was achieved (see **Figure 24**).

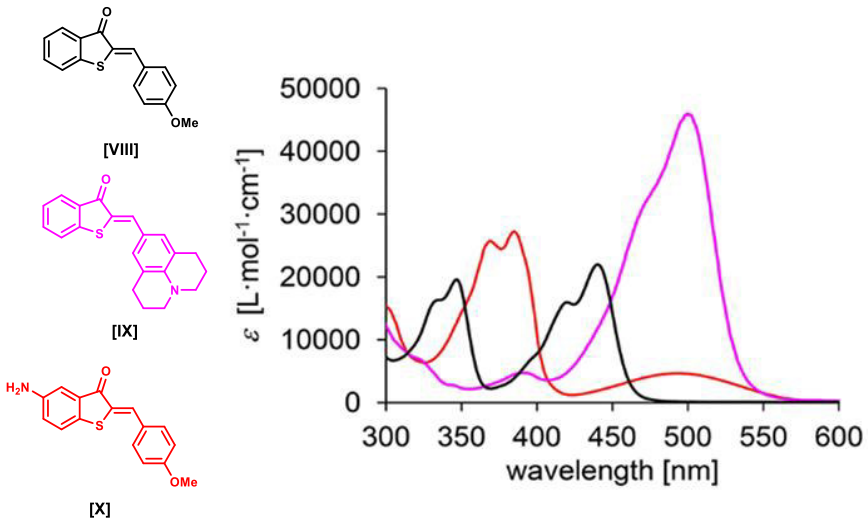

Figure 24: The absorbance can be redshifted by appropriate decoration. Picture modified from reference[38].

A complementary strategy to redshift the absorbance of HTIs was reported by Newhouse and co-workers.[86] Instead of the stilbene's phenyl ring, a pyrrole was used. The electron rich heterocycle led to a moderate redshift of the thermodynamically stable (*Z*)-isomer while the (*E*)-isomer was stabilized by hydrogen bonding which resulted in a stronger redshift for the metastable photo-isomer and in consequence to high isomerization yields due to the clear separation of the absorbance bands (see **Figure 25**).

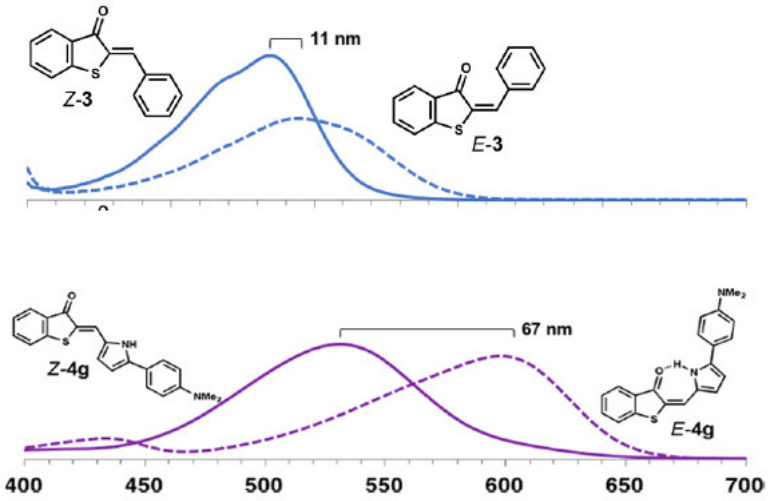

Figure 25: Electron donating features led to a redshifted absorbance which was further redshifted for the (*E*)-isomer due to stabilization through an intramolecular hydrogen bond. Picture modified from reference[86].

When the group of Dube studied the photoisomerization of HTIs with sterically crowded and electron-rich stilbene fragments, they observed a second possible light triggered process. The single bond between the stilbene phenyl ring and the double bond was shown to undergo light induced rotation. The molecule is thought to populate a twisted intramolecular

charge-transfer (TICT) state after irradiation. The process was shown to be highly solvent dependent. In apolar cyclohexane, (*Z*) to (*E*) photoisomerization prevailed while in polar DMSO TICT formation took place (see **Figure 26**).[87]

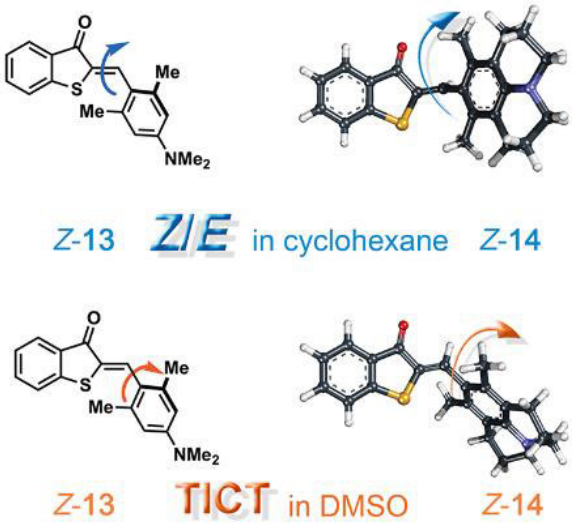

Figure 26: Dependent on the solvent, HTIs can display a different photo induced rotation. Picture taken from reference[38].

B IV Photopharmacology - examples

As already mentioned earlier, azobenzenes are most frequently applied in photopharmacology. Up to date, a wide range of processes and bio-molecules has been targeted. Two concepts are regularly used to design azobenzene containing small molecules. Via "azologization" isosters of azobenzene can be identified to incorporate the switchable motif in known inhibitors and the like (see **Figure 27**).[21, 88] Secondly, in an "azo-extension" approach, the azobenzene motif is attached to a part of the molecule where SAR data suggests that variations are tolerated.

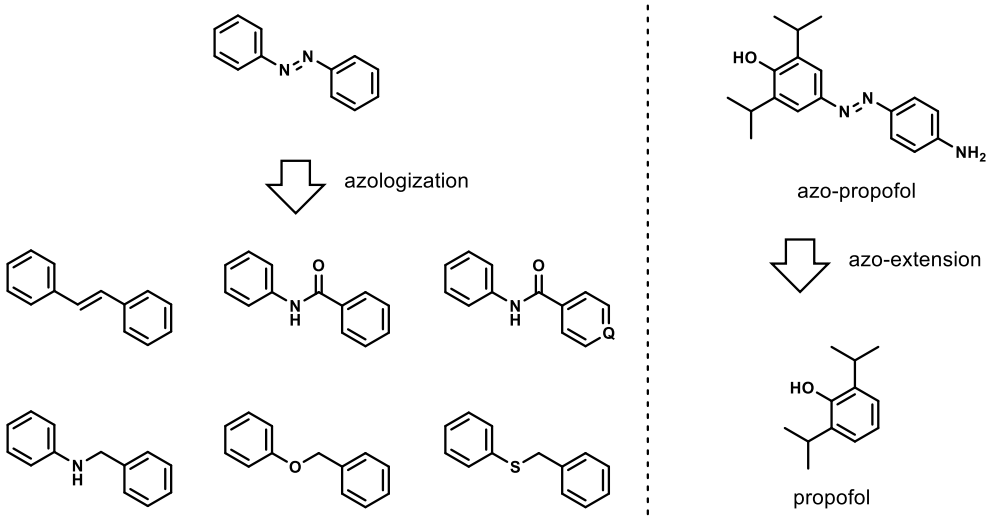

Figure 27: Two frequently applied strategies: Isosters of azobenzene can be replaced by the photoswitchable moiety (azologization) or the photoswitchable moiety can be attached to an existing scaffold (azo-extension).

The vast diversity of successful literature examples include among others photo-control over ion channels[89], glutamate receptors[90-92], $GABA_A$ receptors[93, 94], dopamine receptors[95], cannabinoid receptors[96], AMPA receptors[97], kinases[98], opioid receptors[99], nicotinic acetylcholine receptors[100], insulin release[101-104], antibacterial activity[79, 105] and modulation of G protein-coupled receptors[106]. Photoswitchable lipids[107] have been reported as well as photostatins to photocontrol cytotoxicity by targeting microtubule dynamics.[1] Azobenzene based drugs to treat certain types of blindness have progressed significantly, too.[97, 108, 109] **Figure 28** shows a selection of synthesized compounds to reach these remarkable goals.

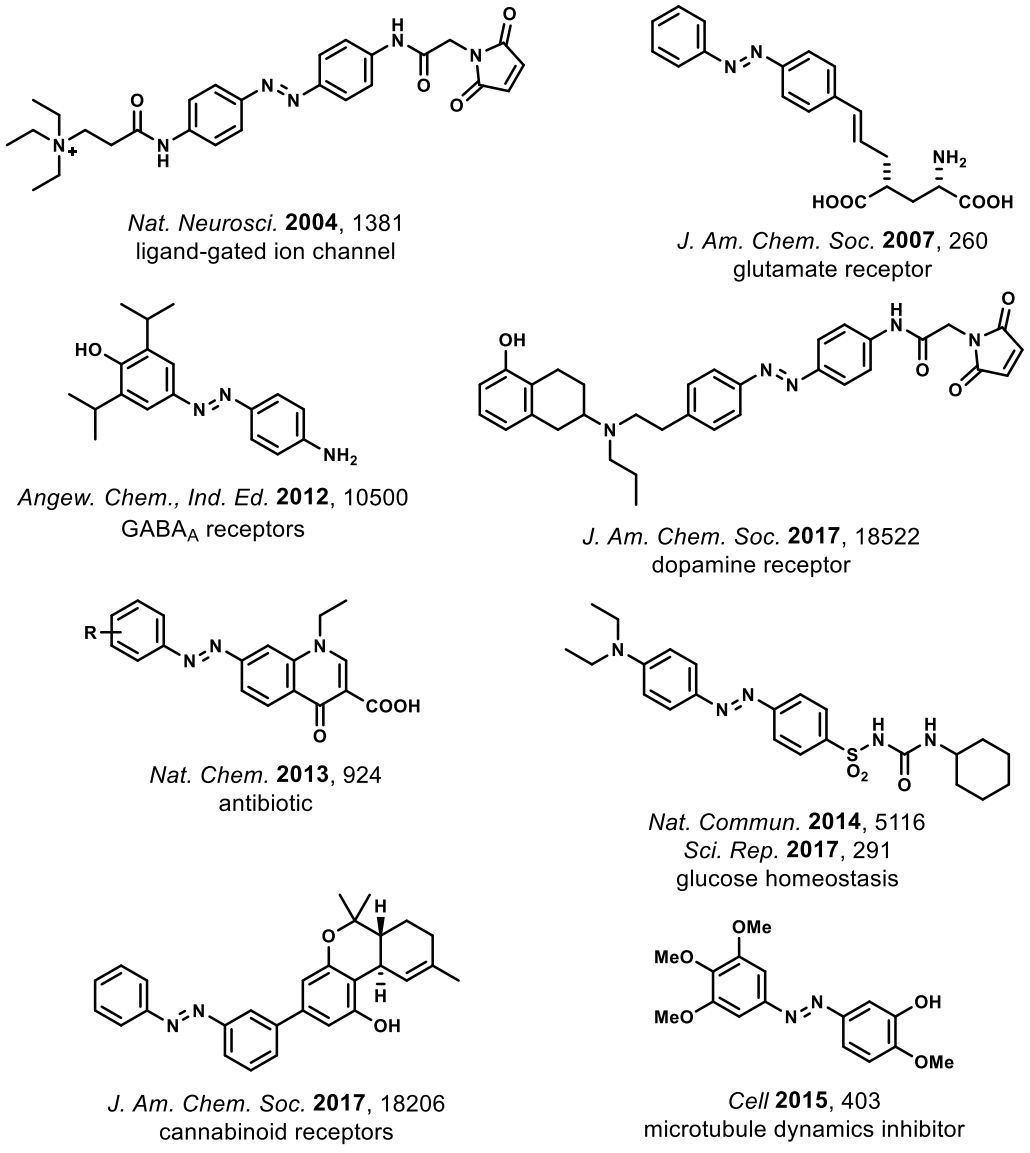

Figure 28: A great variety of azobenzene based photoswitchable compounds have been synthesized for a wide range of photopharmacological applications as photochromic ligands as well as tethered ones.

HTIs have been applied in photoswitchable lipids[110, 111], peptide folding[112-114], enzyme inhibition[115] and gramicidin channels[116].

The first photopharmacological control of a transporter protein was published by Wanner and co-workers on the murine GABA transporter 1 (mGAT1).[58] Based on the known mGAT1 inhibitor **[XI]** (IC_{50} = 0.1 µM) azobenzene containing analogs were synthesized and tested (see **Figure 29**). Compound **[XII]** turned out to exhibit reasonable photodependent activity. The un-irradiated inhibitor displayed an IC_{50} of 0.4 µM (blue dose-response curve) which dropped to 1.66 µM (red dose-response curve) when the compound was switched with 375 nm. With this 4-fold difference in inhibitory activity, the group went on to assess the photodependency in acute murine brain slices via electrophysiology. The more potent (E)-isomer induced a shift in the $GABA_A$ receptor-mediated current which was reversed by application of bicuculline methiodide (BIM), a $GABA_A$ receptor antagonist. When irradiated **[XII]** was used, no shift was induced and thus demonstrating the photodependent transporter inhibition.

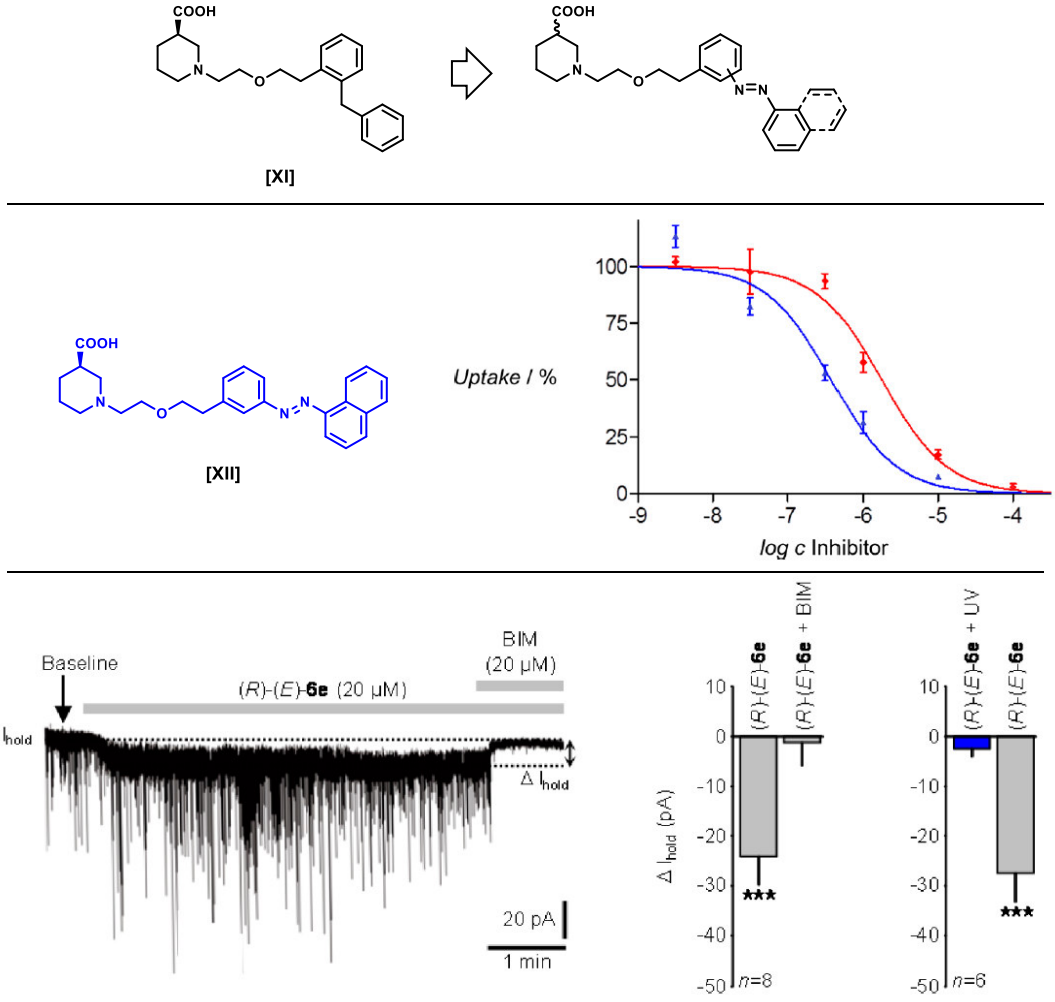

Figure 29: Inspired by mGAT1 inhibitor **[XI]**, photoswitchable inhibitor **[XII]** was found to photodependently block the transporter. Picture modified from reference[58].

Very recently, Trauner's lab reported on photodependent inhibition of a glutamate transporter which is up to date only the second report on a transporter.[59] The literature-

known inhibitor **[XIII]** (low nanomolar IC_{50}) was turned into a photoswitchable analog via azologization (compound **[XIV]**, see **Figure 30**). The compound featured an IC_{50} of 0.9 nM (see dose-response curve, open symbols) on the glutamate transporter EAAT2 (excitory amino acid transporter 2) which decreased to 12.7 nM (closed symbols) when the azobenzene derivative was irradiated with 350 nm, thus a 14-fold difference in activity. When the compound was applied to EAAT2 expressing oocytes, the glutamate uptake dependent voltage was inhibited by compound **[XIV]** (termed ATT in **Figure 30**) in the dark (voltage clamp conditions). L-glutamate only slowly displaced the potent inhibitor. When light of 350 nm was applied and the inhibitor switched into its less active form, displacement took place much more readily.

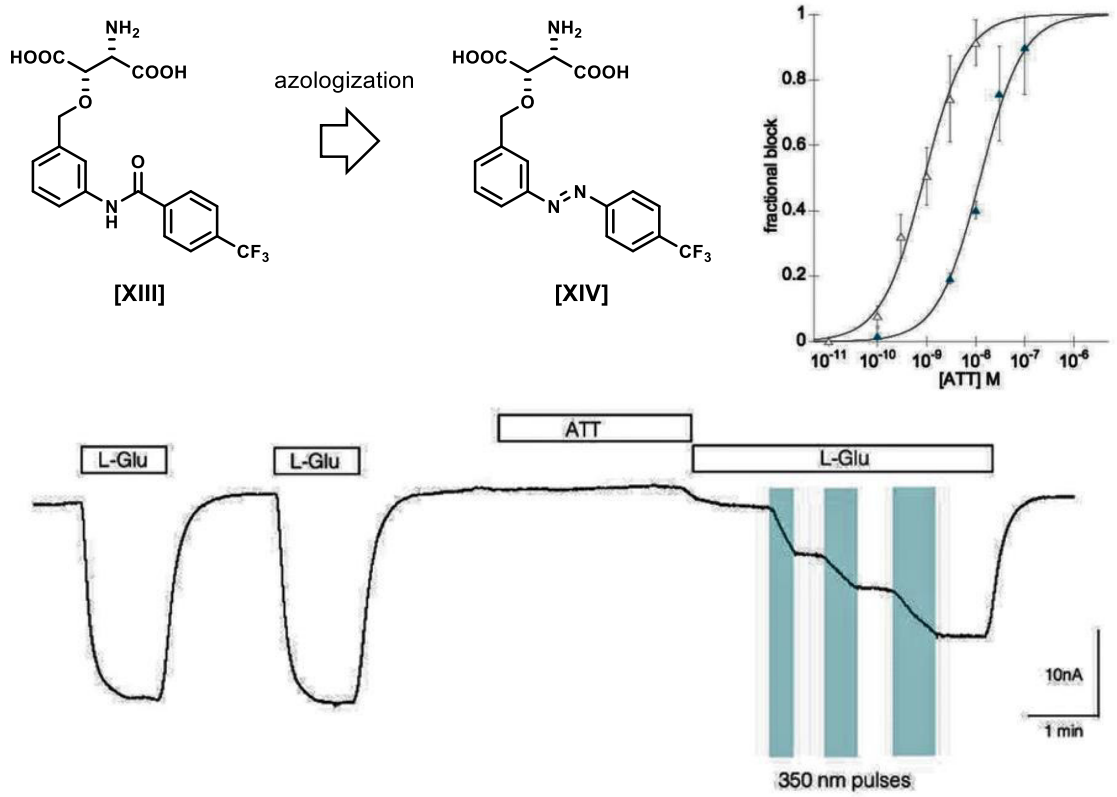

Figure 30: Literature-known compound **[XIII]** served as an inspiration to develop the photoswitchable analog **[XIV]** which was shown to exhibit light dependent inhibitory activity on EAAT2 in oocytes. Picture modified from reference[59].

B V Objective

Within this thesis, we aimed to develop photoswitchable inhibitors of MATs as pharmacological tool compounds. As the SERT attracts the most attention in the scientific community among MATs[3], our research primarily targeted this transporter protein. As NET and DAT are structurally very similar, photodependent inhibition of these two targets would be a secondary, nonetheless likewise desirable goal. **Figure 31** depicts a schematic representation of this thesis' goal: Controlling monoamine uptake by light.

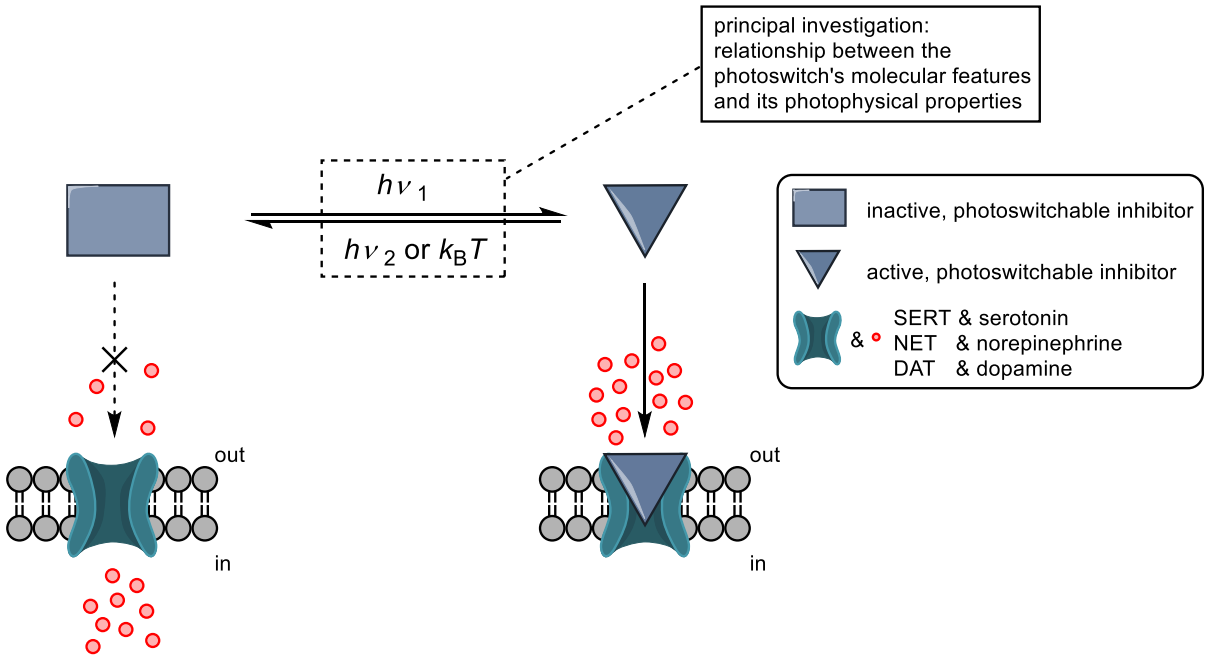

Figure 31: Schematic overview of a photo controlled inhibition of MATs by altering the inhibitor-protein interaction light dependently. The molecule on the left (rectangle) represents an inactive inhibitor of a respective MAT. By irradiation with light of a suitable wavelength (reciprocal ν_1) the molecule can be isomerized and thereby, becomes an active inhibitor (triangle). Consequently, the active monoamine transport is inhibited and extracellular monoamine level rises. The active inhibitor can be switched back to its inactive form with light of a suitable, higher wavelength (reciprocal ν_2) or thermally isomerizes back with a certain velocity. The reverse mode of action is imaginable too: an active inhibitor can be switched into an inactive one by light. For simplification the transporter protein is depicted as a channel.

As outlined in the introduction, MATs play an essential role in neuronal signaling and, hence, in many biological processes associated with the functionality of the CNS. The successful development of photoswitchable MAT inhibitors would provide neuroscientists with novel tools to study transporters in greater detail. Such compounds might pose a valuable addition to the tool-kit of relevant research fields and would facilitate new experiments motivated by the unique features of photoswitches.

Furthermore, we aimed at conducting principal investigations in order to develop a general understanding of the relationship of molecular features of photoswitches and their resulting photophysical properties. In consequence, we would apply this knowledge to the design of the envisaged photoswitches in this explorative project and in addition, this study should lay the groundwork for future projects in this field.

C Results and Discussion

C I Principal investigation: half life time

In this chapter, we took a very general look at azobenzene photoswitches (see **Figure 32**), the most widely applied class in photopharmacology and related fields. As we had yet no experience with photoswitches, we intended to get acquainted with the characteristics of this compound class in terms of synthetic access and practical parameters. By developing a general understanding of these compounds, we aimed to apply this knowledge in later chapters. The later synthesized photoswitchable MAT inhibitors can be seen as functionally decorated azobenzenes. Hence, we wanted to gain knowledge, how the functional group decoration of azobenzenes influences their distinctive properties. Of particular interest were:

- The wavelength of maximal absorbance (λ_{max}) which correlates with the wavelength (reciprocal ν_1) that can effectively trigger the photoisomerism.
- The thermal half life time $\tau_{1/2}$ which represents the stability of the switched state.
- The predictability for future compounds.

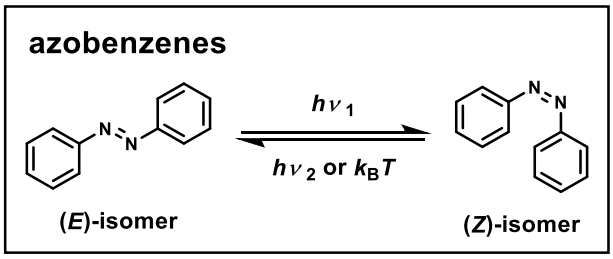

Figure 32: The naturally more stable (*E*)-azobenzene can be converted into its (*Z*)-isomer with UV light. The back isomerization in the dark is a relaxation process with a certain half life time.

While the light induced (*E*) to (*Z*) isomerization and (*Z*) to (*E*) back isomerization are very fast processes, the half life time of the thermal back isomerization varies between μs[66, 117, 118] and years[68, 75]. Spectral properties and half life time can be tuned by decorating the phenyl ring with functional groups.[49, 66] For azobenzenes, the following has been reported in the literature:

- λ_{max} is increased in substituted azobenzenes.[49]
- *para*-substituted azobenzenes have a shorter half life time than unsubstituted azobenzene.[48, 49]
- An increased λ_{max} seems to correlate with a decreased $\tau_{1/2}$ in many cases.[49]

In this context, azoheteroarenes – these are azobenzene derived compounds where one or both phenyl rings are replaced by a heteroaromatic fragment - are significantly less studied. Variations on the heterocyclic scaffold might enable an even deeper influence of the optochemical properties. We aimed to investigate whether what was known for classic azobenzenes holds true for azoheteroarenes as well and planned to conduct a more comprehensive analysis of the substituents' influence.

For practical reasons we wanted to apply a synthetic strategy that would allow rapid and efficient access to a wide range of functional groups. Furthermore, we favored a long half life time of the parent compound as we thought that this would allow appropriate measurability and cover a large range of values. A report by Weston et. al. inspired us to choose arylazopyrazoles as the compound class of choice.[68] In addition, incorporating electron-rich five-membered heterocycles should lead to a higher (redshifted) λ_{max}.[68, 86] In a later chapter (**C I.1.3** and **C I.1.4**) we are going to compare the pyrazoles with other electron-rich heterocycles like thiophenes and investigate the role of the ring structures on the photophysical properties.

C I.1.1 Synthesis of arylazopyrazoles

Unsubstituted 1,3,5-trimethyl-4-(phenyldiazenyl)-1*H*-pyrazole **[3]** investigated by Weston et. al. served as a starting point for this study. The unfunctionalized photoswitch features a thermal half life time of 10 days in acetonitrile at 25 °C as determined by NMR. The compound was synthesized from aniline **[1]** via diazotization, reaction with C-H acidic acetylacetone and subsequent cyclization with methylhydrazine in quantitative yield. Using substituted anilines as starting materials offered the possibility to access a whole library of arylazopyrazoles under these robust and high yielding reaction conditions (see Figure **33**).

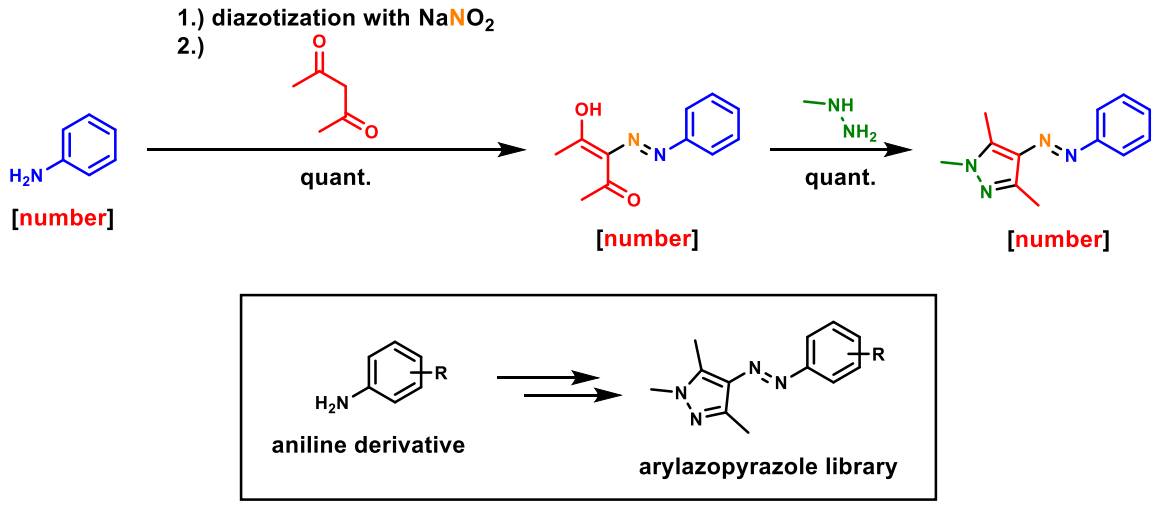

Figure 33: The robust synthesis of arylazopyrazoles promised efficient access to a suitable library to study substitution effects on photophysical parameters.

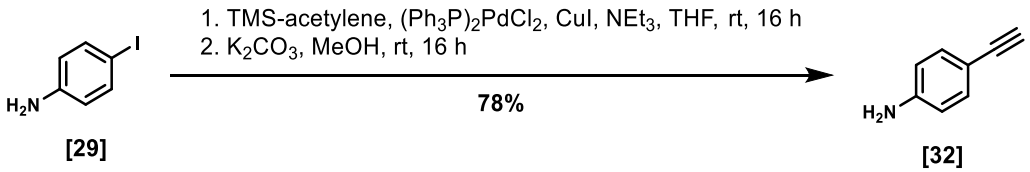

[29] **[32]**

The acetylene substituted aniline **[32]** was obtained via Sonogashira coupling of 4-iodoaniline **[29]** with TMS protected acetylene and subsequent deprotection with K_2CO_3. All other aniline derivatives were commercially available. In the first step of the synthesis, the respective aniline starting material was dissolved in AcOH and conc. HCl. At 0 °C an aqu. solution of $NaNO_2$ was added dropwise while the reaction is maintained at low temperature for one hour. A diazonium intermediate is formed by diazotization that was added as a solution to a suspension of acetylacetone and NaOAc in EtOH/H_2O. The formation of a yellow precipitate indicated formation of the desired product which could be isolated by filtration and which was washed and dried. Most products were obtained in good purity and did not require additional purification. Compound **[24]** (NEt_2 substituted) and compound **[50]** (phenyl substituted) had to be purified by flash column chromatography. Reaction of acetylene substituted aniline **[32]** gave a mixture of the desired product **[33]** and the acetyl side product **[35]** due to partial hydration of the triple bond under the acidic reaction conditions. The two products were separated on silica gel and a combined yield of 52% was achieved.

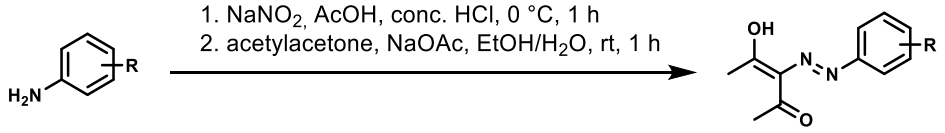

[1] R = H	**[2] R = H**	**73%**
[4] R = *p*-NO_2	**[5] R = *p*-NO_2**	**91%**
[8] R = *p*-OH	**[9] R = *p*-OH**	**66%**
[12] R = *p*-COOH	**[13] R = *p*-COOH**	**87%**
[19] R = *p*-CN	**[20] R = *p*-CN**	**91%**
[23] R = *p*-NEt_2	**[24] R = *p*-NEt_2**	**75%**
[26] R = *p*-F	**[27] R = *p*-F**	**87%**
[29] R = *p*-I	**[30] R = *p*-I**	**92%**
[32] R = *p*-CCH	**[33] R = *p*-CCH**	**34% +**
	[35] R = *p*-Acetyl	**18%**
[37] R = *p*-Me	**[38] R = *p*-Me**	**95%**
[40] R = *p*-Cl	**[41] R = *p*-Cl**	**95%**
[43] R = *p*-Br	**[44] R = *p*-Br**	**94%**
[46] R = *p*-CF_3	**[47] R = *p*-CF_3**	**quant.**
[49] R = *p*-Ph	**[50] R = *p*-Ph**	**44%**
[52] R = *m*-NO_2	**[53] R = *m*-NO_2**	**93%**
[55] R = *o*-NO_2	**[56] R = *o*-NO_2**	**92%**

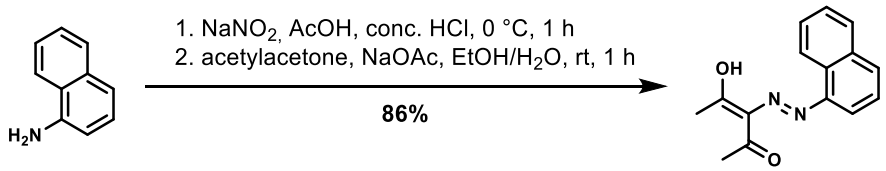

[58] **[59]**

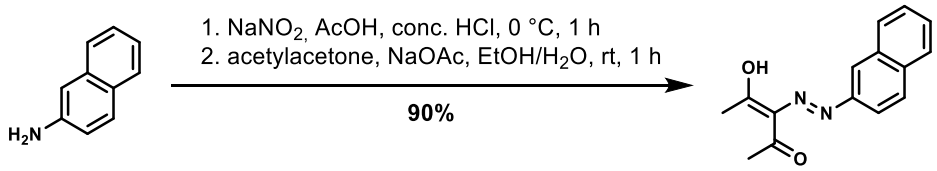

[61] **[62]**

The obtained intermediates could then be used in the second step. Reaction with methylhydrazine in EtOH at reflux temperature led to the cyclization to the desired pyrazole products. Evaporation of volatiles gave the products in very good purity and excellent yields in most cases. Compound **[25]** (NEt_2 substituted), compound **[34]** (acetylene substituted), compound **[36]** (acetyl substituted) and compound **[48]** (CF_3 substituted) had to be purified by flash column chromatography.

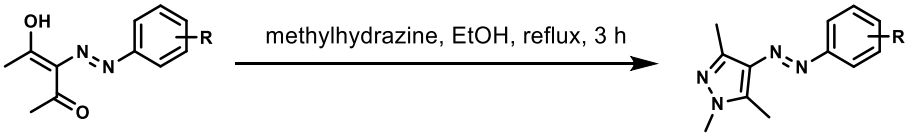

[2] R = H	**[3] R = H**	**quant.**
[5] R = *p*-NO_2	**[6] R = *p*-NO_2**	**99%**
[9] R = *p*-OH	**[10] R = *p*-OH**	**quant.**
[13] R = *p*-COOH	**[14] R = *p*-COOH**	**quant.**
[20] R = *p*-CN	**[21] R = *p*-CN**	**quant.**
[24] R = *p*-NEt_2	**[25] R = *p*-NEt_2**	**86%**
[27] R = *p*-F	**[28] R = *p*-F**	**99%**
[30] R = *p*-I	**[31] R = *p*-I**	**99%**
[33] R = *p*-CCH	**[34] R = *p*-CCH**	**71%**
[35] R = *p*-Acetyl	**[36] R = *p*-Acetyl**	**77%**
[38] R = *p*-Me	**[39] R = *p*-Me**	**quant.**
[41] R = *p*-Cl	**[42] R = *p*-Cl**	**quant.**
[44] R = *p*-Br	**[45] R = *p*-Br**	**quant.**
[47] R = *p*-CF_3	**[48] R = *p*-CF_3**	**90%**
[50] R = *p*-Ph	**[51] R = *p*-Ph**	**97%**
[53] R = *m*-NO_2	**[54] R = *m*-NO_2**	**97%**
[56] R = *o*-NO_2	**[57] R = *o*-NO_2**	**quant.**

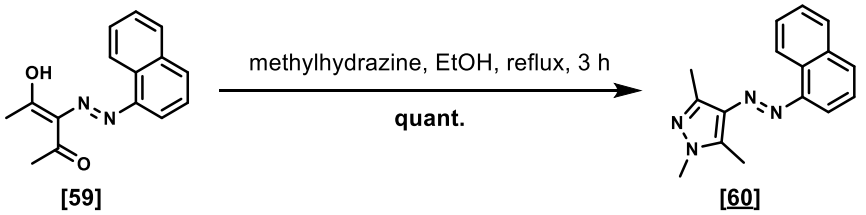

[59] **[60]**

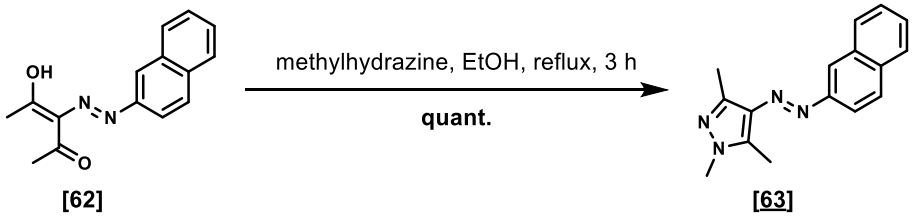

[62] **[63]**

Some of the obtained products were used for follow-up modifications to further diversify the compound library and thereby create a comprehensive collection of substituents.

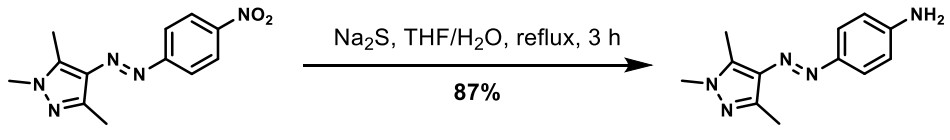

[6] **[7]**

Reduction of nitro derivative **[6]** with Na_2S in THF/H_2O at reflux temperature worked smoothly. After extractive work-up and purification by flash column chromatography, aniline **[7]** was obtained in 87% yield.

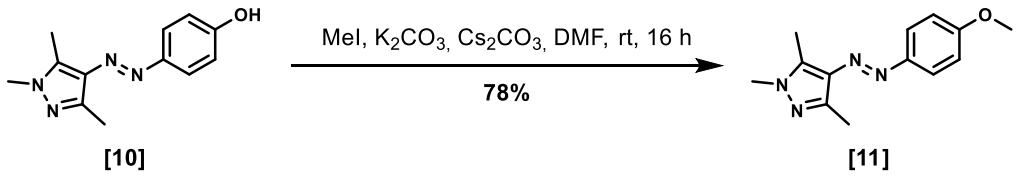

Phenol **[10]** was methylated with MeI under basic conditions in DMF. Isolation by extraction and purification by flash column chromatography afforded anisole derivative **[11]** in 78% yield.

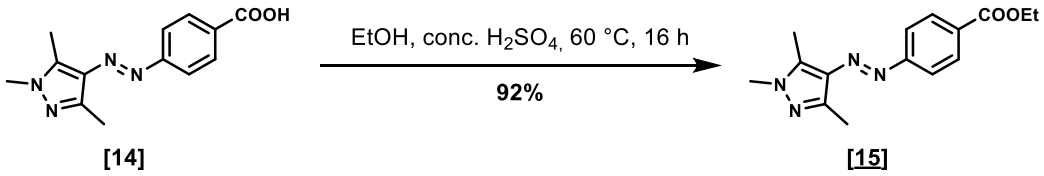

Esterification of acid **[14]** under classic Fischer esterification conditions gave ethyl ester **[15]** after extractive isolation in 92% yield.

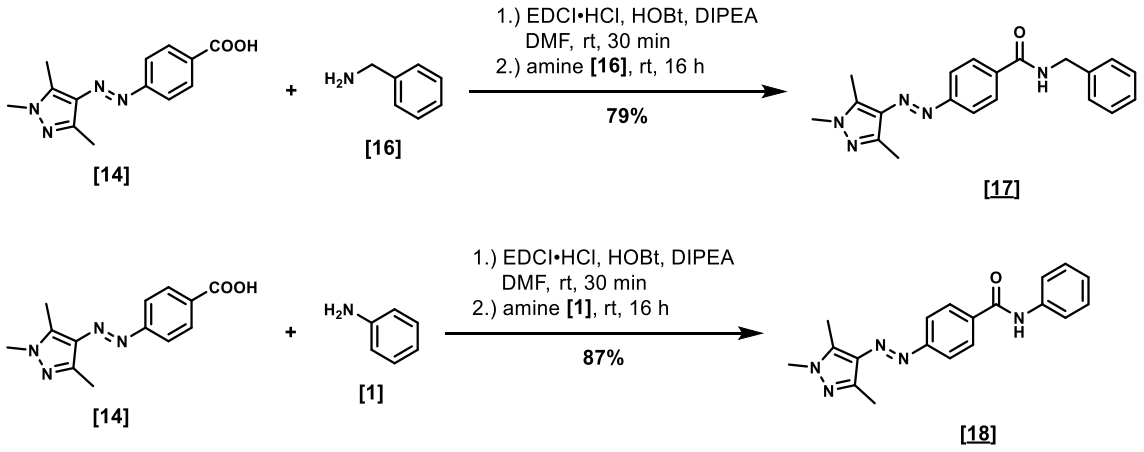

Acid **[14]** was also used for amide coupling. The starting material reacted cleanly under EDCI/HOBt coupling conditions with aniline **[1]** and benzylamine **[16]**, respectively, to afford amides **[17]** and **[18]** after purification by flash column chromatography in very good yields.

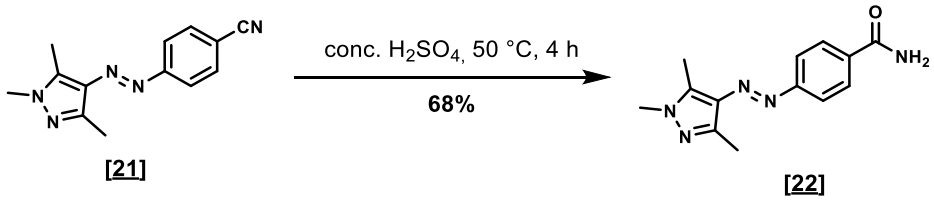

To obtain the corresponding unsubstituted amide analog **[22]**, nitrile **[21]** was hydrolyzed under strongly acidic conditions with conc. H_2SO_4 at 50 °C. The product could be isolated extractively in 68% yield.

C I.1.2 Photophysical characterization of arylazopyrazoles

Table 2: Overview of prepared derivatives and their characteristics.

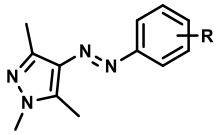

compound	substituent	property	building block potential
[3]	H	literature[68] comparison: half life time of 10 days in MeCN at 25 °C	
[6]	*p*-NO_2	strong -M effect	
[54]	*m*-NO_2	strong -M effect, interaction disabled	
[57]	*o*-NO_2	strong -M effect	
[10]	*p*-OH	electron donor (+M) hydrazone tautomerism	etherification esterification
[11]	*p*-OMe	electron donor (+M)	
[7]	*p*-NH_2	strong electron donor (+M)	amide coupling reductive amination
[25]	*p*-NEt_2	strong electron donor (+M)	
[14]	*p*-COOH	-M effect	esterification amide coupling
[15]	*p*-COOEt	-M effect	
[21]	*p*-CN	-M effect	
[22]	*p*-$CONH_2$	-M effect	
[18]	*p*-CONHPh	-M effect	
[17]	*p*-CONHBz	-M effect	
[28]	*p*-F	halogen series	
[42]	*p*-Cl	halogen series	cross coupling
[45]	*p*-Br	halogen series	cross coupling
[31]	*p*-I	halogen series	cross coupling
[39]	*p*-Me	+I effect	
[34]	*p*-CCH	-I effect	Huisgen click
[36]	*p*-acetyl	-M effect	
[48]	*p*-CF_3	-I effect	
[51]	*p*-Ph	larger π-system	
[60]	1-naphthyl	larger π-system	
[63]	2-naphthyl	larger π-system	

In total, 25 arylazopyrazoles were synthesized, 18 of them unknown to the literature. In **Table 2** the compound library is summarized and the respective features are listed. The substituents were chosen in order to create a broad variety of properties (electron withdrawing and donating capabilities) to sufficiently study their influence on photophysical parameters. The nitro series (compounds **[6]**, **[54]** and **[57]**) should give an insight into the impact of the respective *ortho*, *meta* and *para* substitution position. Some functional groups can be further functionalized and serve as building blocks in a toolkit approach to attach photoswitches to existing molecules. The amides **[22]**, **[18]** and **[17]** were chosen to investigate the predictability of future compounds (e.g. for an analogous MAT inhibitor containing an amide bond).

With the compounds in hand, we went on to measure the photophysical properties. Stock solutions with a concentration of 1 mM in dry DMSO were prepared and stored in brown vials in the darkness. It has to be noted that under standard lab conditions, most of the isolated azopyrazoles contained a measurable amount of (*Z*)-isomer (observed on TLC plates as a second yellow spot and in NMR). To obtain the material in 100% (*E*)-configuration, the isomeric mixtures were heated with an oil bath until the thermal relaxation was complete. Alternatively, conducting the preparation of the photoswitches in a yellow light lab prevented the formation of the (*Z*)-isomer in the first place. DMSO was chosen as solvent as it is non-volatile (required for determination of half life time in an open cuvette), possesses good solubility and is similar to H_2O in polarity which should make the results transferable to biological systems. After measuring the spectrum of the (*E*)-isomer from a 50 μM solution in DMSO, the cuvette was irradiated with OmniCure® LED heads of 365 nm, 385 nm, 400 nm and 460 nm consecutively for five seconds with 100% power (OmniCure® LX400) from the top and associated spectra were recorded. These high performance LEDs emit light with a power of typically 10 – 15 W/cm^2 which usually produced the respective photostationary state (PSS) within one second. The obtained data was processed with Origin 8.5. **Figure 34** shows a representative result. In the initial state, 100% (*E*)-isomer is present which has a characteristically strong absorbance between 340 and 400 nm (black curve). At the maximum absorbance the λ_{max} value can be determined (in this case 352 nm). Irradiation with 365 nm leads to a profound change of the spectrum indicating the successful switch towards the (*Z*)-isomer (red curve). The initial absorbance band disappears and the redshifted band of the (*Z*)-isomer around 450 nm becomes prominent. It is generally believed that the larger the difference of the two absorbance bands is the higher the isomer conversion yields are as it allows the selective excitation of one isomer.[86] With light of increasing wavelengths (385 nm → 460 nm; blue, magenta and green curve) more and more (*E*)-isomer is restored.

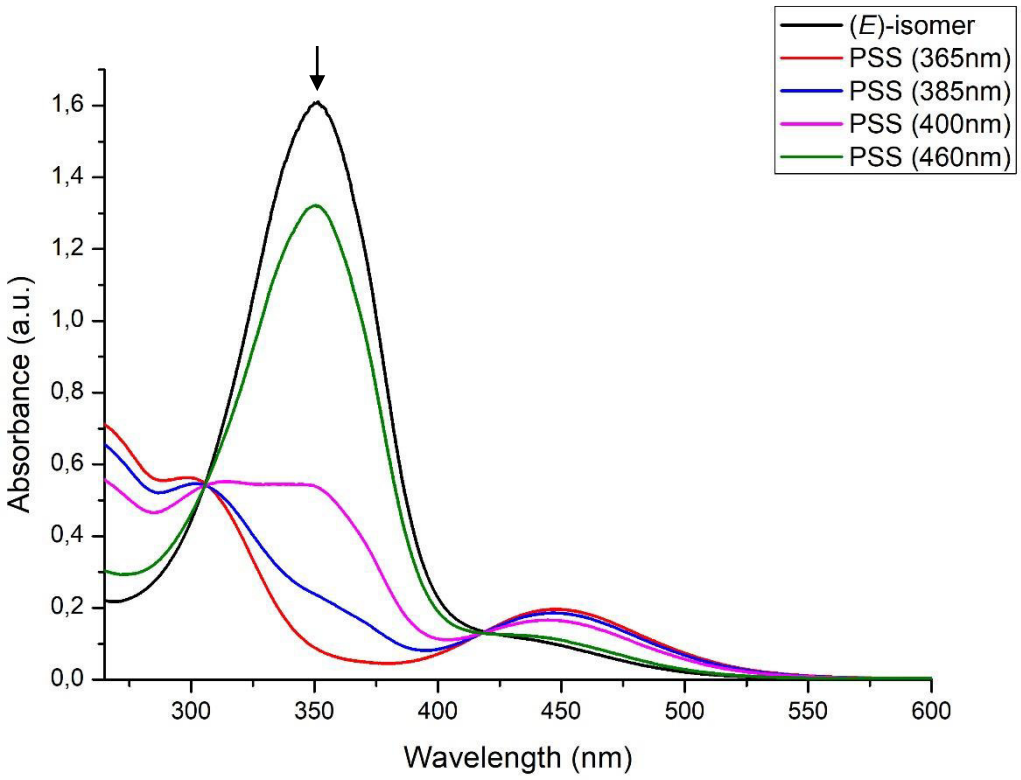

Figure 34: Representative UV-Vis spectra of an arylazopyrazole.

In **Table 3** the λ_{max} values for all synthesized azopyrazoles are summarized. Additionally, the LED wavelength (λ_{switch}) is noted, that produced the highest (*E*) to (*Z*) conversion as determined by the largest difference of spectra.

The parent compound **[3]** exhibits a λ_{max} value of 340 nm. All prepared derivatives have a higher λ_{max}, except fluoro derivative **[28]** which features the same value. Apparently, any substitution leads to a redshift. Most substituents lead to a modest increase of 3 to 17 nm resulting in λ_{max} values in the range of 343 – 357 nm. The strongest effect is observed for amines **[25]** and **[7]** (400 nm and 385 nm) The naphthalene derivative **[60]** with the azo moiety in position 1 has a redshifted λ_{max} of 375 nm which is significantly higher than the 350 nm for the corresponding 2-substituted analog **[63]**. *p*-NO_2 derivative **[6]** too has a substantially redshifted absorbance with a maximum at 375 nm which was only moderately observed for *ortho*-analog **[57]** and basically not the case for *meta*-analog **[54]**. We can only hypothesize that the strong influence of the *p*-NO_2 group might result from the push-pull system, which is weakend for the *ortho*-isomer and not possible for the *meta*-isomer. The best wavelength to switch a specific compound (λ_{switch}) correlates with the λ_{max} value and is 365 nm in most cases but for the most redshifted amine photoswitches.

Table 3: Wavelength of maximal absorbance for the arylazopyrazole (*E*)-isomers and the irradiation wavelength that produced the highest content of (*Z*)-isomer. n.d. (not determined): Due to ultra-fast relaxation, the compound could not be observed in its switched configuration in our setup.

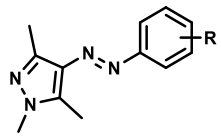

compound	substituent	λ_{max}	λ_{switch}
[3]	H	340 nm	365 nm
[28]	*p*-F	340 nm	365 nm
[39]	*p*-Me	343 nm	365 nm
[42]	*p*-Cl	346 nm	365 nm
[45]	*p*-Br	347 nm	365 nm
[31]	*p*-I	350 nm	365 nm
[48]	*p*-CF_3	346 nm	365 nm
[10]	*p*-OH	352 nm	n.d.
[11]	*p*-OMe	349 nm	365 nm
[14]	*p*-COOH	352 nm	365 nm
[15]	*p*-COOEt	354 nm	365 nm
[22]	*p*-$CONH_2$	351 nm	365 nm
[17]	*p*-CONHBz	351 nm	365 nm
[18]	*p*-CONHPh	355 nm	365 nm
[21]	*p*-CN	356 nm	365 nm
[34]	*p*-CCH	357 nm	365 nm
[36]	*p*-acetyl	357 nm	365 nm
[51]	*p*-Ph	357 nm	365 nm
[63]	2-naphthyl	350 nm	365 nm
[60]	1-naphthyl	375 nm	365 nm
[7]	*p*-NH_2	385 nm	385 nm
[25]	*p*-NEt_2	400 nm	400 nm
[6]	*p*-NO_2	375 nm	n.d.
[54]	*m*-NO_2	344 nm	365 nm
[57]	*o*-NO_2	349 nm	n.d.

With knowledge of the λ_{max} value and the irradiation wavelength that would give the most (*Z*)-isomer (λ_{switch}), we next turned or attention to the half life time. Sample preparation was done as before. The initial absorbance value at λ_{max} was measured (= A_{max}) and the sample was irradiated with λ_{switch} for five seconds. The absorbance at λ_{max} was tracked over time which increased following first order kinetics. If the half life time was sufficiently short (approx. two hours) then the following method was used: The absorbance was plotted over time and an exponential fit function was applied: $A = A_{max} + (A_0 - A_{max}) * e^{-kt}$. A representative example is depicted below (**Figure 35**). The velocity constant *k* was directly obtained from the fit function (*k* = 5.0 * 10^{-4} s^{-1} in this case). The half life time $\tau_{1/2}$ was obtained by applying the following equation: $\tau_{1/2} = \ln(2)/k$ ($\tau_{1/2}$ = 23 min in this case).

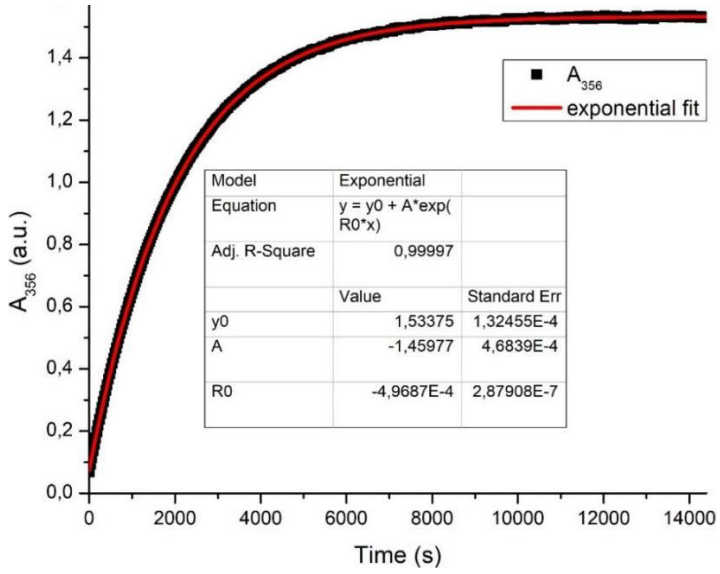

Figure 35: If the compound relaxed completely during the measurement, an exponential fit function delivered the velocity constant *k* directly.

If the half life time was longer and the A_{max} value was not reached over night, a different method was applied. The following formula was applied to linearize the curve: $A_{linearized} = \ln(A_{max} - A_t)$. This value was plotted over time and a linear fit function was applied (see **Figure 36** for a representative example). The slope of the fit function is the velocity constant *k* (1.4 * 10^{-6} s^{-1} in this case). The accuracy of this method depends on the quality of the A_{max} value. It is therefore challenging to spot smaller differences and we put a larger focus on the order of magnitude of these values. For a more accurate determination, ^{1}H-NMR measurements would be feasible.

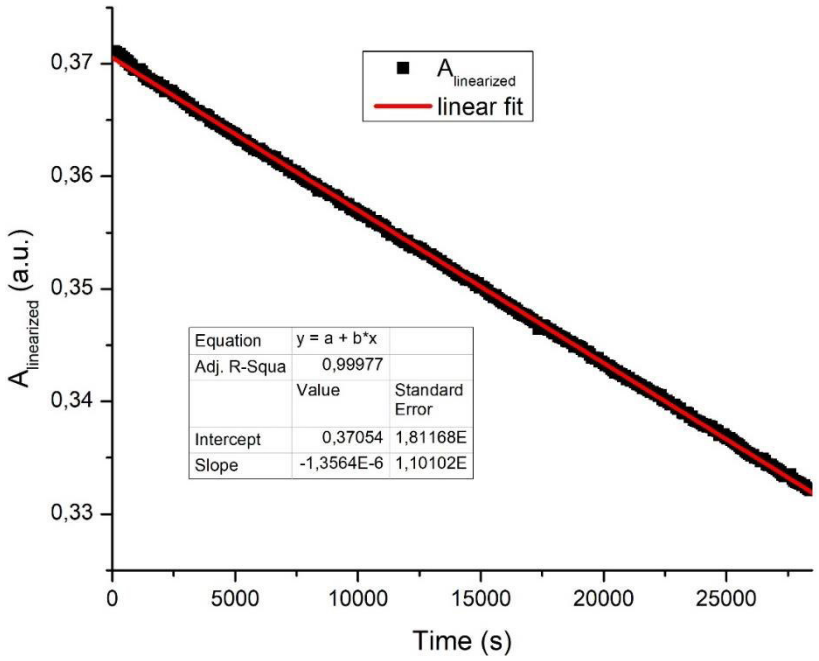

Figure 36: For compounds with a longer half life time, the curve was linearized and the velocity constant *k* was obtained from the slope of a linear fit function.

In **Table 4** all measured half life times are summarized. The obtained values cover a range of 10 days down to sub-hour and three ultra-fast relaxing examples. The ultra-fast relaxation of phenol **[10]** can be attributed to the azo-hydrazone tautomerism which enables facile rotation of the N-N bond.[66, 119, 120] Similarly, the two nitro derivatives **[6]** and **[57]** could enable a rotation due to the push-pull system which is not possible in *meta*-analog **[54]** (see **Figure 37**). The relaxation of the two amines **[25]** and **[7]** was accelerated in the presence of H_2O and in an aqu. system, the relaxation can become ultra-fast (see compound **[115]** in chapter **C II.1.3**). The fact that *para*-substitution always led to an acceleration of the relaxation reaction can be confirmed.[48] As the unsubstituted parent compound has the slowest relaxation rate and both electron-donating and –withdrawing substituents lead to an acceleration, a resonance stabilization of a transition state can be assumed.[49] We sought to investigate, whether the mesomeric effect of the substituents could be correlated with the relaxation rates of azopyrazoles via their Hammett parameter[121] which can be obtained from the literature[122].

Table 4: Measured half life times for the azopyrazoles after irradiation with the respective λ_{switch} at 23 °C in DMSO (50 μM) in the dark.
[§]: The half life times of the two amines were sensitive to H_2O and decreased with increasing H_2O content.
[&]: value for CONHMe. [‡]: value for NMe_2

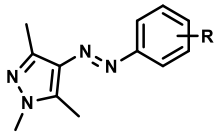

compound	substituent	thermal half life time at 23 °C in DMSO	Hammett parameter σ
[3]	H	10.5 d (k = 7.6 * 10^{-7} s^{-1})	0.00
[28]	*p*-F	10.5 d (k = 7.7 * 10^{-7} s^{-1})	0.06
[39]	*p*-Me	6 d (k = 1.3 * 10^{-6} s^{-1})	-0.17
[42]	*p*-Cl	5.5 d (k = 1.5 * 10^{-6} s^{-1})	0.23
[45]	*p*-Br	5.5 d (k = 1.4 * 10^{-6} s^{-1})	0.23
[31]	*p*-I	6 d (k = 1.4 * 10^{-6} s^{-1})	0.18
[11]	*p*-OMe	3.5 d (k = 2.2 * 10^{-6} s^{-1})	-0.27
[34]	*p*-CCH	3 d (k = 2.7 * 10^{-6} s^{-1})	0.23
[51]	*p*-Ph	2 d (k = 3.5 * 10^{-6} s^{-1})	-0.01
[63]	2-naphthyl	2 d (k = 3.7 * 10^{-6} s^{-1})	
[22]	*p*-$CONH_2$	1 d (k = 9.4 * 10^{-6} s^{-1})	0.36
[17]	*p*-CONHBz	1 d (k = 9.4 * 10^{-6} s^{-1})	0.36[&]
[18]	*p*-CONHPh	10 h (k = 1.9 * 10^{-5} s^{-1})	0.41
[48]	*p*-CF_3	9 h (k = 2.2 * 10^{-5} s^{-1})	0.54
[60]	1-naphthyl	8 h (k = 2.3 * 10^{-5} s^{-1})	
[14]	*p*-COOH	6.5 h (k = 2.9 * 10^{-5} s^{-1})	0.45
[25]	*p*-NEt_2	4.5 h (k = 4.3 * 10^{-5} s^{-1})[§]	-0.83[‡]
[7]	*p*-NH_2	2.5 h (k = 7.2 * 10^{-5} s^{-1})[§]	-0.66
[15]	*p*-COOEt	2 h (k = 9.6 * 10^{-5} s^{-1})	0.45
[36]	*p*-acetyl	55 min (k = 2.1 * 10^{-4} s^{-1})	0.50
[21]	*p*-CN	23 min (k = 5.0 * 10^{-4} s^{-1})	0.66
[6]	*p*-NO_2	< 1 s	
[54]	*m*-NO_2	1.5 d (k = 5.6 * 10^{-6} s^{-1})	
[57]	*o*-NO_2	< 1 s	
[10]	*p*-OH	< 1 s	

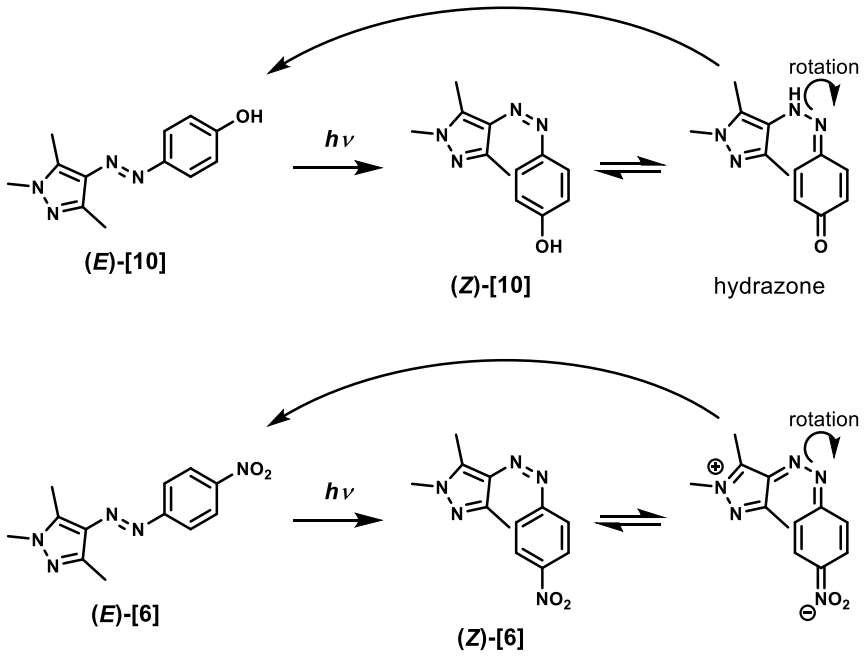

Figure 37: Legitimate relaxation mechanisms for the ultra-fast relaxation of compounds **[10]**, **[6]** and **[57]** involves the rotation of an N-N bond.

log k/k_0 (k_0 = reaction rate of reference compound **[3]**) was plotted against the Hammett parameter σ (Hammett equation) and the result can be seen in **Figure 38**. The V-shaped plot[49] indicates that any mesomeric interaction of *para*-substituents facilitates the relaxation reaction and that the acceleration correlates with the substituent's mesomeric interaction tendency. For phenyl-substituted derivative **[51]** the Hammett parameter of almost zero seems to be a not suitable description for this situation.

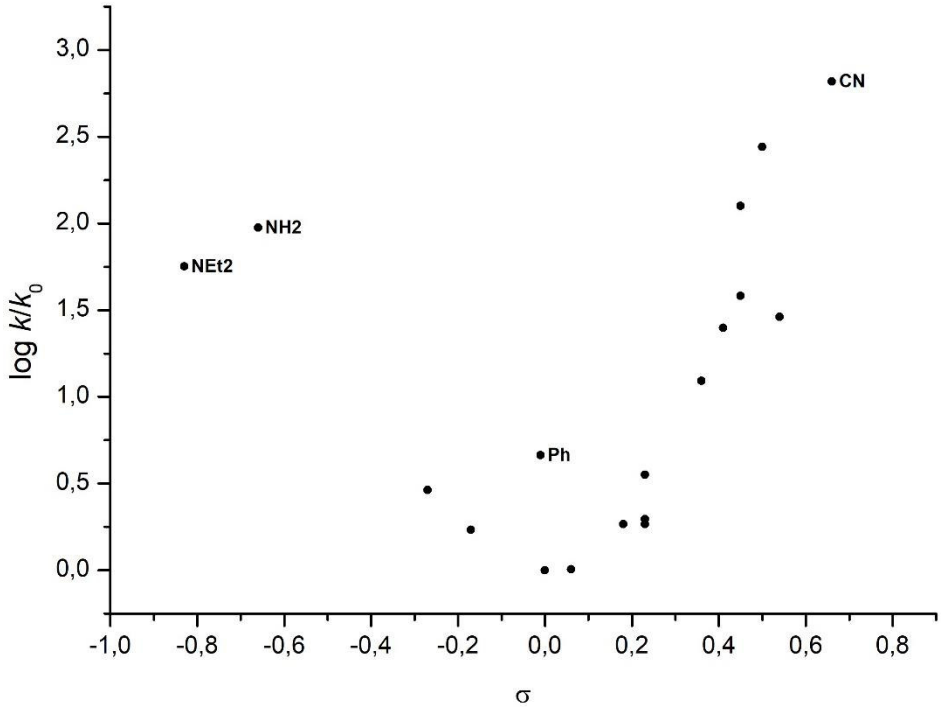

Figure 38: Correlation between log k/k_0 and Hammett parameter σ gives a V-shaped plot.

By comparison of the unsubstituted amide **[22]** with the benzyl substituted amide **[17]** it can be seen that the two similar compounds have the same λ_{max} of 351 nm and the same half life time of approximately one day. This suggested that the properties of future photoswitches can be predicted by comparison with analogous compounds. This was shown to be the case for a subsequent chapter's photoswitchable inhibitor which had the same properties (see compound **[112]**, chapter **C II.1.3**).

C I.1.3 Synthesis of arylazothiophenes

In comparison to azobenzene, unsubstituted arylazopyrazole **[3]** has a 17 nm redshifted absorbance. Arylazothiophenes offer an even larger electron density and, hence, the possibility to further redshift the absorbance. Only a handful of arylazothiophenes are known to the literature[123-129] and their narrow substitution pattern originates from the limited synthetic access. In line with arylazopyrazoles, we planned to synthesize a focused library of arylazothiophenes and to compare them to the current data set. The behavior of an unsubstituted photoswitch was of particular interest as we have seen in the previous chapter that the unsubstituted parent compound determines the limit for both λ_{max} (lowest) and half life time (longest). In addition, two regioisomers of arylazothiophenes are possible, namely arylazo-2-thiophenes and arylazo-3-thiophenes (see **Figure 39**). By comparing the regioisomers we were interested in the influence of the substitution position of the heterocycle. Regioisomers **[60]** and **[63]** from the previous chapter suggested that there might be a profound difference.

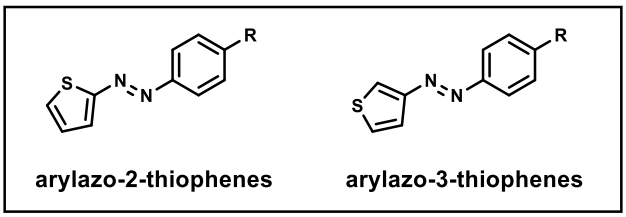

Figure 39: Arylazo-2-thiophenes and arylazo-3-thiophenes were targeted to further investigate the role of the heterocyclic scaffold.

Attempting a classic diazo coupling with thiophene gives aryl-aryl coupling rather than the desired N-aryl coupling.[130] A literature report by Knochel and co-workers encouraged us to target a modular synthesis of arylazo-2-thiophenes.[131] Only one example was reported where thiophene does not bear another substituent which suggests a rather delicate behavior of this compound class. The authors used 2-iodothiophene to form the corresponding Grignard reagent and, via transmetalation, the respective diheteroaryl zinc species was formed which was then coupled with an aryldiazonium tetrafluoroborate to yield the azo product (see **Figure 40**).

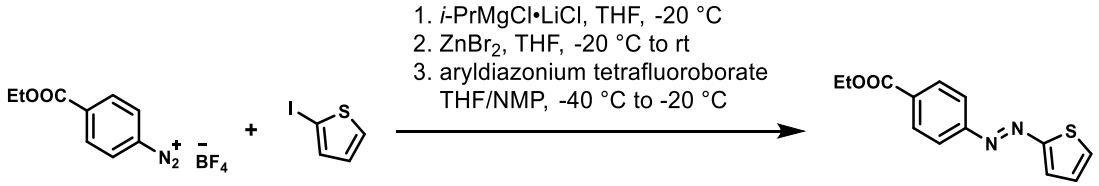

Figure 40: The literature example by Knochel and co-workers provided an opportunity to synthesized thiophene-unsubstituted azoheteroarenes.

To access different arylazo-2-thiophenes, the corresponding benzenediazonium tetrafluoroborates had to be synthesized which represent stable forms of diazonium salts due to the non-coordinative nature of the anion. They can be isolated and dried and, thus, be used under anhydrous reaction conditions like in the present modification of a classical azo coupling reaction.

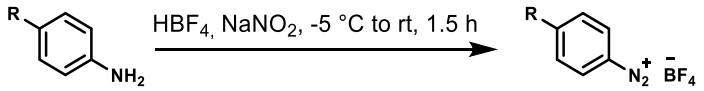

[1] R = H	**[64] R = H**	**84%**
[19] R = CN	**[65] R = CN**	**77%**
[29] R = I	**[66] R = I**	**62%**
[32] R = CCH	**[67] R = CCH**	**85%**
[4] R = NO_2	**[68] R = NO_2**	**72%**
[69] R = COOEt	**[70] R = COOEt**	**99%**
[71] R = OPiv	**[72] R = OPiv**	**72%**
[23] R = NEt_2	**[73] R = NEt_2**	**99%**
[26] R = F	**[74] R = F**	**77%**

The appropriate aniline was dissolved or suspended in HBF_4 (48% in H_2O). The solution or mixture was cooled to -5 °C and aqu. $NaNO_2$ was added while the temperature was maintained at -5 °C. The mixture was stirred for 30 minutes at -5 °C and an additional hour at room temperature. The precipitate was collected by filtration and was washed with cold diethyl ether. If ^{1}H-NMR showed insufficient purity, the crude product was redissolved in acetone and precipitated again by the addition of cold diethyl ether. The product was isolated by filtration, washed with cold Et_2O and dried in vacuo. The stability of the salts was largely different. Unsubstituted **[64]** was freshly prepared regularly while nitro derivative **[68]** is commercially available. The salts were stored in a freezer for prolonged stability.

The subsequent coupling reaction proved to be problematic. In essence, the literature conditions were used but with the difference, that no NMP was added as co-solvent which resulted in poorer solubility of the diazonium salt and might be reason for the moderate performance of this reaction. From trial reactions with NMP, however, we were unable to isolate the products in pure form by flash column chromatography on silica gel due to their very apolar character. Residual NMP led to co-elution.

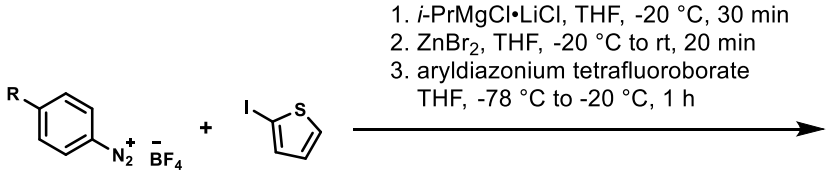

[64] R = H
[65] R = CN
[66] R = I
[67] R = CCH
[68] R = NO_2
[70] R = COOEt
[72] R = OPiv

[75]

[76] R = H 52%
[77] R = CN 40%
[78] R = I 33%
[79] R = CCH 25%
[80] R = NO_2 66%
[82] R = COOEt 40%
[84] R = OPiv 44%

Although the reaction was not high-yielding, most target compounds were successfully synthesized, which is remarkable as most of them are unknown to the literature.

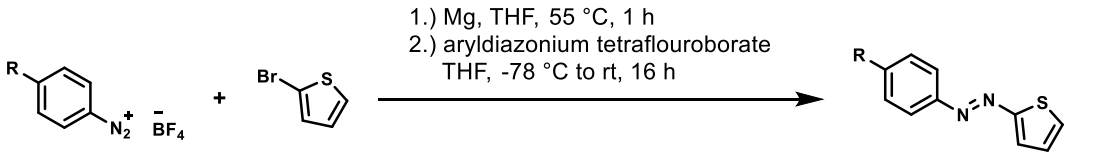

[73] R = NEt_2
[74] R = F

[86]

[87] R = NEt_2 63%
[88] R = F 47%

For the transformation of diazonium tetrafluoroborates **[73]** and **[74]** an alternative procedure[126] was applied as these two substrates performed better when they were directly reacted with the Grignard reagent rather than with the corresponding Zinc species. Selected derivatives were used in follow-up modifications.

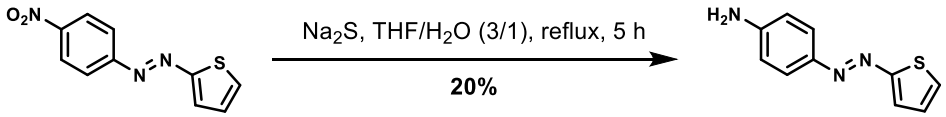

[80] [81]

Nitro compound **[80]** was reduced with Na_2S in a THF/H_2O mixture at reflux temperature. After extractive work-up and purification of the crude material by flash column chromatography on silica gel 20% of the aniline derivative **[81]** (9 mg) were obtained. The low yield can be attributed to the small scale of the reaction.

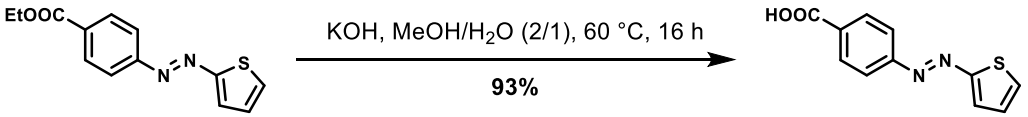

[82] [83]

Hydrolysis of ester **[82]** under basic conditions afforded acid **[83]** which was isolated by extraction and purified by re-dissolving as its carboxylate, washing with Et_2O and precipitation. The product was isolated by filtration in 93% yield.

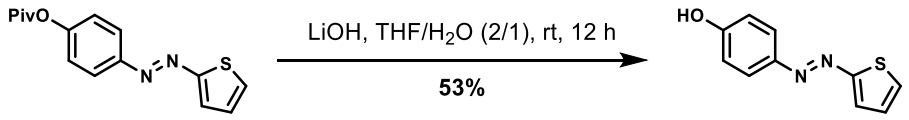

[84] **[85]**

Pivalate **[84]** was hydrolyzed with LiOH in a THF/H_2O mixture. 8 mg of phenol **[85]** (53% yield) were successfully isolated in a small scale experiment.

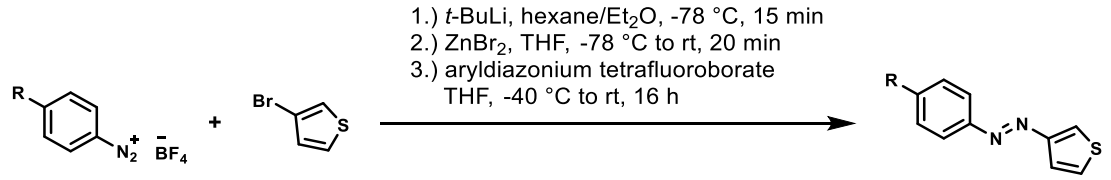

[64] R = H
[68] R = NO_2
[74] R = F

[89]

[90] R = H **24%**
[91] R = NO_2 **36%**
[93] R = F **9%**

Arylazo-3-thiophenes were even more challenging to synthesize. The tendency of the prepared metal species to undergo a metal halogen dance reaction[132] to form the more stable 2-isomer resulted in repeated isolation of the undesired arylazo-2-thiophenes. Our optimization efforts delivered hexane/Et_2O as a suitable solvent mixture that enabled the preparation of the desired metal species which was subsequently reacted with appropriate aryldiazonium tetrafluoroborates to obtain the desired arylazo-3-thiophenes, albeit in poor yields.

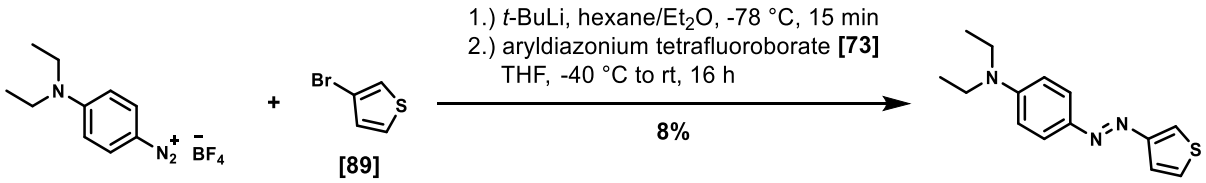

[73]

[89]

[92]

Substrate **[73]** failed to give any product with the previous method but delivered enough material when the lithium species was directly reacted with the diazonium salt to give product **[92]**

In total, 12 arylazo-2-thiophenes were prepared of which nine are unknown to the literature. All four arylazo-3-thiophenes represent novel photoswitches.

C I.1.4 Photophysical characterization of arylazothiophenes

Table 5: Wavelength of maximal absorbance for the arylazothiophene (*E*)-isomers and the irradiation wavelength that produced the highest content of (*Z*)-isomer. n.d. (not determined): Due to ultra-fast relaxation, the compound could not be observed in its switched configuration in our setup.

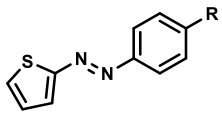

arylazo-2-thiophenes

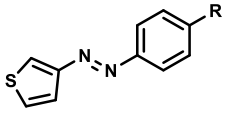

arylazo-3-thiophenes

substituent	compound	λ_{max}	λ_{switch}	compound	λ_{max}	λ_{switch}
H	**[76]**	365 nm	365 nm	**[90]**	331 nm	365 nm
F	**[88]**	365 nm	365 nm	**[93]**	332 nm	365 nm
OPiv	**[84]**	370 nm	365 nm			
COOH	**[83]**	376 nm	365 nm 385 nm			
I	**[78]**	378 nm	365 nm 385 nm			
COOEt	**[82]**	378 nm	365 nm 385 nm			
CN	**[77]**	379 nm	365 nm 385 nm			
CCH	**[79]**	381 nm	385 nm			
NO_2	**[80]**	391 nm	385 nm 400 nm	**[91]**	352 nm	365 nm
OH	**[85]**	393 nm	n.d.			
NH_2	**[81]**	456 nm	400 nm 460 nm			
NEt_2	**[87]**	481 nm	460 nm	**[92]**	439 nm	400 nm

All compounds have been evaluated as before and the results are summarized in **Table 5** (λ_{max} values) and **Table 6** (half life times). The minimal λ_{max} determined by the unsubstituted derivatives **[76]** and **[90]** is 365 nm and 331 nm, respectively, which is in the one case a lot higher than the arylazopyrazole (340 nm) and in the other case not much higher than azobenzene (323 nm). It is remarkable that the position of the azo junction results in a difference of 34 nm. It seems that a C-N bond in the more electrophilic 2-position of thiophene is capable of influencing the important orbitals by its electron-donating properties while the 3-position is not (see **Figure 41**; in analogy to electrophilic substitution principles, electron-donation would be more facile for the arylazo-2-thiophenes as more resonance structures are

possible.). As it has been the case before, any substitution leads to a redshifted absorbance which is most pronounced for the respective amine derivatives. This logically makes higher wavelengths able to switch derivatives of the arylazo-2-thiophene series up to the 400 and 460 nm LED. The influence of the substituents on λ_{max} is similar to the prepared pyrazoles. Notably, phenol **[85]** exhibits a strong redshift too.

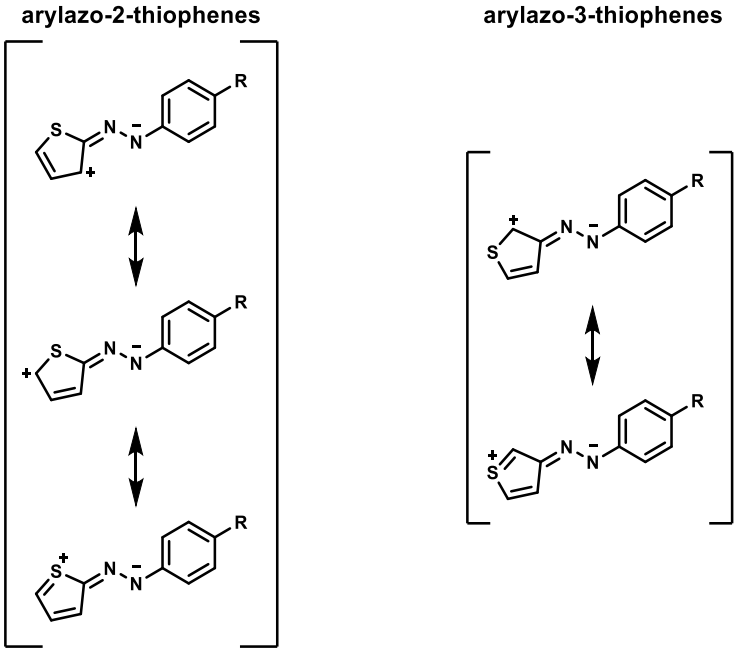

Figure 41: We hypothesize that the arylazo-2-thiophenes have a redshifted absorbance due to a facilitated electron-donation from the 2-position.

The half life time offset for the two thiophene isomers differs by two orders of magnitude. While compound **[76]** has a half life time of three hours, switched compound **[90]** is stable for days. As it has been generally proposed in the literature[35], we observed that the higher the absorbance, the shorter the half life time, possibly due to the dipolar character of the thermal transition state (compare to **Figure 41**). Very recently, Fuchter and co-workers reported on a series of N-heterocyclic azoheteroarenes similarly demonstrating a wide range of half life times for seemingly very similar scaffolds.[69] The two novel unsubstituted thiophenes **[76]** and **[90]** are therefore further examples to corroborate design principles. By choosing the appropriate ring structures and relevant substituents, a whole toolbox of photoswitchable azo compounds can be used to tailor the optochemical properties.

Table 6: Measured half life times for the arylazothiophenes after irradiation with the respective λ_{switch} at 23 °C in DMSO (50 μM) in the dark. [§]: The half life time was sensitive to H_2O and decreased with increasing H_2O content.

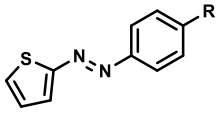

arylazo-2-thiophenes

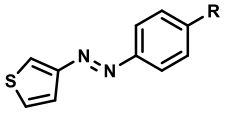

arylazo-3-thiophenes

substituent	compound	thermal half life time at 23 °C in DMSO	compound	thermal half life time at 23 °C in DMSO
H	**[76]**	3.2 h (k = 6.0 * 10^{-5} s^{-1})	**[90]**	11 d (k = 7.1 * 10^{-7} s^{-1})
COOEt	**[82]**	3.1 h (k = 6.1 * 10^{-5} s^{-1})		
CN	**[77]**	3.1 h (k = 6.3 * 10^{-5} s^{-1})		
F	**[88]**	2.6 h (k = 7.3 * 10^{-5} s^{-1})	**[93]**	8 d (k = 1.0 * 10^{-6} s^{-1})
OPiv	**[84]**	1.7 h (k = 1.1 * 10^{-4} s^{-1})		
I	**[78]**	1.5 h (k = 1.3 * 10^{-4} s^{-1})		
COOH	**[83]**	1.2 h (k = 1.6 * 10^{-4} s^{-1})		
NO_2	**[80]**	1.1 h (k = 1.8 * 10^{-4} s^{-1})	**[91]**	2 h (k = 9.1 * 10^{-5} s^{-1})
CCH	**[79]**	0.5 h (k = 3.6 * 10^{-4} s^{-1})		
NH_2	**[81]**	16 sec (k = 4.3 * 10^{-2} s^{-1})[§]		
NEt_2	**[87]**	7 sec (k = 1.0 * 10^{-1} s^{-1})[§]	**[92]**	1 h (k = 2.1 * 10^{-4} s^{-1})[§]
OH	**[85]**	< 1 s		

For the upcoming photopharmacological part, the following guidelines summarize design principles that can be used to predict the photophysical properties of azobenzene based photoswitches.

- The unsubstituted scaffold (e.g. azobenzene, arylazo-2-thiophene, …) features the lowest possible λ_{max} and the highest possible half life time of a compound class. Any modification redshifts the absorbance and destabilizes the (*Z*)-isomer. Generally, predictions can be made by comparison with similar library-compounds.
- The absorbance can be redshifted the most via amine substitution in *para* and *ortho* position.
- For long half life times a stable scaffold should be chosen and the linkage to the photoswitch should feature hardly any mesomeric interaction (e.g. alkyl) and/or the meta position should be addressed.
- For short half life times a fast-relaxing scaffold could be used. Functional groups with strong mesomeric interactions shorten the half life time. Phenol (para and

ortho) and push-pull systems enable ultra-fast relaxation. Amine become ultra-fast too in aqu. systems.

C II Photoswitchable MAT inhibitors

C II.1 Escitalopram based azo photoswitches

C II.1.1 Inhibitor design

In the introduction (chapter **B II**) three different approaches of synthetic pharmacological ligands were explained in detail:

- caged ligands
- photochromic ligands
- photoswitchable tethered ligands

As we value the reversibility of light as a stimulus, caged ligands were of no interest to us for this particular reason. Tethered ligands are inevitably more elaborate in terms of synthetic challenges, protein engineering that might be necessary and the need of structural information. As there was no crystal structure of SERT available in the beginning of the project, we favored a solely synthetic approach and aimed to design photochromic ligands. We were looking for a well-studied, potent inhibitor of SERT which is commercially available and would also allow efficient chemical modifications. Escitalopram (see **Figure 42**) met our requirements and this chapter will discuss our approach based on this SSRI. As azobenzene based photoswitches are used predominantly in successful literature examples, this photoswitchable fragment was the logical starting point for our investigations and this chapter will be limited to azobenzenes and related azo photoswitches.

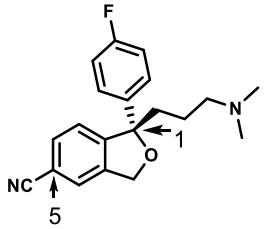

racemate: **citalopram**
S-enantiomer: **escitalopram**

Figure 42: The SSRI escitalopram served as a starting point for the ligand design.

In order to choose a position where to introduce an azo containing modification, we looked at available structure activity relationship (SAR) data[133-137] from the literature. It became apparent that substituents in position 5 were, on the one hand, well tolerated in many cases. Very encouraging examples (see **Figure 43**) were published by Newman and co-workers

who developed fluorescent probes by attaching fluorophores (compounds **[XV]** and **[XVI]**) in that position. A particularly interesting example is compound **[XVII]**. The C-C double could be exchanged with an N-N double bond and the resulting azobenzene analog would be a promising target compound. On the other hand, there are also a number of 5-substituted citalopram and escitalopram analogs where the introduction of the substituent reduced the activity significantly. We hypothesized that the conformational change of a photoswitchable moiety in that position could have a similar effect: different activity of the two different isomers. In addition, this data suggests that the amine and the fluorophenyl fragments are involved in crucial molecular interactions and are not suitable for derivatization. This has also been supported by molecular docking studies[138] which aimed to identify the location of a second, allosteric binding site. Guided by this SAR data, we concluded that a 5-substituted photoswitchable escitalopram analog was a reasonable approach. Furthermore, the nitrile group offers a versatile platform for numerous chemical manipulations in contrast to the other molecular features of escitalopram and the published literature should provide useful synthetic procedures for initial syntheses.

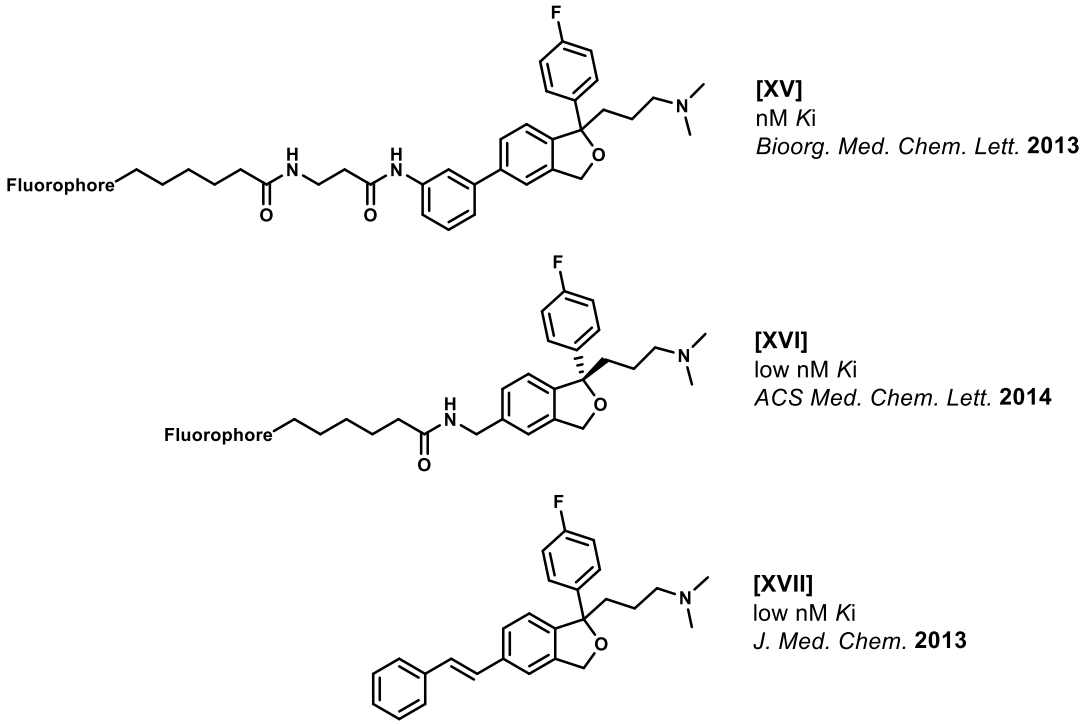

Figure 43: 5-Substituted citalopram and escitalopram analogs from the literature.

In a later phase of the project the crystal structure of hSERT, co-crystallized with escitalopram[9, 10] became available and provided valuable insights. **Figure 44** shows hSERT in an outward-open conformation, locked by the antidepressant. Two molecules escitalopram were located in the crystal structure; one occupying the central binding site (green molecule) and one binding to the allosteric binding site (cyan molecule). The nitrile group of the central escitalopram molecule (blue atom on the left is the nitrogen) is directed towards the open

channel and hence, some space is available for modifications in that position, as hypothesized earlier.

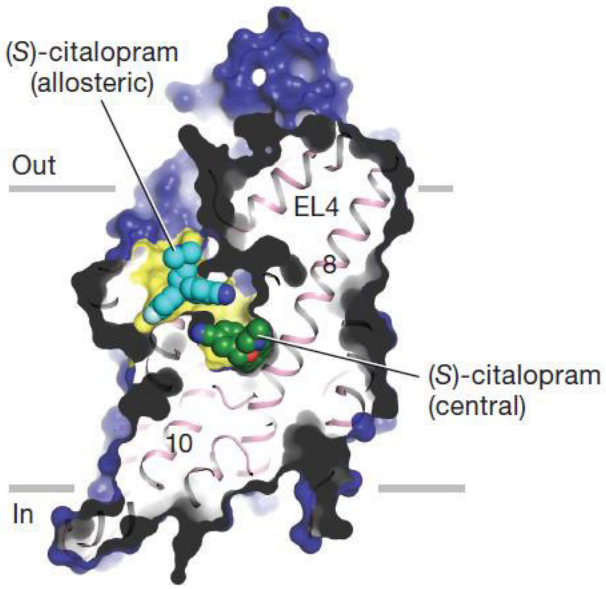

Figure 44[9]: The crystal structure of hSERT, co-crystallized with escitalopram, supported our considerations.

In order to combine the molecular features of escitalopram and azobenzene, we designed two different classes of molecules (see **Figure 45**). In an "elongation approach" we aimed to attach azobenzene fragments onto the escitalopram scaffold via different linkers. The nitrile group can be transformed into a number of different functional groups which can subsequently be used to attach a photoswitchable building block. This approach is potentially quite straight-forward but places the molecular features, that are affected by photo-isomerization, in significant distance to the parent scaffold. Nevertheless, successful literature examples[91] make this approach a legitimate option. In a second approach we aimed to reduce this distance. As azobenzenes consists of two aromatic rings and escitalopram features an accessible phenyl ring, we wanted to incorporate this parent phenyl ring into the new azobenzene motif (see **Figure 43**, compound **[XVII]** for comparison). We termed this approach "incorporation approach". This poses a more elaborate synthetic challenge as the azobenzene has to be synthesized on the parent scaffold by different means (see introduction for comparison).

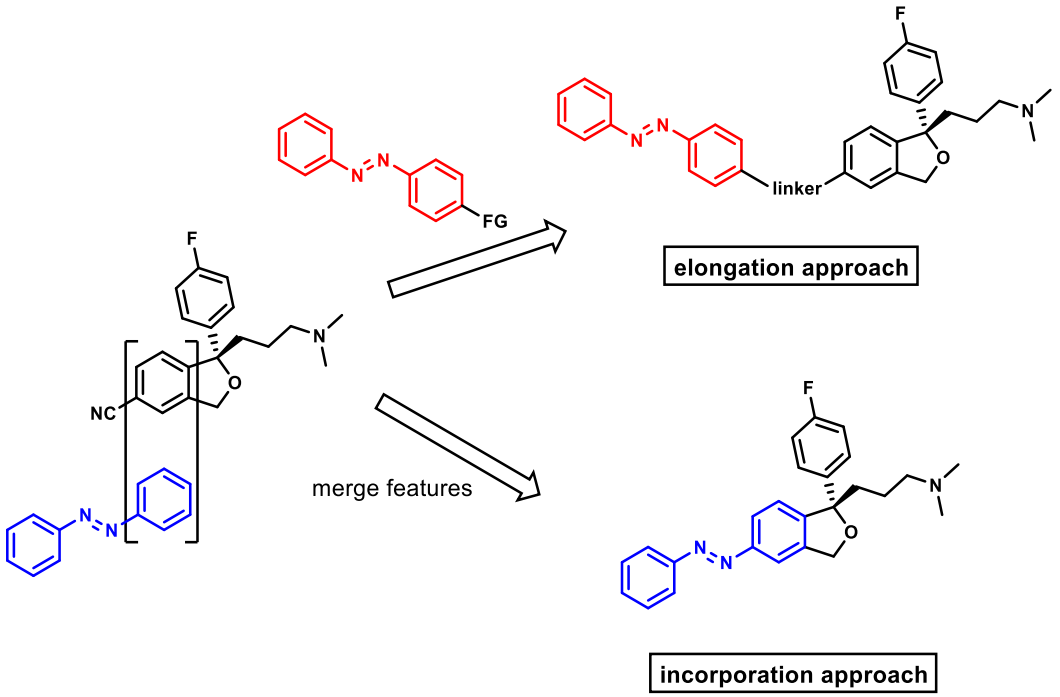

Figure 45: Our ligand design foresaw two different approaches to introduce photoswitchable moieties into the escitalopram parent compound.

C II.1.2 Synthesis

With a rational ligand design in hand we went on to investigate the synthetic feasibility of our approach. As mentioned before, the functionalization of the nitrile group with azobenzene building blocks (elongation approach, see **Figure 45**) is a matter of basic functional group interconversions. More interestingly, the synthesis of compounds of the incorporation approach require an intermediate unknown to the literature. Retrosynthetically, we considered two different cuts (see **Figure 46**). Cut **a** leaves us with an electrophilic N-species and the aryl ring as the nucleophile. This classical azo coupling chemistry is described in more detail in chapter **B III** and requires an aniline version of escitalopram. If we consider cut **b**, we require an electrophilic N-species on the one side and a nucleophilic N-species on the other one. This can be realized with a Mills condensation (see chapter **B III**) of a nitroso compound and an aniline and hence, requires again aniline escitalopram. A third possible cut would be between the azo group and the second phenyl ring but this would require a "naked" escitalopram which would be even more complicated to prepare from commercial material and the regioselectivity of the azo coupling would compromise this proposal. The synthesis of an aniline analog of escitalopram was therefore a centerpiece of our outlined synthetic routes.

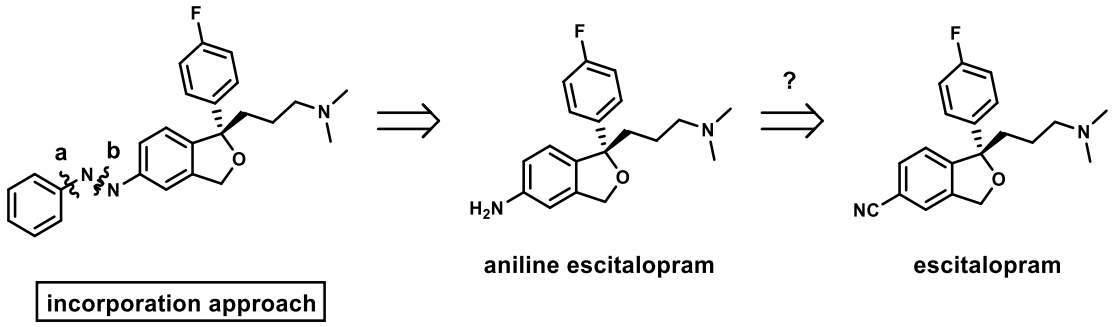

Figure 46: Retrosynthetic considerations.

Escitalopram was purchased from TCI as its oxalate and served as a suitable starting material for our purposes. The oxalate had to be treated with diluted NH_4OH (H_2O/conc. NH_4OH = 10/1) to liberate the free base. Extraction with EtOAc gave the free base as a colorless oil after evaporation of the solvent. In a very first reaction we wanted to reduce the nitrile to the corresponding primary amine, which could be used to attach an azobenzene building block afterwards. For this exact reduction we applied a literature protocol[137].

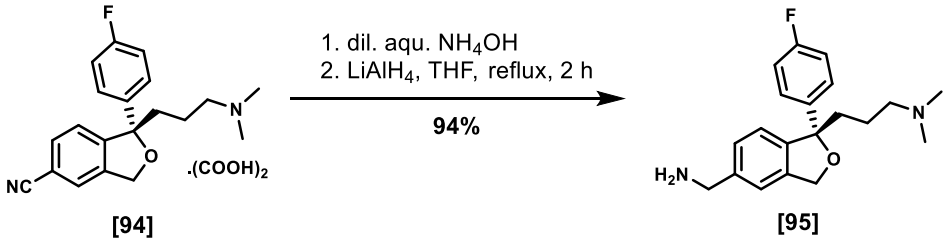

Escitalopram oxalate **[94]** was transferred into the free base which was subsequently reduced with $LiAlH_4$ in dry THF at reflux temperature. As the transformation happened very cleanly (spot-to-spot on TLC), the primary amine **[95]** could be isolated by simple extractive work-up as described in the literature and was obtained in satisfying purity in 94% yield. The reactivity of the primary amine was exploited in the next reaction step to form an amide via well-established amide coupling conditions. Commercial 4-(phenylazo)benzoic acid **[110]** and the previously prepared 4-((1,3,5-trimethyl-1*H*-pyrazol-4-yl)diazenyl)benzoic acid **[14]** (see chapter **C I.1.1**) served as suitable reaction partners. Acid **[110]** and acid **[14]**, respectively, was activated by treatment with EDCI•HCl, HOBt and DIPEA in dry DMF. Afterwards, the primary amine **[95]** was added and the reaction was stirred until TLC indicated full consumption of the amine **[95]**. The crude material was purified by preparative HPLC and the photoswitches **[111]** and **[112]** were obtained in 88% and 66% yield, respectively.

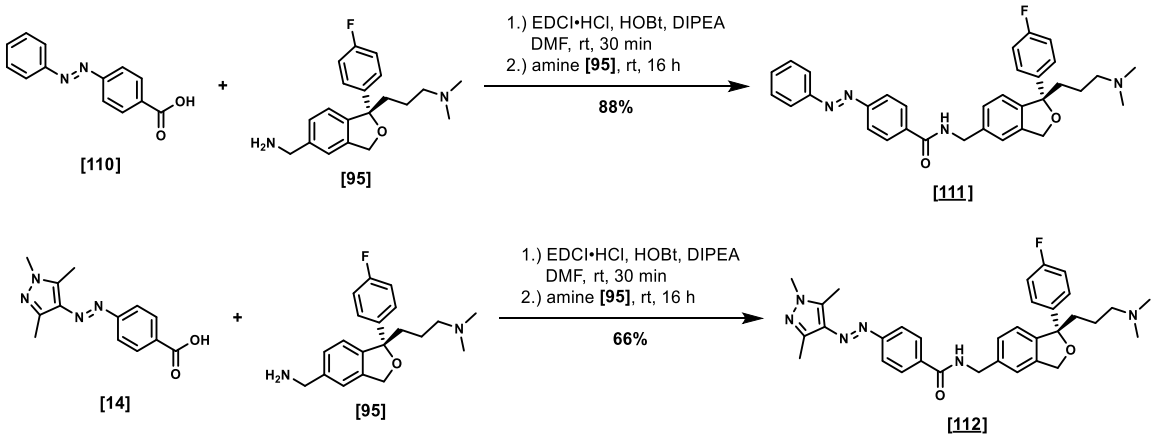

For a different linkage to the azobenzene we applied a different reduction protocol to escitalopram[137] in order to access a different building block. Treatment of the free base with Ni-Al alloy in formic acid at reflux temperature gave clean reduction to the corresponding aldehyde **[96]**. After extractive work-up the product was obtained in 90% yield with satisfying purity.

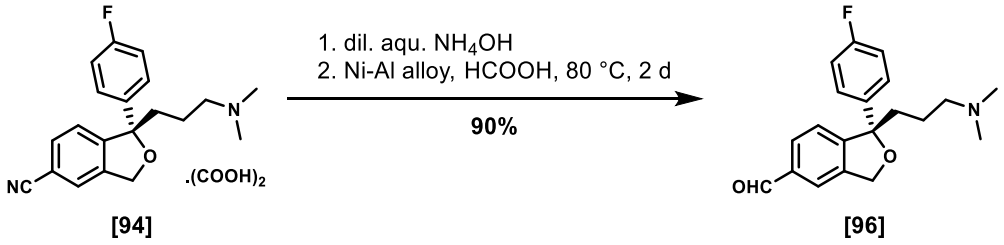

The obtained aldehyde **[96]** was then used to carry out a reductive amination with commercial 4-(phenyldiazenyl)aniline **[114]** following a literature procedure[139] for similar substrates. The two reaction partners were reacted in DCE under acidic conditions (AcOH) and $NaBH(OAc)_3$ was used as the reducing agent. Extractive work-up gave the crude product which was purified by preparative HPLC. Photoswitch **[115]** was obtained in 54% yield.

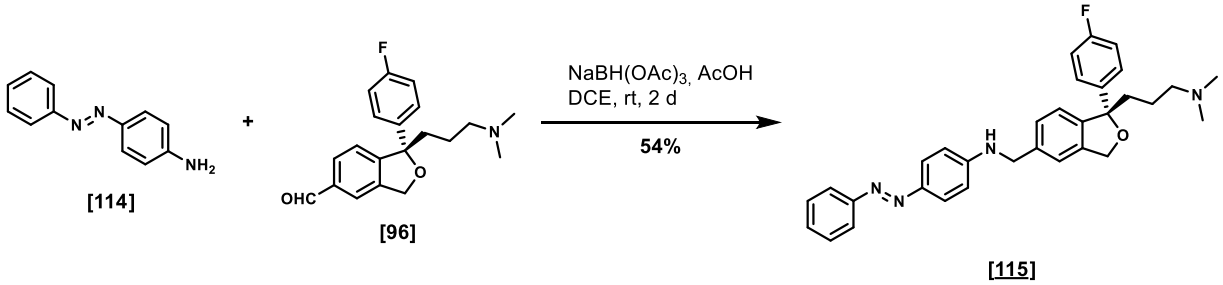

After obtaining the first photoswitchable analogs of escitalopram, we turned our attention to the challenging preparation of the aniline derivative of escitalopram. The aniline could also be used for another amide formation to obtain a shorter version of compound **[111]** by one methylene group. As escitalopram features a C-aryl bond in position 5 where we desired an N-aryl bond in the envisaged aniline escitalopram, a substitution in this position or a degradation of the C-species comes to mind. A degradation of a C-species to introduce an

NH_2 group can be realized via a Curtius rearrangement (hydrolysis of the intermediary isocyanate) of the corresponding carboxylic acid. Fortunately, a carboxylic acid can be accessed directly from the nitrile analog, which enables us to use escitalopram as the starting material (see **Figure 47**).

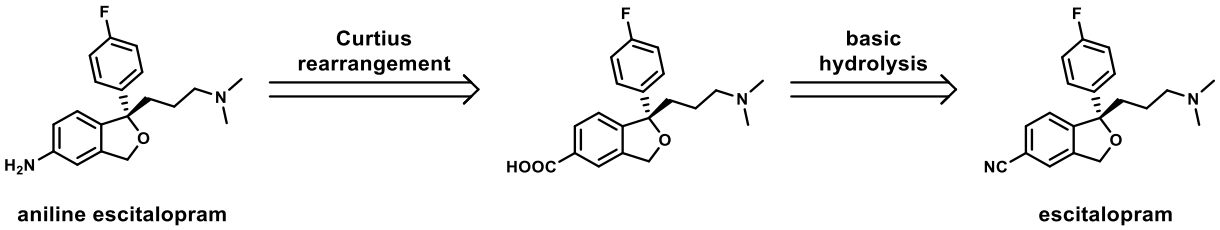

Figure 47: Retrosynthetic analysis of aniline escitalopram.

The corresponding carboxylic acid of escitalopram has so far never been isolated but was used directly to obtain the methyl ester[139]. In an attempt to isolate this compound we stirred escitalopram oxalate **[94]** with NaOH (7 equiv.) in EtOH/H_2O (1/1) at reflux temperature until full consumption of the starting material was observed by TLC (48 hours). The mixture was acidified with 2 N HCl and the product was extracted several times with EtOAc. The efficiency of the extraction was strongly dependent on the pH and complete extraction was tracked via TLC. Product **[97]** was obtained as colorless crystals in quantitative yield after evaporation of the solvent and drying in high vacuum under heating.

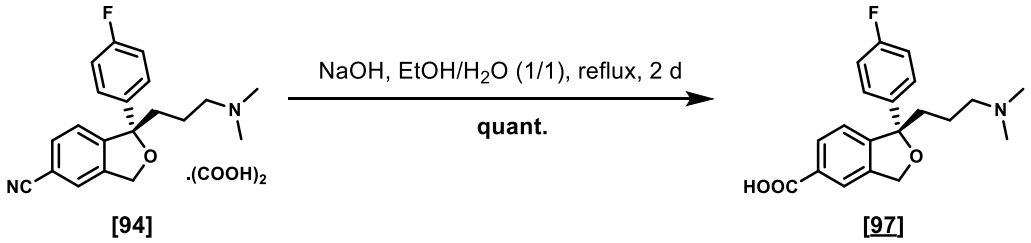

For the subsequent Curtius rearrangement it is necessary to transfer the carboxylic acid **[97]** into its acid chloride, which can be used to obtain the acid azide after substitution. Under loss of nitrogen the thermal Curtius rearrangement gives an isocyanate, which hydrolyses to the corresponding unstable carbamic acid delivering the desired aniline escitalopram upon loss of CO_2. Acid chloride formation was carried out with oxalyl chloride under DMF catalysis[140] in dry DCM. Formation of gas indicated the ongoing transformation. After TLC analysis showed full conversion (MeOH-quenched sample delivers the methyl ester), volatiles were removed in vacuo. The acid chloride was obtained as a colorless foam if purity was satisfying. The acid chloride was dissolved in dioxane and a solution of NaN_3 in dioxane/H_2O (1/1) was added dropwise which immediately gave the formation of a precipitate (NaCl). After complete conversion volatiles were removed in vacuo and the residue was treated with $CHCl_3$. While the product is soluble the by-product NaCl remains undissolved and can be removed by filtration. After evaporation of the solvent the crude acid azide was obtained as a pale yellow

oil in quantitative yield and purity was usually very good according to ^{1}H-NMR. This intermediate was then dissolved in a mixture of DMF and H_2O (2/1) and stirred at reflux temperature where excessive gas formation indicated that the desired reaction occurred. The crude product was obtained after evaporation of the volatiles which was purified by flash column chromatography and the desired product aniline escitalopram **[98]** was obtained in excellent 87% yield.

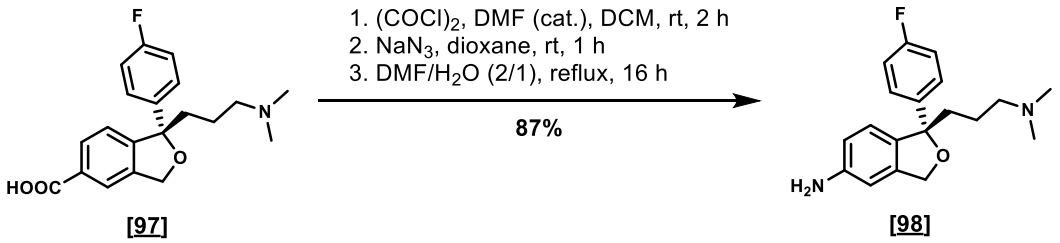

With this valuable building block in hand we first targeted the before mentioned shorter version of compound **[111]**. Applying the amide coupling conditions from above to acid **[110]** and aniline **[98]** afforded amide **[113]** in 62% yield after purification by flash column chromatography.

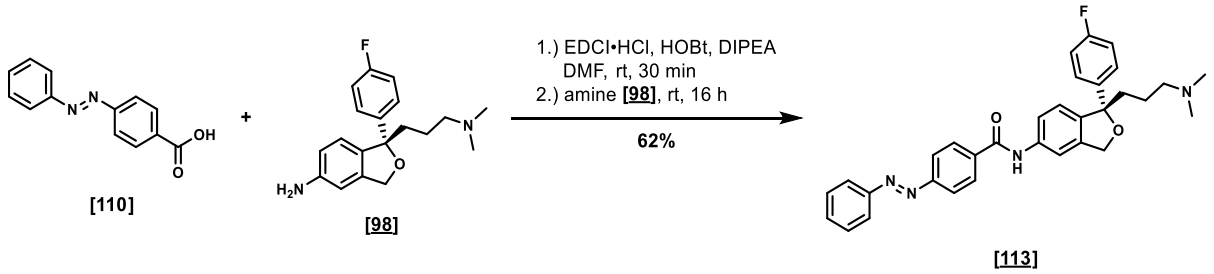

The photoswitches **[111]**, **[112]**, **[115]** and **[113]** conclude the examples of the elongation approach and biological results in combination with photophysical characterization will rate the feasibility of this approach (see chapter **C II.1.3** and **C II.1.4**).

Next, we targeted possible synthetic pathways to access molecules of the incorporation approach. Aniline **[98]** can be a versatile building block if diazotization and condensations conditions can be successfully applied. In a first approach we investigated if conditions used in chapter **C I.1.1** to access arylazopyrazoles are applicable. Due to limited quantities of available starting material, a small scale synthesis had to be conducted and therefore, it was decided to carry out the reaction sequence without isolation of the intermediate. Addition of an aqu. $NaNO_2$ solution to a cold solution of aniline **[98]** in AcOH and conc. HCl led to the formation of the diazonium chloride. This solution was then added to a solution of acetylacetone and NaOAc in EtOH/H_2O (7/4) which resulted in the desired formation of the new C-N bond. The crude intermediate was isolated by extraction and was treated with methylhydrazine in EtOH at reflux temperature. Purification of the crude material by preparative HPLC afforded arylazopyrazole **[116]** in 50% as a first example of compounds

following the incorporation approach. The combination of the arylazopyrazole moiety and the escitalopram scaffold links this two investigations nicely and lessons learned in chapter **C I.1.2** can be directly applied.

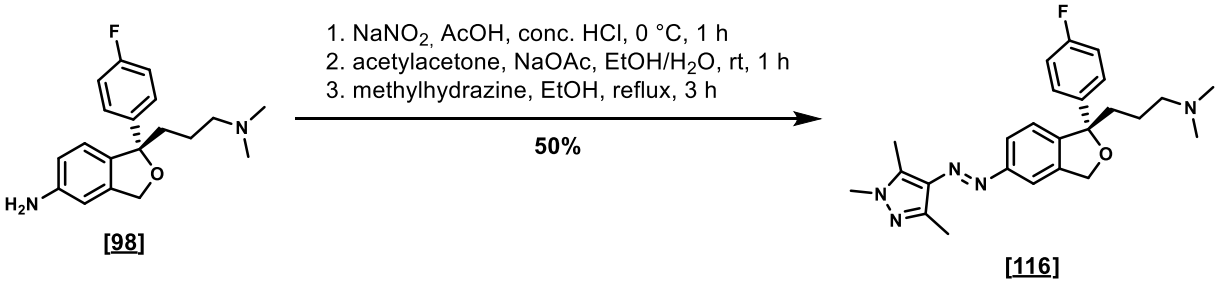

[98] **[116]**

As these diazotization conditions were well tolerated, we went on to prepare a photoswitch by classical azo coupling. 2-Naphthol **[125]** was chosen as a suitable reaction partner and the resulting molecule would feature an extended π-system and in combination with the hydroxy group a pronounced redshift of the absorbance could be expected from studies carried out in chapter **C I.1.2**. Diazotization was conducted similarly and the diazonium solution was added to a solution of 2-naphthol **[125]** in 2 N NaOH, which gave the instant formation of a red precipitate. The crude product was isolated by extraction and purified by flash column chromatography to obtain photoswitch **[126]** in striking 85 % yield.

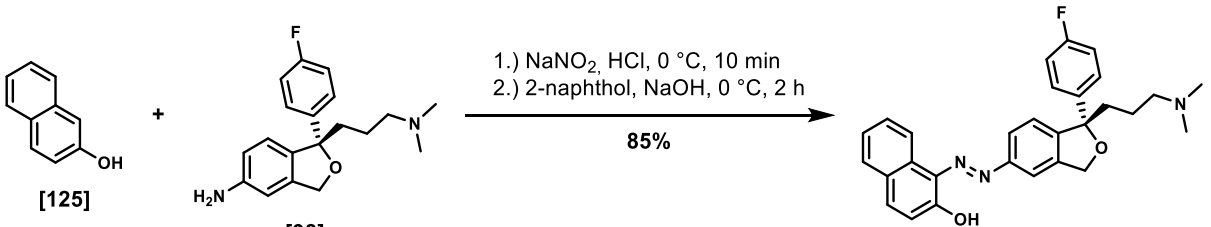

[125] **[98]** **[126]**

In order to expand the accessibility to photoswitches of the incorporation type, we considered the Mills condensation[56] as a potential route to a whole library of compounds (see **Figure 48**). This approach requires nitroso compounds, which potentially react with aniline escitalopram **[98]** in a condensation reaction. While the Mills reaction is a straight-forward reaction to obtain azobenzenes, the stability and accessibility of nitroso compounds is a notable limitation. After examination of available literature we focused on two different oxidative approaches to synthesize the necessary nitroso building blocks from readily available anilines.

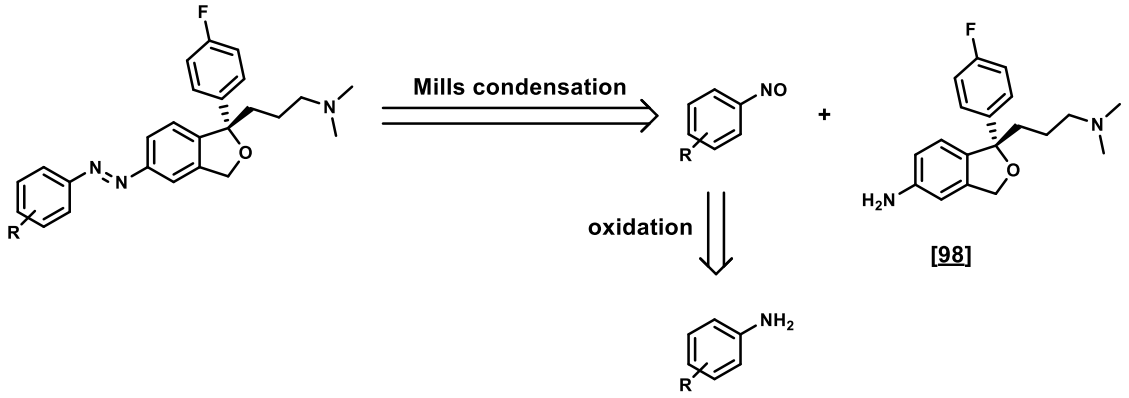

Figure 48: A Mills condensation of aniline **[98]** and nitroso compounds potentially gives access to a small library of escitalopram based photoswitches.

The two chosen procedures featured an oxidation protocol with Oxone®[141, 142] ($KHSO_5$•½$KHSO_4$•½K_2SO_4) and a protocol with H_2O_2, catalyzed by MoO_3 and KOH[143]. According to the literature the oxidation with Oxone® (1 - 2 equiv.) in H_2O at room temperature gives predominantly the nitroso compound accompanied by azoxy and *N*-aryl hydroxylamine intermediates. Furthermore, over-oxidation to the corresponding nitro compounds is often observed. It was reported that a biphasic mixture of H_2O and DCM gives satisfying results in terms of consumption of starting material, reaction time, isolated yields and purity. Preparatively, the aniline starting material was dissolved in DCM. A solution of Oxone® in H_2O was then added under argon and the biphasic mixture was stirred until TLC analysis showed full consumption of the aniline. After an extractive work-up the crude products were purified where necessary and possible by sublimation or recrystallization (see experimental part for details). This procedure was successfully applied to aniline **[1]**, 4-bromoaniline **[43]**, 4-aminobenzoic acid **[12]**, methyl 4-aminobenzoate **[106]** and 3-aminobenzonitrile **[108]** to obtain the corresponding nitroso compounds **[99]**, **[101]**, **[105]**, **[107]** and **[109]** in yields of 50% - 92%.

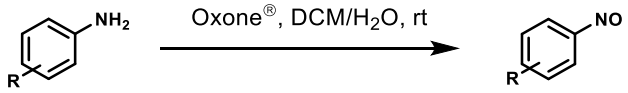

[1] R = H	**[99] R = H,**	**50%**
[43] R = *p*-Br	**[101] R = *p*-Br**	**72%**
[12] R = *p*-COOH	**[105] R = *p*-COOH**	**92%**
[106] R = *p*-COOMe	**[107] R = *p*-COOMe**	**73%**
[108] R = *m*-CN	**[109] R = *m*-CN**	**80%**

In an explorative trial the literature-unknown transformation of naphthalen-2-amine **[157]** and naphthalen-1-amine **[158]** to the corresponding nitroso compounds 2-nitrosonaphthalene **[XVIII]** and 1-nitrosonaphthalene **[XIX]** was attempted. The photoswitches which would result from these building blocks would feature increased steric bulk compared to a single phenyl ring without the addition of a functional group. The π-system

could be extended like in compound **[126]** without reducing the half life time as extensively as in the hydroxy analog.

When the same conditions from above were applied to naphthalen-1-amine **[158]**, a colorless precipitate appeared. The identity of the precipitate remained unclear. During the reaction, gas formation was observed and TLC analysis showed multiple spots while GC-MS analysis showed a mixture of starting material mass, product mass and the mass of the over-oxidized nitro compound. Crude material was isolated via extraction and by sublimation a small amount (3%) of orange-brown crystals was isolated. FTIR analysis of the material indicated the presence of a carbonyl functional group and a ^{13}C-NMR spectrum showed only five carbons, indicating the formation of a symmetric compound. By comparison to a literature spectrum[144] the material was confirmed to be 1,4-naphthoquinone, resulting from oxidation in both positions. Repetition of the experiment with varying amounts of oxidant and different reaction times did not succeed.

In a similar fashion, naphthalen-2-amine **[157]** was used as the starting material but oxidation with Oxone® as before was not successful. Monitoring the reaction with GC-MS indicated formation of the desired nitroso product **[XVIII]** and the corresponding nitro compound but the crude material which was obtained after extraction contained no nitroso product **[XVIII]** according to ^{1}H-NMR. As before, varying the reaction conditions did not lead to the isolation of any nitroso product **[XVIII]**.

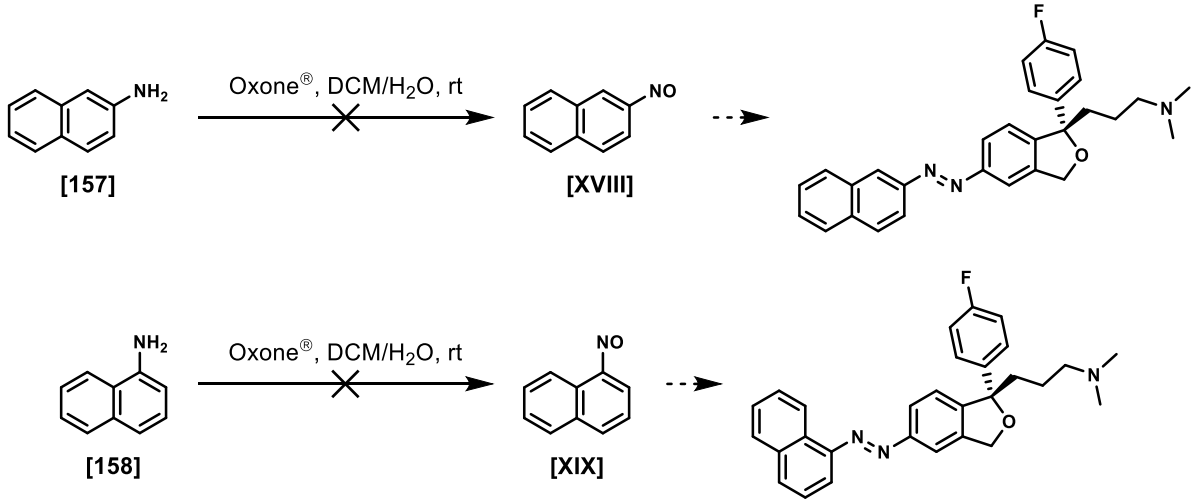

The second oxidation protocol for the preparation of nitroso compounds used in this thesis featured H_2O_2 as the oxidizing agent, catalyzed by MoO_3 and KOH[143]. Other catalytic methods using H_2O_2 for the synthesis of aromatic nitroso compounds have been published and according to the literature the formation of dimeric products like azo or azoxy analogs and over-oxidation to the nitro compounds were often observed as side products or main products.[145-148] A mixture of the respective aniline starting material in MeOH/H_2O was treated with 10 mol% MoO_3, 10 mol% KOH and 4 equiv. 30% H_2O_2. Usually, the nitroso product was

not soluble and could be isolated by filtration once TLC indicated full conversion. 1-Chloro-4-nitrosobenzene **[100]** was synthesized from 4-chloroaniline **[40]** and was obtained in 59% yield after purification by sublimation. 4-Nitrosotoluene **[102]** was obtained in 81% after filtration using *p*-toluidine **[37]**. The oxidation of 4-methoxyaniline **[103]** led to the formation of 1-methoxy-4-nitrosobenzene **[104]** which was soluble in the reaction mixture but could be extracted using *n*-heptane and was isolated in 79% yield after concentration of the organic phase and crystallization from it at -30 °C.

The same procedure was then used to attempt the oxidation of 4-iodoaniline **[29]** which was not covered by the original literature report but the formed precipitate was not the desired nitroso product **[XX]** and remained unidentified. Applying these conditions to 2-nitroaniline **[55]** did not give any consumption of starting material. Similarly, also naphthalen-1-amine **[158]** gave no consumption of starting material. For the reaction of 4-nitroaniline **[4]** no base was used as described in the original publication. The consumption of starting material was very sluggish (as reported) but the formation of nitroso compound **[XXII]** could not be reproduced and instead, only over-oxidation to the corresponding di-nitro compound was observed according to GC-MS. When the synthesis of nitroso compound **[XVIII]** from naphthalen-2-amine **[157]** was attempted, GC-MS and TLC analysis showed the formation of undesired side products like the corresponding azoxy and azo compounds.

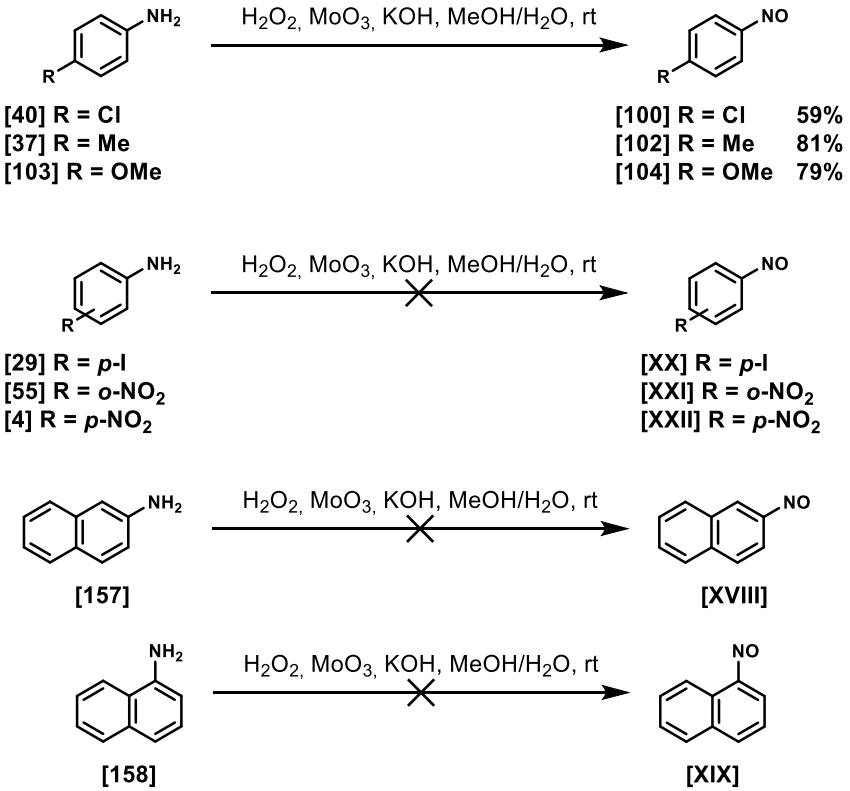

In summary, applying these two oxidation procedures, a number of nitroso compounds were obtained and in cases where the desired oxidation reaction took place, the isolation of

the material was straight-forward. However, some nitroso compounds proved to be troublesome to synthesize or to isolate, respectively. Nevertheless, the rapid access and preparative simplicity of this approach makes this pathway a reasonable strategy. For the azo compounds that were not obtained via this route, an alternative approach could be attempted in follow-up projects. Functional group interconversions at the azo stage, access via an azo coupling strategy or a more elaborate coupling of hydrazines and a subsequent oxidation might be suitable alternatives.

With seven nitroso compounds in hand we went on to investigate the feasibility of the subsequent Mills reaction. Aniline escitalopram **[98]** was dissolved in acetic acid and a solution of the corresponding nitroso compound in AcOH (and DMSO, where necessary, as a homogeneous reaction allowed faster kinetics) was added and the resulting solution was stirred at room temperature until TLC analysis showed full conversion. 2 equiv. of the nitroso compound were used to compensate for over-oxidation to the nitro analog. Typically, the solution turned red over time, indicating the successful formation of the azo dye. On TLC plates the products were visible as characteristic yellow spots. The novel photoswitches were isolated by flash column chromatography in yields up to 95% demonstrating the efficiency for most cases. Surprisingly, when using 1-methoxy-4-nitrosobenzene **[104]**, a demethylation took place. The free phenol **[121]** was suggested as the putative product as HR-MS, NMR characterization and the resulting photophysical behavior actually support the proposed structure. No precedence of the observed demethylation was found in the literature and no Mills condensation using 1-methoxy-4-nitrosobenzene **[104]** has been reported either.

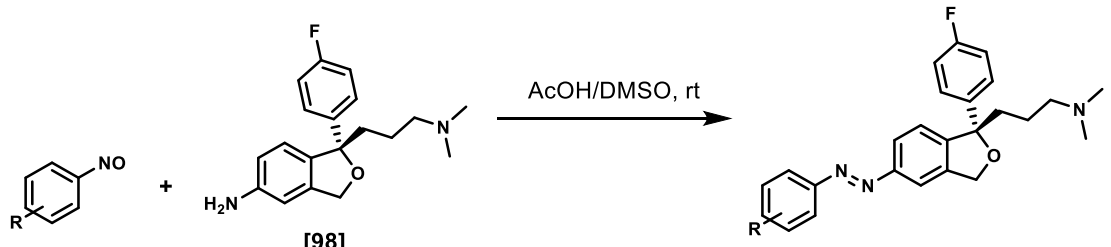

[99] R = H,
[100] R = *p*-Cl
[101] R = *p*-Br
[102] R = *p*-Me
[104] R = *p*-OMe
[105] R = *p*-COOH
[107] R = *p*-COOMe
[109] R = *m*-CN

[117] R = H,	**58%**
[118] R = *p*-Cl	**91%**
[119] R = *p*-Br	**61%**
[120] R = *p*-Me	**81%**
[121] R = *p*-OH	**95%**
[122] R = *p*-COOH	**69%**
[123] R = *p*-COOMe	**79%**
[124] R = *m*-CN	**92%**

After the successful synthesis of this small library, we had 14 photoswitchable escitalopram analogs available: Four elongated versions and ten incorporated ones. A versatile platform for the synthesis of these compounds was established and we expect to benefit from the lessons learned in this chapter. With this set of photoswitches in hand, we moved on to investigate the photophysical behavior which will be covered in the following chapter.

C II.1.3 Photophysical characterization

The photophysical characterization was carried out like in previous chapters (see chapter **C I.1.2**). Based on the lessons learned in the principal investigation, we had a good idea of the resulting switching behavior of the synthesized escitalopram based azobenzenes. In contrast to previous chapters, we had to keep one additional aspect in mind when thinking ahead of the biological evaluation. As the bio assays are performed in an aqu. buffer, the behavior in that aqu. system was arguably more important to investigate. Hence, in addition to measurements in DMSO, we conducted the same measurements in a system mimicking assay conditions (experimental details see chapter **E I.6**). Spectra were recorded right after preparation of the sample (black curve; completely relaxed = (*E*)-isomer) and after irradiation with light of 365 nm (red curve), 385 nm (blue curve), 400 nm (magenta curve) and 460 nm (green curve). In **Figure 49** the absorbance spectra for the photoswitchable inhibitors of the elongation approach are depicted (compounds **[111]**, **[112]**, **[115]** and **[113]**). In **Table 7** the wavelength of maximal absorbance (λ_{max}) for the corresponding (*E*)-isomers are summarized. The two amides **[111]** and **[113]** gave very similar values and are effectively switched (λ_{switch}) with 365 nm while light of higher wavelengths causes the back switch. The amide **[112]** has a 22 nm higher λ_{max} compared to **[111]** which is caused by the electron richer pyrazole. Hence, 365 nm is still the most effective wavelength to cause the switch but 385 nm and 400 nm also cause a fairly significant switch due to the redshifted λ_{max}. In the case of the amine **[115]** the strong electron donating effect of the substituent leads to a significantly higher λ_{max} of 414 nm. The compound is not effectively switched anymore with 365 nm while light of 400 nm gave the most content of (*Z*)-isomer. The λ_{max} values in the buffer system are very similar to DMSO but consistently a little lower. As already pointed out in chapter **C I.1.2** the half life time of amino substituted azo compounds is decreased in the presence of water. In the aqu. buffer the half life time of amine **[115]** is reduced to such a small value (less than one second) that the switched state could not be observed with the used instrument. As the measurements in DMSO are in general transferable to the aqu. system it can be expected, that light of 400 nm would be suitable to switch amine **[115]** in the biological evaluation as well.

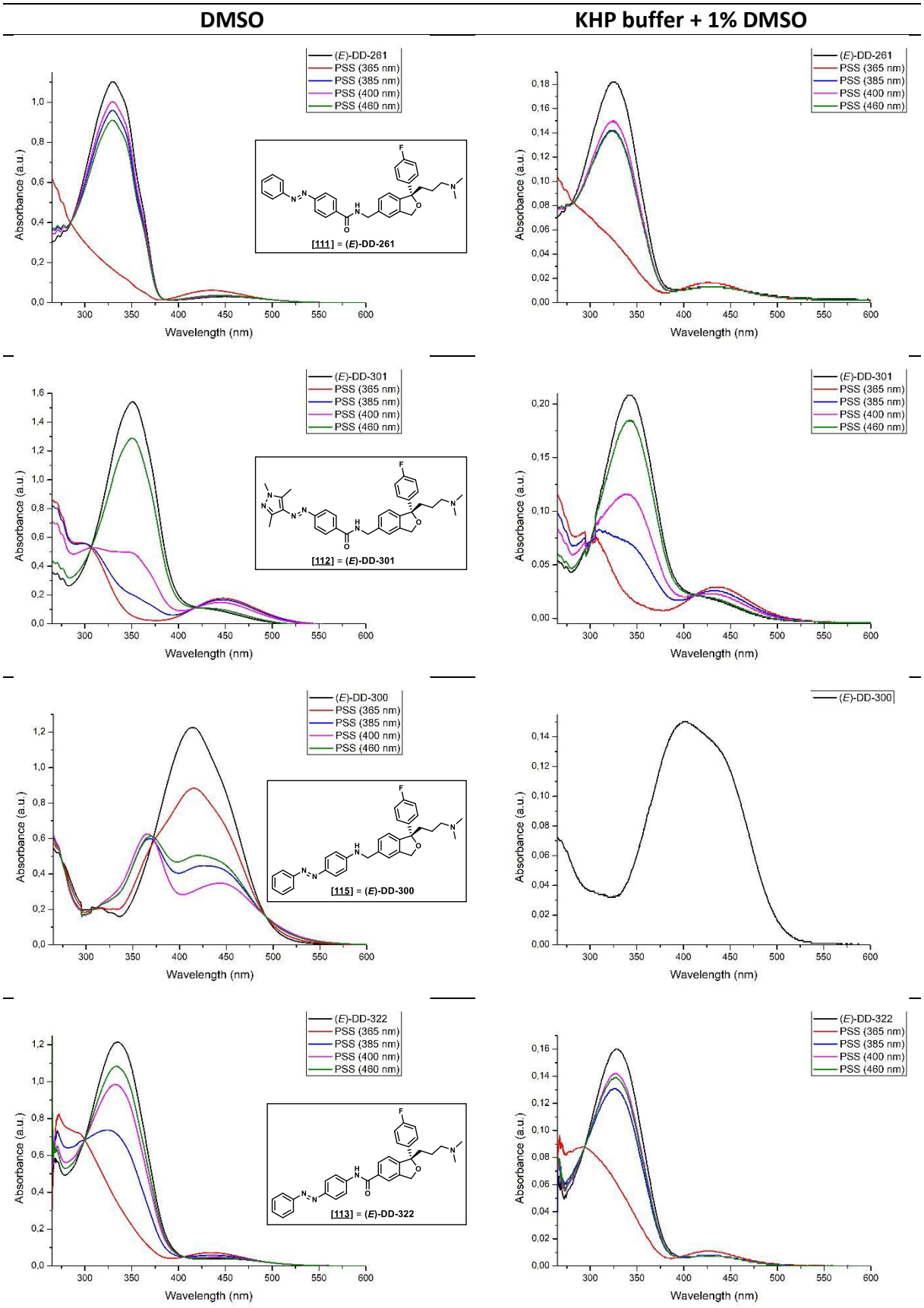

Figure 49: UV-Vis absorbance spectra of photoswitches **[111]**, **[112]**, **[115]** and **[113]** in the dark and after irradiation with 365 nm, 385 nm, 400 nm and 460 nm in DMSO and KHP buffer + 1% DMSO.

Table 7: Wavelength of maximal absorbance for the (*E*)-isomer of compounds **[111]**, **[112]**, **[115]** and **[113]**.

compound	λ_{max} DMSO	λ_{max} KHP buffer + 1% DMSO	λ_{switch}
[111] = DD-261 (amide+)	330 nm	325 nm	365 nm
[112] = DD-301 (prz. amide)	352 nm	342 nm	365 nm
[115] = DD-300 (amine)	414 nm	402 nm	400 nm
[113] = DD-322 (amide)	336 nm	329 nm	365 nm

Figure 50 shows the absorbance spectra for the photoswitchable compounds of the incorporation approach (compounds **[116]**, **[126]**, **[117]**, **[118]**, **[119]**, **[120]**, **[121]**, **[122]**, **[123]** and **[124]**). In **Table 8** λ_{max} values for the corresponding (*E*)-isomers are listed. The two hydroxy analogs **[126]** and **[121]** behave differently and will be discussed at the end of this paragraph. Among all the observed escitalopram analogs, unsubstituted **[117]** has the lowest λ_{max} with 332 nm which was already observed in earlier chapters for completely unsubstituted azo compounds. The escitalopram scaffold leads to a slight increase in λ_{max} compared to azobenzene itself (323 nm in DMSO, data not shown). The pyrazole analog **[116]** has a higher λ_{max} than all the substituted azobenzenes (hydroxy analogs excluded) as it was the case with the photoswitches of the elongation approach (comparison of **[112]** with **[111]**). The value of λ_{max} correlates with the wavelength suitable for the (*E*) to (*Z*) switch. All the substituted azobenzenes (hydroxy analogs excluded) can be effectively switched (λ_{switch}) with 365 nm while light of 385 nm is already a lot less effective. In contrast, the pyrazole analog can be switched considerably with 385 nm and 400 nm although 365 nm remains the most effective wavelength. Again, the λ_{max} in the aqu. system were slightly decreased and, hence, the effectiveness of 365 nm to cause the switch persisted. The phenol **[121]** features a strongly increased λ_{max} of 436 nm which is surprising. On the one hand phenol **[85]** also had a significantly redshifted absorbance in a previous chapter but the azobenzene analog 4-phenylazophenol has a λ_{max} of only 356 nm. The naphthol **[126]** has an even larger π-sytem and exhibits an impressive λ_{max} of 490 nm in KHP buffer (comparable with Sudan I: 490 nm[149]). Due to feasible formation of the hydrazone tautomers[119] (see **Figure 51**), *p*- and *o*-hydroxy substituted azo compounds feature an ultra-short half life time and therefore, the switched state could not be observed with our setup. Hence, we were unable to determine the effectiveness of the available irradiation wavelengths.

In accordance with the conducted principal investigation (see chapter **C I.1.2**) it was demonstrated that azo compounds bearing substituents with moderate electronic effects behave almost as azobenzene itself: The λ_{max} range from 332 nm to 346 nm and the compounds can very effectively be switched with 365 nm and backswitched with 400 – 460

nm. If the substituents are placed in *m*-position, the difference to azobenzene is even smaller. Stronger electronic effects like in aniline and phenol analogs (**[115]**, **[126]** and **[121]**) lead to a strong redshift of the λ_{max}.

Table 8: Wavelength of maximal absorbance for the (*E*)-isomer of compounds **[116]**, **[126]**, **[117]**, **[118]**, **[119]**, **[120]**, **[121]**, **[122]**, **[123]** and **[124]**.

compound	λ_{max} DMSO	λ_{max} KHP buffer + 1% DMSO	λ_{switch}
[116] = DD-293 (pyrazole)	346 nm	341 nm	365 nm
[126] = DD-406 (naphthol)	484 nm	490 nm	n.d.
[117] = DD-321 (H)	332 nm	329 nm	365 nm
[118] = DD-401 (*p*-Cl)	339 nm	336 nm	365 nm
[119] = DD-309 (*p*-Br)	342 nm	339 nm	365 nm
[120] = DD-400 (*p*-Me)	342 nm	338 nm	365 nm
[121] = DD-402 (*p*-OH)	436 nm	444 nm	n.d.
[122] = DD-403 (*p*-COOH)	339 nm	334 nm	365 nm
[123] = DD-404 (*p*-COOMe)	340 nm	333 nm	365 nm
[124] = DD-405 (*m*-CN)	333 nm	328 nm	365 nm

DMSO	KHP buffer + 1% DMSO
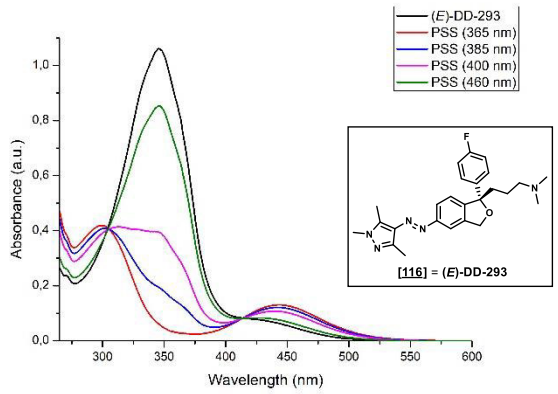	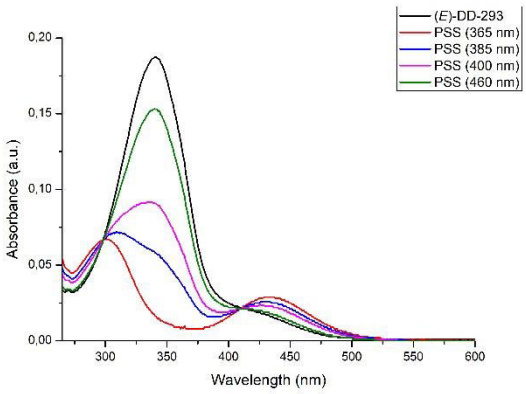
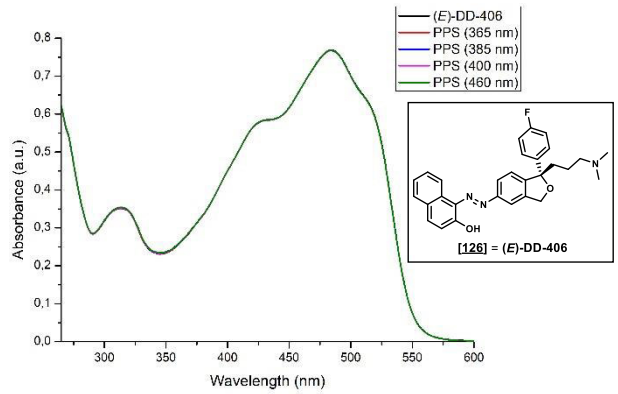	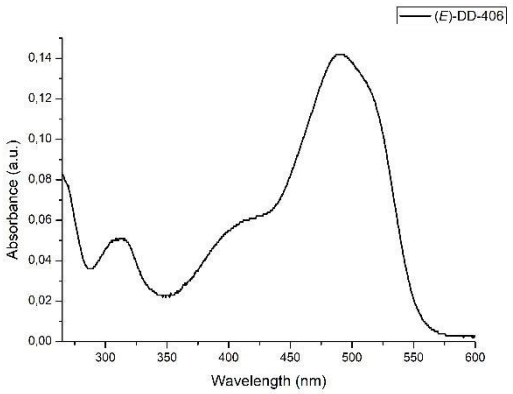
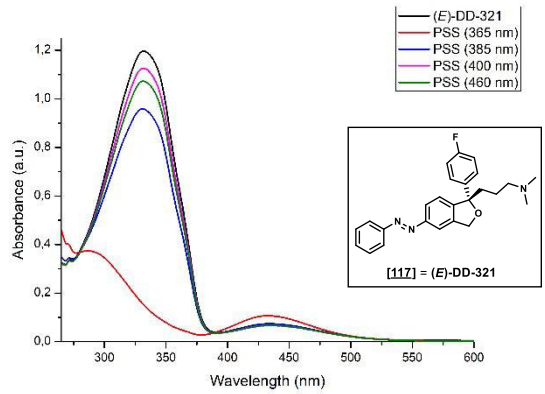	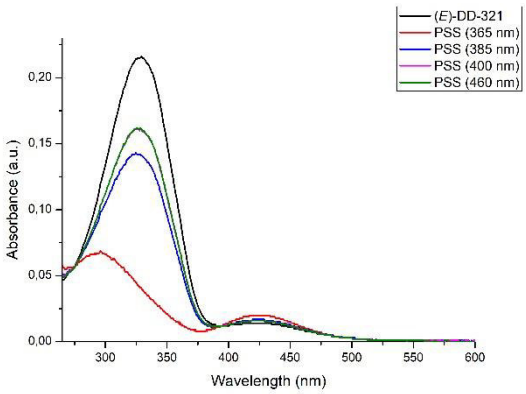
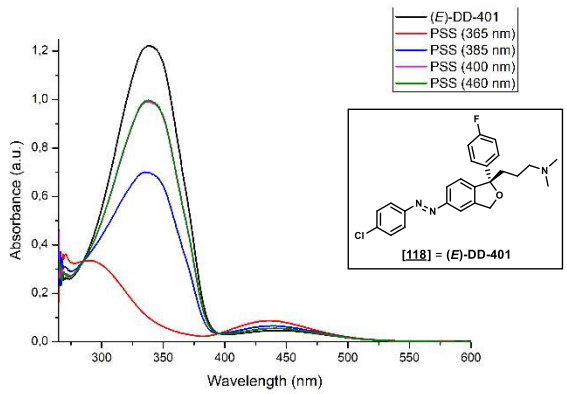	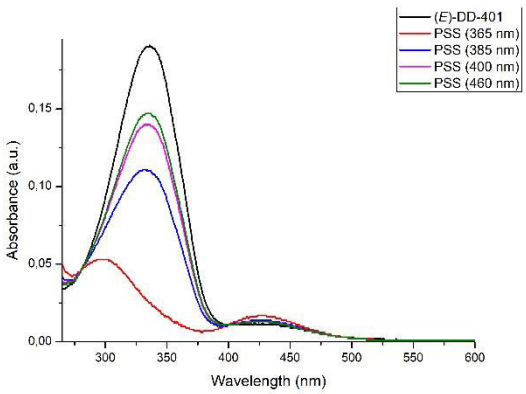

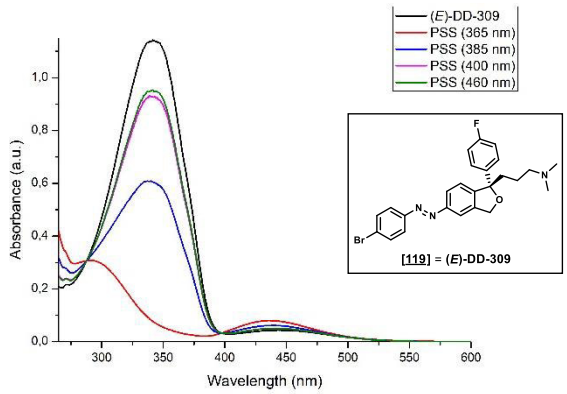
(E)-DD-309
PSS (365 nm)
PSS (385 nm)
PSS (400 nm)
PSS (460 nm)
Absorbance (a.u.)
Wavelength (nm)
[119] = (E)-DD-309

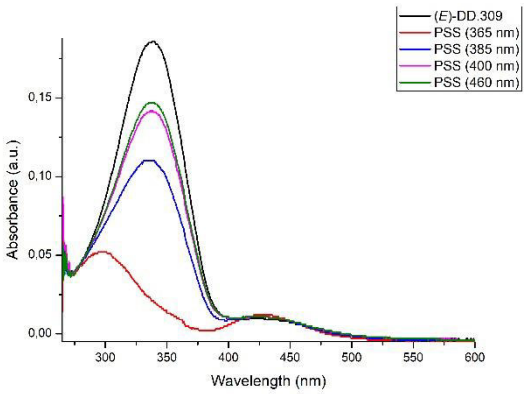
(E)-DD-309
PSS (365 nm)
PSS (385 nm)
PSS (400 nm)
PSS (460 nm)
Absorbance (a.u.)
Wavelength (nm)

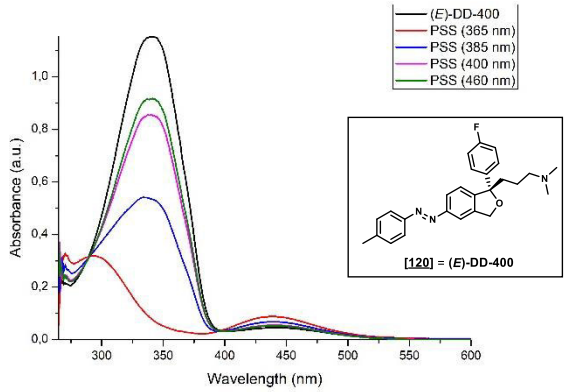
(E)-DD-400
PSS (365 nm)
PSS (385 nm)
PSS (400 nm)
PSS (460 nm)
Absorbance (a.u.)
Wavelength (nm)
[120] = (E)-DD-400

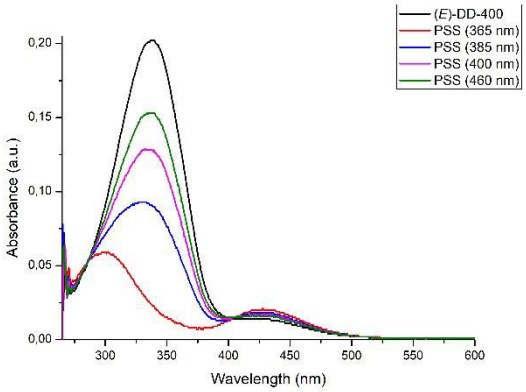
(E)-DD-400
PSS (365 nm)
PSS (385 nm)
PSS (400 nm)
PSS (460 nm)
Absorbance (a.u.)
Wavelength (nm)

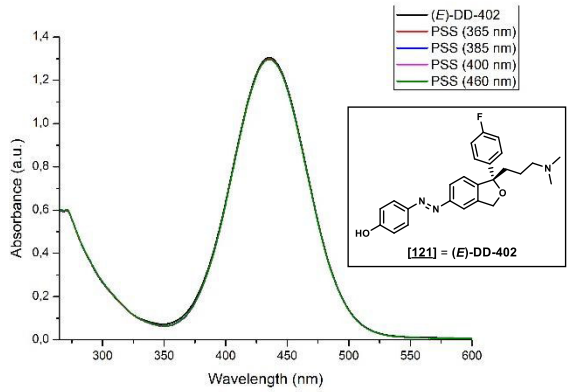
(E)-DD-402
PSS (365 nm)
PSS (385 nm)
PSS (400 nm)
PSS (460 nm)
Absorbance (a.u.)
Wavelength (nm)
[121] = (E)-DD-402

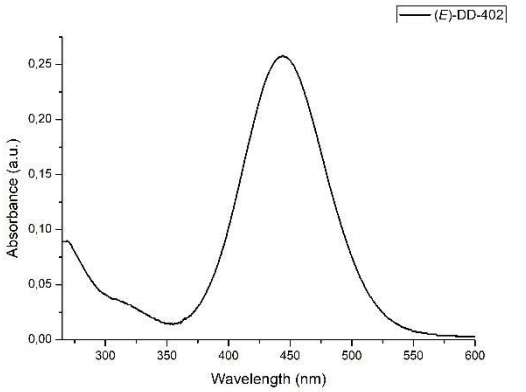
(E)-DD-402
Absorbance (a.u.)
Wavelength (nm)

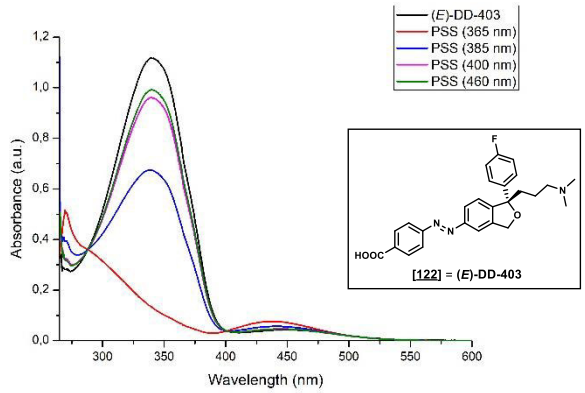
(E)-DD-403
PSS (365 nm)
PSS (385 nm)
PSS (400 nm)
PSS (460 nm)
Absorbance (a.u.)
Wavelength (nm)
[122] = (E)-DD-403

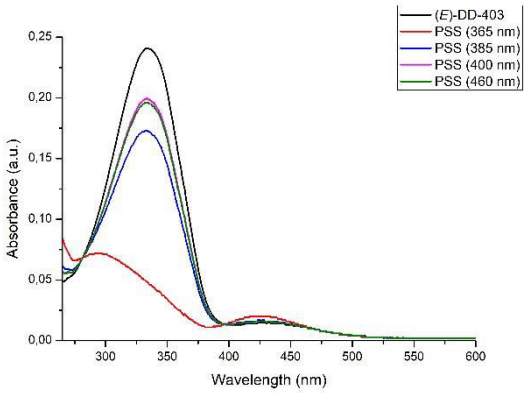
(E)-DD-403
PSS (365 nm)
PSS (385 nm)
PSS (400 nm)
PSS (460 nm)
Absorbance (a.u.)
Wavelength (nm)

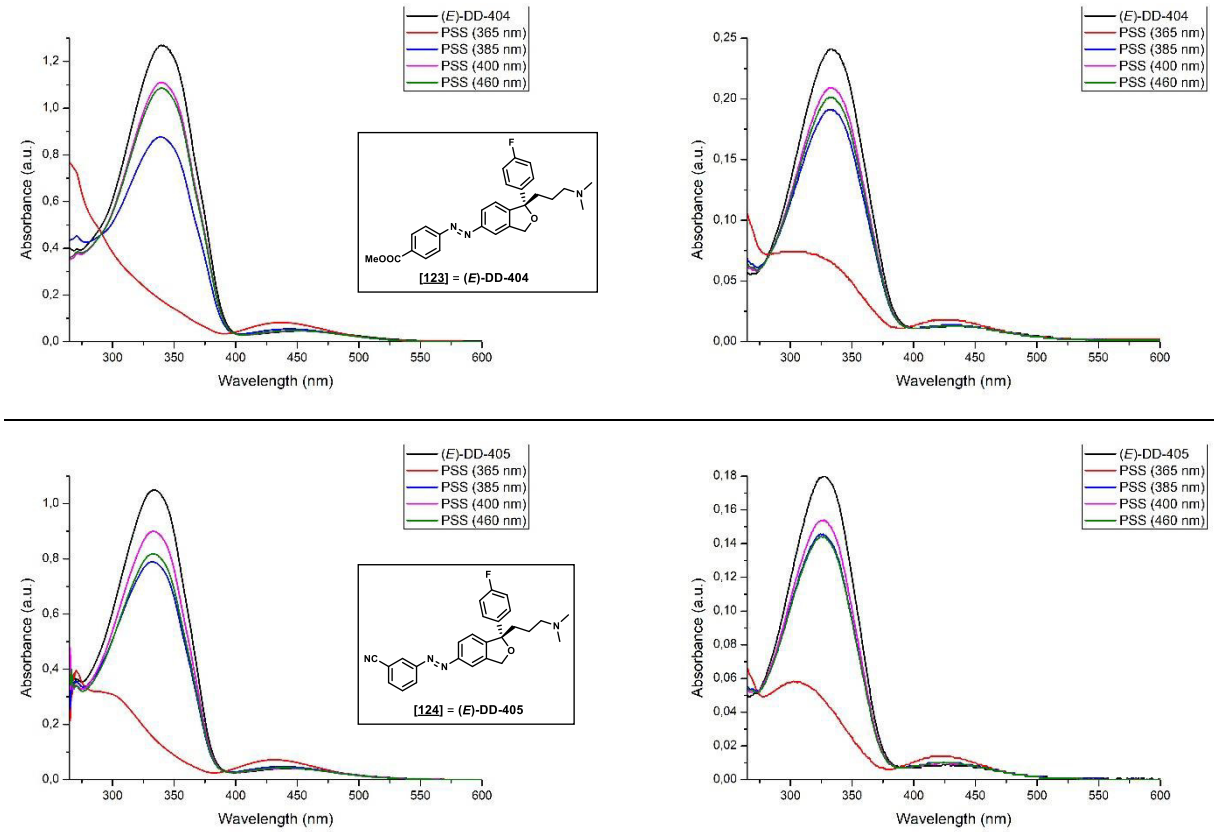

Figure 50: UV-Vis absorbance spectra of photoswitches **[116]**, **[126]**, **[117]**, **[118]**, **[119]**, **[120]**, **[121]**, **[122]**, **[123]** and **[124]** in the dark and after irradiation with 365 nm, 385 nm, 400 nm and 460 nm in DMSO and KHP buffer + 1% DMSO.

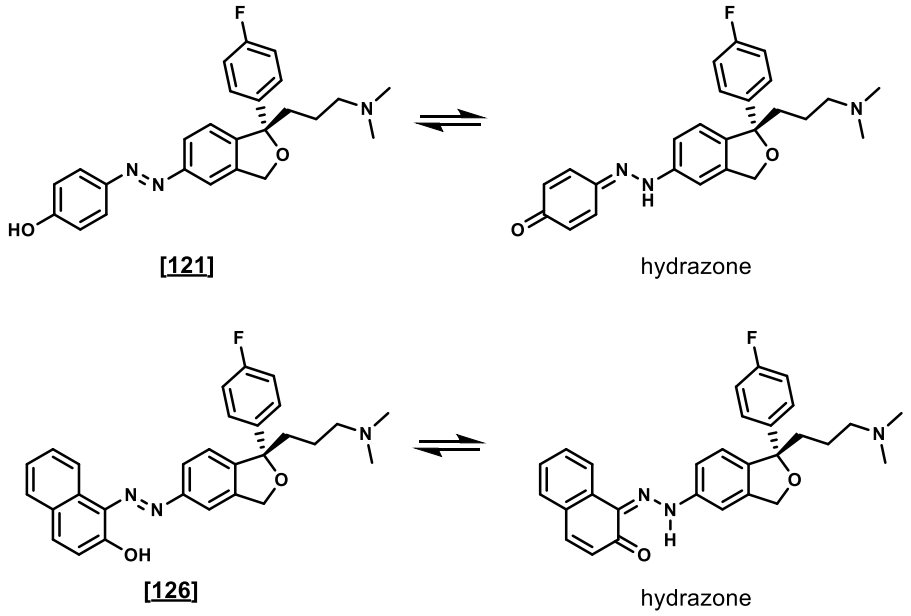

Figure 51: Azo-hydrazone tautomerism of hydroxy bearing photoswitches leads to a strong redshift of the λ_{max} and to ultra-short half life times.

Looking ahead to the biological evaluation, the critical information obtained in that section was that almost all synthesized escitalopram based azo photoswitches can be effectively switched with light of 365 nm. For the aniline derivative **[115]** 400 nm was found

to be the most effective wavelength. With our current setup we were unable to determine the required wavelength to switch hydroxy derivatives **[126]** and **[121]**, but in analogy to aniline **[115]** we expect that higher wavelengths are required.

In addition to this vital piece of information, the thermal half life time ($\tau_{½}$) of the excited state has to be considered as the less stable (*Z*)-isomer will undergo relaxation to the more stable (*E*)-isomer. Hence, we measured the thermal half life time for all the prepared photoswitches in DMSO (50 µM) and in KHP buffer + 1% DMSO (10 µM) after switching the compounds with the suitable wavelength. As before, we expected to apply the guidelines formulated in the principal investigation (see chapter **C I.1.2**). For very long half life times we applied the method explained in chapter **C I.1.2** and hence, have to acknowledge that relative differences are challenging to spot (for reasons outlined in the respective chapter). In general, we only consider the order of magnitude of these values. In **Table 9** the respective values are summarized and grouped by similarities.

The photoswitches bearing substituents with weak electronic effects in *para* position (unsubstituted **[117]**, amides **[111]** and **[113]**, chloride **[118]**, bromide **[119]** and methyl **[120]**) show very similar half life times of multiple days (4 – 7 days) and this value stays in the same order of magnitude in the KHP buffer. Compound **[124]** with a substituent in *meta* position is similarly stable in the (*Z*)-form despite that the nitrile is a strong electron withdrawing group but cannot interact with the π-system from the *meta* position. The somewhat better interacting acid **[122]** and methyl ester **[123]** gave half life times of 2 – 3 days in DMSO which interestingly increased to larger values in KHP buffer. This is in stark contrast to aniline **[115]** which showed the opposite trend. The unsubstituted arylazopyrazole **[116]** has a comparable half life time of 7 days which heavily decreased to 4 hours in the aqu. system while the amide substituted pyrazole **[112]** had a half life time of only 1 day which also decreased strongly to half an hour in the KHP buffer. A possible explanation for this phenomenon could be that the hydrogen bond acceptor ability of the pyrazole destabilizes the (*Z*)-isomer in the aqu. buffer which would mean the potential hydrogen bond facilitates the relaxation reaction. The difference between the unsubstituted (7 days) and the amide substituted arylazopyrazole (1 day) was already observed in chapter **C I.1.2** and, interestingly, does not appear in the case of the phenyl analogs (**[117]**: 6 days, in comparison to amides **[111]** and **[113]**: 7 days). As we already hypothesized in the former chapter, the amide in combination with the electron rich pyrazole might act as a weak push-pull system in contrast to the amide phenyl combination and thereby weaken the N-N double bond in the excited state which makes compound **[112]** more prone to relaxation. The aniline **[115]** with its strong +M effect on the aryl system had a half life time of just 3.5 hours in DMSO which decreased to a not measurable (too fast) value in buffer. Similarly, the two hydroxy derivatives **[126]** and **[121]** are also relaxing ultra-fast due

to the feasible formation of the hydrazone form (see **Figure 51**) of the (*Z*)-isomer where the N-N single bond can rotate freely.

Table 9: Measured half life times $\tau_{½}$ and associated reaction rate constant of escitalopram based azo analogs in DMSO and aqu. buffer + 1% DMSO.

compound	DMSO	KHP buffer + 1% DMSO
[117] = DD-321 (H)	6 d (k = 1.3 * 10^{-6} s^{-1})	10 d (k = 7.7 * 10^{-7} s^{-1})
[111] = DD-261 (amide+)	7 d (k = 1.1 * 10^{-6} s^{-1})	5 d (k = 1.7 * 10^{-6} s^{-1})
[113] = DD-322 (amide)	7 d (k = 1.2 * 10^{-6} s^{-1})	6 d (k = 1.4 * 10^{-6} s^{-1})
[118] = DD-401 (*p*-Cl)	4.2 d (k = 1.9 * 10^{-6} s^{-1})	9 d (k = 9.1 * 10^{-7} s^{-1})
[119] = DD-309 (*p*-Br)	4.5 d (k = 1.8 * 10^{-6} s^{-1})	8 d (k = 1.0 * 10^{-6} s^{-1})
[120] = DD-400 (*p*-Me)	5 d (k = 1.5 * 10^{-6} s^{-1})	10 d (k = 8.0 * 10^{-7} s^{-1})
[124] = DD-405 (*m*-CN)	11 d (k = 7.3 * 10^{-7} s^{-1})	12 d (k = 6.6 * 10^{-7} s^{-1})
[122] = DD-403 (*p*-COOH)	2.6 d (k = 3.1 * 10^{-6} s^{-1})	9 d (k = 8.8 * 10^{-7} s^{-1})
[123] = DD-404 (*p*-COOMe)	2.2 d (k = 3.7 * 10^{-6} s^{-1})	5.5 d (k = 1.5 * 10^{-6} s^{-1})
[116] = DD-293 (pyrazole)	7 d (k = 1.2 * 10^{-6} s^{-1})	4 h (k = 4.6 * 10^{-5} s^{-1})
[112] = DD-301 (prz. amide)	1.0 d (k = 8.2 * 10^{-6} s^{-1})	0.5 h (k = 3.5 * 10^{-4} s^{-1})
[115] = DD-300 (amine)	3.5 h (k = 4.8 * 10^{-5} s^{-1})	< 1 s
[126] = DD-406 (naphthol)	< 1 s	< 1 s
[121] = DD-402 (*p*-OH)	< 1 s	< 1 s

To assess the significance of the measured values for slowly relaxing compounds, we decided to perform a determination of the half life time via NMR. Compound **[117]** was dissolved in DMSO-d_6 and was irradiated with light of 365 nm. It was crucial to directly irradiate the solution and stir it too (see **Figure 52**). After irradiation the solution was transferred into an amberized NMR tube which ensured protection from light. With the used 365 nm UV LED head and the controller unit LX400 from OmniCure® 5 minutes of irradiation were sufficient to switch 85% of a 10 mM solution (≈ 4 mg/mL) of the compound. In periodic intervals a ^{1}H-NMR spectrum was recorded and the integrals of the protons in position 3 for the (*Z*)- and the (*E*)-isomer were used to determine the content of (*Z*)-isomer. This content was plotted against the time (see **Figure 52**) and a half life time of 4 days and 19 hours was determined. This is comparable to the value of 6 days obtained with the UV-Vis method. This result shows that the two different methods give similar values and allow for a cross-validation of results by independent methods. However, the experimental conditions in these two methods vary to some extend. It has to be kept in mind that the difference in concentration (50 μM vs. 10 mM) could potentially cause a difference in half life time but this was not

investigated within this thesis. As the UV-Vis method is operatively simpler and immensely less time consuming, it was the method of choice for our requirements.

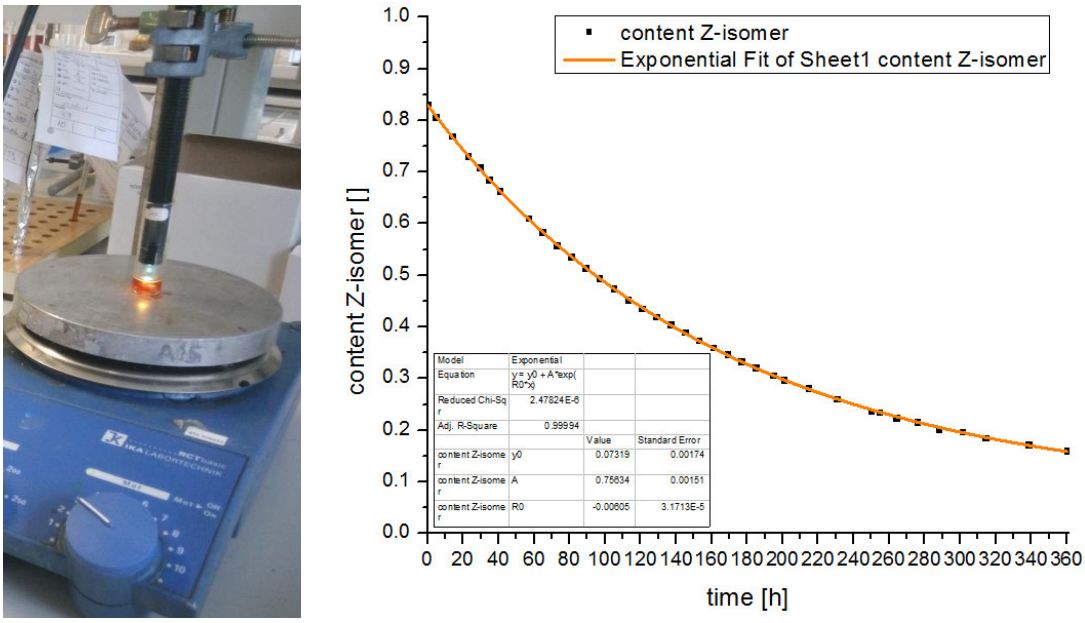

Figure 52: Left: Switching of a 10 mM solution of photoswitch **[117]** in DMSO-d_6 for NMR measurements. Right: The content of (*Z*)-isomer decreases over time because of thermal relaxation and can be used to determine the thermal half life time.

Having determined suitable wavelengths for switching the escitalopram based azo analogs and their respective thermal half life time, we can assume that in the following biological evaluation, compounds can be successfully switched and many of them would exhibit a considerably stable excited state in the aqu. system. Compounds with ultra-fast relaxation however, can not be applied in a switched state as they completely relax back to the natural (*E*)-form once irradiation is halted and with our means we are also not able to tell, to which content these azo benzenes can be switched while irradiated with certain light sources. It will be discussed at appropriate sections how this challenge was tackled.

As it has been mentioned before, the strongly redshifted λ_{max} value of phenol **[121]** (436 nm) is surprisingly high in comparison to the related 4-phenylazophenol with 356 nm. However, a re-evaluation of the structure was not considered within this project as the resulting biological activity (see chapter **C II.1.4**) did not justify the effort. If the compound would be revisited in future projects, mechanistic considerations should help to elucidate the structure. As the experimental data show that a demethylation has happened at some point, the nitroso compound upon tautomerism might behave differently and undergo an alternative pathway.

C II.1.4 Biological evaluation

As outlined in chapter **C II.1.1**, the 14 in chapter **C II.1.2** synthesized photoswitchable inhibitors were designed to inhibit the human serotonin transporter. In the previous chapter **C II.1.3** we have shown that:

- 11 of these novel inhibitors are very effectively switched with 365 nm in KHP buffer and feature long half life times from half an hour to multiple days.
- Amine **[115]** was successfully switched with 400 nm in DMSO. As the switching wavelength (λ_{switch}) can be directly transferred to the aqu. system, we believe that 400 nm light is applicable in the KHP buffer too where the amine exhibits an ultra-fast relaxation.
- The two hydroxy derivatives **[126]** and **[121]** have ultra-short half life times as well and hence, no λ_{switch} could be determined. By comparison of the UV-Vis spectra we expect that significantly higher wavelengths than 365 nm will be necessary.

This chapter will deal with the biological evaluation of the novel inhibitors (inhibition of neurotransmitter uptake) that has been conducted until this thesis was submitted. For the light dependent evaluation, we developed LED well plates for two different wavelengths (365 nm and 410 nm) which is described in detail in chapter **C III**. For the sake of a concise interpretation, results obtained with the aid of the LED well plate are reported in favor of results, where a preceding method was used as this procedure is believed to deliver more robust and reliable results (for respective arguments see development chapter).

The uptake inhibition assays were carried out at the Medical University of Vienna in the laboratory of Prof. Harald Sitte by Marion Holy and Kathrin Jäntsch. A detailed description of the assay procedure can be found in the literature[150]. In short:

- HEK cells expressing the hSERT were grown and placed in a 96 well plate.
- The cells were preincubated (typically for six minutes) in triplicates with a dilution series of the inhibitor.
- The solution was exchanged for a solution of the inhibitor containing additional 100 nM [^{3}H]serotonin and the cells were incubated for one minute (uptake time).
- The uptake reaction was stopped and cells were lysed with 1% SDS.
- The amount of [^{3}H]serotonin was counted on a Liquid Scintillation Analyzer.
- The counts were plotted after subtraction of the counts related to unspecific uptake (blank = 100 μM paroxetine).

- From the resulting dose response curve the half maximal inhibitory concentration (IC_{50}) was obtained.
- This assay was carried out independently one to three times for the assessment of the inhibitor in its (*E*)-form and analogously in its (*Z*)-form under the influence of 365 nm, supplied by the 365 nm LED well plate.

In **Figure 53** the measured IC_{50} values are summarized. At this point in time **DD-300** (aniline derivative) which would require the 410 nm LED well plate, has not been measured, yet. Compared to the parent compound escitalopram (IC_{50} = 0.05 μM), all synthesized inhibitor exhibit a decreased potency ranging from 0.2 μM (**(*Z*)-DD-322**) to 3.6 μM (**(*Z*)-DD-309**) which still makes all of these compounds useful inhibitors. When comparing the IC_{50} values for the switched compounds (red bars) and the native compound (black bar), unfortunately no pronounced differences were found. In relative terms, **DD-403** (acid) showed the largest difference when switched as the IC_{50} more than doubled. This is, however, only a modest photo-effect. When we designed the ligands, we hoped that azobenzene **DD-321**, which is the N-N analog to the corresponding literature know stilbene analog (low nM K_i)[139], would result in a light-dependent binding. Surprisingly, this was not the case.

DD-301 and **DD-261** were still evaluated with an older method where the solutions of the dilution series were irradiated prior to application. In the case of **DD-301** this could have a significant effect as the half life time in aqu. buffer was determined to be half an hour, which can become significantly shorter when ambient light leads to relaxation (see chapter **C III**). It is therefore strongly suggested to repeat this measurement with the 365 nm LED well plate.

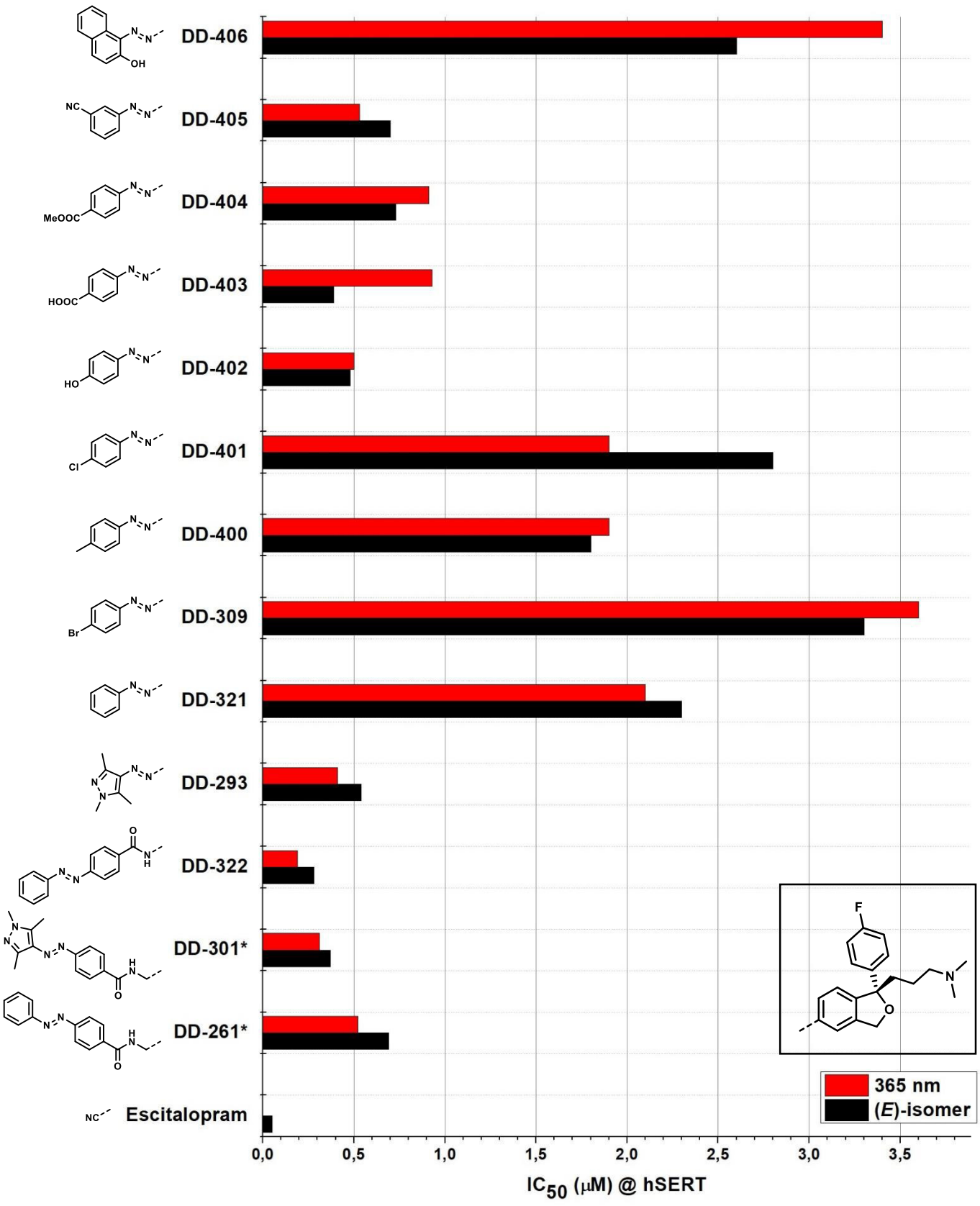

Figure 53: Biological evaluation of 13 escitalopram based azobenzene photoswitches on hSERT. *: **DD-301** and **DD-261** were assessed without the 365 nm LED well plate but with irradiation of the solutions prior to application.

For the hSERT activity data being rather disappointing, we decided to evaluate the synthesized compound on the related hNET and hDAT, too, as these transporters are considerably similar and share a number of same or comparable amino acids in the central binding site.[13, 151] The uptake inhibition assay remained the same. The cells expressing the corresponding transporter were grown. [^{3}H]MPP+ in 0.015 μM concentration was used for uptake with both, hNET and hDAT. For the blank value, hNET was blocked with 30 μM cocaine and hDAT was blocked with 10 μM paroxetine. The data available at this point is depicted in **Figure 54** for hNET. The data for hDAT so far has been ambiguous and is not considered. Unfortunately, the data on hNET is similarly discouraging. No pronounced differences were observed. It has to be noted, that in the case of **DD-309** (Br) in some cases an improvement of the potency by a factor of five was observed. However, these findings were not reproduced in other cases and the pooled data led only to a poor photo-dependent behavior. **DD-401** gave similar data while the individual experiments displayed a reduced variance.

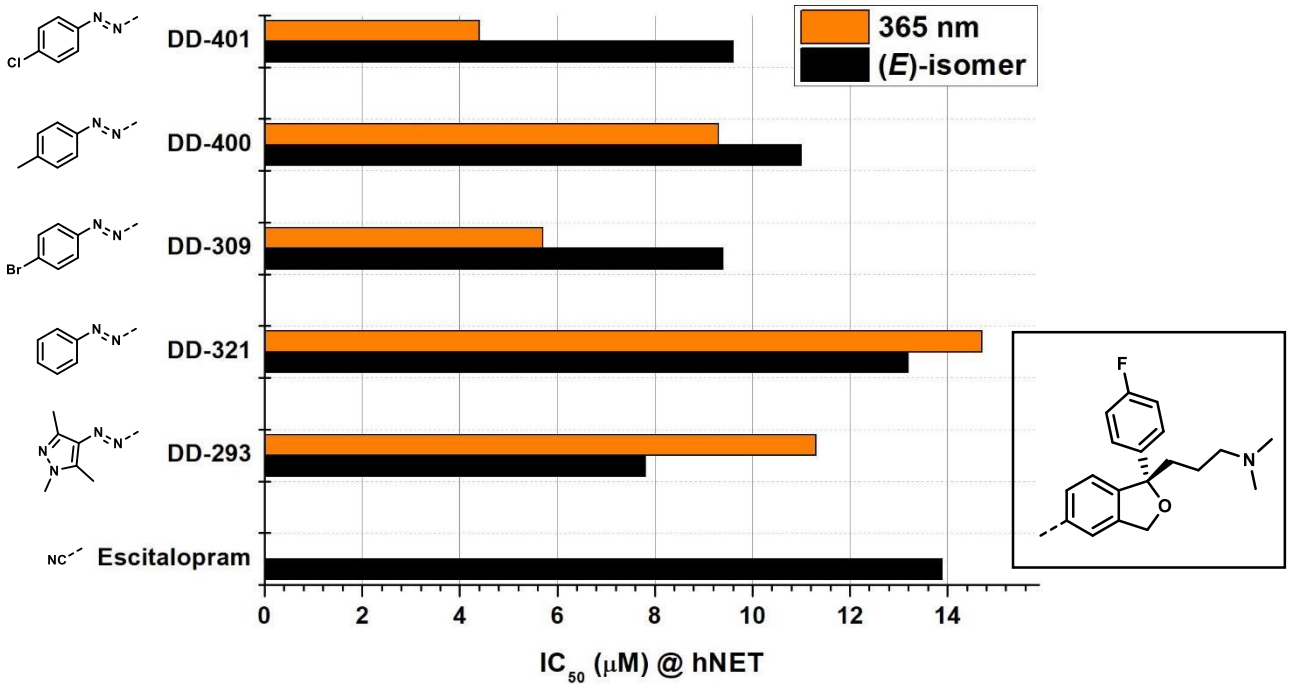

Figure 54: Biological evaluation of escitalopram based azobenzene photoswitches on hNET.

The biological impact of the designed escitalopram and azobenzene based photoswitches was, so far, comparatively modest. The following chapters will deal with alternative approaches to tackle this thesis' objective. That includes the exploration of an alternative class of photoswitchable ligands and a different parent compound.

C II.2 Escitalopram based HTI photoswitches

C II.2.1 Inhibitor design

In the previous chapter **C II.1** we designed, synthesized and evaluated azobenzene derivatives of escitalopram. The universal use of light of 365 nm to switch most of those azobenzene photoswitches was demonstrated. Using UV light in biological systems, however, is necessarily linked to two important disadvantages. High energy light potentially exhibits damaging effects[152] and the depth of penetration with short-wavelength light is greatly reduced in comparison to light of higher wavelengths,[153, 154] which becomes problematic if the compound of interest should be used in a more complex biological environment involving tissue. It is therefore generally appealing to increase (redshift) the wavelength that is required to trigger the photoisomerism of molecular photoswitches. One strategy is to redshift this wavelength by appropriate substitution of the parent scaffold. Very recently, remarkable results have been reported on azobenzenes e.g. through late-stage *ortho*-chlorination by C-H activation.[80] A second, complementary strategy is to use a scaffold, that has an intrinsically redshifted absorbance. Hemithioindigo (HTI) photoswitches are such a class of compounds. Similarly to azobenzenes they undergo a light induced *E*/*Z* isomerism. In contrast however, HTIs can be switched with blue light (typically 410 nm), which makes them a particularly interesting compound class (see **Figure 55**). In comparison to well-known azobenzenes, HTIs have been studied less but are considered an emerging class of photoswitches.[39] In order to expand the scope of our approach towards photoswitchable MAT inhibitors, we decided to investigate the feasibility of an HTI based access to novel derivatives. In addition to the redshifted absorbance, exploring a different photoswitch would expand the chemical space of potential inhibitors and offer additional synthetic opportunities.

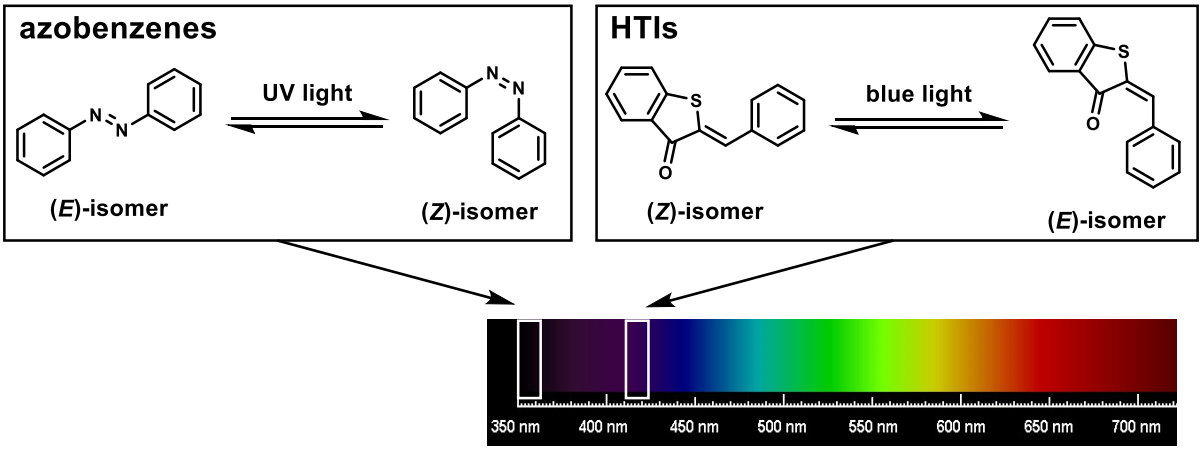

Figure 55: HTIs can be switched from their stable (*Z*)-form into their corresponding (*E*)-isomer with blue light.

In analogy to the ligand design in chapter **C II.1.1**, we aimed for compounds of the incorporation approach only, as the lack of available building blocks for a building block

approach made this synthetically undesirable in addition to the fact that the center of isomerism would be placed in remote distance to the biologically important molecular features. By merging the molecular features of escitalopram and the unsubstituted HTI, we designed an appropriate target molecule (see **Figure 56**).

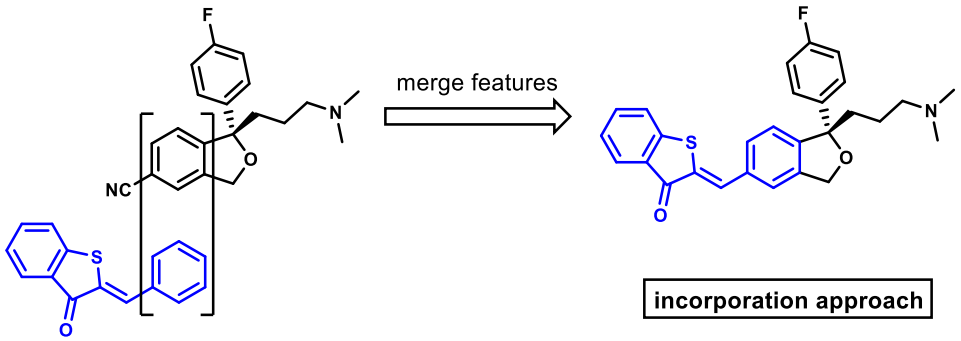

Figure 56: Ligand design of HTI analogs of escitalopram following the incorporation approach.

Retrosynthetically, we favored a condensation reaction (see **Figure 57**) as this would require the literature known aldehyde **[96]** which we have already used in a previous reductive amination reaction. Access to benzothiophene **[130]** can be achieved via a classical Friedel-Crafts acylation reaction.

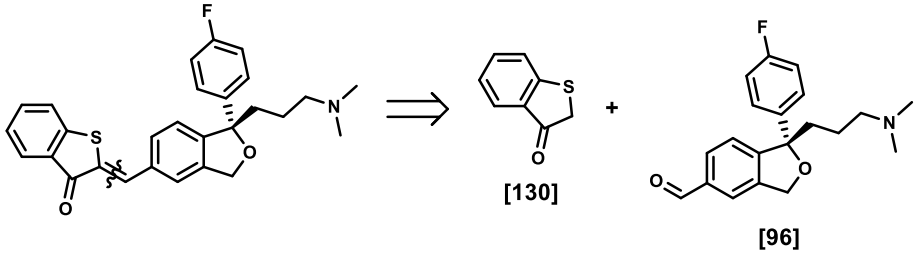

Figure 57: The envisaged target molecule could be synthesized via a condensation of aldehyde **[96]** with benzothiophene **[130]**.

C II.2.2 Synthesis

In the first synthetic step, commercially available thiophenol **[127]** was reacted with bromoacetic acid **[128]** in a substitution reaction which installs the acid functional group for the Friedel-Crafts acylation later.[155]

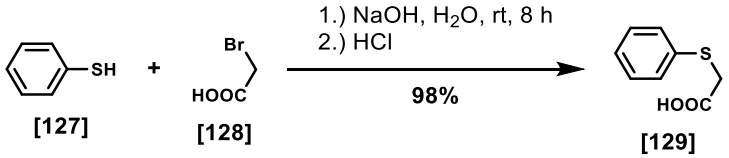

Freshly distilled thiophenol **[127]** was treated with bromoacetic acid **[128]** and aqu. NaOH (2 equiv.). After full consumption of starting material, the reaction was acidified and the product **[129]** was obtained by extractive work-up in 98% yield.

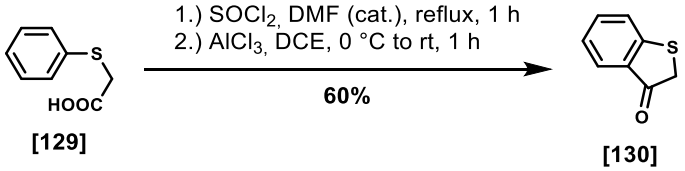

The obtained acid **[129]** was then stirred with $SOCl_2$ under DMF catalysis at reflux temperature to prepare the intermediary acid chloride as a suitable starting material for the subsequent Friedel-Crafts acylation. The acid chloride was isolated after evaporation of volatiles in vacuo. The Lewis acid $AlCl_3$ was suspended in dry DCE. At 0 °C the acid chloride intermediate was added dropwise which underwent the desired cyclization towards the five-membered ring readily. The reaction was quenched with cold H_2O. Extraction provided the product **[130]** as a reddish solid in 60% yield.[111]

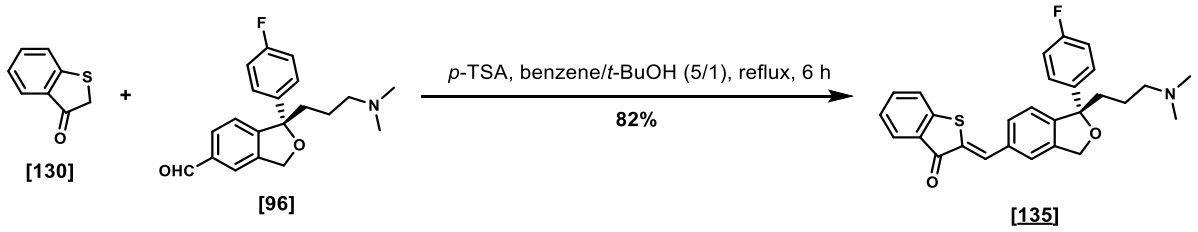

With the cyclic ketone **[130]** in hand, we could proceed to the Aldol condensation reaction with escitalopram aldehyde **[96]**. To catalyze the desired reaction, we used *p*-TSA. As the solubility of reactant **[130]** in the reaction solvent benzene was poor, *t*-BuOH was added to guarantee a homogenous reaction. The two starting materials were stirred at reflux temperature under argon until TLC analysis indicated full conversion. The appearance of a yellow spot on TLC was characteristic for the formation of the desired dye. The crude material was isolated by extraction and purification by flash column chromatography on silica gel afforded the target compound **[135]** in 82% yield.

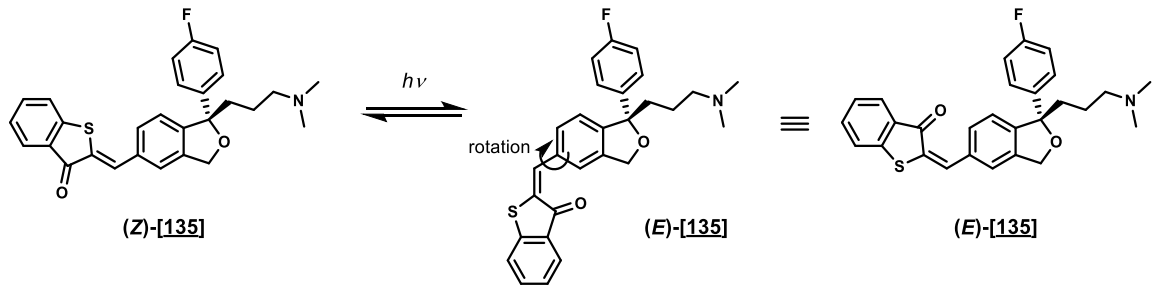

Figure 58: Photoisomers of escitalopram analog **[135]**.

With this most basic HTI analog of escitalopram we had rapidly accessed a novel photoswitch and got ourselves acquainted with the underlying chemistry. However, if we look at the two photoisomers **(*Z*)-[135]** and **(*E*)-[135]**, the geometric differences look huge on first glance (see **Figure 58**). But as the single bond can rotate, we have to acknowledge that the sterics are rather small when the carbon scaffold aligns with the (*Z*)-isomer. Nevertheless,

specific interactions of the sulfur and/or the ketone could lead to differences in biological activity. In order to increase structural differences of the shape of the two photoisomers, we concluded to place a substituent as perpendicular as possible to the axis of the double bond where the photoswitch occurs. The aromatic *ortho* positions next to the sulfur and the ketone, respectively, pose therefore the most promising opportunity to make the (*Z*)- and (*E*)-isomers less similar. In the case of the *ortho* position relative to the ketone, retrosynthesis delivered an intermediate that would not result in the desired product in the planned Friedel-Crafts acylation as due to sterics the other regioisomer would be the predominant product. The retrosynthesis of the second target compound circumvents this selectivity issue by blocking the competing *ortho* position with the desired substituent (see **Figure 59**).

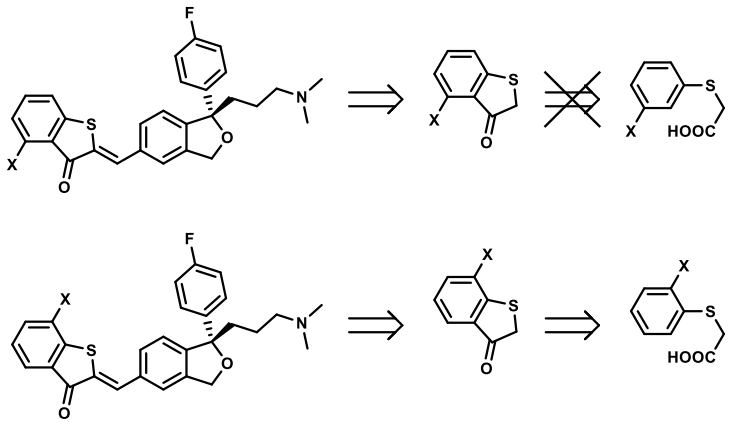

Figure 59: Substitution of the two *ortho* positions constitutes a possibility to make the two photoisomers more distinctive. The second proposed structure is synthetically feasible.

A number of *ortho* substituted commercial starting materials is available. We desired a building block that would allow further chemical modification in order to enable access to a number of photoswitches from a late-stage intermediate. Hence, thiosalicylic acid **[131]** represented a reasonable candidate based on the prospective follow-up chemistry of a carboxylic acid function.

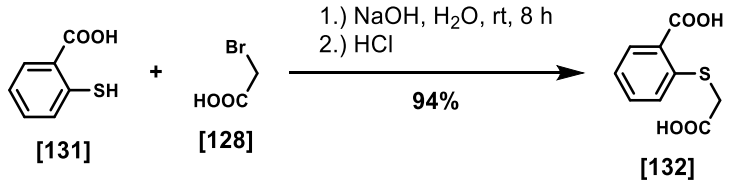

In analogy to the synthesis above, thiosalicylic acid **[131]** was reacted with bromoacetic acid **[128]** and aqu. NaOH (4 equiv.).[155] After complete conversion, the reaction was acidified and the product **[132]** was collected by vacuum filtration and after washing and drying in high vacuum 98% of pure product were obtained.

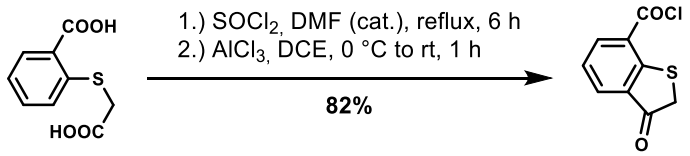

[132] [133]

Stirring dicarboxylic acid **[132]** in $SOCl_2$ with a catalytic amount of DMF at reflux temperature resulted in formation of the corresponding dicaboxylic acid chloride which was isolated after evaporation of volatiles. This intermediate was then added as a solution in DCE to a suspension of $AlCl_3$ in DCE at 0 °C. The intramolecular reaction took place selectively and after full conversion was observed by TLC analysis, the reaction was quenched with 2 N HCl. After extractive work-up, product **[133]** was isolated in 82% yield. Interestingly, the carboxylic acid chloride function was recovered and proved to be considerably stable which had already been reported in the literature[156]. The acid chloride **[133]** could directly be used in the Aldol condensation to form HTIs if a nucleophile (alcohols, amines) was provided to react with the acid chloride. Although products were obtained, the isolated yields in this one pot reaction were in the range of 20 – 40 %. In order to improve the yield and to access an additional target compound, we aimed for the hydrolysis of the acid chloride prior to condensation with escitalopram aldehyde **[96]**. The acid functional group could then be used to introduce further modifications. Stirring compound **[133]** with H_2O or 1 N NaOH did not give any conversion. When the mixture was heated, side reactions resulted in lousy purity. The target structure is prone to dimerization towards thioindigo derivatives and this was encountered under various conditions. Ultimately, homogenous reaction conditions were found to be crucial.

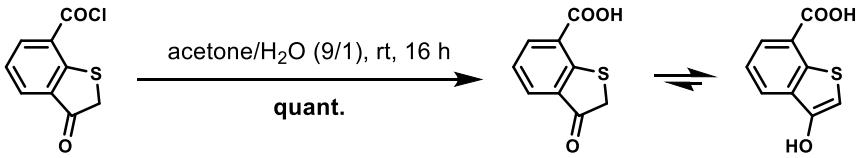

[133] [134]

When acid chloride **[133]** was dissolved in acetone and mixed with H_2O, the desired reaction took place at room temperature. After evaporation of volatiles, product **[134]** was obtained quantitatively. According to NMR analysis, the compound existed predominantly in its enol form, probably due to the resulting larger aromatic system.

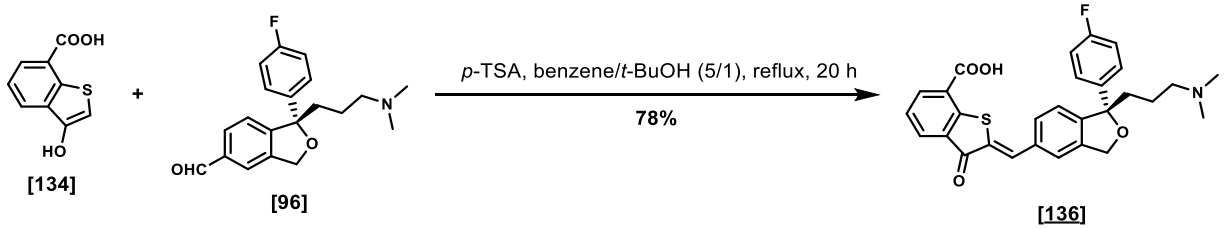

[134] [96] [136]

When acid **[134]** was reacted with escitalopram aldehyde **[96]** under the same conditions as before (*p*-TSA catalysis, reflux in benzene/*t*-BuOH), full conversion was observed after 20 hours and a characteristic yellow spot on TLC indicated the success of the desired reaction. After volatiles had been removed in vacuo, purification by flash column chromatography on silica gel provided compound **[136]** in 78% yield with a purity of approximately 90%. For analytically pure material, the compound was further purified by preparative HPLC. The purity after flash column chromatography however proved to be sufficient for the next reaction step and follow-up purification effectively removed the residual impurities. In the following derivatization of the carboxylic acid we aimed to introduce esters in order to eliminate the hydrogen donor capability at that position and a piperidine amide to introduce ample steric bulk. In a side project (Sophia Schnabl's master thesis) docking studies indicated that the piperidine ring reaches into the allosteric S2 binding site of hSERT. This offers the opportunity to introduce molecular features in that region to undergo interactions with amino acids of the S2 site.

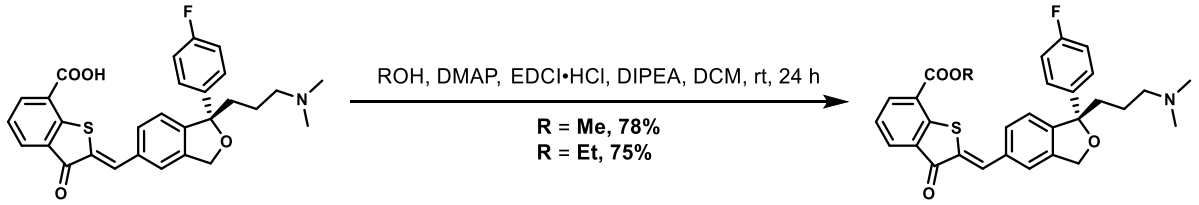

[136]

R = Me [137]
R = Et [138]

Under Steglich conditions, acid **[136]** was treated with EDCI•HCl, DIPEA and DMAP in a mixture of DCM and MeOH or EtOH. The crude material was isolated by extraction and after purification by flash column chromatography on silica gel, the desired target compounds **[137]** and **[138]** were obtained in 78% and 75% yield, respectively.

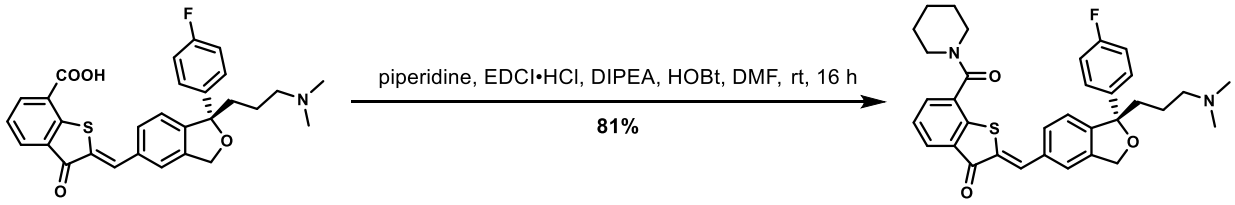

[136] [139]

Amide coupling of acid **[136]** with piperidine, EDCI•HCl, DIPEA and HOBt in DMF worked well and after extractive work-up and purification by flash column chromatography on silica gel, product **[139]** was isolated in 81 % yield.

In essence, we established the required chemistry to access HTI analogs of escitalopram. Unsubstituted **[135]** represents the most basic photoswitch of this compound class. With acid **[136]** we introduced an additional chemical handle to access a wider range of compounds which was successfully demonstrated with the preparation of esters **[137]** and

[138] and amide **[139]**. We hypothesized that a substituent *ortho* to the sulfur would render the two photoisomers more distinctive in their dimensions.

C II.2.3 Photophysical characterization

With the five new HTI photoswitches in hand, we went on to investigate their photophysical properties. As with the analogous azobenzenes in chapter **C II.1.3**, we recorded UV-Vis spectra in DMSO (50 μM) after sample preparation ((*Z*)-isomer) and after irradiation with the available LEDs. The obtained data is summarized in **Figure 60**. The black curve represents the initial state of the compound and is assumed to be exclusively the (*Z*)-isomer. The λ_{max} of the unsubstituted HTI **[135]**, the esters **[137]** and **[138]**, and amide **[139]** is very similar and ranges from 438 nm to 440 nm (see **Table 10**). Thus, they show very similar switching behavior. The acid **[136]** has a 10 nm higher λ_{max} of 450 nm and, hence, reacts a little bit different. In comparison to azobenzenes (e.g. compare unsubstituted HTI **[135]** with unsubstituted azobenzene **[117]**) this is a more than 100 nm redshifted λ_{max}. When the HTI compounds are irradiated with 365 nm (red curve), 385 nm (blue curve), 400 nm (magenta curve) or 460 nm (green curve), their respective photostationary state is obtained. As the λ_{max} values for the (*Z*)-isomer and the (*E*)-isomer of an HTI are closer together than it is the case for azobenzenes, the resulting spectra are more similar for HTIs (compare with **Figure 25** in chapter **B III**). While 365 nm is able to cause a significant switch, light of 400 nm was the best of the available wavelengths to obtain the highest quantities of (*E*)-isomer - which is in accordance with literature values[85, 115, 156, 157] – while 365 nm was generally used to switch azobenzenes. 460 nm was able to restore some (*Z*)-isomer. This effect was less pronounced in the case of the acid **[136]** which has a 10 nm higher λ_{max} and, hence, demonstrates the relationship of redshifted λ_{max} and the required wavelength for the (*Z*) to (*E*) isomerism. From comparison of the obtained spectra to literature data and the therein investigated isomer yield[39], we could estimate that the observed behavior corresponds to a successful switch in more than 90% conversion. Further in-depth investigations can be conducted by NMR and HPLC analysis, but at this stage of the project a different focus was considered.

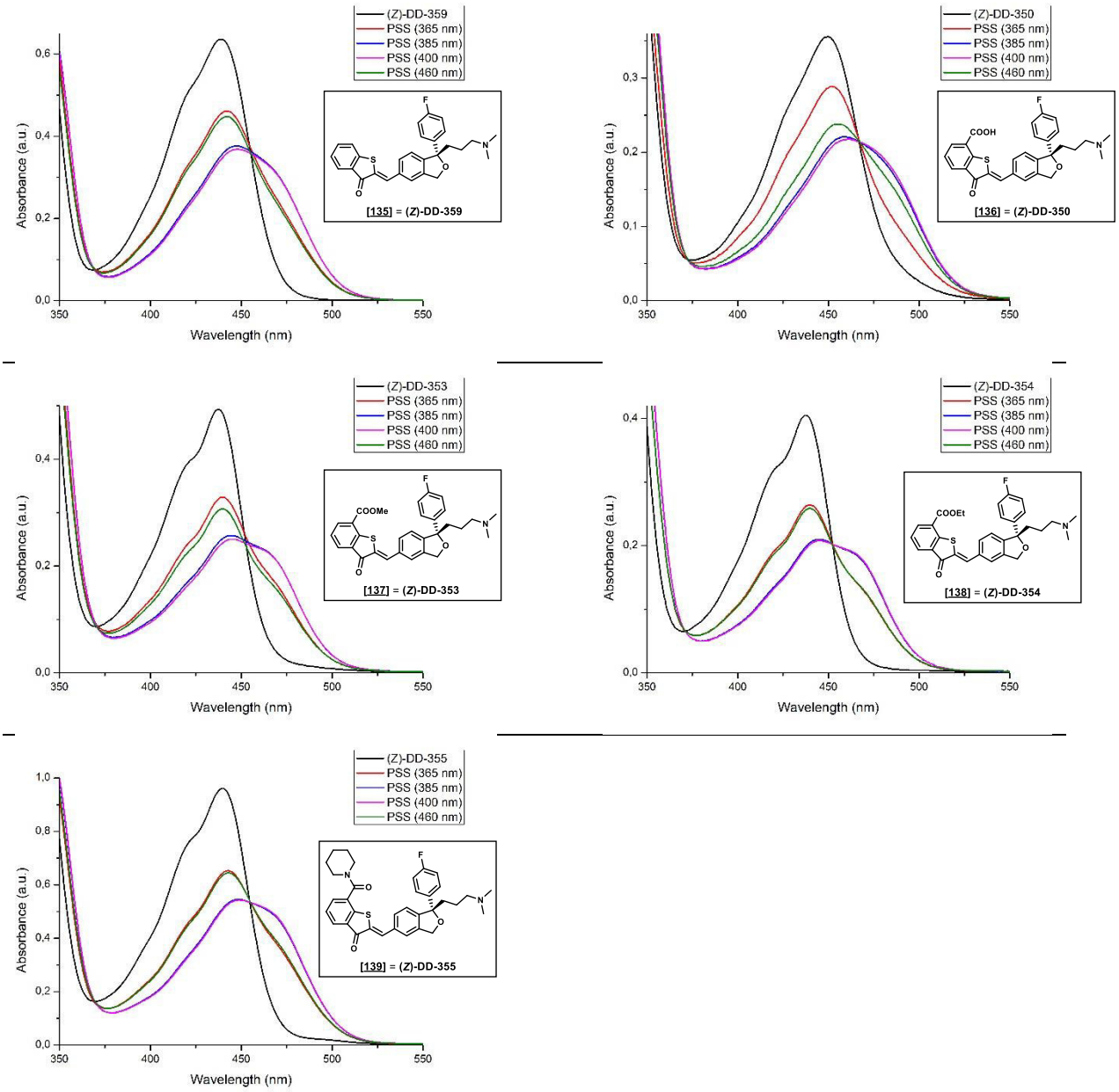

Figure 60: UV-Vis absorbance spectra of photoswitches **[135]**, **[136]**, **[137]**, **[138]** and **[139]** in the dark and after irradiation with 365 nm, 385 nm, 400 nm and 460 nm in DMSO.

Table 10: Wavelength of maximal absorbance for the (*Z*)-isomer of compounds **[135]**, **[136]**, **[137]**, **[138]** and **[139]**.

compound	λ_{max} DMSO	λ_{switch}
[135] = DD-359 (H)	439 nm	400 nm
[136] = DD-350 (acid)	450 nm	400 nm
[137] = DD-353 (Me ester)	438 nm	400 nm
[138] = DD-354 (Et ester)	438 nm	400 nm
[139] = DD-355 (amide)	440 nm	400 nm

As before with the azobenzene analogs, we were interested in the stability of the switched state and. consequently, measured the half life time of the excited state. The obtained data is summarized in **Table 11**. In general, the synthesized compounds display rather short half life times. The group of unsubstituted HTI **[135]**, the esters **[137]** and **[138]**, and amide **[139]** were determined to feature half life times between five and 15 minutes. The acid **[136]** has a longer half life time of 2.5 hours. This is particularly different to azobenzenes where the unsubstituted photoswitch generally features the longest half life time and any substitution leads to a destabilization. Interestingly, the carboxylic acid function prolonged the excited state while the esters and amide shortened it.

Table 11: Measured half life times $\tau_{½}$ and associated reaction rate constant of escitalopram based HTI analogs in DMSO.

compound	DMSO
[135] = DD-359 (H)	16 min (k = 7.0 * 10^{-4} s^{-1})
[136] = DD-350 (acid)	2.5 h (k = 7.6 * 10^{-5} s^{-1})
[137] = DD-353 (Me ester)	4.5 min (k = 2.6 * 10^{-3} s^{-1})
[138] = DD-354 (Et ester)	6 min (k = 2.0 * 10^{-3} s^{-1})
[139] = DD-355 (amide)	9 min (k = 1.3 * 10^{-3} s^{-1})

When we tried to investigate the photoswitches in the aqu. KHP buffer, we observed some difficulties. Overall, the results were problematic to interpret. The absorbance of freshly prepared samples (addition of 5 µL of a 100 mM DMSO stock to 495 µL KHP buffer) reduced over time. When the sample was irradiated with the appropriate wavelengths, the compound first appeared to switch but very surprisingly, irradiation with 460 nm did not lead to a regain in absorbance but to a further decline. In addition, no half life time could be measured as the resulting curve did not follow the expected first order kinetics, but rather seemed to be a combination of several processes. A recent literature report[86] came to our attention where the authors stated, that photoswitching of related HTIs in aqu. media was less successful in contrast to other solvents. They observed that as the proportion of H_2O increased, the efficacy of photoswitching decreased. Intrigued by this information we set out to examine how the behavior of the synthesized HTIs changed when transitioning from DMSO to aqu. KHP buffer. We chose methylester **[137]** as a representative example as this compound featured the shortest half life time and would therefore be most convenient to investigate as we aimed to look at the relaxation behavior. **Figure 61** and **Figure 62** show the obtained data in DMSO/buffer mixtures.

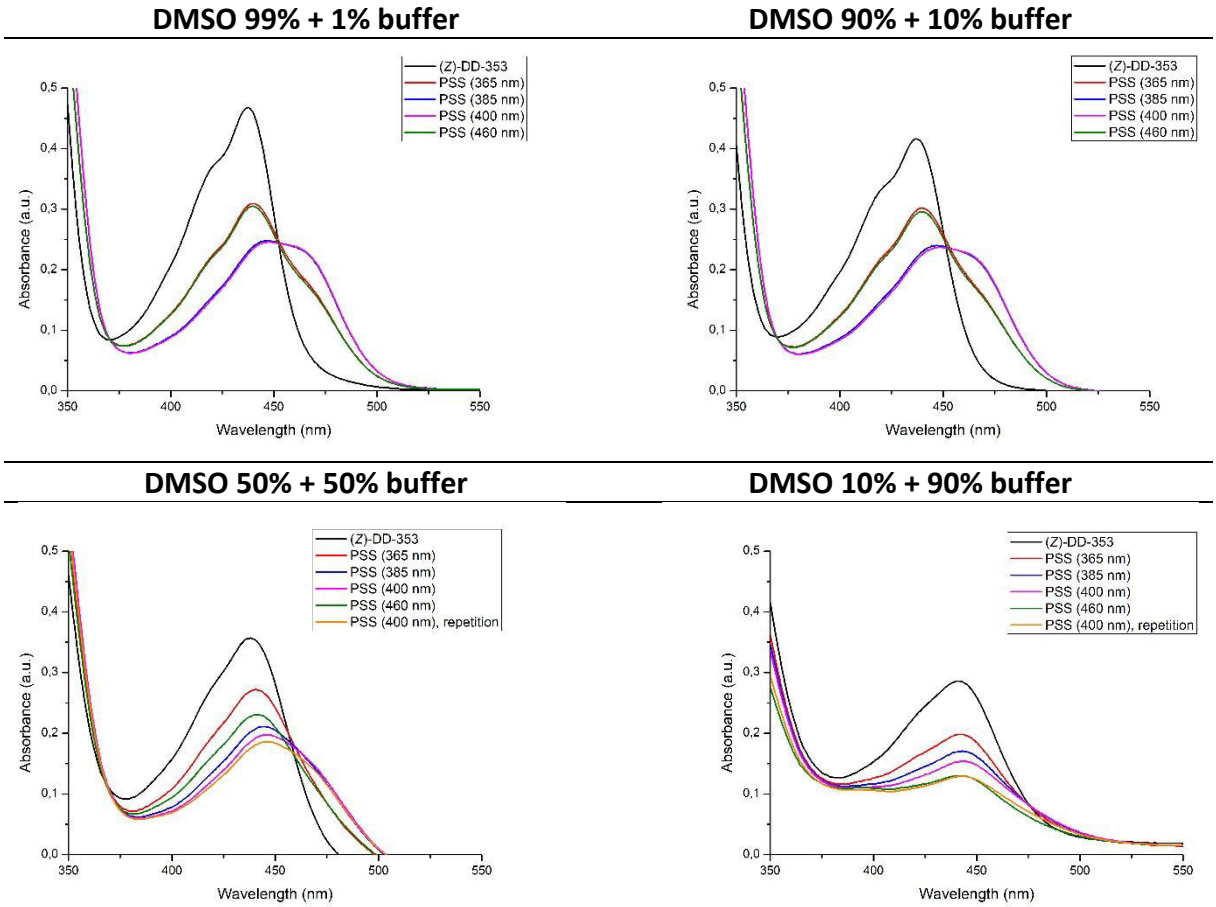

Figure 61: UV-Vis spectra of HTI **[137]** in dependence of increasing H_2O content.

In mixtures containing 1% buffer and 10% buffer, the switchability remained basically the same in comparison to the behavior in DMSO (compare to **Figure 60**). Interestingly, the half life time increased from 4.5 minutes in DMSO to 12 minutes (k = 9.7 * 10^{-4} s^{-1}) when 1% buffer was present and to 31 minutes (k = 3.7 * 10^{-4} s^{-1}) when 10% buffer was used. It also appears that in comparison to the data in DMSO, the (*Z*)-isomer is either not completely recovered or the extinction coefficient in the presence of buffer decreases as the absorbance reaches a lower level. When a balanced mixture of DMSO and buffer was used, the compound reacted differently (as described above) which became even more pronounced when using excessive KHP buffer. The absorbance continuously decreased with changing wavelengths and the first measurement after irradiation with 400 nm could not be reproduced which indicates an ongoing process. In the 50% DMSO/50% buffer mixture, a relaxation could be observed which gave a half life time of 21 minutes (k = 5.5 * 10^{-4} s^{-1}) but the mathematical function was not unambiguous anymore and as we expect a second process to be going on, this value is not considered to be valid. With 90% buffer the relaxation was even harder to interpret.

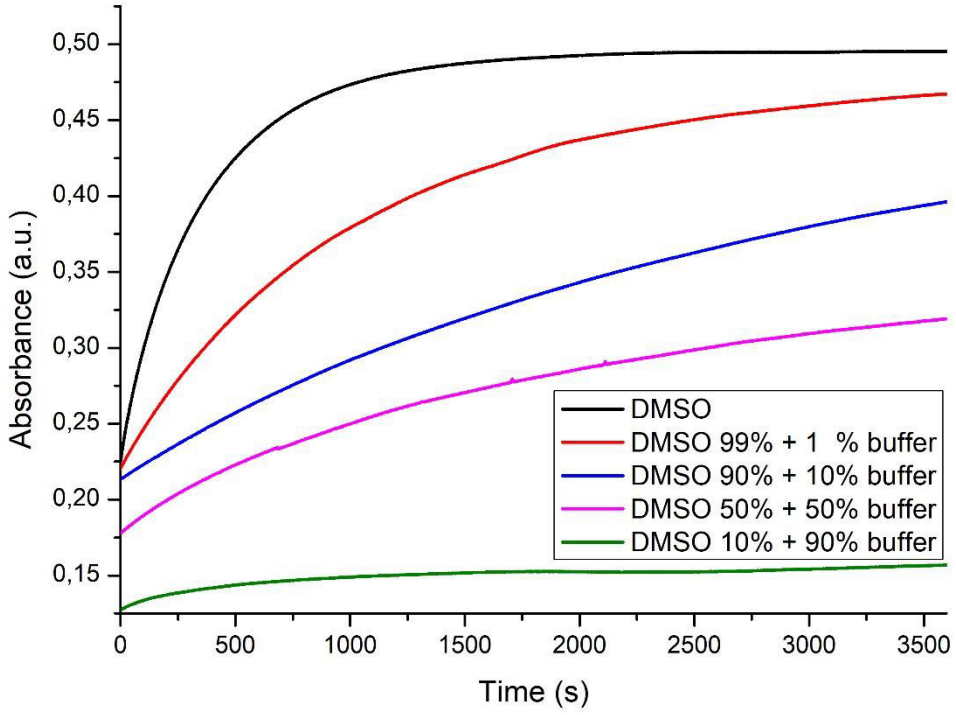

Figure 62: Relaxation behavior of HTI **[137]** in dependence of increasing H_2O content.

Taking these results into account, we have to acknowledge the peculiar behavior of the synthesized HTIs in KHP buffer. At this point it is not clear, if and with which isomeric yield the compounds can be switched in an aqu. solution. The implications for the planned biological evaluation are currently uncertain. As HTIs have been shown to work in biological systems[116] they might as well isomerize as intended in a protein environment. Further research is necessary to gain more insight. It is suggested to investigate the stability and the actual content of photoisomers with HPLC in dependence of wavelengths, sample preparation and storage, and content of aqu. buffer. This should give a clearer picture of the situation.

C II.3 Paroxetine based azo photoswitches

C II.3.1 Inhibitor design

While chapters **C II.1** and **C II.2** dealt with escitalopram based photoswitchable inhibitors, this chapter will expand our work by using a different parent compound. Motivated by the crystal structure of hSERT we looked at the second inhibitor that was successfully co-crystallized with the transporter in this report[9]. Paroxetine (see **Figure 63**) too is an inhibitor of the SSRI class and has an even higher binding affinity to hSERT. In addition, paroxetine only binds to the central binding site while escitalopram also binds to the allosteric binding site. **Figure 63** shows the paroxetine bound hSERT. The maltose molecule in the crystal structure is an artifact from the crystallization procedure. The binding of paroxetine to hSERT is further substantiated by mutational[13] and computational studies[158].

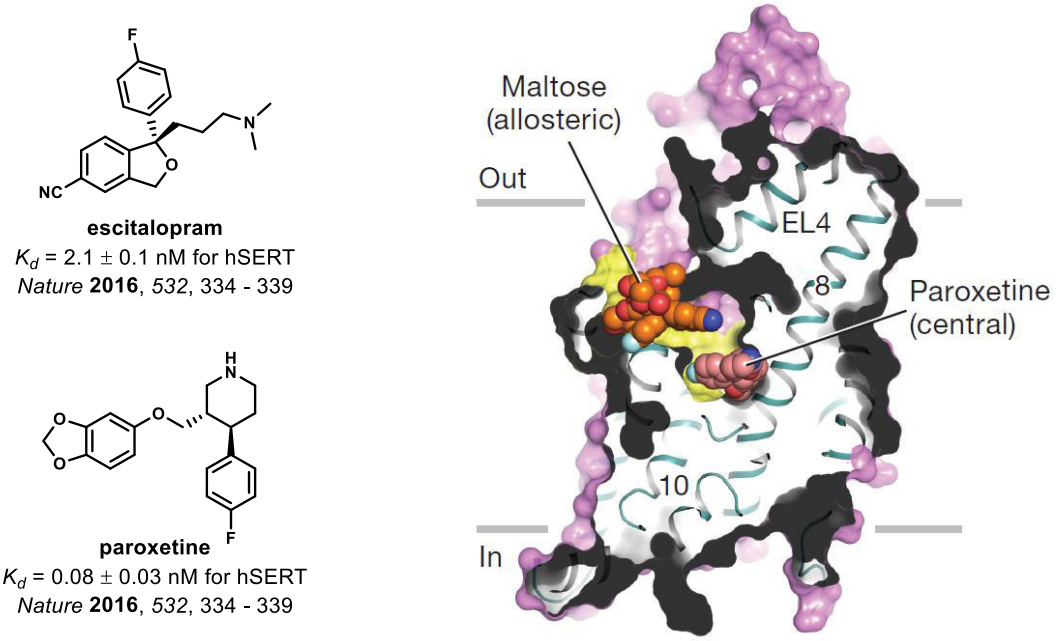

Figure 63[9]: Left: The structure of the two SSRIs escitalopram and paroxetine and their binding affinity to hSERT. Right: The crystal structure of hSERT with paroxetine bound to the central binding site.

In order to rationally design a photoswitchable SERT inhibitor based on paroxetine, we wanted to place the photoswitchable motif in a region, where the protein offers some but not too much available space (compare to the ligand design in chapter **C II.1.1**). In case of escitalopram, this space was available where the nitrile group was pointing. Therefore, we compared the position of the two inhibitors in order to find the respective position in paroxetine (see **Figure 64**). The individual parts of the two molecules occupy three sub-pockets: A, B and C. In sub-pocket A, the tertiary amine of escitalopram and the secondary amine of paroxetine interact strongly with aspartate 98 via a salt bridge. Sub-pocket B hosts the fluorophenyl fragment of escitalopram and the benzodioxol fragment of paroxetine.

Interestingly, the fluorophenyl fragment of paroxetine is located in sub-pocket C where the escitalopram's nitrile is found. In accordance with the escitalopram based inhibitor design, we decided to place the photoswitch on the fluoro bearing phenyl ring. In line with the incorporation approach used with escitalopram, we planned to exchange the fluoro substituent with the azo group. While potentially *ortho*, *meta* and *para* position are imaginable, we decided to place the new moiety in *para* position as this probably is the synthetically most feasible option keeping structural complexity under control. **Figure 65** depicts the proposed target compound.

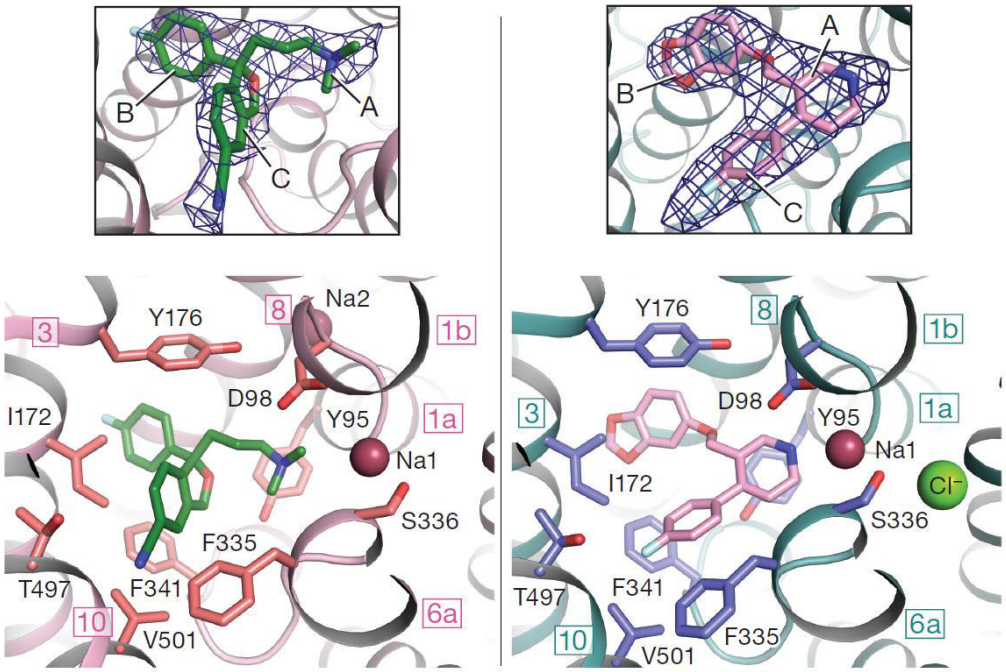

Figure 64[9]: Left: Orientation of escitalopram in the central binding site. The nitrile (sub-pocket C) points towards a region where some space is available. Right: Orientation of paroxetine in the central binding site. The fluorophenyl fragment occupies sub-pocket C.

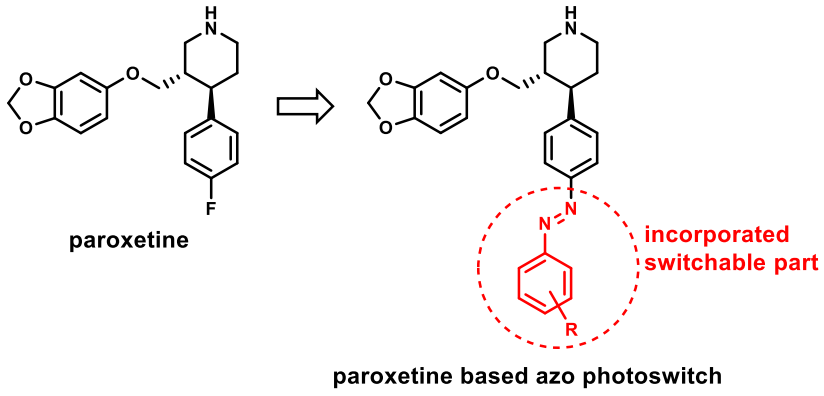

Figure 65: An azobenzene based photoswitchable version of paroxetine.

C II.3.2 Retrosynthetic analysis

While the nitrile group of escitalopram proved to be a versatile handle to introduce a variety of different residues, the fluorophenyl fragment of paroxetine is a considerably inert chemical group. For the synthesis of escitalopram based photoswitches, we could use commercially available escitalopram as the starting material. In case of the envisaged paroxetine analogs, commercially available paroxetine is not a suitable starting point. Considering that the target compounds could be synthesized via a Mills condensation, we would need to prepare the corresponding paroxetine aniline for the reaction with various nitroso compounds (see **Figure 66**). An aniline version of paroxetine is unknown to the literature and, hence, we needed to develop a de-novo synthesis.

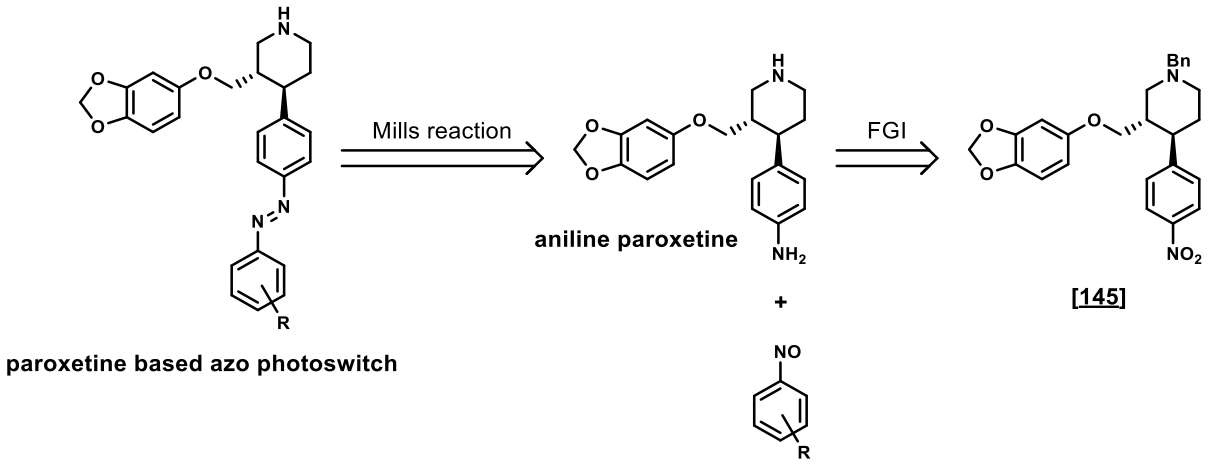

Figure 66: We planned to access the target compounds via a Mills condensation of an aniline analog of paroxetine and corresponding nitroso compounds.

As the envisaged aniline is a considerable nucleophile, we thought to not have the reactive species present in reactions leading up to the crucial intermediate, but to either protect the aniline or introduce it in a late synthetic stage from a suitable precursor via functional group interconversion. Protection of the secondary amine in the piperine ring is probably required for the same reasons. We favored a strategy where we synthesized the aniline analog from the corresponding nitro derivative **[145]** as the nitro group is expected to not be affected by the applied reactions and the reduction of a nitro to the amine is a facile process. Therefore, we screened the literature for total and formal syntheses of paroxetine where we could use an analogous nitro starting material instead of the published fluoro starting material. A number of literature reports[159-163] used elaborate catalytic protocols with novel catalysts and/or ligands. We were particularly inspired by the straightforwardness of a publication by Takasu et. al.[164] The authors reported the synthesis of substituted piperidinones from α,β-unsaturated amides (see **Figure 67**). The *trans*-lactam **[XXIII]** was transferred into racemic alcohol **[XXIV]** which is an intermediate in the synthesis of paroxetine[165].

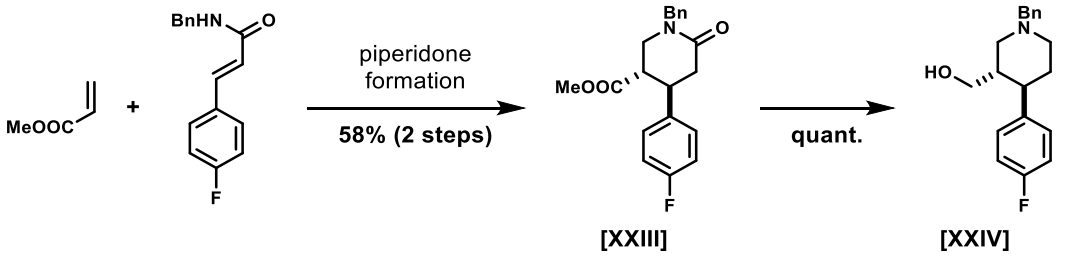

Figure 67: The literature reported synthesis[164] of lactam **[XXIII]** served as an inspiration for our synthetic plan.

Consequently, we decided to use the corresponding nitro starting material for our de-novo synthesis. **Figure 68** outlines the resulting retrosynthetic rationale. Nitro compound **[145]** could be obtained from alcohol **(3*S*,4*R*)-[143]** via an etherification. Alcohol **(3*S*,4*R*)-[143]** has to be accessed by some kind of optical resolution as the envisaged racemic alcohol ***rac*-[143]** should be prepared from racemic piperidinone ***trans*-[142]** after reduction. ***trans*-[142]** could be synthesized by the beforementioned literature protocol which faces no stereo-selective influence when prepared from literature known α,β-unsaturated amide **[141]**. This leaves us with 4-nitrocinnamic acid **[140]** as a suitable, commercially available starting material.

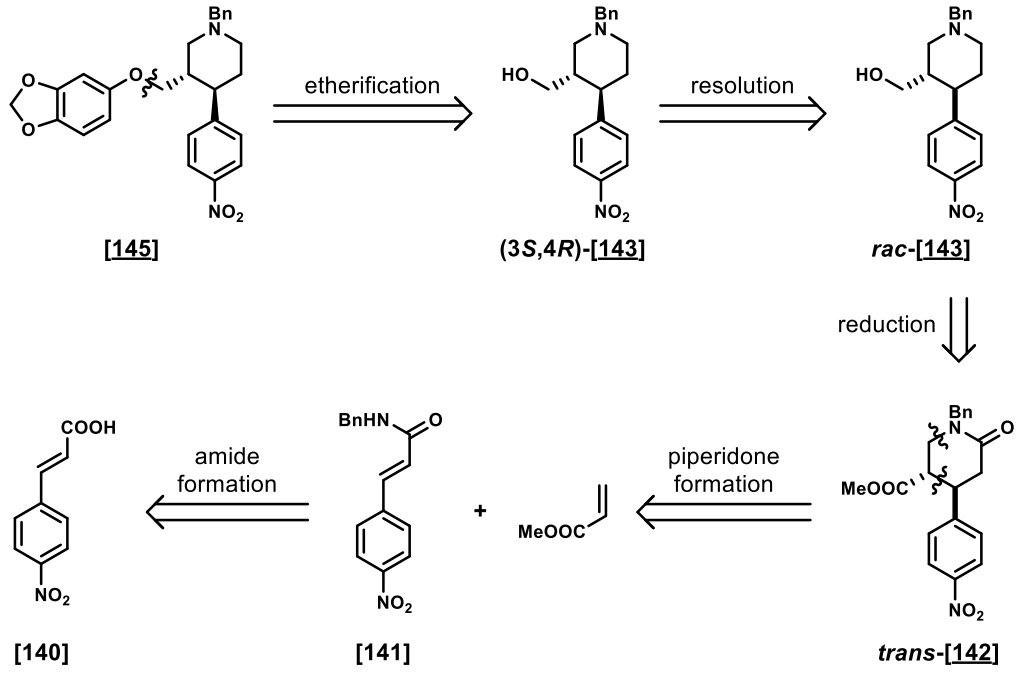

Figure 68: Retrosynthetic analysis of nitro compound **[145]**.

C II.3.3 Synthesis

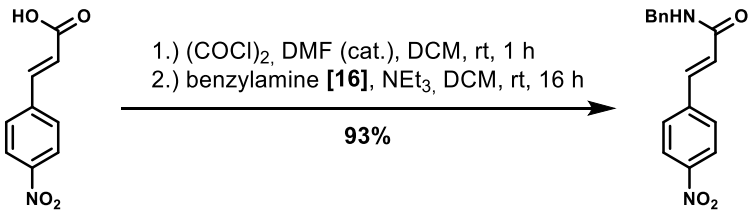

[140] [141]

The synthetic route commenced with the synthesis of amide **[141]** from commercially available 4-nitrocinnamic acid **[140]**. Amidation with benzylamine **[16]** introduces the nitrogen of the piperidine ring of paroxetine and makes the product a nucleophile for the upcoming Michael addition. In subsequent reaction stepy the benzyl also serves as a protecting group. To activate the acid **[140]**, acid chloride formation with oxalyl chloride, catalyzed by DMF, was conducted. Freshly distilled oxalyl chloride was added dropwise to a solution of the starting material in dry DCM and a catalytic amount of dry DMF under argon. Gas formation indicated the desired transformation to take place. TLC analysis (MeOH-quenched sample gives the corresponding methyl ester) showed full conversion after one hour. After volatiles had been evaporated in vacuo, the crude acid chloride was dissolved in dry DCM again, and benzylamine **[16]** and NEt_3, which quenches the formed HCl, were added. The reaction was stirred over night whereupon TLC analysis indicated full conversion. Washing with 1 N HCl and 1 N NaOH should remove any acidic and basic residues. The crude material was recrystallized from toluene and 93% of crystalline product **[141]** were obtained.

The amide **[141]** could then be used to attempt the cyclization to the piperidinone with methyl acrylate based on the literature report.[164] The ring is formed by a double Michael addition. The mechanism is depicted in **Figure 69**. The amide's nitrogen attacks the α,β-unsaturated olefin as the nucleophile. The resulting enolate attacks in a very similar fashion intramolecularly the α,β-unsaturated double bond of the amide and thereby, forms a stable six-membered ring.

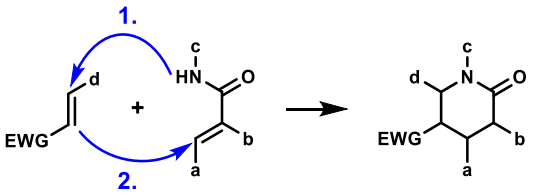

Figure 69: The piperidinone ring is formed by a double Michael reaction.

In our synthesis, residue *a* is the aryl, residues *b* and *d* are hydrogens, residue *c* is the benzyl protecting group and the *EWG* is the methyl ester. As there is very little stereo-control when the enolate attacks the amide in the second Michael addition, a balanced mixture of *cis*-

and *trans*-products is to be expected. Furthermore, as there is no chiral induction, the two products are formed as racemates.

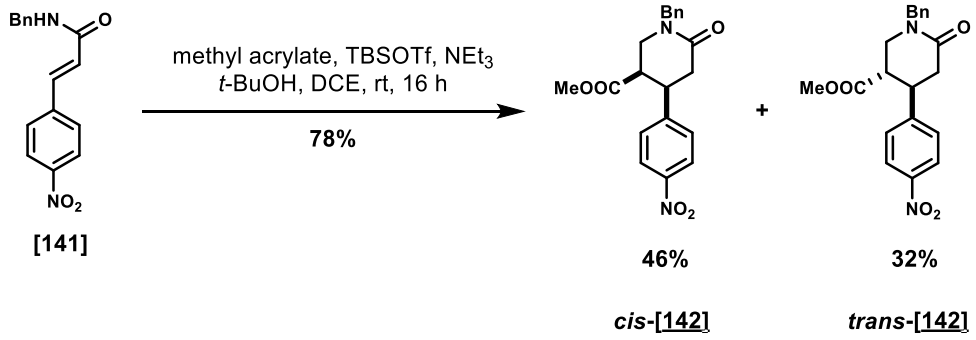

When conducting the synthesis of the piperidinones ***cis*-[142]** and ***trans*-[142]** it was crucial to use the literature concentration of 1 M relative to the starting material **[141]** as a lower concentration in an initial trial gave no conversion, at all. Distilled methyl acrylate (1 equiv.) and dry NEt_3 (0.7 equiv.) were added to a suspension of the amide **[141]** (1 equiv.) in dry DCE in a Schlenk flask. TBSOTf (1.2 equiv.) was added dropwise under. After complete addition, *t*-BuOH (0.25 equiv.) was added and the suspension was stirred at room temperature. After approximately one hour the suspension became homogenous. In all conducted experiments, full conversion was not achieved according to TLC analysis. As there was little starting material found in crude NMRs, small amounts of starting material must be easily detectible under UV. The two products ***cis*-[142]** and ***trans*-[142]** were almost not visible under UV but could be stained with basic $KMnO_4$. Analysis of the reaction by GC-MS confirmed the desired transformation to take place. The crude material was isolated by an extractive work-up. When DCM was added to dissolve the material, remaining starting material precipitated and could be removed by filtration. The two products ***cis*-[142]** and ***trans*-[142]** were successfully separated by flash column chromatography on silica gel. 46% of ***cis*-[142]** and 32% of ***trans*-[142]** were isolated which results in a combined yield of 78%. As conversion was incomplete under the applied literature conditions, we tried to push conversion to completion by changing some of the reaction parameters (see **Table 12**).

Table 12: In order to try to achieve full consumption of the starting material **[141]**, the following reaction conditions were varied.

reaction	TBSOTf	methyl acrylate	temperature	yield
A	1.2	1	rt	78%
B	1.5	1	rt	37%
C	1.2	1	50 °C	<40%
D	1.2	1.5	rt	53%

When increasing the amount of used TBSOTf (reaction B), again full conversion was not observed and the yield dropped to 37%. When the reaction was carried out at 50 °C, less than 40% of products were isolated. Using a higher amount of methyl acrylate led to a yield of 53% and a prominent side product formed which was confirmed to be the result of a third Michael addition (see **Figure 70**) by ^{1}H-NMR and LC-MS. The formation of this side product was already reported in the original reference[164]. Hence, the best result was achieved applying the exact literature conditions (reaction A).

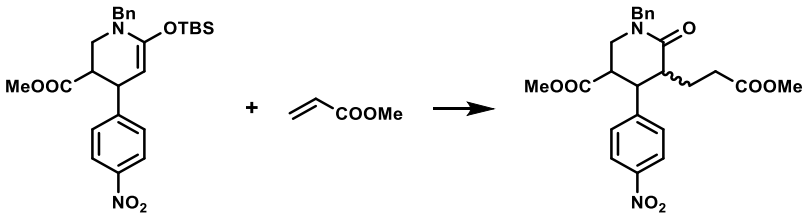

Figure 70: Formation of the side product by a third Michael addition.

As paroxetine features a *trans*-configuration, only the piperidinone ***trans*-[142]** could be used in the next reaction step. However, ***cis*-[142]** can be transformed into ***trans*-[142]** because the α-position of the ester is C-H acidic and the proton can be abstracted, leading to a planar enolate configuration. After restoration of the ester in a protic solvent, the molecule can either adopt the *cis*-configuration from before or the more stable *trans*-configuration. An epimerization of ***cis*-[142]** with a strong base in presence of a protic solvent is expected to give an equilibrium of the two products with preference for ***trans*-[142]** which would boost the total yield of the desired product.

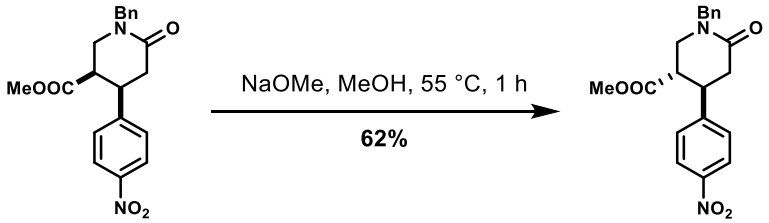

***cis*-[142]** ***trans*-[142]**

***cis*-[142]** was dissolved in dry MeOH and NaOMe was added. The reaction was stirred at 55 °C oil bath temperature under argon until TLC analysis showed no change in the composition of products. After extractive work-up and purification by flash column chromatography, 62% of the desired ***trans*-[142]** were isolated while 15% of ***cis*-[142]** remained unconverted. The total yield of ***trans*-[142]** could thereby be increased to 61% after two steps. In a later phase of the project it came to our attention that the used NaOMe might contain unknown quantities of NaOH which would result in ester hydrolysis and loss of the resulting acid upon aqu. work-up. Therefore, we expect that the yield of this step could be improved in follow-up projects by using a freshly prepared solution of NaOMe in MeOH

(reaction of Na with dry MeOH). We also tried to apply the epimerization protocol directly to the crude mixture of ***cis*-[142]** and ***trans*-[142]** after the cyclization which would reduce labor (one purification by flash column chromatography fewer). Unfortunately, this approach led to a lower yield of 39% of isolated ***trans*-[142]** and, hence, we stuck to the described two-step procedure (however, there may be additional room for optimization upon more detailed variation of conditions).

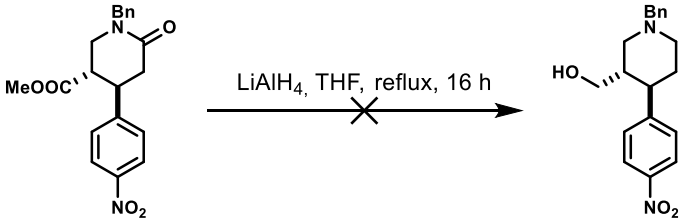

***trans*-[142]** **rac-[143]**

In the next step we attempted the reduction of ***trans*-[142]**. Following the original publication[164] (towards paroxetine), ***trans*-[142]** was dissolved in dry THF, $LiAlH_4$ was added and the reaction was stirred at reflux temperature under argon for 16 hours. TLC analysis afterwards showed multiple spots and ^{1}H-NMR of the crude material showed an unidentifiable mixture of undesired compounds. In a second attempt, the solution of the starting material was cooled with an ice bath and after addition of the reducing agent, TLC analysis was conducted immediately but already showed multiple spots. Therefore, it was concluded that the nitro substituent was not compatible with these reaction conditions. In consequence, we decided to look for milder reducing conditions and screened the literature for the reduction of similar substrates. As the reduction of the less reactive amide is probably the more challenging transformation, we looked for the reduction of similar amides in the presence of a nitro group.

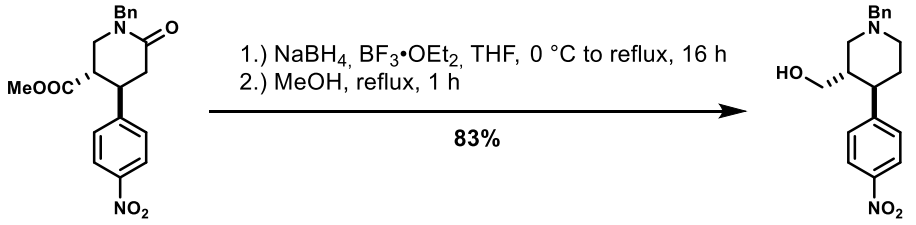

***trans*-[142]** **rac-[143]**

Conditions from a work by Norris et. al.[166] seemed applicable. $BF_3 \bullet Et_2O$ (4 equiv.) was added dropwise under argon to a cooled suspension of $NaBH_4$ (4 equiv.) in dry THF and the reaction was stirred for one hour at 0 °C. The two reagents react according to the following equation:

$$4\ NaBH_4 + 4\ BF_3 \rightarrow 4\ BH_3 + NaBH_4 + 3\ NaBF_4$$

BH_3 is generated in situ and one equiv. of $NaBH_4$ remains which is necessary for the complete reduction of both functional groups, ester and amide. The starting material ***trans*-[142]** was dissolved in dry THF and added to this reducing suspension whereupon the reaction was stirred at reflux temperature for 16 hours. After quenching with 1 N NaOH and extractive work-up, the crude product was obtained which was purified by flash column chromatography on silica gel. The isolated colorless solid was thought to be the desired product, as NMR spectra were in accordance with the structure and HR-MS confirmed the sum formula. The isolated yield however, was only 41% which was surprising as the crude material was obtained almost quantitatively and the purity was already quite good. As this crude material also formed nice crystals, a second attempt was carried out and the obtained crude material was tried to recrystallize from ligroin and toluene. Interestingly, the material dissolved well at first but then a poorly soluble precipitate formed which could not be dissolved at reflux temperature and the recrystallization process was stopped. The material was purified by flash column chromatography as before but to our surprise, a different solid material was obtained. The HR-MS gave the same mass and spectral data also matched expectations based on the product's structure but were different from the previously isolated material. A re-examination of the literature made us realize that the initially obtained material was the amine-borane complex[167] of the product and the product can be liberated from this adduct; in the case of the recrystallization attempt the thermal stress must have caused the transformation. In order to liberate the amine from the amine-borane complex in a more controlled fashion, we applied conditions from the literature[168]. The intermediate was dissolved in MeOH and stirred at reflux temperature. Methanolysis was complete after one hour and after evaporation of the solvent and purification by flash column chromatography on silica gel the desired product ***rac*-[143]** was obtained in very satisfying 83% yield.

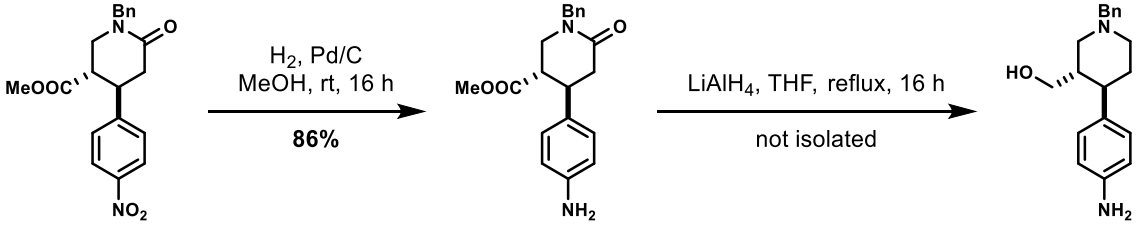

trans-[142] [159] [160]

In parallel, we telescoped alternative synthetic routes towards the target compound. As the nitro substituent in ***trans*-[142]** was not tolerating $LiAlH_4$ and should be reduced to the aniline later, we thought to change the order of events and reduce the nitro earlier. Classic reduction by hydrogen, catalyzed by Pd/C in MeOH gave 86% of the corresponding aniline **[159]**. This substrate was perfectly compatible with the $LiAlH_4$ conditions and alcohol **[160]** was formed cleanly but not isolated as we established the borane reduction protocol in the

meantime and the free aniline would probably require additional protection. Nevertheless, this route could have been a valuable back-up strategy.

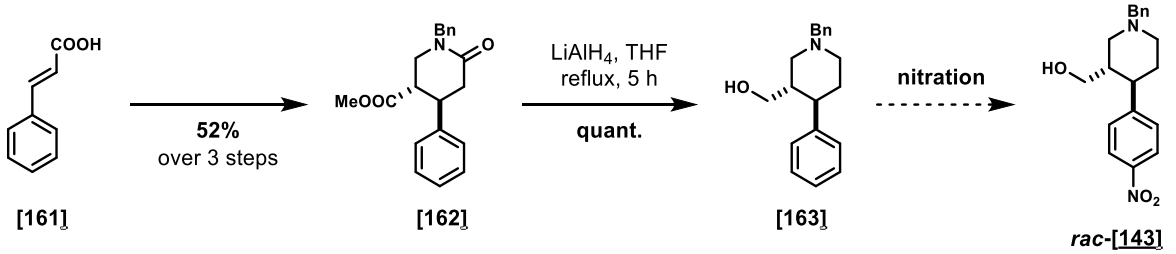

In a second alternative scenario, we prepared piperidinone **[162]** starting from cinnamic acid **[161]** in 52% yield over three steps following the established synthetic route. Piperidinone **[162]** was quantitatively reduced to alcohol **[163]** with $LiAlH_4$. This product could potentially be used to access ***rac*-[143]** via nitration but was not followed as we had already found a robust access to this key intermediate.

Inspired by a report on similar substrates[169], we planned to use key intermediate ***rac*-[143]** to conduct an enzymatic kinetic resolution at this stage. An alternative would have been the optical resolution by crystallization. In the literature, a paroxetine precursor was successfully resolved using L-*o*-chlorotartranilic acid.[170] Based on the reported protocol[169], we desired to convert one of the two enantiomers of ***rac*-[143]** into the corresponding acetate catalyzed by a Lipase. First, we needed to prepare the racemic acetate which would serve as reference material to develop an analytic method on a chiral HPLC as well as for TLC analysis.

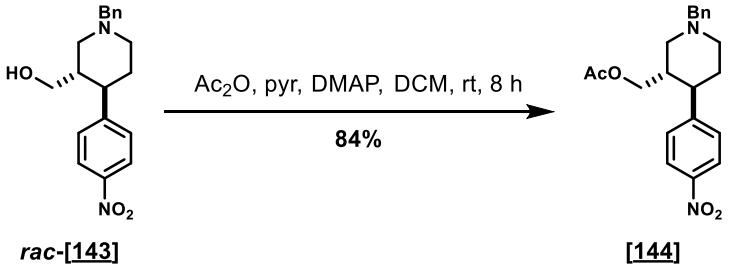

***rac*-[143]** was dissolved in DCM and pyridine (2 equiv.), a catalytic amount of DMAP and acetic anhydride (2 equiv.) was added at 0 °C. After complete conversion of the starting material the crude product was isolated by extraction and purification by flash column chromatography afforded the required acetate **[144]** in 84% yield. Racemic alcohol ***rac*-[143]** and racemic acetate **[144]** were then used to develop an analytical HPLC method (see **Figure 71**) on a ChiralPak AS-H column.

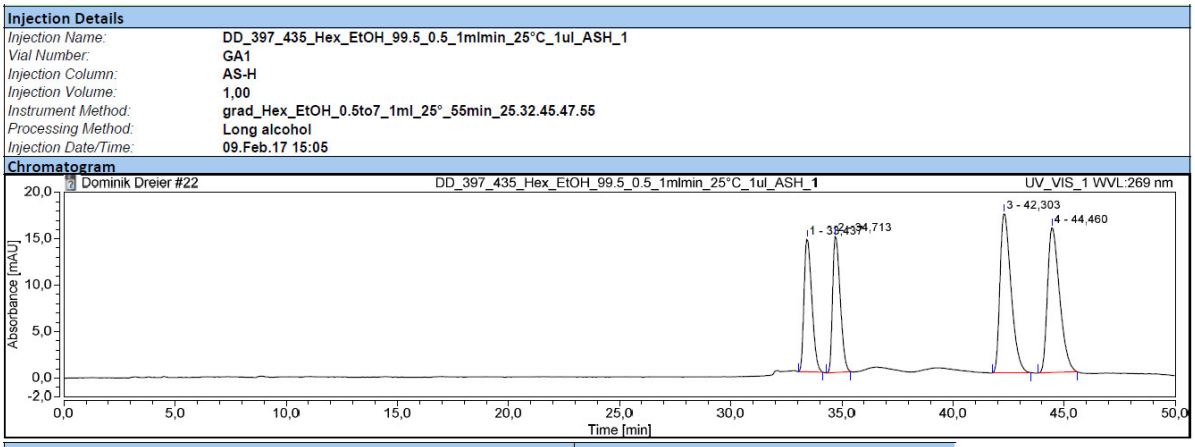

Integration Results

No.	Retention Time min	Area mAU*min	Rel.Area %
1,0	33,437	5,820	18,54
2,0	34,713	5,817	18,53
3,0	42,303	9,924	31,62
4,0	44,460	9,828	31,31

Figure 71: The two pairs of enantiomers were successfully separated on a ChiralPak AS-H column by HPLC.

Next, the Lipases CAL-A, CAL-B and Amano Lipase were used to investigate whether they would convert the alcohol ***rac*-[143]** into the acetate **[144]**. The first two were chosen as they gave very good results on the related substrate in the literature[169] and the latter Amano Lipase because we have had good experience with this particular Lipase in past projects in our research group. ***rac*-[143]** was dissolved in DIPE (20 mM), which is a common solvent in Lipase catalyzed acetylation. The respective Lipase (100 w%) and vinyl acetate (10 equiv.) were added and the mixture was stirred at room temperature. To our delight, all three Lipases showed conversion according to TLC analysis. Among the used Lipases, the Amano Lipase gave the best selectivity (see **Table 13**).

Table 13: First attempt to enantioselectively acetylate ***rac*-[143]** by three different Lipases.

Lipase	time (h)	conv. (%)	remaining alcohol ee (%)	acetate ee (%)
Amano	16	16	12	89
CAL-A	1	48	25	35
CAL-B	3	30	25	79

In order to optimize the reaction conditions towards the desired absolute configuration dictated by paroxetine's absolute configuration, we needed to assign absolute configuration to our literature-unknown compounds and determine the Lipase's stereo-preference. We intended to transfer an enantiomerically enriched compound into a substance known to the literature; by comparison of the respective optical rotations we would then be able to assign absolute configuration.

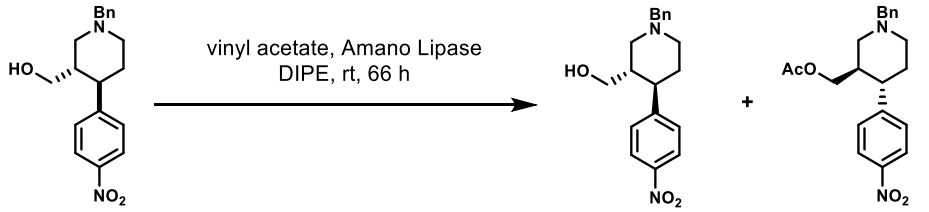

rac-[143] (3*S*,4*R*)-[143] (3*R*,4*S*)-[144]

43 % 55 %
56 %ee 89 %ee

In a preparative experiment, 100 mg of the starting material ***rac*-[143]** were used as described before and after conversion reached 55% as monitored by chiral HPLC, the catalyst was removed by filtration through celite. Volatiles were removed in vacuo and after purification by flash column chromatography 43 mg of unreacted alcohol **[143]** with an ee of 56% and 62 mg of acetate **[144]** with an ee of 89% were isolated.

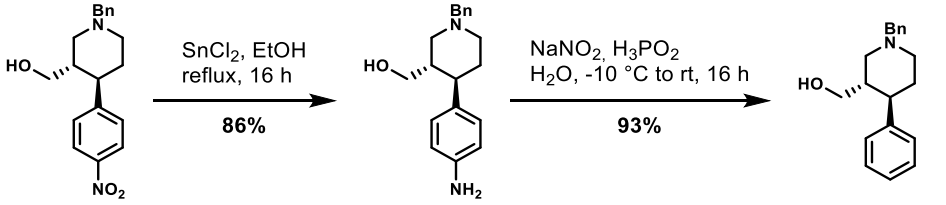

(3*S*,4*R*)-[143] (3*S*,4*R*)-[160] (3*S*,4*R*)-[163]

56 %ee 56 %ee 56 %ee

$SnCl_2$ (4 equiv.) was added to a solution of the enantiomerically enriched alcohol (56% ee) in EtOH and the mixture was stirred at reflux temperature for 16 hours. The aniline **[160]** was obtained as a pure product in 86% yield after extractive work-up. This material was then dissolved in 50% H_3PO_2 (1.11 mL) and H_2O (0.37 mL) and the solution was cooled to -10 °C. An aqu. solution of $NaNO_2$ (1 equiv.) was added to this solution. The reaction was stirred for 16 hours. Extraction afforded pure product **[163]** in 93% yield. The specific optical rotation was determined ($[\alpha]_D^{23}$ = -8.2, c = 1.0, $CHCl_3$, 56% ee) and compared with the literature value[171] for compound **[163]** with an absolute configuration of (3*R*,4*S*) ($[\alpha]_D^{23}$ = +15.1, c = 1.0, $CHCl_3$, 90% ee). As the synthesized material had the opposite optical rotation it was concluded that the Amano Lipase preferably acetylates the alcohol with (3*R*,4*S*) configuration and, hence, the remaining alcohol can be obtained in the desired (3*S*,4*R*) configuration of clinically used paroxetine. In contrast to that, the other two Lipases, CAL-A and CAL-B, had the opposite stereo-preference and preferentially acetylated the (3*S*,4*R*)-alcohol.

In an effort to optimize the stereoselectivity of the used Lipases, we varied the solvent in the acetylation reaction. **Table 14** summarizes the results of this screening. Reactions were run until approximately 50% conversion for a maximum of 72 hours while monitored by chiral HPLC. The two Lipases CAL-A and CAL-B displayed higher activity and converted alcohol ***rac*-[143]** faster but with poorer selectivity compared to the Amano Lipase which gave reasonable

selectivity but exhibited slow conversion. Reactions in THF and DCM turned out to be very slow with less than 5% conversion after 48 hours in most cases. When the acetate donor vinyl acetate (VA) was used as solvent, selectivity dropped considerably. Promising results were obtained with the Amano Lipase in MTBE, toluene and DIPE.

Table 14: Results of the solvent screening in the Lipase catalyzed acetylation of alcohol ***rac*-[143]**. Conditions were as before: concentration of 20 mM, 100 w% Lipase, 10 equiv. vinyl acetate, room temperature.

				remaining alcohol		**acetate**	
Lipase	**solvent**	**time (h)**	**conv. (%)**	**config.**	**ee (%)**	**config.**	**ee (%)**
Amano	MTBE	48	44	(3*S*,4*R*)	46	(3*R*,4*S*)	85
CAL-A	MTBE	1	44	(3*R*,4*S*)	8	(3*S*,4*R*)	14
CAL-B	MTBE	3	47	(3*R*,4*S*)	47	(3*S*,4*R*)	72
Amano	toluene	48	16	(3*S*,4*R*)	14	(3*R*,4*S*)	92
CAL-A	toluene	3	38	(3*R*,4*S*)	23	(3*S*,4*R*)	48
CAL-B	Toluene	3	16	(3*R*,4*S*)	11	(3*S*,4*R*)	77
Amano	DIPE	72	47	(3*S*,4*R*)	48	(3*R*,4*S*)	90
CAL-A	DIPE	1	48	(3*R*,4*S*)	25	(3*S*,4*R*)	35
CAL-B	DIPE	3	30	(3*R*,4*S*)	25	(3*S*,4*R*)	79
Amano	VA	25	4	(3*S*,4*R*)	2	(3*R*,4*S*)	74
CAL-A	VA	2	23	(3*R*,4*S*)	10	(3*S*,4*R*)	43
CAL-B	VA	25	18	(3*R*,4*S*)	10	(3*S*,4*R*)	65
Amano	THF	48	<5	-	-	-	-
CAL-A	THF	48	<5	-	-	-	-
CAL-B	THF	48	15	(3*R*,4*S*)	11	(3*S*,4*R*)	83
Amano	DCM	48	<5	-	-	-	-
CAL-A	DCM	48	<5	-	-	-	-
CAL-B	DCM	48	16	(3*R*,4*S*)	11	(3*S*,4*R*)	75

For the synthesis of a preparative amount of the desired chiral alcohol, the reaction in toluene was considered too slow. As the reaction in DIPE featured better selectivity, we opted to use this solvent within the optimized protocol. In order to shorten the reaction time, we increased the concentration to 50 mM and used 200 w% of the Amano Lipase.

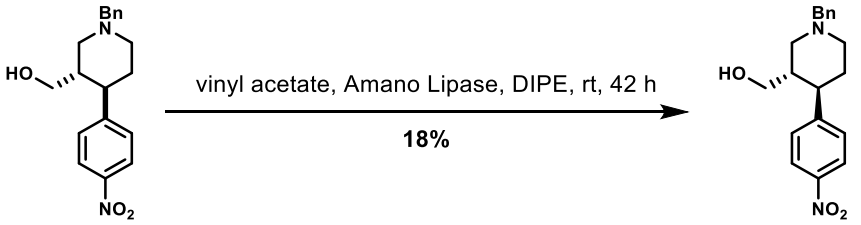

rac-[143] (3*S*,4*R*)-[143]

94% ee

500 mg ***rac*-[143]** were dissolved in DIPE (30.6 mL, 50 mM) and vinyl acetate (10 equiv.) and Amano Lipase (1000 mg) were added and after stirring the suspension for 42 hours at room temperature the suspension was filtered through a pad of celite. Separation by flash column chromatography provided 91 mg of pure chiral alcohol **(3*S*,4*R*)-[143]** with an ee of 94%. The obtained yield of 18% from a theoretical maximum of 50% yield is only moderate but was attributed to the generally poorer selectivity for Lipases when using primary alcohols as substrates. In the future, the reaction should be carried out at lower temperature in order to achieve better selectivity. 15 °C proved to be a reasonable compromise in preliminary experiments. Another option would be to re-visit the reaction in MTBE or even toluene under same considerations.

With the chiral alcohol **(3*S*,4*R*)-[143]** in hand, we were now ready to move on in our synthetic plan to prepare the next intermediate and introduce the benzodioxol fragment. In order to form the ether linkage, the alcohol should be transformed into the corresponding mesylate which turns the alcohol into a powerful leaving group that can be substituted with the appropriate nucleophile.[172]

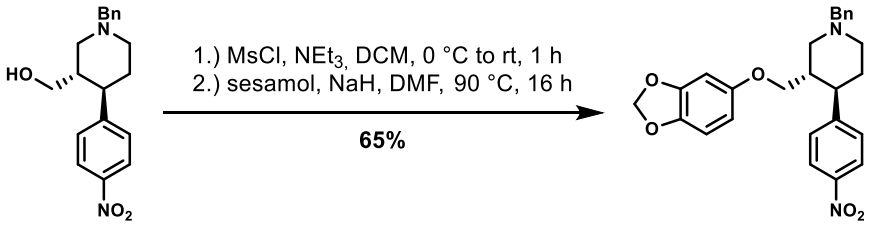

(3*S*,4*R*)-[143] [145]

Chiral alcohol **(3*S*,4*R*)-[143]** was dissolved in dry DCM and MsCl (1.44 equiv.) and NEt_3 (1.44 equiv.) as the base were added at 0 °C under argon. The reaction was stirred at room temperature until TLC analysis showed full conversion and the mesylate intermediate was obtained after extraction. In order to turn the phenol into a stronger nucleophile, it can be deprotonated with a strong base. Sesamol was dissolved in dry DMF and NaH (equimolar) was added at 0 °C under argon. This solution was stirred at room temperature for 20 minutes and afterwards a solution of the mesylate in dry DMF was added and the reaction was stirred at 90 °C until TLC analysis showed full conversion. Excessive sesamol was removed by washing with 1 N NaOH in the extractive work-up and purification of the crude material by flash column

chromatography in silica gel provided the ether **[145]** in 65% yield. In the next step, the nitro substituent should be reduced to the corresponding amine. Reduction with hydrogen, catalyzed by Pd/C is a versatile method for this transformation. In this case, it is a particularly good choice as we could simultaneously cleave the benzyl protecting group and thereby, save one synthetic step in the overall synthesis if the secondary amine does not require protection anymore. In case this proves to be not the case, alternative methods for the reduction of the nitro group in the presence of the benzyl protected amine exist. For example $SnCl_2$ was used in the preparation of aniline **[160]**.

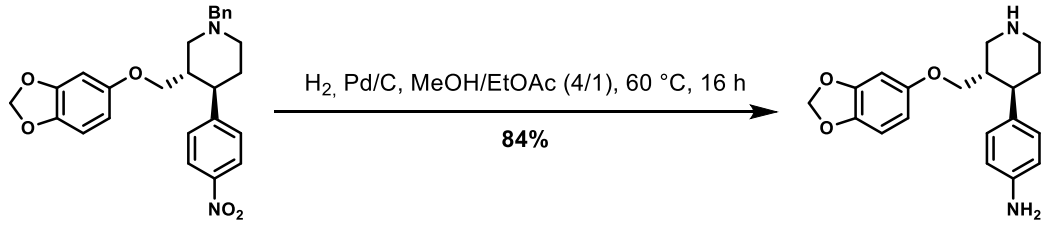

[145] [146]

The starting material **[145]** was dissolved in MeOH/EtOAc (4/1). The EtOAc was necessary in order to dissolve the material completely. 10% Pd/C (10 mol%) was added and the suspension was stirred under an atmosphere of hydrogen while heated with an oilbath to 60 °C. TLC analysis showed full conversion after stirring the reaction over night and solids were subsequently removed by filtration through celite. The crude material was purified by flash column chromatography on silica gel. Due to the very polar character of the obtained compound, a mixture of $CHCl_3$/MeOH/NH_4OH (80/20/1) was used as the eluent which gave very good results for polar compounds. Aniline **[146]** was obtained in wonderful 84% yield. After successful installation of the aniline, the right nucleophile was now in place for the envisaged condensation with nitrosobenzenes. As the Mills reaction is typically conducted in AcOH, we expected the secondary amine to get protonated under the reaction conditions. Protonation would render the secondary amine non-nucleophilic while the aniline would undergo the desired transformation.

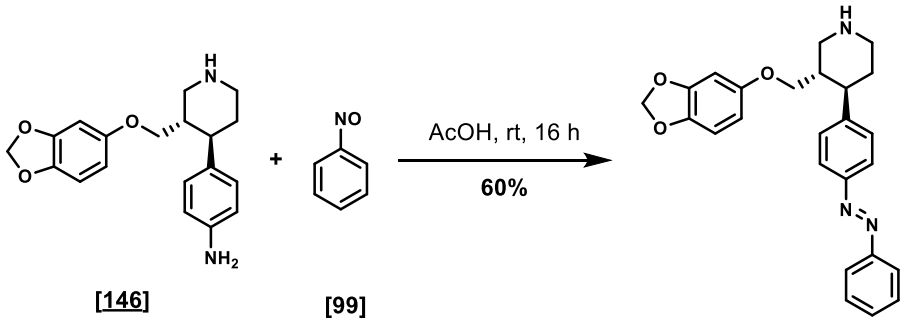

[146] [99] [147]

Nitrosobenzene **[99]** (2 equiv.) was added to a solution of aniline **[146]** in AcOH. The solution was stirred at room temperature over night whereupon the solution had turned

orange which hinted formation of an azo compound. TLC analysis indicated full consumption of starting material. After extractive work-up and purification by flash column chromatography on silica gel ($CHCl_3$/MeOH/NH_4OH = 100/10/1) the target compound **[147]** was isolated in 60% yield.

In summary, the paroxetine based azo photoswitch **[147]** (94% ee) was successfully synthesized in a de-novo synthesis over 8 steps in 2.8 % overall yield starting from 4-nitrocinnamic acid **[140]** with the enzymatic kinetic resolution of key intermediate ***rac*-[143]** being the bottle neck.

C II.3.4 Photophysical characterization

As in previous chapters (see **C II.1.3**), azo compound **[147]** was photophysically characterized. Spectra were recorded in DMSO (50 μM) and in KHP buffer + 1% DMO (10 μM). The results are displayed in **Figure 72**. As it was expected for a typical azobenzene bearing a substituent with little influence on the photophysical parameters (see chapter **C I.1.2**), photoswitch **[147]** features a λ_{max} of 331 nm in DMSO and 328 nm in the aqu. buffer (comparable to azobenzene's 323 nm in DMSO, data not shown). Irradiation with 365 nm was very effective in switching the compound to the corresponding (*Z*)-isomer. Light of 400 nm and 460 nm was able to switch the (*Z*)-isomer back to the relaxed (*E*)-isomer. The thermal half life time in DMSO was determined to be 6.5 days (k = 1.2 * 10^{-6} s^{-1}) in DMSO and comparable 8 days (k = 1.0 * 10^{-6} s^{-1}) in the KHP buffer which makes the paroxetine based azo compound very bistable (**Figure 73**).

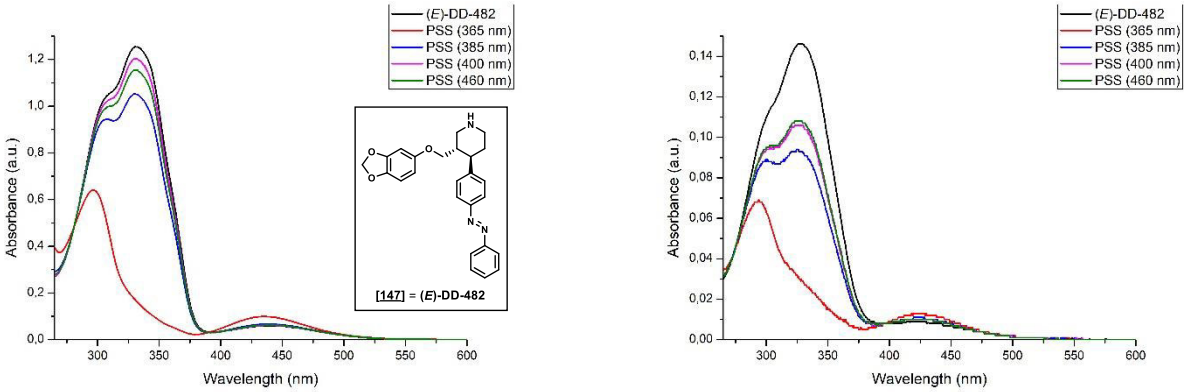

Figure 72: UV-Vis absorbance spectra of photoswitch **[147]** in the dark and after irradiation with 365 nm, 385 nm, 400 nm and 460 nm in DMSO and KHP buffer + 1% DMSO.

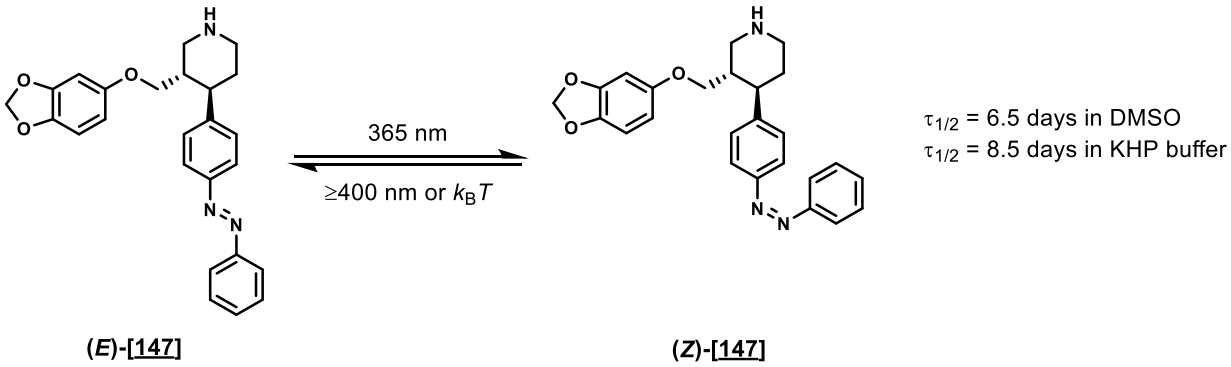

Figure 73: Photoswitch **[147]** can be switched effectively with 365 nm and possesses a long half life time.

C II.3.5 Biological evaluation

With the novel photoswitch **[147]** in hand, we conducted a comprehensive biological assessment. The compound's ability to inhibit the reuptake of the associated neurotransmitter was measured on hSERT and hNET; both in its natural (*E*)-configuration as wells as its excited (*Z*)-configuration. For the photodependent measurement under the influence of light of 365 nm, our newly constructed UV-LED well plate (365 nm) was used (see **C III**). In 96-well plates the cells, over-expressing the corresponding transporter, were grown. The cells were pre-incubated with a dilution series of the compound in KHP buffer + 1% DMSO for 10 minutes to reach the equilibrium binding to the transporter dependent on the concentration. The solution was removed and the same dilution series containing the corresponding radioactively labeled neurotransmitter was added to enable reuptake into the cells for a certain time (typically 1 – 3 minutes). The solution was removed again to stop the reuptake process and the cells were washed with buffer. Afterwards, the cells were disrupted and the radioactivity was measured. Higher radioactivity equals more radioactively labeled neurotransmitter inside the cells and therefore, a worse inhibition of reuptake. For the blank value, a high concentration of a very potent inhibitor was used (e.g. 30 μM paroxetine for hSERT). The measured values were used to create dose-response curves and the respective IC_{50} was determined. This assay was carried out conventionally to assess the activity of the (*E*)-isomer and with the UV-LED well plate (365 nm), applying 20 V and 0.23 A, to assess the (*Z*)-isomer.

As mentioned in the beginning, the SERT is of highest interest and as paroxetine is a representative of the SSRIs and the ligand design was based on structural hSERT data, we hoped to observe a photodependent behavior on hSERT and less activity on the two other transporters, hNET and hDAT. The crucial dose-response curves on hSERT are depicted in **Figure 74**. To our utmost delight and the author's personal relief, the results were very encouraging. **[147]** in its stable (*E*)-configuration showed an IC_{50} of 8.7 μM while the potency increased by more than one order of magnitude to 0.8 μM when measured under the

influence of 365 nm on the UV-LED well plate (365 nm). Irradiation with this wavelength makes the compound a much better inhibitor. Therefore, we hoped to photo-block serotonin reuptake with this novel tool compound.

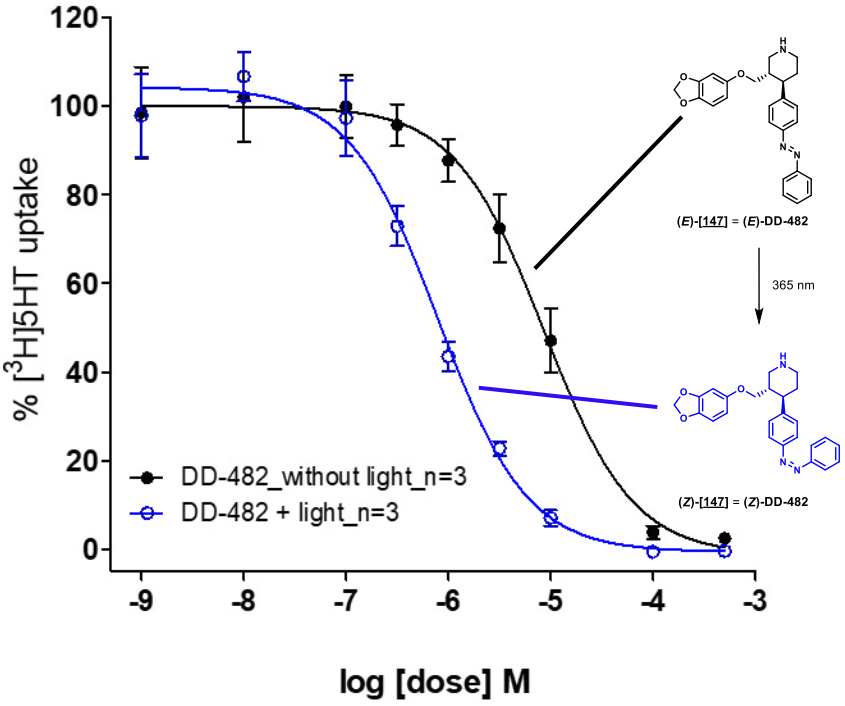

Figure 74: Dose-response curve of photoswitch **[147]**. The relaxed (*E*)-isomer displayed an IC_{50} of 8.7 µM which was improved by approximately one order of magnitude to 0.8 µM when the compound was irradiated with 365 nm.

On hNET, the compound showed reasonable activity as well as a photo effect, albeit to a smaller extent. Without any influence of artificial light, the IC_{50} was determined to be 14 µM which improved to a more potent IC_{50} of 2.6 µM when irradiated with 365 nm as before (data not shown). When this thesis was submitted, no data on hDAT was yet available.

To support the new data, we conducted a number of control experiments. Under our assay conditions, the parent compound paroxetine produced an IC_{50} of 56 nM (n = 4) when not irradiated and a value of 64 nM (n = 4) when irradiated with 365 nm and hence, displayed no photo dependent behavior as expected. Azobenzene gave no inhibition on hSERT; neither without nor under irradiation with 365 nm. On hNET an IC_{50} of 2.7 µM (n = 3) and on hDAT an IC_{50} of 15 µM (n = 3) were measured for paroxetine.

In order to further evaluate the compound's ability to block the transporter, we performed electrophysiology experiments with the whole cell patch clamp technique. Upon administration of serotonin the SERT displays currents. These currents arise when all transporters enter the transport cycle. During each cycle one serotonin molecule is transported into the cell and released from the inward facing conformation together with one Na^+ and one Cl^- ion. The transporter then returns to the outward facing conformation loaded with K^+. The currents carried by SERT are comprised of two components: an initial peak current

and a steady state current. The initial peak current represents a synchronized conformational change during which the substrate is carried through the membrane. The steady state current is a read out of transporters operating in the forward transport mode. Inhibitors of substrate uptake block the steady currents carried by SERT. The apparent association rate of an inhibitor can be estimated by measuring the time required to reach a steady level of current block. The dissociation rate of the inhibitor on the other hand can be obtained by measuring the time of current recovery following removal of the inhibitor from the bath solution. We analyzed the level of current block upon administration of the two isomers of **[147]**, respectively. While 10 µM of the active form **(*Z*)-[147]** fully blocked the current, the same concentration of the inactivate form **(*E*)-[147]** had no effect (see **Figure 75**) which further demonstrates the potential of the photoswitchable SERT inhibitor.

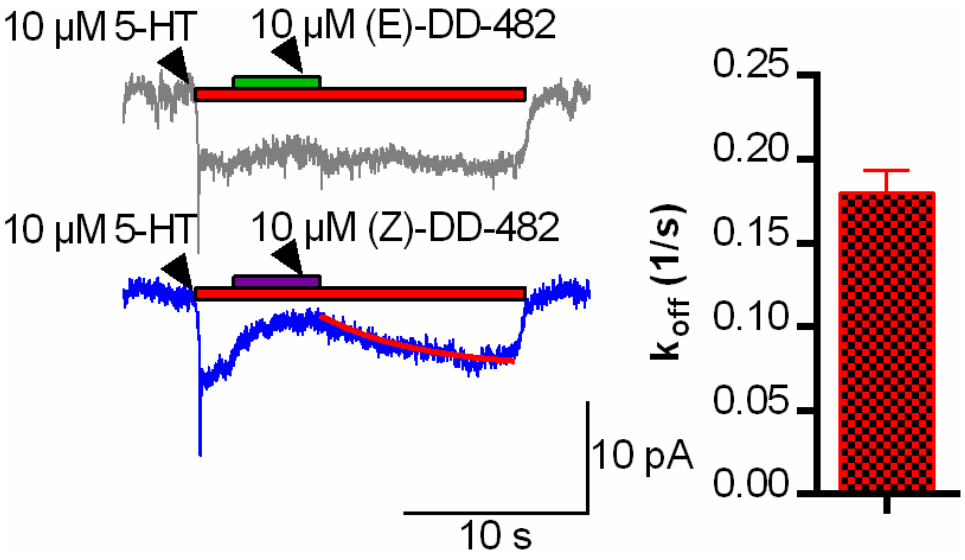

Figure 75: Electrophysiology experiments demonstrated that **(*Z*)-[147]** blocks the transporter (blue curve) while **(*E*)-[147]** does not (grey curve). The dissociation rate k_{off} of **(*Z*)-[147]** was obtained by measuring the time of current recovery.

The absence of blockage in the electrophysiology experiments with **(*E*)-[147]** was considerably intriguing as the previously determined IC_{50} of 8.7 µM could result in some activity under the applied conditions. To rule out the influence of toxicity on the dose response curve, we conducted a toxicological study (trypan blue accumulation by dead cells, see **Figure 76**). No alarming toxicity was observed.

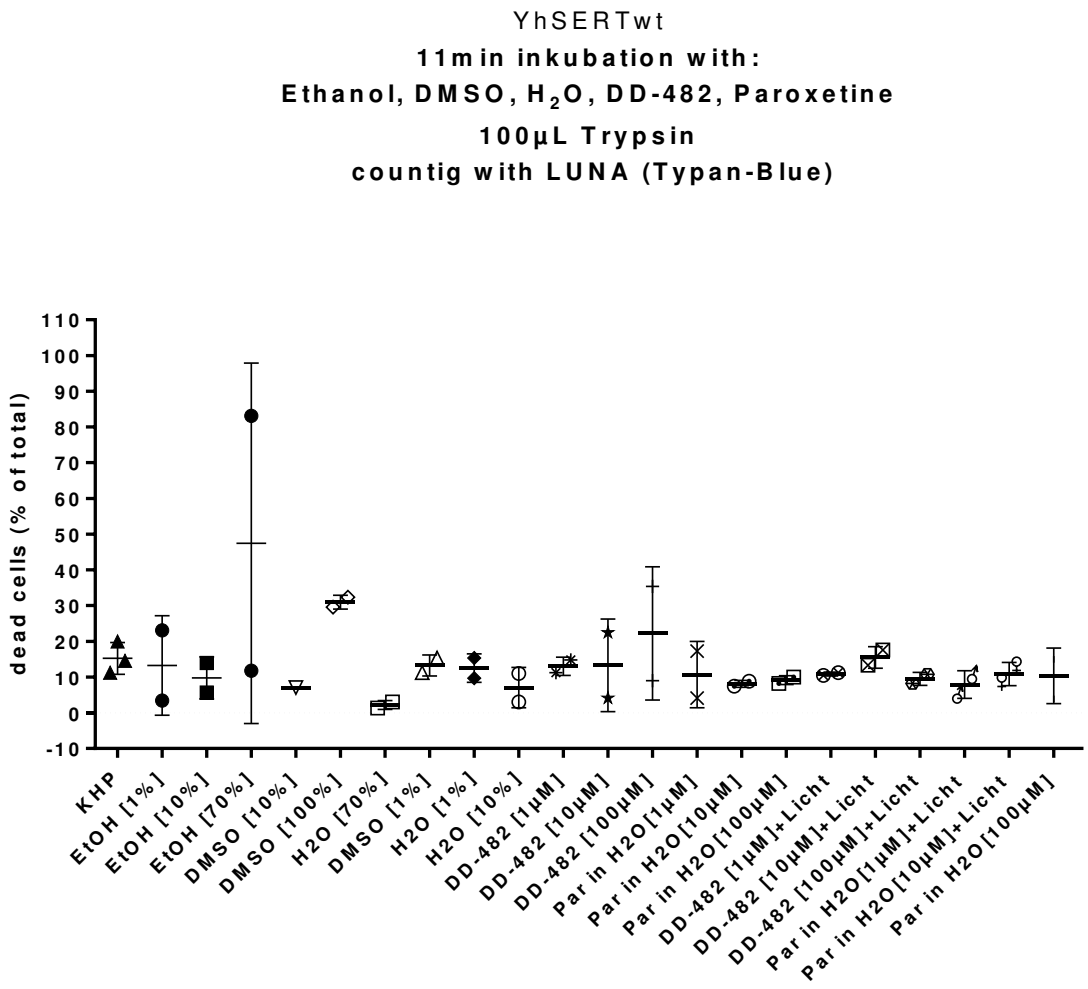

Figure 76: The conducted cell viability assay showed no significant toxicity. Dead cells accumulate the dye trypan blue and can be distinguished from viable cells.

C II.3.6 Computational studies

In order to get a better understanding of the molecular reasons for the observed potency difference of **(*Z*)-[147]** and **(*E*)-[147]** on hSERT, we decided to carry out molecular docking studies[173]. The crystal structure of ts3 hSERT complexed with paroxetine at the central binding site (protein data bank ID: 5I6X, resolution: 3.14 Å) was used for docking. The ts3 structure is a thermostabilized variant of the wild-type hSERT featuring some thermostabilizing mutations necessary for successful crystallization.[9] The protein was prepared with the ligand inside the protein complex using the Preparation Wizard implemented in the Schrödinger Suite.[174] During the preparation, hydrogen atoms were added and optimal protonation states were determined, followed by energy minimization.

Four compounds were applied in these docking studies (see **Figure 77**): paroxetine, **[147]**, the corresponding *meta*-analog **[XXV]** and *ortho*-analog **[XXVI]**. The photoswitches were used in their (*E*)-configuration as well as their (*Z*)-configuration. In chapter **C II.3.1** we argued that the synthesis of *para*-substituted **[147]** would probably be more straight-forward

than the synthesis of *meta*-analog **[XXV]** and *ortho*-analog **[XXVI]**. However, if the docking results would indicate that one of the two hypothetical molecules or both are interesting in terms of expected activity and pronounced difference of the two photo-isomers, we would consider a de-novo synthesis in follow-up projects based on the established biological performance of the para-scaffold.

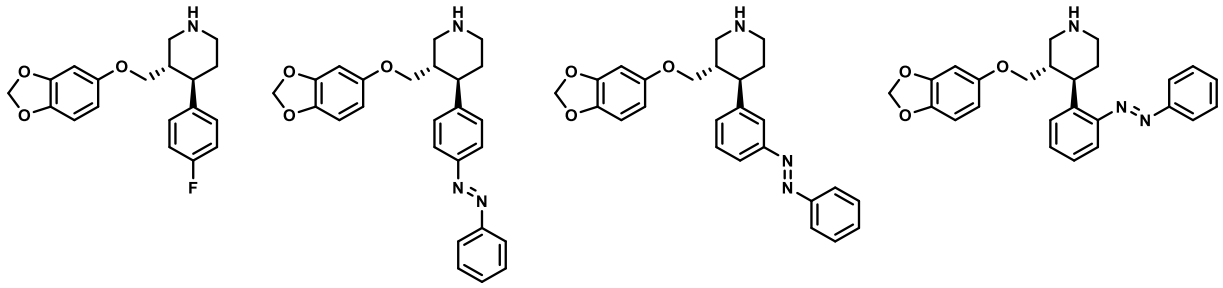

Figure 77: Paroxetine and the photoswitches **[147]**, **[XXV]** and **[XXVI]** were used in docking studies on hSERT.

The binding site for paroxetine and its analogs was defined by the 25 residues around the central binding site within a distance of 4.5 Å: TYR95, ALA96, ASP98, ARG104, ILE168, ALA169, ILE172, ALA173, SER174, TYR175, TYR176, PHE335, SER336, LEU337, GLY338, PHE341, VAL343, GLY435, SER438, SER439, ALA441, GLY442, LEU443, THR497, and VAL501.

The docking studies were carried using GOLD 5.1[175], Autodock 4.2[176], and Autodock Vina 1.1[177]. The Autodock and Autodock Vina were implemented in the Ligandscout 4.1 software package[178]. In the parameter settings of GOLD, genetic algorithm (GA) was used in the docking and the maximum number of the generated poses was set to 100. "Allow early termination" was deactivated and all the remaining parameters were left as default.

In GOLD, for each ligand, 100 docking poses were generated. GOLD PLP was used as scoring function. On basis of the common scaffold, an RMSD (root-mean-square deviation) matrix of all four ligands (including the redocking of paroxetine) was generated and used for clustering. The matrix was clustered with the software RStudio using hierarchical clustering algorithm in which complete linkage was used for merging the clusters. A threshold of 3 Å was set to cut the cluster tree. RMSD calculations between the common scaffolds of all docked poses and paroxetine in the crystal structure was performed using the inbuilt function in the Schrödinger Suite, as we assume that the shared scaffold will be orientated in the pocket in a similar fashion as in the crystal structure. MM/GBSA (Molecular Mechanics/Generalized Born Surface Area) calculations[179, 180] were performed to estimate the binding free energy of the best pose of each ligand for the comparison of the (*E*)- and (*Z*)-configuration.

The poses in two of the largest clusters (#1 and #11) had the lowest mean (1.68±0.48 and 1.95±0.44 Å) RMSD compared to the paroxetine pose in the crystal structure. In addition, these two clusters also showed highest GOLD PLP fitness (89.2±6.6 and 86.5±6.6), indicating

that the poses of these two clusters fit the paroxetine binding pose in the crystal. Only two poses of **(*E*)-DD-482** were found in these two clusters while 32 poses of **(*Z*)-DD-482** were found. These two poses of **(*E*)-DD-482** had a mean RMSD of 1.88 Å and a GOLD PLP fitness of 83.0, while the 32 poses of **(*Z*)-DD-482** had a much lower mean RMSD (0.84 Å) and a higher GOLD PLP fitness (86.1). These results could explain the increased activity of **(*Z*)-DD-482** compared to **(*E*)-DD-482**, most probably due to a better fit in the pocket as indicated by the lower RMSD value (relative to the paroxetine pose in the crystal structure).

The best poses (lowest RMSD) derived from Autodock and Autodock Vina docking results also agree with the results above in terms of RMSD values. **(*Z*)-DD-482** has a significantly lower RMSD compared to **(*E*)-DD-482** (1.62 Å to 2.27 Å in Autodock and 1.32 Å to 3.92 Å in Autodock Vina). Clustering analysis was not performed in Autodock and Autodock Vina as they normally only produce 10 to 20 poses for each ligand, which were too few for clustering.

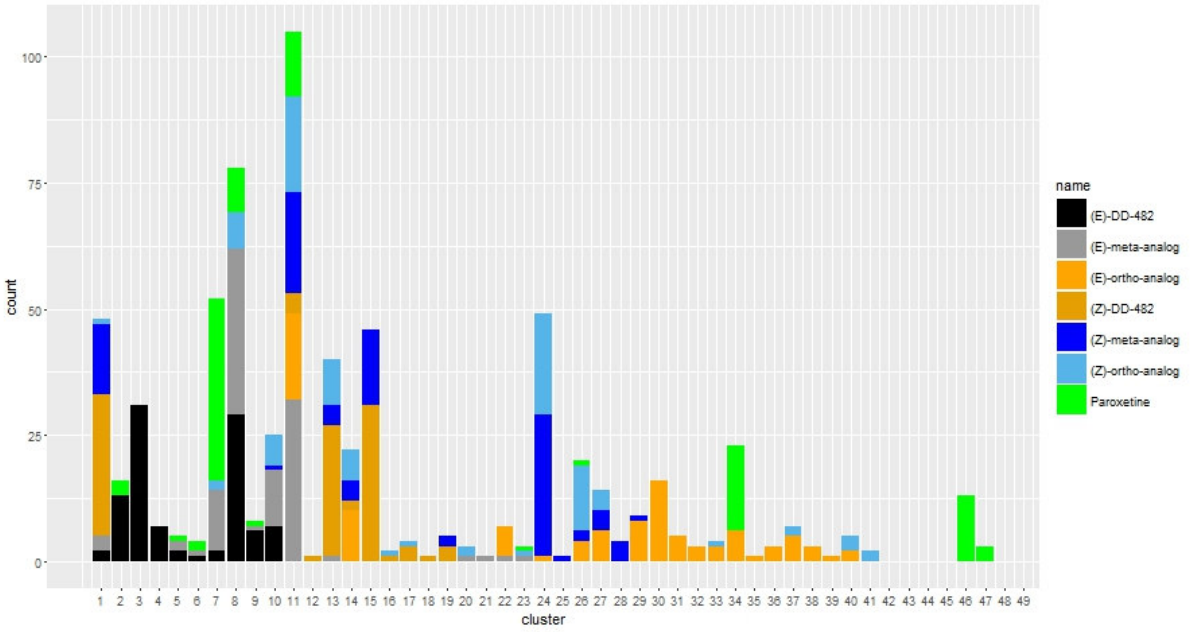

Figure 78: Common scaffold clustering of poses of paroxetine, **DD-482** and its hypothetical analogs in GOLD.

(*Z*)-DD-482 (-75.5 kcal/mol in GOLD and -71.1 kcal/mol in Autodock) exhibits lower MM/GBSA binding energy compared to paroxetine (-67.7 kcal/mol in GOLD and -35.4 kcal/mol in Autodock) and **(*E*)-DD-482** (-61.5 kcal/mol in GOLD and -61.8 kcal/mol in Autodock), implying higher binding affinity of **(*Z*)-DD-482**. Using Autodock Vina, **(*E*)-DD-482** has lower binding energy, which is different compared to the results above. This is most likely because the **(*E*)-DD-482** pose in Autodock Vina was significantly different compared to the Gold and Autodock poses (compare the poses for **(*E*)-DD-482** in **Figure 79**).

Visual inspection of (*E*)- and (*Z*)-poses showed that the benzodioxol moiety of **(*E*/*Z*)-DD-482** is positioned in the hydrophobic ridge formed by Ile172 and Phe341 in sub-pocket B

(compare to **Figure 64**) whereas the amine group of the piperidine moiety is positioned in sub-pocket A forming a hydrogen bond with the sidechain of Tyr497 (see **Figure 79**). The hydrogen bond with the sidechain of Asp98 shown in the crystal structure is not observed due to the unfavorable rotamer position of Asp98. Further inspection of sub-pocket B revealed that the azobenzene fragment of the (*E*)-configuration needs to shift towards the extracellular vestibule in order to be accommodated because the space of sub-pocket C is limited by Thr497 and Gly498. This leaves sub-pocket C unoccupied which accounts for the unfavorable inhibitory activity (IC_{50} = 8.7 μM) of **(*E*)-DD-482**. The (*Z*)-configuration of the azobenzene fragment allows still a partial occupation of sub-pocket C because the azobenzene moiety can be oriented toward the extracellular vestibule without sterically interfering with Thr497 and Gly498. The partial occupations of sub-pocket C also explains the higher activity of **(*Z*)-DD-482** (IC_{50} = 0.8 μM) compared to **(*E*)-DD-482**, but also the lower activity compared to paroxetine (IC_{50} ≈ 60 nM). The docking pose for **(*E*)-DD-482** created by Autodock Vina has to be disregarded as (*E*)-azobenzenes are planar and the program allowed twisted conformations.

In summary, these docking results are able to explain the observed activity difference between **(*E*)-DD-482** and **(*Z*)-DD-482**. We believe that the (*Z*)-configuration shows better activity as this compound can adopt a conformation much more similar to the paroxetine crystal structure than the (*E*)-configuration. **(*Z*)-DD-482** is able to significantly occupy sub-pocket C while the occupation of that pocket by **(*Z*)-DD-482** is sterically hindered. Furthermore, MM/GBSA calculations support this notion by estimating a better binding free energy for the (*Z*)-configuration.

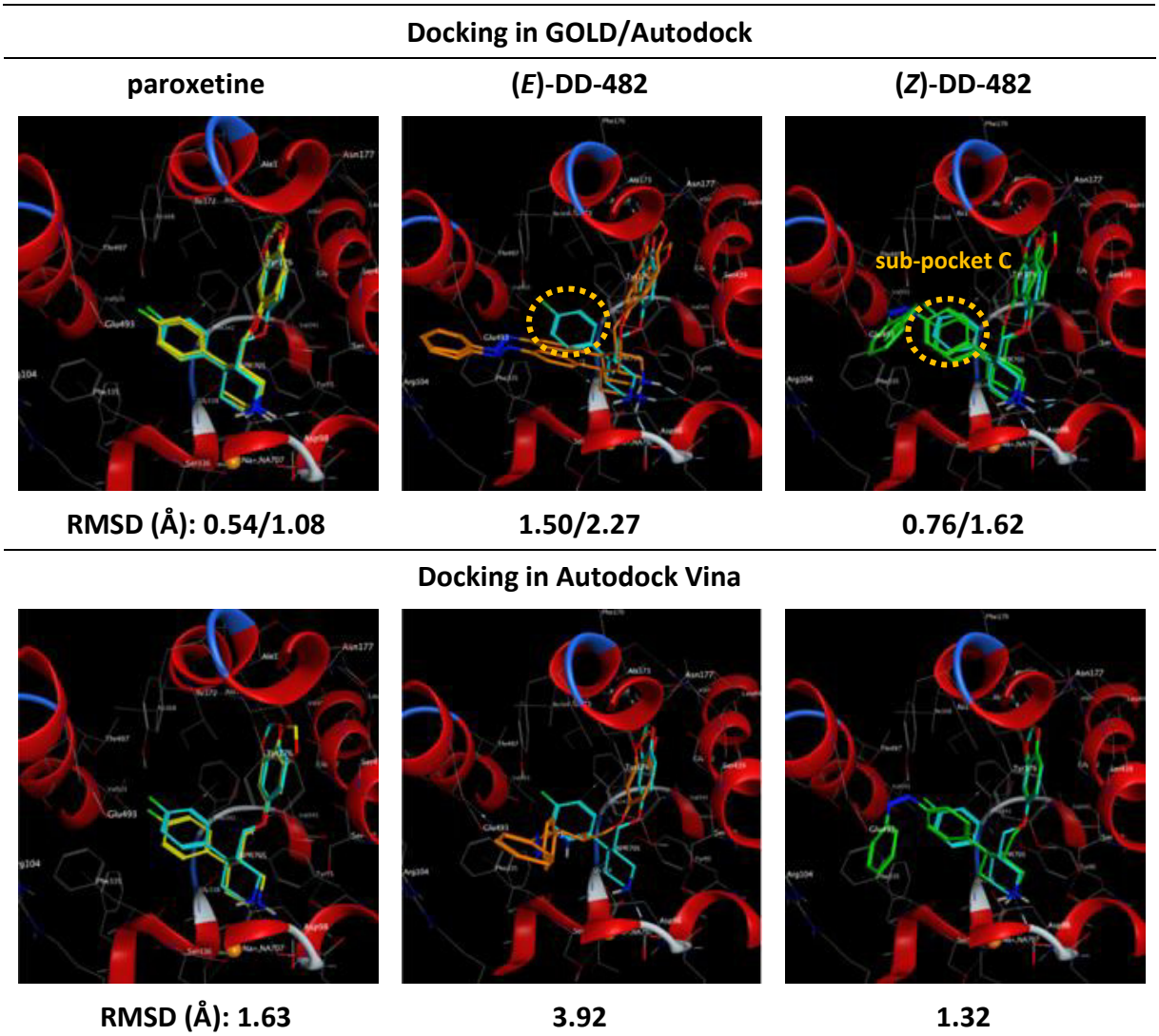

Figure 79: Best docking poses (lowest RMSD) of paroxetine (yellow molecule: docked; cyan molecule: crystal structure pose), **(*E*)-DD-482** (orange molecule) and **(*Z*)-DD-482** (green molecule) in GOLD, Autodock and Autodock Vina with RMSD values. Nitrogen atoms are depicted in blue, oxygen atoms in red.

Regarding the *ortho*- and *meta*-analogs, more poses of the *meta*-analog are found in the important clusters #1 and #11 but a similar number of (*E*)- and (*Z*)-poses is found in these two clusters for both compounds suggesting little light dependency is to be expected. At this stage, the two compounds are not particularly interesting and further research is necessary. Substituted derivatives might be more interesting target compounds and input from ongoing computational studies should guide further synthesis.

C II.4 Paroxetine based HTI photoswitches

C II.4.1 Inhibitor design

After the valuable experience we gained in the total synthesis of paroxetine based azo photoswitch **[147]**, we sought to expand our approach to a HTI version of paroxetine. Considering the line of argumentation in chapter **C II.3.1** (rational design of **[147]**) and in comparison to chapter **C II.2** (escitalopram based HTI photoswitches), the logic target compound was the compound depicted in **Figure 80**.

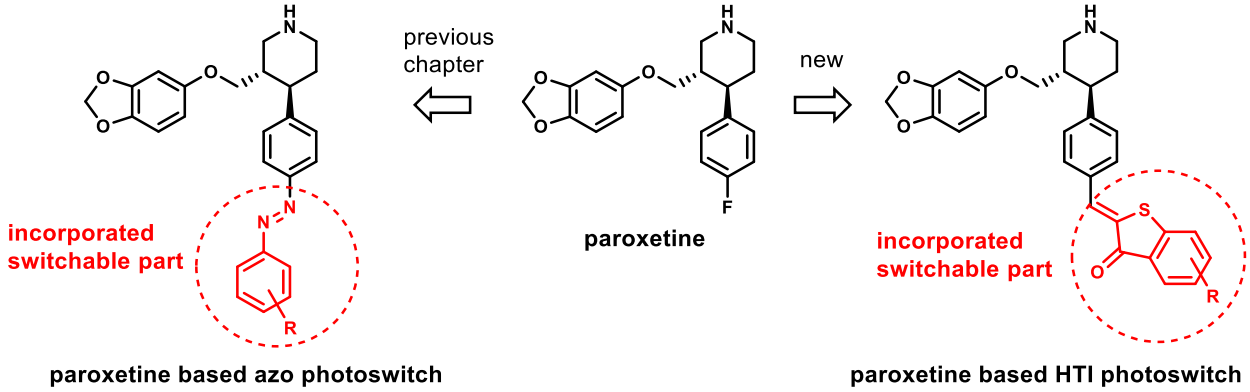

Figure 80: Rationale for a photoswitchable HTI analog of paroxetine.

C II.4.2 Retrosynthetic analysis

As it has already been described in chapter **C II.2.2**, a reliable method to synthesize HTIs is the condensation reaction of a benzaldehyde derivative with an appropriate cyclic ketone. In order to access the envisaged HTI target compound, we would require aldehyde **(3*S*,4*R*)-[154]** and one of the HTI building blocks from previous chapter **C II.2.2** (e.g. compound **[130]**). The benzyl protecting group is required as in the previous synthesis in order to avoid undesired side reactions. One method to synthesize a benzaldehyde derivative is the reaction of the corresponding aryl lithium species with DMF which requires bromo compound **(3*S*,4*R*)-[153]**. This method should be orthogonal to the applied chemistry up to this point as we sought to synthesize bromide **(3*S*,4*R*)-[153]** in analogy to the synthesis of the corresponding nitro compound **[145]** which makes 4-bromocinnamic acid **[148]** a suitable starting material.

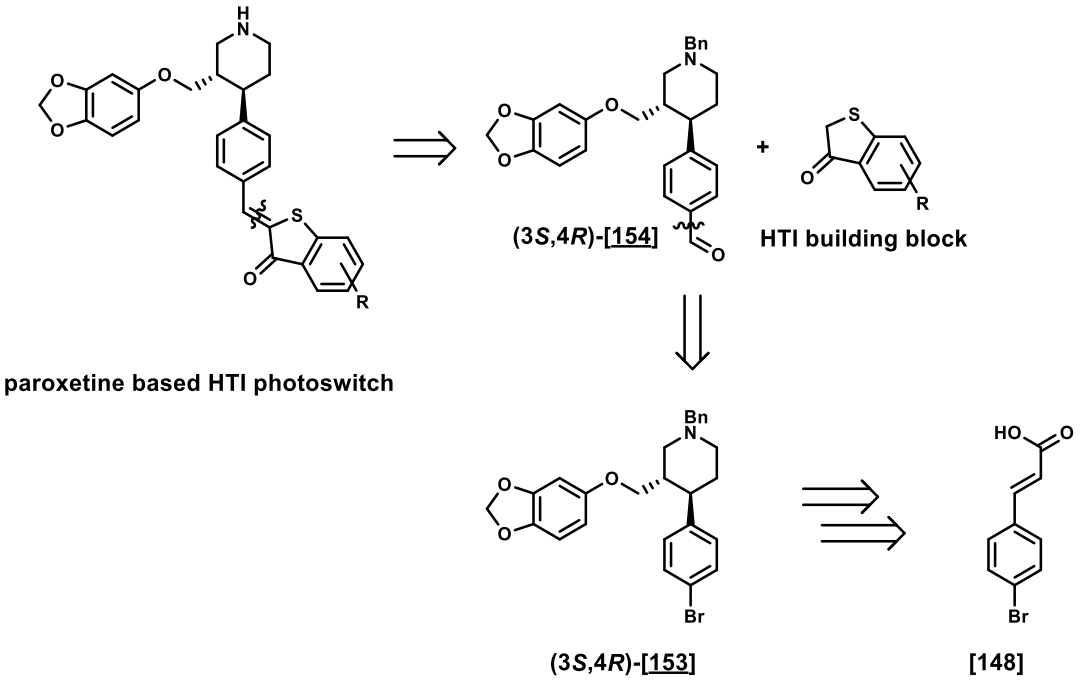

Figure 81: Retrosynthetic analysis of the paroxetine based HTI target compound.

C II.4.3 Synthesis

Transformations already carried out in chapter **C II.3.3** are not discussed in detail as they gave the same characteristics in the following reactions. For more details the reader is referred to the respective previous reactions.

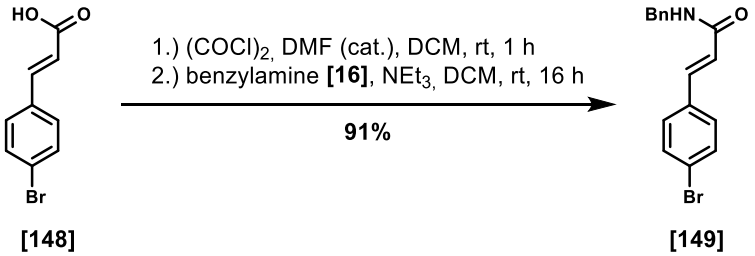

After 4-bromocinnamic acid **[148]** was identified as a convenient starting material, the synthesis of amide **[149]** was the first step of the synthesis. In analogy to the synthesis of the corresponding nitro derivative **[141]**, a suspension of the starting material in dry DCM was reacted with oxalyl chloride under DMF catalysis to afford the acid chloride intermediate. After evaporation of the solvent, the intermediate was dissolved in dry DCM and treated with NEt_3 and benzylamine **[16]**. Stirring over night led to full conversion and the reaction mixture was washed with 1 N HCl and 1 N NaOH to remove acidic and basic impurities. The crude product was isolated by filtration and dried in vacuo. Recrystallization from toluene gave 91% of pure amide **[149]** as colorless needles.

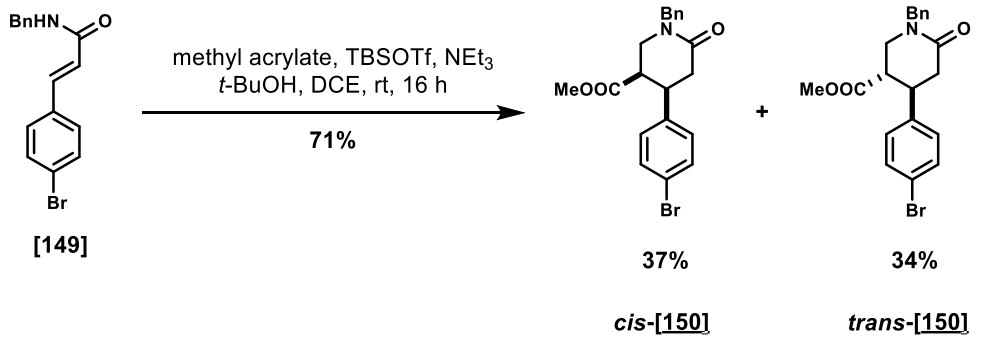

In the next reaction step, reaction of amide **[149]** with methyl acrylate in a double Michael addition led to the formation about equivalent amounts of the two products ***cis*-[150]** and ***trans*-[150]** in a combined yield of 71% under the same conditions as before (TBSOTf, NEt_3, *t*-BuOH in DCE)[164]. The two compounds were isolated separately by flash column chromatography on silica gel.

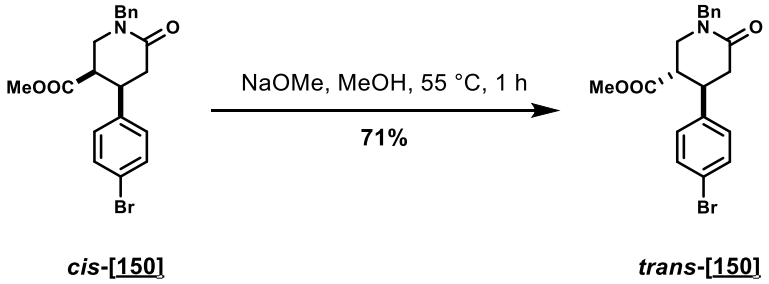

To increase the amount of desired ***trans*-[150]**, ***cis*-[150]** was epimerized with NaOMe in dry MeOH. 71% of ***trans*-[150]** was obtained after chromatographic purification which resulted in a yield of 60% ***trans*-[150]** over the two reaction steps.

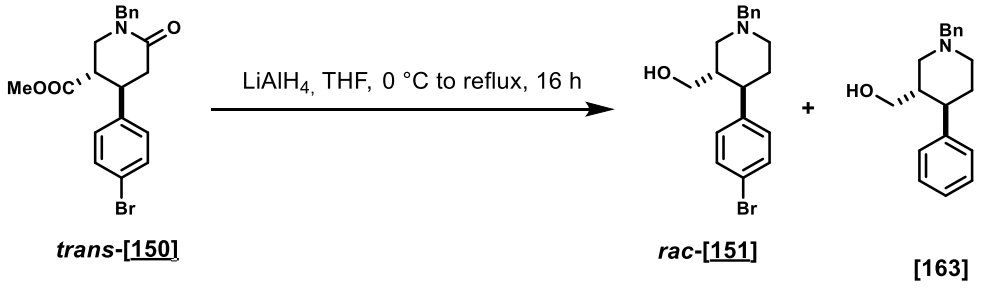

When the reduction of ***trans*-[150]** with $LiAlH_4$ in dry THF was attempted, varying amounts of the debrominated side product **[163]** were obtained which resulted in significant loss of material and, furthermore, the debrominated compound **[163]** co-eluted with the desired product ***rac*-[151]** on silica gel; hence, this approach turned out as not feasible.

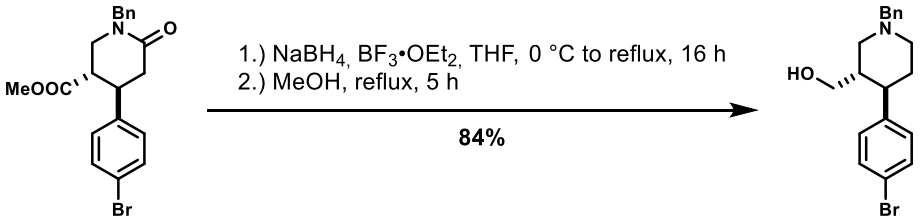

trans-[150] *rac*-[151]

Since the reduction protocol with $NaBH_4$ and BF_3 (in situ generation of BH_3) worked very well in the synthesis of nitro analog ***rac*-[143]**, the same conditions were applied to ***trans*-[150]**. The desired alcohol ***rac*-[151]** was isolated in a very good yield of 84% after purification by flash column chromatography on silica gel.

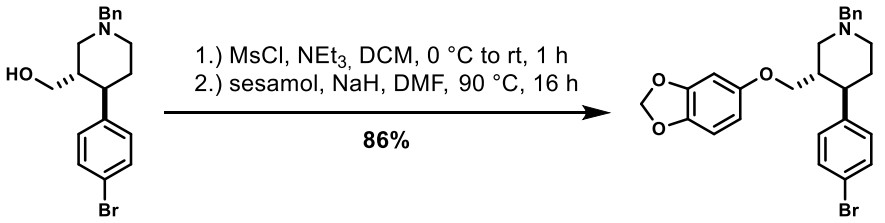

rac-[151] [153]

***rac*-[151]** was then reacted with MsCl and NEt_3 in dry DCM to prepare the corresponding mesylate as an intermediate. The mesylate was isolated by extraction. Sesamol was deprotonated with NaH in dry DMF and a solution of the mesylate in dry DMF was added. The substitution reaction took place at 90 °C and after full conversion, the product was isolated by extraction and subsequent chromatographic purification. A great yield of 86% was achieved. Up to this point the applied protocols were the same as in the corresponding nitro series. With bromide **[153]** in hand, the next step was the crucial introduction of the aldehyde moiety which serves as the necessary handle to introduce the photoswitchable HTI fragment.

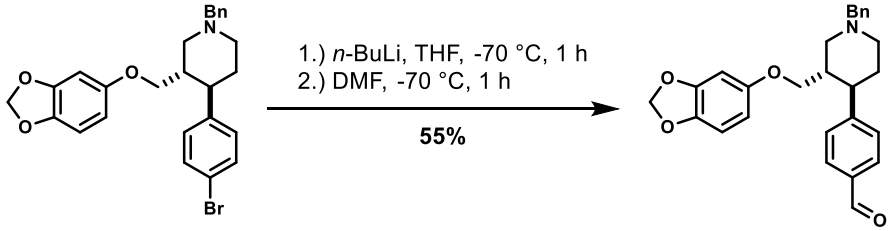

[153] [154]

Bromide **[153]** was treated with *n*-BuLi (1.5 equiv., 1.45 M in hexane) in dry THF at -70 °C (internal temperature) to form the corresponding lithium species via metal halogen exchange. After stirring the reaction at that temperature for one hour, dry DMF (1.05 equiv.) was added and the reaction was stirred at -70 °C for one hour. The reaction was quenched with satd. aqu. NH_4Cl. The crude material was obtained after extractive work-up. Purification by flash column chromatography on silica gel with common LP/EtOAc gave the desired product **[154]** contaminated with a side product. Using toluene/MeCN (2/1) as the mobile

phase, the side product could be isolated which co-eluted with the product **[154]** when using LP/EtOAc mixture. From HPLC-MS, ^{1}H-NMR and ^{13}C-NMR data we concluded, that the side product was the corresponding phenol. In mechanistic terms, a phenol can be formed if the lithium species reacts with oxygen. Therefore, we used degassed solvents (bubbling with argon under sonication for 10 minutes) in an optimized experiment. In this new attempt and using the toluene/MeCN mixture for flash column chromatography we isolated 55% of **[154]**. A considerable amount of debrominated side product reduced the yield which originates from the reaction of the lithium species with residual moisture, which could be subject for future optimization. With the reactive aldehyde **[154]** available, we focused on the condensation reaction to generate the chromophore. As the HTI building block, we used compound **[130]** which was already available from earlier synthetic work (see chapter **C II.2.2**)

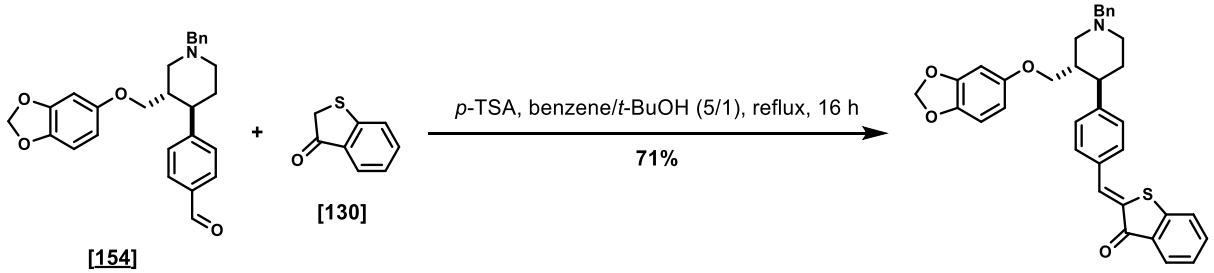

[154] [130] [155]

The aldehyde **[154]** and *p*-TSA (1.5 equiv.) were dissolved in a degassed benzene/*t*-BuOH mixture. HTI building block **[130]** was dissolved under sonication in a degassed benzene/*t*-BuOH mixture and afterwards, the two solutions were combined and stirred at reflux temperature for 16 hours. Volatiles were removed in vacuo and the crude material was purified by flash column chromatography on silica gel with an optimized gradient of toluene/MeCN. The desired product **[155]** was isolated in 71% yield and had the characteristic yellow appearance in isolated form as well as on TLC plates.

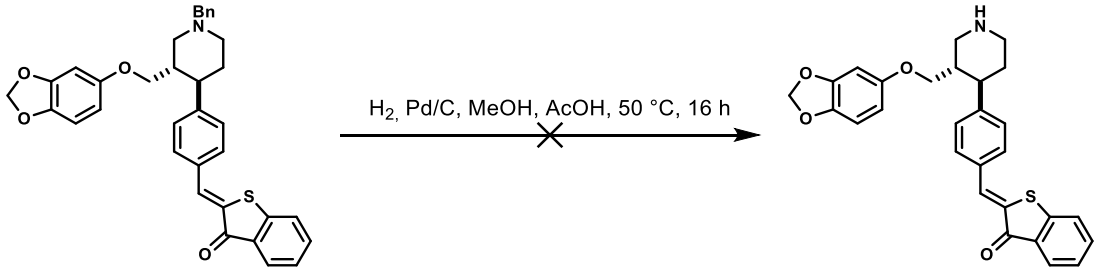

[155] [156]

In order to debenzylate the protected amine, we applied classical hydration conditions. No catalytic hydration in the presence of an HTI fragment was reported in the literature which could be attributed to the sulfur content. Nevertheless, in a small scale experiment, a solution of the starting material **[155]** in MeOH (+ 1 drop of AcOH) was treated with 10% Pd/C. The suspension was stirred under an atmosphere of hydrogen at 50 °C for 16 hours. The desired

product **[156]** could not be obtained. The sulfur containing compound might inhibit the catalytic activity of the Pd/C as it was expected. Therefore, we required non-standard deprotection conditions. A method using 1-chloroethyl chloroformate came to our attention.[181] The reagent can be used to substitute the benzyl residue and form the resulting carbamate as an intermediate which conveniently can be cleaved by heating the compound to reflux in MeOH. The liberated HCl forms a hydrochloride with the product. Basification would deliver the free base.

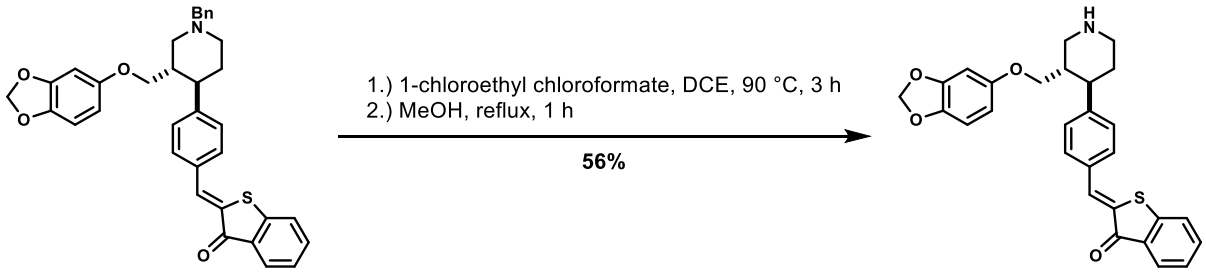

[155] [156]

A solution of the starting material **[155]** in DCE was treated with 1-chloroethyl chloroformate (10 equiv.) at 0 °C and the reaction was stirred at reflux temperature. Volatiles were removed in vacuo after complete conversion (3 hours). Toluene was added and removed in vacuo. This step was repeated two times to completely remove the benzyl chloride byproduct. The isolated intermediate was dissolved in MeOH and heated to reflux temperature. After one hour, TLC analysis indicated complete conversion. After basification, the crude product was isolated by extraction and purification by flash column chromatography on silica gel with $CHCl_3$/MeOH/NH_4OH (100/10/1) afforded 56% of the final product **[156]**. The moderate yield can be attributed to the small scale of the synthesis in this late stage. The racemic target compound, a paroxetine based HTI photoswitch was successfully synthesized. A good yield of 9% over eight steps was achieved.

In analogy to the synthesis of chiral azo paroxetine **[147]** we planned to separate the two enantiomers at the alcohol stage by an enzymatic kinetic resolution (see respective section in chapter **C II.3.3**). As in the previous nitro series, an acetylation of the alcohol was envisaged. Hence, we needed to prepare the chiral acetate first.

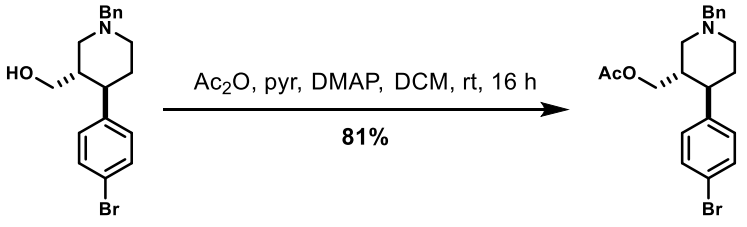

***rac*-[151]** **[152]**

***rac*-[151]** was dissolved in dry DCM and reacted with pyridine (2 equiv.) and acetic anhydride (2 equiv.) under DMAP catalysis. Conversion was complete after stirring the

reaction for 16 hours and the crude material was isolated by an extractive work-up. Purification by flash column chromatography gave racemic acetate **[152]** in 81% yield. The same analytical method as before gave a good separation of the two alcohol enantiomers and the two acetate enantiomers on a ChiralPak AS-H column by HPLC.

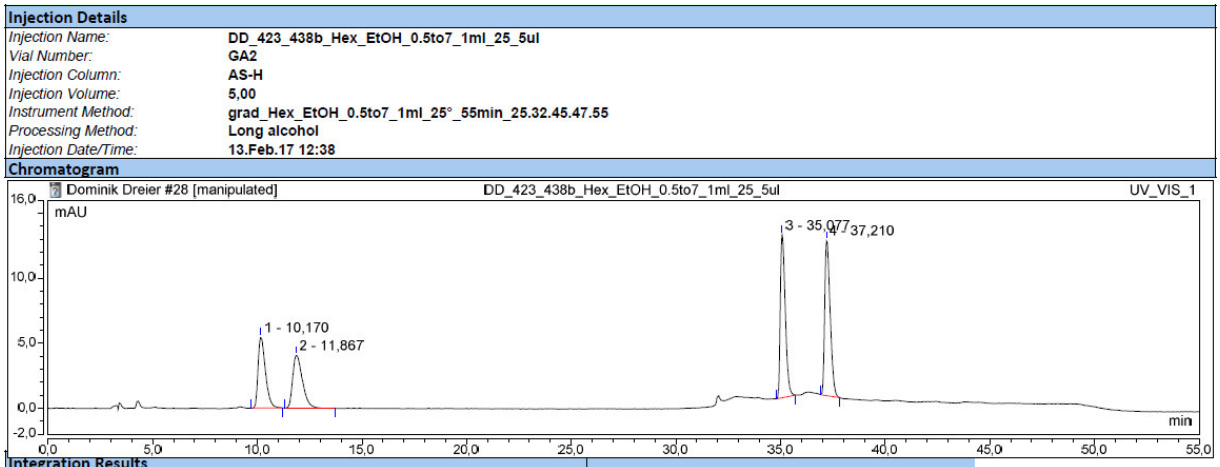

Integration Results

No.	Retention Time min	Area mAU*min	Rel.Area %
1,0	10,170	2,210	19,26
2,0	11,867	2,185	19,04
3,0	35,077	3,522	30,70
4,0	37,210	3,556	30,99

Figure 82: The two pairs of enantiomers were successfully separated on a ChiralPak AS-H column by HPLC.

The bio-catalysts CAL-A, CAL-B and Amano Lipase were all able to convert ***rac*-[151]** to acetate **[152]** in DIPE with vinyl acetate as the acetate donor (see **Table 15**) but with different stereo-preference for CAL-A.

Table 15: First attempt to enantioselectively acetylate ***rac*-[151]** by three different Lipases.

Lipase	time (h)	conv. (%)	remaining alcohol ee (%)	acetate ee (%)
Amano	56	33	28	84
CAL-A	4	59	39	32
CAL-B	4	35	35	84

From preliminary experiments it became evident that CAL-B catalyzed the acetylation considerably fast with a reasonable selectivity. Therefore, this Lipase was used to prepare optically enriched material in order to determine the absolute configuration of the individual enantiomers.

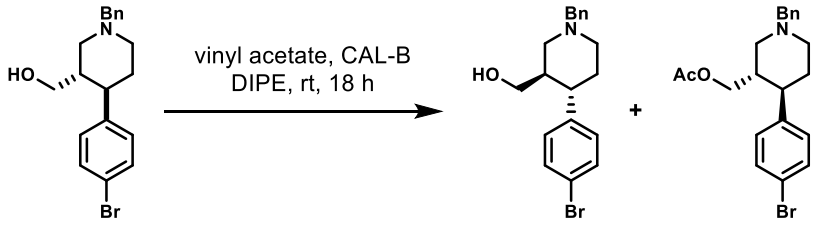

***rac*-[151]** **(3*R*,4*S*)-[151]** **(3*S*,4*R*)-[152]**

40 %
80 %ee

54 %
59 %ee

100 mg of ***rac*-[151]** were dissolved in DIPE (13.9 mL, 20 mM) and vinyl acetate (10 equiv.) and CAL-B (100 w%) were added and the suspension was stirred at room temperature for 18 hours whereupon monitoring by chiral HPLC indicated reasonable conversion and ee values. The bio-catalyst was removed by filtration through a short pad of celite and after evaporation of the solvent the crude material was purified by flash column chromatography on silica gel (EtOAc in LP, 20% → 100%) and alcohol **[151]** and acetate **[152]** were successfully separated. Unconverted alcohol **[151]** was obtained in 40% yield with an ee of 80% and acetate **[152]** was isolated in 54% yield with an ee of 59%. The isolated alcohol **[151]** (80% ee) was then used for its transfer into a compound known to the literature. Comparison of the specific optical rotation should then provide the desired information to assign absolute configuration.

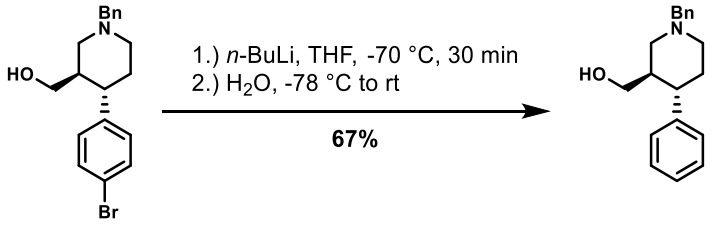

(3*R*,4*S*)-[151] **(3*R*,4*S*)-[163]**

80 %ee **80 %ee**

Alcohol **[151]** (80% ee) was dissolved in dry THF and cooled to -70 °C under argon. At this temperature *n*-BuLi (2.5 equiv., 1.6 M in hexane) was added and the reaction was stirred at -70 °C for 30 minutes. Satd. aqu. NH_4Cl was added and the reaction was slowly warmed to room temperature. The crude product was isolated by extraction and after purification by flash column chromatography on silica gel (EtOAc in LP, 20% → 100%) pure product **[163]** was obtained in 67% yield. The specific optical rotation was determined ($[\alpha]_D^{23}$ = +13.4, c = 1.0, $CHCl_3$, 80% ee) and compared with the literature value[171] for compound **[163]** with an absolute configuration of (3*R*,4*S*) ($[\alpha]_D^{23}$ = +15.1, c = 1.0, $CHCl_3$, 90% ee). As the synthesized material had the same optical rotation it was concluded that the CAL-B preferably acetylates the alcohol with (3*S*,4*R*) configuration and, hence, the remaining alcohol can be obtained in (3*R*,4*S*) configuration. In contrast to that, the other two Lipases, Amano Lipase and CAL-A, had

the opposite stereo-preference and preferentially acetylated the (3*R*,4*S*)-alcohol. Therefore, we could ether use CAL-B to isolate the acetate in the desired (3*S*,4*R*) configuration of paroxetine or use Amano Lipase or CAL-A to isolate the alcohol in the very same configuration. It is noteworthy that the stereo-preference for the Amano Lipase and CAL-B remained the same as in the nitro series but changed in case of CAL-A.

After we established the absolute configuration of the respective enantiomers we carried out a solvent screening in order to find good conditions for a preparative synthesis of the chiral bromo alcohol **[151]**. In **Table 16** the results of that screening are displayed. CAL-A gave only poor selectivity and is synthetically not feasible. CAL-B performed a little worse than the Amano Lipase in terms of selectivity. The results for the Amano Lipase in MTBE and DIPE were reasonable, albeit worse than in the nitro series. In order to increase the selectivity the reaction temperature can be lowered which leads to slower kinetics as well. In preliminary experiments, 10 °C and 15 °C gave encouraging results and the reaction can be accelerated by doubling the Lipase load and an increase in concentration to 50 mM.

Table 16: Results of the solvent screening in the Lipase catalyzed acetylation of alcohol ***rac*-[151]**. Conditions were as before: concentration of 20 mM, 100 w% Lipase, 10 equiv. vinyl acetate, room temperature.

				remaining alcohol		**acetate**	
Lipase	**solvent**	**time (h)**	**conv. (%)**	**config.**	**ee (%)**	**config.**	**ee (%)**
Amano	MTBE	48	50	(3*S*,4*R*)	56	(3*R*,4*S*)	82
CAL-A	MTBE	3	54	(3*S*,4*R*)	33	(3*R*,4*S*)	36
CAL-B	MTBE	3	42	(3*R*,4*S*)	47	(3*S*,4*R*)	80
Amano	toluene	48	21	(3*S*,4*R*)	18	(3*R*,4*S*)	72
CAL-A	toluene	24	42	(3*S*,4*R*)	16	(3*R*,4*S*)	23
CAL-B	Toluene	24	46	(3*R*,4*S*)	38	(3*S*,4*R*)	68
Amano	DIPE	48	31	(3*S*,4*R*)	21	(3*R*,4*S*)	88
CAL-A	DIPE	4	59	(3*S*,4*R*)	39	(3*R*,4*S*)	32
CAL-B	DIPE	4	35	(3*R*,4*S*)	35	(3*S*,4*R*)	84
Amano	VA	48	10	(3*S*,4*R*)	6	(3*R*,4*S*)	63
CAL-A	VA	6	27	(3*S*,4*R*)	10	(3*R*,4*S*)	32
CAL-B	VA	48	42	(3*R*,4*S*)	33	(3*S*,4*R*)	66
Amano	THF	48	<5	-	-	-	-
CAL-A/B	THF	48	<5	-	-	-	-
Amano	DCM	48	<5	-	-	-	-
CAL-A/B	DCM	48	<5	-	-	-	-

Due to time constraints, the chiral alcohol **[151]** had not yet been synthesized when this thesis was written. Further optimization is necessary to obtain the compound in sufficient optical purity (the nitro analog was isolated with 94% ee). This will be addressed in follow-up projects. The chemistry to access the target compound was successfully developed in this thesis as demonstrated with the racemic material and can be directly applied once the chiral material is available.

C II.4.4 Photophysical characterization

After the successful preparation of paroxetine based HTI derivative **[156]**, we conducted the photophysical characterization like in previous chapters (**C II.1.3**, **C II.2.3** and **C II.3.4**). A 50 μM solution in DMSO of the compound was used to determine a λ_{max} of 439 nm (see **Figure 83**) which is exactly the same λ_{max} of the analogous escitalopram based HTI **[135]**. Irradiation with 400 nm was very effective in switching the compound to the corresponding (*E*)-isomer. The thermal half life time in DMSO was determined to be 8 minutes (k = 1.4 * 10^{-3} s^{-1}). The evaluation of the photoswitch in KHP buffer requires further research (see chapter **C II.2.3**).

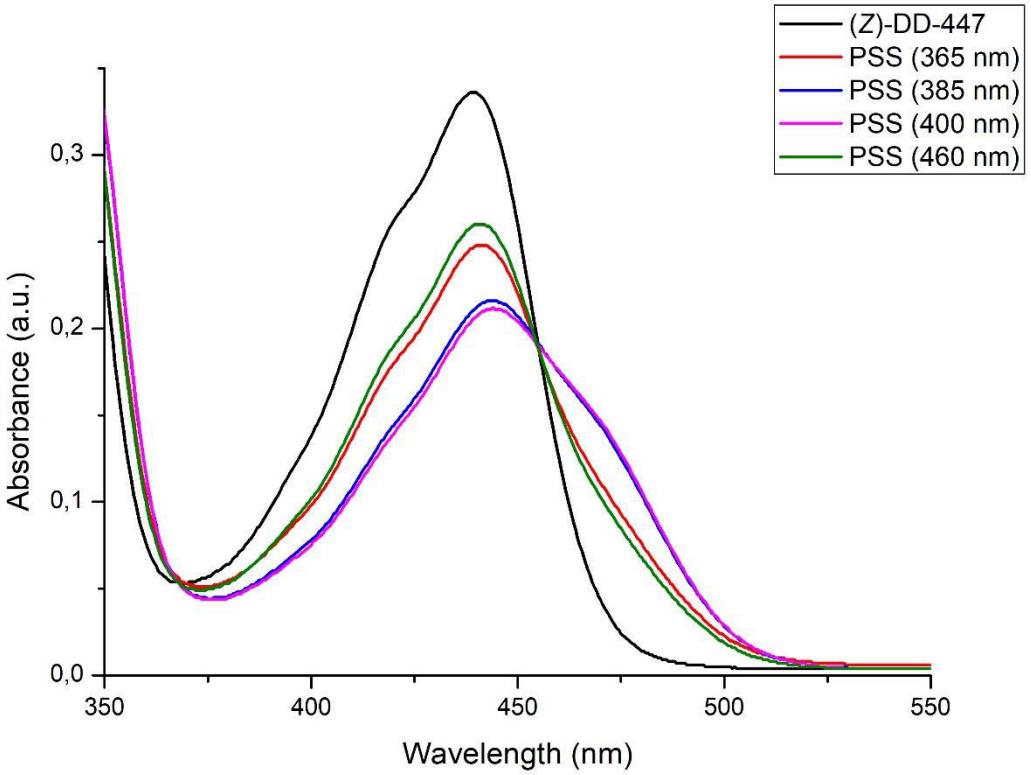

Figure 83: UV-Vis spectra of paroxetine based HTI derivative **[156]** in DMSO in the dark and after irradiation with the respective wavelength.

C II.4.5 Computational studies

As the docking studies carried out in chapter **C II.3.6** nicely explained the observations made in the biological experiments, we had reasonable confidence in the computer model. Therefore, we decided to carry out the same computational experiments with the four compounds shown in **Figure 84**. The results should give an outlook on the expected behavior of chiral paroxetine HTI analog **[156]** (**DD-447**) which we only accessed in racemic form in this thesis. In consistency with the earlier chapter, paroxetine served as the reference point. In addition, we were interested in the predicted behavior of analogous *meta*- and *ortho*-compounds **[XXVII]** and **[XXVIII]** as they could be interesting future target molecules. The molecular docking was carried out as described in the respective previous chapter. The three photoswitchable HTI compounds were docked in their stable (*Z*)-configuration and excited (*E*)-configuration.

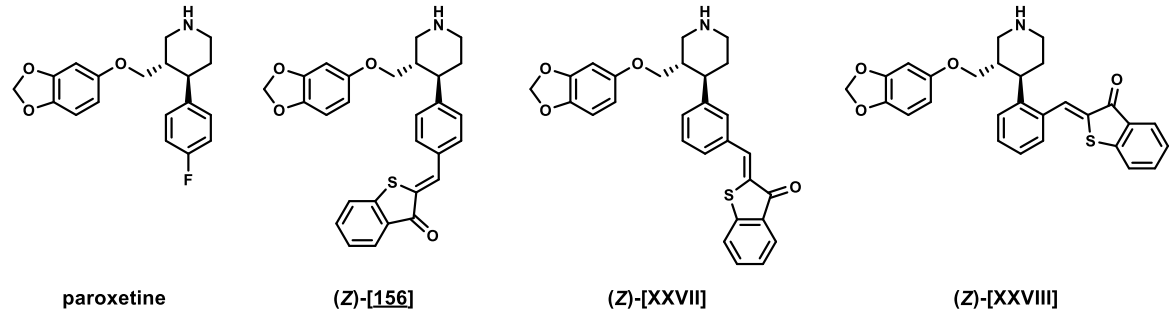

Figure 84: Paroxetine and the photoswitches **[156]**, **[XXVII]** and **[XXVIII]** were used in docking studies on hSERT.

As stated in the previous docking chapter, clusters #1 and #11 had the lowest RMSD and the highest GOLD PLP fitness, indicating that poses of these two clusters mimic the paroxetine binding pose in the crystal. However, both **(*Z*)-DD-447** and **(*E*)-DD-447** did not show similar poses in GOLD compared to the paroxetine crystal structure as only one pose of **(*Z*)-DD-447** was found in these two clusters. Most poses of **(*Z*)-DD-447** and **(*E*)-DD-447** were found in clusters 2, 3, 8 and 9, which had mean RMSD of 6.98 Å to 7.24 Å.

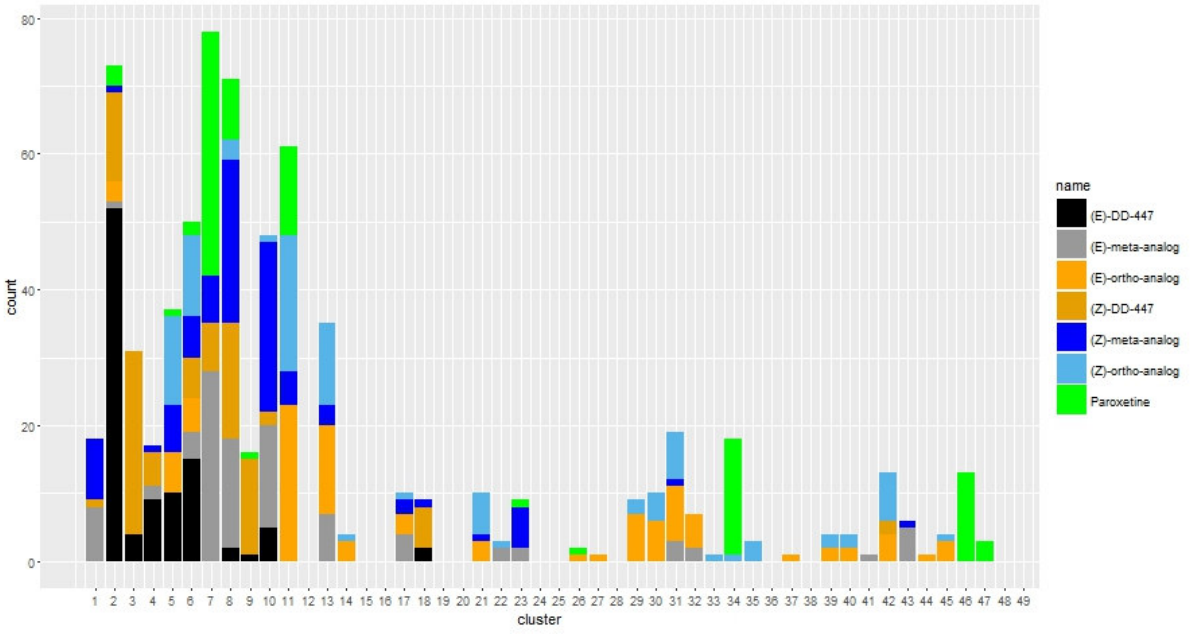

Figure 85: Common scaffold clustering of poses of paroxetine, **DD-447** and its hypothetical analogs in GOLD.

All three docking algorithms were able to reproduce the original paroxetine pose observed in the crystal structure with a RMSD of less than 1.63 Å. According to the earlier docking results of the paroxetine based azo photoswitch (**DD-482**), GOLD and Autodock produced comparable docking poses. In the case of the corresponding HTI photoswitch (**DD-447**), they unfortunately generated contradictory results (see **Figure 86**). In GOLD, only the (*Z*)-configuration fits into the central binding site (RMSD value of 1.21 Å), while in Autodock, only the (*E*)-configuration fits (RMSD value of 2.32 Å). Although Autodock Vina gave good RMSD values, these results are not considered. As already observed with the azobenzene analog, the program allows the HTI fragment to adopt impossible configurations which makes a conclusion for a photodependent behavior illegitimate.

Consequently, we were unable to make a proper prediction whether one configuration would fit better in the central binding site than the other. From a comparison of the best docking pose in GOLD (**Figure 86**, top left) and Autodock (**Figure 86** center bottom) it can be seen that the poses are relatively similar and, importantly, the isomerism of the HTI part leads only to a comparatively small change in the molecule's geometry. In accordance with considerations conducted in chapter **C II.2**, a substitution on the benzothiophene would be a possibility to introduce more significant differences in the molecule's architecture when switched. Further computational experiments should support future ligand design in this direction and suggest promising HTI photoswitches.

(*Z*)-DD-447		
GOLD	**Autodock**	**Autodock Vina**
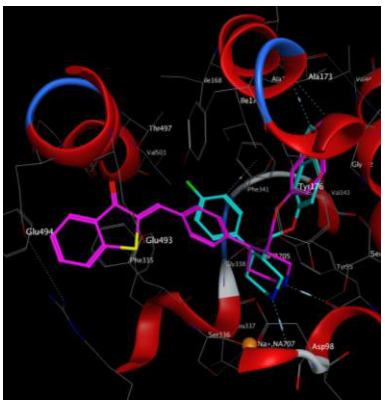	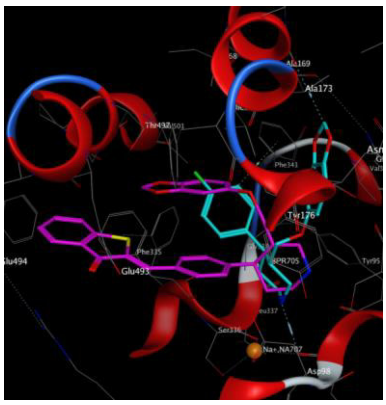	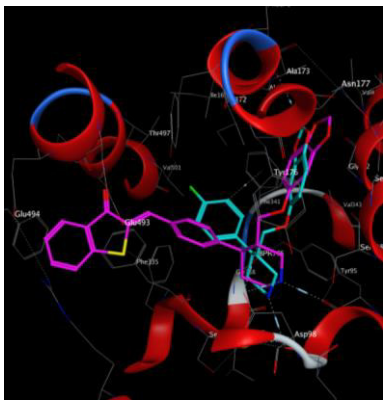
RMSD (Å): 1.21	**5.60**	**2.12**
(*E*)-DD-447		
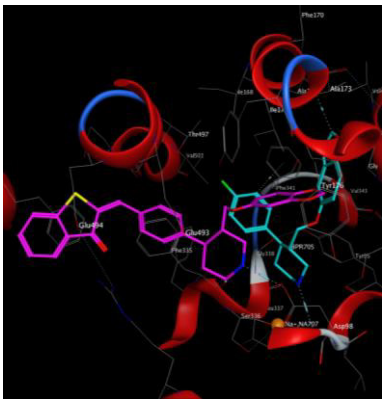	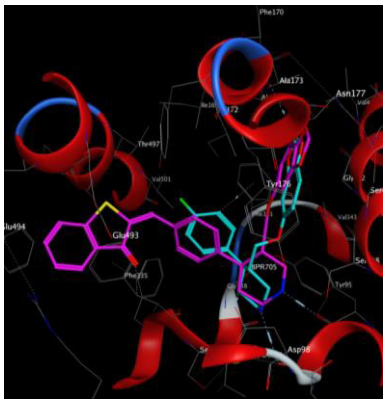	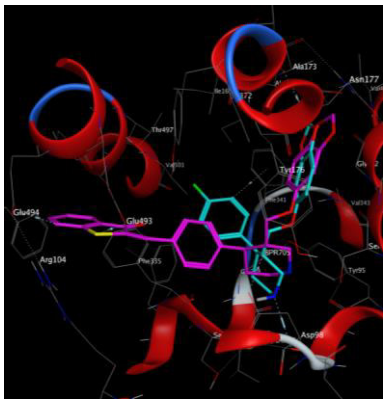
RMSD (Å): 5.40	**2.32**	**2.65**

Figure 86: Best docking poses (lowest RMSD) of **(*Z*)-DD-447** and **(*E*)-DD-447** in GOLD, Autodock and Autodock Vina with RMSD values.

Regarding the *meta*- and *ortho*-analogs, a similar number of poses for (*Z*)- and (*E*)-*meta*-analog was found in cluster #1 and likewise, a similar number of poses of (*Z*)- and (*E*)-*ortho*-analog was found in cluster #11 which are the two clusters of interest. A good number of *ortho*-poses were found in cluster #11 which could suggest that the *ortho*-analog could be a reasonable inhibitor according to GOLD. However, as both configurations populated this cluster evenly, this preliminary data suggested that there is no photo-dependent behavior to be expected and the introduction of substituents could therefore be a more promising strategy.

C III Development of LED well plates

In an early phase of the project, after we had the first few photoswitchable inhibitors synthesized, we sought to find a possibility to biologically evaluate these compounds in their switched state. We knew from thorough photophysical characterization of the target molecules (see chapter **C II.1.3** and chapter **C II.3.4**) that most azobenzenes were effectively switched with 365 nm. We also determined that the prepared inhibitors feature half life times of the switched state typically of several days in the medium used in the biological evaluation (KHP buffer + 1% DMSO). For the bio-assay, HEK cells expressing the corresponding transporter protein were grown in 96 well plates. Pre-incubation and incubation with solutions of inhibitor usually takes five to ten minutes in total. In comparison to that, the half life time of the excited (*Z*)-azobenzenes was orders of magnitude larger. It seemed therefore reasonable, to irradiate the inhibitor solutions with 365 nm (see **Figure 87**) until they reached their photostationary state (five seconds were sufficient as determined by UV-Vis experiments) prior to application and used them as such. Irradiation would convert most of the (*E*)-molecules into (*Z*)-molecules and due to the long half life times only neglectable relaxation should occur on the time scale of the bio-assay. This approach was successfully used in preliminary experiments. With this method we observed moderately different potencies (IC_{50}) when measured after irradiation with 365 nm and without irradiation in isolated cases. For example, compound **[119]** had an IC_{50} of 8.1 µM on hNET, which improved to 1.7 µM when the irradiated inhibitor was tested. However, the reproducibility of these preliminary findings proved to be modest. In order to find the cause of this problem, we took a closer look at the behavior of the switched compound during the bio-assay. We were absolutely certain, that the irradiation with the 365 nm LED switched the compounds as we had observed by UV-Vis experiment on multiple occasions. The long half life times made the compounds very stable in their switched state during the incubation. However, there was one difference we neglected up to this point. The thermal half life time, determined by UV-Vis absorbance, was measured in the dark. The bio-assay on the other hand is carried out on a lab bench under ambient conditions. Hence, we sought to understand the difference under these two conditions.

Figure 87: Switching a solution of an azobenzene analog was done by irradiation with 365 nm.

In order to do so, we conducted an UV-Vis experiment, where we investigated in how far the determined half life time in the dark was still valid under a couple of reasonable conditions in the lab. We used a representative azobenzene derivative in KHP buffer + 1% DMSO with a concentration of 10 µM. The half life time of this compound in the aqu. buffer was multiple days. In **Figure 88** the corresponding measurements are displayed. The pure (*E*)-

isomer shows a strong absorbance with a λ_{max} of 338nm (black curve). After irradiation with 365 nm, the compound is effectively switched into its (*Z*)-isomer (red curve). Next, the compound was kept two minutes inside the spectrometer in complete darkness, whereupon no relaxation was observed (navy curve, overlayed by red curve) as it was expected. Afterwards the cuvette was removed from the dark chamber and placed on the bench. The room was considerably dark as the sun-blinds were closed and the lights were off. After two minutes another spectrum was recorded (cyan curve). Relaxation has occurred to some degree as the absorbance increased more in two minutes than a half life time of multiple days would dictate. From the absorbance value it was calculated, that 2% of the molecules relaxed in this time. The sample was irradiated again with 365 nm to re-establish the initially switched state. When the sample was placed for two minutes in the same room but with artificial light being turned on, 11% relaxation was measured (blue curve). When the sun-blinders were removed and the switched sample was placed for two minutes on the bench as it would typically be the case on any sunny day, already 25% of the molecules were in (*E*)-configuration (green curve) which is a tremendous decrease in half life time. The most relaxation (48%) was observed when the switched sample was placed on a window bench with the window being open (orange curve). Compared with the initial half life time of multiple days this is an incredible acceleration of the relaxation process.

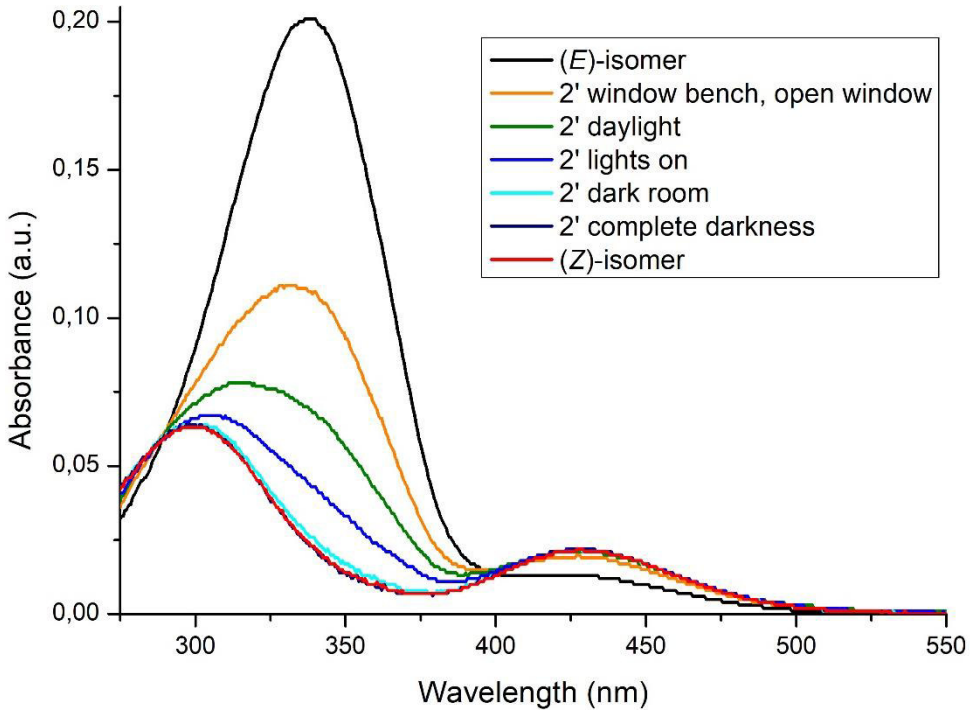

Figure 88: Typical lab conditions led to a vast acceleration of the relaxation process.

This phenomenon can be explained if we consider the possibilities for relaxation. Azobenzenes can relax thermally with the given half life time. In addition, the restoration of the (*E*)-configuration can be achieved by irradiation with light of higher wavelengths (visible

light). This was shown in earlier chapters when the azobenzene analogs were irradiated with 460 nm (see chapter **C II.1.3** and chapter **C II.3.4**). As sunlight contains all wavelengths of the visible spectrum, this light induces relaxation pathway would lead to a new photostationary state dependent of the sunlight spectrum. As the (*E*)-isomer is the more stable configuration, this state would feature mainly relaxed azobenzene molecules. Hence, a sample containing excited (*Z*)-isomers would undergo light induced relaxation under the influence of sunlight much faster than the half life time would suggest. As sunlight is omnipresent under normal working conditions, this phenomenon poses a considerable limitation to our efforts. In consequence, we carried out the bio-assay in a red light room in order to eliminate the influence of sunlight. As expected, no noteworthy relaxation was observed under these conditions (measured by UV-Vis, data not shown). However, performing the bio-assay in a red light room was impractical due to reduced visibility and therefore, did not offer a sustainable alternative.

In addition, we faced a second limitation when we relied on the stability of the excited (*Z*)-configuration. As it was determined in chapter **C II.1.3**, a number of photoswitchable inhibitors exhibit ultra-short half life times. Inevitably, these compounds would be completely relaxed before one could add them to the HEK cells.

We therefore had to acknowledge the fundamental need for a more robust experimental setup that would solve these two problems. A work published by Oliver Thorn-Seshold and Dirk Trauner & co-workers[1] prompted us to rethink our strategy in the light dependent bio-assay. The authors incubated cells with photoswitchable cytotoxic agents termed photostatins in 96 and 24 well plates. To ensure the properties of photoswitched compounds over time, they developed a computer controlled system that irradiates the cells-containing well plates with the solutions every five minutes (irradiation for 0.25 – 0.6 seconds; see **Figure 89**). Inspired by this approach, we sought to develop similar 96 well plate constructs that would allow continuous irradiation of the HEK cells during the bio-assay. Under continuous irradiation with the appropriate wavelength we expected to counteract the effect of ambient light. Molecules that undergo relaxation would immediately switch back to the (*Z*)-form and the photostationary state at the corresponding wavelength would be maintained. Furthermore, we hoped that compounds with ultra-short half life time would also be kept in (*Z*)-configuration while irradiated as the (*E*) to (*Z*) isomerization using high intensity light should be a faster process than the backisomerization. As seen

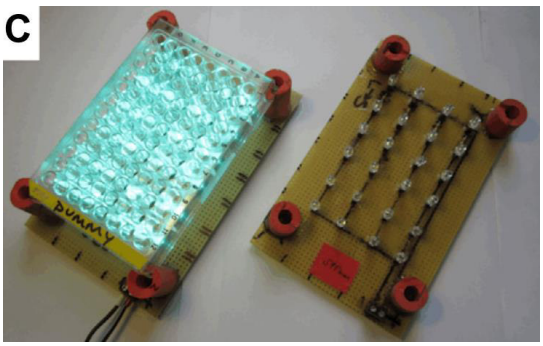

Figure 89: Thorn-Seshold and Dir Trauner & co-worker developed a construct to put well plates under irradiation with LEDs (picture taken from the literature[1]).

in **Figure 89** we aimed for a similar construct on which we could place the 96 well plates. The construct should be assembled in a way that the light sources align with the position of the wells and allow convenient irradiation of the wells from beneath.

We wanted to test our rationale with the development of a cheaper prototype and in case of promising results, expand the concept to a more sophisticated setup. As before, we planned to demonstrate the switchability of azobenzene analogs and hence, required a light source that emits 365 nm. The emitted light should also be focused on the dimension of a well plate and not be distributed over larger areas. We purchased eight 365 nm LEDs (article XSL-365-5E) from Roithner Lasertechnik GmbH with an optical power of 2.4 – 6.0 mW which should be arranged in a 4 x 2 matrix. Wolfgang Tomischko from the Institute of Chemical Technologies and Analytics of TU Wien kindly assembled the prototype. The circuit diagram can be seen in **Figure 91** and the finished prototype is displayed in **Figure 90**. The supply current of 48 V and 0.3 A can be regulated with a potentiometer.

Figure 90: The prototype consisted of eight 365 nm LEDs arranged in a 4 x 2 matrix. The supply current can be modified with a potentiometer.

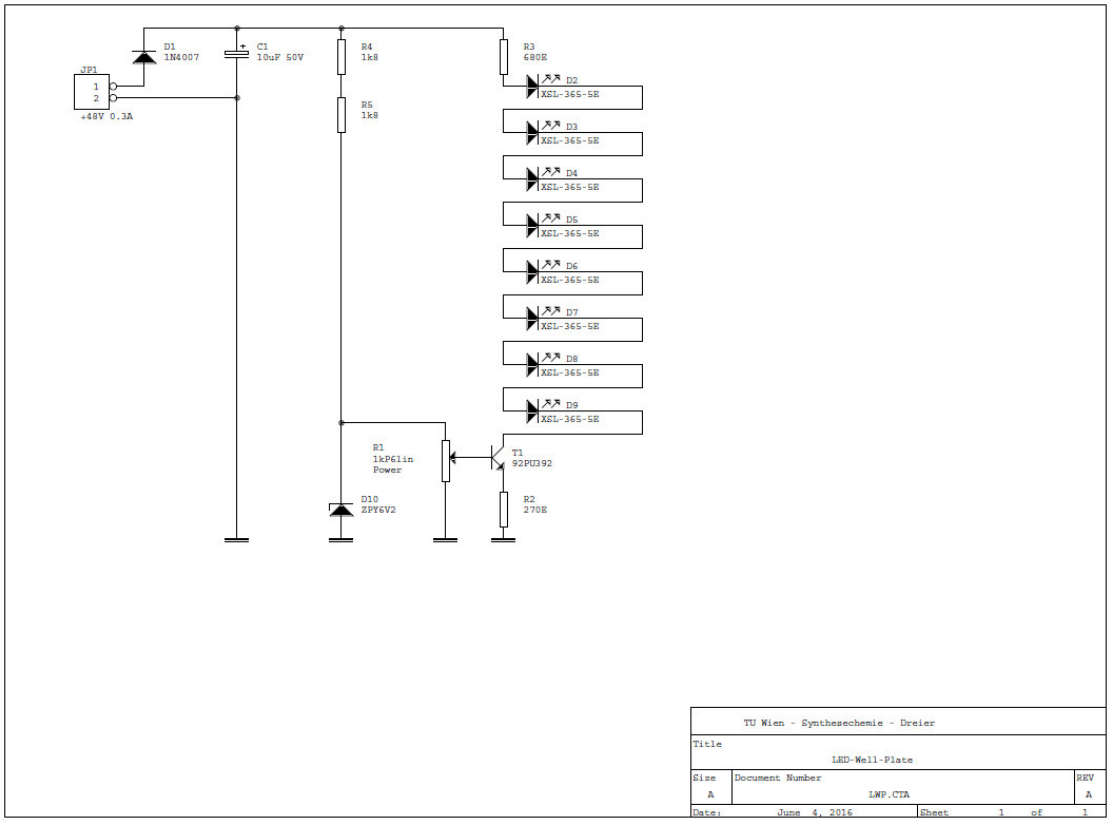

Figure 91: Circuit diagram of the prototype.

To assess whether a photoswitchable azobenzene analog would be successfully switched, we conducted UV-Vis measurements of a representative synthetic compound in KHP buffer under a few conditions. The following observations were made (data not shown):

- Irradiation for 60 seconds with maximum intensity switched the compound completely when the light was passed through the well plate material (polystyrene) from beneath.
- Irradiation for 60 seconds with maximum intensity switched the compound completely when the light was passed through the well plate material (polystyrene) from beneath and the wells contained a monolayer of HEK cells with the same density used in the bio assay.
- No difference was observed whether the compound was switched with the prototype in a red light room or under ambient light on a lab bench.
- Irradiation for ten minutes with maximum intensity led to no difference in the microscopic appearance of the HEK cells.

From these findings we concluded that the light emitted from the LEDs was capable of switching azobenzenes in the bio assay when the well plate was placed on top of the LED well plate construct. Therefore, we felt comfortable expanding our approach to a more sophisticated design. The number of LEDs should be increased to an amount where we could

perform enough measurements for one dose response curve. The intensity of the emitted light should be increased to make the (*E*) to (*Z*) isomerization as fast as possible. The new design should also allow a firm fixation of 96 well plates. We purchased 36 high-performance LED chips from RS Components (RS order number 890-3954) with a radiant flux of 780 mW and arranged them in a 12 x 3 matrix as the individual concentrations of a dose response curve are measured in triplicates. Two fans were used to cool the device (RS order number 758-8229). The conductor board was produced by Conrad Leiterplattenservice. Wolfgang Tomischko kindly designed and built the new 365 nm LED well plate according to the circuit diagram in **Figure 92**.

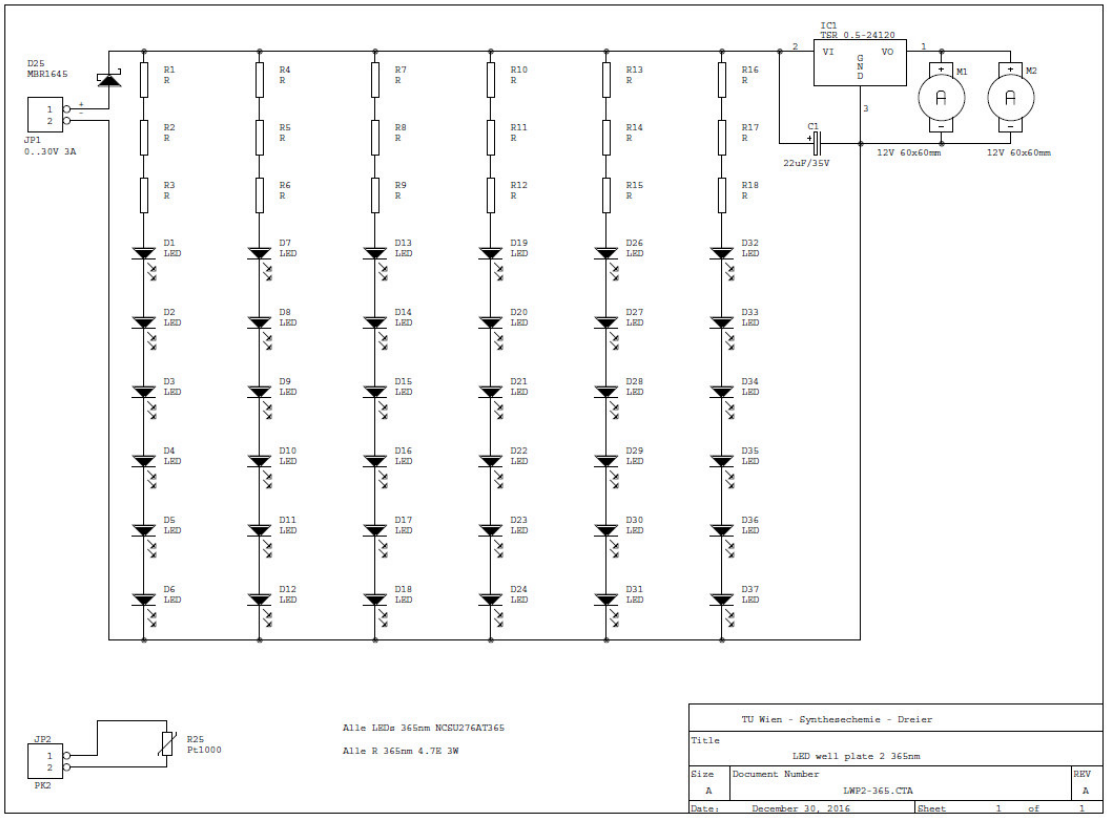

Figure 92: Circuit diagram of the 365 nm LED well plate.

In addition to a 365 nm version for most of the azobenzene analogs, we aimed to develop a second LED well plate for the realm of photoswitchable HTIs which require a different wavelength. In chapter **C II.2.3** and chapter **C II.4.4** we have seen that from the to us available wavelengths, 400 nm was always the most effective one to switch the synthesized HTI analogs. Comparable HTI examples from the literature[85, 115, 156, 157] suggested the range of 400 – 410 nm. 36 high-performance LED chips from RS Components (RS order number 894-7761) were purchased with a radiant flux of 990 mW. The 410 nm version was constructed in analogy to the 365 nm version (see **Figure 93**) by Wolfgang Tomischko.

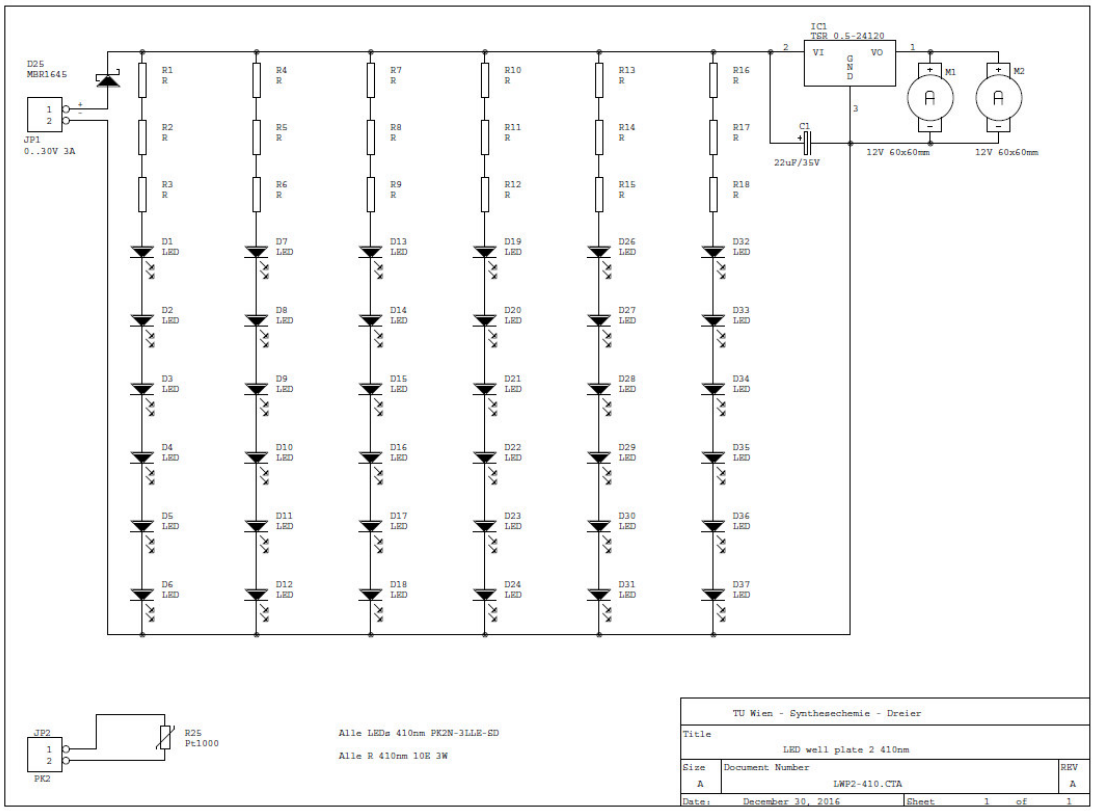

Figure 93: Circuit diagram of the 410 nm LED well plate.

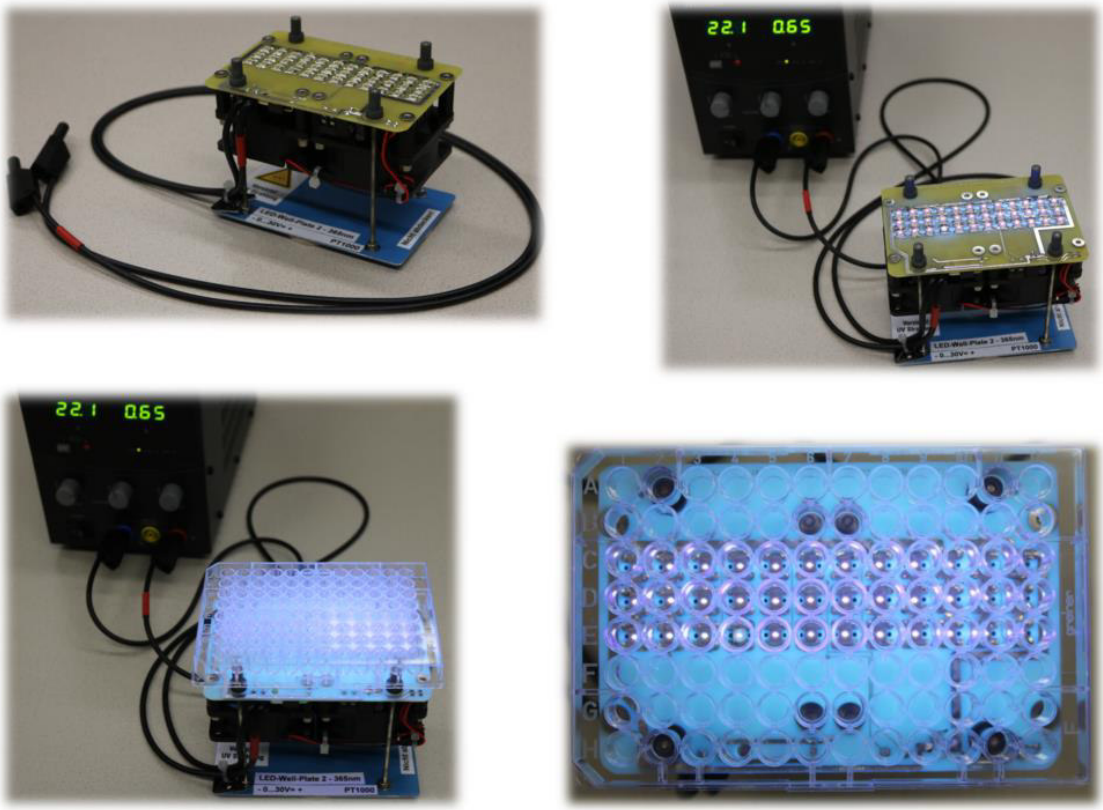

Figure 94: Top left: the 365 nm LED well plate. Top right: with power supply. Bottom left: with 96 well plate on top. Bottom right: 12 x 3 matrix aligns with the wells.

Figure 94 depicts the finished 365 nm LED well plate (the 410 nm version looks almost the same). To supply the respective device with electricity, a power supply unit with adjustable settings is used. When testing the device, it became apparent that the LEDs become very hot when a high voltage is used (80 °C at 29 V and 3 A) which can lead to softening and deformation of the 96 well plate. As a temperature increase could be harmful for the HEK cells and would probably alter their behavior in the bio assay compared to the non-light dependent measurement we investigated this effect in dependence of the used voltage. 250 µL of KHP buffer was placed in the wells and with a conventional lab thermosensor the temperature was monitored over time while the well plate was irradiated. We screened for a voltage that would not heat the solution for more than 2 °C over a period of ten minutes (the pre incubation time in the bio assay is typically five minutes). 20.0 V were found to be a reasonable voltage for the 365 nm LED well plate which led to a temperature increase of only 1.3 °C within five minutes (see **Figure 95**). For the 410 nm LED well plate 22.0 V were found to be suitable (data similar to **Figure 95**, not shown). It has to be noted that when starting the device, the voltage had to be increased to a larger value first (e.g. 25 V) and then reduced to the desired value. Otherwise the LEDs would emit light with starkly varying intensity.

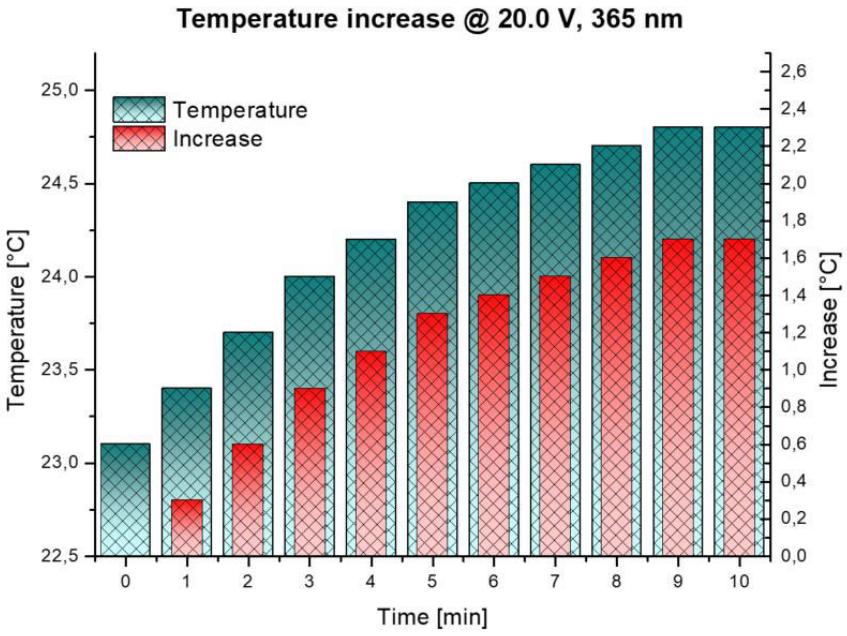

Figure 95: Temperature profile of the 365 nm LED well plate with a 20.0 V supply.

In order to assess the homogeneity of the emitted light over the 12 x 3 well area, a power measurement was conducted. A FieldMaxII-TO from Coherent was used. The sensor was placed centric over one well – containing 250 µL of KHP buffer - and the power of the emitted light was measured over each well. The measurements for the 365 nm LED well plate were done at 400 nm which is the lower limit of the measurement device but the relative value should nevertheless be representative for the homogeneity. In **Figure 96** the relative power values can be seen. The values vary from 1.2 – 2.7 mW/cm^2 and are lowest on the left

and right side probably due to a more pronounced cumulative effect in the more central wells. If the rows 1, 2, 11 and 12 are not considered, the power varies only between 1.9 – 2.7 mW/cm^2 which appears to be reasonably homogeneous. The rows 3 – 10 (orange area) should be used for the light dependent triplicates. The other rows could be used for light independent triplicates like the blank determination. **Figure 97** depicts the results for the 410 nm LED well plate. Interestingly, rows 11 and 12 emit a lot less which makes them less feasible for the light dependent measurement points. This can be attributed to the peculiarities of such an electronic device at an early development stage. Rows 1 – 10 vary from 9 – 13 mW/cm^2 which should be reasonably homogeneous as well and are therefore recommended to be used.

	1	2	3	4	5	6	7	8	9	10	11	12
C	1.3	1.6	2.0	2.0	2.0	2.1	2.2	2.4	2.2	2.3	2.1	1.7
D	1.4	1.9	2.1	2.3	2.3	2.2	2.5	2.7	2.5	2.5	2.3	1.4
E	1.2	1.6	1.9	1.9	1.9	1.9	2.2	2.3	2.2	2.2	1.7	1.5

Figure 96: Power of the emitted light measured central over the corresponding well in mW/cm^2 for the 365 nm LED well plate (measured at 400 nm) at 20.0 V. The orange area marks the recommended wells for the light dependent concentrations.

	1	2	3	4	5	6	7	8	9	10	11	12
C	10	11	10	10	9	9	9	10	10	10	6	4
D	11	13	12	10	9	10	11	11	11	11	7	4
E	9	12	11	9	9	9	9	10	10	11	6	4

Figure 97: Power of the emitted light measured central over the corresponding well in mW/cm^2 for the 410 nm LED well plate at 22.0 V. The orange area marks the recommended wells for the light dependent concentrations.

To prove that the two developed LED well plates are in fact able to switch azobenzene and HTI analogs under assay conditions, we conducted the following experiment. A 96 well plate containing HEK cells intended for the bio assay was mounted on the 365 nm LED well plate device and the wells were filled with 250 µL of a 50 µM solution of a representative azobenzene derivative in KHP buffer. A UV-Vis spectrum was measured to record the starting composition ((*E*)-isomer). The continuous irradiation of the wells was started and sampled were taken after 30 seconds, 90 seconds, 3 minutes and 5 minutes. By UV-Vis measurements it was shown that the first sample after 30 seconds was already completely switched (data not

shown) and hence, it was concluded that indeed, the device is able to switch the compound during the bio assay. For the assessment of the 410 nm LED well plate the procedure was repeated with a representative HTI analog but in DMSO as the poorer solubility in KHP buffer gave a reduced absorbance. In accordance with the first experiment, the HTI compound was already effectively switched after 30 seconds (first data point, data not shown).

As a negative control, escitalopram (for hSERT and hNET) and cocaine (hDAT) were subjected to the bio assay under irradiation and without irradiation. No significant difference was found. As it can be seen in the respective chapters (e.g. chapter **C II.3.5**), the developed LED well plate proved to deliver reliable and robust results. In comparison to the procedure we used in the beginning of the project where we irradiated the dilution series prior to application (see **Figure 87**), the established protocol is an efficient process which enables the convenient assessment of photoswitchable MAT inhibitors almost identical to the execution of the conventional assay and is potentials a sustainable solution for future projects.

In-depth manuals for all three devices were stored on the university's server and can be found in the author's personal project folder.

D Summary and outlook

In the first experimental chapter (**C I**) considerable experience was gained in order to synthesized and characterized azo based photoswitches. Standard procedures were established to determined photophysical properties. A library of 25 arylazopyrazoles formed the basis for a comprehensive evaluation of substituents' influence on absorbance and half life time while the ring structures determine the offset for λ_{max} (e.g. 365 nm for arylazo-2-thiophenes) and the upper limit for the resulting half life time. The guidelines for photophysical properties could steer ligand design. By comparison to similar library compounds, the resulting properties of future photoswitches can be estimated.

Based on well-studied SERT inhibitors, their SAR data and hSERT structural data, photoswitchable variations of two different SERT blockers (escitalopram and paroxetine) were designed, synthesized, photophysically assessed and biologically evaluated. As photoswitchable moieties azobenzenes and hemithioindigos were utilized (see **Figure 98**).

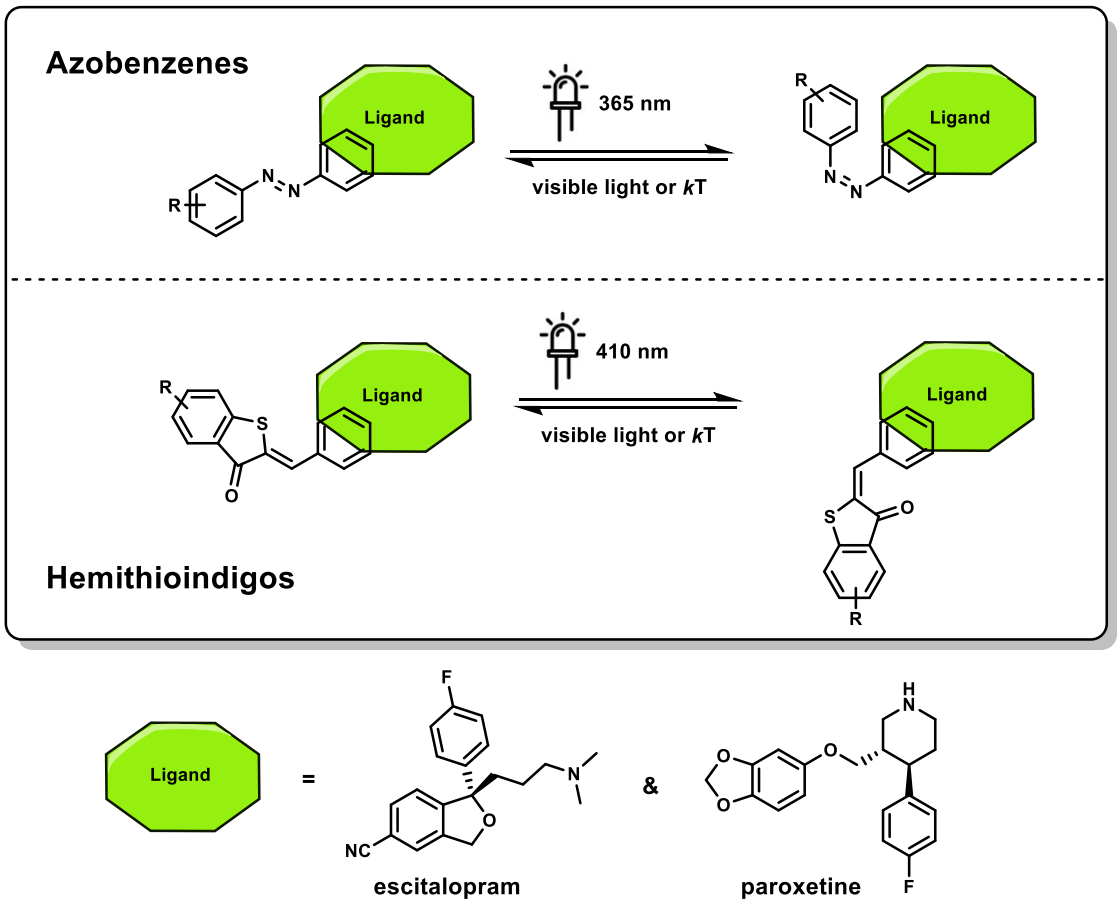

Figure 98: Escitalopram and paroxetine based azobenzene and HTI analogs were designed, synthesized, photophysically assessed and biologically evaluated.

Starting from commercial escitalopram, a number of building blocks were prepared that allowed access to a large number of photoswitchable derivatives. Many azobenzenes were synthesized via Mills condensation which required the synthesis of several nitroso compounds.

In accordance with knowledge about the photophysical behavior from the first chapter, an extensive optochemical assessment was conducted prior to biological evaluation. Results for HTIs measured in DMSO proved to be not directly transferable into aqu. systems. This behavior remains not fully understood and, hence, more research is necessary to rate the potential in biological systems.

Unfortunately, the escitalopram based analogs display only modest photo-dependent inhibition of MATs.

Based on paroxetine an eight step total synthesis of a racemic HTI analog and an eight step total synthesis of a chiral azobenzene analog (**DD-482**) was successfully tackled. The synthesis of a chiral HTI analog could be realized in a future project.

Most importantly, **DD-482** displays a greatly enhanced inhibition (IC_{50} = 0.8 μM) when activated with light of 365 nm than compared to its natural (*E*)-configuration (IC_{50} = 8.7 μM).

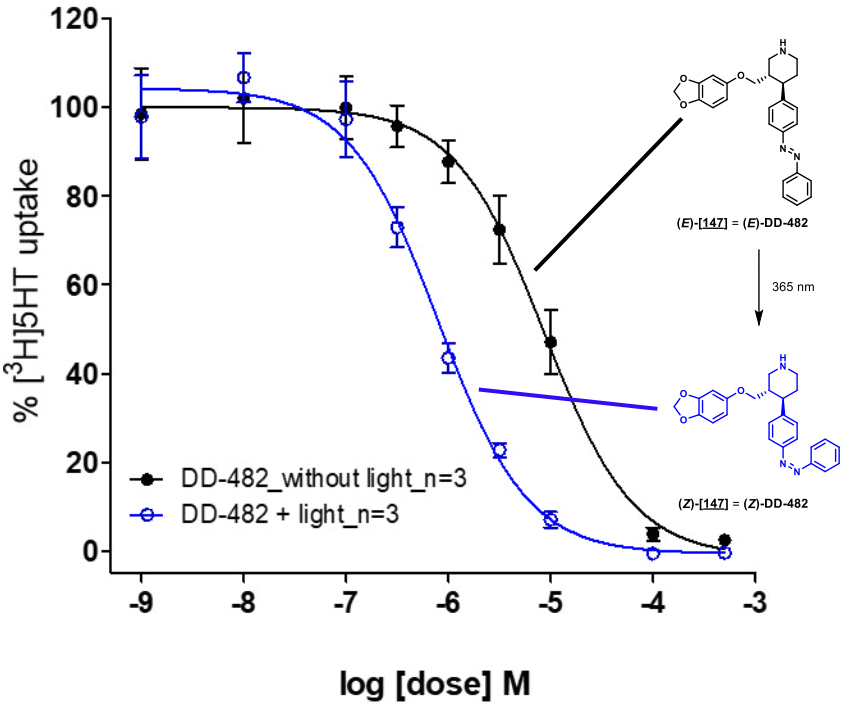

Figure 99: Dose-response curve of photoswitch **DD-482**. The relaxed (*E*)-isomer displayed an IC_{50} of 8.7 μM which was improved by approximately one order of magnitude to 0.8 μM when the compound was irradiated with 365 nm.

In electrophysiology experiments the light dependent uptake inhibition was further substantiated (see **Figure 100**).

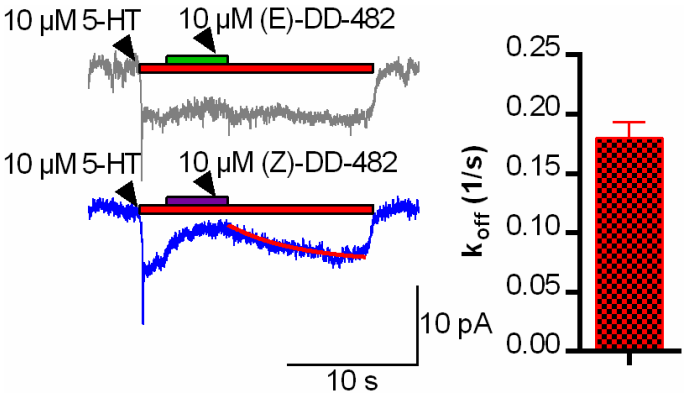

Figure 100: Electrophysiology experiments demonstrated that **(*Z*)-DD-482** blocks the transporter (blue curve) while **(*E*)-DD-482** does not (grey curve). The dissociation rate k_{off} of **(*Z*)-DD-482** was obtained by measuring the time of current recovery.

In computational docking studies (see **Figure 101**) we rationalized the activity difference by a more favorable binding of **(*Z*)-DD-482** due to reduced steric bulk after irradiation in a specific sub-pocket. This pharmacological tool compound promises great potential in future light dependent experiments on hSERT.

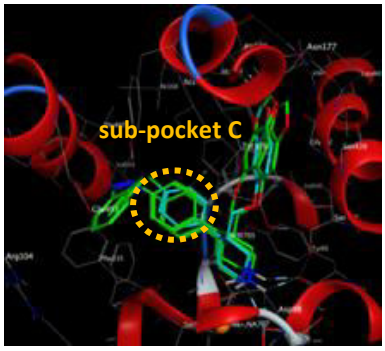

Figure 101: Docking pose of **(*Z*)-DD-482** (green molecule) in hSERT. The cyan molecule is paroxetine from the crystal structure.

In chapter **C III** the development of LED well plates (see **Figure 102**) is described which hold great potential to enable robust and reliable assay performance under the influence of 365 nm (common for many azobenzenes) and 410 nm (common for many HTIs).

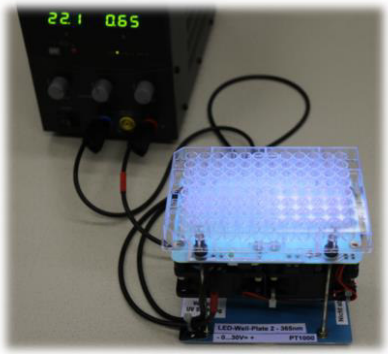

Figure 102: The developed LED well plates can be used to irradiate 96 well plates with light of 365 nm or 410 nm during the assay.

E Experimental part

E I Materials and methods – chemical synthesis

Unless otherwise noted, chemicals were purchased from commercial suppliers and used without further purification. The purity of the reported compounds is > 95% according to NMR.

E I.1 NMR spectroscopy

NMR spectra were recorded on a Bruker *AC 200* (^{1}H: 200 MHz, ^{13}C: 50 MHz), Bruker *Avance Ultrashield 400* (^{1}H: 400 MHz, ^{13}C: 101 MHz) and Bruker *Avance IIIHD 600* spectrometer equipped with a Prodigy BBO cryo probe (^{1}H: 600 MHz, ^{13}C: 151MHz). Chemical shifts are given in parts per million (ppm) and were calibrated with internal standards of deuterium labeled solvents $CDCl_3$ (^{1}H 7.26 ppm, ^{13}C 77.16 ppm), MeOD (^{1}H 3.31 ppm, ^{13}C 49.00 ppm) and DMSO-d_6 (^{1}H 2.50 ppm, ^{13}C 39.52 ppm). NMR assignments of unknown compounds were confirmed by ^{1}H - ^{1}H COSY, ^{1}H - ^{13}C, HSQC and ^{1}H - ^{13}C, HMBC and by comparison to predicted spectra. Ambiguous assignment is marked with an asterisk. Proton multiplicities are denoted by the following abbreviations: s (singlet), br s (broad singlet), d (doublet), dd (doublet of a doublet), ddd (doublet of a doublet of a doublet), t (triplet), dt (doublet of a triplet), q (quartet), dq (doublet of a quartet), p (quintet), hep (septet), m (multiplet). Coupling constants (*J*) are presented in Hz (Hertz). Carbon multiplicities (suppressed CH coupling) are denoted by the following abbreviations: s (singlet), d (doublet), t (triplet) and q (quartet). In case of fluoro structures the coupling constant is denoted generally as " x/y, $^{z}J_{CF}$ = …Hz " whereby x represents the multiplicity of the CH coupling, y the multiplicity of the CF coupling and z the order of spin-spin coupling.

E I.2 Chromatographic methods

TLC was performed using silica gel 60 aluminum plates containing fluorescent indicator from Merck and detected either with UV light at 254 nm or by staining in ninhydrin solution (300 mg ninhydrin, 3 mL acetic acid, 100 mL butanol) or potassium permanganate (1 g $KMnO_4$, 6.6 g K_2CO_3, 100 mg NaOH, 100 mL H_2O in 1M NaOH) with heating.

HPLC chromatography was carried out with an Autopurification system of Waters using an ACQUITY QDa Detector in combination with a 2998 Photodiode Array Detector. Analytical separation was conducted using XSELECT CSH Fluoro-Phenyl 5 µm 4.6 x 150 mm and XSELECT CSH C18 5 µm 4.6 x 150 mm columns. Preparative separation was performed using XSELECT CSH Prep Fluoro-Phenyl 5 µm 30 x 150 mm and XSELECT CSH Prep C18 5 µm OBD 30 x 150 mm columns. As solvents HPLC grade methanol and HPLC grade H_2O were used containing 0.1% formic acid.

Flash column chromatography (FC) was carried out with a Büchi Sepacore^{TM} MPLC system using silica gel 60 M (particle size 40-63 µm, 230-400 mesh ASTM, Macherey Nagel, Düren). Unless otherwise noted all compounds were purified with a ratio of 1/100 (weight (compound)/ weight (silica)).

GC/MS spectra were measured on a Thermo Trace 1300 / ISQ LT (single quadrupole MS (EI)) using a standard capillary column BGB 5 (30 m x 0.25 mm ID).

Enantiomeric excess was determined via HPLC with a ChiralPak AS-H (250 mm x 4.6 mm ID) column on a Thermo Scientific/Dionex Ultimate 3000 HPLC using mixtures of *n*-hexane/EtOH 0.5 - 7% over 55 minutes at 25 °C as mobile phase.

E I.3 Melting point

Melting points were determined by a Leica Galen III Kofler or a Büchi Melting Point B-545 and are uncorrected.

E I.4 HR-MS

An Agilent 6230 LC TOFMS mass spectrometer equipped with an Agilent Dual AJS ESI-Source was used for HR-MS analysis. The mass spectrometer was connected to a liquid chromatography system of the 1100/1200 series from Agilent Technologies, Palo Alto, CA, USA. The system consisted of a 1200SL binary gradient pump, a degasser, column thermostat, and an HTC PAL autosampler (CTC Analytics AG, Zwingen, Switzerland). A silica-based Phenomenex C-18 Security Guard Cartridge was used as stationary phase.

Data evaluation was performed using Agilent MassHunter Qualitative Analysis B.07.00. Identification was based on peaks obtained from extracted ion chromatograms (extraction width ± 20 ppm).

E I.5 Specific rotation

Specific rotation $[\alpha]_D^{20}$ was determined using an MCP 500 polarimeter from Anton Paar by the following equation: $[\alpha]_D^{20} = 100*\alpha/[c]*l$; c in [g/100 mL], l in [dm]

E I.6 UV-Vis spectroscopy

UV-Vis measurements were conducted on a UV-1800 UV-Vis spectrophotometer from Shimadzu. Spectra were recorded in a range from 265 nm to 600 nm with incremental steps of 0.5 nm and fast settings. Spectra were recorded in triplicates to spot potential instabilities. Measurements in DMSO: For baseline correction a 500 µL quartz cuvette was charged with dry DMSO (475 µL). Afterwards, 25 µL of the 1 mM stock solution in DMSO were added resulting in a concentration of 50 µM.
Measurements in KHP buffer + 1% DMSO: In the bio assay, a 100 mM stock solution of the synthetic compound in DMSO is used. In the dilution series the compound is dissolved in Krebs-HEPES buffer (KHP, 25 mM HEPES, 120 mM NaCl, 5 mM KCl, 1.2 mM $CaCl_2$, 1.2 mM $MgSO_4$, 5 mM D-glucose, pH adjusted to 7.3 with NaOH) containing 1% DMSO (details see **C II.1.4**). To mimic these conditions, we had to add 1% of our 1 mM DMSO stock solution to the KHP buffer. Practically, in a 500 µL cuvette, 495 µL KHP buffer were placed and used for the blank measurement. Afterwards, 5 µL of the DMSO stock solution were added and mixed, resulting in a concentration of 10 µM which is five times lower than the concentration used in the DMSO measurement and therefore, absorbance values in the buffer measurements are proportionally lower. Spectra were recorded right after preparation of the sample (completely relaxed = (*E*)-isomer) and after irradiation with light of 365 nm, 385 nm, 400 nm and 460 nm.

E II General procedures

E II.1 General procedure A: Synthesis of arylazopyrazole intermediates

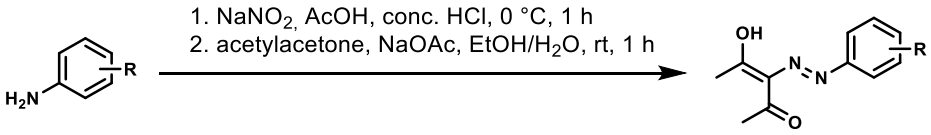

Arylazopyrazole intermediates were synthesized according to a modified literature procedure[68]. $NaNO_2$ (1.2 equiv.) in H_2O (≈0.25 g/mL) was added dropwise to a solution of the respective aniline (1 equiv.) in AcOH and conc. HCl at 0 °C. The resulting solution was stirred at 0 °C for one hour. Then, the solution was added to a suspension of NaOAc (3 equiv.) and acetylacetone (1.3 equiv.) in EtOH/H_2O (7/4, 2 M relative to NaOAc). The reaction mixture was stirred at room temperature for one hour. The precipitate was collected by filtration, washed with little cold H_2O followed by little cold H_2O/EtOH (1/1) and dried in vacuo to afford the azo intermediate.

E II.2 General procedure B: Synthesis of arylazopyrazoles

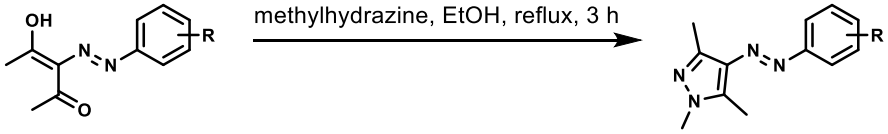

Methylhydrazine (1 equiv.) was added to a solution of the corresponding azo intermediate (1 equiv.) in EtOH and the resulting solution was stirred at reflux temperature for 3 hours. Evaporation of the solvent in vacuo afforded the desired product.[68]

E II.3 General procedure C: Synthesis of aryldiazonium tetrafluoroborates

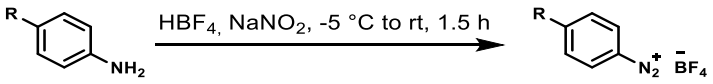

Aryldiazonium tetrafluoroborates were synthesized according to a modified literature procedure[182]. The corresponding aniline (1 equiv.) was dissolved in HBF_4 (48% in H_2O). In cases where the aniline did not dissolve completely, the mixture was heated until a homogeneous solution was obtained and then cooled again to precipitate the aniline as fine crystals to ensure a well-stirred mixture. The solution or mixture was cooled to -5 °C. An aqu. solution of $NaNO_2$ (1.14 equiv., approx. 4 M) was added dropwise while the temperature was maintained

at -5 °C. The mixture was stirred for 30 minutes at -5 °C and an additional hour at room temperature. The precipitate was collected by filtration and was washed with cold diethyl ether. If ^{1}H-NMR showed insufficient purity, the crude product was redissolved in acetone and precipitated again by the addition of cold diethyl ether. The product was isolated by filtration, washed with cold diethyl ether and dried in vacuo.

E II.4 General procedure D: Synthesis of arylazo-2-thiophenes – Method A

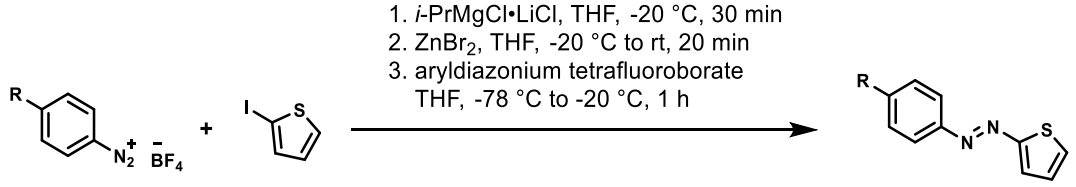

Preparation of $ZnBr_2$ (1.0 M in dry THF): A dry and argon flask was charged with $ZnBr_2$ (9.325 g, 41.41 mmol). The salt was heated to 140 °C under high vacuum for at least 4 hours. After cooling to room temperature, one glass joint was replaced by a septum. Dry THF (41 mL) was added via syringe and the suspension was stirred for 16 hours under argon atmosphere. In most cases, the salt was not completely dissolved but the fine suspension was transferable anyway. The reagent was stored under argon atmosphere, but not longer than one week.

Arylazo-2-thiophenes were synthesized from the corresponding diazonium tetrafluoroborates by a modified literature protocol[131]. A solution of *i*-PrMgCl•LiCl (2.00 mL, 1.3 M in THF, 2.54 mmol, 1.6 equiv.) was added dropwise to a solution of 2-iodothiophene (501 mg, 2.385 mmol, 1.5 equiv., scaled down on some instances, freshly distilled prior to use) in dry THF (1.6 mL) at -20 °C. The mixture was stirred for 30 minutes at the same temperature. Then, $ZnBr_2$ (1.30 mL, 1.0 M in dry THF, 1.27 mmol, 0.8 equiv.) was added dropwise to the Grignard-reagent at -20 °C. The reaction mixture was warm to room temperature and was stirred for further 20 minutes at the same temperature. Meanwhile, a suspension of the previously synthesized diazonium tetrafluoroborate (1.59 mmol, 1 equiv.) in dry THF (6 mL) was prepared and cooled to -78 °C. Subsequently, the formed zinc reagent was added dropwise to the suspension not exceeding -70 °C. After complete addition, the reaction mixture was slowly warmed to -20 °C and was stirred for one hour at that temperature. The mixture was then quenched with satd. aqu. NH_4Cl (4.5 mL) and extracted four times with DCM (20 mL aliquots). The combined organic phases were washed once with brine (30 mL) and dried over $MgSO_4$. Filtration and evaporation of the solvent in vacuo provided the crude product.

E II.5 General procedure E: Synthesis of arylazo-2-thiophenes – Method B

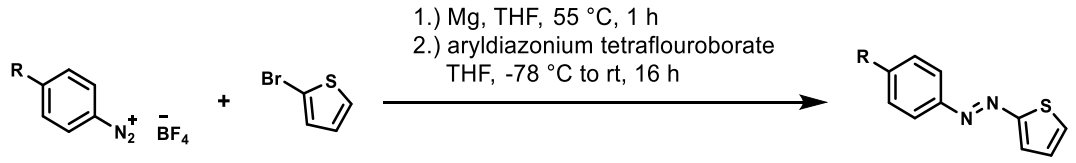

For two arylazo-2-thiophenes alternative literature conditions[126] were applied. A flask was charged with Mg (39 mg, 1.61 mmol, 1.01 equiv.) and dry THF (4 mL). Then, a small amount of 2-bromothiophene (257 mg, 1.59 mmol, 1 equiv.) was added. In order to start the Grignard reaction, a crystal of iodine was added and the reaction mixture was heated to 55 °C. After the reaction had started, the rest of the 2-bromothiophene was added dropwise to the reaction mixture. The mixture was then stirred till all the magnesium was consumed (approximately one hour). The yellow solution was subsequently added via syringe to a suspension of the diazonium tetrafluoroborate (1.59 mmol, 1 equiv.) in dry THF (8 mL) at -78 °C. After complete addition, the reaction mixture was slowly warmed to room temperature and was stirred for 16 hours. Subsequently, the black reaction mixture was quenched with H_2O (5 mL) and was extracted with DCM, (5 x 20 mL). The combined organic phases were dried over $MgSO_4$ and volatiles were removed in vacuo to afford the crude product.

E II.6 General procedure F: Synthesis of arylazo-3-thiophenes

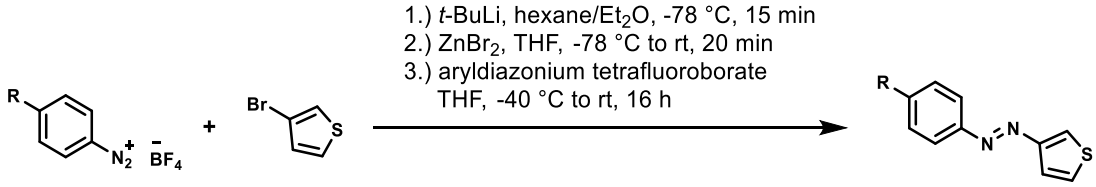

Arylazo-3-thiophenes were accessed by applying a modified combination of literature conditions[131, 183]. 3-Bromothiophene (470 mg, 2.88 mmol, 1.6 equiv.) was placed in a flask. The flask was closed with a septum and was evacuated and flushed with argon three times. Dry hexane (12.8 mL) and dry diethyl ether (8 mL) were added via syringe and the solution was cooled to -78 °C. A solution of *t*-BuLi (1.7M in pentane, 3.39 mL, 5.76 mmol, 3.2 equiv.) was added dropwise via syringe while the temperature was maintained at -78 °C (internal thermometer). The solution was stirred at that temperature for 15 minutes. A syringe was preloaded with a dimethyl disulfide solution in dry THF and was used to quench an aliquot of the reaction directly in the syringe. TLC and GC-MS analysis of that quenched material showed complete lithiation. $ZnBr_2$ (2.16 mL, 1.0 M in dry THF, 2.16 mmol, 1.2 equiv., see preparation

in **General procedure D**) was added via syringe. The reaction was warmed to room temperature and was stirred for 20 minutes at that temperature. The diazonium tetrafluoroborate analog (1.80 mmol, 1 equiv.) was placed in a 100 mL round bottom flask. The flask was closed with a septum and was evacuated and flushed with argon three times. Dry THF (25 mL) was added via syringe and the suspension was cooled to -40 °C. The zinc organyl solution was added to that suspension via syringe. The reaction was stirred for 16 hours while slowly warming up in the cooling bath. Satd. aqu. NH_4Cl (10 mL) was added and the phases were separated. The aqu. phase was extracted with DCM (3 x 10 mL). The combined organic phases were washed with brine (50 mL) and dried over $MgSO_4$. After evaporation of the solvent in vacuo, the crude product was obtained.

E III Chemical synthesis

E III.1 Arylazopyrazoles

E III.1.1 4-Hydroxy-3-(phenyldiazenyl)pent-3-en-2-one [2]

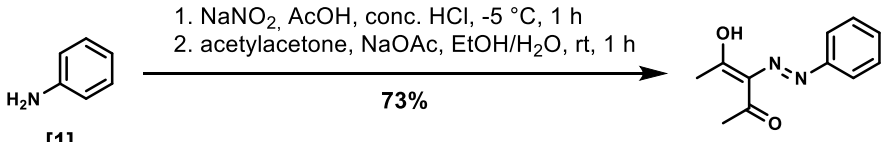

[1]
93.13 g/mol

[2]
204.23 g/mol

4-Hydroxy-3-(phenyldiazenyl)pent-3-en-2-one **[2]** was synthesized according to **General procedure A** using aniline **[1]** (0.69 g, 7.40 mmol), AcOH (10 mL) and conc. HCl (1.7 mL) with the temperature during the formation of the diazonium salt being held at -5 °C.

Yield	73% (1.10 g, 5.40 mmol)
Appearance	yellow crystals
Melting point	86.0 – 86.5 °C (Lit.[184]: 85 – 86 °C)
TLC-Analysis	R_f = 0.40 (LP/EtOAc = 20/1)
Sum formula	$C_{11}H_{12}N_2O_2$
^{1}H-NMR (200 MHz, $CDCl_3$)	δ = 2.49 (s, 3H, CH_3), 2.61 (s, 3H, CH_3), 7.13 – 7.25 (m, 1H, H4'), 7.36 – 7.45 (m, 4H, H2' & H3' & H5' & H6'), 14.73 (br s, 1H, enol-H) ppm.

^{13}C-NMR (101 MHz, $CDCl_3$) δ = 26.7 (q, CH_3), 31.7 (q, CH_3), 116.3 (d, 2C, C2' & C6' or C3' & C5'), 126.0 (d, C4'), 129.7 (d, 2C, C2' & C6' or C3' & C5'), 133.3 & 141.6 (2xs, 2C, C3 & C1'), 197.1 & 198.0 (2xs, 2C, carbonyl-C & enol-C) ppm.

The assignments of protons and carbon atoms in the NMR codes of compounds **[2]**, **[5]**, **[9]**, **[13]**, **[20]**, **[24]**, **[27]**, **[30]**, **[33]**, **[35]**, **[38]**, **[41]**, **[44]** and **[47]** were carried out as follows:

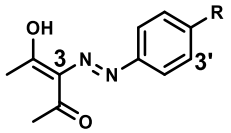

E III.1.2 1,3,5-Trimethyl-4-(phenyldiazenyl)-1*H*-pyrazole [3]

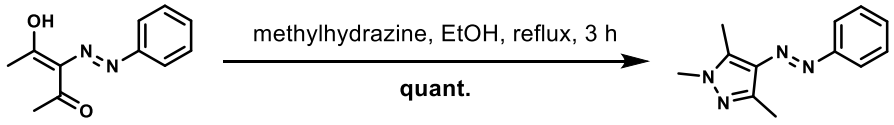

[2]
204.23 g/mol

[3]
214.27 g/mol

1,3,5-Trimethyl-4-(phenyldiazenyl)-1*H*-pyrazole **[3]** was synthesized according to **General procedure B** using azo intermediate **[2]** (1.00 g, 4.90 mmol) and EtOH (25 mL).

Yield quant. (1.05 g, 4.90 mmol)

Appearance yellow crystals

Melting point 61.0 – 61.5 °C (Lit.[185, 186]: 60 – 63 °C)

TLC-Analysis R_f = 0.45 (LP/EtOAc = 1/1)

Sum formula $C_{12}H_{14}N_4$

GC-MS 215 (10), 214 (76, M^+), 137 (100), 109 (86)

^{1}H-NMR (400 MHz, $CDCl_3$) δ = 2.51 (s, 3H, CH_3), 2.58 (s, 3H, CH_3), 3.78 (s, 3H, N-CH_3), 7.33 – 7.40 (m, 1H, H4'), 7.43 – 7.48 (m, 2H, H3' & H5'), 7.76 – 7.80 (m, 2H, H2' & H6') ppm.

^{13}C-NMR (101 MHz, $CDCl_3$) δ = 10.1 (q, CH_3), 14.0 (q, CH_3), 36.1 (q, N-CH_3), 121.9 & 129.0 (2xd, 4C, C2' & C6' & C3' & C5'), 129.4 (d, C4'), 135.3 & 138.8 & 142.6 & 153.7 (4xs, 4C, C3 & C4 & C5 & C1') ppm.

The assignments of protons and carbon atoms in the NMR codes of compounds **[3]**, **[6]**, **[7]**, **[10]**, **[11]**, **[14]**, **[15]**, **[15]**, **[17]**, **[18]**, **[21]**, **[22]**, **[25]**, **[28]**, **[31]**, **[34]**, **[36]**, **[39]**, **[42]**, **[45]**, **[48]** and **[51]** were carried out as follows:

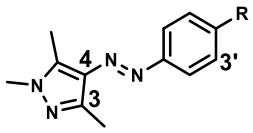

E III.1.3 4-Hydroxy-3-((4-nitrophenyl)diazenyl)pent-3-en-2-one [5]

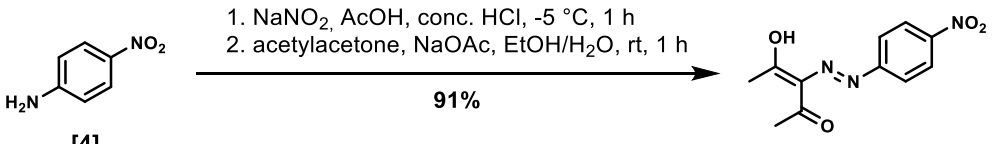

[4]
138.13 g/mol

[5]
249.23 g/mol

4-Hydroxy-3-((4-nitrophenyl)diazenyl)pent-3-en-2-one **[5]** was synthesized according to **General procedure A** using 4-nitroaniline **[4]** (1.02 g, 7.40 mmol), AcOH (10 mL) and conc. HCl (1.7 mL) with the temperature during the formation of the diazonium salt being held at -5 °C.

Yield	91% (1.67 g, 6.70 mmol)
Appearance	yellow crystals
Melting point	224.0 – 225.5 °C (Lit.[184]: 220 – 222 °C)
TLC-Analysis	R_f = 0.60 (LP/EtOAc = 3/1)
Sum formula	$C_{11}H_{11}N_3O_4$
^{1}H-NMR (400 MHz, $CDCl_3$)	δ = 2.53 (s, 3H, CH_3), 2.64 (s, 3H, CH_3), 7.49 (d, *J* = 9.1 Hz, 2H, H2' & H6'), 8.30 (d, *J* = 9.1 Hz, 2H, H3' & H5'), 14.53 (br s, 1H, enol-H) ppm.
^{13}C-NMR (101 MHz, DMSO-d_6)	δ = 26.1 (q, CH_3), 31.2 (q, CH_3), 116.0 & 125.5 (2xd, 4C, C2' & C3' & C5' & C6'), 137.1 & 143.0 & 148.0 (3xs, 3C, C3 & C1' & C4'), 196.4 & 198.1 (2xs, 2C, carbonyl-C & enol-C) ppm.
Comment	Residual solvent signal of DMSO-d_6 overlapped with a methyl signal in ^{1}H-NMR, hence, ^{1}H-NMR was recorded in $CDCl_3$. Solubility in $CDCl_3$ was too bad for ^{13}C-NMR measurements

E III.1.4 1,3,5-Trimethyl-4-((4-nitrophenyl)diazenyl)-1*H*-pyrazole [6]

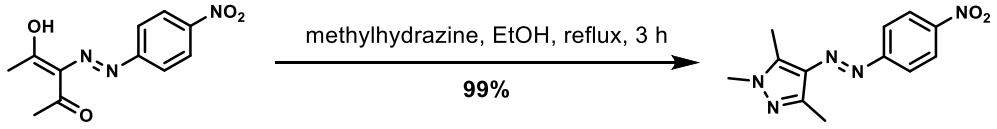

[5]
249.23 g/mol

[6]
259.27 g/mol

1,3,5-Trimethyl-4-((4-nitrophenyl)diazenyl)-1*H*-pyrazole **[6]** was synthesized according to **General procedure B** using azo intermediate **[5]** (900 mg, 3.61 mmol) and EtOH (19 mL).

Yield	99% (924 mg, 3.56 mmol)
Appearance	orange crystals
Melting point	149.0 – 151.0 °C (Lit.[186]: 128 – 129 °C)
TLC-Analysis	R_f = 0.30 (LP/EtOAc = 1/1)
Sum formula	$C_{12}H_{13}N_5O_2$
GC-MS	259 (22, M^+), 137 (100), 109 (71)
^{1}H-NMR (400 MHz, $CDCl_3$)	δ = 2.50 (s, 3H, CH_3), 2.61 (s, 3H, CH_3), 3.81 (s, 3H, N-CH_3), 7.87 (d, *J* = 9.0 Hz, 2H, H2' & H6' or H3' & H5'), 8.32 (d, *J* = 9.0 Hz, 2H, H2' & H6' or H3' & H5') ppm.
^{13}C-NMR (101 MHz, $CDCl_3$)	δ = 10.2 (q, CH_3), 14.2 (q, CH_3), 36.3 (q, N-CH_3), 122.4 & 124.8 (2xd, 4C, C2' & C6' & C3' & C5'), 136.0 & 140.8 & 143.1 & 147.7 & 157.3 (5xs, 5C, C3 & C4 & C5 & C1' & C4') ppm.
Comment	^{1}H-NMR data is in accordance with the literature[186]. The in the literature reported ^{13}C-NMR data seems to be flawed as the authors report a physically impossible number of signals.

E III.1.5 4-((1,3,5-Trimethyl-1*H*-pyrazol-4-yl)diazenyl)aniline [7]

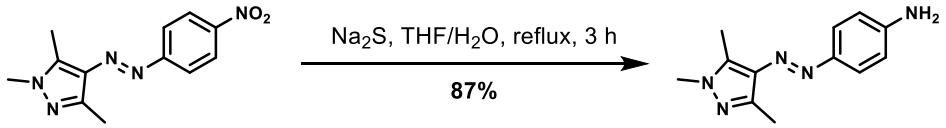

[6]
259.27 g/mol

[7]
229.29 g/mol

4-((1,3,5-Trimethyl-1*H*-pyrazol-4-yl)diazenyl)aniline **[7]** was prepared by applying literature conditions[187] for similar substrates. Na_2S (1.25 g, 5.21 mmol, 3 equiv.) was added to a solution of 1,3,5-trimethyl-4-((4-nitrophenyl)diazenyl)-1*H*-pyrazole **[6]** (451 mg, 1.74 mmol, 1 equiv.) in THF/H_2O (3/1, 22.8 mL). The suspension was stirred at reflux temperature for 3 hours. THF was removed in vacuo and the residue was partitioned between EtOAc (28.5 mL) and 1 N

NaOH (9.5 mL). The organic phase was washed with 1 N NaOH, satd. aqu. $NaHCO_3$ (10 mL) and brine (10 mL) and was dried over $MgSO_4$ and concentrated in vacuo, affording the crude product. After purification by flash column chromatography (silica gel/crude material = 100/1, LP/EtOAc = 3/1) the pure product was obtained.

Yield	87% (347 mg, 1.51 mmol)
Appearance	yellow crystals
Melting point	198.0 – 201.0 °C
TLC-Analysis	R_f = 0.40 (LP/EtOAc = 1/2)
Sum formula	$C_{12}H_{15}N_5$
HR-MS	$[M+H]^+$: calculated: 230.1400 Da, found: 230.1425 Da, difference: 2.5 mDa
GC-MS	230 (15), 229 (100, M^+), 137 (79), 109 (78)
^{1}H-NMR (400 MHz, $CDCl_3$)	δ = 2.48 (s, 3H, CH_3), 2.54 (s, 3H, CH_3), 3.76 (s, 3H, N-CH_3), 3.90 (br s, 2H, NH_2), 6.72 (d, *J* = 8.7 Hz, 2H, H3' & H5'), 7.66 (d, *J* = 8.7 Hz, 2H, H2' & H6') ppm.
^{13}C-NMR (101 MHz, $CDCl_3$)	δ = 10.1 (q, CH_3), 13.8 (q, CH_3), 36.0 (q, N-CH_3), 114.9 & 123.6 (2xd, 4C, C2' & C6' & C3' & C5'), 135.0 & 137.4 & 142.2 & 146.7 & 148.1 (5xs, 5C, C3 & C4 & C5 & C1' & C4') ppm.

E III.1.6 4-Hydroxy-3-((4-hydroxyphenyl)diazenyl)pent-3-en-2-one [9]

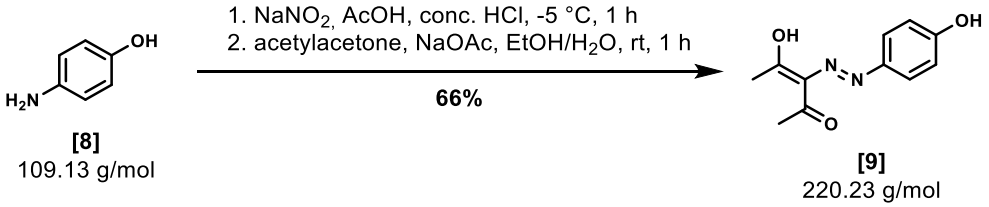

[8]
109.13 g/mol

[9]
220.23 g/mol

4-Hydroxy-3-((4-hydroxyphenyl)diazenyl)pent-3-en-2-one **[9]** was synthesized according to **General procedure A** using 4-aminophenol **[8]** (808 mg, 7.40 mmol), AcOH (10 mL) and conc. HCl (1.7 mL) with the temperature during the formation of the diazonium salt being held at -5 °C.

Yield	66% (1.07 g, 4.84 mmol)
Appearance	brown crystals
Melting point	240.5 – 241.0 °C
TLC-Analysis	R_f = 0.40 (LP/EtOAc = 3/1)

Sum formula $C_{11}H_{12}N_2O_3$

^{1}H-NMR (400 MHz, DMSO-d_6) δ = 2.37 (s, 3H, CH_3), 2.45 (s, 3H, CH_3), 6.83 (d, *J* = 8.9 Hz, 2H, H2' & H6'), 7.42 (d, *J* = 8.8 Hz, 2H, H3' & H5'), 9.65 (s, 1H, OH), 14.50 (br s, 1H, enol-H) ppm.

^{13}C-NMR (151 MHz, DMSO-d_6) δ = 26.4 (q, CH_3), 31.1 (q, CH_3), 116.1 & 118.1 (2xd, 4C, C2' & C3' & C5' & C6'), 132.1 & 133.7 & 155.9 (3xs, 3C, C3 & C1' & C4'), 195.9 & 196.0 (2xs, 2C, carbonyl-C & enol-C) ppm.

Comment Spectral data is in accordance with the literature[188]

E III.1.7 4-((1,3,5-Trimethyl-1*H*-pyrazol-4-yl)diazenyl)phenol [10]

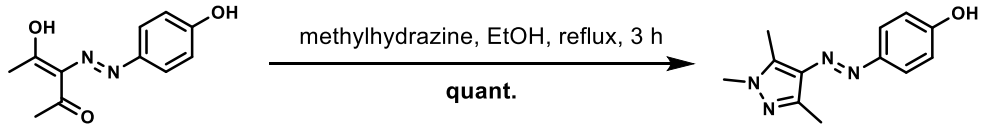

[9] 220.23 g/mol

[10] 230.27 g/mol

4-((1,3,5-Trimethyl-1*H*-pyrazol-4-yl)diazenyl)phenol **[10]** was synthesized according to **General procedure B** using azo intermediate **[9]** (500 mg, 2.27 mmol) and EtOH (12 mL).

Yield quant. (523 mg, 2.27 mmol)

Appearance yellow crystals

Melting point 232.5 – 233.5 °C

TLC-Analysis R_f = 0.40 (LP/EtOAc = 1/2)

Sum formula $C_{12}H_{14}N_4O$

GC-MS 230 (27, M^+), 137 (41), 113 (15), 109 (38)

^{1}H-NMR (400 MHz, DMSO-d_6) δ = 2.34 (s, 3H, CH_3), 2.51 (s, 3H, CH_3), 3.71 (s, 3H, N-CH_3), 6.87 (d, *J* = 8.8 Hz, 2H, H2' & H6' or H3' & H5'), 7.61 (d, *J* = 8.8 Hz, 2H, H2' & H6' or H3' & H5'), 9.93 (br s, 1H, OH) ppm.

^{13}C-NMR (101 MHz, DMSO-d_6) δ = 9.4 (q, CH_3), 13.7 (q, CH_3), 35.8 (q, N-CH_3), 115.6 & 123.1 (2xd, 4C, C2' & C6' & C3' & C5'), 134.0 & 138.1 & 139.9 & 146.1 & 159.1 (5xs, 5C, C3 & C4 & C5 & C1' & C4') ppm.

Comment Spectral data are in accordance with literature data.[188]

E III.1.8 4-((4-Methoxyphenyl)diazenyl)-1,3,5-trimethyl-1*H*-pyrazole [11]

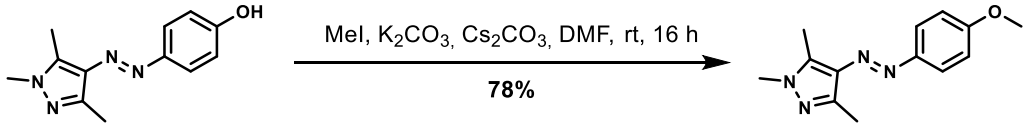

[10]
230.27 g/mol

[11]
244.30 g/mol

4-((1,3,5-Trimethyl-1*H*-pyrazol-4-yl)diazenyl)phenol **[10]** (100 mg, 0.43 mmol, 1 equiv.) was added to a stirred suspension of K_2CO_3 (120 mg, 0.87 mmol, 2 equiv.) and Cs_2CO_3 (71 mg, 0.21 mmol, 0.5 equiv.) in DMF (2.2 mL). After stirring at room temperature for 10 minutes methyl iodide (123 mg, 0.87 mmol, 2 equiv.) was added to the reaction. After stirring at room temperature for 16 hours, complete conversion was observed by GC-MS and TLC analysis. H_2O (10 mL) was added and the mixture was extracted with EtOAc (3 x 10 mL). The combined organic phases were washed with H_2O (2 × 10 mL) and dried over $MgSO_4$. The solvent was removed in vacuo and the crude product was purified by flash column chromatography (silica gel/crude material = 100/1, LP/EtOAc = 17/3) yielding 4-((4-methoxyphenyl)diazenyl)-1,3,5-trimethyl-1*H*-pyrazole **[11]**.

Yield	78% (83 mg, 0.34 mmol)
Appearance	yellow crystals
Melting point	104.0 – 104.5 °C (Lit.[186]: 62 – 64 °C)
TLC-Analysis	R_f = 0.45 (LP/EtOAc = 1/1)
Sum formula	$C_{13}H_{16}N_4O$
HR-MS	$[M+H]^+$: calculated: 245.1397 Da, found: 245.1426 Da, difference: 2.9 mDa
GC-MS	245 (15), 244 (100, M^+), 137 (100), 122 (11), 109 (65)
^{1}H-NMR (400 MHz, $CDCl_3$)	δ = 2.49 (s, 3H, CH_3), 2.56 (s, 3H, CH_3), 3.77 (s, 3H, CH_3), 3.87 (s, 3H, CH_3), 6.97 (d, *J* = 9.0 Hz, 2H, H3' & H5'), 7.77 (d, *J* = 9.0 Hz, 2H, H2' & H6') ppm.
^{13}C-NMR (101 MHz, $CDCl_3$)	δ = 10.1 (q, CH_3), 13.9 (q, CH_3), 36.1 (q, N-CH_3), 55.7 (q, O-CH_3), 114.2 & 123.4 (2xd, 4C, C2' & C6'& C3' & C5'), 135.0 & 138.1 & 142.3 & 148.1 & 160.9 (5xs, 5C, C3 & C4 & C5 & C1' & C4') ppm.
Comment	^{1}H-NMR data is in accordance with the literature[186]. The in the literature reported ^{13}C-NMR data seems to be flawed as the authors report a physically impossible number of signals. As the measured melting point was considerably higher, we measured

HR-MS to further substantiate the identity of the synthesized material

E III.1.9 4-((2-Hydroxy-4-oxopent-2-en-3-yl)diazenyl)benzoic acid [13]

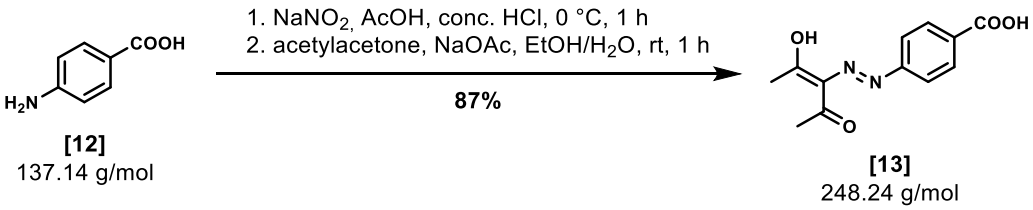

[12]
137.14 g/mol

[13]
248.24 g/mol

4-((2-Hydroxy-4-oxopent-2-en-3-yl)diazenyl)benzoic acid **[13]** was synthesized according to **General procedure A** using 4-aminobenzoic acid **[12]** (1.02 g, 7.40 mmol), AcOH (10 mL) and conc. HCl (1.7 mL).

Yield 87% (1.60 g, 6.45 mmol)

Appearance yellow crystals

Melting point 268.5 – 269.0 °C

TLC-Analysis R_f = 0.70 (EtOAc + 3% conc. HCl)

Sum formula $C_{12}H_{12}N_2O_4$

^{1}H-NMR (400 MHz, DMSO-d_6) δ = 2.43 (s, 3H, CH_3), 2.47 (s, 3H, CH_3), 7.63 (d, J = 8.4 Hz, 2H, H2' & H6'), 7.96 (d, J = 8.5 Hz, 2H, H3' & H5'), 13.68 (br s, 1H, enol-H) ppm. acid not detected

^{13}C-NMR (101 MHz, DMSO-d_6) δ = 26.3 (q, CH_3), 31.2 (q, CH_3), 115.7 (d, 2C, C2' & C6' or C3' & C5'), 126.9 (s, C3 or C1' or C4'), 130.9 (d, 2C, C2' & C6' or C3' & C5'), 134.8 (s, C3 or C1' or C4'), 145.4 (s, C3 or C1' or C4'), 166.8 (s, acid), 196.4 & 197.3 (2xs, 2C, carbonyl-C & enol-C) ppm.

Comment The compound was described in the literature as an intermediate but no analytical data was available.

E III.1.10 4-((1,3,5-Trimethyl-1*H*-pyrazol-4-yl)diazenyl)benzoic acid [14]

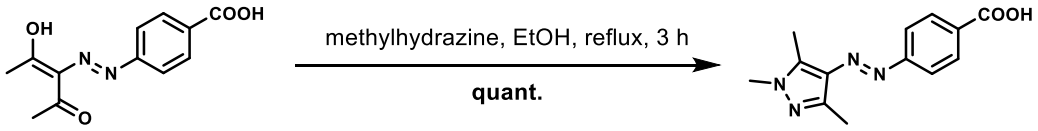

[13]
248.24 g/mol

[14]
258.28 g/mol

4-((1,3,5-Trimethyl-1*H*-pyrazol-4-yl)diazenyl)benzoic acid **[14]** was synthesized according to **General procedure B** using azo intermediate **[13]** (750 mg, 3.02 mmol) and EtOH (16 mL).

Yield quant. (778 mg, 3.02mmol)

Appearance yellow crystals

Melting point 278.0 – 279.0 °C (Lit.[189]: 271 – 272 °C)

TLC-Analysis R_f = 0.40 (EtOAc + 3% conc. HCl)

Sum formula $C_{13}H_{14}N_4O_2$

^{1}H-NMR (400 MHz, DMSO-d_6) δ = 2.38 (s, 3H, CH_3), 2.56 (s, 3H, CH_3), 3.74 (s, 3H, N-CH_3), 7.78 (d, *J* = 8.5 Hz, 2H, H2' & H6' or H3' & H5'), 8.06 (d, *J* = 8.5 Hz, 2H, H2' & H6' or H3' & H5'), 13.06 (br s, 1H, acid) ppm.

^{13}C-NMR (101 MHz, DMSO-d_6) δ = 9.5 (q, CH_3), 13.8 (q, CH_3), 36.0 (q, N-CH_3), 121.3 & 130.4 (2xd, 4C, C2' & C6' & C3' & C5'), 131.0 & 134.8 & 104.5 & 140.7 & 155.5 (5xs, 5C, C3 & C4 & C5 & C1' & C4'), 166.9 (s, acid) ppm.

E III.1.11 Ethyl 4-((1,3,5-trimethyl-1*H*-pyrazol-4-yl)diazenyl)benzoate [15]

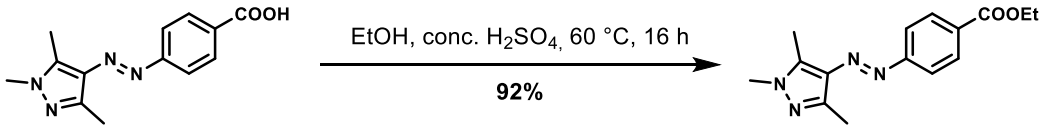

[14]
258.28 g/mol

[15]
286.34 g/mol

Acid **[14]** (300 mg, 1.16 mmol) was placed in an 8 mL vial. EtOH (5 mL) and conc. H_2SO_4 (3 drops) were added and the suspension was stirred for 16 hours at 60 °C in a thermo block (thermo sensor was set to 66 °C). The reaction was extracted with diethyl ether (2 x 20 mL). The combined organic phases were washed with 1 N NaOH (20 mL), satd. aqu. $NaHCO_3$ (2 x 15 mL) and brine (2 x 15 mL). After evaporation of the solvent in vacuo ethyl 4-((1,3,5-trimethyl-1*H*-pyrazol-4-yl)diazenyl)benzoate **[15]** was obtained.

Yield 92% (305 mg, 1.07 mmol)

Appearance orange crystals

Melting point	132.0 – 133.0 °C
TLC-Analysis	R_f = 0.30 (LP/EtOAc = 5/1)
Sum formula	$C_{15}H_{18}N_4O_2$
HR-MS	$[M+H]^+$: calculated: 287.1503 Da, found: 287.1509 Da, difference: 0.6 mDa
GC-MS	286 (29, M^+), 137 (100), 109 (58)
^{1}H-NMR (400 MHz, $CDCl_3$)	δ = 1.42 (t, *J* = 7.1 Hz, 3H, CH_2-C<u>H</u>$_3$), 2.51 (s, 3H, CH_3), 2.60 (s, 3H, CH_3), 3.80 (s, 3H, N-CH_3), 4.40 (q, *J* = 7.1 Hz, 2H, C<u>H</u>$_2$-C<u>H</u>$_3$), 7.80 (d, *J* = 8.8 Hz, 2H, H2' & H6' or H3' & H5'), 8.13 (d, *J* = 8.8 Hz, 2H, H2' & H6' or H3' & H5') ppm.
^{13}C-NMR (101 MHz, $CDCl_3$)	δ = 10.2 (q, CH_3), 14.1 (q, CH_3), 14.5 (q, CH_3), 36.2 (q, N-CH_3), 61.2 (t, CH_2), 121.7 & 130.6 (2xd, 4C, C2' & C6' & C3' & C5'), 130.7 & 135.7 & 139.8 & 142.9 & 156.5 (5xs, 5C, C3 & C4 & C5 & C1' & C4'), 166.5 (s, ester) ppm.

E III.1.12 *N*-Benzyl-4-((1,3,5-trimethyl-1*H*-pyrazol-4-yl)diazenyl)benzamide [<u>17</u>]

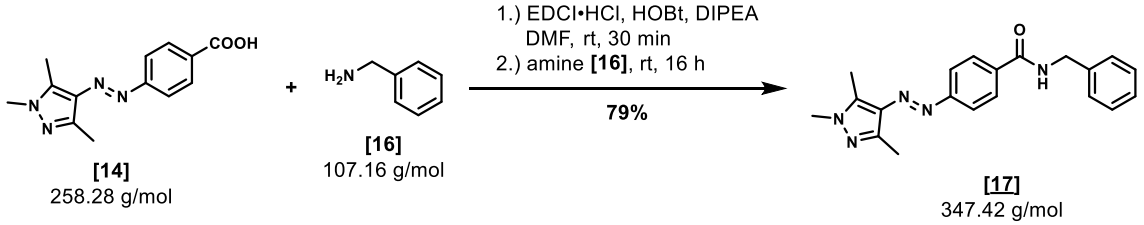

Acid **[14]** (37.2 mg, 0.144 mmol, 1 equiv.), EDCI•HCl (30.3 mg, 0.158 mmol, 1.1 equiv.), HOBt (24.2 mg, 0.158 mmol, 1.1 equiv.) and DIPEA (39.1 mg, 0.302 mmol, 2.1 equiv.) were dissolved in dry DMF (1.5 mL) and were stirred under argon at room temperature for 30 minutes. Then a solution of benzylamine **[16]** (15.4 mg, 0.144 mmol, 1 equiv.) in DMF (1.5 mL) was added via syringe and the reaction was stirred at room temperature for 16 hours. Volatiles were removed in vacuo. Purification by flash column chromatography (silica gel/crude material = 100/1, LP/EtOAc = 4/1) afforded *N*-benzyl-4-((1,3,5-trimethyl-1*H*-pyrazol-4-yl)diazenyl)benzamide **[<u>17</u>]**.

Yield	79% (39.5 mg, 0.114 mmol)
Appearance	yellow crystals
Melting point	177.0 – 178.0 °C
TLC-Analysis	R_f = 0.50 (LP/EtOAc = 2/1)

Sum formula	$C_{20}H_{21}N_5O$
HR-MS	$[M+H]^+$: calculated: 348.1819 Da, found: 348.1843 Da, difference: 2.4 mDa
^{1}H-NMR (400 MHz, $CDCl_3$)	δ = 2.50 (s, 3H, CH_3), 2.59 (s, 3H, CH_3), 3.79 (s, 3H, N-CH_3), 4.68 (d, *J* = 5.6 Hz, 2H, CH_2), 6.43 (br t, *J* = 4.9 Hz, 1H, NH), 7.28 – 7.40 (m, 5H, H2'' & H3'' & H4'' & H5'' & H6''), 7.81 (d, *J* = 8.7 Hz, 2H, H2' & H6' or H3' & H5'), 7.89 (d, *J* = 8.6 Hz, 2H, H2' & H6' or H3' & H5') ppm.
^{13}C-NMR (101 MHz, $CDCl_3$)	δ = 10.2 (q, CH_3), 14.1 (q, CH_3), 36.2 (q, N-CH_3), 44.4 (t, CH_2), 122.0 & 128.0 & 128.1 & 129.0 (4xd, 8C, C2' & C6' & C3' & C5' & C2'' & C6'' & C3'' & C5''), 127.8 (d, C4''), 134.5 & 135.6 & 138.3 & 139.7 & 142.8 & 155.7 (6xs, 6C, C3 & C4 & C5 & C1' & C4' & C1''), 167.0 (s, amide) ppm.

E III.1.13 *N*-Phenyl-4-((1,3,5-trimethyl-1*H*-pyrazol-4-yl)diazenyl)benzamide [18]

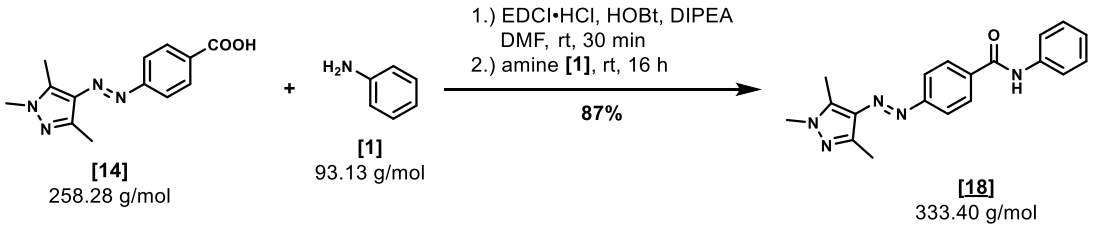

Acid **[14]** (38.7 mg, 0.150 mmol, 1 equiv.), EDCI•HCl (31.4 mg, 0.165 mmol, 1.1 equiv.), HOBt (25.2 mg, 0.165 mmol, 1.1 equiv.) and DIPEA (40.7 mg, 0.315 mmol, 2.1 equiv.) were dissolved in dry DMF (1.5 mL) and were stirred under argon at room temperature for 30 minutes. Then a solution of aniline **[1]** (14.0 mg, 0.150 mmol, 1 equiv.) in DMF (1.5 mL) was added via syringe and the reaction was stirred at room temperature for 16 hours. Volatiles were removed in vacuo. Purification by flash column chromatography (silica gel/crude material = 100/1, LP/EtOAc = 4/1) afforded *N*-phenyl-4-((1,3,5-trimethyl-1*H*-pyrazol-4-yl)diazenyl)benzamide **[18]**.

Yield	87% (43.5 mg, 0.130 mmol)
Appearance	yellow crystals
Melting point	168.0 – 170.0 °C
TLC-Analysis	R_f = 0.35 (LP/EtOAc = 1/2)
Sum formula	$C_{19}H_{19}N_5O$

HR-MS [M+H]$^+$: calculated: 334.1663 Da, found: 334.1687 Da, difference: 2.4 mDa

^{1}H-NMR (400 MHz, $CDCl_3$) δ = 2.51 (s, 3H, CH_3), 2.61 (s, 3H, CH_3), 3.80 (s, 3H, N-CH_3), 7.17 (t, *J* = 7.4 Hz, 1H, H4''), 7.39 (t, *J* = 7.9 Hz, H3'' & H5''), 7.67 (d, *J* = 7.7 Hz, 2H, H2'' & H6''), 7.84 – 7.89 (m, 3H, NH & H2' & H6' or H3' & H5'), 7.97 (d, *J* = 8.5 Hz, 2H, H2' & H6' or H3' & H5') ppm.

^{13}C-NMR (101 MHz, $CDCl_3$) δ = 10.2 (q, CH_3), 14.1 (q, CH_3), 36.2 (q, N-CH_3), 120.3 & 122.2 & 128.0 & 129.3 (4xd, 8C, C2' & C6'& C3' & C5' & C2'' & C6'' & C3'' & C5''), 124.8 (d, C4''), 135.1 & 135.6 & 138.1 & 139.8 & 142.9 & 155.9 (6xs, 6C, C3 & C4 & C5 & C1' & C4' & C1''), 165.3 (s, amide) ppm.

E III.1.14 4-((2-Hydroxy-4-oxopent-2-en-3-yl)diazenyl)benzonitrile [20]

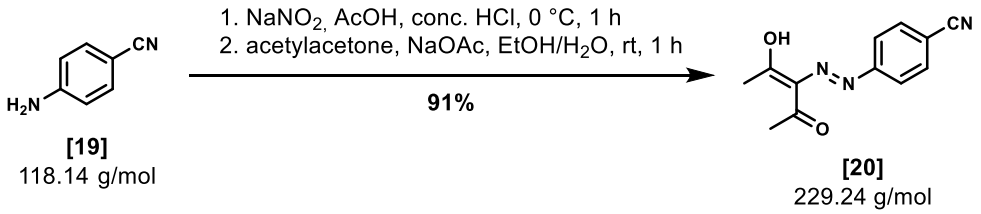

[19]
118.14 g/mol

[20]
229.24 g/mol

4-((2-Hydroxy-4-oxopent-2-en-3-yl)diazenyl)benzonitrile **[20]** was synthesized according to **General procedure A** using 4-aminobenzonitril **[19]** (874 mg, 7.40 mmol), AcOH (10 mL) and conc. HCl (1.7 mL).

Yield 91% (1.54 g, 6.73 mmol)

Appearance yellow crystals

Melting point 190.5 – 191.0 °C

TLC-Analysis R_f = 0.55 (LP/EtOAc = 3/1)

Sum formula $C_{12}H_{11}N_3O_2$

^{1}H-NMR (400 MHz, $CDCl_3$) δ = 2.49 (s, 3H, CH_3), 2.60 (s, 3H, CH_3), 7.45 (d, *J* = 8.8 Hz, 2H, H2' & H6'), 7.68 (d, *J* = 8.8 Hz, 2H, H3' & H5'), 14.48 (br s, 1H, enol-H) ppm.

^{13}C-NMR (101 MHz, $CDCl_3$) δ = 26.7 (q, CH_3), 31.9 (q, CH_3), 108.4 (s, C3 or C1' or C4' or CN), 116.4 (d, 2C, C2' & C6' or C3' & C5'), 118.6 (s, C3 or C1' or C4' or CN), 134.0 (d, 2C, C2' & C6' or C3' & C5'), 134.7 (s, C3 or C1' or C4' or CN), 145.1 (s, C3 or C1' or C4' or CN), 196.9 & 198.7 (2xs, 2C, carbonyl-C & enol-C) ppm.

Comment Spectral data is in accordance with the literature[190].

E III.1.15 4-((1,3,5-Trimethyl-1*H*-pyrazol-4-yl)diazenyl)benzonitrile [21]

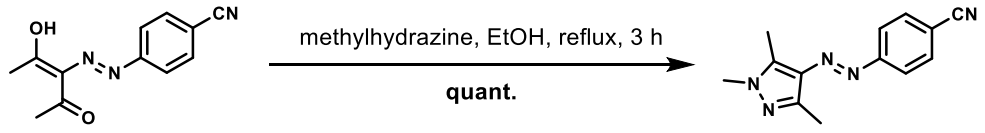

[20]
229.24 g/mol

[21]
239.28 g/mol

4-((1,3,5-Trimethyl-1*H*-pyrazol-4-yl)diazenyl)benzonitrile **[21]** was synthesized according to **General procedure B** using azo intermediate **[20]** (750 mg, 3.27 mmol) and EtOH (17 mL).

Yield quant. (782 mg, 3.27 mmol)

Appearance orange crystals

Melting point 141.0 – 141.5 °C

TLC-Analysis R_f = 0.40 (LP/EtOAc = 1/1)

Sum formula $C_{13}H_{13}N_5$

HR-MS $[M+H]^+$: calculated: 240.1244 Da, found: 240.1257 Da, difference: 1.3 mDa

GC-MS 239 (42, M^+), 137 (100), 109 (77), 102 (10)

^{1}H-NMR (400 MHz, $CDCl_3$) δ = 2.48 (s, 3H, CH_3), 2.58 (s, 3H, CH_3), 3.79 (s, 3H, N-CH_3), 7.73 (d, *J* = 8.8 Hz, 2H, H2' & H6' or H3' & H5'), 7.82 (d, *J* = 8.7 Hz, 2H, H2' & H6' or H3' & H5') ppm.

^{13}C-NMR (101 MHz, $CDCl_3$) δ = 10.1 (q, CH_3), 14.1 (q, CH_3), 36.2 (q, N-CH_3), 112.1 (s, C4'), 119.0 (s, CN), 122.4 & 133.2 (2xd, 4C, C2' & C6' & C3' & C5'), 135.7 & 140.4 & 143.0 & 155.9 (4xs, 4C, C3 & C4 & C5 & C1') ppm.

E III.1.16 4-((1,3,5-Trimethyl-1*H*-pyrazol-4-yl)diazenyl)benzamide [22]

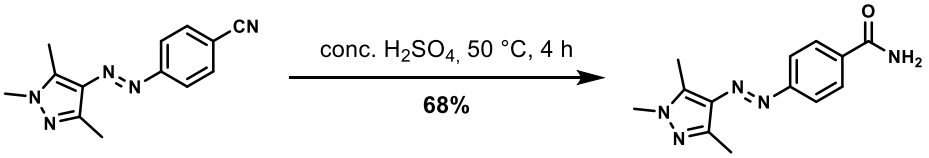

[21]
239.28 g/mol

[22]
257.30 g/mol

4-((1,3,5-Trimethyl-1*H*-pyrazol-4-yl)diazenyl)benzonitrile **[21]** (46.5 mg, 0.19 mmol, 1 equiv.) was dissolved in conc. H_2SO_4 (0.5 mL) and stirred at 50 °C for 4 hours. Then it was slowly poured into ice/H_2O and basified using 6 N NaOH followed by satd. aqu. $NaHCO_3$. The aqu.

mixture was extracted with EtOAc (3 x 5 mL), dried over $MgSO_4$ and concentrated in vacuo to provide 4-((1,3,5-trimethyl-1*H*-pyrazol-4-yl)diazenyl)benzamide **[22]**.

Yield	68% (34 mg, 0.13 mmol)
Appearance	orange crystals
Melting point	198.0 – 201.0 °C
TLC-Analysis	R_f = 0.40 (LP/EtOAc = 4/1)
Sum formula	$C_{13}H_{15}N_5O$
HR-MS	$[M+H]^+$: calculated: 258.1350 Da, found: 258.1357 Da, difference: 0.7 mDa
GC-MS	257 (46, M^+), 208 (10), 207 (56), 137 (100), 109 (76)
^{1}H-NMR (400 MHz, $CDCl_3$)	δ = 2.50 (s, 3H, CH_3), 2.60 (s, 3H, CH_3), 3.80 (s, 3H, N-CH_3), 5.63 (br s, 1H, NH) 6.09 (br s, 1H, NH) 7.83 (d, *J* = 8.7 Hz, 2H, H2' & H6' or H3' & H5'), 7.91 (d, *J* = 8.7 Hz, 2H, H2' & H6' or H3' & H5') ppm.
^{13}C-NMR (101 MHz, $CDCl_3$)	δ = 10.2 (q, CH_3), 14.1 (q, CH_3), 36.2 (q, N-CH_3), 122.0 & 128.4 2x(d, 4C, C2' & C6' & C3' & C5'), 133.4 & 135.6 & 139.8 & 142.9 & 156.0 (5xs, 5C, C3 & C4 & C5 & C1' & C4'), 168.8 (s, amide) ppm.

E III.1.17 3-((4-(Diethylamino)phenyl)diazenyl)-4-hydroxypent-3-en-2-one [24]

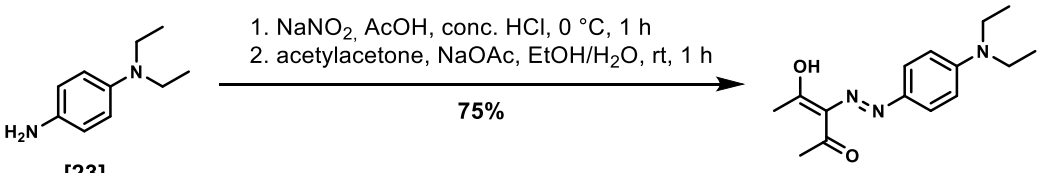

[23]
164.25 g/mol

[24]
275.35 g/mol

3-((4-(Diethylamino)phenyl)diazenyl)-4-hydroxypent-3-en-2-one **[24]** was synthesized according to **General procedure A** using *N*^{1},*N*^{1}-diethylbenzene-1,4-diamine **[23]** (1.22 g, 7.40 mmol), AcOH (10 mL) and conc. HCl (1.7 mL). The obtained crude product was purified by flash column chromatography (silica gel/crude material = 100/1, LP/EtOAc = 19/1).

Yield	75% (1.543 g, 5.56 mmol)
Appearance	red crystals
Melting point	67.5 – 68.0 °C (Lit.[191]: 68 – 69 °C)
TLC-Analysis	R_f = 0.60 (LP/EtOAc = 5/1)

Sum formula $C_{15}H_{21}N_3O_2$

^{1}H-NMR (400 MHz, $CDCl_3$) δ = 1.18 (t, *J* = 7.1 Hz, 6H, $CH_2C\underline{H}_3$), 2.45 (s, 3H, CH_3), 2.58 (s, 3H, CH_3), 3.38 (q, *J* = 7.1, 4H, $C\underline{H}_2CH_3$), 6.68 (d, *J* = 9.1 Hz, 2H, H3' & H5'), 7.31 (d, *J* = 9.1 Hz, 2H, H2' & H6'), 15.27 (br s, 1H, enol-H) ppm.

^{13}C-NMR (101 MHz, $CDCl_3$) δ = 12.7 (q, 2C, $CH_2\underline{C}H_3$), 26.8 (q, CH_3), 31.5 (q, CH_3), 44.8 (t, 2C, $\underline{C}H_2CH_3$), 112.4 & 118.3 (2xd, 4C, C2' & C3' & C5' & C6'), 130.7 & 132.2 & 146.8 (3xs, 3C, C3 & C1' & C4'), 197.0 & 197.1 (2xs, 2C, carbonyl-C & enol-C) ppm.

E III.1.18 *N*,*N*-Diethyl-4-((1,3,5-trimethyl-1*H*-pyrazol-4-yl)diazenyl)aniline [25]

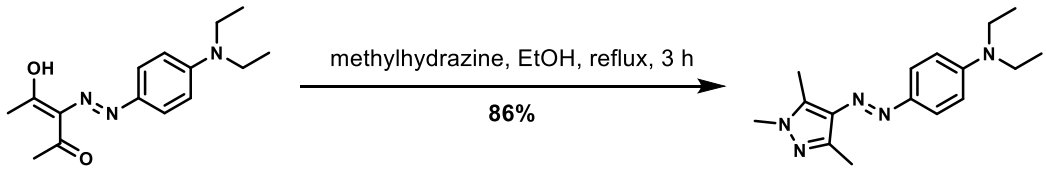

[24]
275.35 g/mol

[25]
285.40 g/mol

N,*N*-Diethyl-4-((1,3,5-trimethyl-1*H*-pyrazol-4-yl)diazenyl)aniline **[25]** was synthesized according to **General procedure B** using azo intermediate **[24]** (750 mg, 2.72 mmol) and EtOH (14 mL). Purification by flash column chromatography (silica gel/crude material = 100/1, LP/EtOAc = 4/1) provided the pure product.

Yield 86% (668 mg, 2.34 mmol)

Appearance orange crystals

Melting point 102.0 – 102.5 °C

TLC-Analysis R_f = 0.35 (LP/EtOAc = 1/1)

Sum formula $C_{16}H_{23}N_5$

HR-MS $[M+H]^+$: calculated: 286.2026 Da, found: 286.2040 Da, difference: 1.4 mDa

GC-MS 286 (17), 285 (85, M^+), 271 (19), 270 (100)

^{1}H-NMR (400 MHz, $CDCl_3$) δ = 1.21 (t, *J* = 7.1 Hz, 6H, $CH_2C\underline{H}_3$), 2.48 (s, 3H, CH_3), 2.54 (s, 3H, CH_3), 3.43 (q, *J* = 7.1 Hz, 4H, $C\underline{H}_2CH_3$), 3.76 (s, 3H, N-CH_3), 6.70 (d, *J* = 9.1 Hz, 2H, H3' & H5'), 7.72 (d, *J* = 9.2 Hz, 2H, H2' & H6') ppm.

^{13}C-NMR (101 MHz, $CDCl_3$) δ = 10.1 (q, CH_3), 12.8 (q, 2C, $CH_2\underline{C}H_3$), 13.8 (q, CH_3), 36.0 (q, N-CH_3), 44.8 (t, 2C, $\underline{C}H_2CH_3$), 111.3 & 123.7 (2xd, 4C, C2' & C3' & C5' & C6'), 135.1 & 136.7 & 142.1 & 144.1 & 149.1 (5xs, 5C, C3 & C4 & C5 & C1' & C4') ppm.

E III.1.19 3-((4-Fluorophenyl)diazenyl)-4-hydroxypent-3-en-2-one [27]

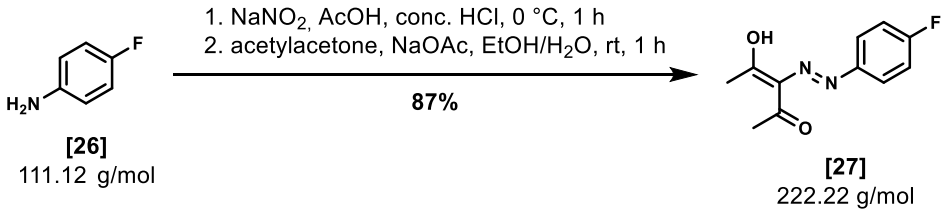

[26]
111.12 g/mol

[27]
222.22 g/mol

3-((4-Fluorophenyl)diazenyl)-4-hydroxypent-3-en-2-one **[27]** was synthesized according to **General procedure A** using 4-fluoroaniline **[26]** (822 mg, 7.40 mmol), AcOH (10 mL) and conc. HCl (1.7 mL).

Yield 87% (1.43 g, 6.44 mmol)

Appearance yellow crystals

Melting point 115.0 – 115.5 °C (Lit.[192]: 117 °C)

TLC-Analysis R_f = 0.60 (LP/EtOAc = 8/1)

Sum formula $C_{11}H_{11}FN_2O_2$

^{1}H-NMR (400 MHz, $CDCl_3$) δ = 2.48 (s, 3H, CH_3), 2.60 (s, 3H, CH_3), 7.11 (dd, *J* = 9.0, 8.1 Hz, 2H, H3' & H5'), 7.38 (dd, *J* = 9.1, 4.6 Hz, 2H, H2' & H6'), 14.80 (br s, 1H, enol-H) ppm.

^{13}C-NMR (101 MHz, $CDCl_3$) δ = 26.7 (q, CH_3), 31.8 (q, CH_3), 116.7 (d/d, $^2J_{CF}$ = 23.3 Hz, 2C, C3' & C5'), 117.8 (d/d, $^3J_{CF}$ = 8.2 Hz, 2C, C2' & C6'), 133.4 (s, C3), 138.0 (s/d, $^4J_{CF}$ = 2.8 Hz, C1'), 160.8 (s/d, $^1J_{CF}$ = 245.9 Hz, C4'), 197.1 & 198.2 (2xs, 2C, carbonyl-C & enol-C) ppm.

E III.1.20 4-((4-Fluorophenyl)diazenyl)-1,3,5-trimethyl-1*H*-pyrazole [<u>28</u>]

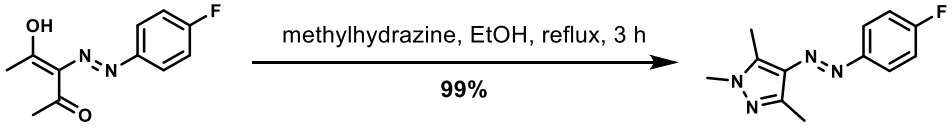

[27]
222.22 g/mol

[<u>28</u>]
232.26 g/mol

4-((4-Fluorophenyl)diazenyl)-1,3,5-trimethyl-1*H*-pyrazole **[<u>28</u>]** was synthesized according to **General procedure B** using azo intermediate **[27]** (700 mg, 3.15 mmol) and EtOH (16 mL).

Yield	99% (724 mg, 3.12 mmol)
Appearance	yellow crystals
Melting point	76.0 – 76.5 °C
TLC-Analysis	R_f = 0.40 (LP/EtOAc = 1/1)
Sum formula	$C_{12}H_{13}FN_4$
HR-MS	$[M+H]^+$: calculated: 233.1197 Da, found: 233.1210 Da, difference: 1.3 mDa
GC-MS	232 (55, M^+), 137 (90), 109 (100)
^{1}H-NMR (400 MHz, $CDCl_3$)	δ = 2.48 (s, 3H, CH_3), 2.56 (s, 3H, CH_3), 3.77 (s, 3H, N-CH_3), 7.09 – 7.15 (m, 2H, H3' & H5'), 7.75 – 7.80 (m, 2H, H2' & H6') ppm.
^{13}C-NMR (101 MHz, $CDCl_3$)	δ = 10.1 (q, CH_3), 14.0 (q, CH_3), 36.1 (q, N-CH_3), 115.8 (d/d, $^2J_{CF}$ = 22.8 Hz, 2C, C3' & C5'), 123.6 (d/d, $^3J_{CF}$ = 8.5 Hz, 2C, C2' & C6'), 135.1 & 138.9 & 142.5 (3xs, C3 & C4 & C5), 150.2 (s/d, $^4J_{CF}$ = 3.1 Hz, C1'), 163.5 (s/d, $^1J_{CF}$ = 249.1 Hz, C4') ppm.

E III.1.21 4-Hydroxy-3-((4-iodophenyl)diazenyl)pent-3-en-2-one [30]

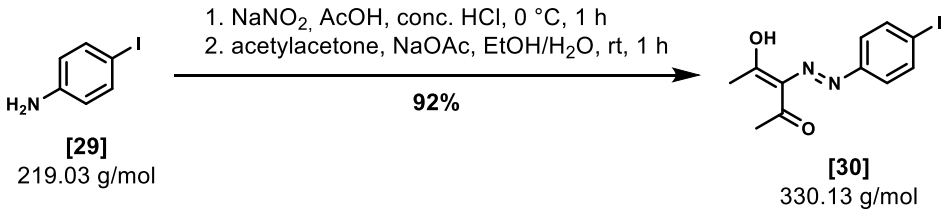

[29]
219.03 g/mol

[30]
330.13 g/mol

4-Hydroxy-3-((4-iodophenyl)diazenyl)pent-3-en-2-one **[30]** was synthesized according to **General procedure A** using 4-iodoaniline **[29]** (1.62 g, 7.40 mmol), AcOH (10 mL) and conc. HCl (1.7 mL).

Yield	92% (2.25 g, 6.80 mmol)
Appearance	yellow crystals
Melting point	152.5 – 153.0 °C (Lit.[193]: 150 °C)
TLC-Analysis	R_f = 0.50 (LP/EtOAc = 8/1)
Sum formula	$C_{11}H_{11}IN_2O_2$
^{1}H-NMR (400 MHz, $CDCl_3$)	δ = 2.47 (s, 3H, CH_3), 2.59 (s, 3H, CH_3), 7.15 (d, *J* = 8.8 Hz, 2H, H2' & H6' or H3' & H5'), 7.69 (d, *J* = 8.8 Hz, 2H, H2' & H6' or H3' & H5'), 14.62 (br s, 1H, enol-H) ppm.

^{13}C-NMR (101 MHz, $CDCl_3$) δ = 26.7 (q, CH_3), 31.8 (q, CH_3), 89.4 (s, C4'), 118.1 (d, 2C, C2' & C6' or C3' & C5'), 133.7 (s, C3 or C1'), 138.7 (d, 2C, C2' & C6' or C3' & C5'), 141.5 (s, C3 or C1'), 197.0 & 198.3 (2xs, 2C, carbonyl-C & enol-C) ppm.

E III.1.22 4-((4-Iodophenyl)diazenyl)-1,3,5-trimethyl-1*H*-pyrazole [31]

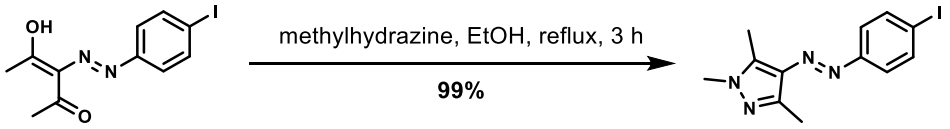

[30]
330.13 g/mol

[31]
340.17 g/mol

4-((4-Iodophenyl)diazenyl)-1,3,5-trimethyl-1*H*-pyrazole **[31]** was synthesized according to **General procedure B** using azo intermediate **[30]** (1.10 g, 3.33 mmol) and EtOH (17 mL).

Yield 99% (1.13 g, 3.33 mmol)

Appearance orange crystals

Melting point 116.5 – 117.5 °C (Lit.[194]: 104 – 106 °C)

TLC-Analysis R_f = 0.35 (LP/EtOAc = 1/1)

Sum formula $C_{12}H_{13}IN_4$

GC-MS 340 (43, M^+), 137 (100), 109 (70)

^{1}H-NMR (400 MHz, $CDCl_3$) δ = 2.48 (s, 3H, CH_3), 2.56 (s, 3H, CH_3), 3.78 (s, 3H, N-CH_3), 7.51 (d, *J* = 8.6 Hz, 2H, H2' & H6' or H3' & H5'), 7.78 (d, *J* = 8.7 Hz, 2H, H2' & H6' or H3' & H5') ppm.

^{13}C-NMR (101 MHz, $CDCl_3$) δ = 10.1 (q, CH_3), 14.0 (q, CH_3), 36.2 (q, N-CH_3), 95.2 (s, C4'), 123.6 (d, 2C, C2' & C6'), 135.3 (s, C3 or C4 or C5 or C1'), 138.2 (d, 2C, C3' & C5'), 139.3 (s, C3 or C4 or C5 or C1'), 142.7 (s, C3 or C4 or C5 or C1'), 153.1 (s, C3 or C4 or C5 or C1') ppm.

E III.1.23 4-Ethynylaniline [32]

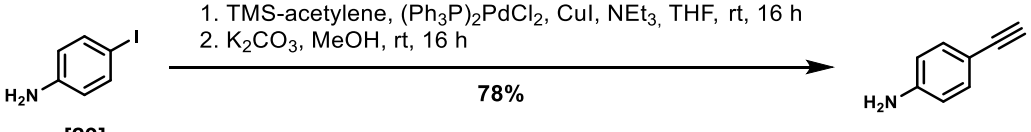

[29]
219.03 g/mol

[32]
117.15 g/mol

4-Ethynylaniline **[32]** was prepared via Sonogashira coupling.[195] An oven-dried round bottom flask equipped with a magnetic stirring bar was charged with 4-iodoaniline **[29]** (9.35 g, 42.7 mmol, 1 equiv.), bis(triphenylphosphine)palladium(II) dichloride (599 mg, 0.85 mmol, 2 mol%),

and copper(I) iodide (163 mg, 0.85 mmol, 2 mol%). The flask was closed with a septum, evacuated and flushed with argon three times. Triethylamine (35 mL) and dry THF (71 mL) were added via syringe. The suspension was stirred for 5 minutes at room temperature and then trimethylsilylacetylene (5.59 g, 56.9 mmol, 1.33 equiv.) was added via syringe and the reaction mixture was stirred for 16 hours. TLC and GC-MS analysis showed full conversion. Volatiles were removed in vacuo. The residue was dissolved in DCM and the solution was filtered through a short pad of silica gel using DCM as eluent. The solvent was removed in vacuo providing the TMS-protected product. The material was dissolved in MeOH (71 mL). K_2CO_3 (5.89 g, 42.7 mmol, 1 equiv.) was added and the reaction was stirred at room temperature for 16 hours. K_2CO_3 was removed by filtration. MeOH was used for washing and the filtrate was concentrated in vacuo. The residue was distributed between H_2O (100 mL) and DCM (100 mL) and phases were separated. The aqu. phase was extracted with DCM (3 x 50 mL). The combined organic phases were washed with brine (150 mL) and dried over $MgSO_4$. After evaporation of the solvent in vacuo the product was obtained in 96% purity.

Yield: 78% (3.91 g, 33.4 mmol)

Appearance brown solid

Melting point 101.0 – 102.0 °C (Lit.[196]: 104 – 105 °C)

TLC-Analysis R_f = 0.50 (LP/EtOAc = 4/1)

Sum formula C_8H_7N

^{1}H-NMR (400 MHz, DMSO-d_6) δ = 3.75 (s, 1H, CCH), 5.50 (br s, 2H, NH_2), 6.52 (d, *J* = 8.6 Hz, 2H, H2 & H6), 7.12 (d, *J* = 8.5 Hz, 2H, H3 & H5) ppm.

^{13}C-NMR (101 MHz, DMSO-d_6) δ = 77.1 (d, C<u>C</u>H), 85.1 (s, <u>C</u>CH), 107.7 (s, C4), 113.5 (d, 2C, C2 & C6), 132.8 (d, 2C, C3 & C5), 149.5 (s, C1) ppm.

E III.1.24 3-((4-Ethynylphenyl)diazenyl)-4-hydroxypent-3-en-2-one [<u>33</u>]

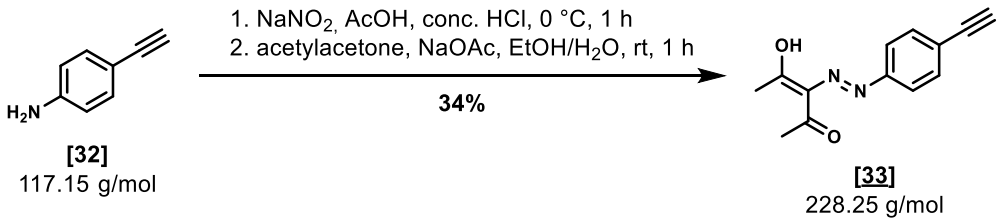

[32]
117.15 g/mol

[<u>33</u>]
228.25 g/mol

3-((4-Ethynylphenyl)diazenyl)-4-hydroxypent-3-en-2-one **[<u>33</u>]** was synthesized according to **General procedure A** using 4-ethynylaniline **[32]** (443 mg, 3.70 mmol), AcOH (5 mL) and conc. HCl (0.85 mL). The product was obtained after purification by flash column chromatography (silica gel/crude material = 100/1, LP/EtOAc = 50/1).

Yield	34% (285 mg, 1.25 mmol), 52% based on combined yield with side product **[35]**.
Appearance	yellow crystals
Melting point	190.0 – 191.0 °C
TLC-Analysis	R_f = 0.40 (LP/EtOAc = 20/1)
Sum formula	$C_{13}H_{12}N_2O_2$
^{1}H-NMR (400 MHz, $CDCl_3$)	δ = 2.49 (s, 3H, CH_3), 2.60 (s, 3H, CH_3), 3.12 (s, 1H, CCH), 7.35 (d, *J* = 8.7 Hz, 2H, H2' & H6' or H3' & H5'), 7.52 (d, *J* = 8.7 Hz, 2H, H2' & H6' or H3' & H5'), 14.65 (br s, 1H, enol-H) ppm.
^{13}C-NMR (101 MHz, $CDCl_3$)	δ = 26.8 (q, CH_3), 31.8 (q, CH_3), 78.1 (d, C<u>C</u>H), 83.2 (s, <u>C</u>CH), 116.1 (d, 2C, C2' & C6' or C3' & C5'), 119.4 (s, C3 or C1' or C4'), 133.7 (d, 2C, C2' & C6' or C3' & C5'), 133.7 (s, C3 or C1' or C4'), 141.8 (s, C3 or C1' or C4'), 197.1 & 198.3 (2xs, 2C, carbonyl-C & enol-C) ppm.

E III.1.25 4-((4-Ethynylphenyl)diazenyl)-1,3,5-trimethyl-1*H*-pyrazole [<u>34</u>]

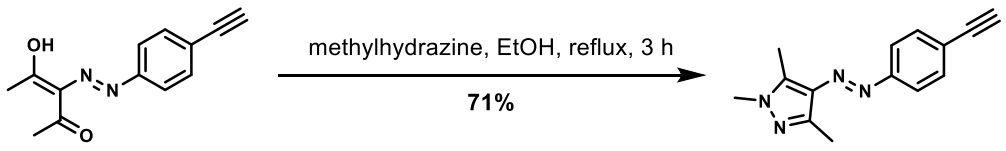

[<u>33</u>]
228.25 g/mol

[<u>34</u>]
238.29 g/mol

4-((4-Ethynylphenyl)diazenyl)-1,3,5-trimethyl-1*H*-pyrazole **[<u>34</u>]** was synthesized according to **General procedure B** using azo intermediate **[<u>33</u>]** (100 mg, 0.44 mmol) and EtOH (2.3 mL). Purification by flash column chromatography provided (silica gel/crude material = 100/1, LP/EtOAc = 4/1) the desired product.

Yield	71% (74 mg, 0.31 mmol)
Appearance	yellow crystals
Melting point	102.5 – 103.5 °C
TLC-Analysis	R_f = 0.45 (LP/EtOAc = 1/1)
Sum formula	$C_{14}H_{14}N_4$
HR-MS	$[M+H]^+$: calculated: 239.1291 Da, found: 239.1309 Da, difference: 1.8 mDa
GC-MS	238 (49, M^+), 137 (100), 109 (71), 101 (15)

^{1}H-NMR (400 MHz, $CDCl_3$) δ = 2.49 (s, 3H, CH_3), 2.58 (s, 3H, CH_3), 3.17 (s, 1H, CCH), 3.78 (s, 3H, N-CH_3), 7.57 (d, *J* = 8.7 Hz, 2H, H2' & H6' or H3' & H5'), 7.74 (d, *J* = 8.6 Hz, 2H, H2' & H6' or H3' & H5') ppm.

^{13}C-NMR (101 MHz, $CDCl_3$) δ = 10.1 (q, CH_3), 14.0 (q, CH_3), 36.2 (q, N-CH_3), 78.7 & 83.8 (s & d, CCH), 121.9 (d, 2C, C2' & C6'), 122.9 (s, C3 or C4 or C5 or C1' or C4'), 133.0 (d, 2C, C3' & C5'), 135.5 (s, C3 or C4 or C5 or C1' or C4'), 139.4 (s, C3 or C4 or C5 or C1' or C4'), 142.7 (s, C3 or C4 or C5 or C1' or C4'), 153.5 (s, C3 or C4 or C5 or C1' or C4') ppm.

E III.1.26 3-((4-Acetylphenyl)diazenyl)-4-hydroxypent-3-en-2-one [35]

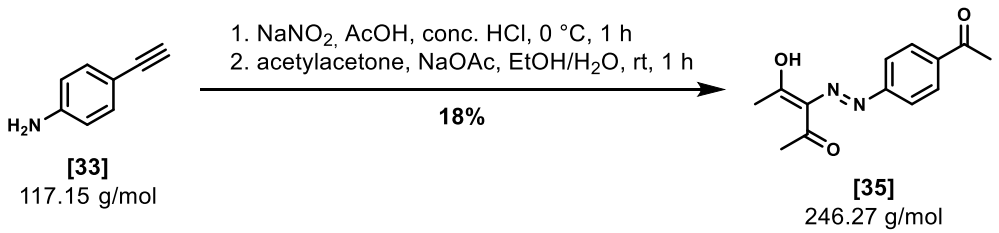

[33]
117.15 g/mol

[35]
246.27 g/mol

3-((4-Acetylphenyl)diazenyl)-4-hydroxypent-3-en-2-one **[35]** was obtained as a side product in the preparation of alkyne **[33]** due to partial hydration of the triple bond. The product was isolated through separation via flash column chromatography (silica gel/crude material = 100/1, LP/EtOAc = 50/1).

Yield 18% (285 mg, 0.68 mmol), 52% based on combined yield with main product **[33]**.

Appearance orange crystals

Melting point 143.0 – 143.5 °C (Lit.[197]: 150 °C)

TLC-Analysis R_f = 0.60 (LP/EtOAc = 4/1)

Sum formula $C_{13}H_{14}N_2O_3$

^{1}H-NMR (400 MHz, $CDCl_3$) δ = 2.49 (s, 3H, CH_3), 2.57 (s, 3H, CH_3), 2.59 (s, 3H, CH_3), 7.43 (d, *J* = 8.8 Hz, 2H, H2' & H6' or H3' & H5'), 7.99 (d, *J* = 8.7 Hz, 2H, H2' & H6' or H3' & H5'), 14.54 (br s, 1H, enol-H) ppm.

^{13}C-NMR (101 MHz, $CDCl_3$) δ = 26.6 (q, CH_3), 26.7 (q, CH_3), 31.8 (q, CH_3), 115.8 & 130.4 (2xd, 4C, C2' & C3' & C5' & C6'), 134.2 & 134.4 & 145.3 (3xs, 3C, C3 & C1' & C4'), 196.6 & 197.0 & 198.4 (3xs, 3C, 2 x carbonyl-C & enol-C) ppm.

E III.1.27 1-(4-((1,3,5-Trimethyl-1*H*-pyrazol-4-yl)diazenyl)phenyl)ethan-1-one [36]

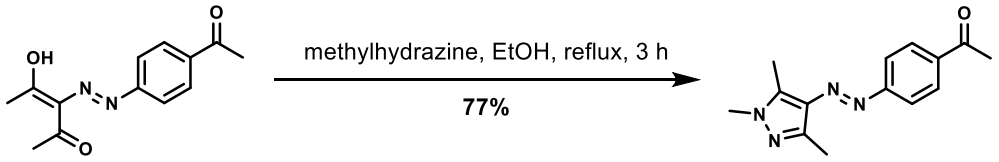

[35]
246.27 g/mol

[36]
256.31 g/mol

1-(4-((1,3,5-Trimethyl-1*H*-pyrazol-4-yl)diazenyl)phenyl)ethan-1-one **[36]** was synthesized according to **General procedure B** using azo intermediate **[35]** (50 mg, 0.20 mmol) and EtOH (1.0 mL). Purification by flash column chromatography (silica gel/crude material = 100/1, LP/EtOAc = 4/1) provided the pure product.

Yield	77% (39 mg, 0.15 mmol)
Appearance	orange crystals
Melting point	111.5 – 112.5 °C
TLC-Analysis	R_f = 0.40 (LP/EtOAc = 1/2)
Sum formula	$C_{14}H_{16}N_4O$
HR-MS	$[M+H]^+$: calculated: 257.1397 Da, found: 257.1406 Da, difference: 0.9 mDa
GC-MS	256 (46, M^+), 137 (100), 109 (76)
^{1}H-NMR (400 MHz, $CDCl_3$)	δ = 2.50 (s, 3H, CH_3), 2.60 (s, 3H, CH_3), 2.64 (s, 3H, CH_3), 3.79 (s, 3H, N-CH_3), 7.82 (d, *J* = 8.6 Hz, 2H, H2' & H6' or H3' & H5'), 8.05 (d, *J* = 8.7 Hz, 2H, H2' & H6' or H3' & H5') ppm.
^{13}C-NMR (101 MHz, $CDCl_3$)	δ = 10.2 (q, CH_3), 14.1 (q, CH_3), 26.9 (q, CH_3), 36.2 (q, N-CH_3), 121.9 & 129.5 (2xd, 4C, C2' & C6' & C3' & C5'), 135.8 & 137.2 & 139.9 & 142.9 & 156.5 (5xs, 5C, C3 & C4 & C5 & C1' & C4'), 197.7 (s, ketone) ppm.

E III.1.28 4-Hydroxy-3-(*p*-tolyldiazenyl)pent-3-en-2-one [38]

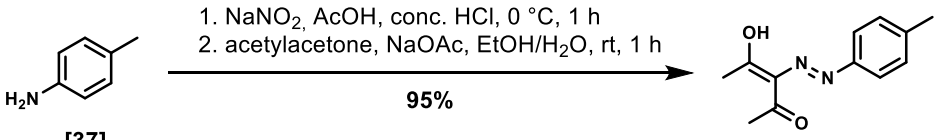

[37]
107.16 g/mol

[38]
218.26 g/mol

4-Hydroxy-3-(*p*-tolyldiazenyl)pent-3-en-2-one **[38]** was synthesized according to **General procedure A** using *p*-toluidine **[37]** (2.00 g, 18.66 mmol), AcOH (25 mL) and conc. HCl (4.25 mL).

Yield	95% (3.878 g, 17.77 mmol)
Appearance	yellow crystals
Melting point	97.0 – 98.0 °C (Lit.[184, 198]: 94 – 96 °C)
TLC-Analysis	R_f = 0.75 (LP/EtOAc = 5/1)
Sum formula	$C_{12}H_{14}N_2O_2$
^{1}H-NMR (400 MHz, $CDCl_3$)	δ = 2.36 (s, 3H, CH_3), 2.49 (s, 3H, CH_3), 2.60 (s, 3H, CH_3), 7.21 (d, *J* = 8.3 Hz, 2H, H2' & H6'), 7.31 (d, *J* = 8.5 Hz, 2H, H3' & H5'), 14.81 (br s, 1H, enol-H) ppm.
^{13}C-NMR (101 MHz, $CDCl_3$)	δ = 21.2 (q, Ph-CH_3), 26.8 (q, CH_3), 31.8 (q, CH_3), 116.4 (d, 2C, C2' & C6' or C3' & C5'), 130.4 (d, 2C, C2' & C6' or C3' & C5'), 133.1 & 136.1 & 139.4 (3xs, 3C, C3 & C1' & C4'), 197.2 & 197.9 (2xs, 2C, carbonyl-C & enol-C) ppm.

E III.1.29 1,3,5-Trimethyl-4-(*p*-tolyldiazenyl)-1*H*-pyrazole [39]

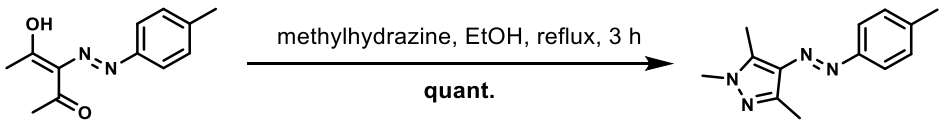

[38]
218.26 g/mol

[39]
228.30 g/mol

1,3,5-Trimethyl-4-(*p*-tolyldiazenyl)-1*H*-pyrazole **[39]** was synthesized according to **General procedure B** using azo intermediate **[38]** (1.50 g, 6.87 mmol) and EtOH (38 mL).

Yield	quant. (1.57 g, 6.87 mmol)
Appearance	yellow crystals
Melting point	81.0 – 83.0 °C
TLC-Analysis	R_f = 0.25 (LP/EtOAc = 5/1)

Sum formula	$C_{13}H_{16}N_4$
HR-MS	$[M+H]^+$: calculated: 229.1448 Da, found: 229.1458 Da, difference: 1.0 mDa
GC-MS	228 (67, M^+), 137 (100), 109 (81)
^{1}H-NMR (400 MHz, $CDCl_3$)	δ = 2.41 (s, 3H, CH_3), 2.49 (s, 3H, CH_3), 2.57 (s, 3H, CH_3), 3.78 (s, 3H, N-CH_3), 7.25 (d, *J* = 8.0 Hz, 2H, H3' & H5'), 7.69 (d, *J* = 8.2 Hz, 2H, H2' & H6') ppm.
^{13}C-NMR (101 MHz, $CDCl_3$)	δ = 10.1 (q, CH_3), 13.9 (q, CH_3), 21.5 (q, Ph-CH_3), 36.1 (q, N-CH_3), 121.8 & 129.7 (2xd, 4C, C2' & C6' & C3' & C5'), 135.2 & 138.5 & 139.7 & 142.5 & 151.8 (5xs, 5C, C3 & C4 & C5 & C1' & C4') ppm.

E III.1.30 3-((4-Chlorophenyl)diazenyl)-4-hydroxypent-3-en-2-one [41]

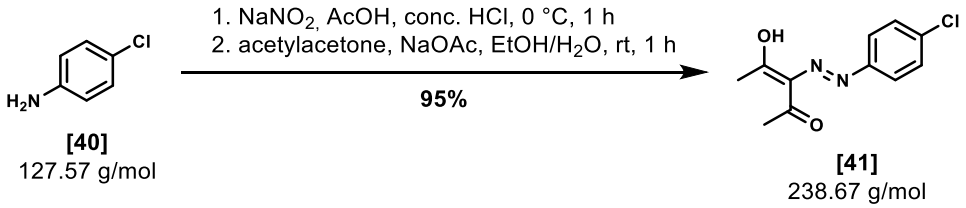

[40]
127.57 g/mol

[41]
238.67 g/mol

3-((4-Chlorophenyl)diazenyl)-4-hydroxypent-3-en-2-one **[41]** was synthesized according to **General procedure A** using 4-chloroaniline **[40]** (2.380 g, 18.66 mmol), AcOH (25 mL) and conc. HCl (4.25 mL).

Yield	95% (4.252 g, 17.81 mmol)
Appearance	yellow crystals
Melting point	135.0 – 135.5 °C (Lit.[184]: 128 – 130 °C)
TLC-Analysis	R_f = 0.60 (LP/EtOAc = 5/1)
Sum formula	$C_{11}H_{11}ClN_2O_2$
^{1}H-NMR (400 MHz, $CDCl_3$)	δ = 2.49 (s, 3H, CH_3), 2.61 (s, 3H, CH_3), 7.33 – 7.40 (m, 4H, H2' & H3' & H5' & H6'), 14.70 (br s, 1H, enol-H) ppm.
^{13}C-NMR (101 MHz, $CDCl_3$)	δ = 26.8 (q, CH_3), 31.8 (q, CH_3), 117.5 (d, 2C, C2' & C6' or C3' & C5'), 129.9 (d, 2C, C2' & C6' or C3' & C5'), 131.2 & 133.6 & 140.3 (3xs, 3C, C3 & C1' & C4'), 197.1 & 198.3 (2xs, 2C, carbonyl-C & enol-C) ppm.

E III.1.31 4-((4-Chlorophenyl)diazenyl)-1,3,5-trimethyl-1*H*-pyrazole [42]

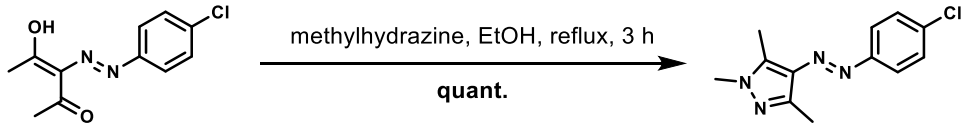

[41]
238.67 g/mol

[42]
248.17 g/mol

4-((4-Chlorophenyl)diazenyl)-1,3,5-trimethyl-1*H*-pyrazole **[42]** was synthesized according to **General procedure B** using azo intermediate **[41]** (1.64 g, 6.87 mmol) and EtOH (38 mL).

Yield	quant. (1.71 g, 6.87 mmol)
Appearance	yellow crystals
Melting point	85.0 – 86.0 °C
TLC-Analysis	R_f = 0.10 (LP/EtOAc = 5/1)
Sum formula	$C_{12}H_{13}ClN_4$
HR-MS	$[M+H]^+$: calculated: 249.0902 Da, found: 249.0912 Da, difference: 1.0 mDa
GC-MS	250 (13, M^+), 248 (41, M^+), 137 (100), 109 (69)
^{1}H-NMR (400 MHz, $CDCl_3$)	δ = 2.48 (s, 3H, CH_3), 2.57 (s, 3H, CH_3), 3.78 (s, 3H, N-CH_3), 7.42 (d, *J* = 8.7 Hz, 2H, H2' & H6' or H3' & H5'), 7.72 (d, *J* = 8.7 Hz, 2H, H2' & H6' or H3' & H5') ppm.
^{13}C-NMR (101 MHz, $CDCl_3$)	δ = 10.1 (q, CH_3), 14.0 (q, CH_3), 36.2 (q, N-CH_3), 123.1 & 129.2 (2xd, 4C, C2' & C6' & C3' & C5'), 135.0 & 135.2 & 139.2 & 142.7 & 152.2 (5xs, 5C, C3 & C4 & C5 & C1' & C4') ppm.

E III.1.32 3-((4-Bromophenyl)diazenyl)-4-hydroxypent-3-en-2-one [44]

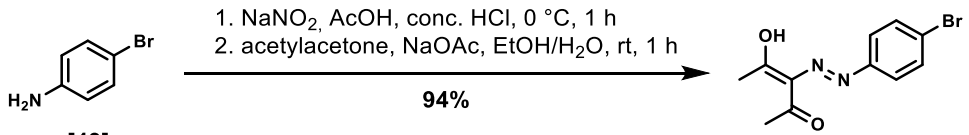

[43]
172.03 g/mol

[44]
283.13 g/mol

3-((4-Bromophenyl)diazenyl)-4-hydroxypent-3-en-2-one **[44]** was synthesized according to **General procedure A** using 4-bromoaniline **[43]** (3.210 g, 18.66 mmol), AcOH (25 mL) and conc. HCl (4.25 mL).

Yield	94% (4.991 g, 17.62 mmol)
Appearance	yellow crystals

Melting point	143.0 – 143.5 °C (Lit.[184]: 136 – 138 °C)
TLC-Analysis	R_f = 0.65 (LP/EtOAc = 5/1)
Sum formula	$C_{11}H_{11}BrN_2O_2$
^{1}H-NMR (400 MHz, $CDCl_3$)	δ = 2.48 (s, 3H, CH_3), 2.61 (s, 3H, CH_3), 7.29 (d, *J* = 8.8 Hz, 2H, H2' & H6' or H3' & H5'), 7.52 (d, *J* = 8.8 Hz, 2H, H2' & H6' or H3' & H5'), 14.67 (br s, 1H, enol-H) ppm.
^{13}C-NMR (101 MHz, $CDCl_3$)	δ = 26.8 (q, CH_3), 31.9 (q, CH_3), 117.8 (d, 2C, C2' & C6' or C3' & C5'), 118.8 (s, C3), 132.9 (d, 2C, C2' & C6' or C3' & C5'), 133.7 & 140.8 (2xs, 2C, C4' & C1'), 197.1 & 198.4 (2xs, 2C, carbonyl-C & enol-C) ppm.

E III.1.33 4-((4-Bromophenyl)diazenyl)-1,3,5-trimethyl-1*H*-pyrazole [45]

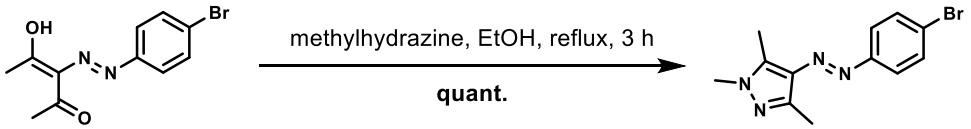

[44]
283.13 g/mol

[45]
293.17 g/mol

4-((4-Bromophenyl)diazenyl)-1,3,5-trimethyl-1*H*-pyrazole **[45]** was synthesized according to **General procedure B** using azo intermediate **[44]** (1.945 g, 6.87 mmol) and EtOH (38 mL).

Yield	quant. (2.014 g, 6.87 mmol)
Appearance	yellow crystals
Melting point	88.0 – 90.0 °C
TLC-Analysis	R_f = 0.10 (LP/EtOAc = 5/1)
Sum formula	$C_{12}H_{13}BrN_4$
HR-MS	$[M+H]^+$: calculated: 293.0396 Da, found: 293.0408 Da, difference: 1.2 mDa
GC-MS	294 (23, M^+), 292 (24, M^+), 137 (100), 109 (62)
^{1}H-NMR (400 MHz, $CDCl_3$)	δ = 2.48 (s, 3H, CH_3), 2.57 (s, 3H, CH_3), 3.78 (s, 3H, N-CH_3), 7.57 (d, *J* = 8.9 Hz, 2H, H2' & H6' or H3' & H5'), 7.66 (d, *J* = 8.8 Hz, 2H, H2' & H6' or H3' & H5') ppm.
^{13}C-NMR (101 MHz, $CDCl_3$)	δ = 10.1 (q, CH_3), 14.0 (q, CH_3), 36.2 (q, N-CH_3), 123.3 (s, C4'), 123.4 & 132.2 (2xd, 4C, C2' & C6' & C3' & C5'), 135.3 & 139.3 & 142.7 & 152.5 (4xs, 4C, C3 & C4 & C5 & C1') ppm.

E III.1.34 4-Hydroxy-3-((4-(trifluoromethyl)phenyl)diazenyl)pent-3-en-2-one [47]

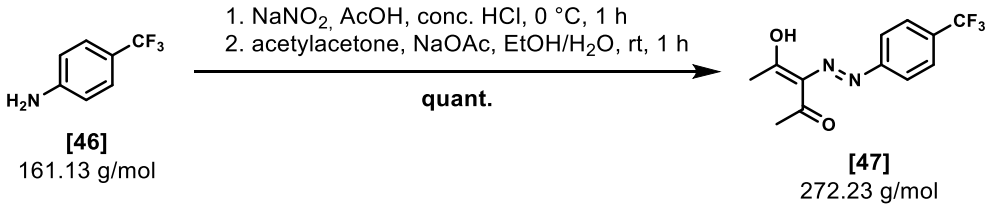

[46]
161.13 g/mol

[47]
272.23 g/mol

4-Hydroxy-3-((4-(trifluoromethyl)phenyl)diazenyl)pent-3-en-2-one **[47]** was synthesized according to **General procedure A** using 4-(trifluoromethyl)aniline **[46]** (500 mg, 3.10 mmol), AcOH (5 mL) and conc. HCl (0.85 mL).

Yield	quant. (836 mg, 3.10 mmol)
Appearance	yellow crystals
Melting point	179.0 – 180.0 °C
TLC analysis	R_f = 0.6 (LP/EtOAc = 5/1)
Sum formula	$C_{12}H_{11}F_3N_2O_2$
^{1}H-NMR (400 MHz, $CDCl_3$)	δ = 2.50 (s, 3H, CH_3), 2.61 (s, 3H, CH_3), 7.47 (d, J = 8.4 Hz, 2H, H2' & H6' or H3' & H5'), 7.65 (d, J = 8.5 Hz, 2H, H2' & H6' or H3' & H5'), 14.58 (br s, 1H, enol-H) ppm.
^{13}C-NMR (101 MHz, $CDCl_3$)	δ = 26.8 (q, CH_3), 31.9 (q, CH_3), 116.2 (d, 2C, C2' & C6'), 124.1 (s/q, $^1J_{CF}$ = 271.7 Hz, CF_3), 127.1 (d/q, $^3J_{CF}$ = 3.8 Hz, 2C, C3' & C5'), 127.5 (s/q, $^2J_{CF}$ = 32.9 Hz, C4'), 134.3 & 144.4 (2xs, 2C, C3 & C1'), 197.1 & 198.6 (2xs, 2C, carbonyl-C & enol-C) ppm.
Comment	^{1}H-NMR data is in accordance with the literature[199].

E III.1.35 1,3,5-Trimethyl-4-((4-(trifluoromethyl)phenyl)diazenyl)-1*H*-pyrazole [48]

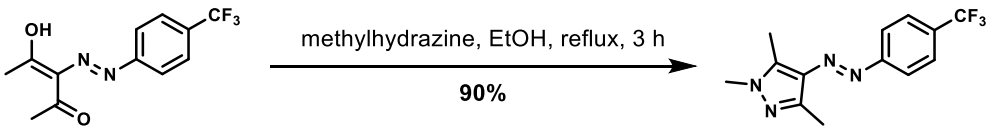

[47]
272.23 g/mol

[48]
282.27 g/mol

1,3,5-Trimethyl-4-((4-(trifluoromethyl)phenyl)diazenyl)-1*H*-pyrazole **[48]** was synthesized according to **General procedure B** using azo intermediate **[47]** (425 mg, 1.56 mmol) and EtOH (8.5 mL). The crude material was purified by flash column chromatography (silica gel/crude material = 100/1, LP → LP/EtOAc = 1/1),

Yield	90% (397 mg, 1.41 mmol)
Appearance	yellow crystals
Melting point	80.0 – 81.0 °C
TLC-Analysis	R_f = 0.15 (LP/EtOAc = 5/1)
Sum formula	$C_{13}H_{13}F_3N_4$
HR-MS	$[M+H]^+$: calculated: 283.1165 Da, found: 283.1187 Da, difference: 2.2 mDa
GC-MS	282 (49, M^+), 144 (11), 137 (100), 109 (79)
^{1}H-NMR (600 MHz, $CDCl_3$)	δ = 2.50 (s, 3H, CH_3), 2.59 (s, 3H, CH_3), 3.80 (s, 3H, N-CH_3), 7.71 (d, J = 8.3 Hz, 2H, H2' & H6' or H3' & H5'), 7.85 (d, J = 8.1 Hz, 2H, H2' & H6' or H3' & H5') ppm.
^{13}C-NMR (151 MHz, $CDCl_3$)	δ = 10.2 (q, CH_3), 14.1 (q, CH_3), 36.2 (q, N-CH_3), 122.1 (d, 2C, C2' & C6'), 124.3 (s/q, $^1J_{CF}$ = 272.2 Hz, CF_3), 126.2 (d/q, $^3J_{CF}$ = 3.8 Hz, 2C, C3' & C5'), 130.7 (s/q, $^2J_{CF}$ = 32.2 Hz, C4'), 135.5 & 140.0 & 142.8 & 155.7 (4xs, 4C, C3 & C4 & C5' & C1') ppm.

E III.1.36 3-([1,1'-Biphenyl]-4-yldiazenyl)-4-hydroxypent-3-en-2-one [50]

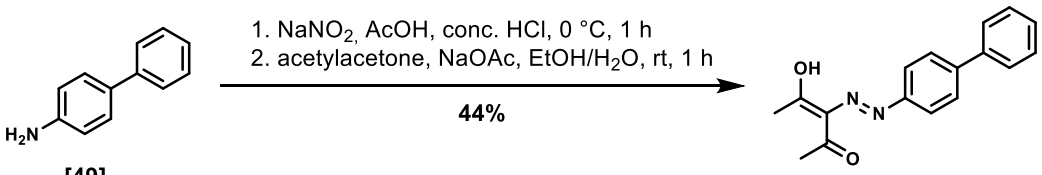

[49]
169.23 g/mol

[50]
280.33 g/mol

3-([1,1'-Biphenyl]-4-yldiazenyl)-4-hydroxypent-3-en-2-one **[50]** was synthesized according to **General procedure A** using [1,1'-biphenyl]-4-amine **[49]** (1.00 g, 5.91 mmol), AcOH (25 mL) and conc. HCl (1.36 mL). Ice was added to the filtrate and the precipitate was combined with the precipitate from the first step. The combined crude material was purified by flash column chromatography (silica gel/crude material = 100/1, LP/EtOAc = 9/1 → 1/1).

Yield	44% (737 mg, 2.63 mmol)
Appearance	yellow crystals
Melting point	137.5 – 140.0 °C
TLC-Analysis	R_f = 0.55 (LP/EtOAc = 5/1)
Sum formula	$C_{17}H_{16}N_2O_2$

^{1}H-NMR (400 MHz, $CDCl_3$) δ = 2.52 (s, 3H, CH_3), 2.63 (s, 3H, CH_3), 7.34 – 7.39 (m, 1H, Ar-H), 7.43 – 7.52 (m, 4H, Ar-H), 7.58 – 7.62 (m, 2H, Ar-H), 7.67 – 7.73 (m, 2H, Ar-H), 14.83 (br s, 1H, enol-H) ppm.

^{13}C-NMR (101 MHz, $CDCl_3$) δ = 26.8 (q, CH_3), 31.8 (q, CH_3), 116.8 (d, 2C, Ar-C), 127.0 (d, 2C, Ar-C), 127.7 (d, C4''), 128.5 (d, 2C, Ar-C), 129.1 (d, 2C, Ar-C), 133.5 & 139.0 & 140.2 & 140.9 (4xs, 4C, C3 & C1' & C4' & C1''), 197.2 & 198.1 (2xs, 2C, carbonyl-C & enol-C) ppm.

E III.1.37 4-([1,1'-Biphenyl]-4-yldiazenyl)-1,3,5-trimethyl-1*H*-pyrazole [51]

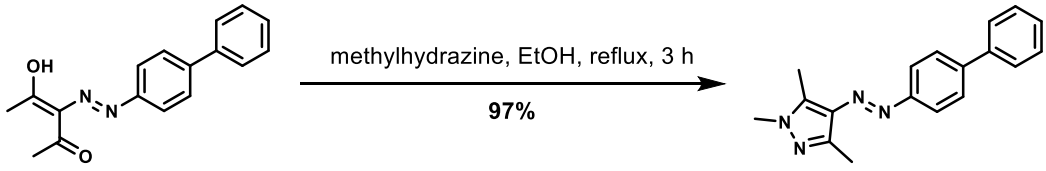

[50]
280.33 g/mol

[51]
290.37 g/mol

4-([1,1'-Biphenyl]-4-yldiazenyl)-1,3,5-trimethyl-1*H*-pyrazole **[51]** was synthesized according to **General procedure B** using azo intermediate **[50]** (359 mg, 1.28 mmol) and EtOH (7 mL).

Yield 97% (361 mg, 1.24 mmol)

Appearance yellow crystals

Melting point 141.0 – 142.0 °C

TLC-Analysis R_f = 0.10 (LP/EtOAc = 5/1)

Sum formula $C_{18}H_{18}N_4$

HR-MS $[M+H]^+$: calculated: 291.1604 Da, found: 291.1631 Da, difference: 2.7 mDa

GC-MS 290 (47, M^+), 152 (13), 137 (100), 109 (53)

^{1}H-NMR (400 MHz, $CDCl_3$) δ = 2.52 (s, 3H, CH_3), 2.60 (s, 3H, CH_3), 3.80 (s, 3H, N-CH_3), 7.35 – 7.40 (m, 1H, H4''), 7.44 – 7.49 (m, 2H, Ar-H), 7.63 – 7.72 (m, 4H, Ar-H), 7.86 (d, *J* = 8.6 Hz, 2H, Ar-H), ppm.

^{13}C-NMR (101 MHz, $CDCl_3$) δ = 10.2 (q, CH_3), 14.0 (q, CH_3), 36.2 (q, N-CH_3), 122.4 (d, 2C, Ar-C), 127.2 (d, 2C, Ar-C), 127.7 (d, C4''), 127.8 (d, 2C, Ar-C), 129.0 (d, 2C, Ar-C), 135.4 & 138.9 & 140.7 & 142.2 & 142.7 & 153.0 (6xs, 6C, C3 & C4 & C5 & C1' & C4' & C1'') ppm.

E III.1.38 4-Hydroxy-3-((3-nitrophenyl)diazenyl)pent-3-en-2-one [53]

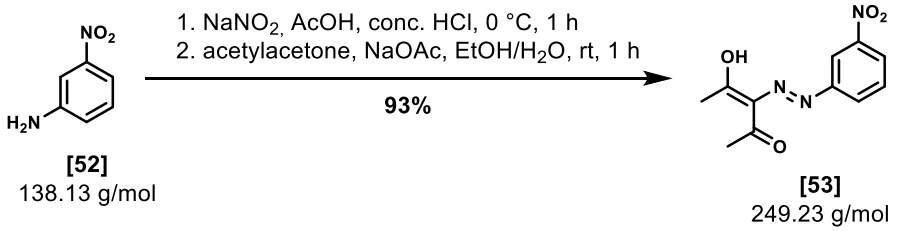

[52]
138.13 g/mol

[53]
249.23 g/mol

4-Hydroxy-3-((3-nitrophenyl)diazenyl)pent-3-en-2-one **[53]** was synthesized according to **General procedure A** using 3-nitroaniline **[52]** (2.577 g, 18.66 mmol), AcOH (25 mL) and conc. HCl (4.25 mL).

Yield	93% (4.373 g, 17.55 mmol)
Appearance	yellow crystals
Melting point	142.0 – 142.5 °C (Lit.[200]: 146 °C)
TLC-Analysis	R_f = 0.75 (LP/EtOAc = 5/1)
Sum formula	$C_{11}H_{11}N_3O_4$
^{1}H-NMR (400 MHz, $CDCl_3$)	δ = 2.54 (s, 3H, CH_3), 2.63 (s, 3H, CH_3), 7.58 (t, *J* = 8.1 Hz, 1H, H5'), 7.68 (ddd, *J* = 8.2, 2.2, 1.1 Hz, 1H, H4' or H6'), 8.03 (ddd, *J* = 8.1, 2.2, 1.1 Hz, 1H, H4' or H6'), 8.26 (t, *J* = 2.2 Hz, 1H, H2'), 14.64 (br s, 1H, enol-H) ppm.
^{13}C-NMR (101 MHz, $CDCl_3$)	δ = 26.8 (q, CH_3), 31.9 (q, CH_3), 110.9 & 119.9 & 121.7 & 130.7 (4xd, 4C, C2' & C4' & C5' & C6'), 134.5 & 143.0 & 149.5 (3xs, 3C, C3 & C1' & C3'), 197.0 & 198.8 (2xs, 2C, carbonyl-C & enol-C) ppm.

E III.1.39 1,3,5-Trimethyl-4-((3-nitrophenyl)diazenyl)-1*H*-pyrazole [54]

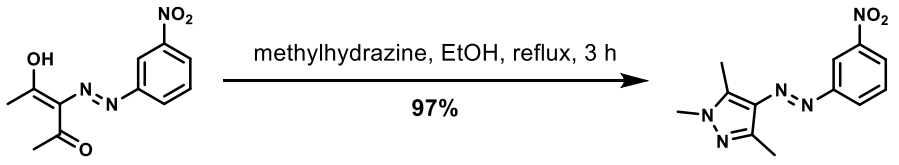

[53]
249.23 g/mol

[54]
259.27 g/mol

1,3,5-Trimethyl-4-((3-nitrophenyl)diazenyl)-1*H*-pyrazole **[54]** was synthesized according to **General procedure B** using azo intermediate **[53]** (1.712 g, 6.87 mmol) and EtOH (38 mL).

Yield	97% (1.728 g, 6.66 mmol)
Appearance	yellow crystals

Melting point	203.0 – 204.0 °C
TLC-Analysis	R_f = 0.15 (LP/EtOAc = 5/1)
Sum formula	$C_{12}H_{13}N_5O_2$
HR-MS	$[M+H]^+$: calculated: 260.1142 Da, found: 260.1147 Da, difference: 0.5 mDa
GC-MS	259 (34, M^+), 137 (100), 109 (67)
^{1}H-NMR (400 MHz, $CDCl_3$)	δ = 2.51 (s, 3H, CH_3), 2.61 (s, 3H, CH_3), 3.81 (s, 3H, N-CH_3), 7.63 (t, *J* = 8.0 Hz, 1H, H5'), 8.10 (ddd, *J* = 7.9, 1.9, 1.1 Hz, 1H, H4' or H6'), 8.21 (ddd, *J* = 8.2, 2.3, 1.1 Hz, 1H, H4' or H6'), 8.58 (t, *J* = 2.1 Hz, 1H, H2') ppm.
^{13}C-NMR (101 MHz, $CDCl_3$)	δ = 10.2 (q, CH_3), 14.2 (q, CH_3), 36.3 (q, N-CH_3), 116.1 & 123.4 & 128.4 & 129.8 (4xd, 4C, C2' & C4' & C5' & C6'), 135.4 & 140.4 & 142.9 & 149.2 & 154.4 (5xs, 5C, C3 & C4 & C5 & C1' & C3') ppm.

E III.1.40 4-Hydroxy-3-((2-nitrophenyl)diazenyl)pent-3-en-2-one [56]

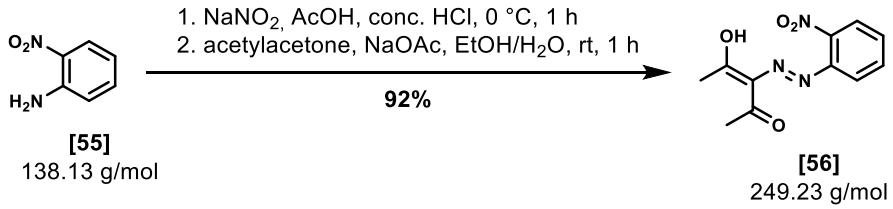

[55]
138.13 g/mol

[56]
249.23 g/mol

4-Hydroxy-3-((2-nitrophenyl)diazenyl)pent-3-en-2-one **[56]** was synthesized according to **General procedure A** using 2-nitroaniline **[55]** (2.577 g, 18.66 mmol), AcOH (25 mL) and conc. HCl (4.25 mL).

Yield	92% (4.314 g, 17.31 mmol)
Appearance	yellow crystals
Melting point	184.0 – 184.5 °C (Lit.[184]: 182 – 184 °C)
TLC-Analysis	R_f = 0.30 (LP/EtOAc = 5/1)
Sum formula	$C_{11}H_{11}N_3O_4$
^{1}H-NMR (400 MHz, $CDCl_3$)	δ = 2.55 (s, 3H, CH_3), 2.65 (s, 3H, CH_3), 7.24 – 7.28 (m, 1H, H4’ or H5’), 7.72 (dddd, *J* = 8.6, 7.9, 1.5, 0.7 Hz, 1H, H4’ or H5’), 8.14 (dd, *J* = 8.5, 1.3 Hz, 1H, H3’ or H6’), 8.29 (dd, *J* = 8.5, 1.5 Hz, 1H, H3’ or H6’), 15.49 (br s, 1H, enol-H) ppm.

^{13}C-NMR (151 MHz, $CDCl_3$) δ = 26.9 (q, CH_3), 31.9 (q, CH_3), 117.4 & 124.2 & 126.3 & 136.0 (4xd, 4C, C3' & C4' & C5' & C6'), 135.9 & 136.4 & 138.5 (3xs, 3C, C3 & C1' & C2'), 197.2 & 197.3 (2xs, 2C, carbonyl-C & enol-C) ppm.

E III.1.41 1,3,5-Trimethyl-4-((2-nitrophenyl)diazenyl)-1*H*-pyrazole [57]

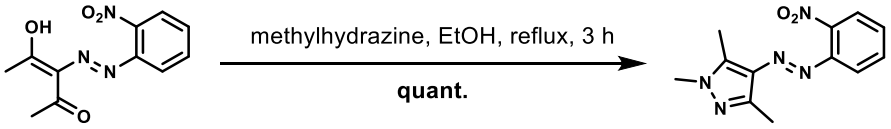

[56]
249.23 g/mol

[57]
259.27 g/mol

1,3,5-Trimethyl-4-((2-nitrophenyl)diazenyl)-1*H*-pyrazole **[57]** was synthesized according to **General procedure B** using azo intermediate **[56]** (1.712 g, 6.87 mmol) and EtOH (38 mL).

Yield quant. (1.781 g, 6.87 mmol)

Appearance yellow crystals

Melting point 133.0 – 136.0 °C (Lit.[186]: 101 – 102 °C)

TLC-Analysis R_f = 0.65 (LP/EtOAc = 5/1)

Sum formula $C_{12}H_{13}N_5O_2$

HR-MS $[M+H]^+$: calculated: 260.1142 Da, found: 260.1153 Da, difference: 1.1 mDa

GC-MS 259 (21, M^+), 227 (33), 213 (13), 144 (12), 138 (10), 137 (100), 119 (14), 109 (71)

^{1}H-NMR (400 MHz, $CDCl_3$) δ = 2.45 (s, 3H, CH_3), 2.55 (s, 3H, CH_3), 3.78 (s, 3H, N-CH_3), 7.44 (ddd, *J* = 8.0, 7.3, 1.4 Hz, 1H, H4' or H5'), 7.60 (ddd, *J* = 8.1, 7.3, 1.4 Hz, 1H, H4' or H5'), 7.69 (dd, *J* = 8.1, 1.3 Hz, 1H, H3' or H6') 7.79 (dd, *J* = 8.0, 1.2 Hz, 1H, H3' or H6') ppm.

^{13}C-NMR (101 MHz, $CDCl_3$) δ = 10.3 (q, CH_3), 13.8 (q, CH_3), 36.2 (q, N-CH_3), 118.4 & 123.8 & 128.9 & 132.6 (4xd, 4C, C3' & C4' & C5' & C6'), 136.1 & 139.9 & 144.1 & 146.2 & 147.4 (5xs, 5C, C3 & C4 & C5 & C1' & C2') ppm.

Comment Spectral data are in accordance with the literature[186].

E III.1.42 4-Hydroxy-3-(naphthalen-1-yldiazenyl)pent-3-en-2-one [59]

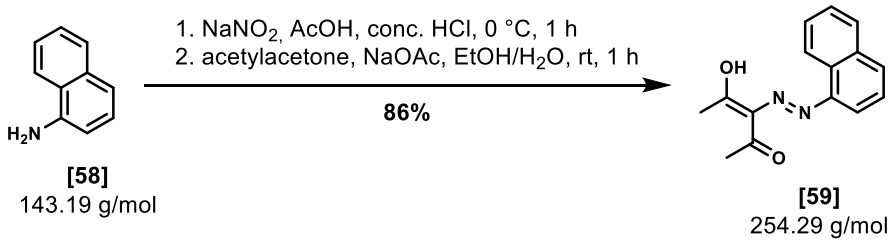

[58]
143.19 g/mol

[59]
254.29 g/mol

4-Hydroxy-3-(naphthalen-1-yldiazenyl)pent-3-en-2-one[201] **[59]** was synthesized according to **General procedure A** using naphthalen-1-amine **[58]** (2.672 g, 18.66 mmol), AcOH (25 mL) and conc. HCl (4.25 mL).

Yield	86% (4.076, 16.03 mmol)
Appearance	brown solid
Melting point	144.0 – 145.0 °C
TLC-Analysis	R_f = 0.60 (LP/EtOAc = 5/1)
Sum formula	$C_{15}H_{14}N_2O_2$
^{1}H-NMR (400 MHz, $CDCl_3$)	δ = 2.57 (s, 3H, CH_3), 2.69 (s, 3H, CH_3), 7.53 – 7.65 (m, 3H, Ar-H), 7,74 (d, *J* = 8.2 Hz, 1H, Ar-H), 7.92 (d, *J* = 7.5 Hz, 2H, Ar-H), 8.04 (d, *J* = 8.8 Hz, 1H, Ar-H) 15.74 (br s, 1H, enol-H) ppm.
^{13}C-NMR (101 MHz, $CDCl_3$)	δ = 26.9 (q, CH_3), 31.9 (q, CH_3), 112.2 (d, Ar-C), 119.7 (d, Ar-C), 123.6 (s, C3), 126.2 (d, Ar-C), 126.2 (d, Ar-C), 126.6 (d, Ar-C), 127.2 (d, Ar-C), 129.0 (d, Ar-C), 134.2 & 134.5 & 136.7 (3xs, 3C, C4a' & C8a' & C1'), 197.4 & 198.4 (2xs, 2C, carbonyl-C & enol-C) ppm.
Comment	The compound was described in the literature as an intermediate but no analytical data was available.

E III.1.43 1,3,5-Trimethyl-4-(naphthalen-1-yldiazenyl)-1*H*-pyrazole [60]

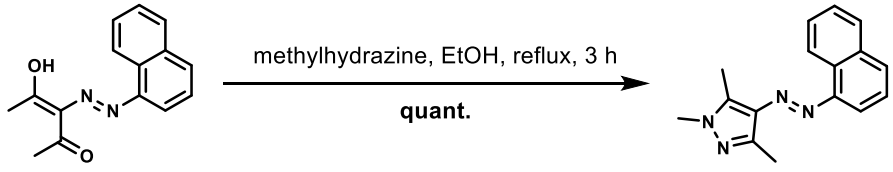

[59]
254.29 g/mol

[60]
264.33 g/mol

1,3,5-Trimethyl-4-(naphthalen-1-yldiazenyl)-1*H*-pyrazole **[60]** was synthesized according to **General procedure B** using azo intermediate **[59]** (1.747 g, 6.87 mmol) and EtOH (38 mL).

Yield	quant. (1.816 mg, 6.87 mmol)
Appearance	yellow crystals
Melting point	115.0 – 118.0 °C
TLC-Analysis	R_f = 0.10 (LP/EtOAc = 5/1)
Sum formula	$C_{16}H_{16}N_4$
HR-MS	$[M+H]^+$: calculated: 265.1448 Da, found: 265.1457 Da, difference: 0.9 mDa
GC-MS	264 (52, M^+), 137 (100), 127 (19), 109 (75)
^{1}H-NMR (400 MHz, $CDCl_3$)	δ = 2.64 (s, 3H, CH_3), 2.67 (s, 3H, CH_3), 3.83 (s, 3H, N-CH_3), 7.52 – 7.63 (m, 3H, Ar-H), 7.76 (dd, *J* = 7.6 & 1.1 Hz, 1H, Ar-H), 7.87 – 7.92 (m, 2H, Ar-H), 8.79 (d, *J* = 8.4 Hz, 1H, Ar-H) ppm.
^{13}C-NMR (101 MHz, $CDCl_3$)	δ = 10.2 (q, CH_3), 14.5 (q, CH_3), 36.2 (q, N-CH_3), 110.8 & 123.7 & 125.8 & 126.3 & 126.5 & 128.0 & 129.6 (7xd, 7C, C2' & C3' & C4' & C5' & C6' & C7' & C8'), 131.1 & 134.4 & 136.4 & 139.6 & 142.2 & 148.9 (6xs, 6C, C3 & C4 & C5 & C1' & C4a' & C8a') ppm.

E III.1.44 4-Hydroxy-3-(naphthalen-2-yldiazenyl)pent-3-en-2-one [62]

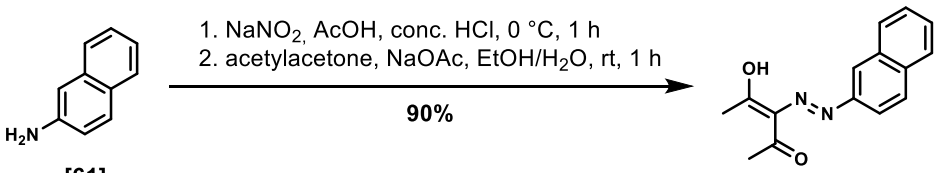

[61]
143.19 g/mol

[62]
254.29 g/mol

4-Hydroxy-3-(naphthalen-2-yldiazenyl)pent-3-en-2-one **[62]** was synthesized according to **General procedure A** using naphthalen-2-amine **[61]** (2.672 g, 18.66 mmol), AcOH (25 mL) and conc. HCl (4.25 mL).

Yield	90% (4.270 g, 16.79 mmol)
Appearance	brown solid
Melting point	131.0 – 133.0 °C (Lit.[202]: 125 °C)
TLC-Analysis	R_f = 0.60 (LP/EtOAc = 5/1)
Sum formula	$C_{15}H_{14}N_2O_2$

^{1}H-NMR (400 MHz, $CDCl_3$) δ = 2.56 (s, 3H, CH_3), 2.64 (s, 3H, CH_3), 7.46 (ddd, *J* = 8.0, 6.9, 1.3 Hz, 1H, Ar-H), 7.52 (ddd, *J* = 8.4, 6.8, 1.3 Hz, 1H, Ar-H), 7.67 – 7.73 (m, 2H, Ar-H), 7.83 (d, *J* = 8.9 Hz, 2H, Ar-H), 7.90 (d, *J* = 8.8 Hz, 2H, Ar-H), 14.98 (br s, 1H, enol-H) ppm.

^{13}C-NMR (101 MHz, $CDCl_3$) δ = 26.9 (q, CH_3), 31.8 (q, CH_3), 113.7 (d, Ar-C), 115.7 (d, Ar-C), 125.9 (d, Ar-C), 127.4 (d, Ar-C), 127.8 (d, Ar-C), 128.2 (d, Ar-C), 130.2 (d, Ar-C), 131.9 & 133.6 & 133.8 & 139.3 (4xs, 4C, C3 & C1' & C4a' & C8a'), 197.2 & 198.1 (2xs, 2C, carbonyl-C & enol-C) ppm.

E III.1.45 1,3,5-Trimethyl-4-(naphthalen-2-yldiazenyl)-1*H*-pyrazole [63]

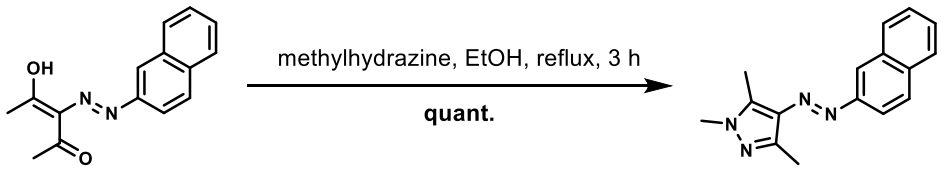

[62]
254.29 g/mol

[63]
264.33 g/mol

1,3,5-Trimethyl-4-(naphthalen-2-yldiazenyl)-1*H*-pyrazole **[63]** was synthesized according to **General procedure B** using azo intermediate **[62]** (1.747 g, 6.87 mmol) and EtOH (38 mL).

Yield quant. (1.816 mg, 6.87 mmol)

Appearance yellow crystals

Melting point 120.0 – 121.0 °C

TLC-Analysis R_f = 0.10 (LP/EtOAc = 5/1)

Sum formula $C_{16}H_{16}N_4$

HR-MS $[M+H]^+$: calculated: 265.1448 Da, found: 265.1457 Da, difference: 0.9 mDa

GC-MS 264 (54, M^+), 236 (10), 235 (11), 137 (100), 127 (19), 109 (76)

^{1}H-NMR (400 MHz, $CDCl_3$) δ = 2.56 (s, 3H, CH_3), 2.63 (s, 3H, CH_3), 3.80 (s, 3H, N-CH_3), 7.48 – 7.55 (m, 2H, Ar-H), 7.84 – 7.89 (m, 2H, Ar-H), 7.94 – 8.01 (m, 2H, Ar-H), 8.26 (d, *J* = 1.5 Hz, 1H, H1') ppm.

^{13}C-NMR (101 MHz, $CDCl_3$) δ = 10.2 (q, CH_3), 14.1 (q, CH_3), 36.2 (q, N-CH_3), 117.2 & 125.4 & 126.6 & 126.8 & 128.0 & 129.0 & 129.1 (7xd, 7C, C1 & C3 & C4 & C5 & C6 & C7 & C8), 133.9 & 134.2 & 135.4 & 138.9 & 142.7 & 151.4 (6xs, 6C, C3 & C4 & C5 & C2' & C4a' & C8a') ppm.

E III.2 Aryldiazonium tetrafluoroborates

E III.2.1 Benzenediazonium tetrafluoroborate [64]

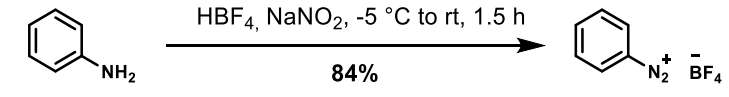

[1]
93.13 g/mol

[64]
191.92 g/mol

Benzenediazonium tetrafluoroborate **[64]** was synthesized according to **General procedure C** using aniline **[1]** (1.62 g, 17.40 mmol) and HBF_4 (11 mL).

Yield 84% (2.80 g, 14.61 mmol)

Appearance colorless crystals

Sum formula $C_6H_5BF_4N_2$

^{1}H-NMR (400 MHz, DMSO-d_6) δ = 7.98 (dd, *J* = 8.8, 7.7 Hz, 2H, H3 & H5), 8.26 (t, *J* = 7.7 Hz, 1H, H4), 8.66 (dd, *J* = 8.9, 1.2 Hz, 2H, H2 & H6) ppm.

^{13}C-NMR (101 MHz, DMSO-d_6) δ = 115.2 (d, 2C, C3 & C5), 118.8 (d, C4), 129.4 (d, 2C, C2 & C6), 157.2 (s, C1) ppm.

E III.2.2 4-Cyanobenzenediazonium tetrafluoroborate [65]

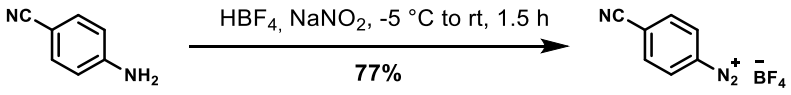

[19]
118.14 g/mol

[65]
216.93 g/mol

4-Cyanobenzenediazonium tetrafluoroborate **[65]** was synthesized according to **General procedure C** using 4-aminobenzonitrile **[19]** (796 mg, 6.74 mmol) and HBF_4 (4.3 mL).

Yield 77% (1.13 g, 5.21 mmol)

Appearance colorless crystals

Sum formula $C_7H_4BF_4N_3$

^{1}H-NMR (400 MHz, DMSO-d_6) δ = 8.46 (d, *J* = 8.9 Hz, 2H, H3 & H5), 8.84 (d, *J* = 9.0 Hz, 2H, H2 & H6) ppm.

^{13}C-NMR (101 MHz, DMSO-d_6) δ = 116.3 (s, C1), 121.0 & 121.7 (2xs, 2C, C4 & CN), 133.0 (d, 2C, C2 & C6), 134.8 (d, 2C, C3 & C5) ppm.

E III.2.3 4-Iodobenzenediazonium tetrafluoroborate [66]

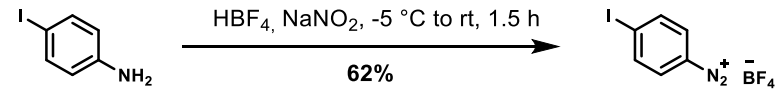

[29]
219.03 g/mol

[66]
317.82 g/mol

4-Iodobenzenediazonium tetrafluoroborate **[66]** was synthesized according to **General procedure C** using 4-iodoaniline **[29]** (1095 mg, 5.00 mmol) and HBF_4 (3.2 mL).

Yield 62% (983 mg, 3.09 mmol)

Appearance pale gray crystals

Sum formula $C_6H_4BF_4IN_2$

^{1}H-NMR (400 MHz, DMSO-d_6) δ = 8.35 (d, *J* = 9.1 Hz, 2H, H2 & H6), 8.43 (d, *J* = 9.0 Hz, 2H, H3 & H5) ppm.

^{13}C-NMR (101 MHz, DMSO-d_6) δ = 113.6 (s, C4), 115.2 (s, C1), 132.8 (d, 2C, C2 & C6), 140.2 (d, 2C, C3 & C5) ppm.

E III.2.4 4-Ethynylbenzenediazonium tetrafluoroborate [67]

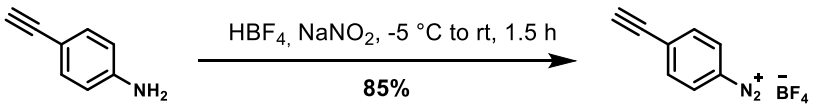

[32]
117.15 g/mol

[67]
215.95 g/mol

4-Ethynylbenzenediazonium tetrafluoroborate **[67]** was synthesized according to **General procedure C** using 4-ethynylaniline **[32]** (367 mg, 3.13 mmol) and HBF_4 (2 mL).

Yield 85% (574 mg, 2.65 mmol)

Appearance brown crystals

Sum formula $C_8H_5BF_4N_2$

^{1}H-NMR (400 MHz, DMSO-d_6) δ = 5.15 (s, 1H, CCH), 8.06 (d, *J* = 8.8 Hz, 2H, H2 & H6), 8.67 (d, *J* = 8.9 Hz, 2H, H3 & H5) ppm.

^{13}C-NMR (101 MHz, DMSO-d_6) δ = 81.3 (d, C<u>C</u>H), 91.4 (s, <u>C</u>CH), 115.5 (s, C1), 133.0 (d, 2C, C2 & C6 or C3 & C5), 133.6 (s, C4), 134.0 (d, 2C, C2 & C6 or C3 & C5) ppm.

E III.2.5 4-Nitrobenzenediazonium tetrafluoroborate [68]

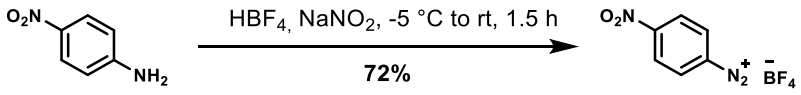

[4] 138.13 g/mol

[68] 236.92 g/mol

4-Nitrobenzenediazonium tetrafluoroborate **[68]** was synthesized according to **General procedure C** using 4-nitroaniline **[4]** (1058 mg, 7.66 mmol) and HBF_4 (4.8 mL).

Yield 72% (1.31 g, 5.52 mmol)

Appearance beige crystals

Sum formula $C_6H_4BF_4N_3O_2$

^{1}H-NMR (400 MHz, DMSO-d_6) δ = 8.72 (d, *J* = 9.2 Hz, 2H, H2 & H6), 8.93 (d, *J* = 9.2 Hz, 2H, H3 & H5) ppm.

^{13}C-NMR (101 MHz, DMSO-d_6) δ = 121.9 (s, C1), 126.0 (d, 2C, C3 & C5), 134.5 (d, 2C, C2 & C6), 153.2 (s, C4) ppm.

E III.2.6 4-(Ethoxycarbonyl)benzenediazonium tetrafluoroborate [70]

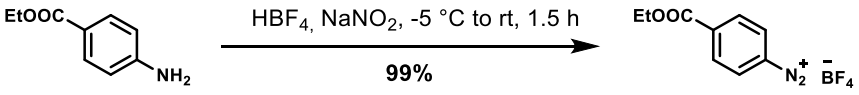

[69] 165.19 g/mol

[70] 263.99 g/mol

4-(Ethoxycarbonyl)benzenediazonium tetrafluoroborate **[70]** was synthesized according to **General procedure C** using ethyl 4-aminobenzoate **[69]** (915 mg, 5.54 mmol) and HBF_4 (3.5 mL).

Yield 99% (1.44 g, 5.46 mmol)

Appearance colorless crystals

Sum formula $C_9H_9BF_4N_2O_2$

^{1}H-NMR (400 MHz, DMSO-d_6) δ = 1.36 (t, *J* = 7.1 Hz, 3H, CH_3), 4.41 (q, *J* = 7.1 Hz, 2H, CH_2), 8.44 (d, *J* = 8.9 Hz, 2H, H2 & H6), 8.79 (d, *J* = 8.9 Hz, 2H, H3 & H5) ppm.

^{13}C-NMR (101 MHz, DMSO-d_6) δ = 13.9 (q, CH_3), 62.4 (t, CH_2), 120.2 (s, C1), 131.2 (d, 2C, C3 & C5), 133.1 (d, 2C, C2 & C6), 139.4 (s, C4), 163.3 (s, ester) ppm.

E III.2.7 4-Aminophenyl pivalate [71]

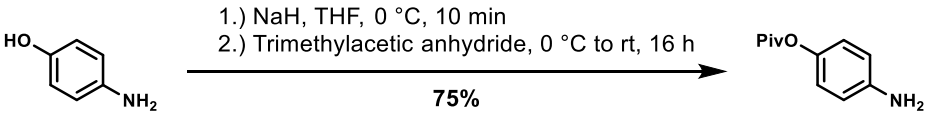

[8]
109.13 g/mol

[71]
193.25 g/mol

4-Aminophenyl pivalate **[71]** was prepared according to a literature protocol[203]. A solution of 4-aminophenol **[8]** (627 mg, 5.74 mmol, 1 equiv.) in dry THF (25 mL) was added to a suspension of NaH (287 mg, 60% dispersion in mineral oil, 7.175 mmol, 1.25 equiv.) in dry THF (25 mL) at 0 °C, followed by stirring for 10 minutes at 0 °C. Trimethylacetic anhydride (1.07 g, 5.74 mmol, 1 equiv.) was added dropwise to the resultant mixture. Thereby, the light purple solution turned brown and a precipitate appeared. The reaction mixture was slowly warmed to room temperature and was stirred for 16 hours. TLC analysis did not show full conversion and further 0.11 g trimethylacetic anhydride (0.1 equiv.) were added. After one hour of additional stirring, starting material was completely consumed and the reaction mixture was treated with satd. aqu. NH_4Cl and extracted with EtOAc (4 x 40 mL). The combined organic phases were washed with brine and volatiles were removed in vacuo. Purification by flash column chromatography (silica gel/crude material = 100/1, LP/EtOAc = 5/1) provided the desired product.

Yield	75% (831 mg, 4.30 mmol)
Appearance	orange liquid
TLC-Analysis	R_f = 0.30 (LP/EtOAc = 3/1)
Sum formula	$C_{11}H_{15}NO_2$
GC-MS	193 (13, M^+), 109 (100)
^{1}H-NMR (400 MHz, $CDCl_3$)	δ = 1.33 (s, 9H, Piv), 3.72 (br s, 2H, NH_2), 6.66 (d, *J* = 8.8 Hz, 2H, H2 & H6 or H3 & H5), 6.83 (d, *J* = 8.8 Hz, 2H, H2 & H6 or H3 & H5) ppm.
^{13}C-NMR (101 MHz, $CDCl_3$)	δ = 27.3 (q, 3C, Piv), 39.1 (s, Piv), 115.8 (d, 2C, C2 & C6 or C3 & C5), 122.2 (d, 2C, C2 & C6 or C3 & C5), 143.4 (s, C1 or C4), 144.1 (s, C1 or C4), 177.7 (s, ester) ppm.

E III.2.8 4-(Pivaloyloxy)benzenediazonium tetrafluoroborate [72]

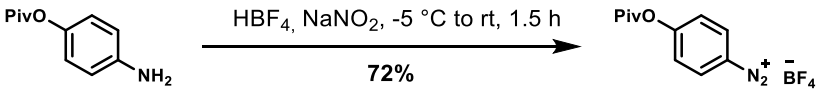

[71]
193.25 g/mol

[72]
292.04 g/mol

4-(Pivaloyloxy)benzenediazonium tetrafluoroborate **[72]** was synthesized according to **General procedure C** using 4-aminophenyl pivalate **[71]** (201 mg, 1.04 mmol) and HBF_4 (0.7 mL).

Yield 72% (216 mg, 0.74 mmol)

Appearance brown-red crystals

Sum formula $C_{11}H_{13}BF_4N_2O_2$

^{1}H-NMR (400 MHz, DMSO-d_6) δ = 1.34 (s, 9H, Piv), 7.81 (d, J = 9.2 Hz, 2H, H3 & H5), 8.76 (d, J = 9.2 Hz, 2H, H2 & H6) ppm.

Compound decomposed in DMSO-d_6 solution while recording ^{13}C-NMR.

E III.2.9 4-(Diethylamino)benzenediazonium tetrafluoroborate [73]

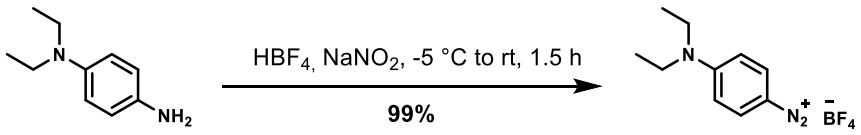

[23]
164.25 g/mol

[73]
263.05 g/mol

4-(Diethylamino)benzenediazonium tetrafluoroborate **[73]** was synthesized according to **General procedure C** using N^1,N^1-diethylbenzene-1,4-diamine **[23]** (1.26 g, 7.66 mmol) and HBF_4 (4.8 mL).

Yield 99% (1.99 g, 7.58 mmol)

Appearance brown-red crystals

Sum formula $C_{10}H_{14}BF_4N_3$

^{1}H-NMR (400 MHz, DMSO-d_6) δ = 1.17 (t, J = 7.1 Hz, 6H, 2 x CH_3), 3.63 (q, J = 7.1 Hz, 4H, 2 x CH_2), 7.09 (d, J = 9.7 Hz, 2H, H3 & H5), 8.21 (d, J = 9.7 Hz, 2H, H2 & H6) ppm.

^{13}C-NMR (101 MHz, DMSO-d_6) δ = 12.1 (q, 2C, 2 x CH_3), 45.3 (t, 2C, 2 x CH_2), 88.6 (d, 2C, C3 & C5), 113.8 (s, C1), 134.4 (d, 2C, C2 & C6), 154.6 (s, C4) ppm.

E III.2.10 4-Fluorobenzenediazonium tetrafluoroborate [74]

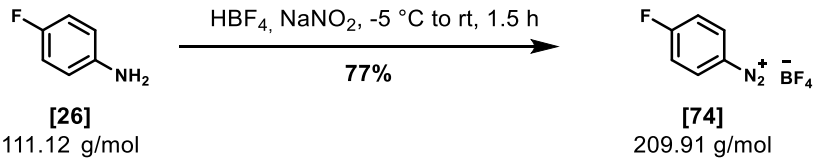

[26]
111.12 g/mol

[74]
209.91 g/mol

4-Fluorobenzenediazonium tetrafluoroborate **[74]** was synthesized according to **General procedure C** using 4-fluoroaniline **[26]** (876 mg, 7.88 mmol) and HBF_4 (5 mL).

Yield 77% (1.24 g, 5.90 mmol)

Appearance colorless crystals

Sum formula $C_6H_4BF_5N_2$

^{1}H-NMR (400 MHz, DMSO-d_6) δ = 7.89 (dd, J = 9.4, 8.3 Hz, 2H, H3 & H5), 8.80 (dd, J = 9.4, 4.5 Hz, 2H, H2 & H6) ppm.

^{13}C-NMR (101 MHz, DMSO-d_6) δ = 111.8 (s/d, $^4J_{CF}$ = 2.8 Hz, C1), 119.4 (d/d, $^2J_{CF}$ = 25.3 Hz, 2C, C3 & C5), 137.0 (d/d, $^3J_{CF}$ = 12.3 Hz, 2C, C2 & C6), 168.4 (s/d, $^1J_{CF}$ = 267.0 Hz, C4) ppm.

E III.3 Arylazo-2-thiophenes

E III.3.1 1-Phenyl-2-(thiophen-2-yl)diazene [76]

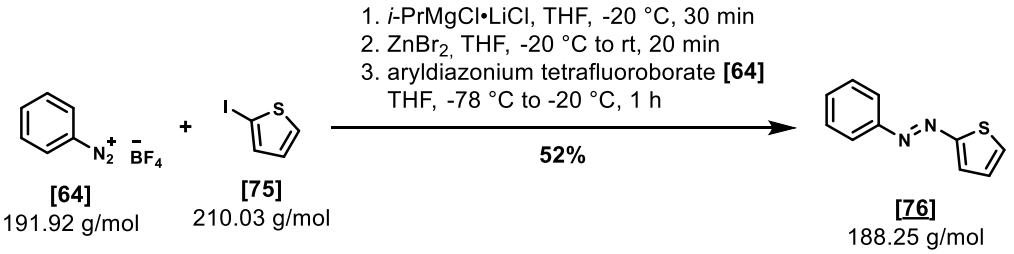

[64]
191.92 g/mol

[75]
210.03 g/mol

[76]
188.25 g/mol

1-Phenyl-2-(thiophen-2-yl)diazene **[76]** was synthesized according to **General procedure D** using 2-iodothiophene **[75]** (501 mg, 2.385 mmol, 1.5 equiv.) and benzenediazonium tetrafluoroborate **[64]** (305 mg, 1.59 mmol). The pure product was obtained after purification by flash column chromatography (silica gel/crude material = 100/1, LP/EtOAc = 19/1).

Yield 52% (156 mg, 0.83 mmol)

Appearance red crystals

Melting point 71.5 – 72.0 °C

TLC-Analysis R_f = 0.50 (LP/EtOAc = 10/1)

Sum formula $C_{10}H_8N_2S$

HR-MS	$[M+H]^+$: calculated: 189.0481 Da, found: 189.0501 Da, difference: 2.0 mDa
GC-MS	188 (73, M^+), 111 (81), 77 (100)
^{1}H-NMR (600 MHz, $CDCl_3$)	δ = 7.17 (dd, *J* = 5.3, 3.8 Hz, 1H, H4), 7.42 (dd, *J* = 5.4, 1.3 Hz, 1H, H5), 7.45 (t, *J* = 7.3 Hz, 1H, H4'), 7.50 (t, *J* = 7.5 Hz, 2H, H3' & H5'), 7.82 (dd, *J* = 3.8 , 1.3 Hz, 1H, H3), 7.87 – 7.89 (m, 2H, H2' & H6') ppm.
^{13}C-NMR (151 MHz, $CDCl_3$)	δ = 122.9 (d, 2C, C2' & C6'), 127.6 (d, C3 or C4 or C5 or C4'), 128.6 (d, C3 or C4 or C5 or C4'), 129.2 (d, 2C, C3' & C5'), 130.9 (d, C3 or C4 or C5 or C4'), 131.9 (d, C3 or C4 or C5 or C4'), 152.2 (s, C1'), 160.5 (s, C2) ppm.

The assignments of protons and carbon atoms in the NMR codes of compounds **[76]**, **[77]**, **[78]**, **[79]**, **[80]**, **[81]**, **[82]**, **[83]**, **[84]**, **[85]**, **[87]**, and **[88]** were carried out as follows:

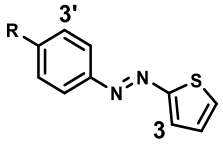

E III.3.2 4-(Thiophen-2-yldiazenyl)benzonitrile [77]

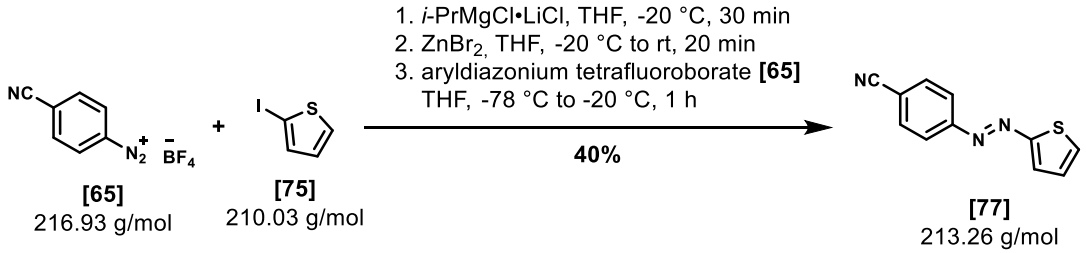

4-(Thiophen-2-yldiazenyl)benzonitrile **[77]** was synthesized according to **General procedure D** using 2-iodothiophene **[75]** (501 mg, 2.385 mmol, 1.5 equiv.) and 4-cyanobenzenediazonium tetrafluoroborate **[65]** (345 mg, 1.59 mmol). The pure product was obtained after purification by flash column chromatography (silica gel/crude material = 100/1, LP/EtOAc = 19/1).

Yield	40% (136 mg, 0.64 mmol)
Appearance	dark red crystals
Melting point	164.0 – 166.0 °C (Lit.[127]: 182 – 183 °C)
TLC-Analysis	R_f = 0.60 (LP/EtOAc = 10/1)
Sum formula	$C_{11}H_7N_3S$
GC-MS	213 (51, M^+), 111 (100), 102 (36)

^{1}H-NMR (400 MHz, $CDCl_3$) δ = 7.21 (dd, *J* = 5.3, 3.9 Hz, 1H, H4), 7.52 (dd, *J* = 5.4, 1.4 Hz, 1H, H5), 7.78 (d, *J* = 8.8 Hz, 2H, H3' & H5'), 7.90 (dd, *J* = 3.9, 1.3 Hz, 1H, H3), 7.93 (d, *J* = 8.8 Hz, 2H, H2' & H6') ppm.

^{13}C-NMR (101 MHz, $CDCl_3$) δ = 113.7 (s, C4'), 118.7 (s, CN), 123.4 (d, 2C, C2' & C6'), 128.1 (d, C3 or C4 or C5), 130.8 (d, C3 or C4 or C5), 133.3 (d, 2C, C3' & C5'), 134.2 (d, C3 or C4 or C5), 154.3 (s, C1'), 160.1 (s, C2) ppm.

Comment ^{1}H-NMR data is in accordance with the literature[127]. The in the literature reported ^{13}C-NMR data seems to be flawed as a comparison of the spectral data with the second literature known compound **[82]** supports our data.

E III.3.3 1-(4-Iodophenyl)-2-(thiophen-2-yl)diazene [78]

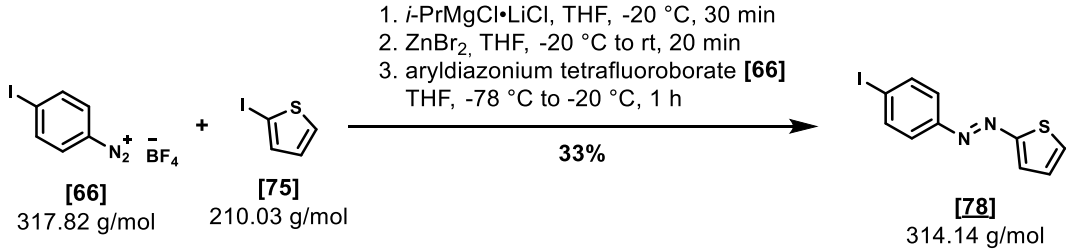

1-(4-Iodophenyl)-2-(thiophen-2-yl)diazene **[78]** was synthesized according to **General procedure D** using 2-iodothiophene **[75]** (501 mg, 2.385 mmol, 1.5 equiv.) and 4-iodobenzenediazonium tetrafluoroborate **[66]** (505 mg, 1.59 mmol). The pure product was obtained after purification by flash column chromatography (silica gel/crude material = 100/1, LP/EtOAc = 98/2).

Yield 33% (165 mg, 0.52 mmol)

Appearance orange-red crystals

Melting point 158.5 – 159.5 °C

TLC-Analysis R_f = 0.60 (LP/EtOAc = 5/1)

Sum formula $C_{10}H_7IN_2S$

HR-MS $[M+H]^+$: calculated: 314.9448 Da, found: 314.9469 Da, difference: 2.1 mDa

GC-MS 314 (53, M^+), 203 (43), 111 (100)

^{1}H-NMR (400 MHz, $CDCl_3$) δ = 7.17 (dd, *J* = 5.3, 3.8 Hz, 1H, H4), 7.44 (dd, *J* = 5.4, 1.3 Hz, 1H, H5), 7.59 (d, *J* = 8.7 Hz, 2H, H3' & H5'), 7.80 – 7.85 (m, 3H, H3 & H2' & H6') ppm.

^{13}C-NMR (101 MHz, $CDCl_3$) δ = 97.4 (s, C4'), 124.5 (d, 2C, C3' & C5'), 127.8 (d, C3 or C4 or C5), 129.3 (d, C3 or C4 or C5), 132.5 (d, C3 or C4 or C5), 138.5 (d, 2C, C3' & C5'), 151.6 (s, C1'), 160.3 (s, C2) ppm.

E III.3.4 1-(4-Ethynylphenyl)-2-(thiophen-2-yl)diazene [79]

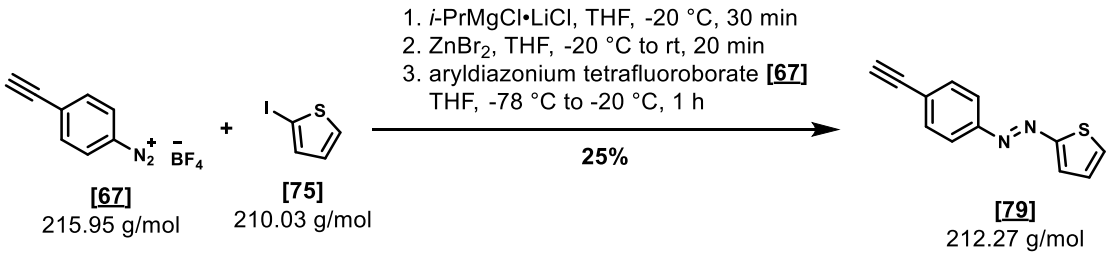

1-(4-Ethynylphenyl)-2-(thiophen-2-yl)diazene **[79]** was synthesized according to **General procedure D** using 2-iodothiophene **[75]** (227 mg, 1.08 mmol, 1.5 equiv.) and 4-ethynylbenzenediazonium tetrafluoroborate **[67]** (155 mg, 0.72 mmol). The pure product was obtained after purification by flash column chromatography (silica gel/crude material = 100/1, LP/EtOAc = 98/2).

Yield 25% (38 mg, 0.18 mmol)

Appearance yellow-orange crystals

Melting point 140.0 – 141.0 °C

TLC-Analysis R_f = 0.60 (LP/EtOAc = 20/1)

Sum formula $C_{12}H_8N_2S$

HR-MS $[M+H]^+$: calculated: 213.0481 Da, found: 213.0494 Da, difference: 1.3 mDa

GC-MS 213 (13, M^+), 212 (90, M^+) 129 (13), 111 (100), 101 (91)

^{1}H-NMR (400 MHz, $CDCl_3$) δ = 3.23 (s, 1H, CCH), 7.18 (dd, *J* = 5.4, 3.9 Hz, 1H, H4), 7.44 (dd, *J* = 5.3, 1.3 Hz, 1H, H5), 7.60 (d, *J* = 8.6 Hz, 2H, H3' & H5'), 7.80 – 7.84 (m, 3H, H2' & H4' & H6') ppm.

^{13}C-NMR (101 MHz, $CDCl_3$) δ = 79.6 (d, C<u>C</u>H), 83.5 (s, <u>C</u>CH), 122.9 (d, 2C, C3' & C5'), 124.5 (s, C4'), 127.8 (d, C3 or C4 or C5), 129.3 (d, C3 or C4 or C5), 132.5 (d, C3 or C4 or C5), 133.1 (d, 2C, C2' & C6'), 151.9 (s, C1'), 160.5 (s, C2) ppm.

E III.3.5 1-(4-Nitrophenyl)-2-(thiophen-2-yl)diazene [80]

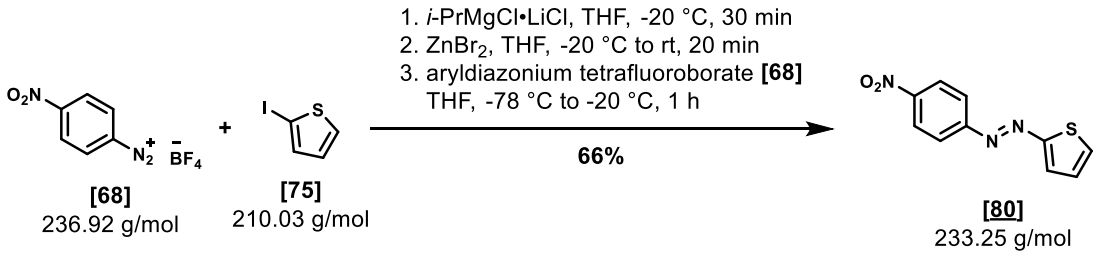

1-(4-Nitrophenyl)-2-(thiophen-2-yl)diazene **[80]** was synthesized according to **General procedure D** using 2-iodothiophene **[75]** (501 mg, 2.385 mmol, 1.5 equiv.) and 4-nitrobenzenediazonium tetrafluoroborate **[68]** (377 mg, 1.59 mmol). The pure product was obtained after purification by flash column chromatography (silica gel/crude material = 100/1, LP/EtOAc = 19/1).

Yield	66% (248 mg, 1.06 mmol)
Appearance	red crystals
Melting point	decomposition at 160 °C
TLC-Analysis	R_f = 0.65 (LP/EtOAc = 10/1)
Sum formula	$C_{10}H_7N_3O_2S$
HR-MS	$[M+H]^+$: calculated: 234.0332 Da, found: 234.0343 Da, difference: 1.1 mDa
GC-MS	233 (40, M^+), 122 (12), 111 (100)
^{1}H-NMR (200 MHz, $CDCl_3$)	δ = 7.19 – 7.28 (m, 1H, H4), 7.55 (d, *J* = 5.0 Hz, 1H, H5), 7.90 – 8.02 (m, 3H, H3 & H2' & H6'), 8.35 (d, *J* = 9.0 Hz, 2H, H3' & H5') ppm.
^{13}C-NMR (101 MHz, $CDCl_3$)	δ = 123.5 (d, C2' & C6'), 124.9 (d, C3' & C5'), 128.3 (d, C3 or C4 or C5), 131.1 (d, C3 or C4 or C5), 134.7 (d, C3 or C4 or C5), 148.6 (s, C4'), 155.6 (s, C1'), 160.1 (s, C2) ppm.

E III.3.6 4-(Thiophen-2-yldiazenyl)aniline [81]

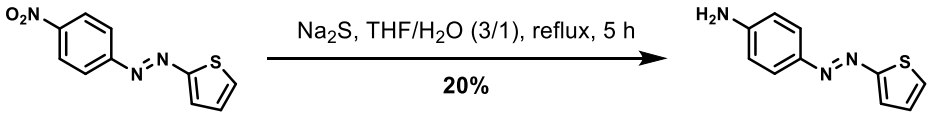

[80]
233.25 g/mol

[81]
203.26 g/mol

4-(Thiophen-2-yldiazenyl)aniline **[81]** was prepared according to a literature protocol[187]. An 8 mL vial was charged with 1-(4-nitrophenyl)-2-(thiophen-2yl)diazene **[80]** (49 mg, 0.21 mmol, 1 equiv.), $Na_2S \bullet 9H_2O$ (151 mg, 0.63 mmol, 3 equiv.) and THF/H_2O (3 mL, 3/1). The black-green reaction mixture was stirred at reflux temperature for 5 hours, whereupon the color turned from black-green to black-red. Subsequently, the reaction mixture was slowly cooled to room temperature (GC-MS analysis and TLC showed full conversion) and volatiles were removed under reduced pressure. The remaining aqu. layer was partitioned between EtOAc (20 mL) and 1 N NaOH (20 mL). The aqu. phase was extracted three times with EtOAc and the combined organic phases were washed once with 1 N NaOH, satd. $NaHCO_3$ and brine (20 mL aliquots), then dried over $MgSO_4$ and volatiles were removed in vacuo. Purification by flash column chromatography (silica gel/crude material = 100/1, LP/EtOAc = 19/1) afforded the desired product).

Yield	20% (9 mg, 0.04 mmol)
Appearance	dark-red crystals
Melting point	120.0 – 122.0 °C
TLC-Analysis	R_f = 0.45 (LP/EtOAc = 2/1)
Sum formula	$C_{10}H_9N_3S$
HR-MS	$[M+H]^+$: calculated: 204.0590 Da, found: 204.0603 Da, difference: 1.3 mDa
^{1}H-NMR (400 MHz, $CDCl_3$)	δ = 4.05 (br s, 2H, NH_2), 6.72 (d, J = 8.8 Hz, 2H, H3' & H5'), 7.11 (dd, J = 5.4, 3.8 Hz, 1H, H4), 7.29 (dd, J = 5.4, 1.3 Hz, 1H, H5), 7.64 (dd, J = 3.8, 1.3 Hz, 1H, H3), 7.74 (d, J = 8.8 Hz, 2H, H2' & H6') ppm.
^{13}C-NMR (101 MHz, $CDCl_3$)	δ = 114.9 (d, 2C, C3' & C5'), 125.2 (d, 2C, C2' & C6'), 126.7 (d, C3 or C4 or C5), 127.3 (d, C3 or C4 or C5), 129.1 (d, C3 or C4 or C5), 145.0 (d, C4'), 149.5 (s, C1'), 161.1 (s, C2) ppm.

E III.3.7 Ethyl-4-(thiophen-2-yldiazenyl)benzoate [82]

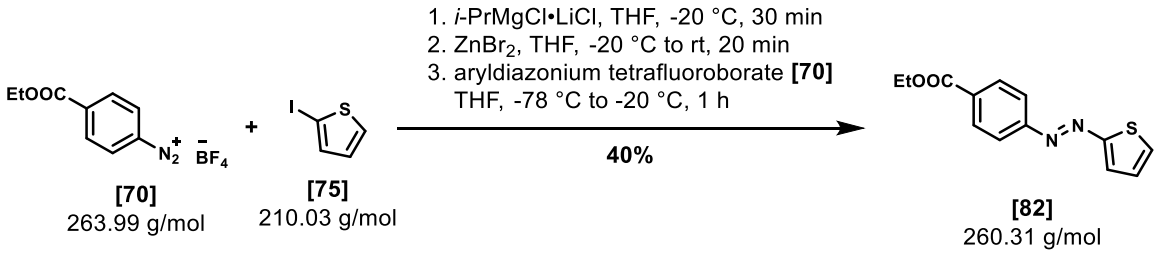

Ethyl-4-(thiophen-2-yldiazenyl)benzoate **[82]** was synthesized according to **General procedure D** using 2-iodothiophene **[75]** (501 mg, 2.385 mmol, 1.5 equiv.) and 4-(ethoxycarbonyl)benzenediazonium tetrafluoroborate **[70]** (420 mg, 1.59 mmol). The pure product was obtained after purification by flash column chromatography (silica gel/crude material = 100/1, LP/EtOAc = 97/3).

Yield	40% (173 mg, 0.66 mmol)
Appearance	bright orange crystals
Melting point	118.5 – 119.0 °C (Lit.[131]: 115.6 – 117.1 °C)
TLC-Analysis	R_f = 0.55 (LP/EtOAc = 10/1)
Sum formula	$C_{13}H_{12}N_2O_2S$
GC-MS	260 (36, M^+), 149 (23), 111 (100), 103 (14)
^{1}H-NMR (400 MHz, $CDCl_3$)	δ = 1.42 (t, *J* = 7.1 Hz, 3H, CH_3), 4.41 (q, *J* = 7.1 Hz, 2H, CH_2), 7.19 (dd, *J* = 5.3, 3.8 Hz, 1H, H4), 7.47 (dd, *J* = 5.3, 1.3 Hz, 1H, H5), 7.87 (dd, *J* = 3.8, 1.3 Hz, 1H, H3), 7.89 (d, *J* = 8.6 Hz, 2H, H2' & H6'), 8.16 (d, *J* = 8.7 Hz, 2H, H3' & H5') ppm.
^{13}C-NMR (101 MHz, $CDCl_3$)	δ = 14.5 (q, CH_3), 61.4 (t, CH_2), 122.7 (d, 2C, C2' & C6'), 127.9 (d, C3 or C4 or C5), 129.8 (d, C3 or C4 or C5), 130.7 (d, 2C, C3' & C5'), 132.0 (s, C4'), 133.3 (d, C3 or C4 or C5), 154.8 (s, C1'), 160.4 (s, C2), 166.2 (s, ester) ppm.
Comment	Spectral data is in accordance with the literature[131].

E III.3.8 4-(Thiophen-2-yldiazenyl)benzoic acid [83]

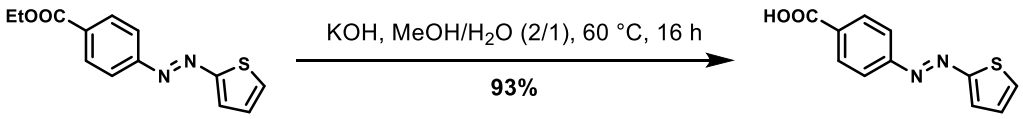

[82]
260.31 g/mol

[83]
232.26 g/mol

4-(Thiophen-2-yldiazenyl)benzoic acid **[83]** was synthesized using a modified literature procedure[204]. The ester **[82]** (62 mg, 0.27 mmol, 1 equiv.) was dissolved in MeOH/H_2O (1 mL, 2/1) and KOH (45 mg, 0.80 mmol, 3 equiv.). The reaction mixture was heated to 60 °C and stirred for 16 hours at that temperature. MeOH was removed in vacuo and the residue was diluted with H_2O (1 mL). Next, conc. HCl was added to adjust an acidic pH. The aqu. layer was then extracted with Et_2O (5 times) and the combined organic phases were dried over $MgSO_4$. Evaporation of the solvent afforded the desired compound. For purification, the acid was dissolved in 0.5 N NaOH and the aqu. layer was extracted 3 times with Et_2O. Conc. HCl was further added to the aqu. layer to precipitate the acid **[83]** as an orange-red solid, which was isolated by filtration.

Yield	93% (55 mg, 0.24 mmol)
Appearance	orange-red crystals
Melting point	decomposition at 191 °C
TLC-Analysis	R_f = 0.45 (EtOAc)
Sum formula	$C_{11}H_8N_2O_2S$
HR-MS	$[M+H]^+$: calculated: 233.0379 Da, found: 233.0391 Da, difference: 1.2 mDa
^{1}H-NMR (400 MHz, DMSO-d_6)	δ = 7.34 (dd, *J* = 5.3, 3.9 Hz, 1H, H4), 7.87 – 7.92 (m, 3H, H5 & H2' & H6'), 8.07 (dd, *J* = 3.9, 1.3 Hz, 1H, H3), 8.11 (d, *J* = 8.7 Hz, 2H, H3' & H5'), 13.21 (br s, 1H) ppm.
^{13}C-NMR (101 MHz, DMSO-d_6)	δ = 122.4 (d, 2C, C2' & C6' or C3' & C5'), 128.6 (d, C3 or C4 or C5), 130.6 (d, 2C, C2' & C6' or C3' & C5'), 131.5 (d, C3 or C4 or C5), 132.5 (s, C4'), 134.4 (d, C3 or C4 or C5), 153.8 (s, C1'), 159.2 (s, C2), 166.6 (s, acid) ppm.

E III.3.9 4-(Thiophen-2yldiazenyl)phenyl pivalate [84]

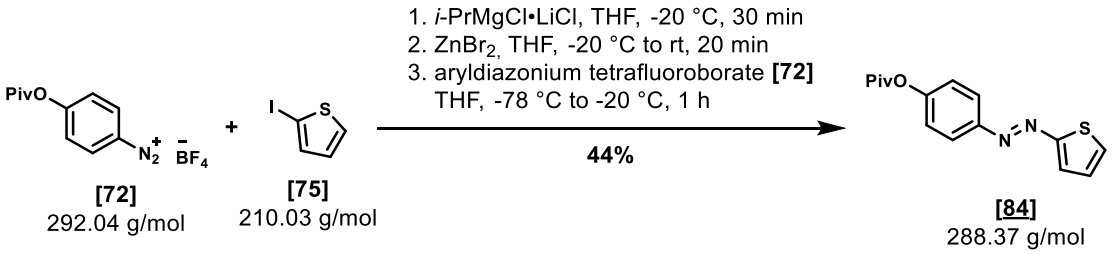

4-(Thiophen-2yldiazenyl)phenyl pivalate **[84]** was synthesized according to **General procedure D** using 2-iodothiophene **[75]** (227 mg, 1.08 mmol, 1.5 equiv.) and 4-(pivaloyloxy)benzenediazonium tetrafluoroborate **[72]** (210 mg, 0.72 mmol). The pure product was obtained after purification by flash column chromatography (silica gel/crude material = 100/1, LP/EtOAc = 97/3).

Yield	44% (86 mg, 0.30 mmol)
Appearance	yellow crystals
Melting point	133.5 – 134.0 °C
TLC-Analysis	R_f = 0.65 (LP/EtOAc = 5/1)
Sum formula	$C_{15}H_{16}N_2O_2S$
HR-MS	$[M+H]^+$: calculated: 289.1005 Da, found: 289.1021 Da, difference: 1.6 mDa
GC-MS	288 (26, M^+), 204 (54), 121 (34), 111 (26)
^{1}H-NMR (400 MHz, $CDCl_3$)	δ = 1.38 (s, 9H, Piv), 7.16 (dd, *J* = 5.4, 3.8 Hz, 1H, H4), 7.19 (d, *J* = 8.9 Hz, 2H, H3' & H5'), 7.41 (dd, *J* = 5.4, 1.3 Hz, 1H, H5), 7.79 (dd, *J* = 3.8, 1.3 Hz, 1H, H3), 7.89 (d, *J* = 8.9 Hz, 2H, H2' & H6') ppm.
^{13}C-NMR (101 MHz, $CDCl_3$)	δ = 27.3 (q, 3C, CH_3-Piv), 39.4 (s, C-Piv), 122.3 (d, 2C, C2' & C6' or C3' & C5'), 124.1 (d, 2C, C2' & C6' or C3' & C5'), 127.6 (d, C3 or C4 or C5), 128.7 (d, C3 or C4 or C5), 131.8 (d, C3 or C4 or C5), 149.7 (s, C4'), 153.1 (s, C1'), 160.4 (s, C2), 176.9 (s, ester) ppm.

E III.3.10 4-(Thiophen-2-yldiazenyl)phenol [85]

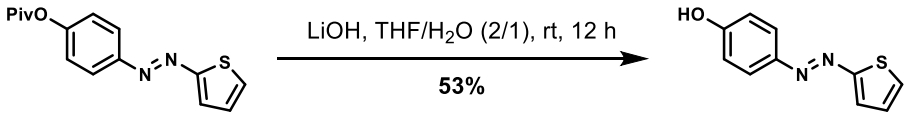

[84]
288.37 g/mol

[85]
204.25 g/mol

4-(Thiophen-2-yldiazenyl)phenol **[85]** was prepared from the corresponding pivalate **[84]** following a literature procedure[131]. The pivalate **[84]** (20 mg, 0.07 mmol, 1 equiv.) was dissolved in THF/H_2O (0.6 mL, 2/1) and LiOH•H_2O (290 mg, 0.69 mmol, 10 equiv.) was added. The reaction mixture was stirred for 12 hours at room temperature. Subsequently, 2 N HCl (0.5 mL) was added to the reaction mixture and the aqu. layer was then extracted with DCM (5 times). The combined organic phases were dried over $MgSO_4$ and volatiles were removed in vacuo. Purification by preparative HPLC provided the desired product.

Yield	53% (8 mg, 0.04 mmol)
Appearance	orange crystals
Melting point	136.0 – 138.0 °C
TLC-Analysis	R_f = 0.40 (LP/EtOAc = 5/1)
Sum formula	$C_{10}H_8N_2OS$
HR-MS	$[M+H]^+$: calculated: 205.0430 Da, found: 205.0445 Da, difference: 1.5 mDa
^{1}H-NMR (400 MHz, $CDCl_3$)	δ = 5.26 (br s, 1H, OH), 6.92 (d, *J* = 8.9 Hz, 2H, H3' & H5'), 7.14 (dd, *J* = 5.4, 3.8 Hz, 1H, H4), 7.35 (dd, *J* = 5.4, 1.4 Hz, 1H, H5), 7.72 (dd, *J* = 3.8, 1.3 Hz, 1H, H3), 7.81 (d, *J* = 8.9 Hz, 2H, H2' & H6') ppm.
^{13}C-NMR (101 MHz, $CDCl_3$)	δ = 116.0 (d, 2C, C3' & C5'), 125.0 (d, 2C, C2' & C6'), 127.5 (d, C3 or C4 or C5), 127.7 (d, C3 or C4 or C5), 130.6 (d, C3 or C4 or C5), 146.7 (s, C4'), 158.2 (s, C1'), 160.7 (s, C2) ppm.

E III.3.11 *N,N*-Diethyl-4-(thiophen-2-diazenyl)aniline [87]

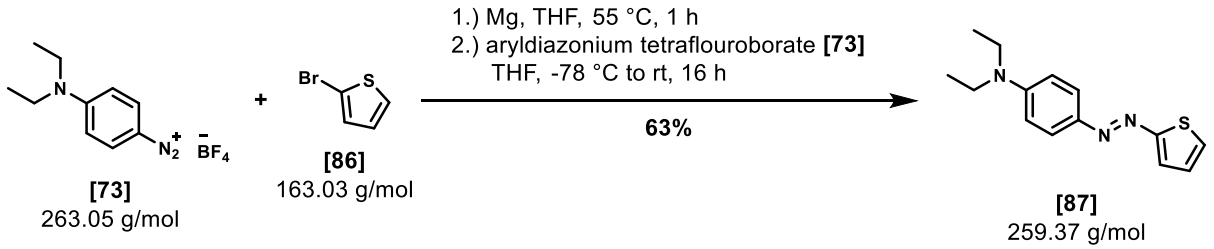

N,N-Diethyl-4-(thiophen-2-diazenyl)aniline **[87]** was synthesized according to **General procedure E** using 2-bromothiophene **[86]** (257 mg, 1.59 mmol, 1 equiv.) and 4-(diethylamino)benzenediazonium tetrafluoroborate **[73]** (418 mg, 1.59 mmol, 1 equiv.). The pure product was obtained after purification by flash column chromatography (silica gel/crude material = 100/1, LP/EtOAc = 19/1).

Yield	63% (256 mg, 0.99 mmol)
Appearance	orange crystals
Melting point	126.5 – 127.0 °C (Lit.[126]: 136 - 138 °C)
TLC-Analysis	R_f = 0.55 (LP/EtOAc = 10/1)
Sum formula	$C_{14}H_{17}N_3S$
^{1}H-NMR (400 MHz, $CDCl_3$)	δ = 1.23 (t, *J* = 7.1 Hz, 6H, 2 x CH_3), 3.45 (q, *J* = 7.1 Hz, 4H, 2 x CH_2), 6.70 (d, *J* = 9.2 Hz, 2H, H3' & H5'), 7.09 (dd, *J* = 5.4, 3.8 Hz, 1H, H4), 7.24 (dd, *J* = 5.4, 1.3 Hz, 1H, H5), 7.57 (dd, *J* = 3.8, 1.3 Hz, 1H, H3), 7.78 (d, *J* = 9.2 Hz, 2H, H2' & H6') ppm.
^{13}C-NMR (101 MHz, $CDCl_3$)	δ = 12.8 (q, 2C, 2 x CH_3), 44.8 (t, 2C, 2 x CH_2), 111.2 (d, 2C, C3' & C5'), 125.4 (d, 2C, C2' & C6'), 125.7 (d, C3 or C4 or C5), 127.2 (d, C3 or C4 or C5), 127.7 (d, C3 or C4 or C5), 142.5 (s, C4'), 150.1 (d, C1'), 161.7 (s, C2) ppm.
Comment	Spectral data are in accordance with the literature[126].

E III.3.12 1-(4-Fluorophenyl)-2-(thiophen-2-yl)diazene [88]

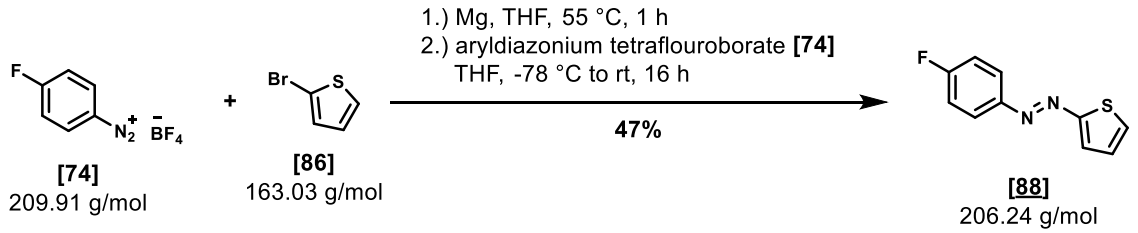

[74]
209.91 g/mol

[86]
163.03 g/mol

[88]
206.24 g/mol

1-(4-Fluorophenyl)-2-(thiophen-2-yl)diazene **[88]** was synthesized according to **General procedure E** using 2-bromothiophene **[86]** (257 mg, 1.59 mmol, 1 equiv.) and 4-fluorobenzenediazonium tetrafluoroborate **[74]** (334 mg, 1.59 mmol, 1 equiv.). The pure product was obtained after purification by flash column chromatography (silica gel/crude material = 100/1, LP/EtOAc = 98/2).

Yield	47% (154 mg, 0.75 mmol)
Appearance	orange crystals
Melting point	88.5 – 89.0 °C
TLC-Analysis	R_f = 0.70 (LP/EtOAc = 10/1)
Sum formula	$C_{10}H_7FN_2S$
HR-MS	$[M+H]^+$: calculated: 207.0387 Da, found: 207.0395 Da, difference: 0.8 mDa
GC-MS	206 (100, M^+), 123 (17), 111 (97)
^{1}H-NMR (400 MHz, $CDCl_3$)	δ = 7.14 – 7.20 (m, 3H, H4 & H3' & H5'), 7.41 (dd, *J* = 5.4, 1.4 Hz, 1H, H5), 7.79 (dd, *J* = 3.8, 1.3 Hz, 1H, H3), 7.87 (dd, *J* = 9.0, 5.3 Hz, 2H, H2' & H6') ppm.
^{13}C-NMR (101 MHz, $CDCl_3$)	δ = 116.2 (d/d, $^2J_{CF}$ = 23.0 Hz, 2C, C3' & C5'), 124.9 (d/d, $^3J_{CF}$ = 8.8 Hz, 2C, C2' & C6'), 127.6 (d, C3 or C4 or C5), 128.6 (d, C3 or C4 or C5), 131.8 (d, C3 or C4 or C5), 148.8 (s/d, $^4J_{CF}$ = 3.1 Hz, C4'), 161.7 (s/d, $^1J_{CF}$ = 275.7 Hz, C4'), 165.43 (s, C2) ppm.

E III.4 Arylazo-3-thiophenes

E III.4.1 1-Phenyl-2-(thiophen-3-yl)diazene [90]

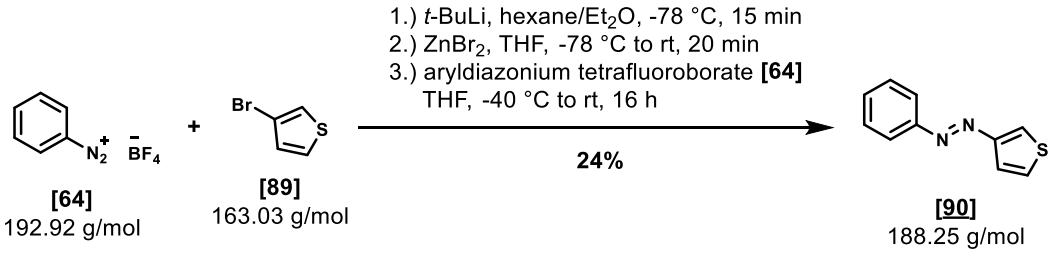

1-Phenyl-2-(thiophen-3-yl)diazene **[90]** was synthesized according to **General procedure F** using 3-bromothiophene **[89]** (470 mg, 2.88 mmol, 1.6 equiv.) and benzenediazonium tetrafluoroborate **[64]** (345 mg, 1.80 mmol, 1 equiv.). The crude product was purified by flash column chromatography (silica gel/crude material = 100/1, LP/EtOAc = 99/1).

Yield	24% (80 mg, 0.42 mmol)
Appearance	orange crystals
Melting point	48.0 – 48.5 °C
Sum formula	$C_{10}H_8N_2S$
TLC-Analysis	R_f = 0.50 (LP/EtOAc = 20/1)
HR-MS	$[M+H]^+$: calculated: 189.0481 Da, found: 189.0490 Da, difference: 0.9 mDa
GC-MS	188 (100, M^+), 115 (11), 111 (82), 105 (10)
^{1}H-NMR (400 MHz, $CDCl_3$)	δ = 7.36 (dd, *J* = 5.1, 3.1 Hz, 1H, H4), 7.45 - 7.53 (m, 3H, H3' & H4' & H5'), 7.61 (dd, *J* = 5.1, 1.2 Hz, 1H, H5), 7.87 (dt, *J* = 6.6, 1.6 Hz, 2H, H3' & H5'), 8.06 (dd, *J* = 3.1, 1.2 Hz, 1H, H2) ppm.
^{13}C-NMR (101 MHz, $CDCl_3$)	δ = 119.0 (d, C2), 122.7 (d, 2C, C2' & C6' or C3' & C5'), 126.4 (d, C4 or C5 or C4'), 126.9 (d, C4 or C5 or C4'), 129.2 (d, 2C, C2' & C6' or C3' & C5'), 130.8 (d, C4 or C5 or C4'), 152.9 & 157.1 (2xs, 2C, C3 & C1') ppm.

The assignments of protons and carbon atoms in the NMR codes of compounds **[90]**, **[91]**, **[92]** and **[93]** were carried out as follows:

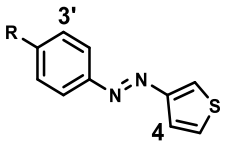

E III.4.2 1-(4-Nitrophenyl)-2-(thiophen-3-yl)diazene [91]

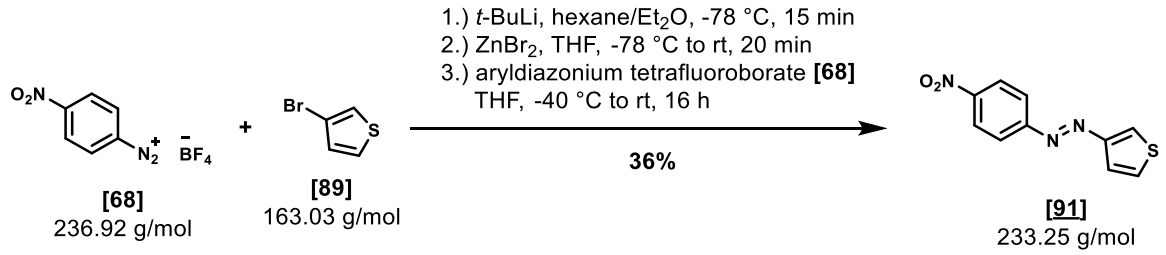

1-(4-Nitrophenyl)-2-(thiophen-3-yl)diazene **[91]** was synthesized according to **General procedure F** using 3-bromothiophene **[89]** (470 mg, 2.88 mmol, 1.6 equiv.) and 4-nitrobenzenediazonium tetrafluoroborate **[68]** (426 mg, 1.80 mmol, 1 equiv.). The crude product was purified by flash column chromatography (silica gel/crude material = 100/1, LP/EtOAc = 97/3).

Yield	36% (150 mg, 0.64 mmol)
Appearance	orange crystals
Melting point	186.5 – 187.0 °C
Sum formula	$C_{10}H_7N_3O_2S$
TLC-Analysis	R_f = 0.60 (LP/EtOAc = 10/1)
HR-MS	$[M+H]^+$: calculated: 234.0332 Da, found: 234.0341 Da, difference: 0.9 mDa
GC-MS	233 (41, M^+), 122 (14), 111 (100)
^{1}H-NMR (400 MHz, $CDCl_3$)	δ = 7.40 (dd, *J* = 5.3, 3.1 Hz, 1H, H4), 7.60 (dd, *J* = 5.3, 1.3 Hz, 1H, H5), 7.98 (d, *J* = 9.1 Hz, 2H, H2' & H6'), 8.21 (dd, *J* = 3.2, 1.2 Hz, 1H, H2), 8.37 (d, *J* = 9.0 Hz, 2H, H3' & H5') ppm.
^{13}C-NMR (101 MHz, $CDCl_3$)	δ = 118.5 (d, C2), 123.3 & 124.9 (2xd, 2C, C2' & C6' & C3' & C5'), 127.0 & 130.2 (2xd, C4 & C5), 148.7 & 156.2 & 157.1 (3xs, 3C, C3 & C1' & C4') ppm.

E III.4.3 *N*,*N*-Diethyl-4-(thiophen-3-yldiazenyl)aniline [92]

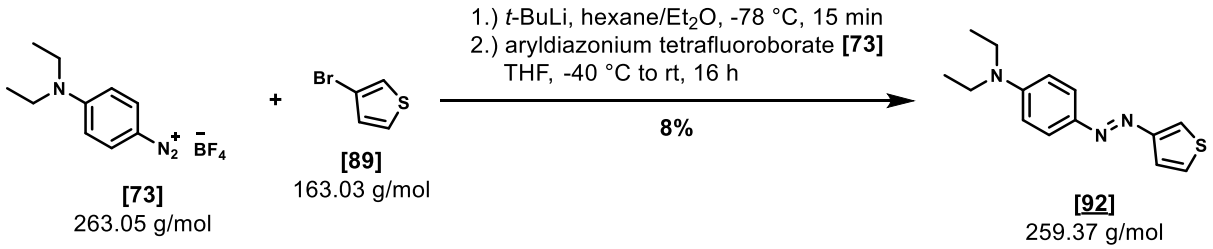

N,*N*-Diethyl-4-(thiophen-3-yldiazenyl)aniline **[92]** was synthesized applying a modified **General procedure F**. 3-Bromothiophene **[89]** (293 mg, 1.80 mmol, 1 equiv.) was placed in a flask. 4-(Diethylamino)benzenediazonium tetrafluoroborate **[73]** (473 mg, 1.80 mmol, 1 equiv.) was placed in a bulb and this bulb was mounted onto one of the necks for convenient addition of the solid material under an inert atmosphere later in the reaction. The flask was closed with a septum and was evacuated and flushed with argon three times. Dry hexane (8 mL) and dry diethyl ether (5 mL) were added via syringe and the solution was cooled to -78 °C. A solution of *t*-BuLi (1.7 M in pentane, 2.12 mL, 3.60 mmol, 2 equiv.) was added dropwise via syringe while the temperature was maintained at -78 °C. The solution was stirred at that temperature for 15 minutes. A syringe was preloaded with a dimethyl disulfide solution in dry THF and was used to quench an aliquot of the reaction directly in the syringe. TLC and GC-MS analysis of that quenched material showed complete lithiation. The bulb containing 4-(diethylamino)benzenediazonium tetrafluoroborate **[73]** was used to add the solid material in portions to the stirred solution. The reaction was stirred for 16 hours slowly warming up in the cooling bath. Satd. aqu. NH_4Cl (5 mL) was added and the phases were separated. The aq. phase was extracted with DCM (3 x 5 mL). The combined organic phases were washed with brine (10 mL) and was dried over $MgSO_4$. After purification by flash column chromatography (silica gel/crude material = 100/1, LP/EtOAc = 98/2) the product was obtained.

Yield	8% (36 mg, 0.14 mmol)
Appearance	orange crystals
Melting point	122.0 – 122.5 °C
Sum formula	$C_{14}H_{17}N_3S$
TLC-Analysis	R_f = 0.50 (LP/EtOAc = 10/1)
HR-MS	$[M+H]^+$: calculated: 260.1216 Da, found: 260.1228 Da, difference: 1.2 mDa
GC-MS	259 (97, M^+), 244 (100), 216 (15), 148 (52), 133 (51), 120 (12), 119 (21), 118 (20), 111 (18), 105 (29), 104 (25)

^{1}H-NMR (400 MHz, $CDCl_3$) δ = 1.23 (t, *J* = 7.1 Hz, 6H, 2 x CH_3), 3.45 (q, *J* = 7.1 Hz, 4H, 2 x CH_2), 6.71 (d, *J* = 9.2 Hz, 2H, H3' & H5'), 7.31 (dd, *J* = 5.2, 3.2 Hz, 1H, H4), 7.57 (dd, *J* = 5.2, 1.2 Hz, 1H, H5), 7.77 – 7.82 (m, 3H, H2 & H2' & H6') ppm.

^{13}C-NMR (101 MHz, $CDCl_3$) δ = 12.8 (q, 2C, 2 x CH_3), 44.8 (t, 2C, 2 x CH_2), 111.2 (d, 2C, C3' & C5'), 119.7 (d, C2 or C4 or C5), 122.5 (d, C2 or C4 or C5), 125.1 (d, 2C, C2' & C6'), 125.8 (d, C2 or C4 or C5), 143.1 & 150.1 & 157.5 (3xs, C3 & C1' & C4') ppm.

E III.4.4 1-(4-Fluorophenyl)-2-(thiophen-3-yl)diazene [93]

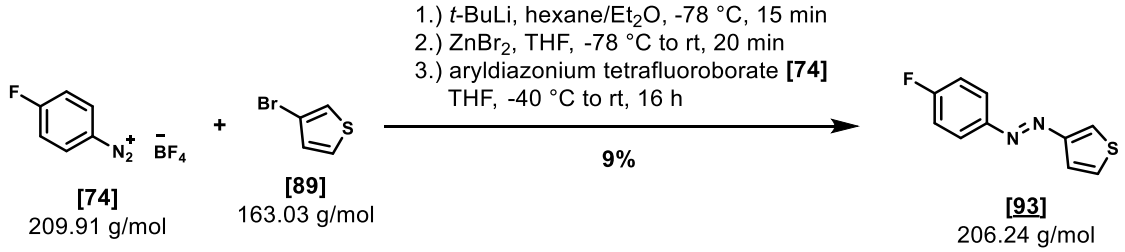

[74] 209.91 g/mol

[89] 163.03 g/mol

[93] 206.24 g/mol

1-(4-Fluorophenyl)-2-(thiophen-3-yl)diazene **[93]** was synthesized according to **General procedure F** using 3-bromothiophene **[89]** (470 mg, 2.88 mmol, 1.6 equiv.) and 4-fluorobenzenediazonium tetrafluoroborate **[74]** (378 mg, 1.80 mmol, 1 equiv.). The crude product was purified by flash column chromatography (silica gel/crude material = 100/1, LP).

Yield 9% (32 mg, 0.16 mmol)

Appearance orange crystals

Melting point 94.0 – 95.0 °C

Sum formula $C_{10}H_7FN_2S$

TLC-Analysis R_f = 0.80 (LP/EtOAc = 10/1)

HR-MS $[M+H]^+$: calculated: 207.0392 Da, found: 207.0394 Da, difference: 0.7 mDa

GC-MS 206 (88, M^+), 123 (17), 111 (75)

^{1}H-NMR (400 MHz, $CDCl_3$) δ = 7.18 (dd, *J* = 9.0, 8.2 Hz, 2H, H3' & H5'), 7.35 (dd, *J* = 5.2, 3.1 Hz, 1H, H4), 7.58 (dd, *J* = 5.3, 1.3 Hz, 1H, H5), 7.88 (dd, *J* = 9.0, 5.3 Hz, 2H, H2' & H6'), 8.03 (dd, *J* = 3.1, 1.2 Hz, 1H, H2) ppm.

^{13}C-NMR (101 MHz, $CDCl_3$) δ = 116.2 (d/d, $^2J_{CF}$ = 22.8 Hz, 2C, C3' & C5'), 118.9 (d, C2 or C4 or C5), 124.7 (d/d, $^3J_{CF}$ = 8.9 Hz, 2C, C2' & C6'), 126.5 (d, C2 or C4 or C5), 126.9 (d, C2 or C4 or C5), 149.4 (s/d, $^4J_{CF}$ = 3.1 Hz, C1'), 156.9 (s, C3), 164.3 (s/d, $^1J_{CF}$ = 251.5 Hz, C4') ppm.

E III.5 Escitalopram building blocks

E III.5.1 (*S*)-3-(5-(Aminomethyl)-1-(4-fluorophenyl)-1,3-dihydroisobenzofuran-1-yl)-*N*,*N*-dimethylpropan-1-amine [95]

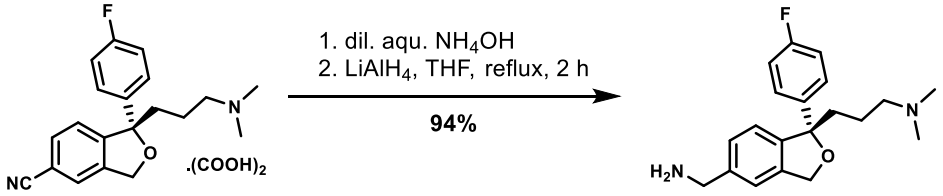

[94]
414.43 g/mol

[95]
328.43 g/mol

Escitalopram amine **[95]** was synthesized according to a literature procedure[137]. Escitalopram oxalate **[94]** (38.6 mg, 0.093 mmol, 1 equiv.) was placed in an 8 mL vial, a dil. solution of aqu. NH_4OH (2.5%, 1 mL) was added and the mixture was stirred for 5 minutes. The mixture was extracted with EtOAc (3 x 1 mL). The combined organic phases were dried over $MgSO_4$. The solvent was evaporated in vacuo giving the free base as a colorless oil. The free base was dissolved in dry THF (2 mL) and $LiAlH_4$ (7.1 mg, 0.186 mmol, 2 equiv.) was added under an argon atmosphere. The reaction mixture was stirred at reflux temperature for 2 hours. Then the reaction was cooled to room temperature and 0.5 N NaOH (1.5 mL) was carefully added to quench the excess $LiAlH_4$. Phases were separated and the aqu. phase was extracted with EtOAc (3 x 1 mL). The combined organic phases were dried over $MgSO_4$ and after evaporation of the solvent in vacuo the product was obtained.

Yield	94% (28.7 mg, 0.087 mmol)
Appearance	colorless oil
TLC analysis	R_f = 0.2 (MeOH + 1% NEt_3)
Sum formula	$C_{20}H_{25}FN_2O$
^{1}H-NMR (400 MHz, $CDCl_3$)	δ = 1.27 – 1.54 (m, 2H, CH_2-C<u>H</u>$_2$-CH_2-N$(CH_3)_2$), 2.03 (br s, 2H, NH_2), 2.06 – 2.21 (m, 2H, C<u>H</u>$_2$-CH_2-CH_2-N$(CH_3)_2$), 2.15 (s, 6H, 2 x CH_3), 2.25 (t, J = 7.9 Hz, 2H, CH_2-CH_2-C<u>H</u>$_2$-N$(CH_3)_2$), 3.85 (s, 2H, NH-CH_2), 5.10 (d, J = 12.4 Hz, 1H, H3), 5.14 (d, J = 12.4 Hz, 1H, H3), 6.96 (dd, $^3J_{HH}$ = 8.8, $^3J_{HF}$ = 8.8 Hz, 2H, H3' & H5'), 7.15 (s, 1H, H4), 7.18 – 7.25 (m, 2H, H6 & H7), 7.44 (dd, $^3J_{HH}$ = 8.5, $^4J_{HF}$ = 5.3 Hz, 2H, H2' & H6') ppm.
^{13}C-NMR (101 MHz, $CDCl_3$)	δ = 22.3 (t, CH_2-<u>C</u>H$_2$-CH_2-N$(CH_3)_2$), 39.5 (t, <u>C</u>H$_2$-CH_2-CH_2-N$(CH_3)_2$), 45.3 (q, 2C, 2 x CH_3), 46.3 (t, <u>C</u>H$_2$-NH_2), 59.7 (t, CH_2-CH_2-<u>C</u>H$_2$-N(CH_3)), 71.9 (t, C3), 90.9 (s, C1), 115.0 (d/d, $^2J_{CF}$ = 21.2 Hz, 2C,

C3‘ & C5‘), 120.0 & 122.0 & 126.7 (3xd, 3C, C4 & C6 & C7), 126.9 (d/d, $^{3}J_{CF}$ = 8.0 Hz, 2C, C2‘ & C6‘), 139.6 (s, C3a or C5 or C7a), 141.3 (s/d, $^{4}J_{CF}$ = 3.1 Hz, C1‘), 142.9 (s, C3a or C5 or C7a), 143.1 (s, C3a or C5 or C7a), 161.9 (s/d, $^{1}J_{CF}$ = 245.0 Hz, C4‘) ppm.

Optical rotation $[\alpha]_D^{25}$ = +4.3 (c = 0.30, MeOH) (Lit.[137]: $[\alpha]_D^{25}$ = +4.26 (c = 0.30, MeOH))The assignments of protons and carbon atoms in the NMR codes of compounds **[95]**, **[96]**, **[97]** and **[98]** were carried out as follows:

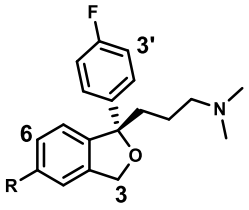

E III.5.2 (*S*)-1-(3-(Dimethylamino)propyl)-1-(4-fluorophenyl)-1,3-dihydroisobenzofuran-5-carbaldehyde [96]

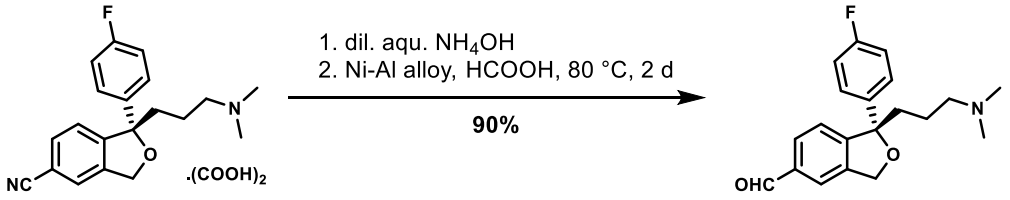

[94]
414.43 g/mol

[96]
327.40 g/mol

Escitalopram aldehyde **[96]** was synthesized according to a literature procedure[137]. Escitalopram oxalate **[94]** (51.5 mg, 0.124 mmol, 1 equiv.) was placed in an 8 mL vial and a dil. solution of aqu. NH_4OH (2.5%, 1 mL) was added and the mixture was stirred for 5 minutes. The mixture was extracted with EtOAc (3 x 1 mL). The combined organic phases were dried over $MgSO_4$. The solvent was evaporated in vacuo giving the free base as a colorless oil. The free base, aluminum-nickel alloy (71.1 mg) and a magnetic stirring bar were placed in an 8 mL vial. Formic acid (1 mL) was added, the vial was flushed with argon and was tightly closed with a screw cap. The mixture was stirred at 80 °C in a thermo block (thermo sensor was set to 88°C) for two days. The mixture was filtered through a pad of celite, neutralized with satd. aqu. $NaHCO_3$ solution and extracted with $CHCl_3$ (3 x 2 mL). The combined organic phases were dried over $MgSO_4$. After evaporation of the solvent in vacuo the product was obtained.

Yield 90% (36.4 mg, 0.111 mmol)

Appearance colorless oil

TLC-Analysis R_f = 0.3 (MeOH + 1% NEt_3)

Sum formula	$C_{20}H_{22}FNO_2$
HR-MS	$[M+H]^+$: calculated: 328.1707 Da, found: 328.1731 Da, difference: 2.4 mDa
^{1}H-NMR (400 MHz, $CDCl_3$)	δ = 1.27 – 1.54 (m, 2H, CH_2-C<u>H</u>$_2$-CH_2-N(CH_3)$_2$), 2.13 (s, 6H, 2 x CH_3), 2.15 – 2.21 (m, 2H, C<u>H</u>$_2$-CH_2-CH_2-N(CH_3)$_2$), 2.23 (t, *J* = 7.2 Hz, 2H, CH_2-CH_2-C<u>H</u>$_2$-N(CH_3)$_2$), 5.18 (d, *J* = 12.7 Hz, 1H, H3), 5.23 (d, *J* = 12.7 Hz, 1H, H3), 7.00 (dd, $^3J_{HH}$ = 8.7, $^3J_{HF}$ = 8.7 Hz, 2H, H3' & H5'), 7.41 – 7.48 (m, 3H, H2' & H6' & H6), 7.73 (s, 1H, H4), 7.81 (d, *J* = 7.7 Hz, 1H, H7), 9.99 (s, 1H, aldehyde) ppm.
^{13}C-NMR (101 MHz, $CDCl_3$)	δ = 22.3 (t, CH_2-<u>C</u>H$_2$-CH_2-N(CH_3)$_2$), 39.2 (t, <u>C</u>H$_2$-CH_2-CH_2-N(CH_3)$_2$), 45.5 (q, 2C, 2 x CH_3), 59.6 (t, CH_2-CH_2-<u>C</u>H$_2$-N(CH_3)$_2$), 71.5 (t, C3), 91.1 (s, C1), 115.4 (d/d, $^2J_{CF}$ = 21.3 Hz, 2C, C3‘ & C5‘), 122.4 (d, C4 or C6 or C7), 122.6 (d, C4 or C6 or C7), 127.0 (d/d, $^3J_{CF}$ = 8.0 Hz, 2C, C2‘ & C6’), 130.3 (d, C4 or C6 or C7), 136.6 (s, C3a or C5 or C7a), 140.1 (s/d, $^4J_{CF}$ = 3.1 Hz, C1‘), 140.4 (s, C3a or C5 or C7a), 151.1 (s, C3a or C5 or C7a), 162.1 (s/d, $^1J_{CF}$ = 246.0 Hz, C4‘), 191.6 (s, aldehyde) ppm.
Optical rotation	$[\alpha]_D^{25}$ = +14.0 (c = 1.00, MeOH) (Lit.[137]: $[\alpha]_D^{25}$ = +12.74 (c = 1.00, MeOH))

E III.5.3 (*S*)-1-(3-(Dimethylamino)propyl)-1-(4-fluorophenyl)-1,3-dihydroisobenzofuran-5-carboxylic acid [<u>97</u>]

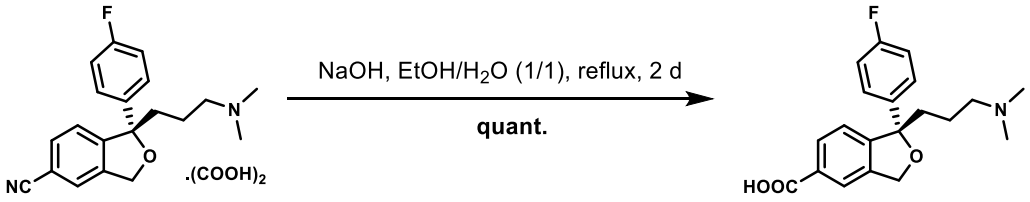

[94] 414.43 g/mol

[<u>97</u>] 343.40 g/mol

Escitalopram oxalate **[94]** (1262 mg, 3.05 mmol, 1 equiv.) and NaOH (853 mg, 21.32 mmol, 7 equiv.) were placed in a 100 mL round bottom flask. EtOH/H_2O (1/1, 50 mL) was added and the reaction was stirred at reflux temperature for two days. The mixture was acidified with 2 N HCl. EtOAc (50 mL) was added and phases were separated. The efficiency of the extraction was followed by TLC and the pH was adjusted if necessary. The aqu. phase was extracted with EtOAc (2 x 50 mL). The combined organic phases were washed with brine (75 mL) and dried over $MgSO_4$. After evaporation of the solvent in vacuo and drying in high vacuum (0.1 mbar, 100°C) Escitalopram acid **[<u>97</u>]** was obtained.

Yield	quant. (1046 mg, 3.05 mmol)
Appearance	colorless crystals
Melting point	117.5 – 118.5 °C
TLC-Analysis	R_f = 0.25 (MeOH)
Sum formula	$C_{20}H_{22}FNO_3$
HR-MS	$[M+H]^+$: calculated: 344.1656 Da, found: 344.1668 Da, difference: 1.2 mDa
^{1}H-NMR (400 MHz, DMSO-d_6)	δ = 1.38 – 1.59 (m, 2H, CH_2-C<u>H</u>$_2$-CH_2-N$(CH_3)_2$), 2.23 (t, J = 7.8 Hz, 2H, C<u>H</u>$_2$-CH_2-CH_2-N$(CH_3)_2$), 2.62 (s, 6H, 2 x CH_3), 2.98 (t, J = 7.9 Hz, 2H, CH_2-CH_2-C<u>H</u>$_2$-N$(CH_3)_2$), 5.16 (d, J = 13.0 Hz, 1H, H3), 5.23 (d, J = 13.0 Hz, 1H, H3), 7.17 (dd, $^3J_{HH}$ = 8.8, $^3J_{HF}$ = 8.8 Hz, 2H, H3' & H5'), 7.60 (dd, $^3J_{HH}$ = 8.8, $^4J_{HF}$ = 5.5 Hz, 2H, H2' & H6'), 7.63 (d, J = 7.8 Hz, 1H, H7), 7.87 (s, 1H, H4), 7.90 (dd, J = 7.9, 1.5 Hz, 1H, H6) ppm. acid not detected
^{13}C-NMR (101 MHz, DMSO-d_6)	δ = 19.2 (t, CH_2-<u>C</u>H$_2$-CH_2-N$(CH_3)_2$), 37.2 (t, <u>C</u>H$_2$-CH_2-CH_2-N$(CH_3)_2$), 42.1 (q, 2C, 2 x CH_3), 56.6 (t, CH_2-CH_2-<u>C</u>H$_2$-N$(CH_3)_2$), 71.3 (t, C3), 90.0 (s, C1), 115.1 (d/d, $^2J_{CF}$ = 21.2 Hz, 2C, C3' & C5'), 122.0 (d, C4, C6 or C7), 122.6 (d, C4, C6 or C7), 126.9 (d/d, $^3J_{CF}$ = 8.2 Hz, 2C, C2' & C6'), 129.1 (d, C4, C6 or C7), 130.7 (s, C5), 139.1 (s, C3a or C7a), 140.5 (s/d, $^4J_{CF}$ = 3.0 Hz, C1'), 148.3 (s, C3a or C7a), 161.3 (s/d, $^1J_{CF}$ = 243.4 Hz, C4'), 166.9 (s, acid) ppm.
Optical rotation	$[\alpha]_D^{25}$ = +9.3 (c = 0.55, MeOH)

E III.5.4 (*S*)-1-(3-(Dimethylamino)propyl)-1-(4-fluorophenyl)-1,3-dihydroisobenzofuran-5-amine [<u>98</u>]

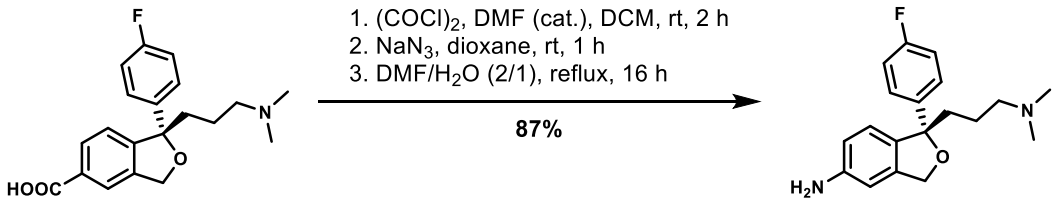

[<u>97</u>] 343.40 g/mol

[<u>98</u>] 314.40 g/mol

A 25 mL round bottom flask was charged with acid **[<u>97</u>]** (500 mg, 1.46 mmol, 1 equiv.). Dry DCM (10 mL) and dry DMF (1 drop) were added via syringe under an argon atmosphere. Oxalyl chloride (0.375 mL, 4.37 mmol, 3 equiv.) was added dropwise under vigorous stirring via syringe. The solution was stirred at room temperature for 2 hours. Volatiles were removed in

vacuo giving a colorless foam. The residue was dissolved in dioxane (10 mL). A solution of NaN_3 (189 mg, 2.91 mmol, 2 equiv.) in H_2O/dioxane (1/1; 1.5 mL) was added dropwise. The reaction was stirred at room temperature for 1 hour. Volatiles were removed in vacuo. The residue was dissolved in $CHCl_3$ and the remaining solids were removed by filtration. After evaporation of the solvent in vacuo the acid azide intermediate was obtained as a pale yellow oil in quant. yield. The crude acid azide intermediate was dissolved in DMF (8 mL) and H_2O (4 mL) and the solution was stirred at reflux temperature for 16 hours. Volatiles were removed in vacuo. The crude material was purified by flash column chromatography (silica gel/crude material = 100/1, MeOH + 1% NEt_3) to afford Escitalopram aniline **[98]**.

Yield	87% (398 mg, 1.27 mmol)
Appearance	colorless oil
TLC-Analysis	R_f = 0.30 (MeOH + 1% NEt_3)
Sum formula	$C_{19}H_{23}FN_2O$
HR-MS	$[M+H]^+$: calculated: 315.1867 Da, found: 315.1866 Da, difference: 0.1 mDa
^{1}H-NMR (400 MHz, $CDCl_3$)	δ = 1.27 – 1.59 (m, 2H, CH_2-C<u>H</u>$_2$-CH_2-N$(CH_3)_2$), 2.03 – 2.12 (m, 2H, C<u>H</u>$_2$-CH_2-CH_2-N$(CH_3)_2$), 2.13 (s, 6H, 2 x CH_3), 2.21 (t, *J* = 7.3 Hz, 2H, CH_2-CH_2-C<u>H</u>$_2$-N$(CH_3)_2$), 3.67 (s, 2H, NH_2), 5.01 (d, *J* = 12.2 Hz, 1H, H3), 5.05 (d, *J* = 12.3 Hz, 1H, H3), 6.48 (d, *J* = 1.2 Hz, 1H, H4), 6.58 (dd, *J* = 8.1, 2.1 Hz, 1H, H6), 6.95 (dd, $^3J_{HH}$ = 8.9, $^3J_{HF}$ = 8.9 Hz, 2H, H3' & H5'), 7.03 (d, *J* = 8.1 Hz, 1H, H7), 7.42 (dd, $^3J_{HH}$ = 8.9, $^4J_{HF}$ = 5.4 Hz, 2H, H2' & H6') ppm.
^{13}C-NMR (101 MHz, $CDCl_3$)	δ = 22.5 (t, CH_2-<u>C</u>H_2-CH_2-N$(CH_3)_2$), 39.7 (t, <u>C</u>H_2-CH_2-CH_2-N$(CH_3)_2$), 45.5 (q, 2C, 2 x CH_3), 59.9 (t, CH_2-CH_2-<u>C</u>H_2-N$(CH_3)_2$), 71.9 (t, C3), 90.8 (s, C1), 107.4 (d, C4), 114.7 (d, C6), 114.9 (d/d, $^2J_{CF}$ = 21.2 Hz, 2C, C3' & C5'), 122.7 (d, C7), 126.9 (d/d, $^3J_{CF}$ = 8.0 Hz, 2C, C2' & C6'), 134.5 (s, C7a), 140.7 (s, C3a), 141.9 (s/d, $^4J_{CF}$ = 3.1 Hz, C1'), 146.3 (s, C5), 161.8 (s/d, $^1J_{CF}$ = 244.6 Hz, C4') ppm.
Optical rotation	$[\alpha]_D^{25}$ = +5.6 (c = 1.25, DCM)

E III.6 Nitroso compounds

E III.6.1 Nitrosobenzene [99]

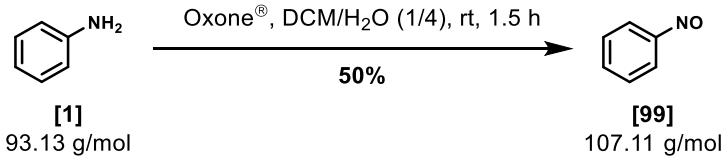

Nitrosobenzene **[99]** was synthesized in analogy to a literature procedure[141]. A solution of Oxone® (33 g, 107.4 mmol, 2 equiv.) in H_2O (200 mL) was added to a solution of aniline **[1]** (5 g, 53.7 mmol, 1 equiv.) in DCM (50 mL) and the reaction was vigorously stirred at room temperature under argon for 1.5 hours until TLC monitoring indicated full consumption of the starting material **[1]**. The reaction mixture was diluted with DCM (100 mL) and H_2O (100 mL) and phases were separated. The organic phase was washed with 1 N HCl (50 mL), satd. aqu. $NaHCO_3$ (50 mL), brine (50 mL) and dried over $MgSO_4$. The solvent was first evaporated at 970 mbar and 40 °C; the pressure was then reduced stepwise down to 840 mbar. The volatile product was purified by sublimation: the flask was heated with a heating jacket in vacuo (15 mbar).

Yield	50% (2.9 g, 27.1 mmol)
Appearance	green crystals (monomer), colorless crystals (dimer)
Melting point	66.5 – 67.0 °C (Lit.[205]: 65 – 67 °C)
TLC-Analysis	R_f = 0.80 (LP/EE = 5/1)
Sum formula	C_6H_5NO
^{1}H-NMR (400 MHz, $CDCl_3$)	δ = 7.63 (t, *J* = 7.5 Hz, 2H, H3 & H5), 7.71 (tt, *J* = 7.3, 1.3 Hz, 1H, H4), 7.89 – 7.93 (m, 2H, H2 & H6) ppm.
^{13}C-NMR (101 MHz, $CDCl_3$)	δ = 121.1 (d, 2C, C2 & C6), 129.4 (d, 2C, C3 & C5), 135.7 (d, C4), 166.0 (s, C1) ppm.

E III.6.2 1-Chloro-4-nitrosobenzene [100]

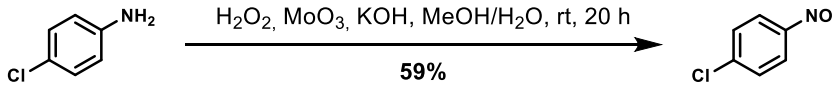

[40]
127.57 g/mol

[100]
141.55 g/mol

1-Chloro-4-nitrosobenzene **[100]** was prepared according to a literature procedure[143]. 30% H_2O_2 (4.2 mL, 40 mmol, 4 equiv.), H_2O (4.5 mL), MoO_3 (144 mg, 1 mmol, 10 mol%) and an aqu. solution of KOH (1 mL, 1 mmol, 10 mol%) were added to a solution of 4-chloroaniline **[40]** (1.28 g, 10 mmol, 1 equiv.) in MeOH (3 mL) under argon. The mixture was stirred at room temperature until monitoring via TLC showed full consumption of the starting material **[40]** (20 hours). H_2O (15 mL) was added and the precipitate was isolated by filtration and was washed with cold MeOH (5 mL). The crude product was purified by sublimation: the flask was heated with a heating jacket in vacuo (15 mbar).

Yield	59% (833 mg, 5.89 mmol)
Appearance	yellow crystals
Melting point	92.5 – 93.0 °C (lit.[206]: 92 °C)
TLC analysis	R_f = 0.90 (DCM/MeOH = 9/1)
Sum formula	C_6H_4ClNO
^{1}H-NMR (400 MHz, $CDCl_3$)	δ = 7.60 (d, *J* = 8.8 Hz, 2H, H2 & H6), 7.86 (d, *J* = 8.6 Hz, 2H, H3 & H5) ppm.
^{13}C-NMR (101 MHz, $CDCl_3$)	δ = 122.3 (d, 2C, C3 & C5), 129.8 (d, 2C, C2 & C6), 142.6 (s, C1), 163.9 (s, C4) ppm.

E III.6.3 1-Bromo-4-nitrosobenzene [101]

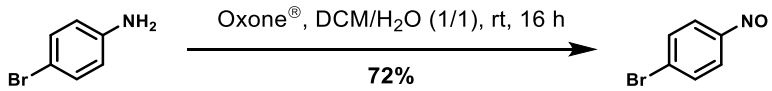

[43]
172.03 g/mol

[101]
186.01 g/mol

1-Bromo-4-nitrosobenzene **[101]** was synthesized according to a literature procedure[141]. A solution of Oxone® (729 mg, 2.37 mmol, 2 equiv.) in H_2O (5 mL) was added to a solution of 4-bromoaniline **[43]** (204 mg, 1.19 mmol, 1 equiv.) in DCM (5 mL) and the reaction was vigorously stirred at room temperature under argon for 16 hours until TLC monitoring indicated full consumption of the starting material **[43]**. Phases were separated and the aqu. phase was extracted with DCM (3 x 5 mL). The combined organic phases were washed with 1 N HCl (10 mL), satd. aqu. $NaHCO_3$ (10 mL), H_2O (10 mL) and brine (10 mL). After drying over

$MgSO_4$ the solution was concentrated under reduced pressure (max. 40 °C water bath temperature at atmospheric pressure followed by max. 750 mbar). The crude product was obtained as a beige solid. The crude product was purified by sublimation: the flask was heated with a heating jacket in vacuo (15 mbar).

Yield	72% (159 mg, 0.85 mmol)
Appearance	turquoise crystals
Melting point	91.0 – 93.0 °C (lit.[207]: 92 – 94 °C)
TLC-Analysis	R_f = 0.90 (DCM/MeOH = 9/1)
Sum formula	C_6H_4BrNO
^{1}H-NMR (400 MHz, $CDCl_3$)	δ = 7.74 – 7.82 (m, 4H, H2 & H3 & H5 & H6) ppm.
^{13}C-NMR (101 MHz, $CDCl_3$)	δ = 122.3 (d, 2C, C3 & C5), 131.8 (s, C1), 132.9 (d, 2C, C2 & C6), 164.0 (s, C4) ppm.

E III.6.4 4-Nitrosotoluene [102]

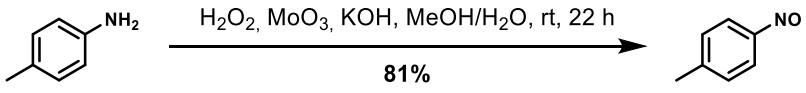

[37] 107.16 g/mol — **[102]** 121.14 g/mol

1-Nitrosotoluene **[102]** was prepared according to a literature procedure[143]. 30% H_2O_2 (4.2 mL, 40 mmol, 4 equiv.), H_2O (4.5 mL), MoO_3 (144 mg, 1 mmol, 10 mol%) and an aqu. solution of KOH (1 mL, 1 mmol, 10 mol%) were added to a solution of *p*-toluidine **[37]** (1.07 g, 10 mmol, 1 equiv.) in MeOH (3 mL) under argon. The mixture was stirred at room temperature until monitoring via TLC showed full consumption of the starting material **[37]** (22 hours). H_2O (15 mL) was added and the precipitate was isolated by filtration and was washed with cold MeOH (5 mL).

Yield	81% (0.98 g, 8.10 mmol)
Appearance	beige crystals
Melting point	44.0 – 44.5 °C (lit.[208]: 45 °C)
TLC-Analysis	R_f = 0.85 (LP/EtOAc = 5/1)
Sum formula	C_7H_7NO
^{1}H-NMR (400 MHz, $CDCl_3$)	δ = 2.45 (s, 3H, CH_3), 7.39 (dd, J = 8.6, 0.8 Hz, 2H, H2 & H6), 7.81 (d, J = 8.3 Hz, 2H, H3 & H5) ppm.

^{13}C-NMR (101 MHz, $CDCl_3$) δ = 22.1 (q, CH_3), 121.4 (d, 2C, C3 & C5), 129.9 (d, 2C, C2 & C6), 147.4 (s, C1), 165.7 (s, C4) ppm.

E III.6.5 1-Methoxy-4-nitrosobenzene [104]

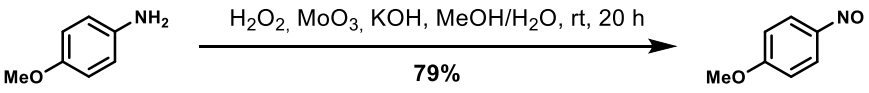

[103] 123.16 g/mol

[104] 137.14 g/mol

1-Methoxy-4-nitrosobenzene **[104]** was prepared according to a literature procedure[143]. 30% H_2O_2 (4.2 mL, 40 mmol, 4 equiv.), H_2O (4.5 mL), MoO_3 (144 mg, 1 mmol, 10 mol%) and an aqu. solution of KOH (1 mL, 1 mmol, 10 mol%) were added to a solution of 4-methoxyaniline **[103]** (1.23 g, 10 mmol, 1 equiv.) in MeOH (3 mL) under argon. The mixture was stirred at room temperature until monitoring via TLC showed full consumption of the starting material **[103]** (20 hours). *n*-Heptane (20 mL) was added and phases were separated. The aqu. phase was extracted with *n*-heptane (3 x 25 mL) and the combined organic phases were concentrated under reduced pressure. The flask was stored at -15 °C and 1-methoxy-4-nitrosobenzene **[104]** crystallized from *n*-heptane as green crystals. The supernatant *n*-heptane was removed and the product was dried in vacuo.

Yield 79% (1.08 g, 7.90 mmol)

Appearance green liquid

Melting point liquid at room temperature (lit.[143]: 20 – 21 °C (hexane))

TLC-Analysis R_f = 0.45 (LP/EtOAc = 10/1)

Sum formula $C_7H_7NO_2$

^{1}H-NMR (400 MHz, $CDCl_3$) δ = 3.95 (s, 3H, CH_3), 7.03 (d, *J* = 9.1 Hz, 2H, H2 & H6), 7.93 (d, *J* = 8.6 Hz, 2H, H3 & H5) ppm.

^{13}C-NMR (101 MHz, $CDCl_3$) δ = 56.1 (q, CH_3), 114.0 (d, 2C, C2 & C6), 126.0 (d, 2C, C3 & C5), 164.1 (s, C4), 165.7 (s, C1) ppm.

E III.6.6 4-Nitrosobenzoic acid [105]

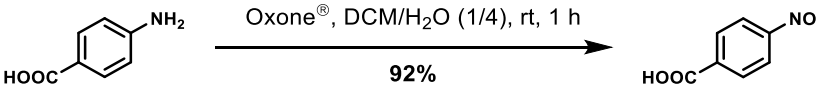

[12] 137.14 g/mol **[105]** 151.12 g/mol

4-Nitrosobenzoic acid **[105]** was synthesized according to a literature procedure[141]. A solution of Oxone® (8.98 g, 14.6 mmol, 2 equiv.) in H_2O (45 mL) was added to a suspension of 4-aminobenzoic acid **[12]** (1.0 g, 7.29 mmol, 1 equiv.) in DCM (11.2 mL) and the reaction was vigorously stirred at room temperature under argon for 1 hour until TLC monitoring indicated full consumption of the starting material **[12]**. The precipitate was isolated by filtration, washed with H_2O and dried in vacuo. The product **[105]** was obtained with a purity of 88% indicated by ^{1}H-NMR and was used as such.

Yield 92% (1.10 g, 6.74 mmol)

Appearance yellow crystals

Melting point decomposition at 215 °C (lit.[209]: decomposition at 250 °C)

TLC-Analysis R_f = 0.10 (DCM/MeOH = 9/1)

Sum formula $C_7H_5NO_3$

^{1}H-NMR (400 MHz, DMSO-d_6) δ = 8.04 (d, *J* = 8.5 Hz, 2H, H3 & H5), 8.26 (d, *J* = 8.5 Hz, 2H, H2 & H6), 13.11 (br s, 1H, acid) ppm.

E III.6.7 Methyl 4-nitrosobenzoate [107]

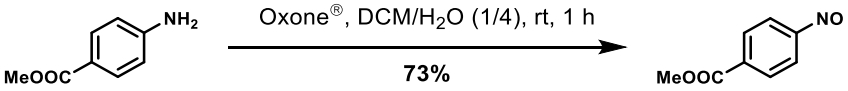

[106] 151.17 g/mol **[107]** 165.15 g/mol

Methyl 4-nitrosobenzoate **[107]** was synthesized according to a literature procedure[141]. A solution of Oxone® (8.14 g, 13.24 mmol, 2 equiv.) in H_2O (80 mL) was added to a solution of methyl 4-aminobenzoate **[106]** (1.0 g, 6.62 mmol, 1 equiv.) in DCM (20 mL) and the reaction was vigorously stirred at room temperature under argon for 1 hour until TLC monitoring indicated full consumption of the starting material **[106]**. Phases were separated and the aqu. phase was extracted with DCM (2 x 25 mL). The combined organic phases were washed with 1 N HCl (50 mL), satd. aqu. $NaHCO_3$ (50 mL) and H_2O (50 mL). After drying over $MgSO_4$ volatiles were removed in vacuo. The pure product **[107]** was obtained after recrystallization from DCM.

Yield 73% (803 mg, 4.86 mmol)

Appearance	yellow crystals
Melting point	128.5 – 129.0 °C (lit.[142]: 126 °C)
TLC-Analysis	R_f = 0.45 (DCM)
Sum formula	$C_8H_7NO_3$
^{1}H-NMR (400 MHz, $CDCl_3$)	δ = 3.98 (s, 3H, CH_3), 7.34 (d, *J* = 8.8 Hz, 2H, H3 & H5), 8.30 (d, *J* = 8.7 Hz, 2H, H2 & H6) ppm.
^{13}C-NMR (101 MHz, $CDCl_3$)	δ = 52.9 (q, CH_3), 120.5 (d, 2C, C3 & C5), 131.2 (d, 2C, C2 & C6), 135.4 (s, C1), 164.5 (s, C4), 165.9 (s, ester) ppm

E III.6.8 3-Nitrosobenzonitrile [109]

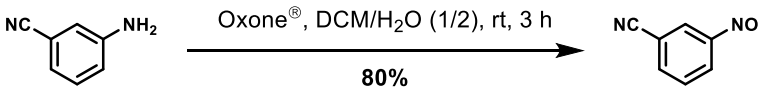

[108] 118.14 g/mol — **[109]** 132.12 g/mol

3-Nitrosobenzonitrile **[109]** was synthesized according to a literature procedure[141]. A solution of Oxone® (10.4 g, 16.92 mmol, 2 equiv.) in H_2O (100 mL) was added to a solution of 3-aminobenzonitrile **[108]** (1 g, 8.46 mmol, 1 equiv.) in DCM (50 mL) and the reaction was vigorously stirred at room temperature under argon for 3 hours until TLC monitoring indicated full consumption of the starting material **[108]**. Phases were separated and the aqu. phase was extracted with DCM (2 x 50 mL). The combined organic phases were washed with 1 N HCl (50 mL), satd. aqu. $NaHCO_3$ (50 mL), H_2O (50 mL) and brine (50 mL). After drying over $MgSO_4$ volatiles were removed in vacuo. The crude product was purified by sublimation: the flask was heated with a heating jacket in vacuo (1 mbar).

Yield	80% (895 mg, 6.77 mmol)
Appearance	green/turquoise crystals
Melting point	decomposition at 105 °C (Lit.[210]: decomposition at 107 °C)
TLC-Analysis	R_f = 0.60 (DCM)
Sum formula	$C_7H_4N_2O$
^{1}H-NMR (400 MHz, $CDCl_3$)	δ = 7.80 (td, *J* = 7.9, 0.6 Hz, 1H, H5), 7.98 (dt, *J* = 7.7, 1.4 Hz, 1H, H4 or H6), 8.13 (ddd, *J* = 8.0, 1.9, 1.2 Hz, 1H, H4 or H6), 8.18 (dt, *J* = 1.7, 0.9 Hz, 1H, H2) ppm.

E III.7 Azo-Escitalopram derivatives

E III.7.1 (*S*)-*N*-((1-(3-(Dimethylamino)propyl)-1-(4-fluorophenyl)-1,3-dihydroisobenzofuran-5-yl)methyl)-4-(phenyldiazenyl)benzamide [<u>111</u>]

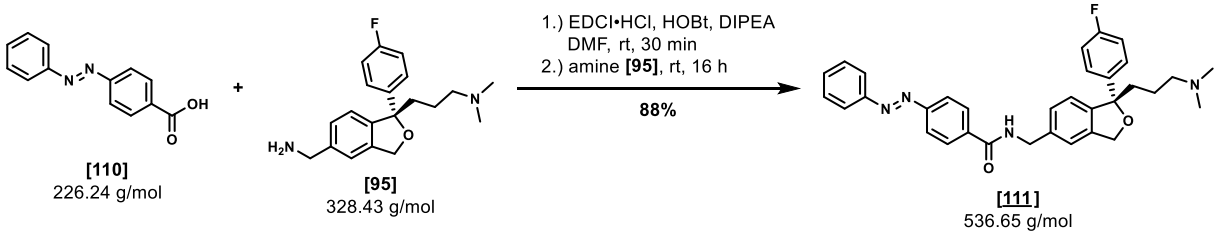

4-(Phenylazo)benzoic acid **[110]** (19.8 mg, 0.09 mmol, 1 equiv.), EDCI•HCl (18.4 mg, 0.10 mmol, 1.1 equiv.) and HOBt (14.7 mg, 0.10 mmol, 1.1 equiv.) and DIPEA (23.7 mg, 0.18 mmol, 2.1 equiv.) were dissolved in dry DMF (1 mL) and were stirred under argon at room temperature for 30 minutes. Then a solution of amine **[95]** (28.7 mg, 0.09 mmol, 1 equiv.) in DMF (1 mL) was added via syringe and the reaction was stirred at room temperature for 16 hours. Volatiles were removed in vacuo and amide **[<u>111</u>]** was obtained after purification by preparative HPLC.

Yield	88% (41.3 mg, 0.08 mmol)
Appearance	orange oil
TLC-Analysis	R_f = 0.25 (MeOH + 1% NEt_3)
Sum formula	$C_{33}H_{33}FN_4O_2$
HR-MS	$[M+H]^+$: calculated: 537.2660 Da, found: 537.2684 Da, difference: 2.4 mDa
^{1}H-NMR (400 MHz, $CDCl_3$)	δ = 1.27 – 1.54 (m, 2H, CH_2-C<u>H</u>$_2$-CH_2-N(CH_3)$_2$), 2.14 (s, 6H, 2 x CH_3), 2.07 – 2.26 (m, 4H, C<u>H</u>$_2$-CH_2-C<u>H</u>$_2$-N(CH_3)$_2$), 4.66 (d, *J* = 5.6 Hz, 2H, NH-C<u>H</u>$_2$), 5.12 (d, *J* = 12.3 Hz, 1H, H3), 5.16 (d, *J* = 12.6 Hz, 1H, H3), 6.53 (t, *J* = 5.6 Hz, 1H, NH), 6.98 (dd, $^3J_{HH}$ = 8.7, $^3J_{HF}$ = 8.7 Hz, 2H, H3' & H5'), 7.22 (s, 1H, H4), 7.25 – 7.31 (m, 2H, H6 & H7), 7.45 (dd, $^3J_{HH}$ = 8.9, $^4J_{HF}$ = 5.3 Hz, 2H, H2' & H6'), 7.49 – 7.56 (m, 3H, H3''' & H4''' & H5'''), 7.91 – 7.98 (m, 6H, H2'' & H3'' & H4'' & H5'' & H2''' & H6''') ppm.

^{13}C-NMR (101 MHz, $CDCl_3$) δ = 22.5 (t, CH_2-$\underline{C}H_2$-CH_2-$N(CH_3)_2$), 39.5 (t, $\underline{C}H_2$-CH_2-CH_2-$N(CH_3)_2$), 44.2 (t, NH-CH_2), 45.5 (q, 2C, 2 x CH_3), 59.8 (t, CH_2-CH_2-$\underline{C}H_2$-$N(CH_3)_2$), 71.9 (t, C3), 91.0 (s, C1), 115.1 (d/d, $^2J_{CF}$ = 21.2 Hz, 2C, C3' & C5'), 121.0 (d, C4), 122.3 (d, C6 or C7), 123.1 & 123.2 (2xd, 4C, C2''' & C6''' & C2'' & C6'' or C3'' & C5''), 126.9 (d/d, $^3J_{CF}$ = 8.0 Hz, 2C, C2' & C6'), 127.6 (d, C6 or C7), 128.1 (d, 2C, C2'' & C6'' or C3'' & C5''), 129.3 (d, 2C, C3''' & C5'''), 131.8 (d, C4'''), 136.0 & 137.9 (2xs, 2C, C5 & C1''), 140.1 (s, C3a or C7a), 141.1 (s/d, $^4J_{CF}$ = 3.1 Hz, C1'), 144.0 (s, C3a or C7a), 152.7 & 154.5 (2xs, 2C, C4'' & C1'''), 162.0 (s/d, $^1J_{CF}$ = 245.2 Hz, C4'), 166.7 (s, amide) ppm.

Optical rotation $[\alpha]_D^{25}$ = +2.2 (c = 0.59, MeOH)

The assignments of protons and carbon atoms in the NMR codes of compounds **[<u>111</u>]**, **[<u>112</u>]**, **[<u>113</u>]** and **[<u>115</u>]** were carried out as follows:

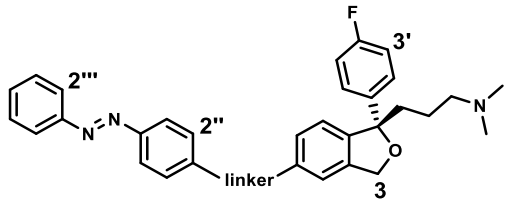

E III.7.2 (*S*)-*N*-((1-(3-(Dimethylamino)propyl)-1-(4-fluorophenyl)-1,3-dihydroisobenzofuran-5-yl)methyl)-4-((1,3,5-trimethyl-1*H*-pyrazol-4-yl)diazenyl)benzamide [<u>112</u>]

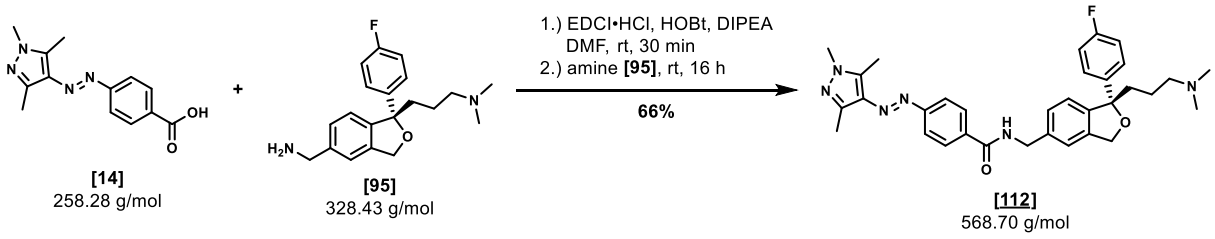

Acid **[14]** (22.7 mg, 0.09 mmol, 1 equiv.), EDCI•HCl (18.3 mg, 0.10 mmol, 1.1 equiv.) and HOBt (14.8 mg, 0.10 mmol, 1.1 equiv.) and DIPEA (23.9 mg, 0.18 mmol, 2.1 equiv.) were dissolved in dry DMF (1 mL) and were stirred under argon at room temperature for 30 minutes. Then a solution of amine **[95]** (28.9 mg, 0.09 mmol, 1 equiv.) in DMF (1 mL) was added via syringe and the reaction was stirred at room temperature for 16 hours. Volatiles were removed in vacuo and amide **[<u>112</u>]** was obtained after purification by preparative HPLC.

Yield 66% (33 mg, 0.06 mmol)

Appearance	orange oil
TLC-Analysis	R_f = 0.3 (MeOH + 1% NEt_3)
Sum formula	$C_{33}H_{37}FN_6O_2$
HR-MS	$[M+H]^+$: calculated: 569.3035 Da, found: 569.3080 Da, difference: 4.5 mDa
^{1}H-NMR (400 MHz, $CDCl_3$)	δ = 1.26 – 1.53 (m, 2H, CH_2-C<u>H</u>$_2$-CH_2-N(CH_3)$_2$), 2.06 – 2.25 (m, 4H, C<u>H</u>$_2$-CH_2-C<u>H</u>$_2$-N(CH_3)$_2$), 2.12 (s, 6H, 2 x CH_3), 2.48 (s, 3H, pyrazole-CH_3), 2.57 (s, 3H, pyrazole-CH_3), 3.77 (s, 3H, N-CH_3), 4.63 (d, *J* = 5.7 Hz, 2H, NH-C<u>H</u>$_2$), 5.10 (d, *J* = 12.5 Hz, 1H, H3), 5.14 (d, *J* = 12.6 Hz, 1H, H3), 6.60 (t, *J* = 5.7 Hz, 1H, NH), 6.96 (dd, $^3J_{HH}$ = 8.7, $^3J_{HF}$ = 8.7 Hz, 2H, H3' & H5'), 7.20 (s, 1H, H4), 7.22 – 7.29 (m, 2H, H6 & H7), 7.44 (dd, $^3J_{HH}$ = 8.9, $^4J_{HF}$ = 5.3 Hz, 2H, H2' & H6'), 7.78 (d, *J* = 8.6 Hz, 2H, H2'' & H6'' or H3'' & H5''), 7.87 (d, *J* = 8.7 Hz, 2H, H2'' & H6'' or H3'' & H5'') ppm.
^{13}C-NMR (101 MHz, $CDCl_3$)	*δ* = 10.1 & 14.0 (2xq, 2C, 2 x pyrazole-CH_3), 22.5 (t, CH_2-<u>C</u>H$_2$-CH_2-N(CH_3)$_2$), 36.2 (q, N-CH_3), 39.5 (t, <u>C</u>H$_2$-CH_2-CH_2-N(CH_3)$_2$), 44.1 (t, N-CH_2), 45.5 (q, 2C, 2 x CH_3), 59.8 (t, CH_2-CH_2-<u>C</u>H$_2$-N(CH_3)$_2$), 71.9 (t, C3), 90.9 (s, C1), 115.1 (d/d, $^2J_{CF}$ = 21.2 Hz, 2C, C3' & C5'), 120.9 (d, C4), 122.0 (d, 2C, C2'' & C6'' or C3'' & C5''), 122.2 (d, C6 or C7), 126.9 (d/d, $^3J_{CF}$ = 8.0n Hz, 2C, C2' & C6'), 127.5 (d, C6 or C7), 128.0 (d, 2C, C2'' & C6'' or C3'' & C5''), 134.3 (s, C1'' or C4''), 135.5 (s, C3''' or C4'''), 138.1 (s, C5), 139.7 (s, C5'''), 140.0 (s, C3a or C7a), 141.1 (s/d, $^4J_{CF}$ = 3.1 Hz, C1'), 142.8 (s, C3''' or C4'''), 143.9 (s, C3a or C7a), 155.7 (s, C1'' or C4''), 161.9 (s/d, $^1J_{CF}$ = 245.2 Hz, C4'), 167.0 (s, amide) ppm.
Optical rotation	$[\alpha]_D^{25}$ = +6.2 (c = 1.25, DCM)

E III.7.3 (*S*)-*N*-(1-(3-(Dimethylamino)propyl)-1-(4-fluorophenyl)-1,3-dihydroisobenzofuran-5-yl)-4-(phenyldiazenyl)benzamide [113]

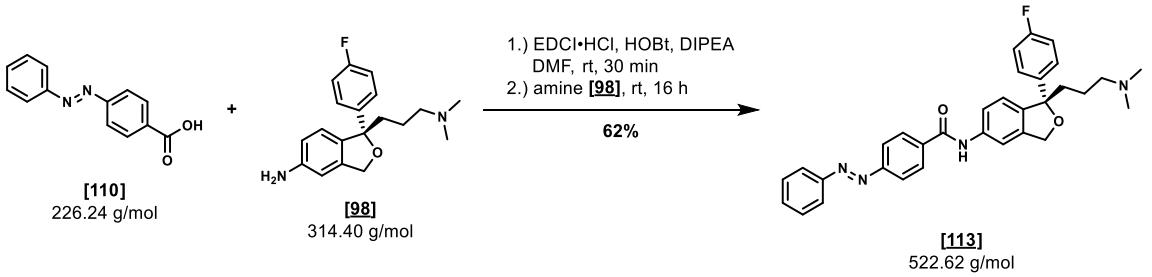

Acid **[110]** (42 mg, 0.19 mmol, 1 equiv.), EDCI•HCl (39 mg, 0.20, 1.1 equiv.) and HOBt (31 mg, 0.20, 1.1 equiv.) and DIPEA (51 mg, 0.39 mmol, 2.1 equiv.) were dissolved in dry DMF (2 mL) and were stirred under argon at room temperature for 30 minutes. Then a solution of aniline **[98]** (59 mg, 0.19 mmol, 1 equiv.) in DMF (2 mL) was added via syringe and the reaction was stirred at room temperature for 16 hours. Volatiles were removed in vacuo and amide **[113]** was obtained after purification by flash column chromatography (silica gel/crude material = 100/1, DCM/MeOH = 19/1 → 8/2).

Yield	62% (62 mg, 0.12 mmol)
Appearance	orange oil
TLC-Analysis	R_f = 0.25 (DCM/MeOH = 9/1)
Sum formula	$C_{32}H_{31}FN_4O_2$
HR-MS	$[M+H]^+$: calculated: 523.2504 Da, found: 523.2523 Da, difference: 1.9 mDa
^{1}H-NMR (400 MHz, $CDCl_3$)	δ = 1.31 – 1.57 (m, 2H, CH_2-C<u>H</u>$_2$-CH_2-N(CH_3)$_2$), 2.08 – 2.23 (m, 2H, C<u>H</u>$_2$-CH_2-CH_2-N(CH_3)$_2$), 2.16 (s, 6H, 2 x CH_3), 2.28 (t, *J* = 7.3 Hz, 2H, CH_2-CH_2-C<u>H</u>$_2$-N(CH_3)$_2$), 5.10 (d, *J* = 12.6 Hz, 1H, H3), 5.15 (d, *J* = 12.6 Hz, 1H, H3), 6.98 (dd, $^3J_{HH}$ = 8.8, $^3J_{HF}$ = 8.8 Hz, 2H, H3' & H5'), 7.25 (d, *J* = 8.8 Hz, 1H, H6 or H7), 7.41 – 7.48 (m, 3H, H6 or H7 & H2’ & H6’), 7.49 – 7.57 (m, 3H, H3’’’ & H4’’’ & H5’’’), 7.70 (d, *J* = 1.0 Hz, 1H, H4), 7.92 – 8.03 (m, 6H, H2’’ & H3’’ & H5’’ & H6’’ & H2’’’ & H6’’’), 8.20 (s, 1H, amide-H) ppm.

^{13}C-NMR (101 MHz, $CDCl_3$) δ = 22.2 (t, CH_2-$\underline{C}H_2$-CH_2-$N(CH_3)_2$), 39.4 (t, $\underline{C}H_2$-CH_2-CH_2-$N(CH_3)_2$), 45.3 (q, 2C, 2 x CH_3), 59.7 (t, CH_2-CH_2-$\underline{C}H_2$-$N(CH_3)_2$), 71.9 (t, C3), 90.9 (s, C1), 113.5 (d, C4), 115.1 (d/d, $^2J_{CF}$ = 21.2 Hz, 2C, C3' & C5'), 120.0 & 122.4 (2xd, 2C, C6 & C7), 123.2 & 123.3 (d, 4C, C3'' & C5'' & C2''' & C6'''), 126.9 (d/d, $^3J_{CF}$ = 8.0 Hz, 2C, C2' & C6'), 128.3 (d, 2C, C2'' & C6''), 129.3 (d, 2C, C3''' & C5'''), 131.9 (d, C4'''), 136.5 (s, C_{quart}), 137.7 (s, C_{quart}), 140.5 (s, C_{quart}), 140.6 (s, C_{quart}), 141.1 (s/d, $^4J_{CF}$ = 3.1 Hz, C1'), 152.6 (s, C_{quart}), 154.6 (s, C_{quart}), 161.9 (s/d, $^1J_{CF}$ = 245.2 Hz, C4'), 165.3 (s, amide) ppm.

Optical rotation $[\alpha]_D^{20}$ = +4.4 (c = 0.50, MeOH)

E III.7.4 (*S*)-*N*-((1-(3-(Dimethylamino)propyl)-1-(4-fluorophenyl)-1,3-dihydroisobenzofuran-5-yl)methyl)-4-(phenyldiazenyl)aniline [115]

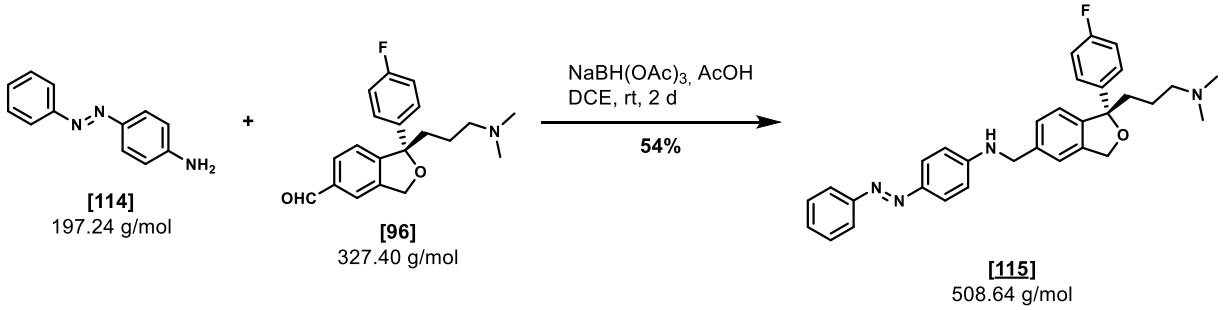

Aniline **[115]** was synthesized according to a literature procedure[135] for similar amines. Aldehyde **[96]** (26.2 mg, 0.080 mmol, 1 equiv.), 4-(phenyldiazenyl)aniline **[114]** (15.8 mg, 0.080 mmol, 1 equiv.), $NaBH(OAc)_3$ (25.4 mg, 0.120 mmol, 1.5 equiv.) and acetic acid (16.0 mg, 0.266 mmol, 3.33 equiv.) were placed in an 8 mL vial. DCE (1 mL) was added. The vial was closed with a screw cap and a septum and was evacuated and flushed with argon three times. The reaction was stirred at room temperature for 48 hours. 1 N NaOH (1 mL) and EtOAc (1.5 mL) were added and phases were separated. The aqu. phase was extracted with EtOAc (3 x 1.5 mL). The combined organic phases were washed with brine (3 mL) and dried over $MgSO_4$. After evaporation of the solvent the crude product was obtained. Purification by preparative HPLC provided the pure compound **[115]**.

Yield 54% (22 mg, 0.043 mmol)

Appearance orange oil

TLC-Analysis R_f = 0.30 (MeOH + 1% NEt_3)

Sum formula $C_{32}H_{33}FN_4O$

HR-MS $[M+H]^+$: calculated: 509.2711 Da, found: 509.2751 Da, difference: 4.0 mDa

^{1}H-NMR (400 MHz, $CDCl_3$) δ = 1.34 – 1.59 (m, 2H, CH_2-C<u>H</u>$_2$-CH_2-N$(CH_3)_2$), 2.09 – 2.21 (m, 2H, C<u>H</u>$_2$-CH_2-CH_2-N$(CH_3)_2$), 2.22 (s, 6H, 2 x CH_3), 2.34 (t, *J* = 7.1 Hz, 2H, CH_2-CH_2-C<u>H</u>$_2$-N$(CH_3)_2$), 4.42 (d, *J* = 5.2 Hz, 2H, NH-C<u>H</u>$_2$), 4.53 (t, *J* = 5.3 Hz, 1H, NH), 5.11 (d, *J* = 12.8 Hz, 1H, H3), 5.16 (d, *J* = 12.7 Hz, 1H, H3), 6.68 (d, *J* = 8.9 Hz, 2H, H2'' & H6''), 6.99 (dd, $^3J_{HH}$ = 8.7, $^3J_{HF}$ = 8.7 Hz, 2H, H3' & H5'), 7.21 (s, 1H, H4), 7.25 – 7.29 (m, 2H, H6 & H7), 7.38 (t, *J* = 7.3 Hz, 1H, H4'''), 7.44 – 7.50 (m, 4H, H2' & H6' & H3''' & H5'''), 7.80 – 7.85 (m, 4H, H3'' & H5'' & H2''' & H6''') ppm.

^{13}C-NMR (101 MHz, $CDCl_3$) δ = 22.0 (t, CH_2-<u>C</u>H_2-CH_2-N$(CH_3)_2$), 39.4 (t, <u>C</u>H_2-CH_2-CH_2-N$(CH_3)_2$), 45.1 (q, 2C, 2 x CH_3), 47.8 (t, NH-CH_2), 59.5 (t, CH_2-CH_2-<u>C</u>H_2-N$(CH_3)_2$), 71.9 (t, C3), 90.9 (s, C1), 112.5 (d, 2C, C2'' & C6''), 115.2 (d/d, $^2J_{CF}$ = 21.2 Hz, 2C, C3' & C5'), 120.4 (d, C4), 122.3 (d, C6 or C7), 122.4 & 125.4 (2xd, 4C, C3'' & C5'' & C3''' & C5'''), 126.9 (d/d, $^3J_{CF}$ = 8.0 Hz, 2C, C2' & C6'), 127.1 (d, C6 or C7), 129.1 (d, 2C, C3''' & C5'''), 129.8 (d, C4'''), 138.5 (s, C5), 139.9 (s, C3a or C7a), 141.0 (s/d, $^4J_{CF}$ = 3.0 Hz, C1'), 143.7 (s, C3a or C7a), 145.2 (s, C4''), 150.7 (s, C1''), 153.2 (s, C1'''), 162.0 (s/d, $^1J_{CF}$ = 245.3 Hz, C4') ppm.

Optical rotation $[\alpha]_D^{20}$ = +9.0 (c = 0.50, MeOH)

E III.7.5 (*S*)-3-(1-(4-Fluorophenyl)-5-((1,3,5-trimethyl-1*H*-pyrazol-4-yl)diazenyl)-1,3-dihydroisobenzofuran-1-yl)-*N*,*N*-dimethylpropan-1-amine [116]

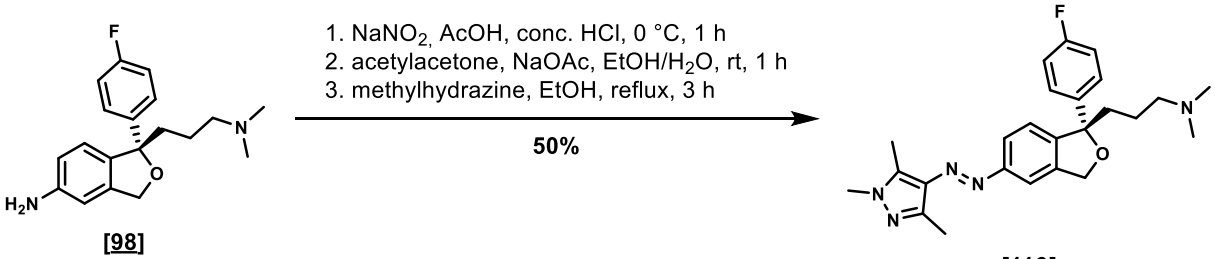

[98]
314.40 g/mol

[116]
435.55 g/mol

Photoswitch **[116]** was synthesized in analogy to a literature procedure[68]. Aniline **[98]** (37.0 mg, 0.118 mmol, 1 equiv.) was dissolved in AcOH (0.67 mL) and conc. HCl (0.11 mL) and the solution was cooled to 0 °C. $NaNO_2$ (9.7 mg, 0.141 mmol, 1.2 equiv.) in H_2O (0.17 mL) was added dropwise at 0 °C. The resulting solution was stirred at 0 °C for 1 hour. The solution was added dropwise via syringe to a suspension of NaOAc (28.9 mg, 0.353 mmol, 3 equiv.) and acetylacetone (15.3 mg, 0.153 mmol, 1.3 equiv.) in EtOH (0.47 mL) and H_2O (0.27 mL). The reaction mixture was stirred at room temperature for 1 hour. Volatiles were removed in vacuo. The residue was dissolved in EtOAc (5 mL) and H_2O (5 mL) and phases were separated. The aqu. phase was extracted with EtOAc (3 x 3 mL) and the combined organic phases were dried over $MgSO_4$. After evaporation of the solvent in vacuo the crude intermediate was obtained, which was directly used for the next reaction step without purification. Crude intermediate (max. 0.118 mmol, 1 equiv.), was dissolved in EtOH (2 mL) in an 8 mL vial. Methylhydrazine (5.4 mg, 0.118 mmol, 1 equiv.) was added. The vial was closed tightly with a screw cap and the solution was stirred at reflux temperature for 3 hours in a thermo block (thermo sensor was set to 85 °C). Volatiles were removed in vacuo. Purification by preparative HPLC afforded the desired product **[116]**.

Yield	50% (25.7 mg, 0.059 mmol)
Appearance	orange oil
TLC analysis	R_f = 0.25 (MeOH + 1% NEt_3)
Sum formula	$C_{25}H_{30}FN_5O$
HR-MS	$[M+H]^+$: calculated: 436.2507 Da, found: 436.2520 Da, difference: 1.3 mDa
^{1}H-NMR (400 MHz, $CDCl_3$)	δ = 1.31 – 1.59 (m, 2H, CH_2-C<u>H</u>$_2$-CH_2-N(CH_3)$_2$), 2.16 (s, 6H, 2 x CH_3), 2.12 – 2.24 (m, 2H, C<u>H</u>$_2$-CH_2-CH_2-N(CH_3)$_2$), 2.27 (t, *J* = 7.3 Hz, 2H, CH_2-CH_2-C<u>H</u>$_2$-N(CH_3)$_2$), 2.47 (s, 3H, pyrazole-CH_3), 2.55 (s,

3H, pyrazole-CH_3), 3.77 (s, 3H, N-CH_3), 5.16 (d, *J* = 12.5 Hz, 1H, H3), 5.21 (d, *J* = 12.4 Hz, 1H, H3), 6.98 (dd, $^3J_{HH}$ = 8.7, $^3J_{HF}$ = 8.7 Hz, 2H, H3' & H5'), 7.34 (d, *J* = 8.1 Hz, 1H, H7), 7.47 (dd, $^3J_{HH}$ = 8.9, $^4J_{HF}$ = 5.4 Hz, 2H, H2' & H6'), 7.59 (s, 1H, H4), 7.71 (dd, *J* = 8.0, 1.4 Hz, 1H, H6) ppm.

^{13}C-NMR (101 MHz, $CDCl_3$) δ = 10.1 & 14.0 (2xq, 2C, 2 x pyrazole-CH_3), 22.2 (t, CH_2-$\underline{C}H_2$-CH_2-$N(CH_3)_2$), 36.1 (q, N-CH_3), 39.3 (t, $\underline{C}H_2$-CH_2-CH_2-$N(CH_3)_2$), 45.3 (q, 2C, 2 x CH_3), 59.6 (t, CH_2-CH_2-$\underline{C}H_2$-$N(CH_3)_2$), 71.8 (t, C3), 90.9 (s, C1), 113.6 (d, C4), 115.1 (d/d, $^2J_{CF}$ = 21.2 Hz, 2C, C3' & C5'), 122.3 (d, C7), 122.8 (d, C6), 127.0 (d/d, $^3J_{CF}$ = 8.0 Hz, 2C, C2' & C6'), 135.2 (s, C4''), 138.9 (s, C5''), 140.3 (s, C3''), 141.0 (s/d, $^4J_{CF}$ = 3.0 Hz, C1'), 142.6 & 145.2 & 153.9 (3xs, 3C, C3a & C5 & C7a), 162.0 (s/d, $^1J_{CF}$ = 245.3 Hz, C4') ppm.

Optical rotation $[\alpha]_D^{25}$ = +18.9 (c = 1.00, MeOH)

E III.7.6 (*S*)-3-(1-(4-Fluorophenyl)-5-(phenyldiazenyl)-1,3-dihydroisobenzofuran-1-yl)-*N*,*N*-dimethylpropan-1-amine [117]

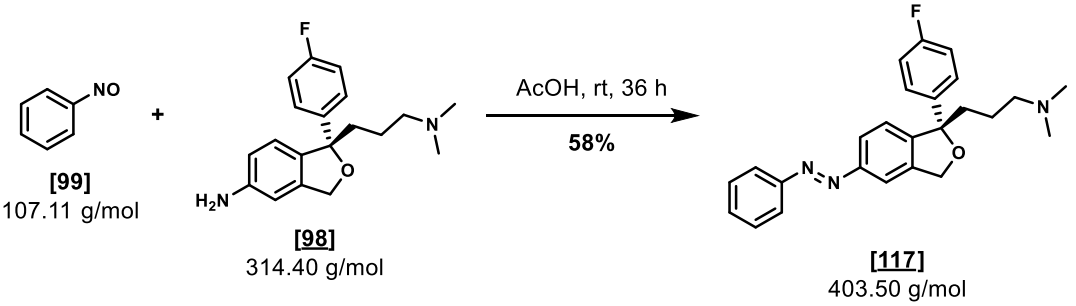

[99]
107.11 g/mol

[98]
314.40 g/mol

[117]
403.50 g/mol

Nitrosobenzene **[99]** (27 mg, 0.254 mmol, 2 equiv.) was placed in a 10 mL round bottom flask. Aniline **[98]** (40 mg, 0.127 mmol, 1 equiv.) and acetic acid (1 mL) was added. The flask was flushed with argon and was closed with a septum. The solution was stirred at room temperature for 36 hours. The solution was basified with 2 N NaOH and the aqu. phase was extracted with $CHCl_3$ (3 x 3 mL). The combined organic phases were dried over $MgSO_4$. Volatiles were evaporated in vacuo. After purification by flash column chromatography (silica gel/crude material = 100/1, DCM/MeOH = 19/1 → 8/2) the pure product **[117]** was obtained.

Yield 58% (30 mg, 0.074 mmol)

Appearance orange oil

TLC analysis R_f = 0.3 (DCM/MeOH = 9/1)

Sum formula $C_{25}H_{26}FN_3O$

HR-MS	$[M+H]^+$: calculated: 404.2133 Da, found: 404.2150 Da, difference: 1.7 mDa
^{1}H-NMR (400 MHz, $CDCl_3$)	δ = 1.35 – 1.61 (m, 2H, CH_2-C<u>H</u>$_2$-CH_2-N(CH_3)$_2$), 2.15 – 2.28 (m, 2H, C<u>H</u>$_2$-CH_2-CH_2-N(CH_3)$_2$), 2.20 (s, 6H, 2 x CH_3), 2.32 (t, *J* = 7.3 Hz, 2H, CH_2-CH_2-C<u>H</u>$_2$-N(CH_3)$_2$), 5.19 (d, *J* = 12.5 Hz, 1H, H3), 5.25 (d, *J* = 12.5 Hz, 1H, H3), 7.01 (dd, $^3J_{HH}$ = 8.7, $^3J_{HF}$ = 8.7 Hz, 2H, H3' & H5'), 7.43 (d, *J* = 8.0 Hz, 1H, H7), 7.46 – 7.54 (m, 5H, H2' & H6' & H3'' & H4'' & H5''), 7.74 (d, *J* = 0.9 Hz, 1H, H4), 7.87 – 7.91 (m, 3H, H6 & H2'' & H6'') ppm.
^{13}C-NMR (101 MHz, $CDCl_3$)	δ 22.2 (t, CH_2-<u>C</u>H_2-CH_2-N(CH_3)$_2$), 39.3 (t, <u>C</u>H_2-CH_2-CH_2-N(CH_3)$_2$), 45.3 (q, 2C, 2 x CH_3), 59.6 (t, CH_2-CH_2-<u>C</u>H_2-N(CH_3)$_2$), 71.8 (t, C3), 90.9 (s, C1), 114.6 (d, C4), 115.3 (d/d, $^2J_{CF}$ = 21.3 Hz, 2C, C3' & C5'), 122.5 (d, C7), 123.0 (d, 2C, C2'' & C6''), 124.2 (d, C6), 127.0 (d/d, $^3J_{CF}$ = 8.0 Hz, 2C, C2' & C6'), 129.2 (d, 2C, C3'' & C5''), 131.2 (d, C4''), 140.5 (s, C7a), 140.6 (s/d, $^4J_{CF}$ = 3.0 Hz, C1'), 147.0 & 152.7 & 152.9 (3xs, 3C, C3a, C5, C1''), 162.1 (s/d, $^1J_{CF}$ = 245.6 Hz, C4') ppm.
Optical rotation	$[\alpha]_D^{20}$ = +16.4 (c = 0.735, MeOH)

The assignments of protons and carbon atoms in the NMR codes of compounds **[<u>117</u>]**, **[<u>118</u>]**, **[<u>119</u>]**, **[<u>120</u>]**, **[<u>121</u>]**, **[<u>122</u>]** and **[<u>123</u>]** were carried out as follows:

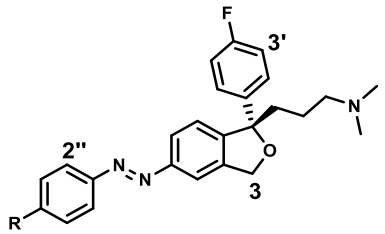

E III.7.7 (*S*)-3-(5-((4-Chlorophenyl)diazenyl)-1-(4-fluorophenyl)-1,3-dihydroisobenzofuran-1-yl)-*N*,*N*-dimethylpropan-1-amine [118]

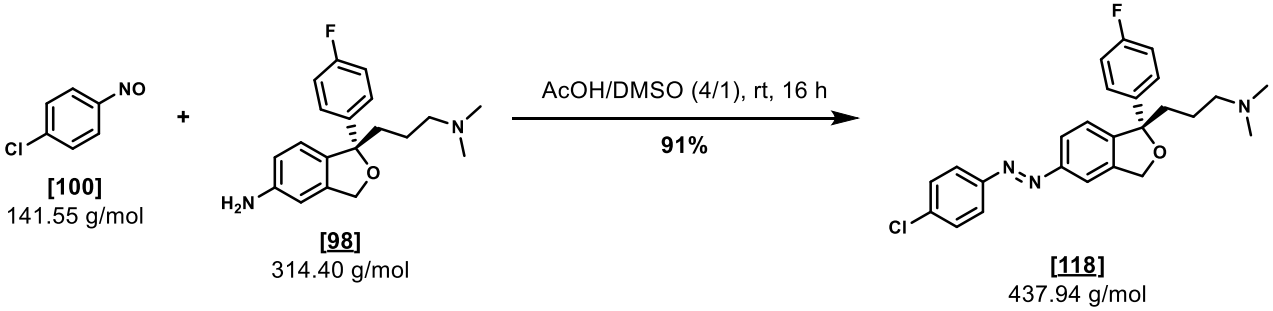

1-Chloro-4-nitrosobenzene **[100]** (31 mg, 0.221 mmol, 2 equiv.) was placed in a 10 mL round bottom flask. Aniline **[98]** (34.7 mg, 0.110 mmol, 1 equiv.) and acetic acid (2 mL) and DMSO (0.5 mL) were added. The flask was flushed with argon and was closed with a septum. The solution was stirred at room temperature for 16 hours. Volatiles were removed in vacuo. The crude material was purified by flash column chromatography (silica gel/crude material = 100/1, $CHCl_3$/MeOH/NH_4OH = 80/20/1) to afford the pure product **[118]**.

Yield	91% (43.7 mg, 0.100 mmol)
Appearance	orange oil
TLC analysis	R_f = 0.2 (DCM/MeOH = 9/1)
Sum formula	$C_{25}H_{25}ClFN_3O$
HR-MS	$[M+H]^+$: calculated: 438.1743 Da, found: 438.1765 Da, difference: 2.2 mDa
^{1}H-NMR (400 MHz, $CDCl_3$)	δ = 1.31 – 1.58 (m, 2H, CH_2-C<u>H</u>$_2$-CH_2-N$(CH_3)_2$), 2.15 (s, 6H, 2 x CH_3), 2.17 – 2.29 (m, 4H, C<u>H</u>$_2$-CH_2-C<u>H</u>$_2$-N$(CH_3)_2$), 5.19 (d, *J* = 12.6 Hz, 1H, H3), 5.24 (d, *J* = 12.6 Hz, 1H, H3), 7.01 (dd, $^3J_{HH}$ = 8.8, $^3J_{HF}$ = 8.8 Hz, 2H, H3' & H5'), 7.42 (d, *J* = 8.0 Hz, 1H, H7), 7.45 – 7.51 (m, 4H, H2' & H6' & H3'' & H5''), 7.73 (d, *J* = 0.9 Hz, 1H, H4), 7.82 – 7.89 (m, 3H, H6 & H2'' & H6'') ppm.
^{13}C-NMR (101 MHz, $CDCl_3$)	δ = 22.4 (t, CH_2-<u>C</u>H$_2$-CH_2-N$(CH_3)_2$), 39.4 (t, <u>C</u>H$_2$-CH_2-CH_2-N$(CH_3)_2$), 45.5 (q, 2C, 2 x CH_3), 59.7 (t, CH_2-CH_2-<u>C</u>H$_2$-N$(CH_3)_2$), 71.7 (t, C3), 90.9 (s, C1), 114.7 (d, C4), 115.2 (d/d, $^2J_{CF}$ = 21.3 Hz, 2C, C3' & C5'), 122.6 (d, C7), 124.2 (d, C6), 124.2 (d, 2C, C2'' & C6''), 127.0 (d/d, $^3J_{CF}$ = 8.0 Hz, 2C, C2' & C6'), 129.5 (d, 2C, C3'' & C5''), 140.5 (s, C3a), 140.5 (s, C4''), 140.6 (s/d, $^4J_{CF}$ = 3.1 Hz, C1'), 147.5 (s, C7a), 151.0 (s, C1''), 152.7 (s, C5), 162.0 (s/d, $^1J_{CF}$ = 245.6 Hz, C4') ppm.

Optical rotation $[\alpha]_D^{20}$ = +19.3 (c = 0.805, MeOH)

E III.7.8 (*S*)-3-(5-((4-Bromophenyl)diazenyl)-1-(4-fluorophenyl)-1,3-dihydroisobenzofuran-1-yl)-*N*,*N*-dimethylpropan-1-amine [119]

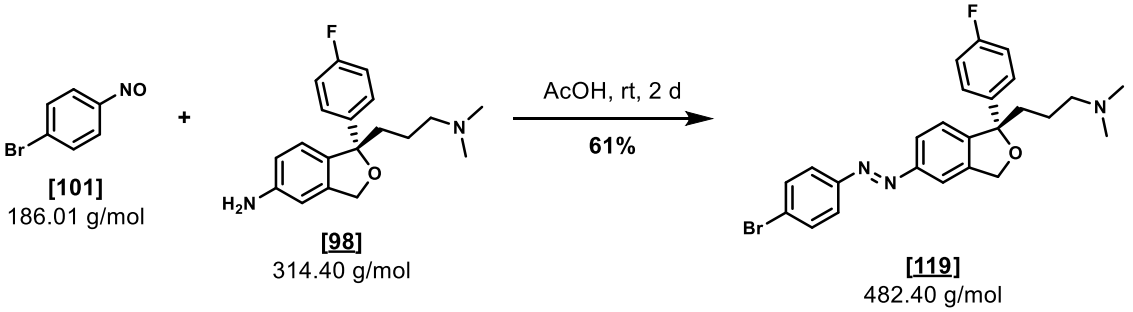

1-Bromo-4-nitrosobenzene **[101]** (12 mg, 0.065 mmol, 1 equiv.) was placed in a 10 mL round bottom flask. Aniline **[98]** (20.3 mg, 0.065 mmol, 1 equiv.) and acetic acid (1 mL) was added. The flask was flushed with argon and was closed with a septum. The solution was stirred at room temperature for 48 hours. The solution was basified with 2 N NaOH and the aqu. phase was extracted with $CHCl_3$ (3 x 3 mL). The combined organic phases were dried over $MgSO_4$. Volatiles were evaporated in vacuo. After purification by flash column chromatography (silica gel/crude material = 100/1, DCM/MeOH = 19/1 → 9/1) the pure product **[119]** was obtained.

Yield 61% (19.0 mg, 0.039 mmol)

Appearance orange oil

TLC analysis R_f = 0.3 (DCM/MeOH = 9/1)

Sum formula $C_{25}H_{25}BrFN_3O$

HR-MS $[M+H]^+$: calculated: 482.1238 Da, found: 482.1254 Da, difference: 1.6 mDa

^{1}H-NMR (600 MHz, $CDCl_3$) δ = 1.42 – 1.61 (m, 2H, CH_2-C<u>H</u>$_2$-CH_2-N(CH_3)$_2$), 2.18 – 2.24 (m, 2H, C<u>H</u>$_2$-CH_2-CH_2-N(CH_3)$_2$), 2.25 (s, 6H, 2 x CH_3), 2.41 (t, *J* = 6.7 Hz, 2H, CH_2-CH_2-C<u>H</u>$_2$-N(CH_3)$_2$), 5.19 (d, *J* = 12.5 Hz, 1H, H3), 5.24 (d, *J* = 12.5 Hz, 1H, H3), 7.01 (dd, $^3J_{HH}$ = 8.7, $^3J_{HF}$ = 8.7 Hz, 2H, H3' & H5'), 7.44 (d, *J* = 8.1 Hz, 1H, H7), 7.49 (dd, $^3J_{HH}$ = 8.9, $^4J_{HF}$ = 5.3 Hz, 2H, H2' & H6'), 7.64 (d, *J* = 8.7 Hz, 2H, H2'' & H6'' or H3'' & H5''), 7.73 (d, *J* = 0.9 Hz, 1H, H4), 7.77 (d, *J* = 8.7 Hz, 2H, H2'' & H6'' or H3'' & H5''), 7.87 (dd, *J* = 8.1, 1.7 Hz, 1H, H6) ppm.

^{13}C-NMR (151 MHz, $CDCl_3$) δ = 21.8 (t, CH_2-$\underline{C}H_2$-CH_2-N(CH_3)$_2$), 39.1 (t, $\underline{C}H_2$-CH_2-CH_2-N(CH_3)$_2$), 45.0 (q, 2C, 2 x CH_3), 59.4 (t, CH_2-CH_2-$\underline{C}H_2$-N(CH_3)$_2$), 71.7 (t, C3), 90.8 (s, C1), 114.7 (d, C4), 115.3 (d/d, $^2J_{CF}$ = 21.3 Hz, 2C, C3' & C5'), 122.6 (d, C7), 124.3 (d, C6), 124.5 (d, 2C, C2'' & C6'' or C3'' & C5''), 125.7 (s, C4''), 127.0 (d/d, $^3J_{CF}$ = 8.0 Hz, 2C, C2' & C6'), 132.9 (d, 2C, C2'' & C6'' or C3'' & C5''), 140.4 (s/d, $^4J_{CF}$ = 3.1 Hz, C1'), 140.5 (s, C7a), 147.3 (s, C3a or C5), 151.3 (s, C1''), 152.7 (s, C3a or C5), 162.1 (s/d, $^1J_{CF}$ = 245.7 Hz, C4') ppm.

Optical rotation $[\alpha]_D^{20}$ = +20.4 (c = 0.765, MeOH)

E III.7.9 (*S*)-3-(1-(4-Fluorophenyl)-5-(*p*-tolyldiazenyl)-1,3-dihydroisobenzofuran-1-yl)-*N*,*N*-dimethylpropan-1-amine [120]

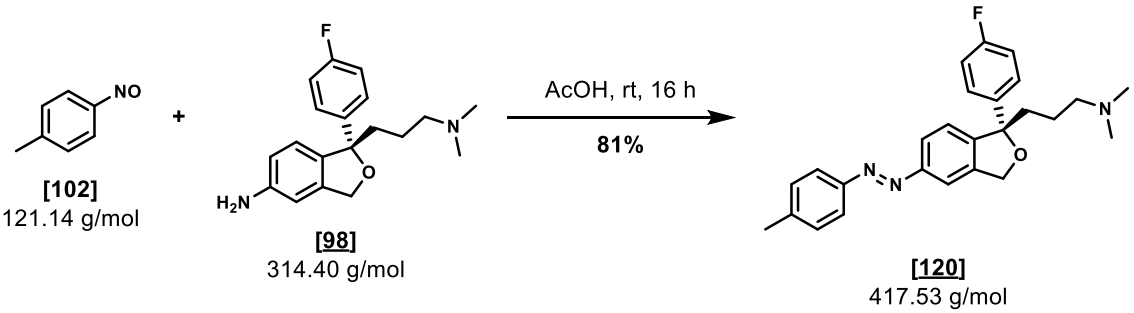

[102]
121.14 g/mol

[98]
314.40 g/mol

[120]
417.53 g/mol

1-Methyl-4-nitrosobenzene **[102]** (26.7 mg, 0.221 mmol, 2 equiv.) was placed in a 10 mL round bottom flask. Aniline **[98]** (34.7 mg, 0.110 mmol, 1 equiv.) and acetic acid (2 mL) was added. The flask was flushed with argon and was closed with a septum. The solution was stirred at room temperature for 16 hours. Volatiles were removed in vacuo. The crude material was purified by flash column chromatography (silica gel/crude material = 100/1, $CHCl_3$/MeOH/NH_4OH = 80/20/1) to afford the pure product **[120]**.

Yield 81% (37.3 mg, 0.089 mmol)

Appearance orange oil

TLC analysis R_f = 0.35 (DCM/MeOH = 1/1)

Sum formula $C_{26}H_{28}FN_3O$

HR-MS $[M+H]^+$: calculated: 418.2289 Da, found: 418.2319 Da, difference: 3.0 mDa

^{1}H-NMR (400 MHz, $CDCl_3$) δ = 1.33 – 1.59 (m, 2H, CH_2-C<u>H</u>$_2$-CH_2-$N(CH_3)_2$), 2.16 (s, 6H, 2 x CH_3), 2.17 – 2.24 (m, 2H, C<u>H</u>$_2$-CH_2-CH_2-$N(CH_3)_2$), 2.26 (t, *J* = 7.2 Hz, 2H, CH_2-CH_2-C<u>H</u>$_2$-$N(CH_3)_2$), 2.43 (s, 3H, Ar-CH_3), 5.19 (d, *J* = 12.5 Hz, 1H, H3), 5.24 (d, *J* = 12.5 Hz, 1H, H3), 7.01 (dd, $^3J_{HH}$ = 8.8, $^3J_{HF}$ = 8.8 Hz, 2H, H3' & H5'), 7.31 (d, *J* = 8.1 Hz, 2H, H3'' & H5''), 7.40 (d, *J* = 8.0 Hz, 1H, H7), 7.49 (dd, $^3J_{HH}$ = 8.9, $^4J_{HF}$ = 5.3 Hz, 2H, H2' & H6'), 7.72 (d, *J* = 1.0 Hz, 1H, H4), 7.81 (d, *J* = 8.3 Hz, 2H, H2'' & H6''), 7.86 (dd, *J* = 8.1, 1.7 Hz, 1H, H6) ppm.

^{13}C-NMR (101 MHz, $CDCl_3$) δ = 21.6 (q, Ar-CH_3), 22.3 (t, CH_2-<u>C</u>H_2-CH_2-$N(CH_3)_2$), 39.4 (t, <u>C</u>H_2-CH_2-CH_2-$N(CH_3)_2$), 45.4 (q, 2C, 2 x CH_3), 59.7 (t, CH_2-CH_2-<u>C</u>H_2-$N(CH_3)_2$), 71.7 (t, C3), 90.9 (s, C1), 114.5 (d, C4), 115.2 (d/d, $^2J_{CF}$ = 21.2 Hz, 2C, C3' & C5'), 122.5 (d, C7), 123.0 (d, 2C, C2'' & C6''), 124.0 (d, C6), 127.0 (d/d, $^3J_{CF}$ = 8.0 Hz, 2C, C2' & C6'), 129.9 (d, 2C, C3'' & C5''), 140.4 (s, C3a), 140.7 (s/d, $^4J_{CF}$ = 3.1 Hz, C1'), 141.8 (s, C4''), 146.8 (s, C7a), 150.8 (s, C1''), 153.0 (s, C5), 162.0 (s/d, $^1J_{CF}$ = 245.4 Hz, C4') ppm

Optical rotation $[\alpha]_D^{20}$ = +17.2 (c = 0.699, MeOH)

E III.7.10 (*S*)-4-((1-(3-(Dimethylamino)propyl)-1-(4-fluorophenyl)-1,3-dihydroisobenzofuran-5-yl)diazenyl)phenol [<u>121</u>]

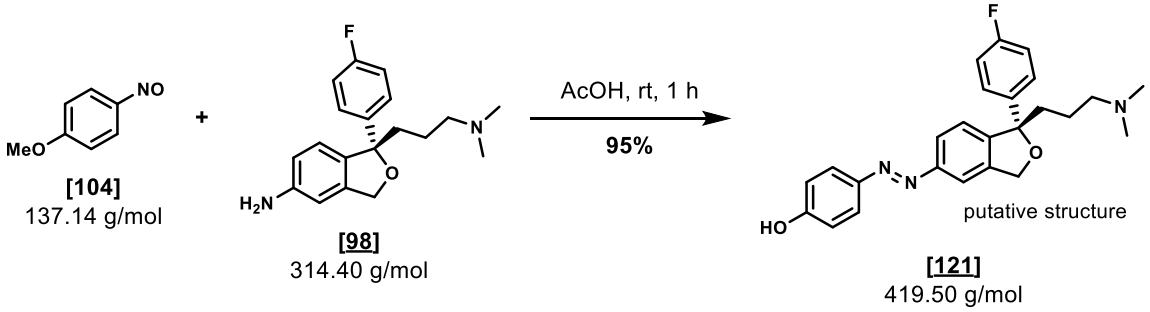

1-Methoxy-4-nitrosobenzene **[104]** (28.8 mg, 0.210 mmol, 2 equiv.) was placed in a 10 mL round bottom flask. Aniline **[<u>98</u>]** (33.0 mg, 0.105 mmol, 1 equiv.) and acetic acid (2 mL) was added. The flask was flushed with argon and was closed with a septum. The solution was stirred at room temperature for 1 hour. The reaction was partitioned between 0.5 N NaOH (10 20 mL) and EtOAc (10 mL) and the aqu. phase was extracted with EtOAc (4 x 10 mL). The combined organic phases were dried over $MgSO_4$ and volatiles were removed in vacuo. The crude material was purified by flash column chromatography (silica gel/crude material = 100/1, DCM/MeOH/NH_4OH = 95/5/0.5 → 90/10/1) to afford the pure product **[<u>121</u>]**.

Yield 95% (41.8 mg, 0.100 mmol)

Appearance	red oil
TLC-Analysis	R_f = 0.15 ($CHCl_3$/MeOH/NH_4OH = 100/10/1)
Sum formula	$C_{25}H_{26}FN_3O_2$
HR-MS	$[M+H]^+$: calculated: 420.2082 Da, found: 420.2109 Da, difference: 2.7 mDa
^{1}H-NMR (400 MHz, $CDCl_3$)	δ = 1.42 – 1.64 (m, 2H, CH_2-C<u>H</u>$_2$-CH_2-N(CH_3)$_2$), 2.10 – 2.27 (m, 2H, C<u>H</u>$_2$-CH_2-CH_2-N(CH_3)$_2$), 2.30 (s, 6H, 2 x CH_3), 2.48 (t, *J* = 7.2 Hz, 2H, CH_2-CH_2-C<u>H</u>$_2$-N(CH_3)$_2$), 5.11 (d, *J* = 12.8 Hz, 1H, H3), 5.15 (d, *J* = 12.7 Hz, 1H, H3), 6.96 (d, *J* = 8.9 Hz, 2H, H2'' & H6'' or H3'' & H5''), 7.00 (dd, $^3J_{HH}$ = 8.8, $^3J_{HF}$ = 8.8 Hz, 2H, H3' & H5'), 7.09 (d, *J* = 1.8 Hz, 1H, H4), 7.15 (dd, *J* = 8.1, 1.9 Hz, 1H, H6), 7.30 (d, *J* = 8.1 Hz, 1H, H7), 7.46 (dd, $^3J_{HH}$ = 8.7, $^4J_{HF}$ = 5.4 Hz, 2H, H2' & H6'), 7.78 (br s, 2H, H2'' & H6'' or H3'' & H5'') ppm. phenolic proton detected at 9.73 ppm in DMSO-d_6
^{13}C-NMR (101 MHz, $CDCl_3$)	δ = 21.6 (t, CH_2-<u>C</u>H_2-CH_2-N(CH_3)$_2$), 39.2 (t, <u>C</u>H_2-CH_2-CH_2-N(CH_3)$_2$), 44.7 (q, 2C, 2 x CH_3), 59.2 (t, CH_2-CH_2-<u>C</u>H_2-N(CH_3)$_2$), 71.7 (t, C3), 90.8 (s, C1), 113.8 (br d, 2C, C2'' & C6'' or C3'' & C5''), 115.3 (d/d, $^2J_{CF}$ = 21.2 Hz, 2C, C3' & C5'), 115.3 (d, C4), 122.2 (d, C6), 123.0 (d, C7), 126.8 (d/d, $^3J_{CF}$ = 8.0 Hz, 2C, C2' & C6'), 139.3 (s, C3a or C5 or C7a), 140.6 (s/d, $^4J_{CF}$ = 3.1 Hz, C1'), 140.9 (s, s, C3a or C5 or C7a), 141.0 (s, s, C3a or C5 or C7a), 151.8 (s, C1''), 162.0 (s/d, $^1J_{CF}$ = 245.7 Hz, C4'), 164.0 (s, C4'') ppm. one tertiary carbon signal of the phenol was detected as a broad peak at 113.8 ppm while the second tertiary carbon signal was not detected
Optical rotation	$[\alpha]_D^{20}$ = +39.4 (c = 0.10, MeOH)

E III.7.11 (*S*)-4-((1-(3-(Dimethylamino)propyl)-1-(4-fluorophenyl)-1,3-dihydroisobenzofuran-5-yl)diazenyl)benzoic acid [122]

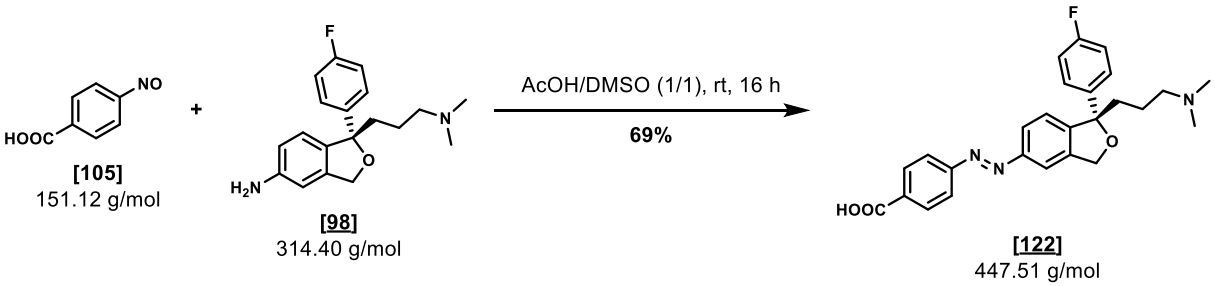

4-Nitrosobenzoic acid **[105]** (33.4 mg, 0.221 mmol, 2 equiv.) was placed in a 10 mL round bottom flask. Aniline **[98]** (34.7 mg, 0.110 mmol, 1 equiv.), acetic acid (2 mL) and DMSO (2 mL) were added. The flask was flushed with argon and was closed with a septum. The solution was stirred at room temperature for 16 hours. Volatiles were removed in vacuo. The crude material was purified by flash column chromatography (silica gel/crude material = 100/1, DCM/MeOH = 1/1) to afford the pure product **[122]**.

Yield	69% (33.9 mg, 0.076 mmol)
Appearance	orange oil
TLC-Analysis	R_f = 0.45 (MeOH)
Sum formula	$C_{26}H_{26}FN_3O_3$
HR-MS	$[M+H]^+$: calculated: 448.2031 Da, found: 448.0250 Da, difference: 1.9 mDa
^{1}H-NMR (400 MHz, $CDCl_3$)	δ = 1.65 – 1.92 (m, 2H, CH_2-C<u>H</u>$_2$-CH_2-N$(CH_3)_2$), 2.18 – 2.42 (m, 2H, C<u>H</u>$_2$-CH_2-CH_2-N$(CH_3)_2$), 2.69 (s, 6H, 2 x CH_3), 2.85 – 3.09 (m, 2H, CH_2-CH_2-C<u>H</u>$_2$-N$(CH_3)_2$), 5.14 (d, *J* = 12.5 Hz, 1H, H3), 5.26 (d, *J* = 12.5 Hz, 1H, H3), 7.00 (dd, $^3J_{HH}$ = 8.7, $^3J_{HF}$ = 8.7 Hz, 2H, H3' & H5'), 7.41 – 7.49 (m, 3H, H7 & H2' & H6'), 7.63 (d, *J* = 0.8 Hz, 1H, H4), 7.70 – 7.77 (m, 3H, H6 & H2'' & H6''), 7.95 (d, *J* = 8.5 Hz, 2H, H3'' & H5'') ppm.

^{13}C-NMR (101 MHz, $CDCl_3$) δ = 20.4 (t, CH_2-$\underline{C}H_2$-CH_2-$N(CH_3)_2$), 38.3 (t, $\underline{C}H_2$-CH_2-CH_2-$N(CH_3)_2$), 42.9 (q, 2C, 2 x CH_3), 58.1 (t, CH_2-CH_2-$\underline{C}H_2$-$N(CH_3)_2$), 71.8 (t, C3), 90.7 (s, C1), 115.4 (d/d, $^2J_{CF}$ = 21.3 Hz, 2C, C3' & C5'), 115.5 (d, C4), 122.5 (d, 2C, C2'' & C6''), 122.6 (d, C7), 123.8 (d, C6), 126.9 (d/d, $^3J_{CF}$ = 8.1 Hz, 2C, C2' & C6'), 130.4 (d, 2C, C3'' & C5''), 137.1 & 140.3 (2xs, 2C, C3a & C4''), 140.4 (s/d, $^4J_{CF}$ = 3.1 Hz, C1'), 145.7 & 152.9 & 153.9 (3xs, 3C, C5 & C7a & C1''), 162.1 (s/d, $^1J_{CF}$ = 246.1 Hz, C4'), 171.2 (s, acid) ppm.

Optical rotation $[\alpha]_D^{20}$ = -73.4 (c = 0.50, MeOH)

E III.7.12 Methyl (*S*)-4-((1-(3-(dimethylamino)propyl)-1-(4-fluorophenyl)-1,3-dihydroisobenzofuran-5-yl)diazenyl)benzoate [123]

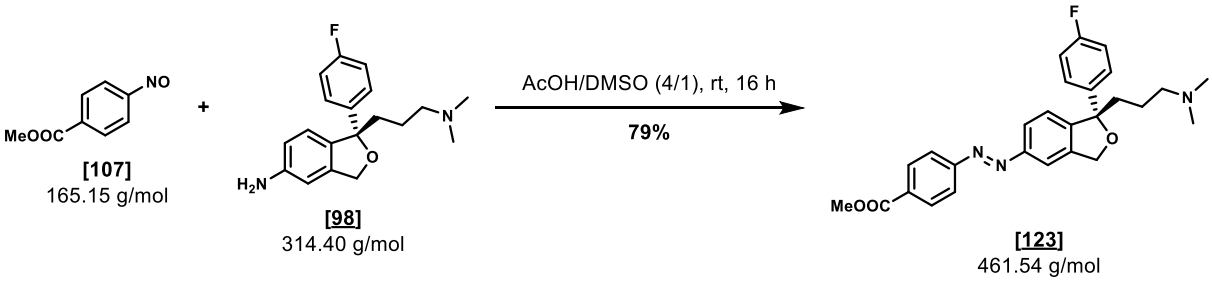

Methyl 4-nitrosobenzoate **[107]** (36.5 mg, 0.221 mmol, 2 equiv.) was placed in a 10 mL round bottom flask. Aniline **[98]** (34.7 mg, 0.110 mmol, 1 equiv.), acetic acid (2 mL) and DMSO (0.5 mL) were added. The flask was flushed with argon and was closed with a septum. The solution was stirred at room temperature for 16 hours. Volatiles were removed in vacuo. The crude material was purified by flash column chromatography (silica gel/crude material = 100/1, $CHCl_3$/MeOH/NH_4OH = 80/20/1) to afford the pure product **[123]**.

Yield 79% (40.3 mg, 0.087 mmol)

Appearance orange oil

TLC-Analysis R_f = 0.45 (DCM/MeOH/NH_4OH = 100/10/1)

Sum formula $C_{27}H_{28}FN_3O_3$

HR-MS $[M+H]^+$: calculated: 462.2187 Da, found: 462.2215 Da, difference: 2.7 mDa

^{1}H-NMR (400 MHz, $CDCl_3$) δ = 1.34 – 1.60 (m, 2H, CH_2-C<u>H</u>$_2$-CH_2-N$(CH_3)_2$), 2.18 (s, 6H, 2 x CH_3), 2.19 – 2.27 (m, 2H, C<u>H</u>$_2$-CH_2-CH_2-N$(CH_3)_2$), 2.30 (t, *J* = 7.3 Hz, 2H, CH_2-CH_2-C<u>H</u>$_2$-N$(CH_3)_2$), 3.95 (s, 3H, COOMe), 5.20 (d, *J* = 12.6 Hz, 1H, H3), 5.25 (d, *J* = 12.6 Hz, 1H, H3), 7.01 (dd, $^3J_{HH}$ = 8.7, $^3J_{HF}$ = 8.7 Hz, 2H, H3' & H5'), 7.44 (d, *J* = 8.1 Hz, 1H, H7), 7.49 (dd, $^3J_{HH}$ = 8.9, $^4J_{HF}$ = 5.3 Hz, 2H, H2' & H6'), 7.76 (d, *J* = 0.9 Hz, 1H, H4), 7.89 – 7.94 (m, 3H, H6 & H2'' & H6''), 8.18 (d, *J* = 8.6 Hz, 2H, H3'' & H5'') ppm.

^{13}C-NMR (101 MHz, $CDCl_3$) δ = 22.2 (t, CH_2-C<u>H</u>$_2$-CH_2-N$(CH_3)_2$), 39.3(t, C<u>H</u>$_2$-CH_2-CH_2-N$(CH_3)_2$), 45.3(q, 2C, 2 x CH_3), 52.5 (q, COOMe), 59.6 (t, CH_2-CH_2-C<u>H</u>$_2$-N$(CH_3)_2$), 71.7 (t, C3), 90.9 (s, C1), 114.9 (d, C4), 115.3 (d/d, $^2J_{CF}$ = 21.3 Hz, 2C, C3' & C5'), 122.6 (d, C7), 122.8 (d, 2C, C2'' & C6''), 124.5 (d, C6), 127.0 (d/d, $^3J_{CF}$ = 8.0 Hz, 2C, C2' & C6'), 130.8 (d, 2C, C3'' & C5''), 132.0 (s, C4''), 140.5 (s/d, $^4J_{CF}$ = 3.1 Hz, C1'), 140.6 (s, C3a), 147.9 & 152.8 & 155.1 (3xs, 3C, C5 & C7a & C1''), 162.1 (s/d, $^1J_{CF}$ = 245.7 Hz, C4'), 166.6 (s, ester) ppm.

Optical rotation $[\alpha]_D^{20}$ = +19.7 (c = 0.50, MeOH)

E III.7.13 (*S*)-3-((1-(3-(Dimethylamino)propyl)-1-(4-fluorophenyl)-1,3-dihydroisobenzofuran-5-yl)diazenyl)benzonitrile [<u>124</u>]

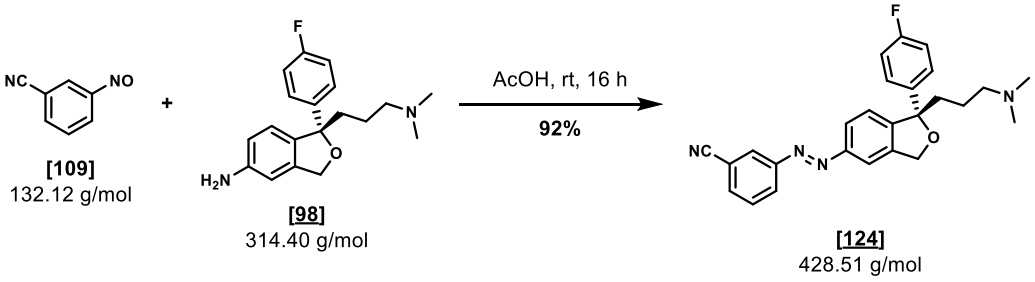

3-Nitrosobenzonitrile **[109]** (29.2 mg, 0.221 mmol, 2 equiv.) was placed in a 10 mL round bottom flask. Aniline **[<u>98</u>]** (34.7 mg, 0.110 mmol, 1 equiv.) and acetic acid (2 mL) was added. The flask was flushed with argon and was closed with a septum. The solution was stirred at room temperature for 16 hours. Volatiles were removed in vacuo. The crude material was purified by flash column chromatography (silica gel/crude material = 100/1, $CHCl_3$/MeOH/NH_4OH = 80/20/1) to afford the pure product **[<u>124</u>]**.

Yield 92% (43.7 mg, 0.102 mmol)

Appearance orange oil

TLC-Analysis R_f = 0.40 (DCM/MeOH/NH_4OH = 100/10/1)

Sum formula $C_{26}H_{25}FN_4O$

HR-MS $[M+H]^+$: calculated: 429.2085 Da, found: 429.2111 Da, difference: 2.6 mDa

^{1}H-NMR (400 MHz, $CDCl_3$) δ = 1.33 – 1.57 (m, 2H, CH_2-C<u>H</u>$_2$-CH_2-N(CH_3)$_2$), 2.15 (s, 6H, 2 x CH_3), 2.18 – 2.28 (m, 4H, C<u>H</u>$_2$-CH_2-C<u>H</u>$_2$-N(CH_3)$_2$), 5.20 (d, *J* = 12.6 Hz, 1H, H3), 5.25 (d, *J* = 12.6 Hz, 1H, H3), 7.01 (dd, $^3J_{HH}$ = 8.7, $^3J_{HF}$ = 8.7 Hz, 2H, H3' & H5'), 7.44 (d, *J* = 8.0 Hz, 1H, H7), 7.49 (dd, $^3J_{HH}$ = 8.9, $^4J_{HF}$ = 5.3 Hz, 2H, H2' & H6'), 7.62 (t, *J* = 7.8 Hz, 1H, H5''), 7.73 (dt, *J* = 7.7, 1.4 Hz, 1H, H4''), 7.76 (d, *J* = 0.9 Hz, 1H, H4), 7.90 (dd, *J* = 8.1, 1.7 Hz, 1H, H6), 8.11 (ddd, *J* = 8.0, 2.0, 1.2 Hz, 1H, H6''), 8.16 (t, *J* = 1.8 Hz, 1H, H2'') ppm.

^{13}C-NMR (101 MHz, $CDCl_3$) δ = 22.3 (t, CH_2-<u>C</u>H$_2$-CH_2-N(CH_3)$_2$), 39.3 (t, <u>C</u>H$_2$-CH_2-CH_2-N(CH_3)$_2$), 45.5 (q, 2C, 2 x CH_3), 59.7 (t, CH_2-CH_2-<u>C</u>H$_2$-N(CH_3)$_2$), 71.6 (t, C3), 90.9 (s, C1), 113.5 (s, C3''), 115.0 (d, C4), 115.3 (d/d, $^2J_{CF}$ = 21.3 Hz, 2C, C3' & C5'), 118.3 (s, CN), 122.7 (d, C7), 124.5 (d, C6), 126.2 (d, C2''), 127.0 (d/d, $^3J_{CF}$ = 8.0 Hz, 2C, C2' & C6'), 127.5 (d, C6''), 130.2 (d, C5''), 133.9 (d, C4''), 140.4 (s/d, $^4J_{CF}$ = 3.1 Hz, C1'), 140.6 (s, C3a), 148.3 & 152.3 & 152.5 (3xs, 3C, C5 & C7a & C1''), 162.0 (s/d, $^1J_{CF}$ = 245.7 Hz, C4') ppm.

Optical rotation $[\alpha]_D^{20}$ = +18.5 (c = 0.50, MeOH)

The assignments of protons and carbon atoms in the NMR codes of compound **[<u>124</u>]** were carried out as follows:

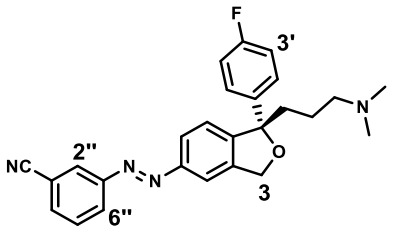

E III.7.14 (*S*)-1-((1-(3-(Dimethylamino)propyl)-1-(4-fluorophenyl)-1,3-dihydroisobenzofuran-5-yl)diazenyl)naphthalen-2-ol [126]

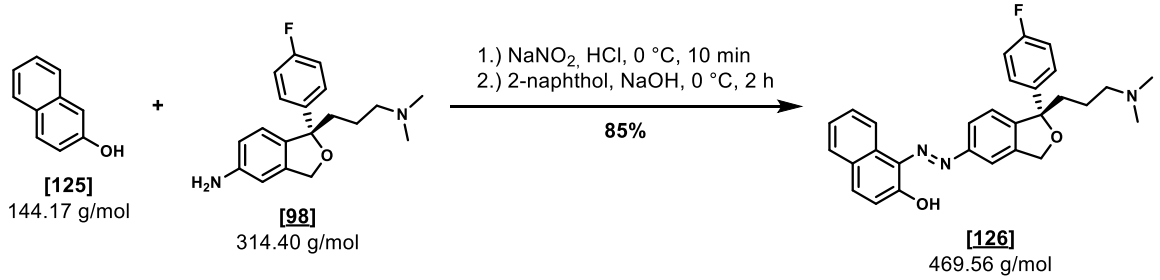

A solution of $NaNO_2$ (8.7 mg, 0.126 mmol, 1.2 equiv.) in H_2O (0.20 mL) was added to a solution of aniline **[98]** (33.0 mg, 0.105 mmol, 1 equiv.) in 2 N HCl (0.14 mL) at 0 °C and the reaction was stirred at 0 °C for 10 minutes. This solution was added dropwise to a solution of 2-naphthol **[125]** (16.6 mg, 0.115 mmol, 1.1 equiv.) in 2 N NaOH (0.20 mL) at 0 °C and was stirred at this temperature for 2 hours. The reaction was diluted with H_2O (5 mL) and was extracted with $CHCl_3$ (3 x 5 mL). The combined organic phases were dried over $MgSO_4$ and after evaporation of the volatiles the crude product was obtained. After purification by flash column chromatography (silica gel/crude material = 100/1, $CHCl_3$/MeOH/NH_4OH = 100/5/0.5) pure product **[126]** was obtained.

Yield	85% (42 mg, 0.089 mmol)
Appearance	orange oil
TLC-Analysis	R_f = 0.40 (DCM/MeOH = 9/1)
Sum formula	$C_{29}H_{28}FN_3O_2$
HR-MS	$[M+H]^+$: calculated: 470.2238 Da, found: 470.2256 Da, difference: 1.8 mDa
^{1}H-NMR (400 MHz, $CDCl_3$)	δ = 1.37 – 1.62 (m, 2H, CH_2-C<u>H</u>$_2$-CH_2-N(CH_3)$_2$), 2.12 – 2.30 (m, 8H, C<u>H</u>$_2$-CH_2-CH_2-N(C<u>H</u>$_3$)$_2$), 2.36 (t, *J* = 7.3 Hz, 2H, CH_2-CH_2-C<u>H</u>$_2$-N(CH_3)$_2$), 5.18 (d, *J* = 12.6 Hz, 1H, H3), 5.24 (d, *J* = 12.6 Hz, 1H, H3), 6.86 (d, *J* = 9.4 Hz, 1H, H3''), 7.01 (dd, $^3J_{HH}$ = 8.7, $^3J_{HF}$ = 8.7 Hz, 2H, H3' & H5'), 7.35 – 7.41 (m, 2H, H7 & H6''), 7.49 (dd, $^3J_{HH}$ = 8.7, $^4J_{HF}$ = 5.5 Hz, 2H, H2' & H6'), 7.54 (ddd, *J* = 8.4, 7.1, 1.3 Hz, 1H, H7''), 7.57 – 7.62 (m, 3H, H4 & H6 & H5''), 7.69 (d, *J* = 9.4 Hz, 1H, H4''), 8.53 (d, *J* = 8.2 Hz, 1H, H8'') ppm.

^{13}C-NMR (101 MHz, $CDCl_3$) δ = 22.0 (t, CH_2-$\underline{C}H_2$-CH_2-N(CH_3)$_2$), 39.3 (t, $\underline{C}H_2$-CH_2-CH_2-N(CH_3)$_2$), 45.2 (q, 2C, 2 x CH_3), 59.5 (t, CH_2-CH_2-$\underline{C}H_2$-N(CH_3)$_2$), 71.8 (t, C3), 90.9 (s, C1), 111.1 (d, C4), 115.3 (d/d, $^2J_{CF}$ = 21.3 Hz, 2C, C3' & C5'), 119.3 (d, C5''), 121.8 (d, C8''), 123.0 (d, C7), 124.5 (d, C3''), 125.9 (d, C6''), 126.9 (d/d, $^3J_{CF}$ = 8.0 Hz, 2C, C2' & C6'), 128.2 (s, C4a''), 128.8 (d, C7), 129.0 (d, C7''), 130.2 (s, C1''), 133.5 (s, C8a''), 140.0 (d, C4''), 140.7 (s/d, $^4J_{CF}$ = 3.1 Hz, C1'), 141.1 & 143.7 & 145.4 (3xs, 3C, C4 & C6 & C7), 162.0 (s/d, $^1J_{CF}$ = 245.6 Hz, C4'), 170.8 (s, C2'') ppm.

Optical rotation $[\alpha]_D^{20}$ = +47.0 (c = 0.50, MeOH)

The assignments of protons and carbon atoms in the NMR codes of compound **[<u>126</u>]** were carried out as follows:

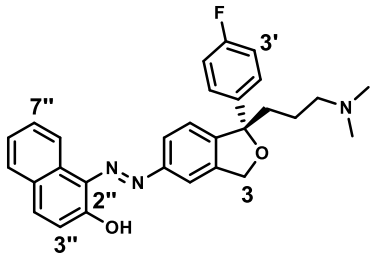

E III.8 HTI building blocks

E III.8.1 2-(Phenylthio)acetic acid [129]

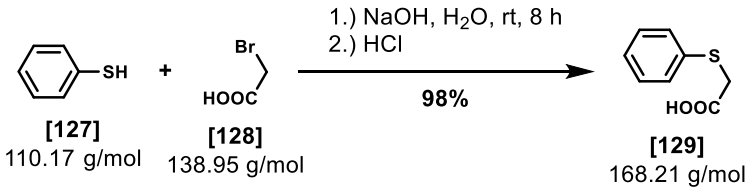

2-(Phenylthio)acetic acid **[129]** was synthesized according to a literature procedure[155]. Thiophenol **[127]** was purified by distillation prior to use. Thiophenol **[127]** (5.5 g, 50 mmol, 1 equiv.) was placed in a 250 mL round bottom flask. H_2O (100 mL), NaOH (4.0 g, 100 mmol, 2 equiv.) and bromoacetic acid **[128]** (6.948 g, 50 mmol, 1 equiv.) were added. The reaction was stirred for 8 hours at room temperature. After TLC analysis indicated the reaction to be finished, the solution was acidified with 2 N HCl and EtOAc was added to dissolve the precipitate. Phases were separated and the aqu. phase was extracted with EtOAc (3 x 30 mL). The combined organic phases were dried over $MgSO_4$, filtered and evaporated to dryness to afford the product.

Yield 98% (8.217 g, 48.8 mmol)

Appearance	Colorless crystals
Melting point	62.0 – 64.0 °C (Lit.[155]: 62 – 64 °C)
TLC-Analysis	R_f = 0.7 (EtOAc + 1 drop conc. HCl)
Sum formula	$C_8H_8O_2S$
^{1}H-NMR (400 MHz, $CDCl_3$)	δ = 3.69 (s, 2H, CH_2), 7.25 – 7.29 (m, 1H, H4), 7.30 – 7.36 (m, 2H, H3 & H5), 7.41 – 7.46 (m, 2H, H2 & H6), 10.20 (br s, 1H, acid) ppm.
^{13}C-NMR (101 MHz, $CDCl_3$)	δ = 36.7 (t, CH_2), 127.4 (d, C4), 129.3 & 130.2 (2xd, 4C, C2 & C3 & C5 & C6), 134.6 (s, C1), 175.5 (s, acid) ppm.

E III.8.2 Benzo[*b*]thiophen-3(2*H*)-one [130]

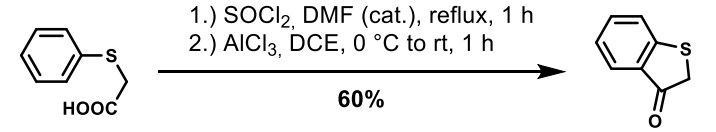

[129]
168.21 g/mol

[130]
150.20 g/mol

Benzo[*b*]thiophen-3(2*H*)-one **[130]** was synthesized by a modified literature procedure[111]. 2-(Phenylthio)acetic acid **[129]** (901 mg, 5.36 mmol, 1 equiv.) was placed in a round bottom flask and freshly distilled $SOCl_2$ (3.9 mL, 53.6 mmol, 10 equiv.) was added under argon. One drop of DMF was added and after stirring the reaction for 1 hour at reflux temperature TLC analysis (MeOH quenched sample) indicated full conversion. Volatiles were removed in vacuo and the acid chloride intermediate was obtained. $AlCl_3$ (0.858 g, 6.43 mmol, 1.1 equiv.) was placed in a round bottom flask and dry DCE (10 mL) was added under argon. The suspension was cooled to 0 °C with a NaCl/ice bath. Then the acid chloride intermediate (1.0 g, 5.36 mmol, 1 equiv.) was added dropwise to the stirred mixture. After 20 minutes the ice bath was removed and the reaction was stirred at room temperature until TLC analysis showed full consumption of the starting material. The reaction was again cooled to 0 °C and was quenched dropwise with degassed ice-cold H_2O. After extraction with DCM (3 x 20 mL) the combined organic phases were dried over $MgSO_4$, filtered and evaporated to dryness to afford the product.

Yield	60% (0.480 g, 3.2 mmol)
Appearance	Reddish solid
Melting point	65.0 – 67.0 °C (Lit.[211]: 64 – 66 °C)
TLC-Analysis	R_f = 0.6 (LP/EtOAc = 5/1)
Sum formula	C_8H_6OS

GC-MS 150 (83, M^+), 122 (32), 121 (100)

^{1}H-NMR (400 MHz, $CDCl_3$) δ = 3.80 (s, 2H, CH_2), 7.22 (ddd, *J* = 7.9, 7.1, 1.0, 1H, Ar-H), 7.43 (d, *J* = 8.0 Hz, 1H, Ar-H), 7.55 (ddd, *J* = 8.3, 7.1, 1.4, 1H, Ar-H), 7.78 (ddd, *J* = 7.8, 1.4, 0.7 Hz, 1H, Ar-H) ppm.

^{13}C-NMR (101 MHz, $CDCl_3$) δ = 39.4 (t, CH_2), 124.7 & 124.9 & 126.8 (3xd, 3C, C4 & C5 & C7), 131.1 (s, C3a), 135.8 (d, C6), 154.4 (s, C7a), 200.2 (s, ketone) ppm.

E III.8.3 2-((Carboxymethyl)thio)benzoic acid [132]

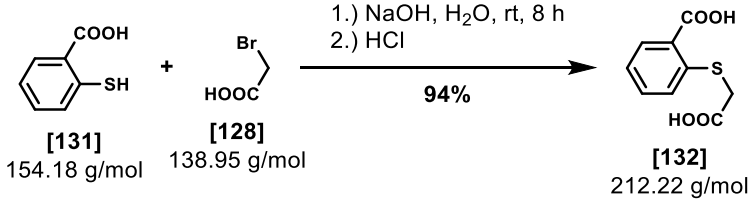

[131] 154.18 g/mol **[128]** 138.95 g/mol **[132]** 212.22 g/mol

2-((Carboxymethyl)thio)benzoic acid **[132]** was synthesized according to a literature procedure[155]. Thiosalicylic acid **[131]** (8.493 g, 55.08 mmol, 1 equiv.) was placed in a 250 mL round bottom flask. H_2O (130 mL), NaOH (8.812 g, 220.32 mmol, 4 equiv.) and bromoacetic acid **[128]** (7.654 g, 55.08 mmol, 1 equiv.) were added. The reaction was stirred for 8 hours at room temperature. After the reaction was finished, the solution was acidified with 2 N HCl. The precipitated product was isolated by filtration and was washed with H_2O. After drying in high vacuum the pure product **[132]** was obtained.

Yield 94% (10.963 g, 51.66 mmol)

Appearance Colorless crystals

Melting point 219.0 – 222.0 °C (Lit.[212]: 219 – 222 °C)

TLC-Analysis R_f = 0.4 (DCM/MeOH = 9/1 + 1 drop AcOH)

Sum formula $C_9H_8O_4S$

^{1}H-NMR (400 MHz, DMSO-d_6) δ = 3.80 (s, 2H, CH_2), 7.22 (td, *J* = 7.5, 1.1 Hz, 1H, Ar-H), 7.36 (dd, *J* = 8.2, 1.0 Hz, 1H, Ar-H), 7.52 (ddd, *J* = 8.2, 7.3, 1.6 Hz, 1H, Ar-H), 7.90 (dd, *J* = 7.8, 1.6 Hz, 1H, Ar-H), 12.96 (br s, 2H, 2 x acid) ppm.

^{13}C NMR (101 MHz, DMSO-d_6) δ = 34.0 (t, CH_2), 124.1 (d, Ar-C), 125.3 (d, Ar-C), 127.7 (s, Ar-C), 131.0 (d, Ar-C), 132.4 (d, Ar-C), 140.4 (s, Ar-C), 167.4 (s, acid), 170.7 (s, acid).

E III.8.4 3-Oxo-2,3-dihydrobenzo[*b*]thiophene-7-carbonyl chloride [133]

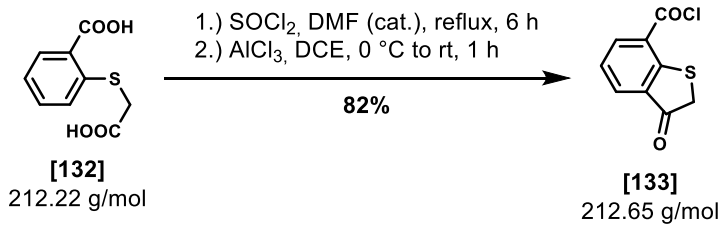

[132]
212.22 g/mol

[133]
212.65 g/mol

3-Oxo-2,3-dihydrobenzo[*b*]thiophene-7-carbonyl chloride **[133]** was synthesized according to a modified literature procedure[111]. 2-((Carboxymethyl)thio)benzoic acid **[132]** (2.83 g, 13.33 mmol, 1 equiv.) was placed in a round bottom flask and freshly distilled $SOCl_2$ (9.65 mL, 133 mmol, 10 equiv.) was added under argon. One drop of DMF was added and after stirring the reaction for 6 hours at reflux temperature TLC analysis (MeOH quenched sample) indicated full conversion. Volatiles were removed in vacuo and the acid chloride intermediate was obtained. $AlCl_3$ (3.91 g, 29.33 mmol, 2.2 equiv.) was placed in a round bottom flask and dry DCE (35 mL) was added under argon. The suspension was cooled to 0 °C with a NaCl/ice bath. Then the acid chloride intermediate (3.32 g, 13.33 mmol, 1 equiv.) was added dropwise as a solution in dry DCE (5 mL) to the stirred mixture. After 20 minutes the ice bath was removed and the reaction was stirred at room temperature until TLC analysis showed full consumption of the starting material. The reaction was again cooled to 0 °C and was quenched dropwise with degassed ice-cold 2 N HCl. After extraction with DCE (4 x 50 mL) the combined organic phases were dried over $MgSO_4$, filtered and evaporated to dryness to afford the product in 93% purity.

Yield	82% (2.33 g, 10.94 mmol)
Appearance	reddish-brown solid
Melting point	100.0 – 109.0 °C (Lit.[212]: 110 – 111 °C)
TLC-Analysis	R_f = 0.4 (LP/EtOAc = 5/1 + 1 drop AcOH)
Sum formula	$C_9H_5ClO_2S$
^{1}H-NMR (400 MHz, $CDCl_3$)	δ = 3.82 (s, 2H, CH_2), 7.42 (t, *J* = 7.7 Hz, 1H, Ar-H), 8.05 (dd, *J* = 7.6, 1.3 Hz, 1H, Ar-H), 8.53 (dd, *J* = 7.8, 1.3 Hz, 1H, Ar-H) ppm.
^{13}C NMR (101 MHz, $CDCl_3$)	δ = 39.9 (t, CH_2), 125.2 (d, Ar-C), 128.7 (s, Ar-C), 132.7 (d, Ar-C), 133.2 (s, Ar-C), 140.9 (d, Ar-C), 158.3 (s, Ar-C), 166.1 (s, acid chloride), 198.8 (s, ketone).

E III.8.5 3-Hydroxybenzo[*b*]thiophene-7-carboxylic acid [134]

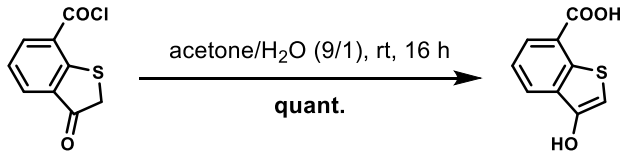

[133]
212.65 g/mol

[134]
194.20 g/mol

A solution of acid chloride **[133]** (2.202 g, 10.36 mmol) in acetone/H_2O (9/1, 150 mL) under argon was stirred at room temperature for 16 hours. TLC analysis showed full consumption of starting material and the solvent was evaporated in vacuo and the product, 3-hydroxybenzo[*b*]thiophene-7-carboxylic acid **[134],** was obtained in 92% purity.

Yield quant. (2.01 g, 10.36 mmol)

Appearance red powder

TLC analysis R_f = 0.7 (DCM/MeOH = 4/1)

Melting point > 300 °C (Lit.[213, 214]: 310 °C; one literature reference[215] wrongly reported the analytical data of the acid chloride **[133]**)

Sum formula $C_9H_6O_3S$

^{1}H-NMR (400 MHz, DMSO-d_6) δ = 6.55 (s, 1H, CH), 7.49 (t, *J* = 7.7 Hz, 1H, Ar-H), 7.98 (dd, *J* = 7.9, 1.2 Hz, 1H, Ar-H), 8.02 (dd, *J* = 7.4, 1.2 Hz, 1H, Ar-H), 10.17 (s, 1H, enol-H), 13.38 (br s, 1H, acid) ppm.

^{13}C NMR (101 MHz, DMSO-d_6) δ = 100.8 (d, CH), 123.6 (d, Ar-C), 124.5 (s, Ar-C), 125.2 (d, Ar-C), 127.1 (d, Ar-C), 133.8 (s, Ar-C), 137.6 (s, Ar-C), 148.0 (s, Ar-C), 167.0 (s, acid).

E III.9 HTI-Escitalopram derivatives

E III.9.1 (*S*)-2-((1-(3-(Dimethylamino)propyl)-1-(4-fluorophenyl)-1,3-dihydroisobenzofuran-5-yl)methylene)benzo[*b*]thiophen-3(2*H*)-one [135]

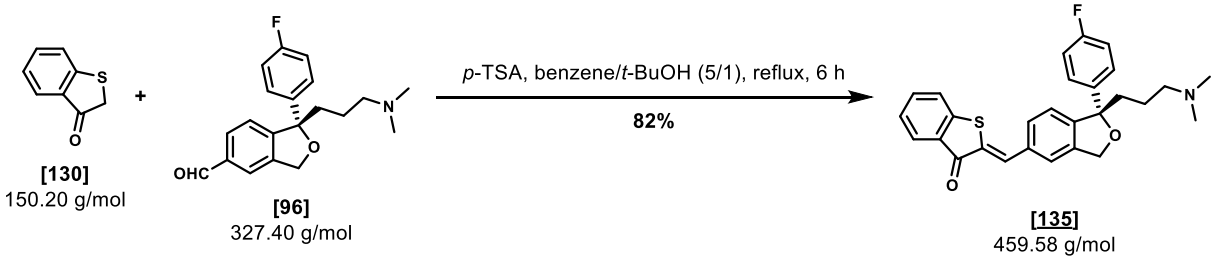

Escitalopram aldehyde **[96]** (63 mg, 0.192 mmol, 1 equiv.) and *p*-TSA•H_2O (55 mg, 0.289 mmol, 1.5 equiv.) were placed in a round bottom flask. The flask was evacuated and flushed with argon three times. Degassed benzene (2.4 mL, degassed by bubbling with argon under sonication for 10 minutes) and degassed *t*-BuOH (0.24 mL) were added via syringe and the solids were dissolved. In a second round bottom flask benzo[*b*]thiophen-3(2*H*)-one **[130]** (43 mg, 0.289 mmol, 1.5 equiv.) was placed. The flask was evacuated and flushed with argon three times. Degassed benzene (2.4 mL) and degassed *t*-BuOH (0.73 mL) were added via syringe and the solid was dissolved under sonication. The benzo[*b*]thiophen-3(2*H*)-one **[130]** solution was added to the starting material **[96]** and the reaction was stirred at reflux temperature until TLC analysis showed full consumption of the starting material (6 hours). Solvents were removed in vacuo. Purification by flash column chromatography (silica gel/crude material = 100/1, DCM/MeOH = 19/1 → 9/1) afforded the pure product **[135]**.

Yield	82% (72.5 mg; 0.158 mmol)
Appearance	yellow oil
TLC-Analysis	0.3 (DCM/MeOH = 9/1)
Sum formula	$C_{28}H_{26}FNO_2S$
HR-MS	$[M+H]^+$: calculated: 460.1741 Da, found: 460.1767 Da, difference: 2.6 mDa

^{1}H-NMR (600 MHz, $CDCl_3$) δ = 1.35 – 1.58 (m, 2H, CH_2-C<u>H</u>$_2$-CH_2-N$(CH_3)_2$), 2.14 – 2.27 (m, 2H, C<u>H</u>$_2$-CH_2-CH_2-N$(CH_3)_2$), 2.21 (s, 6H, 2 x CH_3), 2.31 – 2.36 (m, 2H, CH_2-CH_2-C<u>H</u>$_2$-N$(CH_3)_2$), 5.18 (d, *J* = 12.4 Hz, 1H, H3), 5.23 (d, *J* = 12.4 Hz, 1H, H3), 7.00 (dd, $^3J_{HH}$ = 8.7, $^3J_{HF}$ = 8.7 Hz, 2H, H3' & H5'), 7.28 (td, *J* = 7.5, 1.0 Hz, 1H, H5''), 7.40 (d, *J* = 7.9 Hz, 1H, H7), 7.45 – 7.49 (m, 3H, H2' & H6' & H7''), 7.52 (d, *J* = 1.5 Hz, 1H, H4), 7.56 (ddd, *J* = 8.4, 7.2, 1.3 Hz, 1H, H6''), 7.61 (dd, *J* = 8.2, 1.5 Hz, 1H, H6), 7.90 – 7.93 (m, 2H, olefin-H & H4'') ppm.

^{13}C-NMR (151 MHz, $CDCl_3$) δ = 22.0 (t, CH_2-<u>C</u>H$_2$-CH_2-N$(CH_3)_2$), 39.1 (t, <u>C</u>H$_2$-CH_2-CH_2-N$(CH_3)_2$), 45.1 (q, 2C, 2 x CH_3), 59.4 (t, CH_2-CH_2-<u>C</u>H$_2$-N$(CH_3)_2$), 71.7 (t, C3), 91.0 (s, C1), 115.3 (d/d, $^2J_{CF}$ = 21.3 Hz, 2C, C3' & C5'), 122.6 (d, C7), 123.5 (d, C4), 124.0 (d, C7''), 125.8 (d, C5''), 126.9 (d/d, $^3J_{CF}$ = 8.0 Hz, 2C, C2' & C6'), 127.2 (d, C4''), 130.4 & 130.5 (2xs, 2C, C2'' & C3a'' or C7a''), 131.1 (d, C6), 133.0 (d, olefin-C), 134.2 (s, C3a or C5), 135.5 (d, C6''), 140.3 (s, C3a or C5), 140.3 (s/d, $^4J_{CF}$ = 3.1 Hz, C1'), 146.0 (s, C3a'' or C7a''), 146.5 (s, C7a), 162.0 (s/d, $^1J_{CF}$ = 245.7 Hz, C4'), 188.7 (s, ketone) ppm.

Optical rotation $[\alpha]_D^{20}$ = +18.5 (c = 0.74, DCM)

E III.9.2 (*S*)-2-((1-(3-(Dimethylamino)propyl)-1-(4-fluorophenyl)-1,3-dihydroisobenzofuran-5-yl)methylene)-3-oxo-2,3-dihydrobenzo[*b*]thiophene-7-carboxylic acid [<u>136</u>]

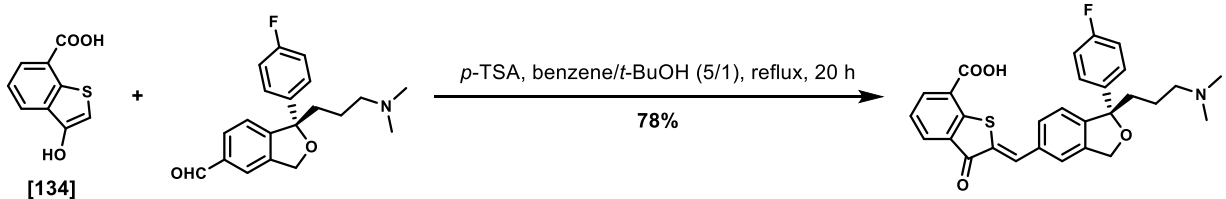

Escitalopram aldehyde **[96]** (522 mg, 1.59 mmol, 1 equiv.) and *p*-TSA•H_2O (455 mg, 2.39 mmol, 1.5 equiv.) were placed in a round bottom flask. The flask was evacuated and flushed with argon three times. Degassed benzene (20 mL, degassed by bubbling with argon under sonication for 10 minutes) and degassed *t*-BuOH (2 mL) were added via syringe and the solids were dissolved. In a second round bottom flask 3-hydroxybenzo[*b*]thiophene-7-carboxylic acid **[134]** (464 mg, 2.39 mmol, 1.5 equiv.) was placed. The flask was evacuated and flushed with argon three times. Degassed benzene (20 mL) and degassed *t*-BuOH (6 mL) were added via syringe and the solid was dissolved under sonication. The 3-hydroxybenzo[*b*]thiophene-7-carboxylic acid **[134]** solution was added to the starting material **[96]** and the reaction was

stirred at reflux temperature until TLC analysis showed full consumption of the starting material (20 hours). Solvents were removed in vacuo. Purification by flash column chromatography (silica gel/crude material = 100/1, DCM/MeOH = 19/1 → MeOH) afforded the pure product **[136]**.

Yield	78% (625 mg; 1.24 mmol)
Appearance	yellow crystals
Melting point	190.0 – 193.0 °C
TLC-Analysis	0.3 (DCM/MeOH = 9/1)
Sum formula	$C_{29}H_{26}FNO_4S$
HR-MS	$[M+H]^+$: calculated: 504.1639 Da, found: 504.1675 Da, difference: 3.6 mDa
^{1}H-NMR (400 MHz, MeOD)	δ = 1.39 – 1.62 (m, 2H, CH_2-C<u>H</u>$_2$-CH_2-N$(CH_3)_2$), 2.21 (t, *J* = 7.9 Hz, 2H, C<u>H</u>$_2$-CH_2-CH_2-N$(CH_3)_2$), 2.32 (s, 6H, 2 x CH_3), 2.52 (t, *J* = 7.8 Hz, 2H, CH_2-CH_2-C<u>H</u>$_2$-N$(CH_3)_2$), 5.16 (d, *J* = 12.7 Hz, 1H, H3), 5.20 (d, *J* = 12.7 Hz, 1H, H3), 7.03 (dd, $^3J_{HH}$ = 8.8, $^3J_{HF}$ = 8.8 Hz, 2H, H3' & H5'), 7.37 (t, *J* = 7.5 Hz, 1H, H5''), 7.49 (d, *J* = 8.1 Hz, 1H, H7), 7.55 (dd, $^3J_{HH}$ = 8.9, $^4J_{HF}$ = 5.3 Hz, 2H, H2' & H6'), 7.63 – 7.68 (m, 2H, H4 & H6), 7.77 (s, 1H, olefin-H), 7.94 (dd, *J* = 7.4, 1.4 Hz, 1H, H4''), 8.26 (dd, *J* = 7.4, 1.4 Hz, 1H, H6'') ppm.
^{13}C-NMR (101 MHz, MeOD)	δ = 22.6 (t, CH_2-<u>C</u>H$_2$-CH_2-N$(CH_3)_2$), 39.7 (t, <u>C</u>H$_2$-CH_2-CH_2-N$(CH_3)_2$), 44.7 (q, 2C, 2 x CH_3), 60.1 (t, CH_2-CH_2-<u>C</u>H$_2$-N$(CH_3)_2$), 72.6 (t, C3), 92.2 (s, C1), 116.0 (d/d, $^2J_{CF}$ = 21.5 Hz, 2C, C3' & C5'), 123.6 (d, C7), 124.8 (d, C4), 126.4 (d, C5''), 128.1 (d/d, $^3J_{CF}$ = 8.1 Hz, 2C, C2' & C6'), 129.1 (d, C4''), 132.3 (d, C6), 132.6 (s, C2'' or C3a'' or C7''), 133.7 (d, olefin-C), 134.0 (s, C2'' or C3a'' or C7''), 134.9 (s, C2'' or C3a'' or C7''), 135.9 (s, C3a or C5), 137.9 (d, C6''), 141.5 (s, C3a or C5), 142.0 (s/d, $^4J_{CF}$ = 3.1 Hz, C1'), 147.4 (s, C7a), 149.0 (s, C7a''), 163.3 (s/d, $^1J_{CF}$ = 244.1 Hz, C4'), 172.2 (s, acid), 191.0 (s, ketone) ppm.
Optical rotation	$[\alpha]_D^{20}$ = +65.7 (c = 0.4, MeOH)

E III.9.3 Methyl *(S)*-2-((1-(3-(dimethylamino)propyl)-1-(4-fluorophenyl)-1,3-dihydroisobenzofuran-5-yl)methylene)-3-oxo-2,3-dihydrobenzo[*b*]thiophene-7-carboxylate [137]

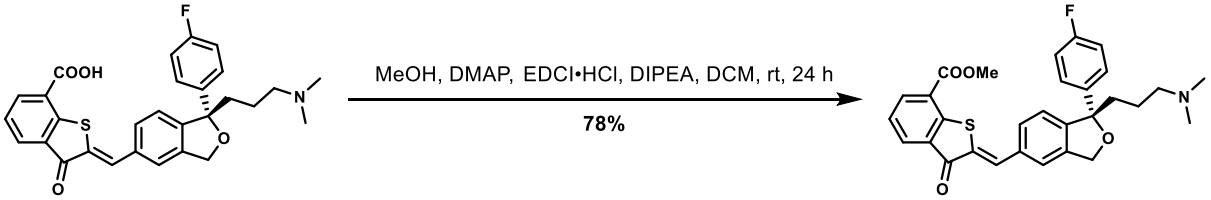

[136]
503.59 g/mol

[137]
517.62 g/mol

Acid **[136]** (50 mg, 0.099 mmol, 1 equiv.) was dissolved in dry MeOH (3 mL) and dry DCM (2 mL). DMAP (6 mg, 0.050 mmol, 0.5 equiv.), EDCI•HCl (29 mg, 0.149 mmol, 1.5 equiv.) and DIPEA (19 mg, 0.149 mmol, 1.5 equiv.) were added. The flask was flushed with argon and the reaction was stirred at room temperature for 24 hours. Solvents were removed in vacuo. The residue was dissolved in $CHCl_3$, washed with satd. aqu. NH_4Cl solution and dried over $MgSO_4$. After evaporation of the solvent purification by flash column chromatography (silica gel/crude material = 100/1, DCM/MeOH = 19/1 → 9/1) afforded the pure product **[137]**.

Yield	78% (40 mg; 0.077 mmol)
Appearance	yellow crystals
Melting point	104.0 – 108.0 °C
TLC-Analysis	R_f = 0.6 (DCM/MeOH = 4/1)
Sum formula	$C_{30}H_{28}FNO_4S$
HR-MS	$[M+H]^+$: calculated: 518.1796 Da, found: 518.1812 Da, difference: 1.6 mDa
^{1}H-NMR (400 MHz, $CDCl_3$)	δ = 1.36 – 1.63 (m, 2H, CH_2-C<u>H</u>$_2$-CH_2-N$(CH_3)_2$), 2.14 – 2.28 (m, 2H, C<u>H</u>$_2$-CH_2-CH_2-N$(CH_3)_2$), 2.24 (s, 6H, 2 x CH_3), 2.38 (t, *J* = 7.0 Hz, 2H, CH_2-CH_2-C<u>H</u>$_2$-N$(CH_3)_2$), 4.02 (s, 3H, COOMe), 5.20 (d, *J* = 12.6 Hz, 1H, H3), 5.25 (d, *J* = 12.6 Hz, 1H, H3), 7.01 (dd, $^3J_{HH}$ = 8.7, $^3J_{HF}$ = 8.7 Hz, 2H, H3' & H5'), 7.37 – 7.43 (m, 2H, H7 & H5''), 7.47 (dd, $^3J_{HH}$ = 8.9, $^4J_{HF}$ = 5.3 Hz, 2H, H2' & H6'), 7.64 (s, 1H, H4), 7.69 (dd, *J* = 8.0, 1.0 Hz, 1H, H6), 7.95 (s, 1H, olefin-H), 8.12 (dd, *J* = 7.5, 1.4 Hz, 1H, H4''), 8.29 (dd, *J* = 7.6, 1.4 Hz, 1H, H6'') ppm.

^{13}C-NMR (101 MHz, $CDCl_3$) δ = 21.9 (t, CH_2-$\underline{C}H_2$-CH_2-$N(CH_3)_2$), 39.1 (t, $\underline{C}H_2$-CH_2-CH_2-$N(CH_3)_2$), 45.0 (q, 2C, 2 x CH_3), 52.8 (q, COOMe), 59.4 (t, CH_2-CH_2-$\underline{C}H_2$-$N(CH_3)_2$), 71.8 (t, C3), 91.0 (s, C1), 115.3 (d/d, $^2J_{CF}$ = 21.3 Hz, 2C, C3' & C5'), 122.7 (d, C7), 123.7 (d, C4), 124.8 (s, C3a'' or C7''), 125.6 (d, C5''), 126.9 (d/d, $^3J_{CF}$ = 8.0 Hz, 2C, C2' & C6'), 131.1 (d, C4''), 131.4 (s, C2''), 131.7 (d, C6), 132.3 (s, C3a'' or C7''), 134.1 (s, C3a or C5), 134.4 (d, olefin-C), 136.7 (d, C6''), 140.3 (s/d, $^4J_{CF}$ = 3.1 Hz, C1'), 140.4 (s, C3a or C5), 146.8 (s, C7a), 148.7 (s, C7a''), 162.1 (s/d, $^1J_{CF}$ = 245.8 Hz, C4'), 165.9 (s, ester), 188.3 (s, ketone) ppm.

Optical rotation $[\alpha]_D^{20}$ = +7.8 (c = 1.0, DCM)

E III.9.4 Ethyl *(S)*-2-((1-(3-(dimethylamino)propyl)-1-(4-fluorophenyl)-1,3-dihydroisobenzofuran-5-yl)methylene)-3-oxo-2,3-dihydrobenzo[*b*]thiophene-7-carboxylate [138]

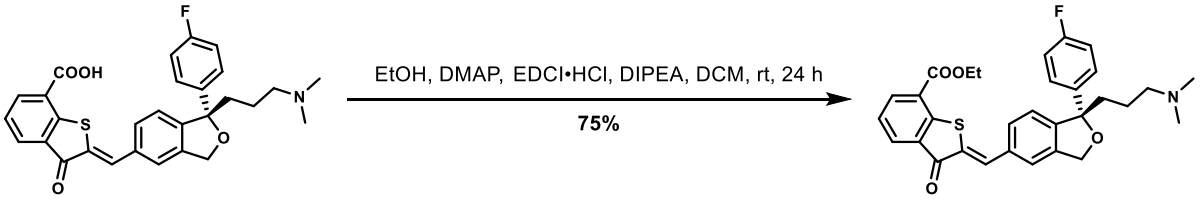

[136]
503.59 g/mol

[138]
531.19 g/mol

Acid **[136]** (50 mg, 0.099 mmol, 1 equiv.) was dissolved in dry EtOH (3 mL) and dry DCM (2 mL). DMAP (6 mg, 0.050 mmol, 0.5 equiv.), EDCI•HCl (29 mg, 0.149 mmol, 1.5 equiv.) and DIPEA (19 mg, 0.149 mmol, 1.5 equiv.) were added. The flask was flushed with argon and the reaction was stirred at room temperature for 24 hours. Solvents were removed in vacuo. The residue was dissolved in $CHCl_3$, washed with satd. aqu. NH_4Cl solution and dried over $MgSO_4$. After evaporation of the solvent purification by flash column chromatography (silica gel/crude material = 100/1, DCM/MeOH = 19/1 → 9/1) afforded the pure product **[138]**.

Yield 75% (39.5 mg; 0.074 mmol)

Appearance yellow crystals

Melting point 106.0 – 110.0 °C

TLC-Analysis R_f = 0.5 (DCM/MeOH = 4/1)

Sum formula $C_{31}H_{30}FNO_4S$

HR-MS $[M+H]^+$: calculated: 532.1952 Da, found: 532.1971 Da, difference: 1.9 mDa

^{1}H-NMR (400 MHz, $CDCl_3$) δ = 1.36 – 1.60 (m, 2H, CH_2-C<u>H</u>$_2$-CH_2-N(CH_3)$_2$), 1.46 (t, *J* = 7.1 Hz, 3H, OCH_2-C<u>H</u>$_3$), 2.14 – 2.26 (m, 2H, C<u>H</u>$_2$-CH_2-CH_2-N(CH_3)$_2$), 2.23 (s, 6H, 2 x CH_3), 2.37 (t, *J* = 7.0 Hz, 2H, CH_2-CH_2-C<u>H</u>$_2$-N(CH_3)$_2$), 4.48 (q, *J* = 7.1 Hz, 2H, OC<u>H</u>$_2$-CH_3), 5.19 (d, *J* = 12.6 Hz, 1H, H3), 5.25 (d, *J* = 12.6 Hz, 1H, H3), 7.00 (dd, $^3J_{HH}$ = 8.7, $^3J_{HF}$ = 8.7 Hz, 2H, H3' & H5'), 7.36 – 7.42 (m, 2H, H7 & H5''), 7.47 (dd, $^3J_{HH}$ = 8.9, $^4J_{HF}$ = 5.3 Hz, 2H, H2' & H6'), 7.64 (s, 1H, H4), 7.69 (dd, *J* = 7.5, 1.2 Hz, 1H, H6), 7.95 (s, 1H, olefin-H), 8.12 (dd, *J* = 7.5, 1.4 Hz, 1H, H4''), 8.29 (dd, *J* = 7.6, 1.4 Hz, 1H, H6'') ppm.

^{13}C-NMR (101 MHz, $CDCl_3$) δ = 14.5 (q, OCH_2-<u>C</u>H_3), 21.9 (t, CH_2-<u>C</u>H_2-CH_2-N(CH_3)$_2$), 39.1 (t, <u>C</u>H_2-CH_2-CH_2-N(CH_3)$_2$), 45.1 (q, 2C, 2 x CH_3), 59.4 (t, CH_2-CH_2-<u>C</u>H_2-N(CH_3)$_2$), 62.0 (t, O<u>C</u>H_2-CH_3), 71.8 (t, C3), 91.0 (s, C1), 115.3 (d/d, $^2J_{CF}$ = 21.3 Hz, 2C, C3' & C5'), 122.6 (d, C7), 123.7 (d, C4), 125.1 (s, C3a'' or C7''), 125.5 (d, C5''), 126.9 (d/d, $^3J_{CF}$ = 8.1 Hz, 2C, C2' & C6'), 131.0 (d, C4''), 131.5 (s, C2''), 131.7 (d, C6), 132.3 (s, C3a'' or C7''), 134.1 (s, C3a or C5), 134.3 (d, olefin-C), 136.6 (d, C6''), 140.3 (s/d, $^4J_{CF}$ = 3.1 Hz, C1'), 140.4 (s, C3a or C5), 146.7 (s, C7a), 148.6 (s, C7a''), 162.0 (s/d, $^1J_{CF}$ = 245.7 Hz, C4'), 165.4 (s, ester), 188.3 (s, ketone) ppm.

Optical rotation $[\alpha]_D^{20}$ = +11.4 (c = 0.975, DCM)

E III.9.5 *(S)*-2-((1-(3-(Dimethylamino)propyl)-1-(4-fluorophenyl)-1,3-dihydroisobenzofuran-5-yl)methylene)-7-(piperidine-1-carbonyl)benzo[*b*]thiophen-3(2*H*)-one [<u>139</u>]

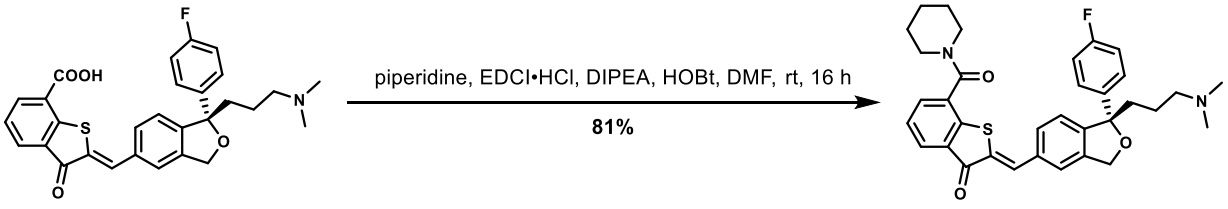

[<u>136</u>]
503.59 g/mol

[<u>139</u>]
570.72 g/mol

Acid **[<u>136</u>]** (50 mg, 0.099 mmol, 1 equiv.) was dissolved in dry DMF (1 mL). EDCI•HCl (21 mg, 0.109 mmol, 1.1 equiv.), HOBt (15 mg, 0.109 mmol, 1.1 equiv.) and DIPEA (27 mg, 0.209 mmol, 2.1 equiv.) were added. The flask was flushed with argon and the reaction was stirred at room temperature for 30 minutes. A solution of piperidine (8.5 mg, 0.099 mmol, 1 equiv.) in dry DMF (1 mL) was added via syringe and the reaction was stirred at room temperature for 16 hours. Solvents were removed in vacuo. The residue was dissolved in $CHCl_3$, washed with satd. aqu. NH_4Cl solution and dried over $MgSO_4$. After evaporation of the solvent purification by

flash column chromatography (silica gel/crude material = 100/1, DCM/MeOH = 19/1 → 9/1) afforded the pure product **[139]**.

Yield	81% (46 mg, 0.081 mmol)
Appearance	orange oil
TLC analysis	R_f = 0.5 (DCM/MeOH = 4/1)
Sum formula	$C_{34}H_{35}FN_2O_3S$
HR-MS	$[M+H]^+$: calculated: 571.2425 Da, found: 571.2442 Da, difference: 1.7 mDa
^{1}H-NMR (400 MHz, $CDCl_3$)	δ = 1.44 – 1.74 (m, 8H, CH_2-C$\underline{H}_2$-CH_2-N(CH_3)$_2$ & 3 x pip-CH_2), 2.17 – 2.30 (m, 2H, C$\underline{H}_2$-CH_2-CH_2-N(CH_3)$_2$), 2.38 (s, 6H, 2 x CH_3), 2.60 (t, *J* = 6.6 Hz, 2H, CH_2-CH_2-C$\underline{H}_2$-N(CH_3)$_2$), 3.27 – 3.86 (m, 4H, 2 x pip-CH_2), 5.17 (d, *J* = 12.6 Hz, 1H, H3), 5.23 (d, *J* = 12.7 Hz, 1H, H3), 6.99 (dd, $^3J_{HH}$ = 8.7, $^3J_{HF}$ = 8.7 Hz, 2H, H3' & H5'), 7.32 (t, *J* = 7.5 Hz, 1H, H5''), 7.42 (d, *J* = 7.9 Hz, 1H, H7), 7.46 (dd, $^3J_{HH}$ = 8.8, $^4J_{HF}$ = 5.3 Hz, 2H, H2' & H6'), 7.52 (dd, *J* = 7.4, 1.3 Hz, 1H, H6''), 7.55 (s, 1H, H4), 7.62 (d, *J* = 8.0 Hz, 1H, H6), 7.93 (s, 1H, olefin-H), 7.94 (dd, *J* = 7.7, 1.3 Hz, 1H, H4'') ppm.
^{13}C-NMR (101 MHz, $CDCl_3$)	δ = 21.0 (t, CH_2-C$\underline{H}_2$-CH_2-N(CH_3)$_2$), 24.5 & 26.0 & 26.6 (3xt, 3C, 3 x pip-C), 38.7 (t, C$\underline{H}_2$-CH_2-CH_2-N(CH_3)$_2$), 43.6 (t, pip-C), 44.2 (q, 2C, 2 x CH_3), 48.7 (t, pip-C), 58.8 (t, CH_2-CH_2-C$\underline{H}_2$-N(CH_3)$_2$), 71.8 (t, C3), 90.8 (s, C1), 115.4 (d/d, $^2J_{CF}$ = 21.3 Hz, 2C, C3' & C5'), 122.6 (d, C7), 123.5 (d, C4), 125.6 (d, C5''), 126.8 (d/d, $^3J_{CF}$ = 8.0 Hz, 2C, C2' & C6'), 127.8 (d, C4''), 130.5 (s, C2a''), 131.4 (s, C3a'' or C7''), 131.5 (d & s, 2C, C6 & C3a'' or C7''), 133.1 (d, C6''), 133.7 (d, olefin-C), 134.1 (s, C3a or C5), 139.9 (s/d, $^4J_{CF}$ = 3.1 Hz, C1'), 140.2 (s, C3a or C5), 145.0 (s, C7a''), 146.4 (s, C7a), 162.0 (s/d, $^1J_{CF}$ = 245.9 Hz, C4'), 167.0 (s, amide), 188.3 (s, ketone) ppm.
Optical rotation	$[\alpha]_D^{20}$ = +16.2 (c = 0.5, DCM)

E III.10 Azo-Paroxetine

E III.10.1 *N*-Benzyl-3-(4-nitrophenyl)acrylamide [141]

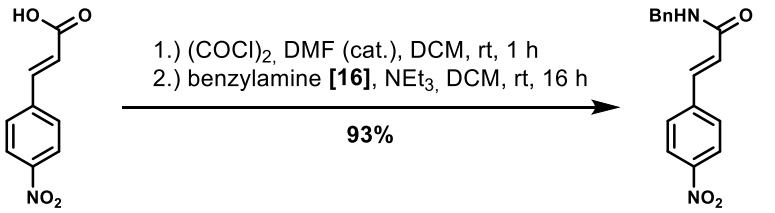

[140]
193.16 g/mol

[141]
282.30 g/mol

4-Nitrocinnamic acid **[140]** (25.00 g, 129 mmol, 1 equiv.) was placed in a round bottom flask and the flask was evacuated and flushed with argon three times. Dry DCM (435 mL, 0.3 M relative to the starting material) and dry DMF (1 drop) were added via syringe. Oxalylchloride (33.3 mL, 388 mmol, 3 equiv.) was added dropwise under argon and the mixture was stirred at room temperature. After 1 hour TLC (sample quenched with MeOH) indicated full consumption of the starting material. The intermediate was obtained by removing the volatiles in vacuo. The isolated acid chloride was dissolved in dry DCM (425 mL) under argon. Benzylamine **[16]** (13.87 g, 129 mmol, 1 equiv.) and NEt_3 (13.10 g, 129 mmol, 1 equiv.) were added and the mixture was stirred at room temperature for 16 hours. The reaction was washed with 1 N HCl (400 mL) and 1 N NaOH (400 mL). Volatiles were removed in vacuo and the obtained crude material was purified by recrystallization from toluene to afford the pure product.

Yield	93% (33.97 g, 120 mmol)
Appearance	pale yellow crystals
Melting point	189.5 – 190.0 °C (Lit.[216]: 188 – 190 °C)
TLC-Analysis	R_f = 0.50 (LP/EtOAc = 1/1)
Sum formula	$C_{16}H_{14}N_2O_3$
GC-MS	282 (17, M^+), 130 (29), 106 (100), 104 (32), 103 (29), 102 (83)
^{1}H-NMR (400 MHz, $CDCl_3$)	δ = 4.60 (d, *J* = 5.7 Hz, 2H, N-CH_2), 5.97 (br s, 1H, NH), 6.53 (d, *J* = 15.6 Hz, 1H, Ar-CH=C<u>H</u>-), 7.28 – 7.40 (m, 5H, H2' & H3' & H4' & H5' & H6'), 7.64 (d, *J* = 8.8 Hz, 2H, H2 & H6), 7.72 (d, *J* = 15.6 Hz, 1H, Ar-C<u>H</u>=CH-), 8.23 (d, *J* = 8.8 Hz, 2H, H3 & H5) ppm.

^{13}C-NMR (101 MHz, $CDCl_3$) δ = 44.2 (t, N-CH_2), 124.3 (d, 2C, C3 & C5), 124.6 (d, Ar-CH=CH-), 128.0 (d, C4'), 128.1 & 128.5 & 129.0 (3xd, 6C, C2 & C6 & C2' & C3' & C5' & C6'), 137.9 (s, C1'), 139.0 (d, Ar-CH=CH-), 141.1 (s, C1), 148.3 (s, C4), 164.7 (s, amide) ppm.

The assignments of protons and carbon atoms in the NMR code of compounds **[141]** and **[149]** were carried out as follows:

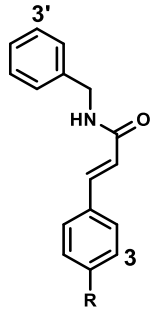

E III.10.2 Methyl (±)-*cis*-1-benzyl-4-(4-nitrophenyl)-6-oxopiperidine-3-carboxylate *cis*-[142]; Methyl (±)-*trans*-1-benzyl-4-(4-nitrophenyl)-6-oxopiperidine-3-carboxylate *trans*-[142]

[141]
282.30 g/mol

46%

***cis*-[142]**
368.39 g/mol

32%

***trans*-[142]**
368.39 g/mol

The piperidinone products ***cis*-[142]** and ***trans*-[142]** were prepared via a double Michael-addition in analogy to a literature procedure[164]. An oven-dried Schlenk flask equipped with a magnetic stirring bar was charged with the amide **[141]** (565 mg, 2 mmol, 1 equiv.). The flask was closed with a septum and evacuated and flushed with argon three times. Dry DCE (2.00 mL, 1.0 M relative to the amide **[141]**), methyl acrylate (172 mg, 2 mmol, 1 equiv.) and dry NEt_3 (195 µL, 1.4 mmol, 0.7 equiv.) were added. TBSOTf (0.55 mL, 2.4 mmol, 1.2 equiv.) was added dropwise via syringe. *t*-BuOH (47.5 µL, 0.5 mmol, 0.25 equiv.) was added to the suspension, which was then stirred at room temperature for 16 hours. In the course of the reaction the mixture became homogeneous. The reaction was partitioned between EtOAc (50 mL) and satd. aqu. $NaHCO_3$ (50 mL). Phases were separated and the aqu. phase was extracted with EtOAc (2 x 20 mL). The combined organic phases were washed with brine (50 mL) and dried over $MgSO_4$. Volatiles were removed in vacuo, affording the crude material. Purification

by flash column chromatography (silica gel/crude material = 100/1, LP/EtOAc = 7/3 → 35/65) afforded the desired products.

Yield	78% (572 mg, 1.55 mmol)
	cis-[142]: 46% (336 mg, 0.91 mmol)
	trans-[142]: 32% (236 mg, 0.64 mmol)

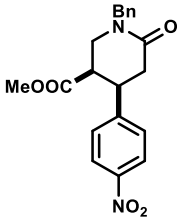

***cis*-[142]**

Appearance	colorless crystals
Melting point	117.5 – 118.0 °C
TLC analysis	R_f = 0.20 (LP/EtOAc = 1/1)
Sum formula	$C_{20}H_{20}N_2O_5$
HR-MS	$[M+H]^+$: calculated: 369.1445 Da, found: 369.1469 Da, difference: 2.4 mDa
GC-MS	368 (33, M^+), 191 (17), 176 (23), 132 (13), 119 (25), 118 (13), 115 (10), 106 (14), 104 (11), 91 (100)
^{1}H-NMR (400 MHz, $CDCl_3$)	δ = 2.97 (d, *J* = 5.7 Hz, 1H, H5), 3.18 – 3.24 (m, 1H, H3), 3.26 – 3.33 (m, 1H, H2), 3.44 (dd, *J* = 12.7, 4.9 Hz, 1H, H2), 3.58 (s, 3H, O-CH_3), 3.77 – 3.82 (m, 1H, H4), 4.53 (d, *J* = 14.3 Hz, 1H, N-CH_2), 4.82 (d, *J* = 14.3 Hz, 1H, N-CH_2), 7.19 – 7.22 (m, 2H, H2' & H6'), 7.29 – 7.39 (m, 5H, H2'' & H3'' & H4'' & H5'' & H6''), 8.08 (d, *J* = 8.8 Hz, 2H, H3' & H5') ppm.
^{13}C-NMR (101 MHz, $CDCl_3$)	δ = 36.0 (t, C5), 39.6 (d, C4), 43.6 (d, C3), 45.0 (t, C2), 50.6 (t, N-CH_2), 52.2 (q, O-CH_3), 123.9 (d, 2C, C3' & C5'), 128.0 (d, C4''), 128.6 & 128.7 & 128.9 (3xd, 6C, C2' & C6' & C2'' & C3'' & C5'' & C6''), 136.4 (s, C1''), 146.9 (s, C1'), 147.4 (s, C4'), 167.9 (s, lactam), 170.6 (s, ester) ppm.

The assignments of protons and carbon atoms in the NMR codes of compounds ***cis*-[142]**, ***trans*-[142]**, ***rac*-[143]**, **[144]**, ***cis*-[150]**, ***trans*-[150]**, ***rac*-[151]** and **[152]** were carried out as follows:

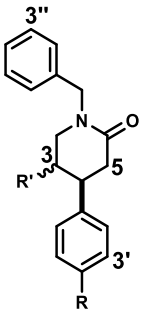

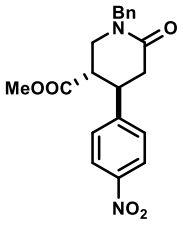

***trans*-[142]**

Appearance	colorless crystals
Melting point	132.0 – 132.5 °C
TLC analysis	R_f = 0.35 (LP/EtOAc = 1/1)
Sum formula	$C_{20}H_{20}N_2O_5$
HR-MS	$[M+H]^+$: calculated: 369.1445 Da, found: 369.1461 Da, difference: 1.6 mDa
GC-MS	68 (23, M^+), 191 (12), 176 (17), 132 (10), 119 (14), 118 (10), 106 (12), 104 (10), 91 (100)
^{1}H-NMR (400 MHz, $CDCl_3$)	δ = 2.65 (dd, *J* = 17.7, 10.7 Hz, 1H, H5), 2.86 (dd, *J* = 17.7, 5.7 Hz, 1H, H5), 3.05 (td, *J* = 9.9, 5.3 Hz, 1H, H3), 3.42 (dd, *J* = 12.5, 5.3 Hz, 1H, H2), 3.46 (s, 3H, O-CH_3), 3.50 – 3.59 (m, 2H, H4 & H2), 4.56 (d, *J* = 14.5 Hz, 1H, N-CH_2), 4.76 (d, *J* = 14.5 Hz, 1H, N-CH_2), 7.27 – 7.39 (m, 7H, H2' & H6' & H2'' & H3'' & H4'' & H5'' & H6''), 8.18 (d, *J* = 8.7 Hz, 2H, H3' & H5') ppm.
^{13}C-NMR (101 MHz, $CDCl_3$)	δ = 38.0 (t, C5), 41.6 (d, C4), 46.2 (d, C3), 47.9 (t, C2), 50.2 (t, N-CH_2), 52.4 (q, O-CH_3), 124.3 (d, 2C, C3' & C5'), 128.0 (d, C4''), 128.2 & 128.4 & 128.9 (3xd, 6C, C2' & C6' & C2'' & C3'' & C5'' & C6''), 136.4 (s, C1''), 147.3 (s, C4'), 148.6 (s, C1'), 167.6 (s, lactam), 171.5 (s, ester) ppm.

E III.10.3 Methyl (±)-*trans*-1-benzyl-4-(4-nitrophenyl)-6-oxopiperidine-3-carboxylate *trans*-[142]

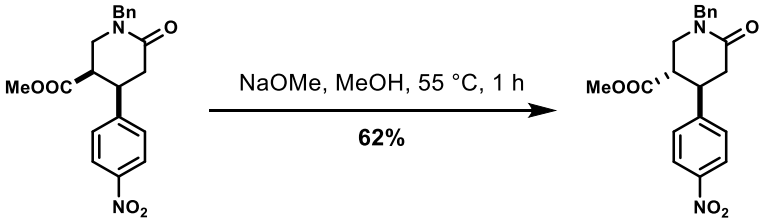

***cis*-[142]**
368.39 g/mol

***trans*-[142]**
368.39 g/mol

Compound ***cis*-[142]** (395 mg, 1.07 mmol, 1 equiv.) was placed in a round bottom flask equipped with a magnetic stirring bar. The flask was closed with a septum and was evacuated and flushed with argon three times. Dry MeOH (16 mL, 0.067 M relative to the starting material) was added to dissolve the starting material. NaOMe (157 mg, 2.9 mmol, 2.7 equiv.) was added to the solution and the reaction was stirred under heating for 1 hour (oilbath set to 55 °C). The reaction mixture was partitioned between EtOAc (200 mL) and satd. aqu. NH_4Cl (150 mL). H_2O (100 mL) was added to dissolve the precipitate. Phases were separated and the aqu. phase was extracted with EtOAc (3 x 50 mL). The combined organic phases were washed with satd. aqu. $NaHCO_3$ (250 mL) and brine (250 mL). Then the organic phase was dried over $MgSO_4$. Volatiles were removed in vacuo to afford the crude material. The product ***trans*-[142]** was obtained after purification via flash column chromatography (silica gel/crude material = 100/1, LP/EtOAc = 3/2 → 1/4).

Yield 62% (244 mg, 0.66 mmol)

Characterization of ***trans*-[142]** see previous section.

E III.10.4 (±)-*trans*-(1-Benzyl-4-(4-nitrophenyl)piperidin-3-yl)methanol *rac*-[143]

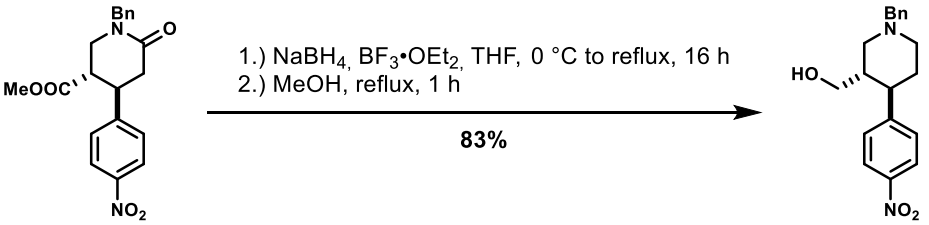

***trans*-[142]**
368.39 g/mol

***rac*-[143]**
326.40 g/mol

Alcohol ***rac*-[143]** was synthesized in analogy to a literature procedure[166]. BF_3•OEt_2 (3.08 mL, 24.95 mmol, 4 equiv.) was added dropwise via syringe to a suspension of $NaBH_4$ (943 mg, 24.95 mmol, 4 equiv.) in dry THF (20.8 mL, 0.3 M relative to the starting material) under argon.

The mixture was stirred at 0 °C for 1 hour. Afterwards, a solution of ***trans*-[142]** (2298 mg, 6.24 mmol, 1 equiv.) in dry THF (31.2 mL, 0.2 M relative to the starting material, final concentration: 0.1 M) was added via syringe. The resulting mixture was stirred at reflux temperature for 16 hours, whereupon it was carefully quenched with 1 N NaOH (60 mL). The reaction was partitioned between EtOAc (400 mL) and 1 N NaOH (400 mL). Phases were separated and the aqu. phase was extracted with EtOAc (3 x 50 mL). The combined organic phases were washed with brine (300 mL). After drying over $MgSO_4$ and evaporation of the solvent the borane complex of the desired product was obtained. MeOH (12.4 mL) was added to the isolated material and the reaction was stirred at reflux temperature for 1 hour. Volatiles were removed in vacuo and the crude material was purified by flash column chromatography (silica gel/crude material = 100/1, $CHCl_3$/MeOH/NH_4OH = 100/10/1) affording the desired product.

Yield	83% (1700 mg, 5.21 mmol)
Appearance	pale yellow crystals
Melting point	104.0 – 105.0 °C
TLC analysis	R_f = 0.40 ($CHCl_3$/MeOH/NH_4OH = 100/10/1)
Sum formula	$C_{19}H_{22}N_2O_3$
HR-MS	$[M+H]^+$: calculated: 327.1703 Da, found: 327.1729 Da, difference: 2.6 mDa
^{1}H-NMR (400 MHz, $CDCl_3$)	δ = 1.25 (s, 1H, OH), 1.75 – 1.91 (m, 2H, H5), 2.01 – 2.12 (m, 3H, H2 & H3 & H6), 2.54 (td, *J* = 11.1, 4.5 Hz, 1H, H4), 2.96 – 3.02 (m, 1H, H6), 3.17 – 3.26 (m, 2H, O-CH_2 & H2), 3.37 (dd, *J* = 10.8, 2.7 Hz, 1H, O-CH_2), 3.56 (d, *J* = 13.1 Hz, 1H, N-CH_2), 3.61 (d, *J* = 13.1 Hz, 1H, N-CH_2), 7.26 – 7.37 (m, 5H, H2'' & H3'' & H4'' & H5'' & H6''), 7.39 (d, *J* = 8.8 Hz, 2H, H2' & H6'), 8.16 (d, *J* = 8.8 Hz, 2H, H3' & H5') ppm.
^{13}C-NMR (101 MHz, $CDCl_3$)	δ = 34.2 (t, C5), 44.0 (d, C3), 45.0 (d, C4), 53.8 (t, C6), 57.2 (t, C2), 63.6 & 63.8 (2xt, 2C, N-CH_2 & O-CH_2), 124.0 (d, 2C, C3' & C5'), 127.3 (d, C4''), 128.4 & 128.5 & 129.3 (3xd, 6C, C2' & C6' & C2'' & C3'' & C5'' & C6''), 138.2 (s, C1''), 146.8 (s, C4'), 152.7 (s, C1') ppm.

E III.10.5 ((±)-*trans*-1-Benzyl-4-(4-nitrophenyl)piperidin-3-yl)methyl acetate [144]

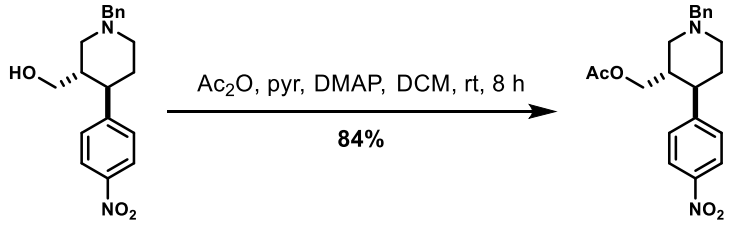

***rac*-[143]**
326.40 g/mol

[144]
368.43 g/mol

Acetic anhydride (26 µL, 0.270 mmol, 2 equiv.) was added to a solution of ***rac*-[143]** (46 mg, 0.135 mmol, 1 equiv.), pyridine (22 µL, 0.270 mmol, 2 equiv.) and DMAP (one crystal, cat.) in DCM (1.35 mL, 0.1 M) at 0 °C. The reaction was stirred at room temperature for 8 hours. Then the resulting mixture was washed with 1 N HCl. The organic phase was dried over $MgSO_4$ and after evaporation of the solvent in vacuo the crude product was obtained. Purification by flash column chromatography (silica gel/crude material = 100/1, LP/EtOAc = 1/1) afforded pure acetate **[144]**.

Yield	84% (50 mg, 0.114 mmol)
Appearance	colorless oil
TLC analysis	R_f = 0.50 (LP/EtOAc = 1/1)
Sum formula	$C_{21}H_{24}N_2O_4$
HR-MS	$[M+H]^+$: calculated: 369.1809 Da, found: 369.1823 Da, difference: 1.4 mDa
^{1}H-NMR (400 MHz, $CDCl_3$)	δ = 1.76 – 1.87 (m, 2H, H5), 1.92 (s, 3H, CH_3), 1.95 (t, *J* = 11.1 Hz, 1H, H2), 2.05 (td, *J* = 11.2, 3.6 Hz, 1H, H6), 2.22 – 2.32 (m, 1H, H3), 2.48 (td, *J* = 11.3, 5.0 Hz, 1H, H4), 2.96 – 3.02 (m, 1H, H6), 3.10 – 3.16 (m, 1H, H2), 3.53 (d, *J* = 13.1 Hz, 1H, N-CH_2), 3.60 – 3.66 (m, 2H, N-CH_2 & O-CH_2), 3.80 (dd, *J* = 11.3, 3.7 Hz, 1H, O-CH_2), 7.24 – 7.35 (m, 5H, H2'' & H3'' & H4'' & H5'' & H6''), 7.37 (d, *J* = 8.8 Hz, 2H, H2' & H6'), 8.16 (d, *J* = 8.7 Hz, 2H, H3' & H5') ppm.
^{13}C-NMR (101 MHz, $CDCl_3$)	δ = 20.8 (q, CH_3), 34.4 (t, C5), 41.0 (d, C3), 45.6 (d, C4), 53.5 (t, C6), 57.2 (t, C2), 63.3 (t, N-CH_2), 65.2 (t, O-CH_2), 124.1 (d, 2C, C3' & C5'), 127.3 (d, C4''), 128.4 & 128.4 & 129.2 (3xd, 6C, C2' & C6' & C2'' & C3'' & C5'' & C6''), 138.1 (s, C1''), 146.9 (s, C4'), 152.0 (s, C1'), 170.9 (s, ester) ppm.

E III.10.6 Determination of absolute configuration

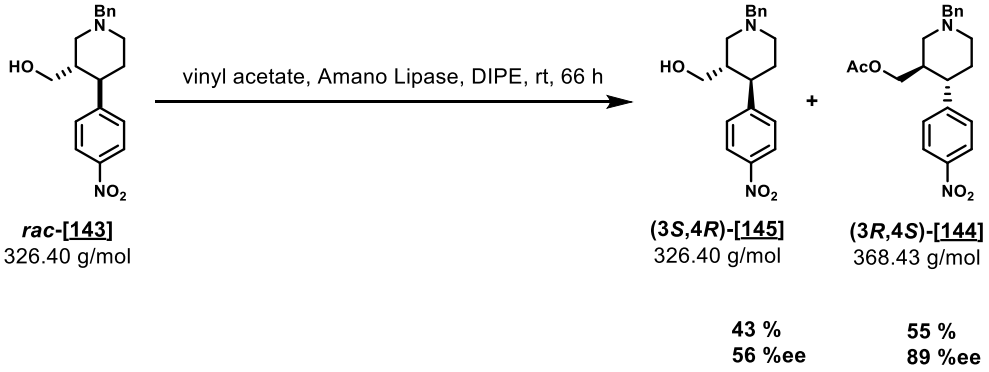

***rac*-[143]**
326.40 g/mol

(3*S*,4*R*)-[145]
326.40 g/mol

(3*R*,4*S*)-[144]
368.43 g/mol

43 %
56 %ee

55 %
89 %ee

Vinyl acetate (264 mg, 3.06 mmol, 10 equiv.) and Amano Lipase PS (100 mg, immobilized on diatomite, product 708011 from Sigma-Aldrich) were added to a solution of ***rac*-[143]** (100 mg, 0.31 mmol, 1 equiv.) in DIPE (15.3 mL, 0.02 M) at room temperature. Conversion and changes in ee composition were monitored by chiral HPLC. The mixture was stirred at room temperature for 66 hours. Then the mixture was filtered through pad of celite and DIPE was used for washing. Volatiles were removed in *vacuo*. Purification of the crude material by flash column chromatography (silica gel/crude material = 100/1, LP/EtOAc = 4/1 → EtOAc) afforded 43 mg of unreacted alcohol with 56% ee and 62 mg of acetate with 89% ee.

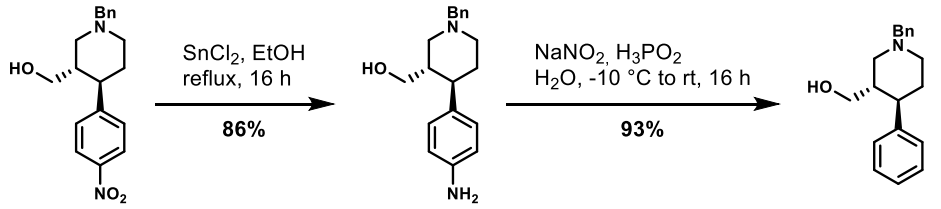

(3*S*,4*R*)-[145]
326.40 g/mol

(3*S*,4*R*)-[160]
326.40 g/mol

(3*S*,4*R*)-[163]
326.40 g/mol

56 %ee

56 %ee

56 %ee

$SnCl_2$ (100 mg, 0.53 mmol, 4 equiv.) was added to a solution of the obtained alcohol (43 mg, 0.13 mmol, 1 equiv., 56% ee) in EtOH (1.32 mL) and the mixture was stirred at reflux temperature for 16 hours. Volatiles were removed in vacuo. The residue was partitioned between EtOAc (2 mL) and satd. aqu. $NaHCO_3$ (2 mL). The mixture was filtered through a pad of celite and EtOAc was used for washing. Phases were separated. The organic phase was washed with brine and dried over $MgSO_4$. After evaporation of the solvent 33.5 mg (86%) of the aniline analog were obtained. The material was dissolved in 50% H_3PO_2 (1.11 mL) and H_2O (0.37 mL) and the solution was cooled to -10 °C. A solution of $NaNO_2$ (8.4 mg, 0.12 mmol, 1 equiv.) in H_2O (0.186 mL) was added to this solution. The reaction was stirred for 16 hours and subsequently partitioned between satd. aqu. $NaHCO_3$ (50 mL) and EtOAc (25 mL). Phases were separated and the aqu. phase was extracted with EtOAc (25 mL). The combined organic phases

were washed with brine and dried over $MgSO_4$. After evaporation of the solvent 29 mg (93%) of the product were obtained as a yellow oil.

Enantiomeric excess (ee) 56%

Optical rotation $[\alpha]_D^{23}$ = -8.2 (c = 1.0, $CHCl_3$)

^{1}H-NMR (400 MHz, $CDCl_3$) δ = 1.76 – 1.83 (m, 1H), 1.86 – 1.97 (m, 1H), 2.00 – 2.15 (m, 3H), 2.35 (td, *J* = 11.5, 4.1 Hz, 1H), 2.98 – 3.04 (m, 1H), 3.20 – 3.30 (m, 2H), 3.39 (dd, *J* = 10.9, 3.2 Hz, 1H), 3.59 (d, *J* = 13.1 Hz, 1H), 3.67 (d, *J* = 13.1 Hz, 1H), 7.19 – 7.40 (m, 10H) ppm.

Comment Spectral data are in accordance with the literature.[171, 217]

E III.10.7 (3*S*,4*R*)-(1-Benzyl-4-(4-nitrophenyl)piperidin-3-yl)methanol (3*S*,4*R*)-[143]

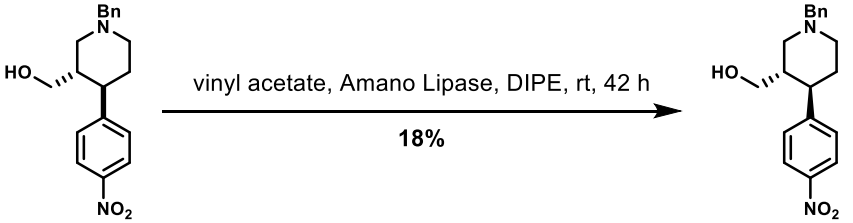

***rac*-[143]**
326.40 g/mol

(3*S*,4*R*)-[143]
326.40 g/mol

Vinyl acetate (1.32 g, 15.3 mmol, 10 equiv.) and Amano Lipase (1000 mg) were added to a solution of ***rac*-[143]** (500 mg, 1.53 mmol, 1 equiv.) in DIPE (30.6 mL, 0.05 M) at room temperature. Conversion and changes in ee composition were monitored by chiral HPLC. The mixture was stirred at room temperature for 42 hours. Then the mixture was filtered through a pad of celite and DIPE was used for washing. Volatiles were removed in vacuo. Purification of the crude material by flash column chromatography (silica gel/crude material = 100/1, silica gel/crude material = 100/1, LP/EtOAc = 4/1 → EtOAc) afforded pure alcohol **(3*S*,4*R*)-[143]**.

Yield 18% (91 mg, 0.28 mmol)

Characterization of **(3*S*,4*R*)-[143]** see previous section.

Enantiomeric excess (ee) 94%

Optical rotation $[\alpha]_D^{20}$ = -18.3 (c = 1.0, $CHCl_3$)

E III.10.8 (3*S*,4*R*)-3-((Benzo[*d*][1,3]dioxol-5-yloxy)methyl)-1-benzyl-4-(4-nitrophenyl)piperidine [145]

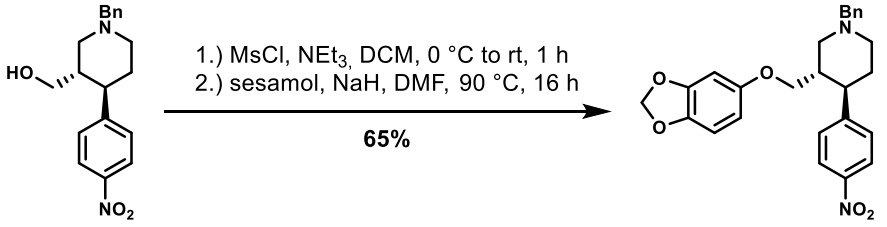

(3*S*,4*R*)-[143]
326.40 g/mol

[145]
446.50 g/mol

Ether **[145]** was synthesized in analogy to a literature procedure[172]. Alcohol **(3*S*,4*R*)-[143]** (91 mg, 0.279 mmol, 1 equiv.) was dissolved in dry DCM (1.39 mL, 0.2 M relative to alcohol **(3*S*,4*R*)-[143]**) and the solution was cooled to 0 °C under argon. NEt_3 (55 µL, 0.401 mmol, 1.44 equiv.) and MsCl (31 µL, 0.401 mmol, 1.44 equiv.) were added via syringe. The mixture was stirred at room temperature for 1 hour and afterwards diluted with H_2O (25 mL). The reaction was partitioned between satd. aqu. $NaHCO_3$ (25 mL) and DCM (50 mL). Phases were separated and the aqu. phase was extracted with DCM (3 x 25 mL). The combined organic phases were washed with brine (50 mL) and dried over $MgSO_4$. After evaporation of the solvent the crude mesylate was obtained. NaH (22 mg, 0.558 mmol, 2 equiv.) was added to a solution of sesamol (77 mg, 0.558 mmol, 2 equiv.) in dry DMF (2.32 mL, 0.24 M relative to sesamol) at 0 °C under argon. The mixture was stirred at room temperature for 20 minutes. A solution of the mesylate in dry DMF (1.16 mL, 0.24 M relative to the mesylate) was added to the phenolate solution via syringe. The reaction mixture was stirred at 90 °C (oil bath set to 96 °C) for 16 hours. The reaction was diluted with EtOAc (50 mL) and washed with H_2O (25 mL) and 1 N NaOH (2 x 25 mL). The combined organic phases were washed with brine (25 mL) and dried over $MgSO_4$. The solvent was removed in vacuo and the crude product was purified by flash column chromatography (silica gel/crude material = 100/1, LP/EtOAc = 9/1 → 6/4) yielding the desired product **[145]**.

Yield	65% (81 mg, 0.181 mmol)
Appearance	colorless oil
TLC analysis	R_f = 0.55 (LP/EtOAc = 1/1)
Sum formula	$C_{26}H_{26}N_2O_5$
HR-MS	$[M+H]^+$: calculated: 447.1915 Da, found: 447.1946 Da, difference: 3.1 mDa

^{1}H-NMR (400 MHz, $CDCl_3$) δ = 1.78 – 1.97 (m, 2H, H5), 2.07 – 2.21 (m, 2H, H2 & H6), 2.23 – 2.35 (m, 1H, H3), 2.70 (td, *J* = 11.6, 4.3 Hz, 1H, H4), 2.99 – 3.07 (m, 1H, H6), 3.18 – 3.26 (m, 1H, H2), 3.43 (dd, *J* = 9.4, 6.1 Hz, 1H, O-CH_2), 3.53 (dd, *J* = 9.4, 3.0 Hz, 1H, O-CH_2), 3.57 (d, *J* = 13.1 Hz, 1H, N-CH_2), 3.65 (d, *J* = 13.1 Hz, 1H, N-CH_2), 5.88 (s, 2H, H2''), 6.08 (dd, *J* = 8.5, 2.5 Hz, 1H, H6''), 6.29 (d, *J* = 2.5 Hz, 1H, H4''), 6.61 (d, *J* = 8.5 Hz, 1H, H7''), 7.27 – 7.40 (m, 7H, H2' & H6' & H2'' & H3'' & H4'' & H5'' & H6''), 8.14 (d, *J* = 8.8 Hz, 2H, H3' & H5') ppm.

^{13}C-NMR (101 MHz, $CDCl_3$) δ = 34.0 (t, C5), 42.1 (d, C3), 44.9 (d, C4), 53.7 (t, C6), 57.3 (t, C2), 63.4 (t, N-CH_2), 69.4 (t, O-CH_2), 98.0 (d, C4''), 101.2 (t, C2''), 105.5 (d, C6''), 108.0 (d, C7''), 124.0 (d, 2C, C3' & C5'), 127.3 (d, C4'''), 128.4 & 128.5 & 129.3 (3xd, 6C, C2' & C6' & C2''' & C3''' & C5''' & C6'''), 138.1 (s, C1'''), 141.8 (s, C7a''), 146.8 (s, C4'), 148.3 (s, C3a''), 152.3 (s, C1'), 154.3 (s, C5'') ppm.

Optical rotation $[\alpha]_D^{20}$ = -63.0 (c = 1.0, $CHCl_3$)

The assignments of protons and carbon atoms in the NMR code of compounds **[145]**, **[146]**, **[153]** and **[154]** were carried out as follows:

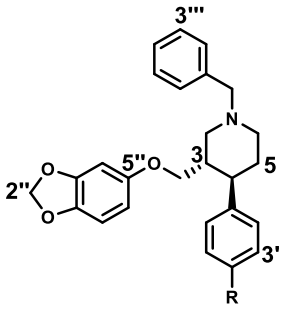

E III.10.9 4-((3*S*,4*R*)-3-((Benzo[*d*][1,3]dioxol-5-yloxy)methyl)piperidin-4-yl)aniline [146]

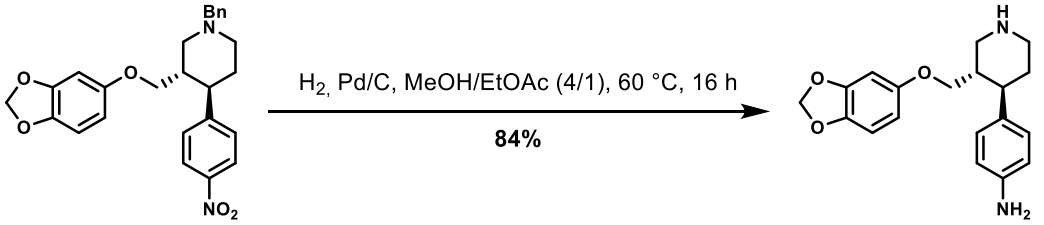

[145]
446.50 g/mol

[146]
326.40 g/mol

10% Pd/C (19 mg, 10 mol%) was added to a solution of the starting material **[145]** (78 mg, 0.175 mmol) in MeOH/EtOAc (1.75 mL, 4/1). The mixture was stirred under an atmosphere of H_2 at 60 °C for 16 hours. The mixture was filtered through a pad of celite (MeOH was used for washing). Volatiles were removed in vacuo and the crude material was purified by flash column chromatography (silica gel/crude material = 100/1, $CHCl_3$/MeOH/NH_4OH = 80/20/1) affording the desired aniline **[146]**.

Yield	84% (48 mg, 0.147 mmol)
Appearance	pale yellow oil
TLC analysis	R_f = 0.25 ($CHCl_3$/MeOH/NH_4OH = 80/20/1)
Sum formula	$C_{19}H_{22}N_2O_3$
HR-MS	$[M+H]^+$: calculated: 327.1703 Da, found: 327.1720 Da, difference: 1.7 mDa
^{1}H-NMR (400 MHz, $CDCl_3$)	δ = 1.65 – 1.83 (m, 2H, H5), 2.00 – 2.10 (m, 1H, H3), 2.45 (td, *J* = 11.6, 4.2 Hz, 1H, H4), 2.64 (t, *J* = 11.6 Hz, 1H, H2), 2.73 (td, *J* = 12.0, 2.9 Hz, 1H, H6), 3.18 (d, *J* = 12.3 Hz, 1H, H6), 3.40 – 3.47 (m, 2H, H2 & O-CH_2), 3.61 (dd, *J* = 9.4, 3.0 Hz, 1H, O-CH_2), 5.86 (s, 2H, H2''), 6.13 (dd, *J* = 8.5, 2.5 Hz, 1H, H6''), 6.34 (d, *J* = 2.5 Hz, 1H, H4''), 6.59 – 6.64 (m, 3H, H3' & H5' & H7''), 6.98 (d, *J* = 8.3 Hz, 2H, H2' & H6') ppm.
^{13}C-NMR (101 MHz, $CDCl_3$)	δ = 35.4 (t, C5), 42.9 (d, C3), 44.5 (d, C4), 47.2 (t, C6), 50.5 (t, C2), 69.8 (t, O-CH_2), 98.1 (d, C4''), 101.1 (t, C2''), 105.7 (d, C6''), 107.9 (d, C7''), 115.5 (d, 2C, C3' & C5'), 128.3 (d, 2C, C2' & C6'), 134.3 (s, C1'), 141.5 (s, C7a''), 144.9 (s, C4'), 148.2 (s, C3a''), 154.6 (s, C5'') ppm.
Optical rotation	$[\alpha]_D^{20}$ = -81.8 (c = 1.0, $CHCl_3$)

E III.10.10 (3*S*,4*R*)-3-((Benzo[*d*][1,3]dioxol-5-yloxy)methyl)-4-(4-(phenyldiazenyl)phenyl)piperidine [147]

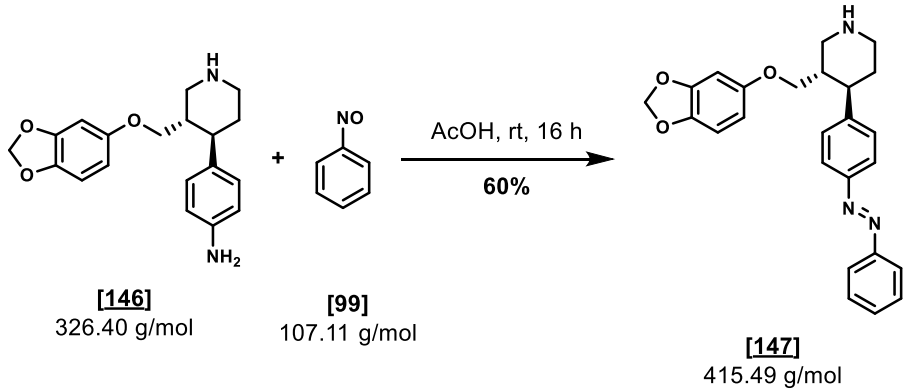

[146]
326.40 g/mol

[99]
107.11 g/mol

[147]
415.49 g/mol

Nitrosobenzene **[99]** (31.5 mg, 0.294 mmol, 2 equiv.) was added to a solution of aniline **[146]** (48 mg, 0.147 mmol, 1 equiv.) in AcOH (1.47 mL, 0.1 M) and the solution was stirred under argon at room temperature for 16 hours. The solution was basified with 1 N NaOH and the mixture was extracted with $CHCl_3$ (3 x 5 mL). The combined organic phases were washed with H_2O (10 mL) and dried over $MgSO_4$. After evaporation of the solvent the crude material was purified by flash column chromatography (silica gel/crude material = 100/1, $CHCl_3$/MeOH/NH_4OH = 100/10/1) affording the desired azo compound **[147]**.

Yield	60% (36.5 mg, 0.088 mmol)
Appearance	orange oil
TLC analysis	R_f = 0.55 ($CHCl_3$/MeOH/NH_4OH = 80/20/1)
Sum formula	$C_{19}H_{22}N_2O_3$
HR-MS	$[M+H]^+$: calculated: 416.1969 Da, found: 416.1987 Da, difference: 1.8 mDa
^{1}H-NMR (400 MHz, $CDCl_3$)	δ = 1.78 – 1.94 (m, 2H, H5), 2.15 – 2.26 (m, 1H, H3), 2.68 – 2.86 (m, 3H, H2 & H4 & H6), 3.26 (d, *J* = 12.2 Hz, 1H, H6), 3.45 – 3.52 (m, 2H, H2 & O-CH_2), 3.62 (dd, *J* = 9.5, 3.0 Hz, 1H, O-CH_2), 5.87 (s, 2H, H2''), 6.13 (dd, *J* = 8.5, 2.5 Hz, 1H, H6''), 6.35 (d, *J* = 2.5 Hz, 1H, H4''), 6.61 (d, *J* = 8.5 Hz, 1H, H7''), 7.37 (d, *J* = 8.4 Hz, 2H, H2' & H6'), 7.44 – 7.48 (m, 1H, H4'''), 7.48 – 7.54 (m, 2H, H3''' & H5'''), 7.86 (d, *J* = 8.4 Hz, 2H, H3' & H5'), 7.88 – 7.91 (m, 2H, H2''' & H6''') ppm.

^{13}C-NMR (101 MHz, $CDCl_3$) δ = 34.9 (t, C5), 42.7 (d, C3), 45.3 (d, C4), 46.9 (t, C6), 50.2 (t, C2), 69.6 (t, O-CH_2), 98.1 (d, C4''), 101.2 (t, C2''), 105.7 (d, C6''), 108.0 (d, C7''), 122.9 (d, 2C, C2''' & C6'''), 123.3 (d, 2C, H3' & H5'), 128.3 (d, 2C, H2' & H6'), 129.2 (d, 2C, C3''' & C5'''), 131.0 (d, C4'''), 141.7 (s, C7a''), 147.6 (s, C1'), 148.3 (s, C3a''), 151.7 (s, C4'), 152.8 (s, C1'''), 154.5 (s, C5'') ppm.

Optical rotation $[\alpha]_D^{20}$ = -109.9 (c = 0.5, $CHCl_3$)

The assignments of protons and carbon atoms in the NMR code of compound **[147]** were carried out as follows:

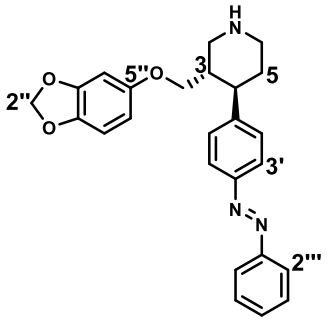

E III.11 HTI-Paroxetine

E III.11.1 *N*-Benzyl-3-(4-bromophenyl)acrylamide [149]

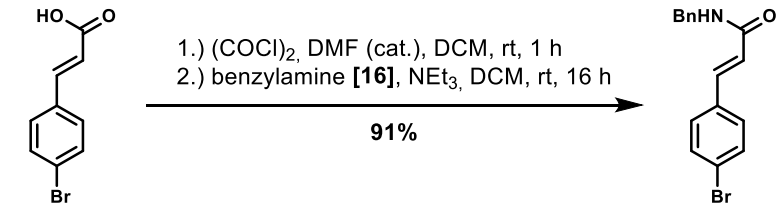

[148]
227.06 g/mol

[149]
316.20 g/mol

4-Bromocinnamic acid **[148]** (10.00 g, 44 mmol, 1 equiv.) was placed in a round bottom flask and the flask was evacuated and flushed with argon three times. Dry DCM (147 mL, 0.3 M relative to the starting material) and dry DMF (1 drop) were added via syringe. Oxalylchloride (11.33 mL, 132 mmol, 3 equiv.) was added dropwise under argon and the mixture was stirred at room temperature. After 1 hour TLC (sample quenched with MeOH) indicated full consumption of the starting material. The intermediate was obtained after removing the volatiles in vacuo. The isolated acid chloride was dissolved in dry DCM (147 mL) under argon. Benzylamine **[16]** (4.72 g, 44 mmol, 1 equiv.) and NEt_3 (4.46 g, 44 mmol, 1 equiv.) were added and the mixture was stirred at room temperature for 16 hours. The reaction was washed with

1 N HCl (100 mL) and 1 N NaOH (100 mL). Volatiles were removed in vacuo and the obtained crude material was purified by recrystallization from toluene to afford the pure product.

Yield 91% (12.64 g, 40 mmol)

Appearance colorless needles

Melting point 170.0 – 171.5 °C (Lit.[218]: 173 – 174 °C)

TLC-Analysis R_f = 0.65 (LP/EtOAc = 1/1)

Sum formula $C_{16}H_{14}BrNO$

GC-MS 317 (7, M^+), 315 (7, M^+), 131 (24), 107 (13), 106 (68), 104 (15), 103 (23), 102 (100), 101 (16)

^{1}H-NMR (400 MHz, $CDCl_3$) δ = 4.57 (d, *J* = 5.7 Hz, 2H, N-CH_2), 5.92 (s, 1H, NH), 6.39 (d, *J* = 15.6 Hz, 1H, Ar-CH=C<u>H</u>-), 7.27 – 7.38 (m, 7H, H2 & H6 or H3 & H5 & benzyl), 7.49 (d, *J* = 8.5 Hz, 2H, H2 & H6 or H3 & H5), 7.61 (d, *J* = 15.6 Hz, 1H, Ar-C<u>H</u>=CH-) ppm.

^{13}C-NMR (101 MHz, $CDCl_3$) δ = 44.1 (t, N-CH_2), 121.2 (d, Ar-CH=<u>C</u>H-), 124.0 (s, C4), 127.8 (d, C4'), 128.1 & 128.9 & 129.3 (3xd, 6C, C2, C6, C2', C3', C5', C6'), 132.2 (d, 2C, C3 & C5), 133.8 (s, C1), 138.2 (s, C1'), 140.3 (d, Ar-<u>C</u>H=CH-), 165.5 (s, amide) ppm.

E III.11.2 Methyl (±)-*cis*-1-benzyl-4-(4-bromophenyl)-6-oxopiperidine-3-carboxylate *cis*-[<u>150</u>]; Methyl (±)-*trans*-1-benzyl-4-(4-bromophenyl)-6-oxopiperidine-3-carboxylate *trans*-[<u>150</u>]

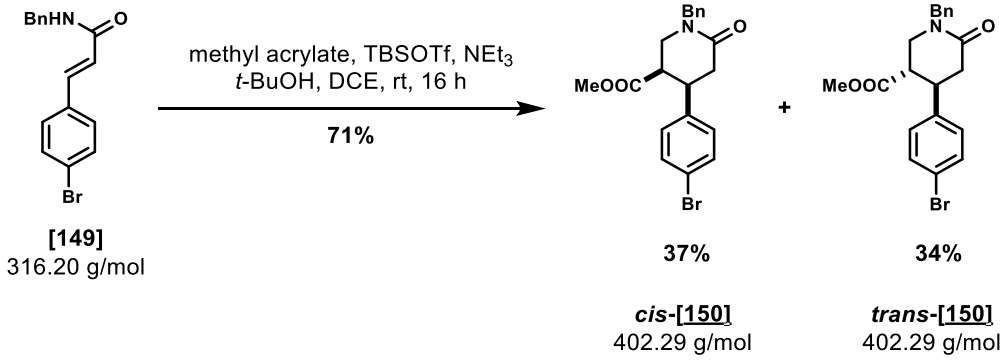

[149]
316.20 g/mol

37%

***cis*-[<u>150</u>]**
402.29 g/mol

34%

***trans*-[<u>150</u>]**
402.29 g/mol

The piperidinone products ***cis*-[<u>150</u>]** and ***trans*-[<u>150</u>]** were prepared via a double Michael-addition in analogy to a literature procedure[164]. The amide **[149]** (11.25 g, 35.6 mmol, 1 equiv.) was placed in a flask and the flask was closed with a septum and evacuated and flushed with argon three times. Dry DCE (35.6 mL, 1.0 M relative to the amide **[149]**), methyl acrylate (3.22 mL, 32.5 mmol, 1 equiv.) and NEt_3 (3.47 mL, 22.75 mmol, 0.7 equiv.) were added under argon. TBSOTf (9.8 mL, 39.0 mmol, 1.2 equiv.) was slowly added to the suspension. Then *t*-BuOH (0.84

mL, 8.125 mmol, 0.25 equiv.) was added and the resulting mixture was stirred at room temperature for 16 hours. The reaction was partitioned between EtOAc and satd. aqu. $NaHCO_3$. The organic phase was washed with brine before being dried over $MgSO_4$. The solvent was removed in vacuo and 17.35 g of crude material were obtained. The crude material was then purified by flash column chromatography (silica gel/crude material = 100/1, LP/EtOAc = 4/1 → 1/9).

Yield 71% (10.11 g, 25.13 mmol)

***cis*-[150]**: 37% (5.20 g, 12.93 mmol)

***trans*-[150]**: 34% (4.91 g, 12.21 mmol)

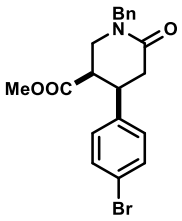

***cis*-[150]**

Appearance colorless oil

TLC analysis R_f = 0.20 (LP/EtOAc = 1/1)

Sum formula $C_{20}H_{20}BrNO_3$

HR-MS $[M+H]^+$: calculated: 402.0699 Da, found: 402.0710 Da, difference: 1.1 mDa

GC-MS 403 (4, M^+), 401 (3, M^+), 118 (10), 116 (14), 115 (13), 106 (10), 104 (14), 103 (13), 102 (15), 91 (100)

^{1}H-NMR (400 MHz, $CDCl_3$) δ = 2.84 – 2.97 (m, 2H, H5), 3.09 – 3.16 (m, 1H, H3), 3.28 (dd, *J* = 12.9, 9.4 Hz, 1H, H2), 3.37 (dd, *J* = 12.8, 5.3 Hz, 1H, H2), 3.58 (s, 3H, O-CH_3), 3.67 (m, 1H, H4), 4.60 (d, *J* = 14.4 Hz, 1H, N-CH_2), 4.71 (d, *J* = 14.4 Hz, 1H, N-CH_2), 6.89 (d, *J* = 8.5 Hz, 2H, H2' & H6'), 7.27 – 7.37 (m, 7H, H3' & H5' & H2'' & H3'' & H4'' & H5'' & H6'') ppm.

^{13}C-NMR (101 MHz, $CDCl_3$) δ = 36.5 (t, C5), 39.3 (d, C4), 43.7 (d, C3), 44.8 (t, C2), 50.6 (t, N-CH_2), 52.0 (q, O-CH_3), 121.6 (s, C4'), 127.9 (d, C4''), 128.6 & 128.8 & 129.4 (3xd, 6C, C2' & C6' & C2'' & C3'' & C5'' & C6''), 131.8 (d, 2C, C3' & C5'), 136.6 (s, C1''), 138.4 (s, C1'), 168.4 (s, lactam), 170.9 (s, ester) ppm.

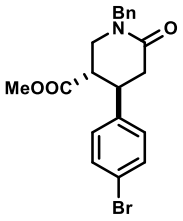

***trans*-[150]**

Appearance	colorless crystals
Melting point	154.5 – 155.0 °C
TLC analysis	R_f = 0.40 (LP/EtOAc = 1/1)
Sum formula	$C_{20}H_{20}BrNO_3$
HR-MS	$[M+H]^+$: calculated: 402.0699 Da, found: 402.0717 Da, difference: 1.8 mDa
GC-MS	403 (6, M^+), 401 (5, M^+), 116 (16), 115 (17), 104 (14), 103 (12), 102 (16), 91 (100)
^{1}H-NMR (400 MHz, $CDCl_3$)	δ = 2.61 (dd, *J* = 17.7, 10.5 Hz, 1H, H5), 2.82 (dd, *J* = 17.7, 5.7 Hz, 1H, H5), 2.96 (td, *J* = 9.6, 5.2 Hz, 1H, H3), 3.37 (dd, *J* = 12.4, 5.2 Hz, 1H, H2), 3.38 (td, *J* = 10.2, 5.7 Hz, 1H, H4), 3.46 (s, 3H, O-CH_3), 3.51 (dd, *J* = 12.4, 9.4 Hz, 1H, H2), 4.55 (d, *J* = 14.5 Hz, 1H, N-CH_2), 4.74 (d, *J* = 14.5 Hz, 1H, N-CH_2), 7.06 (d, *J* = 8.4 Hz, 2H, H2' & H6'), 7.25 – 7.37 (m, 5H, H2'' & H3'' & H4'' & H5'' & H6''), 7.43 (d, *J* = 8.5 Hz, 2H, H3' & H5') ppm.
^{13}C-NMR (101 MHz, $CDCl_3$)	δ = 38.1 (t, C5), 41.2 (d, C4), 46.6 (d, C3), 47.9 (t, C2), 50.2 (t, N-CH_2), 52.2 (q, O-CH_3), 121.3 (s, C4'), 127.8 (d, C4''), 128.4 & 128.9 & 128.9 (3xd, 6C, C2' & C6' & C2'' & C3'' & C5'' & C6''), 132.1 (d, 2C, C3' & C5'), 136.6 (s, C1''), 140.1 (s, C1'), 168.2 (s, lactam), 171.9 (s, ester) ppm.

E III.11.3 Methyl (±)-*trans*-1-benzyl-4-(4-bromophenyl)-6-oxopiperidine-3-carboxylate *trans*-[150]

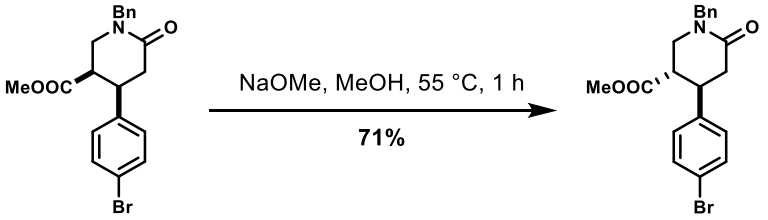

***cis*-[150]**
402.29 g/mol

***trans*-[150]**
402.29 g/mol

Compound ***cis*-[150]** (447 mg, 1.11 mmol, 1 equiv.) was placed in a round bottom flask equipped with a magnetic stirring bar. The flask was closed with a septum and was evacuated and flushed with argon three times. Dry MeOH (16.6 mL, 0.067 M relative to the starting material) was added to dissolve the starting material. NaOMe (166 mg, 3.06 mmol, 2.76 equiv.) was added to the solution and the reaction was stirred under heating for 1 hour (oilbath set to 55 °C). The reaction mixture was partitioned between EtOAc (200 mL) and satd. aqu. NH_4Cl (150 mL). H_2O (100 mL) was added to dissolve the precipitate. Phases were separated and the aqu. phase was extracted with EtOAc (3 x 50 mL). The combined organic phases were washed with satd. aqu. $NaHCO_3$ (150 mL) and brine (250 mL). Then the organic phase was dried over $MgSO_4$. Volatiles were removed in vacuo to afford the crude material. The product ***trans*-[150]** was obtained after purification via flash column chromatography (silica gel/crude material = 100/1, LP/EtOAc = 3/2 → EtOAc).

Yield 71% (317 mg, 0.79 mmol)

Characterization of ***trans*-[150]** see previous section.

E III.11.4 (±)-*trans*-(1-Benzyl-4-(4-nitrophenyl)piperidin-3-yl)methanol *rac*-[151]

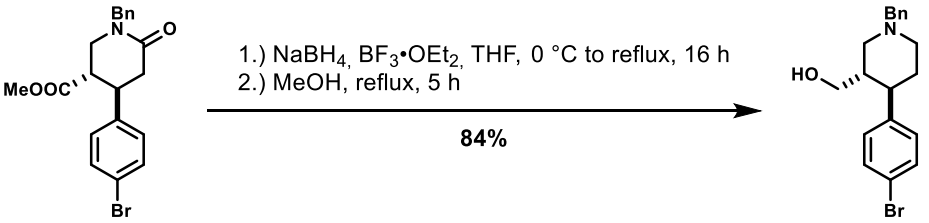

***trans*-[150]**
402.29 g/mol

***rac*-[151]**
360.30 g/mol

Alcohol ***rac*-[151]** was synthesized in analogy to a literature procedure[166]. BF_3•OEt_2 (0.126 mL, 0.99 mmol, 4 equiv.) was added dropwise via syringe to a suspension of $NaBH_4$ (37.6 mg, 0.99 mmol, 4 equiv.) in dry THF (1 mL, 0.25 M relative to the starting material) under argon. The

mixture was stirred at 0 °C for 1 hour. Afterwards, a solution of ***trans*-[150]** (100 mg, 0.25 mmol, 1 equiv.) in dry THF (1 mL + 0.5 mL) was added via syringe. The resulting mixture was stirred at reflux temperature for 16 hours, whereupon it was carefully quenched with 1 N NaOH. The reaction was partitioned between EtOAc and 1 N NaOH. Phases were separated and the aqu. phase was extracted with EtOAc (three times). The combined organic phases were washed with brine. After drying over $MgSO_4$ and evaporation of the solvent, the borane complex of the desired product was obtained. MeOH was added to the isolated material and the reaction was stirred at reflux temperature for 5 hours. Volatiles were removed in vacuo and the crude material was purified by flash column chromatography (silica gel/crude material = 100/1, $CHCl_3$/MeOH/NH_4OH = 100/10/1) affording the desired product.

Yield	84% (75 mg, 0.21 mmol)
Appearance	colorless crystals
Melting point	109.5 – 110.0 °C
TLC analysis	R_f = 0.25 (EtOAc)
Sum formula	$C_{19}H_{22}BrNO$
HR-MS	$[M+H]^+$: calculated: 360.0958 Da, found: 360.0973 Da, difference: 1.5 mDa
^{1}H-NMR (400 MHz, $CDCl_3$)	δ = 1.72 – 1.86 (m, 2H, H5), 1.94 – 2.07 (m, 3H, H2 & H3 & H6), 2.32 (td, *J* = 10.9, 4.9 Hz, 1H, H4), 2.93 – 3.00 (m, 1H, H6), 3.19 (dd, *J* = 7.6, 1.6 Hz, 1H, H2), 3.23 (dd, *J* = 10.9, 6.2 Hz, 1H, O-CH_2), 3.38 (dd, *J* = 11.0, 2.7 Hz, 1H, O-CH_2), 3.54 (d, *J* = 13.1 Hz, 1H, N-CH_2), 3.61 (d, *J* = 13.1 Hz, 1H, N-CH_2), 7.09 (d, *J* = 8.4 Hz, 2H, H2' & H6'), 7.24 – 7.36 (m, 5H, H2'' & H3'' & H4'' & H5'' & H6''), 7.41 (d, *J* = 8.4 Hz, 2H, H3' & H5') ppm.
^{13}C-NMR (101 MHz, $CDCl_3$)	δ = 34.4 (t, C5), 44.1 (d, C3), 44.6 (d, C4), 54.0 (t, C6), 57.4 (t, C2), 63.6 (t, N-CH_2), 64.1 (t, O-CH_2), 120.2 (s, C4'), 127.2 (d, C4''), 128.4 & 129.4 & 129.4 (3xd, 6C, C2' f& C6' & C2'' & C3'' & C5'' & C6''), 131.8 (d, 2C, C3' & C5'), 138.2 (s, C1''), 143.7 (s, C1') ppm.

E III.11.5 ((±)-*trans*-1-Benzyl-4-(4-bromophenyl)piperidin-3-yl)methyl acetate [152]

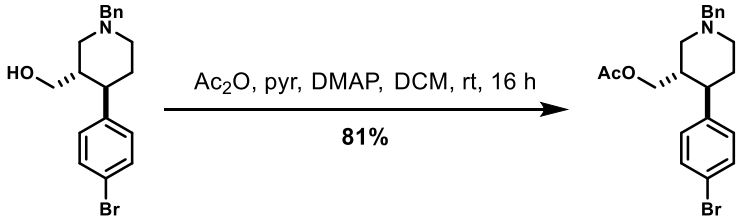

***rac*-[151]**
360.30 g/mol

[152]
402.33 g/mol

Acetic anhydride (23 µL, 0.222 mmol, 2 equiv.) was added to a solution of ***rac*-[151]** (40 mg, 0.111 mmol, 1 equiv.), pyridine (18 µL, 0.222 mmol, 2 equiv.) and DMAP (one crystal, cat.) in DCM (1.11 mL, 0.1 M) at 0 °C. The reaction was stirred at room temperature for 16 hours. Then the resulting mixture was washed with 1 N HCl. The organic phase was dried over $MgSO_4$ and after evaporation of the solvent in vacuo the crude product was obtained. Purification by flash column chromatography (silica gel/crude material = 100/1, LP/EtOAc = 5/1 → 1/1) afforded pure acetate **[152]**.

Yield	81% (36 mg, 0.09 mmol)
Appearance	colorless oil
TLC analysis	R_f = 0.65 (LP/EtOAc = 1/1)
Sum formula	$C_{21}H_{24}BrNO_2$
HR-MS	$[M+H]^+$: calculated: 402.1063 Da, found: 402.1089 Da, difference: 2.6 mDa
^{1}H-NMR (400 MHz, $CDCl_3$)	δ = 1.72 – 1.85 (m, 2H, H5), 1.88 – 1.92 (m, 1H, H2), 1.93 (s, 3H, CH_3), 2.03 (td, *J* = 11.1, 3.5 Hz, 1H, H6), 2.15 – 2.25 (m, 1H, H3), 2.30 (td, *J* = 11.2, 4.8 Hz, 1H, H4), 2.93 – 3.00 (m, 1H, H6), 3.07 – 3.16 (m, 1H, H2), 3.52 (d, *J* = 13.2 Hz, 1H, N-CH_2), 3.60 – 3.66 (m, 2H, N-CH_2 & O-CH_2), 3.81 (dd, *J* = 11.2, 3.5 Hz, 1H, O-CH_2), 7.07 (d, *J* = 8.4 Hz, 2H, H2' & H6'), 7.25 – 7.37 (m, 5H, H2'' & H3'' & H4'' & H5'' & H6''), 7.41 (d, *J* = 8.4 Hz, 2H, H3' & H5') ppm.
^{13}C-NMR (101 MHz, $CDCl_3$)	δ = 20.9 (q, CH_3), 34.5 (t, C5), 41.1 (d, C3), 45.1 (d, C4), 53.8 (t, C6), 57.5 (t, C2), 63.4 (t, N-CH_2), 65.5 (t, O-CH_2), 120.3 (s, C4'), 127.2 (d, C4''), 128.4 & 129.2 & 129.3 (3xd, 6C, C2' & C6' & C2'' & C3'' & C5'' & C6''), 131.8 (d, 2C, C3' & C5'), 138.3 (s, C1''), 143.1 (s, C1'), 171.0 (s, ester) ppm.

E III.11.6 Determination of absolute configuration

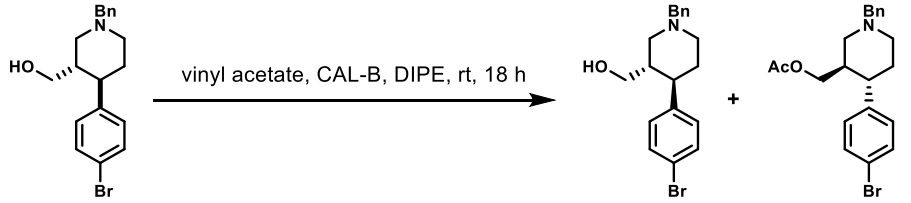

***rac*-[151]**
360.30 g/mol

(3*S*,4*R*)-[151]
360.30 g/mol

(3*R*,4*S*)-[152]
402.33 g/mol

40 %
80 %ee

54 %
59 %ee

Vinyl acetate (239 mg, 2.78 mmol, 10 equiv.) and CAL-B (100 mg, immobilized on Immobead 150, product 54326 from Sigma-Aldrich) were added to a solution of ***rac*-[151]** (100 mg, 0.28 mmol, 1 equiv.) in DIPE (13.9 mL, 0.02 M) at room temperature. Conversion and changes in ee composition were monitored by chiral HPLC. The mixture was stirred at room temperature for 18 hours. Then the mixture was filtered through pad of celite and DIPE was used for washing. Volatiles were removed in vacuo. Purification of the crude material by flash column chromatography (silica gel/crude material = 100/1, LP/EtOAc = 4/1 → EtOAc) afforded 40 mg of unreacted alcohol with 80% ee and 60 mg of acetate with 59% ee.

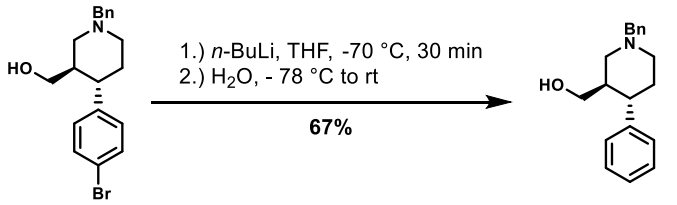

(3*R*,4*S*)-[151]
360.30 g/mol

(3*R*,4*S*)-[163]
326.40 g/mol

80 %ee

80 %ee

The isolated alcohol (80% ee) was dissolved in dry THF (1.11 mL) and cooled to -70 °C under argon. At this temperature *n*-BuLi (0.17 mL, 2.5 equiv., 1.6 M in hexane) was added and the reaction was stirred at -70 °C for 30 minutes. Satd. aqu. NH_4Cl (1 mL) was added and the reaction was slowly warmed to room temperature. The crude product was isolated by extraction with EtOAc (3 x 5 mL) and after purification by flash column chromatography (silica gel/crude material = 100/1, LP/EtOAc = 4/1 → EtOAc) pure product **[163]** was obtained in 67% yield.

Enantiomeric excess (ee) 80%

Optical rotation $[\alpha]_D^{23}$ = +13.4 (c = 1.0, $CHCl_3$)

^{1}H-NMR (400 MHz, $CDCl_3$) δ = 1.76 – 1.83 (m, 1H), 1.86 – 1.97 (m, 1H), 2.00 – 2.15 (m, 3H), 2.35 (td, *J* = 11.5, 4.1 Hz, 1H), 2.98 – 3.04 (m, 1H), 3.20 – 3.30 (m, 2H), 3.39 (dd, *J* = 10.9, 3.2 Hz, 1H), 3.59 (d, *J* = 13.1 Hz, 1H), 3.67 (d, *J* = 13.1 Hz, 1H), 7.19 – 7.40 (m, 10H) ppm.

Comment Spectral data are in accordance with the literature.[171, 217]

E III.11.7 (±)-*trans*-3-((Benzo[*d*][1,3]dioxol-5-yloxy)methyl)-1-benzyl-4-(4-bromophenyl)piperidine [153]

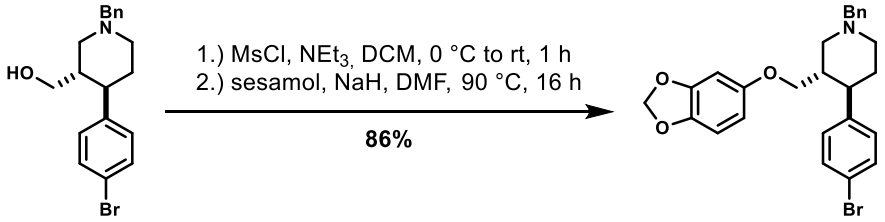

***rac*-[152]**
360.30 g/mol

[153]
480.40 g/mol

Ether **[153]** was synthesized in analogy to a literature procedure[172]. Alcohol ***rac*-[151]** (326 mg, 0.903 mmol, 1 equiv.) was dissolved in dry DCM (4.52 mL, 0.2 M relative to alcohol ***rac*-[151]**) and the solution was cooled to 0 °C under argon. NEt_3 (0.184 mL, 1.30 mmol, 1.44 equiv.) and MsCl (0.100 mL, 1.30 mmol, 1.44 equiv.) were added via syringe. The mixture was stirred at room temperature for 1 hour and afterwards diluted with H_2O (25 mL). The reaction was partitioned between satd. aqu. $NaHCO_3$ (25 mL) and DCM (50 mL). Phases were separated and the aqu. phase was extracted with DCM (3 x 25 mL). The combined organic phases were washed with brine (50 mL) and dried over $MgSO_4$. After evaporation of the solvent the crude mesylate was obtained. NaH (72.5 mg, 60% dispersion in mineral oil, 1.806 mmol, 2 equiv.) was added to a solution of sesamol (250 mg, 1.806 mmol, 2 equiv.) in dry DMF (3.8 mL) at 0 °C under argon. The mixture was stirred at room temperature for 20 minutes. A solution of the mesylate in dry DMF (3.8 mL) was added to the phenolate solution via syringe. The reaction mixture was stirred at 90 °C (oil bath set to 96 °C) for 16 hours. The reaction was diluted with EtOAc (50 mL) and washed with H_2O (25 mL) and 1 N NaOH (2 x 25 mL). The combined organic phases were washed with brine (25 mL) and dried over $MgSO_4$. The solvent was removed in vacuo and the crude product was purified by flash column chromatography (silica gel/crude material = 100/1, LP/EtOAc = 9/1 → 3/2) yielding the desired product **[153]**.

Yield 86% (372 mg, 0.774 mmol)

Appearance yellow oil

TLC analysis R_f = 0.50 (LP/EtOAc = 1/1)

Sum formula $C_{26}H_{26}BrNO_3$

HR-MS $[M+H]^+$: calculated: 480.1169 Da, found: 480.1158 Da, difference: 1.1 mDa

^{1}H-NMR (400 MHz, $CDCl_3$) δ = 1.74 – 1.91 (m, 2H, H5), 2.02 – 2.15 (m, 2H, H2 & H6), 2.17 – 2.27 (m, 1H, H3), 2.48 (td, *J* = 11.5, 4.5 Hz, 1H, H4), 2.96 – 3.02 (m, 1H, H6), 3.20 – 3.27 (m, 1H, H2), 3.44 (dd, *J* = 9.4, 6.7 Hz, 1H, O-CH_2), 3.52 – 3.58 (m, 2H, N-CH_2 & O-CH_2), 3.64 (d, *J* = 13.1 Hz, 1H, N-CH_2), 5.88 (s, 2H, H2''), 6.11 (dd, *J* = 8.5, 2.5 Hz, 1H, H6''), 6.32 (d, *J* = 2.5 Hz, 1H, H4''), 6.62 (d, *J* = 8.5 Hz, 1H, H7''), 7.09 (d, *J* = 8.4 Hz, 2H, H2' & H6'), 7.24 – 7.38 (m, 5H, H2''' & H3''' & H4''' & H5''' & H6'''), 7.40 (d, *J* = 8.4 Hz, 2H, H3' & H5') ppm.

^{13}C-NMR (101 MHz, $CDCl_3$) δ = 34.3 (t, C5), 42.1 (d, C3), 44.5 (d, C4), 53.9 (t, C6), 57.7 (t, C2), 63.5 (t, N-CH_2), 69.7 (t, O-CH_2), 98.1 (d, C4''), 101.2 (t, C2''), 105.7 (d, C6''), 108.0 (d, C7''), 120.2 (s, C4'), 127.2 (d, C4'''), 128.4 & 129.3 & 129.4 (3xd, 6C, C2' & C6' & C2''' & C3''' & C5''' & C6'''), 131.8 (d, 2C, C3' & C5'), 138.4 (s, C1'''), 141.7 (s, C7a''), 143.4 (s, C1'), 148.3 (s, C3a''), 154.5 (s, C5'') ppm.

E III.11.8 4-((±)-*trans*-3-((Benzo[*d*][1,3]dioxol-5-yloxy)methyl)-1-benzylpiperidin-4-yl)benzaldehyde [154]

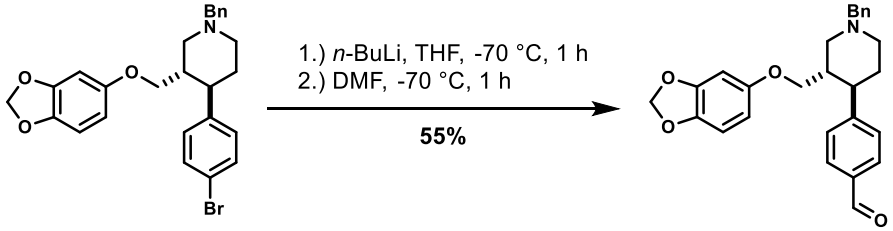

[153] 480.40 g/mol

[154] 429.52 g/mol

Aldehyde **[154]** was synthesized in analogy to a patent procedure[219]. A solution of ether **[153]** (226 mg, 0.470 mmol, 1 equiv.) in dry THF (4.7 mL, degassed by bubbling with argon under sonication for 10 minutes) under argon was cooled to -70 °C (internal temperature). Then *n*-BuLi (0.486 mL, 1.45 M in hexanes, 0.705 mmol, 1.5 equiv.) was added dropwise via syringe and the reaction was stirred at -70 °C for 1 hour. Subsequently, dry DMF (38 µL, 0.494 mmol, 1.05 equiv.) was added via syringe and the resulting mixture was stirred at -70 °C until TLC control showed full conversion (1 hour). The reaction was quenched with satd. aqu. NH_4Cl and transferred into a separatory funnel after reaching room temperature. The reaction was partitioned between EtOAc and satd. aqu. NH_4Cl. The organic phase was washed with brine and dried over $MgSO_4$. After evaporation of the solvent 190 mg crude material (yellow oil)

were obtained. Purification by flash column chromatography (silica gel/crude material = 200/1, toluene/MeCN = 9/1 → 3/2) afforded pure aldehyde **[154]**.

Yield	55% (110 mg; 0.256 mmol)
Appearance	colorless oil
TLC analysis	R_f = 0.30 (LP/EtOAc = 1/1)
Sum formula	$C_{27}H_{27}NO_4$
HR-MS	$[M+H]^+$: calculated: 430.2013 Da, found: 430.2036 Da, difference: 2.3 mDa
^{1}H-NMR (400 MHz, $CDCl_3$)	δ = 1.78 – 1.97 (m, 2H, H5), 2.06 – 2.17 (m, 2H, H2 & H6), 2.26 – 2.36 (m, 1H, H3), 2.62 (td, *J* = 11.6, 4.2 Hz, 1H, H4), 2.98 – 3.04 (m, 1H, H6), 3.21 – 3.27 (m, 1H, H2), 3.44 (dd, *J* = 9.4, 6.6 Hz, 1H, O-CH_2), 3.52 – 3.58 (m, 2H, N-CH_2 & O-CH_2), 3.65 (d, *J* = 13.1 Hz, 1H, N-CH_2), 5.87 (s, 2H, H2''), 6.08 (dd, *J* = 8.5, 2.5 Hz, 1H, H6''), 6.29 (d, *J* = 2.5 Hz, 1H, H4''), 6.60 (d, *J* = 8.5 Hz, 1H, H7''), 7.25 – 7.37 (m, 5H, H2''' & H3''' & H4''' & H5''' & H6'''), 7.38 (d, *J* = 8.2 Hz, 2H, H2' & H6'), 7.80 (d, *J* = 8.2 Hz, 2H, H3' & H5'), 9.96 (s, 1H, aldehyde) ppm.
^{13}C-NMR (101 MHz, $CDCl_3$)	δ = 34.1 (t, C5), 42.0 (d, C3), 45.3 (d, C4), 53.8 (t, C6), 57.5 (t, C2), 63.5 (t, N-CH_2), 69.7 (t, O-CH_2), 98.1 (d, C4''), 101.2 (t, C2''), 105.7 (d, C6''), 108.0 (d, C7''), 127.2 (d, C4'''), 128.4 & 129.3 (2xd, 6C, C2' & C6' & C2''' & C3''' & C5''' & C6'''), 130.3 (d, 2C, C3' & C5'), 135.2 (s, C4'), 138.4 (s, C1'''), 141.7 (s, C7a''), 148.3 (s, C3a''), 151.9 (s, C1'), 154.4 (s, C5''), 192.0 (d, aldehyde) ppm.

E III.11.9 2-(4-((±)-*trans*-3-((Benzo[*d*][1,3]dioxol-5-yloxy)methyl)-1-benzylpiperidin-4-yl)benzylidene)benzo[*b*]thiophen-3(2*H*)-one [155]

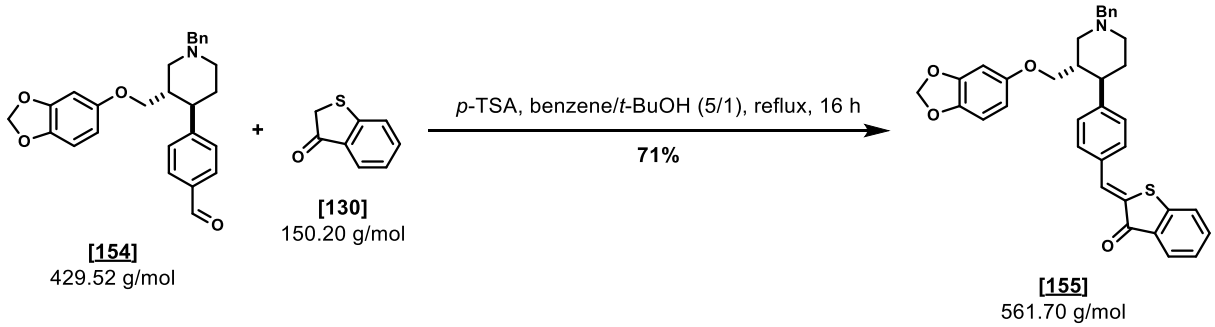

[154]
429.52 g/mol

[130]
150.20 g/mol

[155]
561.70 g/mol

The aldehyde **[154]** (106.5 mg, 0.248 mmol, 1 equiv.) and *p*-TSA•H_2O (71 mg, 0.372 mmol, 1.5 equiv.) were placed in a round bottom flask. The flask was evacuated and flushed with argon three times. Degassed benzene (2.2 mL, degassed by bubbling with argon under sonication for 10 minutes) and degassed *t*-BuOH (0.22 mL) were added via syringe and the solids were dissolved. In a second round bottom flask benzo[*b*]thiophen-3(2*H*)-one **[130]** (56 mg, 0.372 mmol, 1.5 equiv.) was placed. The flask was evacuated and flushed with argon three times. Degassed benzene (2.2 mL) and degassed *t*-BuOH (0.66 mL) were added via syringe and the solid was dissolved under sonication. The benzo[*b*]thiophen-3(2*H*)-one **[130]** solution was added to the starting material **[154]** and the reaction was stirred at reflux temperature until TLC analysis showed full consumption of the starting material (16 hours). Solvents were removed in vacuo. 166 mg of crude material were obtained. Purification by flash column chromatography (silica gel/crude material = 100/1, toluene/MeCN = 9/1 → 3/1) afforded the pure product **[155]**.

Yield	71% (99 mg; 0.176 mmol)
Appearance	yellow oil
TLC analysis	R_f = 0.45 (toluene/MeCN = 3/1)
Sum formula	$C_{35}H_{31}NO_4S$
HR-MS	$[M+H]^+$: calculated: 562.2047 Da, found: 562.2081 Da, difference: 3.4 mDa

^{1}H-NMR (400 MHz, $CDCl_3$) δ = 1.80 – 1.98 (m, 2H, H5), 2.06 – 2.18 (m, 2H, H2 & H6), 2.26 – 2.38 (m, 1H, H3), 2.57 (td, *J* = 11.6, 4.2 Hz, 1H, H4), 2.99 – 3.06 (m, 1H, H6), 3.24 – 3.31 (m, 1H, H2), 3.48 (dd, *J* = 9.8, 6.9 Hz, 1H, O-CH_2), 3.54 – 3.61 (m, 2H, N-CH_2 & O-CH_2), 3.67 (d, *J* = 13.1 Hz, 1H, N-CH_2), 5.86 (s, 2H, H2''), 6.12 (dd, *J* = 8.5, 2.5 Hz, 1H, H6''), 6.33 (d, *J* = 2.5 Hz, 1H, H4''), 6.61 (d, *J* = 8.5 Hz, 1H, H7''), 7.26 – 7.40 (m, 8H, H2' & &6' & H5''' & H2'''' & H3'''' & H4'''' & H5'''' & H6''''), 7.50 (d, *J* = 7.9 Hz, 1H, H7'''), 7.57 (t, *J* = 7.5 Hz, 1H, H6'''), 7.64 (d, *J* = 8.0 Hz, 2H, H3' & H5'), 7.92 – 7.96 (m, 2H, olefin-H & H4''') ppm.

^{13}C-NMR (101 MHz, $CDCl_3$) δ = 34.1 (t, C5), 42.0 (d, C3), 45.0 (d, C4), 53.8 (t, C6), 57.6 (t, C2), 63.5 (t, N-CH_2), 69.7 (t, O-CH_2), 98.1 (d, C4''), 101.2 (t, C2''), 105.7 (d, C6''), 107.9 (d, C7''), 124.0 (d, C7'''), 125.7 (d, C5'''), 127.1 & 127.2 (2xd, 2C, C4''' & C4''''), 128.4 & 128.4 & 129.3 (3xd, 6C, C2' & C6' & C2'''' & C3'''' & C5'''' & C6''''), 129.7 (s, C3a'''), 130.6 (s, C2'''), 131.5 (d, 2C, C3' & C5'), 132.7 (s, C4'), 133.5 (d, olefin-C), 135.3 (d, C6'''), 138.3 (s, C1''''), 141.7 (s, C7a''), 146.1 (s, C7a'''), 147.2 (s, C1'), 148.2 (s, C3a''), 154.4 (s, C5''), 188.7 (s, ketone) ppm.

The assignments of protons and carbon atoms in the NMR codes of compounds **[155]** and **[156]** were carried out as follows:

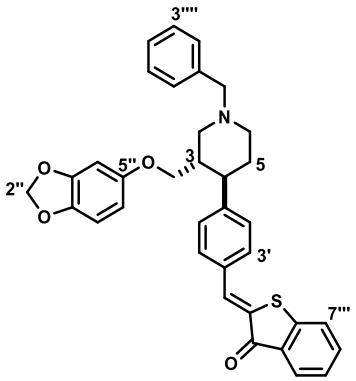

E III.11.10 2-(4-((±)-*trans*-3-((Benzo[*d*][1,3]dioxol-5-yloxy)methyl)-piperidin-4-yl)benzylidene)benzo[*b*]thiophen-3(2*H*)-one [156]

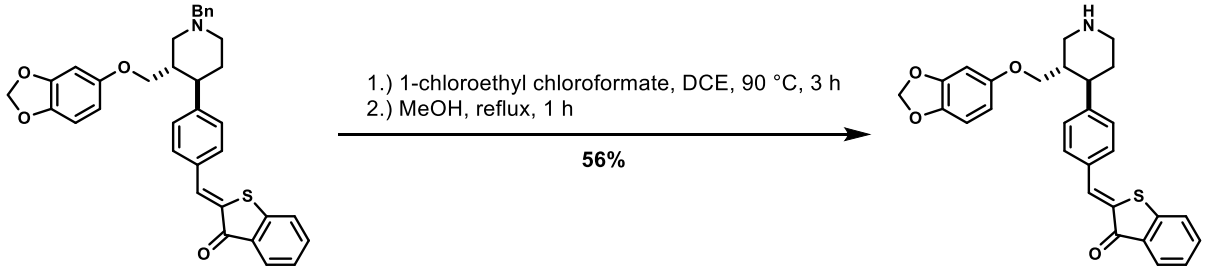

[155]
561.70 g/mol

[156]
471.57 g/mol

Final product **[156]** was obtained after deprotection in analogy to a literature procedure[181]. 1-Chloroethyl chloroformate (38 µL, 0.356 mmol, 10 equiv.) was added to a solution of the starting material **[155]** (20 mg, 36 µmol, 1 equiv.) in DCE (2 mL) at 0 °C via syringe. The flask was flushed with argon and the reaction was stirred at reflux temperature (thermo block set to 90 °C) for 3 hours. Volatiles were removed in vacuo and the crude material was dissolved in toluene and volatiles were again removed in vacuo. This step was repeated two more times. MeOH (2 mL) was added to the residue and the reaction was stirred at reflux temperature (thermo block set to 70 °C) for 1 hour. The solvent was removed in vacuo and the residue was transferred into a separatory funnel using $CHCl_3$. The organic phase was washed with 2 N NaOH. The aqu. phase was extracted with $CHCl_3$ and the combined organic phases were dried over $MgSO_4$. After evaporation of the solvent the crude material (yellow oil) was purified by flash column chromatography (silica gel/crude material = 100/1, $CHCl_3$/MeOH/NH_4OH = 100/10/1) affording pure product **[156]**.

Yield	56% (9.5 mg; 20 µmol)
Appearance	yellow oil
TLC analysis	R_f = 0.45 ($CHCl_3$/MeOH/NH_4OH = 80/20/1)
Sum formula	$C_{28}H_{25}NO_4S$
HR-MS	$[M+H]^+$: calculated: 472.1577 Da, found: 472.1596 Da, difference: 1.9 mDa

^{1}H-NMR (400 MHz, $CDCl_3$) δ = 1.70 – 1.96 (m, 5H, H5 & NH), 2.11 – 2.22 (m, 1H, H3), 2.63 – 2.82 (m, 3H, H2 & H4 & H6), 3.18 – 3.25 (m, 1H, H6), 3.41 – 3.51 (m, 2H, O-CH_2 & H2), 3.59 (dd, *J* = 9.4 Hz, 3.0 Hz, 1H, O-CH_2), 5.86 (s, 2H, H2''), 6.12 (dd, *J* = 8.5 Hz, 2.5 Hz, 1H, H6''), 6.34 (d, *J* = 2.5 Hz, 1H, H4''), 6.61 (d, *J* = 8.5 Hz, 1H, H7''), 7.30 (ddd, *J* = 8.0 Hz, 7.2 Hz, 1.0 Hz, 1H, H5'''), 7.34 (d, *J* = 8.2 Hz, 2H, H2' & H6'), 7.51 (d, *J* = 7.8 Hz, 1H, H7'''), 7.58 (ddd, *J* = 8.3 Hz, 7.1 Hz, 1.4 Hz, 1H, H6'''), 7.65 (d, *J* = 8.0 Hz, 2H, H3' & H5'), 7.92 – 7.96 (m, 2H, olefin-H & H4''') ppm.

^{13}C-NMR (101 MHz, $CDCl_3$) δ = 35.1 (t, C5), 42.8 (d, C3), 45.5 (d, C4), 47.1 (t, C6), 50.4 (t, C2), 69.7 (t, O-CH_2), 98.1 (d, C4''), 101.2 (t, C2''), 105.7 (d, C6''), 108.0 (d, C7''), 124.1 (d, C7'''), 125.7 (d, C5'''), 127.2 (d, C4'''), 128.4 (d, 2C, C2' & C6'), 129.8 (s, C3a'''), 130.7 (s, C2'''), 131.6 (d, 2C, C3' & C5'), 132.8 (s, C4'), 133.5 (d, olefin-C), 135.4 (d, C6'''), 141.7 (s, C7a''), 146.2 (s, C7a'''), 147.2 (s, C1'), 148.3 (s, C3a''), 154.5 (s, C5''), 188.8 (s, ketone) ppm.

E IV Whole cell patch clamp technique

For patch clamp recordings, HEK293 cells stably expressing hSERT (hs4to) were seeded at low density 24 hours before the measurement. To measure substrate-induced hSERT currents, cells were voltage clamped using the whole cell patch clamp technique. Briefly, glass pipettes were filled with a solution consisting of 133 mM potassium gluconate, 5.9 mM NaCl, 1 mM $CaCl_2$, 0.7 mM $MgCl_2$, 10 mM HEPES, 10 mM EGTA, adjusted to pH 7.2 with 30 mM KOH. For some experiments the internal K^+ concentration had to be reduced. In these instances, the pipette solution consisted of 163 mM NMDG, 137 mM MES, 5.9 mM NaCl, 1 mM $CaCl_2$, 0.7 mM $MgCl_2$, 10 mM HEPES, 10 mM EGTA, pH 7.2. The cells were continuously superfused with external solution (140 mM NaCl, 3 mM KCl, 2.5 mM $CaCl_2$, 2 mM $MgCl_2$, 10 mM HEPES, 20 mM glucose, adjusted to pH 7.4 with NaOH).

Currents were recorded at room temperature (20 – 24 °C) using an Axopatch 200B amplifier and pClamp 10.2 software (MDS Analytical Technologies). Unless otherwise stated, cells were voltage clamped to a holding potential of −70 mV, and serotonin was applied for 5 seconds once every 60 seconds. Current traces were filtered at 1 kHz and digitized at 2 kHz using a Digidata 1320A (MDS Analytical Technologies). Liquid junction potential was calculated to be 16 mV and was compensated. Drugs were applied using a DAD-12 (Adams and List, Westbury, NY), which permits complete solution exchange around the cells within 100 ms. Current amplitudes in response to serotonin application were quantified using Clampfit 10.2 software. Passive holding currents were subtracted, and the traces were filtered using a 100-Hz digital Gaussian low pass filter.

F Appendix

F I Publications and conference activities

Journal articles

D. Dreier, M. Holy, K. Jäntsch, S. Kickinger, Y. Hu, E. Hellsberg, G.F. Ecker, W. Sandtner, H.H. Sitte, M.D. Mihovilovic: "*Azo-Paroxetine – A Photoswitchable Serotonin Transporter Inhibitor*"; in preparation

D. Dreier, H. Kalaus, C. Cziegler, P. Miksovsky, M. Schnürch, M.D. Mihovilovic: "*Photophysical Properties of Arylazopyrazoles, Arylazo-2-thiophenes and Arylazo-3-thiophenes* "; European Journal of Organic Chemsitry, in preparation

D. Dreier, M. Resetar, V. Temml, L. Rycek, N. Kratena, M. Schnürch, D. Schuster, V. Dirsch, M.D. Mihovilovic: "*Magnolol dimer-derived fragemtns as PPARγ-selective probes*"; Organic & Biomolecular Chemistry, submitted

I. Corbic Ramljak, J. Stanger, A. Real-Hohn, **D. Dreier**, L. Wimmer, M. Redlberger-Fritz, W. Fischl, K. Klingel, M.D. Mihovilovic, D. Blaas, H. Kowalski: "*Cellular N-Myristoyltransferases play a crucial picornavirus genus-specific role in viral assembly, virion maturation, and infectivity*"; PLOS Pathogens, just accepted

A. Henke, Y. Kovalyova, M. Dunn, **D. Dreier**, N. Gubernator, I. Dincheva, C. Hwu, P. Sebej, M. Ansorge, D. Sulzer, D. Sames: "*Toward Serotonin Fluorescent False Neurotransmitters: Development of Fluorescent Dual Serotonin and Vesicular Monoamine Transporter Substrates for Visualizing Serotonin Neurons*"; ACS Chemical Neuroscience, **9** (2018), 5; S. 925 - 934.

D. Dreier, S. Latkolik, L. Rycek, M. Schnürch, A. Dymáková, A Atanasov, A. Ladurner, E. Heiss, H. Stuppner, D. Schuster, M.D. Mihovilovic, V. Dirsch: "*Linked magnolol dimer as a selective PPARγ agonist - Structure-based rational design, synthesis, and bioactivity evaluation*"; Scientific Reports, **7** (2017), 13002; S. 1 - 10.

F. Rudroff, D. Bianchi, R. Moran-Ramallal, N. Iqbal, **D. Dreier**, M.D. Mihovilovic: "*Synthesis of tetrahydrofuran-based natural products and their carba analogs via stereoselective enzyme mediated Baeyer-Villiger oxidation*"; Tetrahedron, **72** (2016), S. 7212 - 7221.

M. Schön, **D. Dreier**, M. Schnürch, M.D. Mihovilovic: "*Library synthesis of cardiomyogenesis inducing compounds using an efficient two-step-one-flow process*"; Monatshefte für Chemie, **147** (2016), 3; S. 523 - 532.

Conference talks

D. Dreier, L. Rycek, D. Schuster, A Atanasov, V. Dirsch, M. Schnürch, M.D. Mihovilovic: "*Synthesis Of Potential Anti-Inflammatory Agents Inspired By Nature*"; International Symposium: Natural products and drug discovery - future perspectives, Vienna; 2014

Poster Presentations

D. Dreier, M. Holy, K. Jäntsch, H.H. Sitte, M.D. Mihovilovic: "*Synthesis of Photoswitchable Inhibitors for CNS Applications*"; 7th Paul Ehrlich MedChem EuroPhD Network Symposium, Vienna; 2017

D. Dreier, M. Holy, K. Jäntsch, H.H. Sitte, M.D. Mihovilovic: "*Synthesis of Photoswitchable Inhibitors for CNS Applications*"; 10th Joint Meeting on Medicinal Chemistry, Dubrovnik; 2017

D. Dreier, L. Rycek, D. Schuster, A Atanasov, V. Dirsch, M. Schnürch, M.D. Mihovilovic: "*Synthesis and in vitro evaluation of magnolol based dimeric compounds as PPARγ agonists*"; 3rd Prague Summer School: Advances in Drug Discovery, Prague; 2016

D. Dreier, L. Rycek, D. Schuster, A Atanasov, V. Dirsch, M. Schnürch, M.D. Mihovilovic: "*Synthesis and in vitro evaluation of magnolol based dimeric compounds as PPARγ agonists*"; 17th Tetrahedron Symposium - Challenges in Biological, Bioorganic, Organic & Medicinal Chemistry, Sitges; 2016

D. Dreier, M.D. Mihovilovic, H.H. Sitte: "*Optically Switchable Monoamine Transporter Ligands*"; Moltag Science Day, Vienna; 2016

D. Dreier, C. Cziegler, H. Kalaus, E. Horkel, M. Schnürch, M.D. Mihovilovic: "*Azoheteroarene Photoswitches - Effects Of Heteroaromatics And Functional Group Decoration On Their Photophysical Properties*"; 16th Blue Danube Symposium on Heterocyclic Chemistry, Balatonalmadi; 2015

D. Dreier, L. Rycek, D. Schuster, A Atanasov, V. Dirsch, M. Schnürch, M.D. Mihovilovic: "*Synthesis Of Potential Anti-Inflammatory Agents Inspired By Nature*"; IXth Joint Meeting in Medicinal Chemistry, Athens; 2015

D. Dreier, L. Rycek, M. Schnürch, M.D. Mihovilovic: "*Synthesis Of Potential Anti-Inflammatory Agents Inspired By Nature*"; 4th Meeting of the Paul Ehrlich MedChem Euro-PhD Network, Hradec Kralove; 2014

F II Reference list of compounds

[2]	DD-HK-028
[3]	DD-HK-032
[5]	DD-HK-034
[6]	DD-HK-046
[7]	DD-HK-054
[9]	DD-HK-035
[10]	DD-HK-049
[11]	DD-HK-056
[13]	DD-HK-036
[14]	DD-HK-048
[15]	DD-ESC-019
[17]	DD-HK-062
[18]	DD-HK-063
[20]	DD-HK-037
[21]	DD-HK-051
[22]	DD-HK-061
[24]	DD-HK-047
[25]	DD-HK-055
[27]	DD-HK-057
[28]	DD-HK-058
[30]	DD-HK-039
[31]	DD-HK-050
[32]	DD-HK-041
[33]	DD-HK-044
[34]	DD-HK-052
[35]	DD-HK-044b
[36]	DD-HK-053
[38]	DD-ESC-001
[39]	DD-ESC-004
[41]	DD-ESC-002

[42]	DD-ESC-013
[44]	DD-ESC-007
[45]	DD-ESC-015
[47]	DD-ESC-016
[48]	DD-ESC-017
[50]	DD-ESC-011
[51]	DD-ESC-018
[53]	DD-ESC-002
[54]	DD-ESC-008
[56]	DD-ESC-005
[57]	DD-ESC-012
[59]	DD-ESC-003
[60]	DD-ESC-009
[62]	DD-ESC-006
[63]	DD-ESC-014
[64]	DD-CCZ-009
[65]	DD-CCZ-027
[66]	DD-CCZ-025
[67]	DD-CCZ-032
[68]	DD-CHI-005
[70]	DD-CCZ-028
[71]	DD-CCZ-024
[72]	DD-CCZ-033
[73]	DD-CCZ-014
[74]	DD-PM-041
[76]	DD-CCZ-010
[77]	DD-CCZ-012
[78]	DD-CCZ-019
[79]	DD-CCZ-037
[80]	DD-CCZ-013

[81]	DD-CCZ-043
[82]	DD-CCZ-038
[83]	DD-CCZ-049
[84]	DD-CCZ-036
[85]	DD-CCZ-048
[87]	DD-CCZ-047
[88]	DD-PM-002
[90]	DD-PM-036
[91]	DD-PM-037
[92]	DD-PM-044
[93]	DD-PM-042
[95]	DD-261b
[96]	DD-296
[97]	DD-286
[98]	DD-299
[99]	DD-CL-001
[100]	DD-CL-022
[101]	DD-FA-029
[102]	DD-CL-038
[104]	DD-CL-031
[105]	DD-CL-030
[107]	DD-CL-039
[109]	DD-CL-040
[111]	DD-261
[112]	DD-301
[113]	DD-322
[115]	DD-300
[116]	DD-293
[117]	DD-321
[118]	DD-401

[119]	DD-309
[120]	DD-400
[121]	DD-402
[122]	DD-403
[123]	DD-404
[124]	DD-405
[126]	DD-406
[129]	DD-KR-001
[130]	DD-KR-008
[132]	DD-KR-033
[133]	DD-KR-015
[134]	DD-KR-053
[135]	DD-359
[136]	DD-350
[137]	DD-353
[138]	DD-354
[139]	DD-355
[141]	DD-364
cis-[142]	*cis*-DD-369
trans-[142]	*trans*-DD-369
rac-[143]	DD-397
(3*S*,4*R*)-[143]	DD-476
[144]	DD-435
[145]	DD-478
[146]	DD-480
[147]	DD-482
[149]	DD-420
cis-[150]	*cis*-DD-421
trans-[150]	*trans*-DD-421
rac-[151]	DD-423
[152]	DD-438
[153]	DD-428

[154]	DD-436
[155]	DD-441
[156]	DD-447

F III Curriculum vitae

Dominik Dreier, M.Sc.
Mondscheingasse 6/7-8, A-1070 Vienna
+43699/17234427
dominik.dreier@hotmail.com
Date of birth: December 15th, 1989

Education:

May 2014 – present:	**PhD program**: Technical Sciences – Technical Chemistry TU Wien (Prof. Mihovilovic) Doctoral viva presumably end of June 2018 *Research area: Medicinal Chemistry, Organic Synthesis*
May 2015 – present:	**Associate Fellow** of the interdisciplinary doctoral program "Molecular Drug Targets" Institute of Science and Technology Austria, Medical University of Vienna, University of Vienna, TU Wien *Competitive selection process* *Regular presentations and collaborations in an interdisciplinary environment* *Organization of a scientific symposium* *Lab rotations in computational chemistry and neuropharmacology* *Annual scientific retreats*
Oct. 2012 – Apr. 2014:	Master studies: Technical Chemistry - Synthesis TU Wien (Prof. Mihovilovic) *Synthesis of potential anti inflammatory agents inspired by nature* **Master's degree received with distinction** (average grade: 1.0) Received **performance-based scholarship** in 2012/2013 and 2013/2014
Oct. 2009 – Sep. 2012:	Bachelor studies: Technical Chemistry TU Wien **Bachelor's degree received with distinction** (average grade: 1.4) Received **performance-based scholarship** in 2010/2011 and 2011/2012
Jun. 2008:	Matura (final exam) Realgymnasium Völkermarkt Passed with distinction (average grade: 1.3)

Relevant Experience:

Jul. 2017 – Dec. 2017	Research stay, **Columbia University**, New York City (Prof. Sames)
May 2014 – Apr. 2018	**University assistant**, TU Wien, Faculty of Chemistry, Institute of Applied Synthetic Chemistry *Teaching undergraduates in lab courses* *Operator for preparative HPLC and NMR*

Sep. 2012 – Feb. 2014	Lab course assistant, TU Wien, Faculty of Chemistry, Institute of Applied Synthetic Chemistry
Aug. 2010 – Sept. 2010	Internship in the laboratory, Donau Chemie AG, Brückl *Chemical quality control (GC, ICP-OES, titrimetric and gravimetric methods)*

Awards:

2014	"**Würdigungspreis des Bundesministeriums** für Wissenschaft, Forschung und Wirtschaft" *Awarded to the 50 best graduates (master level) of all Austrian universities of an academic year. TU Wien receives two awards per year.*

Scientific output:

Five publications in peer reviewed journals, one manuscript currently submitted, two manuscripts in preparation

Participation (posters and orals) at eight international conferences (e.g. IXth Joint Meeting in Medicinal Chemistry: **best poster award**, Athens, Greece, Jun. 2015; Xth Joint Meeting in Medicinal Chemistry: **best poster award**, Dubrovnik, Croatia, Jun. 2017)

Extracurricular activities:

Feb. 2017 – Jun. 2017	Co-Organizer of TEDxTUWien 2017 *First event took place in May 2017 with 300 attendees.* *Head of the sponsorship team, responsible for finance (20,000€ budget), recruitment of speakers, volunteer manager*
Oct. 2016 – Jun. 2017	TUtheTop program 2016/2017 High potential program of the TU Wien *Assessment center, soft skill training, workshops at Accenture GmbH (e.g. negotiation, project management, business case)*

Language skills:

English	fluent, international working environment for the past five years, semester abroad in New York City
German	native
French	12 ECTS course at WU Wien in 2016/2017

Interests:

Advanced IT skills	programming (PHP, MySQL; programmed quizzes, vocabulary trainers, bots for repetitive tasks)
Running	Marathon sub 4:00, Half Marathon 1:30, 10km sub 0:42

F IV List of abbreviations

[^{3}H]MPP+	tritium labeled 1-methyl-4-phenylpyridinium
Ac	acetate
AcOH	acetic acid
ADHD	attention deficity hyperactivity disorder
aqu.	aqueous
Arg	arginine
Asp	aspartic acid
Bu	butyl
cat.	catalytical
CNS	central nervous system
conc.	concentrated
DAT	dopamine transporter
DCE	1,2-dichloroethane
DCM	dichloromethane
dil.	diluted
DIPE	diisopropyl ether
DIPEA	diisopropylethylamine
DMAP	4-dimethylaminopyridine
DMF	dimethylformamide
DMSO	dimethylsulfoxide
EDCI•HCl	1-ethyl-3-(3-dimethylaminopropyl)carbodiimide hydrochloride
Et	ethyl
GABA	g-aminobutyric acid
HEK cells	human embryonic kidney cells
HOBt	hydroxybenzotriazole
HPLC	high-performance liquid chromatography
HTI	hemithioindigo
IC_{50}	half maximal inhibitory concentration
LED	light-emitting diode
LeuT	leucine transporter
LP	light petroleum
MAT	monoamine transporter
Me	methyl
Ms	mesyl
NCS	*N*-Chlorosuccinimide
NET	norepinephrine transporter
NMR	nuclear magnetic resonance
NSS	neurotransmitter sodium symporter
NTT	neurotransmitter transporter
Ph	phenyl
Phe	phenylalanine
Pr	propyl
p-TSA	*para*-toluenesulfonic acid
pyr	pyridine
rt	room temperature
satd.	saturated
SDS	sodium dodecyl sulfate
SERT	serotonin transporter
SLC	solute carrier
SSRI	selective serotonin reuptake inhibitor
TBSOTf	tert-butyldimethylsilyl trifluoromethanesulfonate
THF	tetrahydrofuran
TM	transmembrane domain
TMS	trimethylsilyl
Tyr	tyrosine
UV-Vis	ultraviolet-visible

F V References

1. Borowiak, M.; Nahaboo, W.; Reynders, M.; Nekolla, K.; Jalinot, P.; Hasserodt, J.; Rehberg, M.; Delattre, M.; Zahler, S.; Vollmar, A.; Trauner, D.; Thorn-Seshold, O., Photoswitchable Inhibitors of Microtubule Dynamics Optically Control Mitosis and Cell Death. *Cell (Cambridge, MA, U. S.)* **2015,** *162*, 403-411.
2. Alivisatos, A. P.; Chun, M.; Church, G. M.; Greenspan, R. J.; Roukes, M. L.; Yuste, R., The Brain Activity Map Project and the Challenge of Functional Connectomics. *Neuron* **2012,** *74*, 970-974.
3. Kristensen, A. S.; Andersen, J.; Joergensen, T. N.; Soerensen, L.; Eriksen, J.; Loland, C. J.; Stroemgaard, K.; Gether, U., SLC6 neurotransmitter transporters: structure, function, and regulation. *Pharmacol. Rev.* **2011,** *63*, 585-640.
4. Rudnick, G.; Kramer, R.; Blakely, R. D.; Murphy, D. L.; Verrey, F., The SLC6 transporters: perspectives on structure, functions, regulation, and models for transporter dysfunction. *Pfluegers Arch.* **2014,** *466*, 25-42.
5. Jessell, T. M.; Kandel, E. R., Synaptic transmission: a bidirectional and self-modifiable form of cell-cell communication. *Cell* **1993,** *72 Suppl*, 1-30.
6. Kurian, M. A.; Gissen, P.; Smith, M.; Heales, S. J. R.; Clayton, P. T., The monoamine neurotransmitter disorders: an expanding range of neurological syndromes. *Lancet Neurol.* **2011,** *10*, 721-733.
7. Yamashita, A.; Singh, S. K.; Kawate, T.; Jin, Y.; Gouaux, E., Crystal structure of a bacterial homologue of Na+/Cl--dependent neurotransmitter transporters. *Nature (London, U. K.)* **2005,** *437*, 215-223.
8. Penmatsa, A.; Wang, K. H.; Gouaux, E., X-ray structure of dopamine transporter elucidates antidepressant mechanism. *Nature* **2013,** *503*, 85-90.
9. Coleman, J. A.; Green, E. M.; Gouaux, E., X-ray structures and mechanism of the human serotonin transporter. *Nature (London, U. K.)* **2016,** *532*, 334-339.
10. Coleman, J. A.; Gouaux, E.; Gouaux, E., Structural basis for recognition of diverse antidepressants by the human serotonin transporter. *Nat Struct Mol Biol* **2018,** *25*, 170-175.
11. Hyttel, J., Comparative pharmacology of selective serotonin re-uptake inhibitors (SSRIs). *Nordic Journal of Psychiatry* **1993,** *47*, 5-12.
12. Glick, S. D.; Haskew, R. E.; Maisonneuve, I. M.; Carlson, J. N.; Jerussi, T. P., Enantioselective behavioral effects of sibutramine metabolites. *Eur. J. Pharmacol.* **2000,** *397*, 93-102.
13. Sorensen, L.; Andersen, J.; Thomsen, M.; Hansen, S. M. R.; Zhao, X.; Sandelin, A.; Stromgaard, K.; Kristensen, A. S., Interaction of Antidepressants with the Serotonin and Norepinephrine Transporters. *J. Biol. Chem.* **2012,** *287*, 43694-43707.
14. Sitte, H. H.; Freissmuth, M., Amphetamines, new psychoactive drugs and the monoamine transporter cycle. *Trends in pharmacological sciences* **2015,** *36*, 41-50.
15. J. Litman, B.; C. Mitchell, D., Rhodopsin structure and function. In *Biomembranes: A Multi-Volume Treatise*, Lee, A. G., Ed. JAI1996; Vol. 2, pp 1-32.
16. Palczewski, K., G Protein–Coupled Receptor Rhodopsin. *Annual Review of Biochemistry* **2006,** *75*, 743-767.
17. Deisseroth, K., Optogenetics. *Nat. Methods* **2011,** *8*, 26-29.
18. Fenno, L.; Yizhar, O.; Deisseroth, K., The Development and Application of Optogenetics. *Annual Review of Neuroscience* **2011,** *34*, 389-412.
19. Fehrentz, T.; Schoenberger, M.; Trauner, D., Optochemical Genetics. *Angew. Chem., Int. Ed.* **2011,** *50*, 12156-12182.
20. Velema, W. A.; Szymanski, W.; Feringa, B. L., Photopharmacology: Beyond Proof of Principle. *J. Am. Chem. Soc.* **2014,** *136*, 2178-2191.
21. Broichhagen, J.; Frank, J. A.; Trauner, D., A Roadmap to Success in Photopharmacology. *Acc. Chem. Res.* **2015,** *48*, 1947-1960.
22. Brieke, C.; Rohrbach, F.; Gottschalk, A.; Mayer, G.; Heckel, A., Light-Controlled Tools. *Angew. Chem., Int. Ed.* **2012,** *51*, 8446-8476.
23. Szymanski, W.; Beierle, J. M.; Kistemaker, H. A. V.; Velema, W. A.; Feringa, B. L., Reversible Photocontrol of Biological Systems by the Incorporation of Molecular Photoswitches. *Chem. Rev. (Washington, DC, U. S.)* **2013,** *113*, 6114-6178.
24. Lerch, M. M.; Hansen, M. J.; van Dam, G. M.; Szymanski, W.; Feringa, B. L., Emerging Targets in Photopharmacology. *Angew. Chem., Int. Ed.* **2016,** *55*, 10978-10999.
25. Zemelman, B. V.; Nesnas, N.; Lee, G. A.; Miesenbock, G., Photochemical gating of heterologous ion channels: Remote control over genetically designated populations of neurons. *Proc. Natl. Acad. Sci. U. S. A.* **2003,** *100*, 1352-1357.
26. Warther, D.; Gug, S.; Specht, A.; Bolze, F.; Nicoud, J. F.; Mourot, A.; Goeldner, M., Two-photon uncaging: New prospects in neuroscience and cellular biology. *Bioorg. Med. Chem.* **2010,** *18*, 7753-7758.
27. Noguchi, J.; Nagaoka, A.; Watanabe, S.; Ellis-Davies, G. C. R.; Kitamura, K.; Kano, M.; Matsuzaki, M.; Kasai, H., In vivo two-photon uncaging of glutamate revealing the structure-function relationships of dendritic spines in the neocortex of adult mice. *J. Physiol. (Oxford, U. K.)* **2011,** *589*, 2447-2457.
28. Leippe, P.; Koehler Leman, J.; Trauner, D., Specificity and Speed: Tethered Photopharmacology. *Biochemistry* **2017,** *56*, 5214-5220.
29. Kawata, S.; Kawata, Y., Three-Dimensional Optical Data Storage Using Photochromic Materials. *Chemical Reviews* **2000,** *100*, 1777-1788.
30. Munenori, Y.; Mizuho, K.; Jun-ichi, M.; Yanlei, Y.; Motoi, K.; J., B. C.; Tomiki, I., Photomobile Polymer Materials: Towards Light-Driven Plastic Motors. *Angewandte Chemie International Edition* **2008,** *47*, 4986-4988.
31. Russew, M.-M.; Hecht, S., Photoswitches: from Molecules to Materials. *Adv. Mater. (Weinheim, Ger.)* **2010,** *22*, 3348-3360.
32. Kucharski, T. J.; Ferralis, N.; Kolpak, A. M.; Zheng, J. O.; Nocera, D. G.; Grossman, J. C., Templated assembly of photoswitches significantly increases the energy-storage capacity of solar thermal fuels. *Nat. Chem.* **2014,** *6*, 441-447.
33. Goestl, R.; Senf, A.; Hecht, S., Remote-controlling chemical reactions by light: Towards chemistry with high spatio-temporal resolution. *Chem. Soc. Rev.* **2014,** *43*, 1982-1996.
34. Bandara, H. M. D.; Burdette, S. C., Photoisomerization in different classes of azobenzene. *Chem. Soc. Rev.* **2012,** *41*, 1809-1825.
35. Beharry, A. A.; Woolley, G. A., Azobenzene photoswitches for biomolecules. *Chem. Soc. Rev.* **2011,** *40*, 4422-4437.
36. Bléger, D.; Hecht, S., Visible-Light-Activated Molecular Switches. *Angewandte Chemie International Edition* **2015,** *54*, 11338-11349.

37. Dong, M.; Babalhavaeji, A.; Samanta, S.; Beharry, A. A.; Woolley, G. A., Red-Shifting Azobenzene Photoswitches for in Vivo Use. *Acc. Chem. Res.* **2015,** *48*, 2662-2670.
38. Waldeck, D. H., Photoisomerization dynamics of stilbenes. *Chem. Rev.* **1991,** *91*, 415-36.
39. Wiedbrauk, S.; Dube, H., Hemithioindigo-an emerging photoswitch. *Tetrahedron Lett.* **2015,** *56*, 4266-4274.
40. Petermayer, C.; Dube, H., Indigoid Photoswitches: Visible Light Responsive Molecular Tools. *Acc. Chem. Res.* **2018,** *51*, 1153-1163.
41. Petermayer, C.; Thumser, S.; Kink, F.; Mayer, P.; Dube, H., Hemiindigo: Highly Bistable Photoswitching at the Biooptical Window. *J. Am. Chem. Soc.* **2017,** *139*, 15060-15067.
42. Lukyanov, B. S.; Lukyanova, M. B., Spiropyrans: Synthesis, properties, and application. *Chem. Heterocycl. Compd. (N. Y., NY, U. S.)* **2005,** *41*, 281-311.
43. Irie, M.; Fukaminato, T.; Matsuda, K.; Kobatake, S., Photochromism of Diarylethene Molecules and Crystals: Memories, Switches, and Actuators. *Chem. Rev. (Washington, DC, U. S.)* **2014,** *114*, 12174-12277.
44. Yokoyama, Y.; Gushiken, T.; Ubukata, T. In *Fulgides and related compounds*2011 Wiley-VCH Verlag GmbH & Co. KGaA; pp 81-95.
45. Lerch, M. M.; Szymanski, W.; Feringa, B. L., The (photo)chemistry of Stenhouse photoswitches: guiding principles and system design. *Chem. Soc. Rev.* **2018,** *47*, 1910-1937.
46. Di Donato, M.; Lerch, M. M.; Lapini, A.; Laurent, A. D.; Iagatti, A.; Bussotti, L.; Ihrig, S. P.; Medved, M.; Jacquemin, D.; Szymanski, W.; Buma, W. J.; Foggi, P.; Feringa, B. L., Shedding Light on the Photoisomerization Pathway of Donor-Acceptor Stenhouse Adducts. *J. Am. Chem. Soc.* **2017,** *139*, 15596-15599.
47. Cattaneo, P.; Persico, M., An ab initio study of the photochemistry of azobenzene. *Phys. Chem. Chem. Phys.* **1999,** *1*, 4739-4743.
48. Talaty, E. R.; Fargo, J. C., Thermal cis-trans isomerization of substituted azobenzenes. Correction of the literature. *Chem. Commun.* **1967**, 65-6.
49. Nishimura, N.; Sueyoshi, T.; Yamanaka, H.; Imai, E.; Yamamoto, S.; Hasegawa, S., Thermal cis-to-trans isomerization of substituted azobenzenes. II. Substituent and solvent effects. *Bull. Chem. Soc. Jpn.* **1976,** *49*, 1381-7.
50. Fliegl, H.; Koehn, A.; Haettig, C.; Ahlrichs, R., Ab Initio Calculation of the Vibrational and Electronic Spectra of trans- and cis-Azobenzene. *J. Am. Chem. Soc.* **2003,** *125*, 9821-9827.
51. Merino, E., Synthesis of azobenzenes, the coloured pieces of molecular materials. *Chem. Soc. Rev.* **2011,** *40*, 3835-3853.
52. Hamon, F.; Djedaini-Pilard, F.; Barbot, F.; Len, C., Azobenzenes-synthesis and carbohydrate applications. *Tetrahedron* **2009,** *65*, 10105-10123.
53. Khan, A.; Hecht, S., Towards photocontrol over the helix-coil transition in foldamers: synthesis and photoresponsive behavior of azobenzene-core amphiphilic oligo(meta-phenyleneethynylene)s. *Chem. - Eur. J.* **2006,** *12*, 4764-4774.
54. Chi, L.; Sadovski, O.; Woolley, G. A., A Blue-Green Absorbing Cross-Linker for Rapid Photoswitching of Peptide Helix Content. *Bioconjugate Chem.* **2006,** *17*, 670-676.
55. Hansen, M. J.; Lerch, M. M.; Szymanski, W.; Feringa, B. L., Direct and Versatile Synthesis of Red-Shifted Azobenzenes. *Angew. Chem., Int. Ed.* **2016,** *55*, 13514-13518.
56. Mills, C., XCIII.-Some new azo-compounds. *Journal of the Chemical Society, Transactions* **1895,** *67*, 925-933.
57. Ueno, K.; Akiyoshi, S., Kinetic study on the condensation reaction of aniline and nitrosobenzenes. *J. Am. Chem. Soc.* **1954,** *76*, 3670-2.
58. Quandt, G.; Hoefner, G.; Pabel, J.; Dine, J.; Eder, M.; Wanner, K. T., First Photoswitchable Neurotransmitter Transporter Inhibitor: Light-Induced Control of γ-Aminobutyric Acid Transporter 1 (GAT1) Activity in Mouse Brain. *J. Med. Chem.* **2014,** *57*, 6809-6821.
59. Cheng, B.; Shchepakin, D.; Kavanaugh, M. P.; Trauner, D., Photoswitchable Inhibitor of a Glutamate Transporter. *ACS Chem. Neurosci.* **2017,** *8*, 1668-1672.
60. Lim, Y.-K.; Lee, K.-S.; Cho, C.-G., Novel Route to Azobenzenes via Pd-Catalyzed Coupling Reactions of Aryl Hydrazides with Aryl Halides, Followed by Direct Oxidations. *Org. Lett.* **2003,** *5*, 979-982.
61. Kang, H.-M.; Kim, H.-Y.; Jung, J.-W.; Cho, C.-G., Practical Synthesis of Azobenzenophanes. *J. Org. Chem.* **2007,** *72*, 679-682.
62. Brash, D. E.; Rudolph, J. A.; Simon, J. A.; Lin, A.; McKenna, G. J.; Baden, H. P.; Halperin, A. J.; Ponten, J., A role for sunlight in skin cancer: UV-induced p53 mutations in squamous cell carcinoma. *Proc. Natl. Acad. Sci. U. S. A.* **1991,** *88*, 10124-8.
63. Matsumura, Y.; Ananthaswamy, H. N., Toxic effects of ultraviolet radiation on the skin. *Toxicol. Appl. Pharmacol.* **2004,** *195*, 298-308.
64. Jacques, S. L., Optical properties of biological tissues: a review. *Phys Med Biol* **2013,** *58*, R37-61.
65. Garcia-Amoros, J.; Diaz-Lobo, M.; Nonell, S.; Velasco, D., Fastest Thermal Isomerization of an Azobenzene for Nanosecond Photoswitching Applications under Physiological Conditions. *Angew. Chem., Int. Ed.* **2012,** *51*, 12820-12823.
66. Garcia-Amoros, J.; Velasco, D., Recent advances towards azobenzene-based light-driven real-time information-transmitting materials. *Beilstein J. Org. Chem.* **2012,** *8*, 1003-1017, No. 113.
67. Wendler, T.; Schütt, C.; Näther, C.; Herges, R., Photoswitchable Azoheterocycles via Coupling of Lithiated Imidazoles with Benzenediazonium Salts. *The Journal of Organic Chemistry* **2012,** *77*, 3284-3287.
68. Weston, C. E.; Richardson, R. D.; Haycock, P. J.; White, A. J. P.; Fuchter, M. J., Arylazopyrazoles: Azoheteroarene Photoswitches Offering Quantitative Isomerization and Long Thermal Half-Lives. *J. Am. Chem. Soc.* **2014,** *136*, 11878-11881.
69. Calbo, J.; Weston, C. E.; White, A. J. P.; Rzepa, H. S.; Contreras-Garcia, J.; Fuchter, M. J., Tuning Azoheteroarene Photoswitch Performance through Heteroaryl Design. *J. Am. Chem. Soc.* **2017,** *139*, 1261-1274.
70. Blevins, A. A.; Blanchard, G. J., Effect of Positional Substitution on the Optical Response of Symmetrically Disubstituted Azobenzene Derivatives. *J. Phys. Chem. B* **2004,** *108*, 4962-4968.
71. Sadovski, O.; Beharry, A. A.; Zhang, F.; Woolley, G. A., Spectral tuning of azobenzene photoswitches for biological applications. *Angew. Chem., Int. Ed.* **2009,** *48*, 1484-1486, S1484/1-S1484/9.
72. Beharry, A. A.; Sadovski, O.; Woolley, G. A., Azobenzene Photoswitching without Ultraviolet Light. *J. Am. Chem. Soc.* **2011,** *133*, 19684-19687.
73. Samanta, S.; Beharry, A. A.; Sadovski, O.; McCormick, T. M.; Babalhavaeji, A.; Tropepe, V.; Woolley, G. A., Photoswitching Azo Compounds in Vivo with Red Light. *J. Am. Chem. Soc.* **2013,** *135*, 9777-9784.
74. Samanta, S.; McCormick, T. M.; Schmidt, S. K.; Seferos, D. S.; Woolley, G. A., Robust visible light photoswitching with ortho-thiol substituted azobenzenes. *Chem. Commun. (Cambridge, U. K.)* **2013,** *49*, 10314-10316.
75. Bléger, D.; Schwarz, J.; Brouwer, A. M.; Hecht, S., o-Fluoroazobenzenes as Readily Synthesized Photoswitches Offering Nearly Quantitative Two-Way Isomerization with Visible Light. *Journal of the American Chemical Society* **2012,** *134*, 20597-20600.

76. Samanta, S.; Babalhavaeji, A.; Dong, M.-x.; Woolley, G. A., Photoswitching of ortho-Substituted Azonium Ions by Red Light in Whole Blood. *Angew. Chem., Int. Ed.* **2013,** *52*, 14127-14130.
77. Sanchez, A. M.; Barra, M.; de Rossi, R. H., On the mechanism of the acid/base-catalyzed thermal cis-trans isomerization of methyl orange. *J. Org. Chem.* **1999,** *64*, 1604-1609.
78. Dong, M.; Babalhavaeji, A.; Collins, C. V.; Jarrah, K.; Sadovski, O.; Dai, Q.; Woolley, G. A., Near-Infrared Photoswitching of Azobenzenes under Physiological Conditions. *J. Am. Chem. Soc.* **2017,** *139*, 13483-13486.
79. Wegener, M.; Hansen, M. J.; Driessen, A. J. M.; Szymanski, W.; Feringa, B. L., Photocontrol of Antibacterial Activity: Shifting from UV to Red Light Activation. *J. Am. Chem. Soc.* **2017,** *139*, 17979-17986.
80. Konrad, D. B.; Frank, J. A.; Trauner, D., Synthesis of Redshifted Azobenzene Photoswitches by Late-Stage Functionalization. *Chem. - Eur. J.* **2016,** *22*, 4364-4368.
81. Nguyen, T. H. L.; Gigant, N.; Joseph, D., Advances in Direct Metal-Catalyzed Functionalization of Azobenzenes. *ACS Catal.* **2018,** *8*, 1546-1579.
82. Yamaguchi, T.; Seki, T.; Tamaki, T.; Ichimura, K., Photochromism of hemithioindigo derivatives. I. Preparation and photochromic properties in organic solvents. *Bull. Chem. Soc. Jpn.* **1992,** *65*, 649-56.
83. Huber, L. A.; Hoffmann, K.; Thumser, S.; Boecher, N.; Mayer, P.; Dube, H., Direct Observation of Hemithioindigo-Motor Unidirectionality. *Angew. Chem., Int. Ed.* **2017,** *56*, 14536-14539.
84. Gerwien, A.; Reinhardt, T.; Mayer, P.; Dube, H., Synthesis of Double-Bond-Substituted Hemithioindigo Photoswitches. *Org. Lett.* **2018,** *20*, 232-235.
85. Maerz, B.; Wiedbrauk, S.; Oesterling, S.; Samoylova, E.; Nenov, A.; Mayer, P.; de Vivie-Riedle, R.; Zinth, W.; Dube, H., Making Fast Photoswitches Faster-Using Hammett Analysis to Understand the Limit of Donor-Acceptor Approaches for Faster Hemithioindigo Photoswitches. *Chem. - Eur. J.* **2014,** *20*, 13984-13992.
86. Zweig, J. E.; Newhouse, T. R., Isomer-Specific Hydrogen Bonding as a Design Principle for Bidirectionally Quantitative and Redshifted Hemithioindigo Photoswitches. *J. Am. Chem. Soc.* **2017,** *139*, 10956-10959.
87. Wiedbrauk, S.; Maerz, B.; Samoylova, E.; Reiner, A.; Trommer, F.; Mayer, P.; Zinth, W.; Dube, H., Twisted Hemithioindigo Photoswitches: Solvent Polarity Determines the Type of Light-Induced Rotations. *J. Am. Chem. Soc.* **2016,** *138*, 12219-12227.
88. Schoenberger, M.; Damjionaitis, A.; Zhang, Z.; Nagel, D.; Trauner, D., Development of a New Photochromic Ion Channel Blocker via Azologization of Fomocaine. *ACS Chem. Neurosci.* **2014,** *5*, 514-518.
89. Banghart, M.; Borges, K.; Isacoff, E.; Trauner, D.; Kramer, R. H., Light-activated ion channels for remote control of neuronal firing. *Nat. Neurosci.* **2004,** *7*, 1381-1386.
90. Volgraf, M.; Gorostiza, P.; Numano, R.; Kramer, R. H.; Isacoff, E. Y.; Trauner, D., Allosteric control of an ionotropic glutamate receptor with an optical switch. *Nat. Chem. Biol.* **2006,** *2*, 47-52.
91. Volgraf, M.; Gorostiza, P.; Szobota, S.; Helix, M. R.; Isacoff, E. Y.; Trauner, D., Reversibly Caged Glutamate: A Photochromic Agonist of Ionotropic Glutamate Receptors. *J. Am. Chem. Soc.* **2007,** *129*, 260-261.
92. Levitz, J.; Pantoja, C.; Gaub, B.; Janovjak, H.; Reiner, A.; Hoagland, A.; Schoppik, D.; Kane, B.; Stawski, P.; Schier, A. F.; Trauner, D.; Isacoff, E. Y., Optical control of metabotropic glutamate receptors. *Nat. Neurosci.* **2013,** *16*, 507-516.
93. Stein, M.; Middendorp, S. J.; Carta, V.; Pejo, E.; Raines, D. E.; Forman, S. A.; Sigel, E.; Trauner, D., Azo-Propofols: Photochromic Potentiators of GABAA Receptors. *Angew. Chem., Int. Ed.* **2012,** *51*, 10500-10504.
94. Lin, W.-C.; Davenport, C. M.; Mourot, A.; Vytla, D.; Smith, C. M.; Medeiros, K. A.; Chambers, J. J.; Kramer, R. H., Engineering a Light-Regulated GABAA Receptor for Optical Control of Neural Inhibition. *ACS Chem. Biol.* **2014,** *9*, 1414-1419.
95. Donthamsetti, P. C.; Winter, N.; Schonberger, M.; Levitz, J.; Stanley, C.; Javitch, J. A.; Isacoff, E. Y.; Trauner, D., Optical Control of Dopamine Receptors Using a Photoswitchable Tethered Inverse Agonist. *J. Am. Chem. Soc.* **2017,** *139*, 18522-18535.
96. Westphal, M. V.; Schafroth, M. A.; Sarott, R. C.; Imhof, M. A.; Bold, C. P.; Leippe, P.; Dhopeshwarkar, A.; Grandner, J. M.; Katritch, V.; Mackie, K.; Trauner, D.; Carreira, E. M.; Frank, J. A., Synthesis of Photoswitchable Δ9-Tetrahydrocannabinol Derivatives Enables Optical Control of Cannabinoid Receptor 1 Signaling. *J. Am. Chem. Soc.* **2017,** *139*, 18206-18212.
97. Laprell, L.; Huell, K.; Stawski, P.; Schoen, C.; Michalakis, S.; Biel, M.; Sumser, M. P.; Trauner, D., Restoring Light Sensitivity in Blind Retinae Using a Photochromic AMPA Receptor Agonist. *ACS Chem. Neurosci.* **2016,** *7*, 15-20.
98. Tsai, Y.-H.; Essig, S.; James, J. R.; Lang, K.; Chin, J. W., Selective, rapid and optically switchable regulation of protein function in live mammalian cells. *Nat. Chem.* **2015,** *7*, 554-561.
99. Schoenberger, M.; Trauner, D., A Photochromic Agonist for μ-Opioid Receptors. *Angew. Chem., Int. Ed.* **2014,** *53*, 3264-3267.
100. Tochitsky, I.; Banghart, M. R.; Mourot, A.; Yao, J. Z.; Gaub, B.; Kramer, R. H.; Trauner, D., Optochemical control of genetically engineered neuronal nicotinic acetylcholine receptors. *Nat. Chem.* **2012,** *4*, 105-111.
101. Broichhagen, J.; Schoenberger, M.; Cork, S. C.; Frank, J. A.; Marchetti, P.; Bugliani, M.; Shapiro, A. M. J.; Trapp, S.; Rutter, G. A.; Hodson, D. J.; Trauner, D., Optical control of insulin release using a photoswitchable sulfonylurea. *Nat. Commun.* **2014,** *5*, 5116.
102. Broichhagen, J.; Podewin, T.; Meyer-Berg, H.; von Ohlen, Y.; Johnston, N. R.; Jones, B. J.; Bloom, S. R.; Rutter, G. A.; Hoffmann-Roeder, A.; Hodson, D. J.; Trauner, D., Optical Control of Insulin Secretion Using an Incretin Switch. *Angew. Chem., Int. Ed.* **2015,** *54*, 15565-15569.
103. Mehta, Z. B.; Johnston, N. R.; Nguyen-Tu, M.-S.; Leclerc, I.; Rutter, G. A.; Broichhagen, J.; Schultz, P.; Trauner, D.; Broichhagen, J.; Larner, D. P.; Hodson, D. J.; Larner, D. P.; Hodson, D. J., Remote control of glucose homeostasis in vivo using photopharmacology. *Sci Rep* **2017,** *7*, 291.
104. Broichhagen, J.; Frank, J. A.; Johnston, N. R.; Mitchell, R. K.; Smid, K.; Marchetti, P.; Bugliani, M.; Rutter, G. A.; Trauner, D.; Hodson, D. J., A red-shifted photochromic sulfonylurea for the remote control of pancreatic beta cell function. *Chem. Commun. (Cambridge, U. K.)* **2015,** *51*, 6018-6021.
105. Velema, W. A.; van der Berg, J. P.; Hansen, M. J.; Szymanski, W.; Driessen, A. J. M.; Feringa, B. L., Optical control of antibacterial activity. *Nat. Chem.* **2013,** *5*, 924-928.
106. Pittolo, S.; Gomez-Santacana, X.; Eckelt, K.; Rovira, X.; Dalton, J.; Goudet, C.; Pin, J.-P.; Llobet, A.; Giraldo, J.; Llebaria, A.; Gorostiza, P., An allosteric modulator to control endogenous G protein-coupled receptors with light. *Nat. Chem. Biol.* **2014,** *10*, 813-815.
107. Frank, J. A.; Franquelim, H. G.; Schwille, P.; Trauner, D., Optical Control of Lipid Rafts with Photoswitchable Ceramides. *J. Am. Chem. Soc.* **2016,** *138*, 12981-12986.
108. Polosukhina, A.; Litt, J.; Tochitsky, I.; Nemargut, J.; Sychev, Y.; De Kouchkovsky, I.; Huang, T.; Borges, K.; Trauner, D.; Van Gelder, R. N.; Kramer, R. H., Photochemical Restoration of Visual Responses in Blind Mice. *Neuron* **2012,** *75*, 271-282.

109. Tochitsky, I.; Polosukhina, A.; Degtyar, V. E.; Gallerani, N.; Smith, C. M.; Friedman, A.; Van Gelder, R. N.; Trauner, D.; Kaufer, D.; Kramer, R. H., Restoring Visual Function to Blind Mice with a Photoswitch that Exploits Electrophysiological Remodeling of Retinal Ganglion Cells. *Neuron* **2014,** *81*, 800-813.
110. Seki, T.; Tamaki, T.; Yamaguchi, T., Photochromism of hemithioindigo derivatives. II. Photochromic behavior in bilayer membranes and related systems. *Bull. Chem. Soc. Jpn.* **1992,** *65*, 657-63.
111. Eggers; Fyles; Montoya, P., Synthesis and characterization of photoswitchable lipids containing hemithioindigo chromophores. *Journal of Organic Chemistry* **2001,** *66*, 2966 - 2977.
112. Kitzig, S.; Thilemann, M.; Cordes, T.; Rueck-Braun, K., Light-switchable peptides with a hemithioindigo unit: Peptide design, photochromism, and optical spectroscopy. *ChemPhysChem* **2016,** *17*, 1252-1263.
113. Cordes, T.; Weinrich, D.; Kempa, S.; Riesselmann, K.; Herre, S.; Hoppmann, C.; Rueck-Braun, K.; Zinth, W., Hemithioindigo-based photoswitches as ultrafast light trigger in chromopeptides. *Chem. Phys. Lett.* **2006,** *428*, 167-173.
114. Regner, N.; Herzog, T. T.; Haiser, K.; Hoppmann, C.; Beyermann, M.; Sauermann, J.; Engelhard, M.; Cordes, T.; Rueck-Braun, K.; Zinth, W., Light-Switchable Hemithioindigo-Hemistilbene-Containing Peptides: Ultrafast Spectroscopy of the Z → E Isomerization of the Chromophore and the Structural Dynamics of the Peptide Moiety. *J. Phys. Chem. B* **2012,** *116*, 4181-4191.
115. Herre, S.; Schadendorf, T.; Ivanov, I.; Herrberger, C.; Steinle, W.; Rueck-Braun, K.; Preissner, R.; Kuhn, H., Photoactivation of an inhibitor of the 12/15-lipoxygenase pathway. *ChemBioChem* **2006,** *7*, 1089-1095.
116. Lougheed, T.; Borisenko, V.; Hennig, T.; Rueck-Braun, K.; Woolley, G. A., Photomodulation of ionic current through hemithioindigo-modified gramicidin channels. *Org. Biomol. Chem.* **2004,** *2*, 2798-2801.
117. Garcia-Amoros, J.; Sanchez-Ferrer, A.; Massad, W. A.; Nonell, S.; Velasco, D., Kinetic study of the fast thermal cis-to-trans isomerisation of para-, ortho- and polyhydroxyazobenzenes. *Phys. Chem. Chem. Phys.* **2010,** *12*, 13238-13242.
118. Garcia-Amoros, J.; Bucinskas, A.; Reig, M.; Nonell, S.; Velasco, D., Fastest molecular photochromic switches based on nanosecond isomerizing benzothiazolium azophenolic salts. *Journal of Materials Chemistry C* **2014,** *2*, 474-480.
119. Gabor, G.; Frei, Y. F.; Fischer, E., Tautomerism and geometric isomerism in arylazophenols and naphthols. IV. Spectra and reversible photoreactions of m- and p-hydroxyazobenzene. *J. Phys. Chem.* **1968,** *72*, 3266-72.
120. Jacques, P.; Strub, H.; See, J.; Fleury, J.-P., A new aspect of azo-hydrazone tautomerism. *Tetrahedron* **1979,** *35*, 2071-2073.
121. Hammett, L. P., Effect of structure upon the reactions of organic compounds. Benzene derivatives. *J. Am. Chem. Soc.* **1937,** *59*, 96-103.
122. Hansch, C.; Leo, A.; Taft, R. W., A survey of Hammett substituent constants and resonance and field parameters. *Chem. Rev.* **1991,** *91*, 165-95.
123. Hallas, G.; Towns, A. D., Dyes derived from aminothiophenes. Part 4: Synthesis of some nitro-substituted thiophene-based azo disperse dyes. *Dyes Pigm.* **1997,** *33*, 319-336.
124. Hallas, G.; Towns, A. D., Dyes derived from aminothiophenes. Part 5. Spectral properties of some nitro-substituted thiophene-based azo disperse dyes. *Dyes Pigm.* **1997,** *34*, 133-146.
125. Hallas, G.; Choi, J.-H., Synthesis and spectral properties of azo dyes derived from 2-aminothiophenes and 2-aminothiazoles. *Dyes Pigm.* **1999,** *42*, 249-265.
126. Moylan, C. R.; McNelis, B. J.; Nathan, L. C.; Marques, M. A.; Hermstad, E. L.; Brichler, B. A., Challenging the Auxiliary Donor Effect on Molecular Hyperpolarizability in Thiophene-Containing Nonlinear Chromophores: X-ray Crystallographic and Optical Measurements on Two New Isomeric Chromophores. *J. Org. Chem.* **2004,** *69*, 8239-8243.
127. Barbero, M.; Cadamuro, S.; Dughera, S.; Giavenoll, C., Reactions of dry arenediazonium o-benzenedisulfonimides with triorganoindium compounds. *Eur. J. Org. Chem.* **2006**, 4884-4890.
128. Kim, J.-H.; Lee, J.-Y.; Bae, J.-H.; Choi, J.-H., Synthesis and spectral characteristics of disazo dyes containing heterocyclic diazo components. *Mol. Cryst. Liq. Cryst.* **2013,** *583*, 70-76.
129. Gore, S. T.; Mackie, R. K.; Tedder, J. M., Reaction of 2,4-dinitrobenzenediazonium ions with thiophenes. Part 2. Coupling reactions, involving unexpected reactions with electron-rich methyl groups in addition to the expected ring attack. *J. Chem. Soc., Perkin Trans. 1* **1976**, 1639-42.
130. Bartle, M.; Gore, S. T.; Mackie, R. K.; Tedder, J. M., Reaction of 2,4-dinitrobenzenediazonium ions with thiophenes. Part 1. An acidic Gomberg reaction. *J. Chem. Soc., Perkin Trans. 1* **1976**, 1636-8.
131. Haag, B.; Peng, Z.; Knochel, P., Preparation of Polyfunctional Indazoles and Heteroarylazo Compounds Using Highly Functionalized Zinc Reagents. *Org. Lett.* **2009,** *11*, 4270-4273.
132. Froehlich, H.; Kalt, W., Base-catalyzed halogen dance reaction at thiophenes: a spectroscopic reinvestigation of the synthesis of 2,5-dibromo-3-(trimethylsilyl)thiophene. *J. Org. Chem.* **1990,** *55*, 2993-5.
133. Madsen, J.; Merachtsaki, P.; Davoodpour, P.; Bergstrom, M.; Langstrom, B.; Andersen, K.; Thomsen, C.; Martiny, L.; Knudsen, G. M., Synthesis and biological evaluation of novel carbon-11-labelled analogues of citalopram as potential radioligands for the serotonin transporter. *Bioorg. Med. Chem.* **2003,** *11*, 3447-3456.
134. Zhang, P.; Cyriac, G.; Kopajtic, T.; Zhao, Y.; Javitch, J. A.; Katz, J. L.; Newman, A. H., Structure-Activity Relationships for a Novel Series of Citalopram (1-[3-(Dimethylamino)propyl]-1-(4-fluorophenyl)-1,3-dihydroisobenzofuran-5-carbonitrile) Analogues at Monoamine Transporters. *J. Med. Chem.* **2010,** *53*, 6112-6121.
135. Banala, A. K.; Zhang, P.; Plenge, P.; Cyriac, G.; Kopajtic, T.; Katz, J. L.; Loland, C. J.; Newman, A. H., Design and synthesis of 1-(3-(dimethylamino)propyl)-1-(4-fluorophenyl)-1,3- dihydroisobenzofuran-5-carbonitrile (citalopram) analogues as novel probes for the serotonin transporter S1 and S2 binding sites. *Journal of Medicinal Chemistry* **2013,** *56*, 9709 - 9724.
136. Zhang, P.; Joergensen, T. N.; Loland, C. J.; Newman, A. H., A rhodamine-labeled citalopram analogue as a high-affinity fluorescent probe for the serotonin transporter. *Bioorg. Med. Chem. Lett.* **2013,** *23*, 323-326.
137. Kumar, V.; Rahbek-Clemmensen, T.; Billesboelle, C. B.; Jorgensen, T. N.; Gether, U.; Newman, A. H., Novel and High Affinity Fluorescent Ligands for the Serotonin Transporter Based on (S)-Citalopram. *ACS Med. Chem. Lett.* **2014,** *5*, 696-699.
138. Plenge, P.; Shi, L.; Beuming, T.; Te, J.; Newman, A. H.; Weinstein, H.; Gether, U.; Loland, C. J., Steric Hindrance Mutagenesis in the Conserved Extracellular Vestibule Impedes Allosteric Binding of Antidepressants to the Serotonin Transporter. *J. Biol. Chem.* **2012,** *287*, 39316-39326.
139. Banala, A. K.; Zhang, P.; Plenge, P.; Cyriac, G.; Kopajtic, T.; Katz, J. L.; Loland, C. J.; Newman, A. H., Design and Synthesis of 1-(3-(Dimethylamino)propyl)-1-(4-fluorophenyl)-1,3-dihydroisobenzofuran-5-carbonitrile (Citalopram) Analogues as Novel Probes for the Serotonin Transporter S1 and S2 Binding Sites. *J. Med. Chem.* **2013,** *56*, 9709-9724.

140. Marson, C. M., Reactions of carbonyl compounds with (monohalo) methyleniminium salts (Vilsmeier reagents). *Tetrahedron* **1992,** *48*, 3659-726.
141. Yu, B.-C.; Shirai, Y.; Tour, J. M., Syntheses of new functionalized azobenzenes for potential molecular electronic devices. *Tetrahedron* **2006,** *62*, 10303-10310.
142. Priewisch, B.; Rueck-Braun, K., Efficient preparation of nitrosoarenes for the synthesis of azobenzenes. *Journal of Organic Chemistry* **2005,** *70*, 2350 - 2352.
143. Defoin, A., Simple preparation of nitrosobenzenes and nitrobenzenes by oxidation of anilines with H2O2 catalyzed with molybdenum salts. *Synthesis* **2004**, 706-710.
144. Bowden, B. F.; Cameron, D. W.; Crossley, M. J.; Feutrill, G. I.; Griffiths, P. G.; Kelly, D. P., Carbon-13 NMR studies of 1,4-naphthoquinones and 9,10-anthraquinones. *Aust. J. Chem.* **1979,** *32*, 769-77.
145. Moeller, E. R.; Joergensen, K. A., Chemistry of molybdenaoxaziridines. A study of oxo(N-phenylhydroxylamido-O,N)-(pyridine-2,6-dicarboxylato)(hexamethylphosphortriamide)molybdenum(VI) and its catalytic properties. *J. Am. Chem. Soc.* **1993,** *115*, 11814-22.
146. Burckard, P.; Fleury, J. P.; Weiss, F., Oxidation of amines by hydrogen peroxide in the presence of alkali pertungstate. *Bull. Soc. Chim. Fr.* **1965**, 2730-3.
147. Sakaue, S.; Tsubakino, T.; Nishiyama, Y.; Ishii, Y., Oxidation of aromatic amines with hydrogen peroxide catalyzed by cetylpyridinium heteropolyoxometalates. *J. Org. Chem.* **1993,** *58*, 3633-8.
148. Sakaue, S.; Sakata, Y.; Nishiyama, Y.; Ishii, Y., Oxidation of aliphatic and aromatic amines with hydrogen peroxide catalyzed by peroxoheteropoly oxometalates. *Chem. Lett.* **1992**, 289-92.
149. Ember, E.; Gazzaz, H. A.; Rothbart, S.; Puchta, R.; van Eldik, R., MnII-A fascinating oxidation catalyst: Mechanistic insight into the catalyzed oxidative degradation of organic dyes by H2O2. *Appl. Catal., B* **2010,** *95*, 179-191.
150. Mayer, F. P.; Holy, M.; Freissmuth, M.; Sitte, H. H.; Luf, A.; Schmid, R.; Nagy, C.; Sitte, H. H., Application of a Combined Approach to Identify New Psychoactive Street Drugs and Decipher Their Mechanisms at Monoamine Transporters. *Curr Top Behav Neurosci* **2017,** *32*, 333-350.
151. Koldsø, H.; Christiansen, A. B.; Sinning, S.; Schiøtt, B., Comparative Modeling of the Human Monoamine Transporters: Similarities in Substrate Binding. *ACS Chemical Neuroscience* **2013,** *4*, 295-309.
152. Kienzler, M. A.; Reiner, A.; Trautman, E.; Yoo, S.; Trauner, D.; Isacoff, E. Y., A Red-Shifted, Fast-Relaxing Azobenzene Photoswitch for Visible Light Control of an Ionotropic Glutamate Receptor. *J. Am. Chem. Soc.* **2013,** *135*, 17683-17686.
153. Kalka, K.; Merk, H.; Mukhtar, H., Photodynamic therapy in dermatology. *J Am Acad Dermatol* **2000,** *42*, 389-413; quiz 414-6.
154. Weissleder, R., A clearer vision for in vivo imaging. *Nat. Biotechnol.* **2001,** *19*, 316-317.
155. Zarei, M.; Mohamadzadeh, M., 3-Thiolated 2-azetidinones: Synthesis and in vitro antibacterial and antifungal activities. *Tetrahedron* **2011,** *67*, 5832 - 5840.
156. Steinle, W.; Rueck-Braun, K., Synthesis and characterization of novel bifunctional hemithioindigo chromophores. *Org. Lett.* **2003,** *5*, 141-144.
157. Cordes, T.; Schadendorf, T.; Priewisch, B.; Rueck-Braun, K.; Zinth, W., The Hammett Relationship and Reactions in the Excited Electronic State: Hemithioindigo Z/E-Photoisomerization. *J. Phys. Chem. A* **2008,** *112*, 581-588.
158. Davis, B. A.; Nagarajan, A.; Forrest, L. R.; Singh, S. K., Mechanism of Paroxetine (Paxil) Inhibition of the Serotonin Transporter. *Sci. Rep.* **2016,** *6*, 23789.
159. Johnson, T. A.; Curtis, M. D.; Beak, P., Highly Diastereoselective and Enantioselective Carbon-Carbon Bond Formations in Conjugate Additions of Lithiated N-Boc Allylamines to Nitroalkenes: Enantioselective Synthesis of 3,4- and 3,4,5-Substituted Piperidines Including (-)-Paroxetine. *J. Am. Chem. Soc.* **2001,** *123*, 1004-1005.
160. Hughes, G.; Kimura, M.; Buchwald, S. L., Catalytic Enantioselective Conjugate Reduction of Lactones and Lactams. *J. Am. Chem. Soc.* **2003,** *125*, 11253-11258.
161. Paraskar, A. S.; Sudalai, A., Co-catalyzed reductive cyclization of azido and cyano substituted α,β-unsaturated esters with NaBH4: enantioselective synthesis of (R)-baclofen and (R)-rolipram. *Tetrahedron* **2006,** *62*, 4907-4916.
162. Ito, M.; Sakaguchi, A.; Kobayashi, C.; Ikariya, T., Chemoselective Hydrogenation of Imides Catalyzed by CpRu(PN) Complexes and Its Application to the Asymmetric Synthesis of Paroxetine. *J. Am. Chem. Soc.* **2007,** *129*, 290-291.
163. Krautwald, S.; Schafroth, M. A.; Sarlah, D.; Carreira, E. M., Stereodivergent α-Allylation of Linear Aldehydes with Dual Iridium and Amine Catalysis. *J. Am. Chem. Soc.* **2014,** *136*, 3020-3023.
164. Takasu, K.; Nishida, N.; Tomimura, A.; Ihara, M., Convenient synthesis of substituted piperidinones from alpha,beta- unsaturated amides: Formal synthesis of deplancheine, tacamonine, and paroxetine. *Journal of Organic Chemistry* **2005,** *70*, 3957 - 3962.
165. Yu, M. S.; Lantos, I.; Peng, Z. Q.; Yu, J.; Cacchio, T., Asymmetric synthesis of (-)-paroxetine using PLE hydrolysis. *Tetrahedron Lett.* **2000,** *41*, 5647-5651.
166. Norris, T.; Braish, T. F.; Butters, M.; DeVries, K. M.; Hawkins, J. M.; Massett, S. S.; Rose, P. R.; Santafianos, D.; Sklavounos, C., Synthesis of trovafloxacin using various (1α,5α,6α)-3-azabicyclo[3.1.0]hexane derivatives. *Perkin 1* **2000**, 1615-1622.
167. Brown, H. C.; Heim, P., Selective reductions. XVIII. Fast reaction of primary, secondary, and tertiary amides with diborane. Simple, convenient procedure for the conversion of amides to the corresponding amines. *J. Org. Chem.* **1973,** *38*, 912-16.
168. Couturier, M.; Tucker, J. L.; Andresen, B. M.; Dube, P.; Negri, J. T., Palladium and Raney Nickel Catalyzed Methanolic Cleavage of Stable Borane-Amine Complexes. *Org. Lett.* **2001,** *3*, 465-467.
169. de Gonzalo, G.; Brieva, R.; Sanchez, V. M.; Bayod, M.; Gotor, V., Enzymatic Resolution of trans-4-(4'-Fluorophenyl)-3-hydroxymethylpiperidines, Key Intermediates in the Synthesis of (-)-Paroxetine. *J. Org. Chem.* **2001,** *66*, 8947-8953.
170. Sugi, K.; Itaya, N.; Katsura, T.; Igi, M.; Yamazaki, S.; Ishibashi, T.; Yamaoka, T.; Kawada, Y.; Tagami, Y.; Otsuki, M.; Ohshima, T., Improved synthesis of paroxetine hydrochloride propan-2-ol solvate through one of metabolites in humans, and characterization of the solvate crystals. *Chem. Pharm. Bull.* **2000,** *48*, 529-536.
171. Brandau, S.; Landa, A.; Franzen, J.; Marigo, M.; Jorgensen, K. A., Organocatalytic conjugate addition of malonates to α,β-unsaturated aldehydes: asymmetric formal synthesis of (-)-paroxetine, chiral lactams, and lactones. *Angew. Chem., Int. Ed.* **2006,** *45*, 4305-4309.
172. Bower, J. F.; Riis-Johannessen, T.; Szeto, P.; Whitehead, A. J.; Gallagher, T., Stereospecific construction of substituted piperidines. Synthesis of (-)-paroxetine and (+)-laccarin. *Chemical Communications* **2007**, 728 - 730.
173. Lengauer, T.; Rarey, M., Computational methods for biomolecular docking. *Curr. Opin. Struct. Biol.* **1996,** *6*, 402-406.

174. Salam, N. K.; Nuti, R.; Sherman, W., Novel Method for Generating Structure-Based Pharmacophores Using Energetic Analysis. *J. Chem. Inf. Model.* **2009,** *49*, 2356-2368.
175. Verdonk, M. L.; Cole, J. C.; Hartshorn, M. J.; Murray, C. W.; Taylor, R. D., Improved protein-ligand docking using GOLD. *Proteins: Struct., Funct., Genet.* **2003,** *52*, 609-623.
176. Morris, G. M.; Huey, R.; Lindstrom, W.; Sanner, M. F.; Belew, R. K.; Goodsell, D. S.; Olson, A. J., AutoDock and AutoDockTools: Automated docking with selective receptor flexibility. *J. Comput. Chem.* **2009,** *30*, 2785-2791.
177. Trott, O.; Olson, A. J., AutoDock Vina: Improving the speed and accuracy of docking with a new scoring function, efficient optimization, and multithreading. *J. Comput. Chem.* **2010,** *31*, 455-461.
178. Wolber, G.; Langer, T., LigandScout: 3-D Pharmacophores Derived from Protein-Bound Ligands and Their Use as Virtual Screening Filters. *J. Chem. Inf. Comput. Sci.* **2005,** *45*, 160-169.
179. Kollman, P. A.; Massova, I.; Reyes, C.; Kuhn, B.; Huo, S.; Chong, L.; Lee, M.; Lee, T.; Duan, Y.; Wang, W.; Donini, O.; Cieplak, P.; Srinivasan, J.; Case, D. A.; Cheatham, T. E., III, Calculating Structures and Free Energies of Complex Molecules: Combining Molecular Mechanics and Continuum Models. *Acc. Chem. Res.* **2000,** *33*, 889-897.
180. Greenidge, P. A.; Kramer, C.; Mozziconacci, J.-C.; Wolf, R. M., MM/GBSA Binding Energy Prediction on the PDBbind Data Set: Successes, Failures, and Directions for Further Improvement. *J. Chem. Inf. Model.* **2013,** *53*, 201-209.
181. Yang, B. V.; O'Rourke, D.; Li, J., Mild and selective debenzylation of tertiary amines using α-chloroethyl chloroformate. *Synlett* **1993**, 195-6.
182. Hanson, P.; Jones, J. R.; Taylor, A. B.; Walton, P. H.; Timms, A. W., Sandmeyer reactions. Part 7.1 An investigation into the reduction steps of Sandmeyer hydroxylation and chlorination reactions. *J. Chem. Soc., Perkin Trans. 2* **2002**, 1135-1150.
183. Roman, B. I.; Monbaliu, J.-C.; De Coen, L. M.; Verhasselt, S.; Schuddinck, B.; Van Hoeylandt, E.; Stevens, C. V., Feruloylbenzotriazole and Weinreb amide as bioinspired building blocks: A reactivity study towards O-, N-, S-, and C-nucleophiles. *Eur. J. Org. Chem.* **2014,** *2014*, 2594-2611.
184. Disli, A.; Kaya, V.; Guelce, A.; Yildirir, Y., Synthesis of 3-(arylazo)-4-hydroxy-3-penten-2-ones. *Org. Prep. Proced. Int.* **2004,** *36*, 96-98.
185. Devi, S.; Saraswat, M.; Grewal, S.; Venkataramani, S., Evaluation of Substituent Effect in Z -Isomer Stability of Arylazo-1 H -3,5-dimethylpyrazoles: Interplay of Steric, Electronic Effects and Hydrogen Bonding. *Journal of Organic Chemistry* **2018,** *83*, 4307 - 4322.
186. Patel; Vyas; Pandey; Fernandes, Reaction of 2,3,4-pentantrione-3-arylhydrazones with N,N-dimethylhydrazine: Formation of substituted 1H-pyrazoles via demethylation. *Synthetic Communications* **1992,** *22*, 3081 - 3087.
187. Schoenberger, M.; Althaus, M.; Fronius, M.; Clauss, W.; Trauner, D., Controlling epithelial sodium channels with light using photoswitchable amilorides. *Nat. Chem.* **2014,** *6*, 712-719.
188. Stricker, L.; Fritz, E.-C.; Peterlechner, M.; Doltsinis, N. L.; Ravoo, B. J., Arylazopyrazoles as Light-Responsive Molecular Switches in Cyclodextrin-Based Supramolecular Systems. *J. Am. Chem. Soc.* **2016,** *138*, 4547-4554.
189. Bekhit, A. A.; Ashour, H. M. A.; Guemei, A. A., Novel pyrazole derivatives as potential promising anti-inflammatory antimicrobial agents. *Archiv der Pharmazie* **2005,** *338*, 167 - 174.
190. Mahmudov, K. T.; Kopylovich, M. N.; Luzyanin, K. V.; Mizar, A.; Guedes da Silva, M. F. C.; Andre, V.; Pombeiro, A. J. L., Structural and thermal properties of three cyano-substituted azoderivatives of β-diketones. *J. Mol. Struct.* **2011,** *992*, 72-76.
191. Mustroph, H.; Henning, L.; Wilde, H., Different substituent effects on the absorption maxima of azomethines and hydrazones. *Z. Chem.* **1989,** *29*, 66-7.
192. Prakash, A.; Gambhir, I. R., Heterocyclic compounds from β-diketones. IV. p-Fluorobenzeneazo oxo esters and azodiketones and their cyclization. *J. Indian Chem. Soc.* **1966,** *43*, 529-35.
193. Pathak, V. N.; Joshi, R.; Gupta, N.; Rao, V. M., Synthesis and biological activities of some 2-alkyl/aryl-4-alkyl/aryl-3-arylazo-(1H)-1,5-benzodiazepines. *Indian J. Heterocycl. Chem.* **2003,** *12*, 331-334.
194. Weston, C. E.; Kramer, A.; Colin, F.; Yildiz, O.; Baud, M. G. J.; Meyer-Almes, F.-J.; Fuchter, M. J., Toward Photopharmacological Antimicrobial Chemotherapy Using Photoswitchable Amidohydrolase Inhibitors. *ACS Infect. Dis.* **2017,** *3*, 152-161.
195. Kosynkin, D. V.; Tour, J. M., Phenylene ethynylene diazonium salts as potential self-assembling molecular devices. *Org. Lett.* **2001,** *3*, 993-995.
196. Takahashi, S.; Kuroyama, Y.; Sonogashira, K.; Hagihara, N., A convenient synthesis of ethynylarenes and diethynylarenes. *Synthesis* **1980**, 627-30.
197. Zsolnai, T., Attempts to discover new fungistats. VIII. Antimicrobial activity of new compounds containing an arylazomethylene group. *Biochem. Pharmacol.* **1965,** *14*, 1325-62.
198. Deeb, A.; Yassin, F.; Ouf, N.; Shehta, W., Pyridazine derivatives and related compounds. 23*. Synthesis of 3-substituted pyrazolo[3,4-c]pyridazines and their application as disperse dyes. *Chem. Heterocycl. Compd. (N. Y., NY, U. S.)* **2010,** *46*, 212-222.
199. Taniguchi, T.; Kawada, A.; Kondo, M.; Quinn, J. F.; Kunitomo, J.; Yoshikawa, M.; Fushimi, M. Preparation of pyridazinone compounds as phosphodiesterase 10A inhibitors for preventing and treating schizophrenia. US20100197651A1, 2010.
200. Masoud, M. S.; Kaddah, A. M.; Khalil, A. M.; Tawfik, N. I., Potentiometric and spectrophotometric determinations of dissociation constants of β-diketoarylazo compounds. *Indian J. Chem., Sect. A* **1979,** *17A*, 502-4.
201. Helal, M. H.; Elgemeie, G. H.; El-kashouti, M. A.; ElMolla, M. M.; Elsayad, H. S.; Ahmed, K. A., Synthesis of new 5-arylazo-3-cyano-4,6-dimethyl-2-acetylchloridethiopyridine reactive disperse dyes and their applications in textile printing. *Pigm. Resin Technol.* **2008,** *37*, 234-242.
202. Ojha; Singh, Synthesis of N1-isonicotinyl-3,5-dimethyl-4-(substituted azo)-1 : 2-diazole. *Journal of the Indian Chemical Society* **1979,** *56*, 1233 - 1236.
203. Dai, W.-M.; Cheung, Y. K.; Tang, K. W.; Choi, P. Y.; Chung, S. L., Highly chemoselective acylation of substituted aminophenols with 3-(trimethylacetyl)-1,3-thiazolidine-2-thione. *Tetrahedron* **1995,** *51*, 12263-76.
204. Khurana, J. M.; Chauhan, S.; Bansal, G., Facile hydrolysis of esters with KOH-methanol at ambient temperature. *Monatsh. Chem.* **2004,** *135*, 83-87.
205. Barton, D. H. R.; Lester, D. J.; Ley, S. V., Oxidation of Ketone and Aldehyde Hydrazones, Oximes, and Semicarbazones and of Hydroxylamines and Hydrazo-compounds, using Benzeneselenic Anhydride. *Journal of the Chemical Society, Perkin Transactions 1: Organic and Bio-Organic Chemistry (1972-1999)* **1980**, 1212 - 1217.
206. Nakamoto, K.; Rundle, R. E., Spectroscopic study of the monomer and the dimer in nitrosobenzene derivatives. *J. Am. Chem. Soc.* **1956,** *78*, 1113-18.

207. Molander, G. A.; Cavalcanti, L. N., Nitrosation of aryl and heteroaryltrifluoroborates with nitrosonium tetrafluoroborate. *Journal of Organic Chemistry* **2012,** *77*, 4402 - 4413.
208. Kamogawa, H.; Kasai, T.; Andoh, T.; Nakamura, T., Liquid Crystalline Compounds Bearing Pyridine Ring: Azoxy Compounds with Alkyl Substituents. *Bulletin of the Chemical Society of Japan* **1987,** *60*, 2905 - 2910.
209. Alway, *Chemische Berichte* **1904,** *37*, 334.
210. Gowenlock, B. G.; Pfab, J.; Young, V. M., Kinetics of the oxidation of aromatic C-nitroso compounds by nitrogen dioxide. *J. Chem. Soc., Perkin Trans. 2* **1997**, 1793-1798.
211. Boyd, D. R.; Sharma, N. D.; Brannigan, I. N.; Evans, T. A.; Haughey, S. A.; McMurray, B. T.; Malone, J. F.; McIntyre, P. B. A.; Stevenson, P. J.; Allen, C. C. R., Toluene dioxygenase-catalyzed cis-dihydroxylation of benzo[b]thiophenes and benzo[b]furans: Synthesis of benzo[b]thiophene 2,3-oxide. *Organic and Biomolecular Chemistry* **2012,** *10*, 7292 - 7304.
212. Varedian, M.; Langer, V.; Bergquist, J.; Gogoll, A., An unexpected triethylsilane-triggered rearrangement of thioaurones to thioflavonols under SPPS conditions. *Tetrahedron Letters* **2008,** *49*, 6033 - 6035.
213. Badger, G. M.; Clark, D. J.; Davies, W.; Farrer, K. T. H.; Kefford, N. P., Thianaphthenecarboxylic acids. *J. Chem. Soc.* **1957**, 2624-30.
214. Irie, M.; Kato, M., Photoresponsive Molecular Tweezers. Photoregulated Ion Capture and Release Using Thioindigo Derivatives Having Ethylenedioxy Side Groups. *Journal of the American Chemical Society* **1985,** *107*, 1024 - 1028.
215. Erdelyi, M.; Varedian, M.; Skoeld, C.; Niklasson, I. B.; Nurbo, J.; Persson, A.; Bergquist, J.; Gogoll, A., Chemistry and folding of photomodulable peptides - stilbene and thioaurone-type candidates for conformational switches. *Org. Biomol. Chem.* **2008,** *6*, 4356-4373.
216. Pardin, C.; Pelletier, J. N.; Lubell, W. D.; Keillor, J. W., Cinnamoyl inhibitors of tissue transglutaminase. *Journal of Organic Chemistry* **2008,** *73*, 5766 - 5775.
217. Kim, J. H.; Shyam, P. K.; Kim, M. J.; Lee, H.-J.; Lee, J. T.; Jang, H.-Y., Enantioselective synthesis and antioxidant activity of 3,4,5-substituted piperidine derivatives. *Bioorg. Med. Chem. Lett.* **2016,** *26*, 3119-3121.
218. Chen, C.-C.; Ho, J.-C.; Chang, N.-C., A practical and efficient synthesis of (E)-beta-aryl-alpha,beta-unsaturated amides. *Tetrahedron* **2008,** *64*, 10350 - 10354.
219. Brenneman, J. B.; Ginn, J. D.; Hopkins, T. D.; Lowe, M. D.; Sarko, C. R.; Westbrook, J. A.; Yu, M.; Zhang, Z. Heterocyclic carboxylic acids as activators of soluble guanylate cyclase. US2016/24059, 2016.